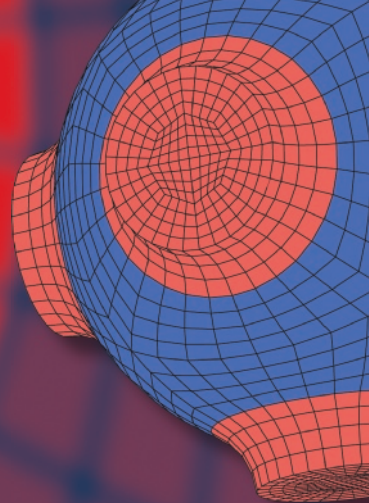


Advanced Structured Materials

Holm Altenbach
Victor A. Eremeyev
Igor S. Pavlov
Alexey V. Porubov *Editors*



Nonlinear Wave Dynamics of Materials and Structures

 Springer


Advanced Structured Materials

Volume 122

Series Editors

Andreas Öchsner, Faculty of Mechanical Engineering, Esslingen University of Applied Sciences, Esslingen, Germany

Lucas F. M. da Silva, Department of Mechanical Engineering, Faculty of Engineering, University of Porto, Porto, Portugal

Holm Altenbach , Faculty of Mechanical Engineering, Otto von Guericke University Magdeburg, Magdeburg, Sachsen-Anhalt, Germany

Common engineering materials reach in many applications their limits and new developments are required to fulfil increasing demands on engineering materials. The performance of materials can be increased by combining different materials to achieve better properties than a single constituent or by shaping the material or constituents in a specific structure. The interaction between material and structure may arise on different length scales, such as micro-, meso- or macroscale, and offers possible applications in quite diverse fields.

This book series addresses the fundamental relationship between materials and their structure on the overall properties (e.g. mechanical, thermal, chemical or magnetic etc) and applications.

The topics of *Advanced Structured Materials* include but are not limited to

- classical fibre-reinforced composites (e.g. glass, carbon or Aramid reinforced plastics)
- metal matrix composites (MMCs)
- micro porous composites
- micro channel materials
- multilayered materials
- cellular materials (e.g., metallic or polymer foams, sponges, hollow sphere structures)
- porous materials
- truss structures
- nanocomposite materials
- biomaterials
- nanoporous metals
- concrete
- coated materials
- smart materials

Advanced Structured Materials is indexed in Google Scholar and Scopus.


More information about this series at <http://www.springer.com/series/8611>


Holm Altenbach · Victor A. Eremeyev ·
Igor S. Pavlov · Alexey V. Porubov
Editors


Nonlinear Wave Dynamics of Materials and Structures


 Springer

Editors

Holm Altenbach 
Faculty of Mechanical Engineering
Otto von Guericke University Magdeburg
Magdeburg, Sachsen-Anhalt, Germany

Igor S. Pavlov 
Mechanical Engineering Research Institute
of the Russian Academy
of Sciences
Nizhny Novgorod, Russia

Victor A. Eremeyev 
Faculty of Civil and Environmental
Engineering
Gdańsk University of Technology
Gdańsk, Poland

Alexey V. Porubov 
Institute for Problems in Mechanical
Engineering of the Russian Academy
of Sciences
St. Petersburg, Russia

ISSN 1869-8433

Advanced Structured Materials

ISBN 978-3-030-38707-5

<https://doi.org/10.1007/978-3-030-38708-2>

ISSN 1869-8441 (electronic)

ISBN 978-3-030-38708-2 (eBook)

© Springer Nature Switzerland AG 2020

This work is subject to copyright. All rights are reserved by the Publisher, whether the whole or part of the material is concerned, specifically the rights of translation, reprinting, reuse of illustrations, recitation, broadcasting, reproduction on microfilms or in any other physical way, and transmission or information storage and retrieval, electronic adaptation, computer software, or by similar or dissimilar methodology now known or hereafter developed.

The use of general descriptive names, registered names, trademarks, service marks, etc. in this publication does not imply, even in the absence of a specific statement, that such names are exempt from the relevant protective laws and regulations and therefore free for general use.

The publisher, the authors and the editors are safe to assume that the advice and information in this book are believed to be true and accurate at the date of publication. Neither the publisher nor the authors or the editors give a warranty, expressed or implied, with respect to the material contained herein or for any errors or omissions that may have been made. The publisher remains neutral with regard to jurisdictional claims in published maps and institutional affiliations.

This Springer imprint is published by the registered company Springer Nature Switzerland AG
The registered company address is: Gewerbestrasse 11, 6330 Cham, Switzerland

Preface



Vladimir Erofeev was born on August 20, 1959, in Gorky (Soviet Union, now Nizhny Novgorod, Russian Federation). In 1981, he graduated from the Faculty of Mechanics and Mathematics of Gorky State University named after N. I. Lobachevsky (now National Research Lobachevsky State University of Nizhny Novgorod), majoring in mechanics.

From 1981 up to 1985, he worked in the department of acoustic diagnostics at the Research Institute for Normalization in Mechanical Engineering of the USSR State Committee for Standards, where, together with the “Molniya” Company Ltd., works were carried out as part of the “Buran” space program. In 1985–1986, he was an employee of the Material Testing Laboratory that paid main attention to full-scale and laboratory tests for the strength of large-diameter pipes used in oil and gas pipelines.

In 1986, at the Leningrad Polytechnic Institute (now Peter the Great St. Petersburg Polytechnic University), Vladimir Erofeev defended his Ph.D. thesis (candidate of physical–mathematical sciences) on “Nonlinear resonant interactions of one-dimensional waves in elastic dispersive media.” In 1986, a branch of the Mechanical Engineering Research Institute named after A.A. Blagonravov of the USSR Academy of Sciences (in 2013, it was transformed into Mechanical Engineering Research Institute of the Russian Academy of Sciences—MERI RAS) was created in Gorky, and Vladimir Erofeev was invited to attend the laboratory of wave processes in materials and structures. In 1990, he received the title of a senior researcher and headed the laboratory.

In 1994, at the Institute for Problems in Mechanical Engineering of the Russian Academy of Sciences (St. Petersburg, Russia) Vladimir Erofeev defended his doctoral dissertation “Wave processes in solids with microstructure” and obtained the scientific degree of Doctor of Physics and Mathematics. In 2003, he was awarded the academic title of professor in acoustics. From 1996 to 2015, Vladimir

Erofeev was the deputy director for Research of MERI RAS, from May 2015 to June 2016, he served as the acting director of this Institute, and in June 2016, he was elected as a director. Now, MERI RAS has the status of a branch of the Federal Research Center “Institute of Applied Physics of the Russian Academy of Sciences.”

Professor Erofeev is a well-known scientist and specialist in such areas as wave processes in continuous media, nonlinear mechanics, and physical acoustics where the following features of the waves are taken into account:

- dispersion of longitudinal and shear (body) waves;
- Rayleigh surface wave dispersion;
- existence of shear surface waves;
- nonlinear self-modulation and self-focusing;
- generation of higher harmonics, including those “forbidden” by the classical theory of elasticity;
- resonant interactions of longitudinal and shear waves with rotational waves;
- formation of strain solitons.

His main scientific results concern

- Development of mathematical models of the dynamics of mechanical systems with material microstructure, damage, geometric and physical nonlinearities, as well as the interaction of deformation, thermal, and magnetic fields.
- Study of dynamic processes in one- and two-dimensional elastic structural elements, in particular, the vibration of rods and plates in the presence of geometric and physical nonlinearities. Discovering of a splitting effect of strain nonlinear localized waves because of their nonlinear interaction.
- Investigation of strain wave processes in solid conductive media subjected to a magnetic field. The possibility of the formation of intense spatially localized magneto-elastic waves (shock waves and strain solitons in a rod, two-dimensional quasi-plane wave beams in a plate, and three-dimensional quasi-plane wave beams in an elastic conductive medium).
- Study of chaotic dynamics of mechanical systems with limited power, e.g., a solid body located on a transport belt is connected with a rigid wall by a viscoelastic connection and is elastically connected with a crank mounted on the motor shaft perpendicularly to the shaft. It is shown that this system has a chaotic dynamics. By averaging, the original system is reduced to a Lorenzian type system.
- Existence and stability of stationary cluster structures in homogeneous chains of dissipative coupled rotators.
- Stability of the movement of high-speed objects along the rail guides of the rocket for methodological and computational support of performing experiments on high-speed acceleration of a payload on a rocket track.

- Spectral acoustic system for testing materials and structures. It is successfully used to determine the accumulated operational damage in the structural elements of pipelines of pressure compensation systems and systems for cleaning and cooling of atomic icebreakers (in the framework of the Russian State program for extending the life of atomic icebreakers).
- Protection systems for machines and structures using inertia and dissipation of rheological (including magnetorheological) media. Original designs of hydraulic vibration mounts have been proposed that effectively reduce vehicle vibration and noise levels.

The list of main publications of Prof. Erofeev (note that there are different variants of writing the family name—Erofeev, Erofeyev):

1. Erofeyev V. I. Wave processes in solids with microstructure. World Scientific Publishing. New Jersey–London–Singapore–Hong Kong–Bangalore–Taipei, 2003
2. Altenbach H., Maugin G., Erofeev V. (Eds) Mechanics of Generalized Continua. Series “Advanced Structured Materials” (Eds A. Öchsner, H. Altenbach, L. F. M. da Silva), Vol. 7. Springer-Verlag, Berlin-Heidelberg, 2011
3. Bagdov A. G., Erofeyev V. I., Shekoyan A. V. Wave Dynamics of Generalized Continua. Series “Advanced Structured Materials” (Eds A. Öchsner, H. Altenbach, L. F. M. da Silva), Vol. 24. Springer-Verlag, Berlin-Heidelberg, 2016
4. Verichev N., Verichev S., Erofeev V. Chaos, Synchronization and Structures in Dynamics of Systems with Cylindrical Phase Space. Springer Nature. Series “Understanding Complex Systems”, 2020 (in press)
5. Erofeyev V. I., Potapov A. I. Longitudinal Strain Waves in Non-Linearly-Elastic Media with Couple Stresses. International Journal of Non-Linear Mechanics. 28(1993)4, pp. 483–488
6. Erofeev V. I., Klyueva N. V. Solitons and nonlinear periodic strain waves in rods, plates, and shells (A Review). Acoustical Physics. 48(2002)6, pp. 643–655
7. Verichev N. N., Verichev S. N., Erofeyev V. I. Chaotic dynamics of simple vibrational systems. Journal of Sound and Vibration. 310(2008)3, pp. 755–767
8. Verichev N. N., Verichev S. N., Erofeyev V. I. Damping lateral vibrations in rotary machinery using motor speed modulation. Journal of Sound and Vibration 329(2010)1, pp. 13–20
9. Butova S. V., Gerasimov S. I., Erofeev V. I., Kamchatnyi V.G. Stability of high-speed objects moving along a rocket track guide. Journal of Machinery and Manufacture and Reliability. 44(2015)1, pp. 1–5
10. Erofeev V. I., Pavlov I. S. Self-modulation of shear waves of deformation propagating in a one-dimensional granular medium with internal stresses. Mathematics and Mechanics of Solids. 21(2016)1, pp. 60–72

11. Erofeev V. I., Dar'enkov A. B., Plekhov A. S., Shokhin A.E. Nonlinear interaction of elastic waves in solid porous material under the condition of phase-group synchronism. *Journal of Vibroengineering*. 18(2016)5, pp. 2926–2935
12. Erofeev V. I., Leontieva A. V., Malkhanov A. O. Stationary longitudinal thermoelastic waves and the waves of the rotational type in the nonlinear micropolar medium. *ZAMM—Journal of Applied Mathematics and Mechanics*. 97(2017)9, pp. 1064–1071
13. Erofeev V. I., Malkhanov A. O. Macromechanical modelling of elastic and visco-elastic Cosserat continuum. *ZAMM—Journal of Applied Mathematics and Mechanics*. 97(2017)9, pp. 1072–1077
14. Erofeev V. I., Malkhanov A. O. Localized strain waves in a nonlinearly elastic conducting medium interacting with a magnetic field. *Mechanics of Solids*. 52(2017)2, pp. 224–231
15. Erofeev V. I., Leontyeva A. V., Pavlov I. S. Propagation of rotational waves in a block geomedium. *Journal of Vibroengineering*. 19(2017)8, pp. 6413–6422
16. Erofeev V. I., Kazhaev V. V., Pavlov I. S. Inelastic interaction and splitting of strain solitons propagating in a rod. *Journal of Sound and Vibration*. 419(2018), pp. 173–182
17. Erofeev V. I., Malkhanov A. O. Dispersion and self-modulation of waves propagating in a solid with dislocations. *Physical Mesomechanics*. 22(2019)3, pp. 173–180
18. Malkhanov A. O., Erofeev V. I., Leontieva A. V. Nonlinear travelling strain waves in a gradient-elastic medium. *Continuum Mechanics and Thermodynamics*. 31(2019)6, pp. 1931–1940

For more than 20 years, Vladimir Erofeev has been teaching as a professor of the Department of Theoretical, Computer and Experimental Mechanics of the Faculty of Mechanics and Mathematics (now: Institute of Information Technologies, Mathematics and Mechanics) of National Research Lobachevsky State University of Nizhny Novgorod. He delivers courses “Wave Processes in Mechanical Systems. Theory and Applications” and “Nonlinear Waves in Continuous Media”. He was the scientific supervisor for two doctors of sciences and 30 candidates of sciences. Three gold medals of the Russian Academy of Sciences awarded the scientific results of young scientists, carried out under the scientific supervision of Prof. Erofeev.

Professor Erofeev is a member of the Russian National Committee on Theoretical and Applied Mechanics, a member of the European Council for Mechanics (EUROMECH), a member of the board of the Russian Acoustic Society, and a member of the Russian Academy of Sciences Academic Council on Acoustics. He was one of the organizers of several all-Russian scientific conferences and participated in the organizing committees of the IUTAM symposium (1999, Sydney, Australia), the EUROMECH colloquia (2006, Delft, the

Netherlands; 2009, Paris, France, devoted to 100 years after the publication of the book of the Cosserat brothers), and the Russian–French–German trilateral seminars on generalized continua (2010, Wittenberg; 2015, Magdeburg, Germany).

Magdeburg, Germany
Gdańsk, Poland/Créteil, France
Nizhny Novgorod, Russia
St. Petersburg, Russia
December 2019

Holm Altenbach
Victor A. Eremeyev
Igor S. Pavlov
Alexey V. Porubov

Contents

1	Elimination of the Flutter Phenomenon in a Forced and Self-excited Nonlinear Beam Using an Improved Saturation Controller Algorithm	1
	Hassan M. Abdelhafez, Andrey V. Nasedkin and Mohamed E. Nassar	
1.1	Introduction	2
1.2	Model of Structure	3
1.3	Mathematical Analysis	5
	1.3.1 Multiple Scale Analysis	5
	1.3.2 Equilibrium Solution	8
	1.3.3 Stability Analysis	10
1.4	Results and Discussions	11
	1.4.1 Nonlinear Beam Without Control	11
	1.4.2 Effects of Velocity Feedback Controller	11
	1.4.3 The Effects of Various Controller Parameters and the Time Margins of Various Time Delays	14
1.5	Conclusions	22
	References	22
2	Use of the Modified Method of Parameter Continuation in Nonlinear Dynamics	25
	Igor V. Andrianov, Viktor I. Olevskyi and Yuliia B. Olevska	
2.1	Introduction	25
2.2	Asymptotic Method for Estimation of Free Vibrations of Beams and Rectangular Plates	27
	2.2.1 Explanation of Main Ideas of the Method on the Base of Calculation of Beam Oscillations	27
	2.2.2 Asymptotic Estimation of Free Vibrations of Nonlinear Plates	31
2.3	Using Asymptotic Method for Estimation of Parameter-Dependent Vibrations of Beams and Rectangular Plates	35

2.3.1	Explanation of the Method on the Base of Parameter-Dependent Beam Oscillations	37
2.3.2	Calculation of Parameter-Dependent Plates Vibrations	39
2.4	Nonlinear Vibration of Integrally Stiffened Cylindrical Shell	42
2.5	Using MMPC for Investigation of Systems with a Finite Number of Degrees of Freedom	46
2.5.1	Duffing Pendulum	47
2.5.2	Application of MMPC for Two Coupled Oscillators	49
2.6	Conclusions	53
	References	53
3	A Mathematically Consistent Vector-Matrix Representation of Generalized Hooke’s Law for Shear-Rigid Plates	57
	Marcus Aßmus and Holm Altenbach	
3.1	Introduction	57
3.1.1	Motivation	57
3.1.2	Organization of the Paper	58
3.1.3	Preliminaries and Notation	59
3.2	Linear Elastic Shear-Rigid Plates	60
3.2.1	Generalized Hooke’s Law	60
3.2.2	Properties of Tensorial Quantities	61
3.3	Vector-Matrix Notation	62
3.3.1	Derivation	62
3.3.2	Mathematical Consistency	65
3.4	Conclusion	66
	References	66
4	Mathematical Simulation of the Plate–Beam Interaction Affected by Colored Noise	69
	Valentin G. Bazhenov, Tatyana V. Yakovleva and Vadim A. Krysko	
4.1	Introduction	70
4.2	Problem Statement	70
4.3	Solution Methods	72
4.4	Numerical Experiment	73
4.5	Conclusion	74
	References	75

5	Dynamic Homogenization of a Chain with Bistable Springs. Statistical Approach	77
	Charlotte Blake and Andrej Cherkaev	
5.1	Introduction	77
5.1.1	Some Previous Results	78
5.1.2	Structure of the Paper	79
5.2	Preliminaries: Single-Spring Dynamics	79
5.2.1	Regimes	80
5.3	Dynamics of a Multi-spring Chain	82
5.3.1	Differential Equations and Numerics	82
5.3.2	Results of Numerical Simulation	83
5.4	Model for Dynamic Homogenization	85
5.4.1	Ansatz: Random Transitions	85
5.4.2	Properties	88
5.5	Validation of the Model	90
5.5.1	Numerical Issues	90
5.5.2	Relationship of Excitation Energy and Dispersion	93
5.6	Conclusions	95
	References	95
6	Analysis of Resistance to Penetration of a Cone into Frozen Sand Based on Data from Inverted Experiments	97
	Anatoliy Bragov, Vladimir V. Balandin, Vladimir VI. Balandin, Leonid Igumnov and Vasilij Kotov	
6.1	Introduction	98
6.2	Measuring Bars Methodology in Inverse Experiment	98
6.3	Mathematical Formulation of the Impact and Penetration Problem	101
6.4	The Data from Inverted Experiments and Calculations	102
6.5	Conclusion	103
	References	104
7	Some Solutions of Dynamic and Static Nonlinear Nonautonomous Klein-Fock-Gordon Equation	107
	Anatolii N. Bulygin and Yuri V. Pavlov	
7.1	Introduction	107
7.2	Methods of Construction of Exact Analytical Solutions of Dynamic and Static Nonautonomous Nonlinear Klein-Fock-Gordon Equations	108
7.3	Ansatzes for Solution of Dynamic Equation	110
7.4	Particular Solutions	112
7.5	Ansatzes for Solution of Static Equation	115
7.6	Conclusion	119
	References	119

8	A Comparison Between Heterogeneous and Homogeneous Layers for Nonlinear Bright Solitary SH Waves in Terms of Heterogeneous Effect	121
	Dilek Demirkuş	
8.1	Introduction	121
8.2	A Review Part for Some Materials in Homogeneous Media	122
8.2.1	Compressible Materials	124
8.2.2	Incompressible Materials	126
8.2.3	Generalized Neo-Hookean Materials	130
8.3	Comparison of Nonlinear Shear Horizontal Waves	132
8.4	Conclusions with Some New Results	134
	References	142
9	On Surface Kinetic Constitutive Relations	145
	Victor A. Eremeyev and Leonid P. Lebedev	
9.1	Introduction	145
9.2	Kinematics and Surface Strain Energy	146
9.3	Kinetic Constitutive Equation	147
9.4	Generalized Young–Laplace Equation	148
9.5	Conclusions	150
	References	151
10	Reduced Linear Viscoelastic Isotropic Cosserat Medium with Translational Viscosity: A Double Negative Acoustic Metamaterial	153
	Elena F. Grekova and Aleksandra P. Piatysheva	
10.1	Introduction	154
10.2	Dynamic Equations and Dispersion Relation	155
10.3	Absence of the Band Gap for an Arbitrary Translational Dissipation n	157
10.4	Asymptotical Approximation for Infinitesimal n	158
10.4.1	Case $ \Omega^2 - \Omega_{1D}^2 \gg n$	158
10.4.2	Case $ \Omega^2 - \Omega_{1D}^2 \ll n$	160
10.4.3	Case $(\Omega^2 - \Omega_{1D}^2)/n = O(1)$	162
10.5	Comparison of Analytical and Numerical Results and Discussion	164
	References	166
11	On Dynamic Model of Structural Transformations in Solids	169
	Dmitry A. Indeitsev, Boris N. Semenov, Dmitry Yu. Skubov and Dmitry S. Vavilov	
11.1	Introduction	170
11.2	Basic Equations of Two-Component Medium	171

11.3	Statement of the Problem. Dispersion Curves	173
11.4	On the Method of Variable Interval	175
11.5	Discrete Model	176
11.6	Continuous Model	180
11.7	Conclusion	184
	References	185
12	Dynamic Penetration into Water Saturated and Frozen Sand: Numerical Analysis of the Inverse Experimental Methodology	187
	Vasiliy Kotov, Vladimir V. Balandin, Vladimir VI. Balandin, Anatoliy Bragov, Andrey Lomunov and Svetlana Litvinchuk	
12.1	Introduction	188
12.2	Grigoryan’s Mathematical Model of the Dynamics of Soil Media	189
12.3	Formulation of Numerical Modeling Problems	191
12.4	Results of Numerical Computations	193
12.5	Conclusion	196
	References	196
13	Extended Model of Surface-Related Effects in Second-Gradient Elasticity. Surface Waves Related to the Nature of Adhesion	199
	Sergey Lurie, Petr Belov and Elena Lykosova	
13.1	Introduction	200
13.2	Formulation of Boundary Value Problems for Elastic Bodies with Adhesion-Active Surfaces	201
13.3	Qualitative Analysis of the Elastic Moduli of Surface Interactions	204
13.4	Extended Continual Adhesion Models of Classical Body	207
	13.4.1 Symmetry Conditions	208
	13.4.2 Frame-Indifference Condition	208
	13.4.3 Weak Frame-Indifference Condition	211
13.5	Surface Waves Related to the Nature of Adhesion	212
	13.5.1 Longitudinal Surface U -waves	213
	13.5.2 Transverse Surface V -Waves	214
	13.5.3 Transverse Surface W -Waves	215
	13.5.4 Surface Θ -Waves and Plane Surface Ω -Waves	216
13.6	Conclusion	218
	References	218
14	Generalized Space–Time Fractional Dynamics in Networks and Lattices	221
	Thomas M. Michelitsch, Alejandro P. Riascos, Bernard A. Collet, Andrzej F. Nowakowski and Franck C. G. A. Nicolleau	
14.1	Introduction	222
14.2	Renewal Process and Continuous-Time Random Walk	222

14.3	Poisson Process	226
14.4	Fractional Poisson Process	227
14.5	Generalization of the Fractional Poisson Process	229
14.6	Continuous-Time Random Walk on Networks	233
14.7	Generalized Space–Time Fractional Diffusion in \mathbb{Z}^d	235
14.8	Diffusion Limit	239
14.9	Conclusions	243
	Appendix: Laplace Transforms and Fractional Operators	243
	References	248
15	Analytical Method for Describing the Dynamics of Mechanical Systems in Variable Time Intervals	251
	Andrey N. Morozov and Andrey L. Nazolin	
15.1	Introduction	252
15.2	Problem of Analytical Description of the Dynamics of Mechanical Systems in Variable Time Intervals	253
15.3	Method of Time Intervals	257
15.4	Relationship of Time Intervals with the Angle of Rotation During Rotational Motion	258
15.5	Relationship of the Period with the Displacement During Oscillatory Motion	263
15.6	Relationship of Time Intervals with Displacement During Reciprocating Motion	267
15.7	Estimation of the Scope of Linear Relations	269
15.8	Conclusion	271
	References	271
16	Propagation of Non-stationary Axisymmetric Perturbations from a Spherical Cavity in Cosserat Medium	273
	Lam V. Nguyen and Dmitry V. Tarlakovskii	
16.1	Introduction	273
16.2	Statement of the Problem	274
16.3	Presentation of the Solution in the Form of Series	277
16.4	General Solution Images	279
16.5	Problem-Solving Images	283
16.6	Linear Approximation of the Solution	285
16.7	Originals of the Solution	289
16.8	Examples	290
16.9	Conclusion	290
	References	291

17 The Equations of Coupled Dynamics of Electromagnetoelastic Thin Shells 293
 Thong D. Pham, Dmitry V. Tarlakovskii and Vladimir A. Vestyak
 17.1 Introduction 293
 17.2 Equations of Motion of the Elastic Shell at Given Loads 295
 17.3 Closed-Form Solution for System of Equations of an Electromagnetoelastic Shell. 296
 17.4 Equations for an Isotropic Conductor Shell 302
 17.5 Equations of Motion of an Electromagnetoelastic Plate 304
 References 305

18 Nonlinear Dynamics of Two-Dimensional Lattices with Complex Structure 309
 Alexey V. Porubov, Alena E. Osokina and Ilya D. Antonov
 18.1 Introduction 309
 18.2 Two-Dimensional Waves in a Generalized Square Lattice 311
 18.2.1 Statement of the Problem 311
 18.2.2 Auxetic Behavior in the Linearized Model. 312
 18.2.3 Continuum Nonlinear Equations 314
 18.2.4 Shear Waves 316
 18.3 Two-Dimensional Nonlinear Waves Propagation in Graphene Lattice. 317
 18.3.1 Continuum Limit for Weakly Transversely Perturbed Waves 320
 18.4 Two-Dimensional Dynamical Strain Processes 324
 18.4.1 Exact Solutions 324
 18.4.2 Transverse Instability of Longitudinal and Shear Waves 325
 18.4.3 Numerical Solutions 326
 18.5 Conclusions 332
 References 333

19 Influence of First to Second Gradient Coupling Tensors Terms with Surface Effects on the Wave Propagation of 2D Network Materials 335
 Yosra Rahali, Hilal Reda, Benoit Vieille, Hassan Lakiss and Jean-François Ganghoffer
 19.1 Introduction 336
 19.2 Second Order Discrete Homogenization for Viscoelastic Network Materials 337
 19.3 Wave Propagation Analysis in Non-centrosymmetric Architectures 342

19.4	Conclusion	348
	Appendix: Transition from Curvilinear to Cartesian Coordinates	349
	References	350
20	A Short Review of Rotations in Rigid Body Mechanics	353
	Wilhelm Rickert, Sebastian Glane and Wolfgang H. Müller	
20.1	Introduction	353
20.2	Rotation and Change of Base	354
	20.2.1 Rotations of Tensors	355
	20.2.2 Representation of the Rotation Tensor	356
20.3	Time Derivatives in Rotating Systems	357
20.4	Analysis of Sequential Rotations	359
	20.4.1 Simplification for Attached Axes	360
	20.4.2 Summary for Sequential Rotations	361
20.5	Treatment of Successive Rotations in the Literature	362
20.6	Conclusion	364
20.7	The LEVI-CIVITA Tensor	365
20.8	Angular Velocity in Terms of Orientation Parameters	365
	References	367
21	A Variant of the Description of the Acoustic and Optical Branches of the Dispersion Law of High-Frequency Waves in an Elastic Medium	369
	Sergey N. Romashin, Margarita V. Khoroshilova and Vladimir S. Shorkin	
21.1	Introduction	370
21.2	General Provisions and Assumptions	370
	21.2.1 An Elastic Medium Model	370
	21.2.2 Expansion Feature of Elastic Material Model	374
21.3	The Optical and Acoustic Branches Model for Dispersion Law	375
21.4	Results and Experimental Data Comparison	377
21.5	Conclusion	377
	References	378
22	Supercomputer Modeling of Wave Propagation in Blocky Media Accounting Fractures of Interlayers	379
	Vladimir M. Sadovskii and Oxana V. Sadovskaya	
22.1	Introduction	380
22.2	Blocky Medium with Elastic-Plastic Interlayers	381
22.3	Simulation of Cracks in Interlayers	384
22.4	Elastic-Plastic Cosserat Continuum	386
22.5	Results of Computation	389
22.6	Concluding Remarks	397
	References	397

23 Structural and Micropolar Beam Models of Nanocrystalline Materials (One-Dimensional Case) 399
 Samvel H. Sargsyan

23.1 Introduction 399

23.2 Discrete-Moment Model of the Atom Chain. Hamilton’s Principle. 400

23.3 One-Dimensional (“Bending”) Continual Model of Linear Chain of Atoms. Hamilton’s Principle for the Continual Model 403

23.4 Equations of the Simple Applied Theory of Micropolar Elastic Thin Beams with Free Fields of Displacements and Rotations. Comparison of the Constructed Models and Determination of the Micropolar Elastic Parameters 406

23.5 Conclusion 408

References 408

24 Circuit Analogies in the Search for New Metamaterials: Phenomenology of a Mechanical Diode 411
 Mario Spagnuolo

24.1 Introduction 411

24.2 Continuum Model of Pantographic Structures 412

 24.2.1 Deformation Energy of a Pantographic Sheet 413

24.3 A Mechanical Diode 414

24.4 Conclusion 417

References 418

25 Damping of Oscillations by a Vibro-Impact System with Serial Magnetic Impact Pairs 423
 Yuri M. Zamuragin, Alexander M. Gousskov and Vitaly L. Krupenin

25.1 Introduction 423

25.2 Problem Statement 424

25.3 Motion Equations 425

25.4 Frequency Response 429

25.5 Conclusion 431

Appendix 431

References 432

26 Exact Solutions of Cubic-Quintic Modified Korteweg-de-Vries Equation 433
 Alexander I. Zemlyanukhin and Andrey V. Bochkarev

26.1 Introduction 433

26.2 Painlevé Analysis 434

26.3 Case 1. $a_1 = 0, a_0 \neq 0$. Periodic and Soliton Solutions. 435

26.4 Case 2. $a_1 = 0, a_0 = 0$. Periodic and Soliton Solutions. 440

26.5	Case 3. Kink-Shaped Solution	441
26.6	Case 4. $a_1 \neq 0$, $a_0 \neq 0$. Approximate Solution	442
	References	445
27	Modelling of Unsteady Elastic Diffusion Oscillations of a Timoshenko Beam	447
	Andrei V. Zemskov and Dmitry V. Tarlakovskii	
27.1	Introduction	447
27.2	Problem Formulation	448
27.3	Integral Representation of the Solution	453
27.4	Solution Algorithm	454
27.5	Example of Computation	456
27.6	Conclusions	458
	References	460

Contributors

Hassan M. Abdelhafez Faculty of Electronic Engineering, Menoufia University, Menouf, Egypt

Holm Altenbach Otto von Guericke University, Magdeburg, Germany

Igor V. Andrianov Institute of General Mechanics RWTH Aachen University, Aachen, Germany

Ilya D. Antonov Institute for Problems in Mechanical Engineering, St. Petersburg, Russian Federation;
Peter the Great St. Petersburg Polytechnic University (SPbPU), St. Petersburg, Russian Federation

Marcus Aßmus Otto von Guericke University, Magdeburg, Germany

Vladimir V. Balandin Research Institute of Mechanics, National Research Lobachevsky State University of Nizhny Novgorod, Nizhny Novgorod, Russian Federation

Vladimir Vl. Balandin Research Institute of Mechanics, National Research Lobachevsky State University of Nizhny Novgorod, Nizhny Novgorod, Russian Federation

Valentin G. Bazhenov Research Institute for Mechanics, Lobachevsky State University of Nizhny Novgorod, Nizhny Novgorod, Russian Federation

Petr Belov Institute of Applied Mechanics of Russian Academy of Science, Moscow, Russian Federation

Charlotte Blake Department of Mathematics, University of Utah, Salt Lake City, UT, USA

Andrey V. Bochkarev Yuri Gagarin State Technical University of Saratov, Saratov, Russian Federation

Anatoliy Bragov Research Institute of Mechanics, National Research Lobachevsky State University of Nizhny Novgorod, Nizhny Novgorod, Russian Federation

Anatolii N. Bulygin Institute for Problems in Mechanical Engineering of Russian Academy of Sciences, Saint Petersburg, Russia

Andrej Cherkaev Department of Mathematics, University of Utah, Salt Lake City, UT, USA

Bernard A. Collet Institut Jean le Rond d'Alembert, Sorbonne Université, Paris, France

Dilek Demirkuş Department of Mathematics, Beykent University, Istanbul, Turkey

Victor A. Eremeyev Faculty of Civil and Environmental Engineering, Gdańsk University of Technology, Gdańsk, Poland;
Southern Federal University, Rostov on Don, Russia;
Southern Scientific Center of RASci, Rostov on Don, Russian Federation

Jean-François Ganghoffer LEM3. Université de Lorraine, CNRS, Metz, France

Sebastian Glane Institute of Mechanics, Chair of Continuum Mechanics and Constitutive Theory, Technische Universität Berlin, Berlin, Germany

Alexander M. Gousskov N.E. Bauman Moscow State Technical University (BMSTU), Moscow, Russian Federation;
A.A. Blagonravov Mechanical Engineering Research Institute of the RAS (IMASH RAN), Moscow, Russian Federation

Elena F. Grekova Institute of Problems in Mechanical Engineering, Russian Academy of Sciences, St. Petersburg, Russian Federation

Leonid Igumnov Research Institute of Mechanics, National Research Lobachevsky State University of Nizhny Novgorod, Nizhny Novgorod, Russian Federation

Dmitry A. Indeitsev Institute for Problems in Mechanical Engineering, St. Petersburg, Russian Federation;
St. Petersburg University, St. Petersburg, Russian Federation;
St. Petersburg Polytechnic University Peter the Great, St. Petersburg, Russian Federation

Margarita V. Khoroshilova Orel State University named after I.S. Turgenev, Orel, Russian Federation

Vasily Kotov Research Institute of Mechanics, National Research Lobachevsky State University of Nizhny Novgorod, Nizhny Novgorod, Russian Federation

Vitaly L. Krupenin A.A. Blagonravov Mechanical Engineering Research Institute of the RAS (IMASH RAN), Moscow, Russian Federation

Vadim A. Krysko Yuri Gagarin State Technical University of Saratov, Saratov, Russian Federation

Hassan Lakiss GPM, INSA Rouen, Université de Rouen, Saint-Étienne-Du-Rouvray, France

Leonid P. Lebedev Universidad Nacional de Colombia, Bogotá, D.C., Colombia

Svetlana Litvinchuk Research Institute of Mechanics, National Research Lobachevsky State University of Nizhny Novgorod, Nizhny Novgorod, Russian Federation

Andrey Lomunov Research Institute of Mechanics, National Research Lobachevsky State University of Nizhny Novgorod, Nizhny Novgorod, Russian Federation

Sergey Lurie Institute of Applied Mechanics of Russian Academy of Science, Moscow, Russian Federation

Elena Lykosova Institute of Applied Mechanics of Russian Academy of Science, Moscow, Russian Federation

Thomas M. Michelitsch Institut Jean le Rond d'Alembert, Sorbonne Université, Paris, France

Andrey N. Morozov Bauman Moscow State Technical University, Moscow, Russian Federation

Wolfgang H. Müller Institute of Mechanics, Chair of Continuum Mechanics and Constitutive Theory, Technische Universität Berlin, Berlin, Germany

Andrey V. Nasedkin Institute of Mathematics, Mechanics and Computer Science, Southern Federal University, Rostov-on-Don, Russian Federation

Mohamed E. Nassar Faculty of Electronic Engineering, Menoufia University, Menouf, Egypt;
Institute of Mathematics, Mechanics and Computer Science, Southern Federal University, Rostov-on-Don, Russian Federation

Andrey L. Nazolin Bauman Moscow State Technical University, Moscow, Russian Federation;
Mechanical Engineering Research Institute of the Russian Academy of Sciences, Moscow, Russian Federation

Lam V. Nguyen Moscow Aviation Institute, Moscow, Russian Federation

Franck C. G. A. Nicolleau Department of Mechanical Engineering, University of Sheffield, Sheffield, UK

Andrzej F. Nowakowski Department of Mechanical Engineering, University of Sheffield, Sheffield, UK

Yuliia B. Olevska Department of Mathematics, National Technical University “Dnipro Polytechnic”, Dnipro, Ukraine

Viktor I. Olevskiy Mathematic Department of State Higher Educational Institution “Ukrainian State University of Chemical Technology”, Dnipro, Ukraine

Alena E. Osokina Peter the Great St. Petersburg Polytechnic University (SPbPU), St. Petersburg, Russian Federation

Yuri V. Pavlov Institute for Problems in Mechanical Engineering of Russian Academy of Sciences, Saint Petersburg, Russia

Thong D. Pham Moscow Aviation Institute, Moscow, Russian Federation

Aleksandra P. Piatysheva Peter the Great St. Petersburg Polytechnic University, St. Petersburg, Russian Federation

Alexey V. Porubov Institute for Problems in Mechanical Engineering, St. Petersburg, Russian Federation;
Peter the Great St. Petersburg Polytechnic University (SPbPU), St. Petersburg, Russian Federation

Yosra Rahali GPM, INSA Rouen, Université de Rouen, Saint-Étienne-Du-Rouvray, France

Hilal Reda Faculty of Engineering, Section III, Lebanese University, Beirut, Lebanon

Alejandro P. Riascos Instituto de Física, Universidad Nacional Autónoma de México, Ciudad de México, Mexico

Wilhelm Rickert Institute of Mechanics, Chair of Continuum Mechanics and Constitutive Theory, Technische Universität Berlin, Berlin, Germany

Sergey N. Romashin Orel State University named after I.S. Turgenev, Orel, Russian Federation

Oxana V. Sadovskaya Institute of Computational Modeling SB RAS, Krasnoyarsk, Russian Federation

Vladimir M. Sadovskii Institute of Computational Modeling SB RAS, Krasnoyarsk, Russian Federation

Samvel H. Sargsyan Shirak State University, Gyumri, Armenia

Boris N. Semenov Institute for Problems in Mechanical Engineering, St. Petersburg, Russian Federation;
St. Petersburg University, St. Petersburg, Russian Federation;
St. Petersburg Polytechnic University Peter the Great, St. Petersburg, Russian Federation

Vladimir S. Shorkin Orel State University named after I.S. Turgenev, Orel, Russian Federation

Dmitry Yu. Skubov Institute for Problems in Mechanical Engineering, St. Petersburg, Russian Federation;
St. Petersburg Polytechnic University Peter the Great, St. Petersburg, Russian Federation

Mario Spagnuolo International Research Center M&MoCS & Università degli Studi dell'Aquila, L'Aquila, Italy

Dmitry V. Tarlakovskii Moscow Aviation Institute, Moscow, Russian Federation;
Institute of Mechanics, Lomonosov Moscow State University, Moscow, Russian Federation

Dmitry S. Vavilov Institute for Problems in Mechanical Engineering, St. Petersburg, Russian Federation;
Mozhaisky Military Space Academy, St. Petersburg, Russian Federation

Vladimir A. Vestyak Moscow Aviation Institute, Moscow, Russian Federation

Benoit Vieille GPM, INSA Rouen, Université de Rouen, Saint-Étienne-Du-Rouvray, France

Tatyana V. Yakovleva Research Institute for Mechanics, Lobachevsky State University of Nizhny Novgorod, Nizhny Novgorod, Russian Federation;
Yuri Gagarin State Technical University of Saratov, Saratov, Russian Federation

Yuri M. Zamuragin N.E. Bauman Moscow State Technical University (BMSTU), Moscow, Russian Federation

Alexander I. Zemlyanukhin Yuri Gagarin State Technical University of Saratov, Saratov, Russian Federation

Andrei V. Zemskov Moscow Aviation Institute, Moscow, Russian Federation;
Institute of Mechanics, Lomonosov Moscow State University, Moscow, Russian Federation

Chapter 1

Elimination of the Flutter Phenomenon in a Forced and Self-excited Nonlinear Beam Using an Improved Saturation Controller Algorithm



Hassan M. Abdelhafez, Andrey V. Nasedkin and Mohamed E. Nassar

Abstract Flutter is a dynamic instability of an elastic structure subjected to fluid flow. Flutter phenomenon of the beam cannot occur unless bending and twisting vibrations occur simultaneously. This paper intends to eliminate the flutter phenomenon by suppressing the bending mode vibrations. The mathematical model under study is the Euler–Bernoulli beam reduced to the bending mode vibrations. The beam operates in the presence of external harmonic excitation on its support and fluid flow. The proposed algorithm uses the saturation controller and the velocity feedback controller together. The improved saturation controller was connected to the primary system by using a quadratic velocity coupling term, which introduces a better vibration reduction than that of the ordinary saturation controller. We applied the multiple-timescale perturbation technique (MSPT) and obtained a first-order approximate solution. We studied the effects of various controller parameters and time delays on the system response. We investigated the stability of the equilibrium solution and the time margins of various time delays and validated some analytical results numerically. Finally, we submitted further improvement to eliminate the undesired regions in the frequency response curve of the saturation controller.

Keywords Active vibration control · Time delay · Improved saturation controller · Velocity feedback controller · Self-excited vibrations · Nonlinear beam oscillations · Multiple timescale method

H. M. Abdelhafez · M. E. Nassar
Faculty of Electronic Engineering, Menoufia University, Menouf 32952, Egypt
e-mail: mohammed.alsayed75@el-eng.menofia.edu.eg

A. V. Nasedkin (✉) · M. E. Nassar
Institute of Mathematics, Mechanics and Computer Science, Southern Federal University,
Milchakova Street 8a, Rostov-on-Don 344090, Russian Federation
e-mail: nasedkin@math.sfedu.ru

© Springer Nature Switzerland AG 2020
H. Altenbach et al. (eds.), *Nonlinear Wave Dynamics of Materials and Structures*, Advanced Structured Materials 122,
https://doi.org/10.1007/978-3-030-38708-2_1

1.1 Introduction

Flutter is a dangerous phenomenon that occurs when an elastic structure is subjected to aerodynamic forces. These aerodynamic forces are exerted on the elastic structure by the fluid flow due to relative motion between the structure and the fluid flow. Interactions between the structure's deflection and the force exerted by the fluid flow can cause positive feedback to the structure. This positive feedback increases oscillations which may lead to instability and flutter phenomenon. So there may be a point at which structure's damping becomes insufficient to damp out these motions. Flutter phenomenon cannot occur unless bending and rotational motions occur simultaneously. For example, the wing of a plane has two basic degrees of freedom or natural modes of vibration: pitch (rotational) and plunge (bending). These elastic structures include aircraft, buildings, telegraph wires, stop signs, and bridges. The mathematical model under study here is an Euler–Bernoulli beam with nonlinear curvature. This model was given in [1]. The beam is subjected to an external harmonic excitation close to its first natural frequency; also, the beam is subjected to a fluid flow which is modeled by nonlinear damping with a negative linear part (Rayleigh's function). This negative damping force causes positive feedback which is proportional to the velocity of motion, so the oscillating system draws energy from the fluid flow and its vibrations increase even in case of free vibrations. However, it vanishes when motion ends, so the fluid flow causes the so-called self-excited vibrations. Self-excited vibrations were studied extensively in [2, 3]. The beam model under study was reduced to a first mode vibration "bending mode" as seen later in the beam model. Interaction between forced vibrations and self-excited vibrations may cause a flutter phenomenon. So our main purpose here is to reduce the bending vibrations in order to restrict this phenomenon.

The saturation phenomenon studied in [4] can be used to design an active vibration controller called a saturation controller. This controller uses the saturation phenomenon with 2:1 internal resonance to suppress the steady-state vibrations of dynamical systems. The ordinary saturation controller was coupled to dynamical systems by using a quadratic position coupling term, as seen in [5, 6]. Authors in [7] used the saturation phenomenon for harvesting energy from the L-shaped vibration system. In [8], a robust saturation controller was designed based on the optimization problem of the linear matrix inequality and applied to a linear system with an active mass damper. A theoretical investigation of a two-degree-of-freedom system subjected to saturation was studied in [9] and applied to a system consisting of a direct current (DC) motor with a nonlinear controller and a harmonic forcing voltage. The effect of dry friction on the response of a system consisting of a saturation controller coupled to a permanent magnet DC motor was discussed in [10] under harmonic excitation. Pai et al. in [11, 12] improved the performance of the saturation controller by using a quadratic velocity coupling term in the controller and adding negative velocity feedback to the system, which enabled the controller from reducing the transient and steady-state vibrations of the system. The positive position feedback controller (PPF) was applied in [13, 14] to suppress vibrations of a nonlinear beam.

In any active control system, loop/time delays are inevitable because of measuring system states, executing the control algorithms, control interfaces, transport delays, and actuation delay. Time delays can reduce the compensation efficiency of the controller and system stability in addition to complications in controller design and operation. Time delays were studied extensively in [15]. The model under discussion here was studied in [16] under the influence of a delayed PPF controller. Lanlan Xu and his colleagues in [17] investigated the active vibration controller for seismically excited building structures in the presence of actuator saturation. In [18], an efficient boundary controller was designed to suppress the undesired vibration of the 1D flexible beam with restricted input.

In this work, we used the improved saturation controller, given in [11, 12], to reduce the bending mode vibrations of the nonlinear beam given in [1]. We proposed an additional improvement for the saturation controller. Warminski et al. in [1] used the nonlinear saturation controller to control the vibrations of this nonlinear beam. They concluded that interaction between external excitation and self-excitation, near the fundamental resonance zone, may lead the system to instability, which in turn can induce flutter phenomenon. They increased the controller damping to overcome this problem. However, increasing the controller damping decreases its efficiency in reducing vibrations. Implementation of the improved controller, presented in [11, 12], led to better vibration suppression. We deduced the effects of various time delays on system response and stability and estimated time margins for different cases of system operation. We utilized the MSPT technique to get a first-order approximate solution and to obtain the equilibrium solution curves under various controller parameters. We studied the stability of the steady-state solution using frequency response equations. We applied the numerical integration and Poincaré map on the original differential equations of the closed-loop system to verify analytical results. All predictions from analytical results are in good agreement with the numerical results.

1.2 Model of Structure

The model of the beam and its physical parameters were given in [1]. The following basic notations are used:

- $x_1, \dot{x}_1, \ddot{x}_1$ are the displacement, the velocity, and the acceleration of the beam, respectively.
- $x_2, \dot{x}_2, \ddot{x}_2$ are the displacement, the velocity, and the acceleration of the controller, respectively.
- α_1 is the negative viscous damping coefficient of the beam.
- α_2 is the linear damping coefficient of the saturation controller.
- α_3 is the control signal gain of the velocity feedback controller.
- β_1 is the cubic damping coefficient of the beam.
- ω_1 is the ratio of the natural frequency of the composite beam with the lumped mass to that of the reference beam without the lumped mass.
- ω_2 is the natural frequency of the saturation controller.

- γ_1 is the coefficient describing the beam geometrical nonlinearity.
- δ is the coefficient describing the beam inertia nonlinearity.
- x_0 is the excitation amplitude.
- Ω is the excitation frequency.
- μ is a constant coefficient.
- λ_1 is the control signal gain of the saturation controller.
- λ_2 is the feedback signal gain of the saturation controller.
- τ_1 and τ_2 are the actuation delays.
- τ_3 is the measurement delay.
- ε is the small dimensionless parameter, i.e., $\varepsilon \ll 1$.

The cantilever beam is mounted on the armature of an electrodynamic shaker, which is a source of external excitation along the X -axis. In practice, this model can be used to describe the aircraft wing such that the wing is suspended to external excitation from the plane body and to self-excitation from the wind flow. The external excitation can be written as

$$x = x_0 \sin(\Omega t).$$

The differential equation which describes the dynamical behavior of the beam was given in [1] in the dimensionless form as follows

$$\ddot{x}_1 + (-\alpha_1 \dot{x}_1 + \beta_1 \dot{x}_1^3) + \omega_1^2 x_1 + \gamma_1 x_1^3 + \delta(x_1 \dot{x}_1^2 + x_1^2 \ddot{x}_1) = x_0 \mu \Omega^2 \sin(\Omega t) + f_1 + f_2.$$

$f_1 = -\alpha_3 \dot{x}_1(t - \tau_1)$ is the feedback control signal from the delayed velocity feedback controller, which was used here to increase system damping and to reduce the effects of self-excited vibrations. $f_2 = \lambda_1 x_2^2(t - \tau_2)$ represents the feedback control signal from the delayed saturation controller. The saturation controller's differential equation is

$$\ddot{x}_2 + \alpha_2 \dot{x}_2 + \omega_2^2 x_2 = f_3.$$

We considered two feedback control strategies for f_3 in the delayed saturation controller:

- First feedback: $f_3 = \lambda_2 x_1(t - \tau_3) x_2(t - \tau_3)$, which represents the ordinary delayed saturation controller.
- Second feedback: $f_3 = \lambda_2 \dot{x}_1(t - \tau_3) \dot{x}_2(t - \tau_3)$. A quadratic velocity coupling was used instead of the ordinary quadratic position coupling to improve the performance of the saturation controller.

Here, we considered extensively the second feedback control strategy. Figure 1.1 presents a block diagram of the closed-loop system. The governing equations of this closed-loop system are

$$\begin{aligned} \ddot{x}_1 + (-\alpha_1 \dot{x}_1 + \beta_1 \dot{x}_1^3) + \omega_1^2 x_1 + \gamma_1 x_1^3 + \delta(x_1 \dot{x}_1^2 + x_1^2 \ddot{x}_1) \\ = x_0 \mu \Omega^2 \sin(\Omega t) - \alpha_3 \dot{x}_1(t - \tau_1) + \lambda_1 x_2^2(t - \tau_2), \end{aligned} \quad (1.1)$$

$$\ddot{x}_2 + \alpha_2 \dot{x}_2 + \omega_2^2 x_2 = \lambda_2 \dot{x}_1(t - \tau_3) \dot{x}_2(t - \tau_3). \quad (1.2)$$

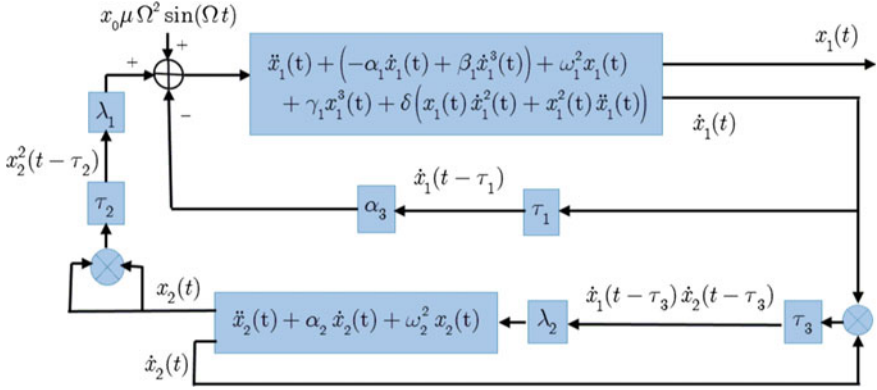


Fig. 1.1 Block diagram of the closed-loop system

1.3 Mathematical Analysis

1.3.1 Multiple Scale Analysis

The MSPT [4] was used here to get a first-order approximate solution of Eqs. (1.1) and (1.2). The first-order uniform expansion was assumed to be in the form

$$x_k(t, \varepsilon) = x_{k0}(T_0, T_1) + \varepsilon x_{k1}(T_0, T_1), \quad (1.3)$$

$$x_k(t - \tau_k, \varepsilon) = x_{k0\tau_k}(T_0, T_1) + \varepsilon x_{k1\tau_k}(T_0, T_1), \quad (1.4)$$

$$x_k(t - \tau_3, \varepsilon) = x_{k0\tau_3}(T_0, T_1) + \varepsilon x_{k1\tau_3}(T_0, T_1), \quad (1.5)$$

where $x_{k0}(T_0, T_1)$, $x_{k1}(T_0, T_1)$ are the zeroth- and first-order perturbations, respectively, $k = 1, 2$, and $T_0 = t$, $T_1 = \varepsilon t$ are fast and slow timescales, respectively. Time derivatives are

$$\frac{d}{dt} = D_0 + \varepsilon D_1, \quad \frac{d^2}{dt^2} = D_0^2 + 2\varepsilon D_0 D_1, \quad D_j = \frac{\partial}{\partial T_j}, \quad j = 0, 1. \quad (1.6)$$

A new scaling is considered for the main system and the controller parameters such that ($m = 1, 2, 3$, $k = 1, 2$)

$$\alpha_m = \varepsilon \hat{\alpha}_m, \quad \beta_1 = \varepsilon \hat{\beta}_1, \quad \gamma_1 = \varepsilon \hat{\gamma}_1, \quad \delta = \varepsilon \hat{\delta}, \quad x_0 = \varepsilon \hat{x}_0, \quad \lambda_k = \varepsilon \hat{\lambda}_k. \quad (1.7)$$

Substituting Eqs. (1.3)–(1.7) into (1.1), (1.2) and equating coefficients of like powers of ε yields the following set of differential equations

$$(D_0^2 + \omega_k^2)x_{k0} = 0, \quad k = 1, 2, \quad (1.8)$$

$$(D_0^2 + \omega_1^2)x_{11} = \mu \hat{x}_0 \Omega^2 \sin(\Omega T_0) - \hat{\gamma}_1 x_{10}^3 + \hat{\lambda}_1 x_{20\tau_2}^2 + \hat{\alpha}_1 D_0 x_{10} - \hat{\delta} x_{10} (D_0 x_{10})^2 - \hat{\beta}_1 (D_0 x_{10})^3 - \hat{\alpha}_3 D_0 x_{10\tau_1} - 2D_0 D_1 x_{10} - \hat{\delta} x_{10}^2 D_0^2 x_{10}, \quad (1.9)$$

$$(D_0^2 + \omega_2^2)x_{21} = \hat{\lambda}_2 D_0 x_{10\tau_3} D_0 x_{20\tau_3} - \hat{\alpha}_2 D_0 x_{20} - 2D_0 D_1 x_{20}. \quad (1.10)$$

The general solutions of Eq. (1.8) can be expressed in the form

$$x_{10}(T_0, T_1) = A(T_1) \exp(i\omega_1 T_0) + \bar{A}(T_1) \exp(-i\omega_1 T_0), \quad (1.11)$$

$$x_{20}(T_0, T_1) = B(T_1) \exp(i\omega_2 T_0) + \bar{B}(T_1) \exp(-i\omega_2 T_0), \quad (1.12)$$

where $A(T_1)$ and $B(T_1)$ are unknown functions of T_1 at this level of approximation. They will be determined later by eliminating the secular and small divisor terms. From Eqs. (1.11) and (1.12), we can get ($l = 1, 3, m = 2, 3$)

$$x_{10\tau_l}(T_0, T_1) = A_{\tau_l}(T_1) \exp[i\omega_1(T_0 - \tau_l)] + \bar{A}_{\tau_l}(T_1) \exp[-i\omega_1(T_0 - \tau_l)], \quad (1.13)$$

$$x_{20\tau_m}(T_0, T_1) = B_{\tau_m}(T_1) \exp[i\omega_2(T_0 - \tau_m)] + \bar{B}_{\tau_m}(T_1) \exp[-i\omega_2(T_0 - \tau_m)]. \quad (1.14)$$

Expanding A_{τ_l} , $l = 1, 3$ and B_{τ_m} , $m = 2, 3$, in Taylor series yields

$$A_{\tau_l}(T_1) = A(T_1 - \varepsilon \tau_l) \approx A(T_1) - \varepsilon \tau_l A'(T_1) + O(\varepsilon^2), \quad (1.15)$$

$$B_{\tau_m}(T_1) = B(T_1 - \varepsilon \tau_m) \approx B(T_1) - \varepsilon \tau_m B'(T_1) + O(\varepsilon^2), \quad (1.16)$$

where the prime denotes derivative with respect to T_1 .

Substituting Eqs. (1.11)–(1.16) into Eqs. (1.9) and (1.10) yields

$$(D_0^2 + \omega_1^2)x_{11} = 2\hat{\lambda}_1 B\bar{B} - \frac{1}{2}i\mu\Omega^2\hat{x}_0 e^{i\Omega T_0} + [iA\omega_1\hat{\alpha}_1 - i\hat{\alpha}_3\omega_1 A e^{-i\omega_1\tau_1} + (2\hat{\delta}\omega_1^2 - 3i\hat{\beta}_1\omega_1^3 - 3\hat{\gamma}_1)A^2\bar{A} - 2i\omega_1 D_1 A] e^{i\omega_1 T_0} + (2\hat{\delta}\omega_1^2 + i\hat{\beta}_1\omega_1^3 - \hat{\gamma}_1)A^3 e^{3i\omega_1 T_0} + \hat{\lambda}_1 B^2 e^{2i\omega_2(T_0 - \tau_2)} + cc, \quad (1.17)$$

$$(D_0^2 + \omega_2^2)x_{21} = \hat{\lambda}_2 A\bar{B}\omega_1\omega_2 e^{i(\omega_1 - \omega_2)(T_0 - \tau_3)} - \hat{\lambda}_2 A B \omega_1 \omega_2 e^{i(\omega_1 + \omega_2)(T_0 - \tau_3)} - (i\hat{\alpha}_2 B + 2i\omega_2 D_1 B)\omega_2 e^{i\omega_2 T_0} + cc, \quad (1.18)$$

where cc means the complex conjugate of the preceding terms and the overbar symbolizes the complex conjugate functions.

From Eqs. (1.17) and (1.18), the associated resonance cases at this approximation order are as follows:

- (I) primary resonance, $\Omega \approx \omega_1$,
- (II) internal resonance, $2\omega_2 \approx \omega_1$,
- (III) simultaneous resonance, $\Omega \approx \omega_1$ and $2\omega_2 \approx \omega_1$.

In this paper, we studied the case of simultaneous resonance and described it by using detuning parameters σ_1 and σ_2 as follows:

$$\Omega = \omega_1 + \sigma_1 = \omega_1 + \varepsilon\hat{\sigma}_1, \quad 2\omega_2 = \omega_1 + \sigma_2 = \omega_1 + \varepsilon\hat{\sigma}_2. \quad (1.19)$$

Inserting Eq. (1.19) into the secular and small divisor terms in Eqs. (1.17) and (1.18) yields the solvability conditions

$$[i\omega_1 A(\hat{\alpha}_1 - \hat{\alpha}_3 e^{-i\omega_1 \tau_1}) + (2\hat{\delta}\omega_1^2 - 3i\hat{\beta}_1\omega_1^3 - 3\hat{\gamma}_1)A^2\bar{A} - 2i\omega_1 D_1 A]e^{i\omega_1 T_0} + \hat{\lambda}_1 B^2 e^{-2i\omega_2 \tau_2} e^{i(\omega_1 + \varepsilon\hat{\sigma}_2)T_0} - \frac{1}{2}\mu\Omega^2 \hat{x}_0 e^{i(\omega_1 + \varepsilon\hat{\sigma}_1)T_0} = 0, \quad (1.20)$$

$$\hat{\lambda}_2 A \bar{B} \omega_1 e^{-i(\omega_1 - \omega_2)\tau_3} e^{i(\omega_2 - \varepsilon\hat{\sigma}_2)T_0} - (i\hat{\alpha}_2 B + 2i\omega_2 D_1 B)e^{i\omega_2 T_0} = 0. \quad (1.21)$$

To analyze the solution of Eqs. (1.20) and (1.21), we introduced the polar notation for A and B as follows:

$$A = \frac{1}{2}a_1 e^{i\theta_1}, \quad D_1 A = \frac{1}{2}(a'_1 + ia_1\theta'_1)e^{i\theta_1}, \quad (1.22)$$

$$B = \frac{1}{2}a_2 e^{i\theta_2}, \quad D_1 B = \frac{1}{2}(a'_2 + ia_2\theta'_2)e^{i\theta_2}. \quad (1.23)$$

where a_1, a_2 are the steady-state displacement amplitudes and θ_1, θ_2 are the phases of the motion of the beam and the controller, respectively.

Inserting Eqs. (1.22) and (1.23) into Eqs. (1.20) and (1.21), returning each scaled parameter to its real value, and separating real and imaginary parts yield

$$Z_s + 4\omega_1 a_1 (2\dot{\theta}_1 - \alpha_3 \sin \psi_3) + a_1^3 (2\delta\omega_1^2 - 3\gamma_1) + 2\lambda_1 a_2^2 \cos(\phi_2 - \psi_1) = 0, \quad (1.24)$$

$$Z_c + 4\omega_1 a_1 (\alpha_3 \cos \psi_3 - \alpha_1) + 3\omega_1^3 \beta_1 a_1^3 - 2\lambda_1 a_2^2 \cos(\phi_2 - \psi_1) + 8\omega_1 \dot{a}_1 = 0, \quad (1.25)$$

$$\omega_1 \lambda_2 a_1 \cos(\phi_2 + \psi_2) + 4\dot{\theta}_2 = 0, \quad (1.26)$$

$$2\alpha_2 a_2 + \omega_1 \lambda_2 a_1 a_2 \sin(\phi_2 + \psi_2) + 4\dot{a}_2 = 0, \quad (1.27)$$

where dot represents derivative with respect to t ,

$$Z_s = 4\mu\Omega^2 x_0 \sin \phi_1, \quad Z_c = 4\mu\Omega^2 x_0 \cos \phi_1.$$

In addition,

$$\begin{aligned}\phi_1 &= \sigma_1 t - \theta_1 = \varepsilon \hat{\sigma}_1 t - \theta_1, & \phi_2 &= \sigma_2 t - \theta_1 + 2\theta_2 = \varepsilon \hat{\sigma}_2 t - \theta_1 + 2\theta_2, \\ \psi_1 &= 2\omega_2 \tau_2, & \psi_2 &= (\omega_1 - \omega_2) \tau_3, & \psi_3 &= \omega_1 \tau_1.\end{aligned}\quad (1.28)$$

By differentiating ϕ_1 and ϕ_2 in Eq. (1.28) w.r.t. t , we get

$$\dot{\theta}_1 = \sigma_1 - \dot{\phi}_1, \quad \dot{\theta}_2 = \frac{1}{2}(\dot{\phi}_2 - \dot{\phi}_1 + \sigma_1 - \sigma_2). \quad (1.29)$$

Inserting Eq. (1.29) into Eqs. (1.24)–(1.27) yields the autonomous amplitude–phase modulating equations as follows

$$\begin{aligned}\dot{a}_1 &= \frac{4\omega_1 a_1 (\alpha_1 - \alpha_3 \cos \psi_3) - 3\omega_1^3 \beta_1 a_1^3 - Z_c + 2\lambda_1 a_2^2 \sin(\phi_2 - \psi_1)}{8\omega_1}, \\ \dot{\phi}_1 &= \frac{Z_s + 4\omega_1 a_1 (2\sigma_1 - \alpha_3 \sin \psi_3) + a_1^3 (2\delta\omega_1^2 - 3\gamma_1) + 2\lambda_1 a_2^2 \cos(\phi_2 - \psi_1)}{8\omega_1 a_1}, \\ \dot{a}_2 &= \frac{1}{4}(-2\alpha_2 a_2 - \omega_1 \lambda_2 a_1 a_2 \sin(\phi_2 + \psi_2)), \\ \dot{\phi}_2 &= \frac{1}{8\omega_1 a_1} [Z_s + 4\omega_1 a_1 (2\sigma_2 - \alpha_3 \sin \psi_3 - \omega_1 \lambda_2 a_1 \cos(\phi_2 + \psi_2)) + \\ &\quad + a_1^3 (2\delta\omega_1^2 - 3\gamma_1) + 2\lambda_1 a_2^2 \cos(\phi_2 - \psi_1)],\end{aligned}\quad (1.30)$$

where, as above, $Z_s = 4\mu\Omega^2 x_0 \sin \phi_1$, $Z_c = 4\mu\Omega^2 x_0 \cos \phi_1$.

1.3.2 Equilibrium Solution

The steady-state response of both the beam and the controller can be obtained as follows

$$\dot{a}_1 = \dot{a}_2 = \dot{\phi}_1 = \dot{\phi}_2 = 0. \quad (1.31)$$

Substituting by (1.31) into (1.29) yields

$$\dot{\theta}_1 = \sigma_1, \quad \dot{\theta}_2 = \frac{1}{2}(\sigma_1 - \sigma_2). \quad (1.32)$$

Substituting by Eqs. (1.31) and (1.32) into Eqs. (1.24)–(1.27), we get

$$4\omega_1 a_1 (2\sigma_1 - \alpha_3 \sin \psi_3) + Z_s + a_1^3 (2\delta\omega_1^2 - 3\gamma_1) + 2\lambda_1 a_2^2 \cos(\phi_2 - \psi_1) = 0, \quad (1.33)$$

$$4\omega_1 a_1 (\alpha_1 - \alpha_3 \cos \psi_3) - Z_c - 3\omega_1^3 \beta_1 a_1^3 + 2\lambda_1 a_2^2 \sin(\phi_2 - \psi_1) = 0, \quad (1.34)$$

$$2(\sigma_1 - \sigma_2) + \omega_1 \lambda_2 a_1 \cos(\phi_2 + \psi_2) = 0, \quad (1.35)$$

$$2\alpha_2 + \omega_1 a_1 \sin(\phi_2 + \psi_2) = 0. \quad (1.36)$$

Extracting $\sin \phi_2$ and $\cos \phi_2$ from Eqs. (1.35) and (1.36) yields

$$\sin \phi_2 = \frac{2(\sigma_1 - \sigma_2) \sin \psi_2 - 2\alpha_2 \cos \psi_2}{a_1 \lambda_2 \omega_1}, \quad (1.37)$$

$$\cos \phi_2 = -\frac{2(\sigma_1 - \sigma_2) \cos \psi_2 + 2\alpha_2 \sin \psi_2}{a_1 \lambda_2 \omega_1}. \quad (1.38)$$

Next, substituting $\sin \phi_2$ and $\cos \phi_2$ in Eqs. (1.33) and (1.34) and extracting values of $\sin \phi_1$ and $\cos \phi_1$, we get

$$\sin \phi_1 = \eta_1 \sin(\psi_1 + \psi_2) + \eta_2 \cos(\psi_1 + \psi_2) + \eta_3 \sin \psi_3 + \eta_4, \quad (1.39)$$

$$\cos \phi_1 = \eta_2 \sin(\psi_1 + \psi_2) - \eta_1 \cos(\psi_1 + \psi_2) - \eta_3 \sin \psi_3 + \eta_5, \quad (1.40)$$

where

$$\eta_1 = \frac{a_2^2 \lambda_1 \alpha_2}{\mu \Omega^2 x_0 a_1 \lambda_2 \omega_1}, \quad \eta_2 = \frac{a_2^2 \lambda_1 (\sigma_1 - \sigma_2)}{\mu \Omega^2 x_0 a_1 \lambda_2 \omega_1}, \quad \eta_3 = \frac{a_1 \omega_1 \alpha_3}{\mu \Omega^2 x_0},$$

$$\eta_4 = \frac{a_1^3 (3\gamma_1 - 2\delta\omega_1^2) - 8a_1 \sigma_1 \omega_1}{4\mu \Omega^2 x_0}, \quad \eta_5 = \frac{4a_1 \omega_1 (\alpha_1 - \alpha_3 \cos \psi_3) - 3a_1^3 \beta_1 \omega_1^3}{4\mu \Omega^2 x_0}.$$

Squaring and adding Eqs. (1.37) and (1.38) produce the first closed-form equation

$$4(\alpha_2^2 + (\sigma_1 - \sigma_2)^2) = a_1^2 \lambda_2^2 \omega_1^2. \quad (1.41)$$

Squaring and adding Eqs. (1.39) and (1.40) generate the second closed-form equation

$$(\eta_1 \sin(\psi_1 + \psi_2) + \eta_2 \cos(\psi_1 + \psi_2) + \eta_3 \sin \psi_3 + \eta_4)^2$$

$$+ (\eta_2 \sin(\psi_1 + \psi_2) - \eta_1 \cos(\psi_1 + \psi_2) - \eta_3 \cos \psi_3 + \eta_5)^2 = 1.$$

Thus, a closed-form equation for the closed-loop system consisting of the beam and the delayed velocity feedback controller can be deduced as follows

$$\begin{aligned} & \omega_1^2(4\alpha_3(\cos \psi_3 - \sigma_1 \tau_1 \sin \psi_3) - 4\alpha_1 + 3a_1^2 \beta_1 \omega_1^2)^2 \\ & + [4\omega_1(\alpha_3 \sin \psi_3 - 2\sigma_1 + \sigma_1 \tau_1 \alpha_3 \cos \psi_3) + a_1^2(3\gamma_1 - 2\delta\omega_1^2)]^2 = \frac{16\mu^2 \Omega^4 x_0^2}{a_1^2}. \end{aligned} \quad (1.42)$$

The closed-form equations for feedback 1 “ordinary saturation controller” can be deduced in the same way.

1.3.3 Stability Analysis

Equation (1.30) can be written in shortened form as follows

$$\dot{a}_j = F_{2j-1}(a_1, \phi_1, a_2, \phi_2), \quad \dot{\phi}_j = F_{2j}(a_1, \phi_1, a_2, \phi_2), \quad j = 1, 2. \quad (1.43)$$

The stability of the equilibrium solution was analyzed by using Jacobian matrix J of the right-hand side of Eq. (1.43). To characterize the system behavior in the neighborhood of equilibrium solution $(a_{10}, \phi_{10}, a_{20}, \phi_{20})$, we expanded functions F_1 , F_2 , F_3 , and F_4 about the equilibrium solution. We assumed that each state of the system consists of its value at equilibrium plus a small perturbation as follows

$$a_j = a_{j1} + a_{j0}, \quad \phi_j = \phi_{j1} + \phi_{j0}, \quad \dot{a}_j = \dot{a}_{j1}, \quad \dot{\phi}_j = \dot{\phi}_{j1}, \quad j = 1, 2, \quad (1.44)$$

where $a_{11}, \phi_{11}, a_{21}, \phi_{21}$ are perturbations which are small with respect to $a_{10}, \phi_{10}, a_{20}, \phi_{20}$. By truncating the series at the linear terms and substituting Eq. (1.44) into Eq. (1.43) yields ($j = 1, 2$)

$$\dot{a}_{j1} = \sum_{m=1}^2 \left(\frac{\partial F_{2j-1}}{\partial a_m} a_{m1} + \frac{\partial F_{2j-1}}{\partial \phi_m} \phi_{m1} \right), \quad \dot{\phi}_{j1} = \sum_{m=1}^2 \left(\frac{\partial F_{2j}}{\partial a_m} a_{m1} + \frac{\partial F_{2j}}{\partial \phi_m} \phi_{m1} \right). \quad (1.45)$$

Thus, we obtained a set of linear differential equations with constant coefficients that govern the components of disturbance. The characteristic determinant of Eq. (1.45) can be expressed as follows

$$\begin{vmatrix} \frac{\partial F_1}{\partial a_1} - \lambda & \frac{\partial F_1}{\partial \phi_1} & \frac{\partial F_1}{\partial a_2} & \frac{\partial F_1}{\partial \phi_2} \\ \frac{\partial F_2}{\partial a_1} & \frac{\partial F_2}{\partial \phi_1} - \lambda & \frac{\partial F_2}{\partial a_2} & \frac{\partial F_2}{\partial \phi_2} \\ \frac{\partial F_3}{\partial a_1} & \frac{\partial F_3}{\partial \phi_1} & \frac{\partial F_3}{\partial a_2} - \lambda & \frac{\partial F_3}{\partial \phi_2} \\ \frac{\partial F_4}{\partial a_1} & \frac{\partial F_4}{\partial \phi_1} & \frac{\partial F_4}{\partial a_2} & \frac{\partial F_4}{\partial \phi_2} - \lambda \end{vmatrix} = 0. \quad (1.46)$$

The stability of the steady-state solution depends on the eigenvalues λ of the Jacobian matrix of Eq. (1.46). The solutions are stable if and only if all roots of the characteristic equation have negative real parts.

1.4 Results and Discussions

The steady-state response of the closed-loop system composed of the beam, the delayed velocity feedback controller, and the improved saturation controller is studied here analytically and numerically. The dimensionless parameters of the beam were given as $\alpha_1 = 0.01$, $\beta_1 = 0.05$, $\omega_1 = 3.06309$, $\gamma_1 = 14.4108$, $\delta = 3.2746$, $\mu = 0.89663$, and $x_0 = 0.01$. We selected the controller parameters as $\alpha_2 = 0.01$, $\lambda_1 = \lambda_2 = 0.5$, $\alpha_3 = 0.05$, and $\sigma_2 = 0$ unless specifying otherwise. In the obtained figures, solid lines correspond to stable solutions while dashed lines correspond to unstable solutions, and the numerical results for steady-state solutions are plotted as small circles. Time history and Poincaré maps were used to validate the results.

1.4.1 *Nonlinear Beam Without Control*

The uncontrolled system was studied extensively in [1, 14]. As the uncontrolled beam is subjected to external excitation and self-excitation, it suffers from the following problems:

1. Self-excitation can build up oscillations even if the external force is very small. As self-excitation is represented by negative damping which causes positive feedback, the displacement amplitude of oscillations increases monotonically with the self-excitation.
2. In the presence of external excitation, self-excitation can interact with it and lead the system to vibrate with an unstable quasi-periodic motion, which may cause the flutter phenomenon.
3. The displacement amplitude of beam vibrations is large when it is externally excited near its natural frequency $\Omega \approx \omega_1$.

Here, we implemented a controller, which consists of a velocity feedback controller and an improved saturation controller, to reduce the bending mode vibrations of the beam.

1.4.2 *Effects of Velocity Feedback Controller*

Effects of velocity feedback controller were studied in two cases.

1.4.2.1 The Saturation Controller Is Not Active

Figure 1.2a presents the frequency response curve (FRC) of the uncontrolled beam at $\alpha_1 = 0.05$. The system vibrates with an unstable quasi-periodic motion in a great part of the FRC due to the interaction between the self-excitation and the external excitation. The eigenvalues of the characteristic equation of the system in intervals AC and DE are conjugate complex values with a positive real part, which corresponds to unstable focus. In interval CD, the eigenvalues are conjugate complex roots with a negative real part, which corresponds to a stable periodic motion. Figure 1.2b shows the effects of α_3 on the FRC of the beam. When α_3 increases, the system damping increases, the peak displacement amplitude of the beam decreases, the effects of self-excitation reduce, and the beam vibrates with a stable periodic motion. From the comparison between Fig. 1.2a and b, we can see that intervals AB and DE, which are unstable in Fig. 1.2a, become stable in Fig. 1.2b. Larger values of α_3 give better results analytically but cause practical problems to the system. So we use values of $\alpha_3 \in [0, 0.1]$.

Figure 1.3 shows the unstable intervals in Fig. 1.2a by taking the point $\sigma_1 = 0.1$ as a sample. Figure 1.3 shows that the beam vibrations are unstable quasi-periodic motions, which verifies results in Fig. 1.2a. After utilizing the velocity feedback controller, the beam vibrates in a stable periodic motion as in Fig. 1.4b. Figure 1.4a shows that the beam vibrations pass through a transient state into a stable periodic steady state.

The previous results confirm that the velocity feedback controller can eliminate the effects of self-excitation and stabilize the system response even if the saturation controller is not active. However, the displacement amplitude of the beam near the

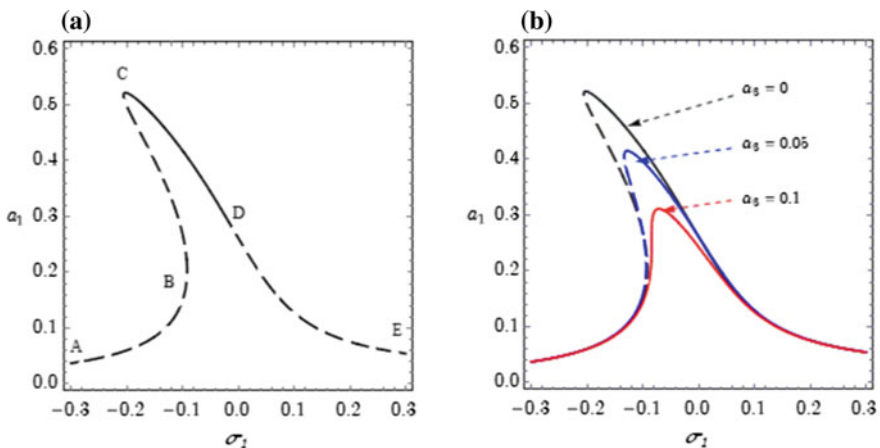


Fig. 1.2 Frequency response curves at $\alpha_1 = 0.05$: **a** uncontrolled beam ($\alpha_3 = 0$), **b** beam with the velocity feedback controller at different values of α_3

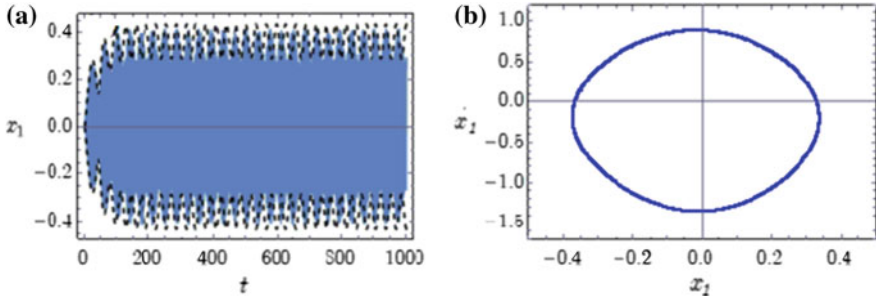


Fig. 1.3 Uncontrolled beam at $\alpha_1 = 0.05$, $\alpha_3 = 0$, and $\sigma_1 = 0.1$: **a** time history, **b** Poincaré map

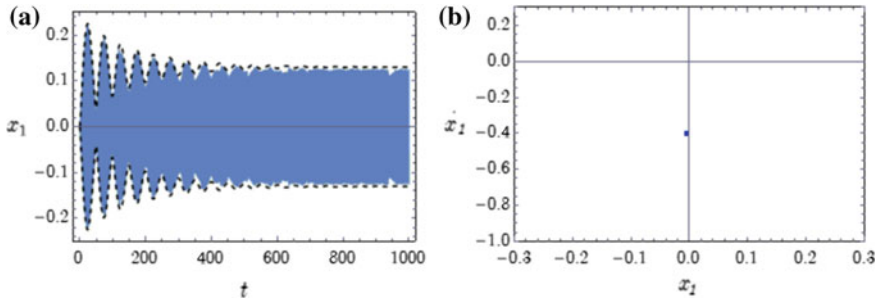


Fig. 1.4 Beam at $\alpha_1 = 0.05$, $\alpha_3 = 0.05$, and $\sigma_1 = 0.1$: **a** time history, **b** Poincaré map

primary resonance ($\Omega \approx \omega_1$) stills large. So we used the improved saturation controller besides the velocity feedback controller to reduce vibrations near the primary resonance ($\Omega \approx \omega_1$ or $\sigma_1 \approx 0$).

1.4.2.2 The Saturation Controller Is Active

We compared FRCs of the ordinary saturation controller “feedback 1” with the FRCs of the improved saturation controller “feedback 2,” and we observed that the improved saturation controller reduces beam vibrations more effectively, but the controller overload risk increases. The overload risk of the controller can be reduced later by increasing λ_1 . Here, we investigated the performance of the improved saturation controller. In the subsequent discussion, the improved saturation controller was called briefly the saturation controller. The peak displacement amplitude in Fig. 1.2 was vanished by using the saturation controller. It is observable from (1.41) that α_3 does not affect the beam displacement amplitude when the saturation controller is active. We employed the velocity feedback controller besides the saturation controller to increase the system damping and to reduce the transient vibrations of the system.

1.4.3 The Effects of Various Controller Parameters and the Time Margins of Various Time Delays

1.4.3.1 Effects of Linear Damping Coefficient of the Saturation Controller α_2

Increasing the damping of the closed-loop system can be done either by increasing α_3 or by increasing α_2 . Figure 1.5 studies the effects of α_2 on the beam and the controller when $\alpha_3 = 0$ (the velocity feedback controller is switched off). The FRCs in Fig. 1.5a of the beam are unstable during the inactivity region of the saturation controller. Also, the FRCs during the activity region of the saturation controller may be unstable, as seen in Fig. 1.5a at $\alpha_1 = 0.01$, $\alpha_2 = 0.05$. It is possible to stabilize system response during the activity region of the saturation controller by increasing α_2 , as seen in Fig. 1.5a when $\alpha_2 = 0.1$. However, increasing α_2 stabilizes the beam response but decreases the controller efficiency. Figure 1.5b shows that the controller overload risk decreases when α_2 increases. Figure 1.5c and d presents the FRC of the beam and the controller at $\alpha_3 = 0.05$ (the velocity feedback controller is switched on) under different values of α_2 . The comparison between Fig. 1.5a and c indicates the important role of the velocity feedback controller besides the saturation controller in increasing system stability and decreasing the controller overload risk.

The effects of α_2 on the stability of system response were studied when the saturation controller is active in Fig. 1.6 under different values of α_3 . The system response may be unstable during the activity region of saturation controller when $\alpha_3 = 0$ as seen in Fig. 1.6a. The arrow plotted in the figure shows that the activity region of the saturation controller at $\alpha_2 = 0.05$ contains unstable bandwidth of frequencies. When a higher value for α_3 was used, a better system response was obtained, as shown in Fig. 1.6b, which confirms the results of Fig. 1.5. Also, we can see that the activity region of the saturation controller decreases by increasing α_2 or α_3 .

1.4.3.2 The Effects of α_3 on Time Margins of τ_1 , τ_2 , and τ_3

Implementing the velocity feedback controller besides the saturation controller increases the time margin of τ_1 , τ_2 , and τ_3 . Figure 1.7 presents the controller's displacement amplitudes versus time delays τ_1 , τ_2 , and τ_3 , respectively, under different values of α_3 . The stable and unstable regions in the amplitude-delay response curves are shown in Fig. 1.7a. Practically, values of time delays are mostly small, so the first stable region, which is the time margin for each time delay, is our main interest. The following amplitude-delay figures concentrate on the first stable region only. When α_3 increases, the time margin of τ_1 , τ_2 , and τ_3 increases, and displacement amplitude a_2 slightly decreases within the time margin. Equation (1.41) shows that α_3 , τ_1 , τ_2 , and τ_3 cannot alter the beam displacement amplitude a_1 during the activity region of the saturation controller.

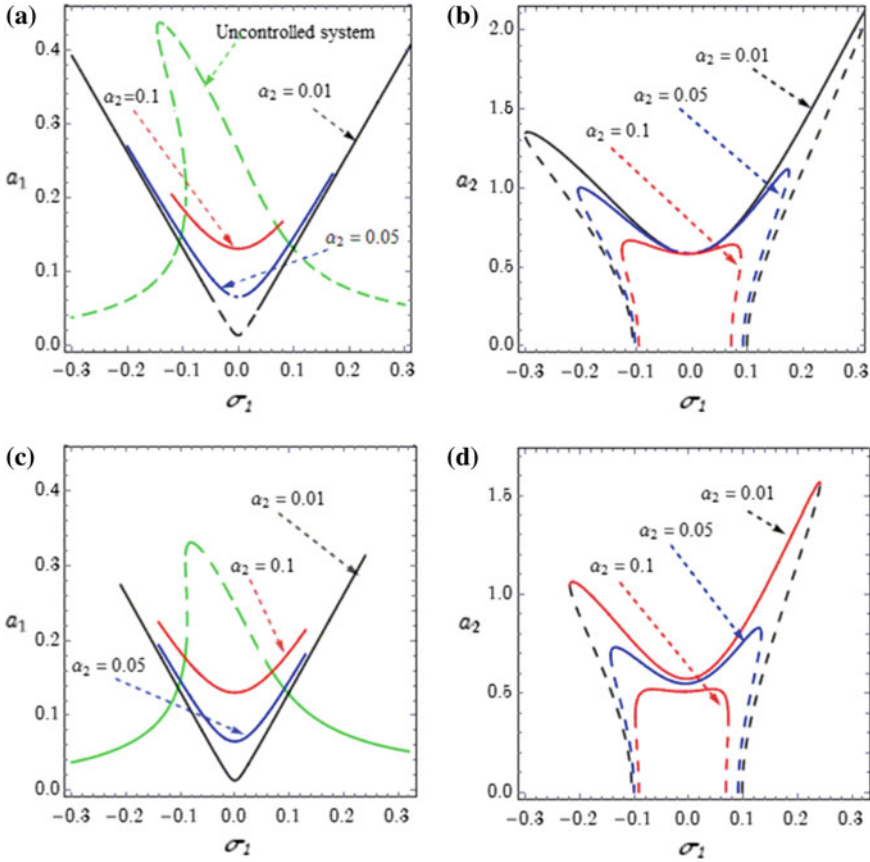


Fig. 1.5 Frequency response curves: **a** beam, **b** controller at $\alpha_3 = 0$, i.e., “controlled only by the saturation controller”; **c** beam, **d** controller at $\alpha_3 = 0.05$, under different values of α_2

1.4.3.3 Effects of Control Gain λ_1

From Eq. (1.41), the controller gain λ_1 does not affect the value of beam displacement amplitude. From the results, we observed that λ_1 does not affect the time margins of τ_1 , τ_2 , and τ_3 . The FRC of the beam and the controller are presented in Fig. 1.8 under different values of λ_1 . Figure 1.8a ensures that λ_1 does not influence the beam displacement amplitude. The controller displacement amplitude decreases when λ_1 increases, as seen in Fig. 1.8b. The controller displacement amplitude is plotted in Fig. 1.8c as a function of the external detuning parameter and control gain λ_1 . Figure 1.8c illustrates that the controller overload decreases while λ_1 increases.

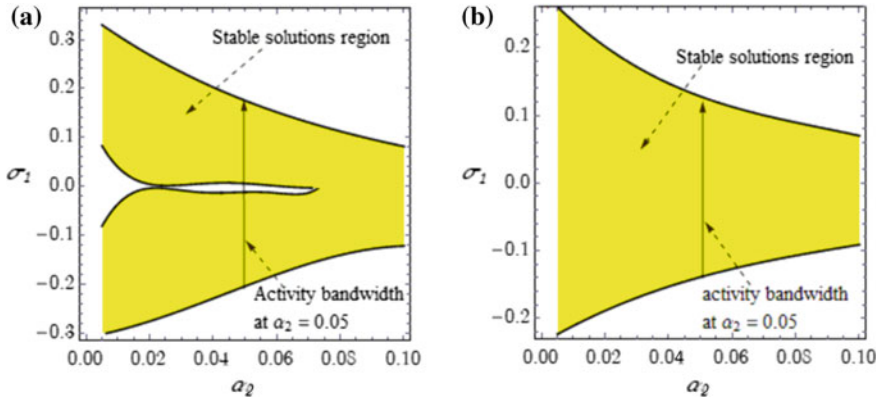


Fig. 1.6 Effects of α_2 on the stability of solutions during activity of saturation controller at: **a** $\alpha_3 = 0$, **b** $\alpha_3 = 0.05$

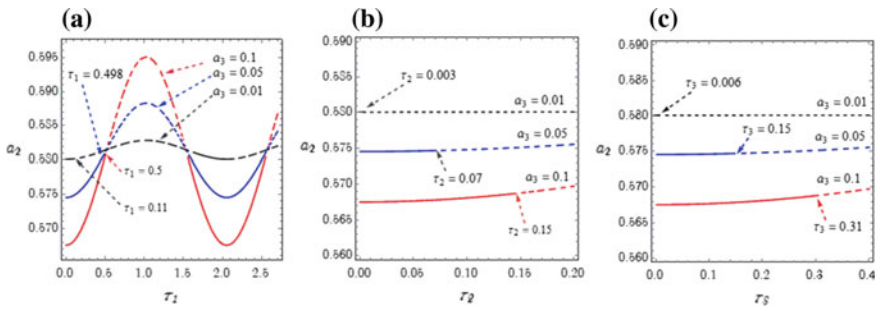


Fig. 1.7 Amplitude a_2 with delay: **a** τ_1 , when $\tau_2 = \tau_3 = 0$, **b** τ_2 , when $\tau_1 = \tau_3 = 0$, **c** τ_3 , when $\tau_2 = \tau_3 = 0$, all at $\sigma_1 = \sigma_2 = 0$

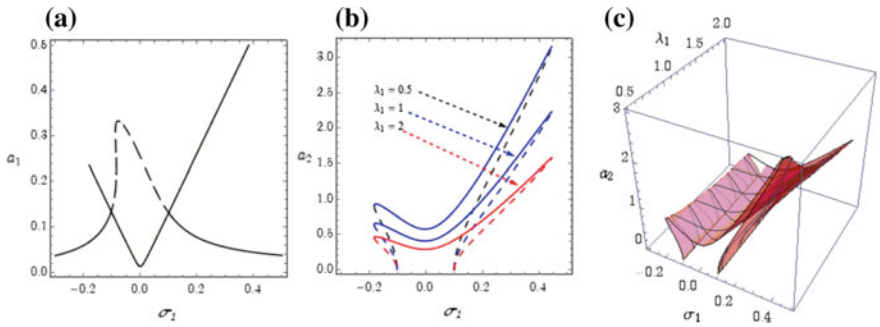


Fig. 1.8 Frequency response curves: **a** beam, **b** controller, under different values of λ_1 at $\tau_1 = 0.05$ and $\tau_2 = \tau_3 = 0.02$, **c** the controller displacement amplitude as a function of excitation frequency σ_1 and controller gain λ_1

1.4.3.4 Effects of Feedback Gain λ_2

Figure 1.9a shows that time margins of τ_2 and τ_3 decrease as λ_2 increases. We observed that increasing λ_2 does not alter the time margin of τ_1 . Also, the controller’s displacement amplitude increases as λ_2 increases. From Fig. 1.9c, we found that increasing the values of τ_1 and τ_2 decreases the time margin of τ_3 and vice versa. The FRCs of the beam and the controller under different values of λ_2 are presented in Fig. 1.10a and b, respectively. From Fig. 1.10a, we can conclude that the vibration suppression bandwidth increases as λ_2 increases. In Fig. 1.10a, there are some regions at which the displacement amplitude of the controlled beam is larger than that of the uncontrolled beam. Consequently, these regions are undesired. In the subsequent section (in Fig. 1.12), we presented an improvement in the controller algorithm to eliminate these regions.

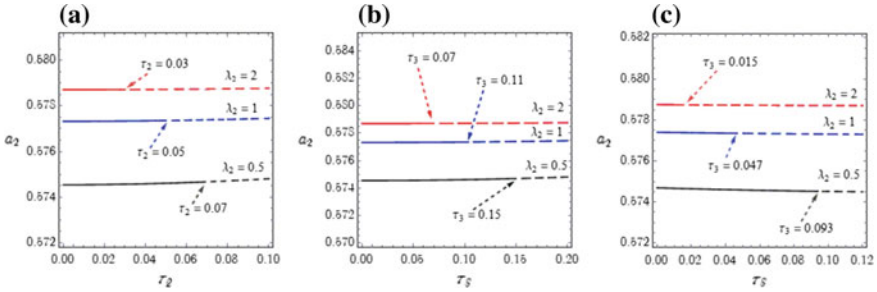


Fig. 1.9 Amplitude a_2 with delay: **a** τ_2 , when $\tau_1 = \tau_3 = 0$, **b** τ_3 , when $\tau_1 = \tau_2 = 0$, and **c** τ_3 , when $\tau_1 = 0.01$, $\tau_2 = 0.03$ under different values of λ_2 at $\sigma_1 = \sigma_2 = 0$

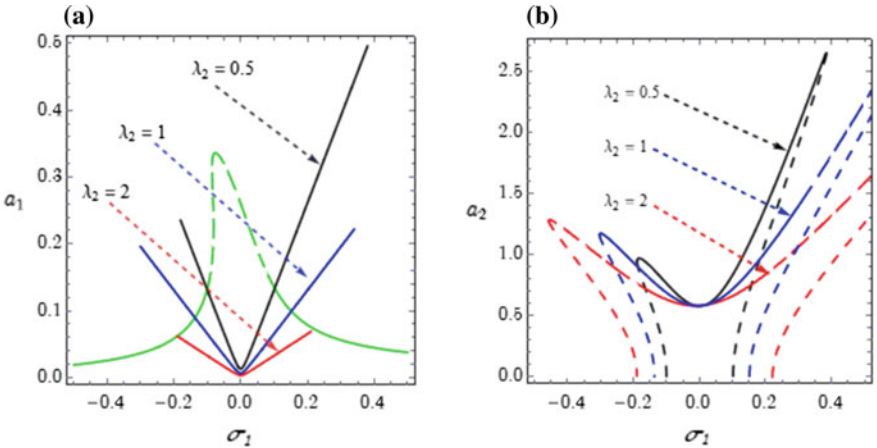


Fig. 1.10 Frequency response curves under different values of λ_2 at $\tau_1 = 0.1$, $\tau_2 = 0.02$ and $\tau_3 = 0.01$: **a** beam, **b** FRC of the controller

1.4.3.5 Effects of Time Delays τ_1 , τ_2 , and τ_3

The effects of τ_1 , τ_2 , and τ_3 on the FRC of the beam and the controller were investigated. The obtained results show that the time delay τ_1 does not affect on the FRC of the beam and the controller and that the activity region of saturation controller decreases when τ_2 or τ_3 increases. We plotted Fig. 1.11 using several results such that given in Figs. 1.7 and 1.9. Figure 1.11a presents the effects of τ_2 and τ_3 on the stability of solutions under different values of feedback gain λ_2 at $\tau_1 = 0.1$. For example, at $\lambda_2 = 0.5$, the analytical solution is stable at $\tau_2 + 0.5\tau_3 \leq 0.076$. So the stable solutions region consists of the red, green, and yellow regions, but the analytical solution is unstable at $\tau_2 + 0.5\tau_3 > 0.076$. The time margins of τ_2 and τ_3 at $\lambda_2 = 0.5$ depend on the equation $\tau_2 + 0.5\tau_3 = 0.076$. So the time margin of τ_2 is inversely proportional to that of τ_3 and vice versa. The red and green regions represent the stable solutions region when $\lambda_2 = 1$. The red region is the only stable solution region when $\lambda_2 = 2$. The stability criteria at $\lambda_2 = 1$ and $\lambda_2 = 2$ are indicated in the figure, respectively. When λ_2 increases, the area of stable solutions region decreases, and the overall time margin decreases.

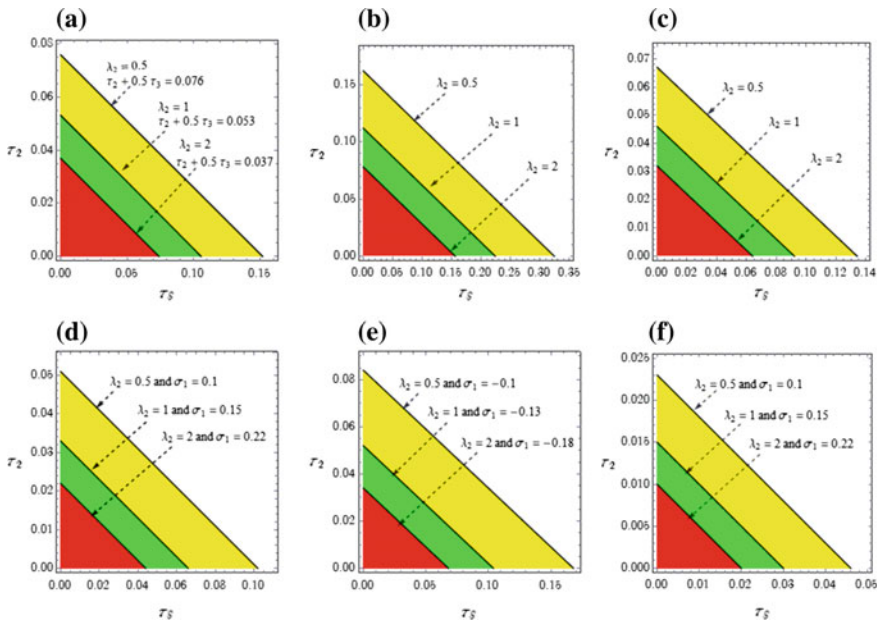


Fig. 1.11 Time margins of τ_2 , τ_3 , and stable solution regions under different values of λ_2 at **a** $\alpha_3 = 0.05$, $\tau_1 = 0.1$, $\sigma_1 = \sigma_2 = 0$, **b** $\alpha_3 = 0.1$, $\tau_1 = 0.1$, $\sigma_1 = \sigma_2 = 0$, **c** $\alpha_3 = 0.05$, $\tau_1 = 0.2$, $\sigma_1 = \sigma_2 = 0$, **d** $\alpha_3 = 0.05$, $\tau_1 = 0.1$ at different positive values of σ_1 , **e** $\alpha_3 = 0.05$, $\tau_1 = 0.1$ at different negative values of σ_1 , and **f** $\alpha_3 = 0.05$, $\tau_1 = 0.1$, $x_0 = 0.1$ at different positive values of σ_1

Comparison of Fig. 1.11b with Fig. 1.11a yields that the area of stable solutions region is directly proportional to the value of α_3 . Comparison between Fig. 1.11c and Fig. 1.11a shows that increasing τ_1 decreases the area of stable solution region. For a constant value of τ_2 , τ_1 and τ_3 are inversely proportional to each other.

The increase of excitation frequency over the beam natural frequency “ σ_1 positive” minimizes the area of stable solutions region, as shown in Fig. 1.11d. However, the area of stable solutions region increases with the decrease of the excitation frequency “ σ_1 negative,” as shown in Fig. 1.11e. The values of sigma 1 implemented in Fig. 1.11a and Fig. 1.11b are the limits of the system stable operation in Fig. 1.10a. Figure 1.11f indicates the effects of τ_2 and τ_3 on the stability of solutions at different values of σ_1 when $x_0 = 0.1$. Comparing Fig. 1.11f with Fig. 1.11d yields that increasing the amplitude of external excitation x_0 decreases the area of stable solution region.

1.4.3.6 A Suggestion for Improving the Saturation Controller Algorithm

The saturation phenomenon was studied extensively in [4]. Numerical validation of the frequency response curves of the beam and the controller at $\lambda_2 = 1$ was presented in Fig. 1.12a and b, respectively. We need to distinguish between three cases of system operation. The first case occurs when excitation frequency increases during system operation. The jump phenomenon, in this case, is indicated by the red arrows in Fig. 1.12a and b for the beam and the controller, respectively. The second case is indicated by green arrows in the figure, and this case occurs when excitation frequency decreases during system operation. In the third case, the system starts vibration from rest, and the FRC is indicated by the path “ABDEFHI.” The beam displacement amplitude in the interval FG is larger than its value in interval FH. Besides, the beam displacement amplitude in the interval DC is larger than its value in interval DB. So intervals FG and DC are undesired system responses. As the result, we improved the control algorithm such that the controller operates only in the region between the points D and F shown in Fig. 1.12a. In other words, after improving the control algorithm, the FRC of the beam is the path “ABDEFHI” in all cases of system operation.

To improve the controller performance, the controller algorithm must be supplied by the ability to detect the region of the optimal operation of the saturation controller (interval between points D and F, as shown in Fig. 1.12a. For example, If the system started operation at $\sigma_1 \in]D, F[$, then the external excitation frequency “ σ_1 ” increases toward the point F during system operation, and the algorithm needs to detect the point F and deactivate the saturation controller; as a result, the FRC takes the path FHI instead of the path FGHI. From Eq. (1.41), we can deduce that the controller parameters that influence the optimal operation region of the controller are α_2 , σ_2 , and λ_2 . From the discussion of Figs. 1.5 and 1.6, α_3 is preferred to control the system damping, so we can assume that α_2 is constant. Also, internal resonance is perfectly tuned, i.e., $\sigma_2 = 0$. So we investigated the optimal operation region (bandwidth of

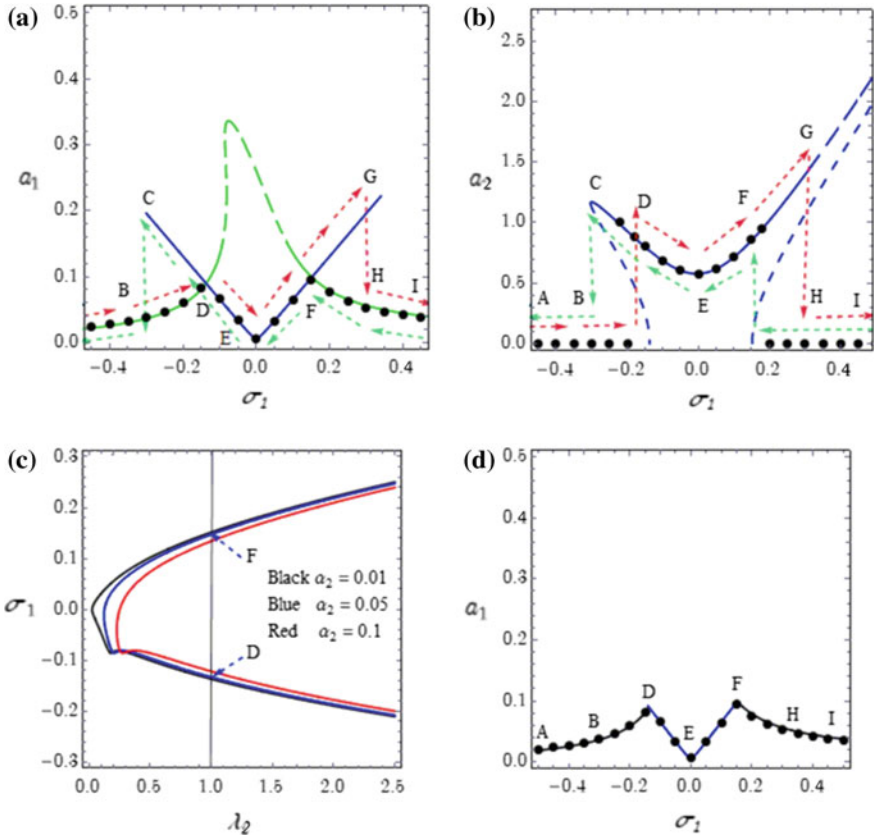


Fig. 1.12 Frequency response curves at $\tau_1 = 0.1$, $\tau_2 = 0.02$, and $\tau_3 = 0.01$: **a** beam, **b** controller at $\lambda_2 = 1$, **c** relation between intersection points “D and F” in **(a)** and λ_2 at different values of α_2 and **d** FRC of the beam at $\lambda_2 = 1$ after the suggested improvement

frequencies between the points D and F in Fig. 1.12a and c under the influence of the controller gain λ_2 .

The condition used to plot Fig. 1.12c can be programmed in the control algorithm to enable the detection of the points D and F. We obtained this condition from Eqs. (1.41) and (1.42). Figure 1.12d presents the FRC of the beam at $\lambda_2 = 1$ after the suggested improvement. In the region DEF, the saturation controller and velocity feedback controller operate simultaneously. In the regions ABD and FHI, only the velocity feedback controller is active.

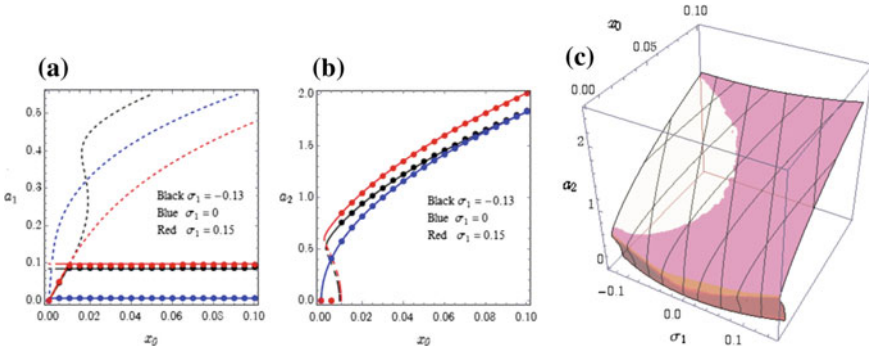


Fig. 1.13 Force–amplitude response curve: **a** beam, **b** controller, **c** controller response versus external detuning parameter σ_1 and excitation amplitude when $\lambda_2 = 1$, $\sigma_2 = 0$, $\tau_1 = 0.01$, $\tau_2 = 0.008$, and $\tau_3 = 0.01$ at different values of σ_1

1.4.3.7 Force Response

The force–amplitude response of the beam and the controller are plotted in Fig. 1.13a and b, respectively. We assumed that the internal resonance is perfectly tuned ($\sigma_2 = 0$), while external resonance σ_1 changes according to the excitation frequency. The uncontrolled beam vibrates with large displacement amplitudes when the system is excited near its natural frequency, as seen in the dashed curves in Fig. 1.13a. From Eqs. (1.1) and (1.2), we can see that $\dot{x}_1(t - \tau_3)$, which depends on x_1 , is a parametric excitation for x_2 . As seen in Fig. 1.13a, the amplitude of parametric excitation a_1 , for the controlled system (solid lines), increases linearly with x_0 until reaching a critical value $2\sqrt{\alpha_2^2 + \sigma_1^2/(\lambda_2\omega_1)}$ then saturates. After the saturation of x_1 mode, the primary system energy is transferred to the controller because of the saturation phenomenon. Figure 1.13a illustrates that the displacement amplitude of the beam after control is extremely smaller than its value before control. The results were verified numerically, as shown by small circles in the figure. Figure 1.13c shows the controller response versus the external detuning parameter σ_1 and the excitation amplitude x_0 . A certain threshold is required for x_0 to turn on the saturation controller, as seen in Fig. 1.13b and c.

The saturation phenomenon needs a specific threshold value of x_0 to be activated. Figure 1.14a, b show the time response of the beam and the controller, respectively, when x_0 is less than the threshold value. The controller operates until vanishing its initial energy, as seen in Fig. 1.14b and deactivates. In this case, the beam is controlled only by the velocity feedback controller. The analytical formula defining the threshold can be deduced from Eqs. (1.41) and (1.42). The threshold value of x_0 is plotted as a function of σ_1 and λ_2 in Fig. 1.14c. It can be seen that the threshold value decreases as the external detuning parameter tends to zero. Also, the threshold value decreases when λ_2 increases for a constant value of σ_1 .

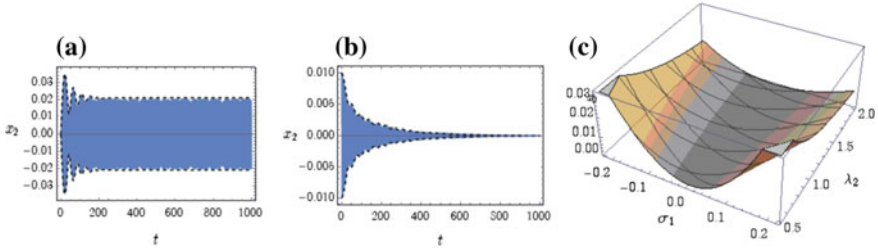


Fig. 1.14 Time history of: **a** beam, **b** controller at $\lambda_2 = 1$, $\sigma_1 = 0.15$, $\tau_1 = 0.1$, $\tau_2 = 0.008$, and $\tau_3 = 0.01$ and **c** the threshold value of x_0 versus σ_1 and λ_2

1.5 Conclusions

The flutter phenomenon of the cantilever beam may occur if bending and twisting mode vibrations occur simultaneously. This work aimed to restrict the flutter phenomenon by reducing the bending mode vibrations of a forced and self-excited nonlinear beam. The control algorithm employed the velocity feedback controller and the saturation controller. Utilizing the velocity feedback controller besides the saturation controller increases system damping without reducing controller efficiency. So, it eliminates the effects of self-excitation, reduces the transient vibrations, and increases the time margin of the system. We concluded the optimal combinations of controller parameters, the time margins, and the stable solution regions for the expected bandwidth of external excitation. Finally, we proposed an improvement to the control algorithm to eliminate the undesired regions from the FRC of the saturation controller. We recommend practicing this algorithm and expect better vibrations reduction.

Acknowledgements We wish to thank Prof. Warminski and his coauthors as we used their proposed model in [1] to be the basic model for this work.

This research for the second author was partially performed in the framework of the project 9.1001.2017/4.6 of Russian Ministry of Education and Sciences.

References

1. Warminski, J., Cartmell, M.P., Mitura, A., Bochenski, M.: Active vibration control of a nonlinear beam with self- and external excitations. *Shock Vib.* **20**, 1033–1047 (2013)
2. Den Hartog, J.P.: *Mechanical Vibrations*. McGraw-Hill, New York (1984)
3. Abadi, A.: *Nonlinear Dynamics of Self-excitation in Autoparametric Systems*. University of Utrecht (2003)
4. Nayfeh, A.H., Mook, D.T.: *Nonlinear Oscillations*. Wiley, New York (1995)
5. Saeed, N.A., Eissa, M.: Nonlinear time delay saturation-based controller for suppression of nonlinear beam vibrations. *Appl. Math. Model.* **37**, 8846–8864 (2013)

6. Eissa, M., Kandil, A., Kamel, M.: Vibration suppression of a nonlinear magnetic levitation system via time delayed nonlinear saturation controller. *Int. J. Non-linear Mech.* **72**, 23–41 (2015)
7. Harne, R.L., Sun, A., Wang, K.W.: Leveraging nonlinear saturation-based phenomena in an L-shaped vibration energy harvesting system. *J. Sound Vib.* **363**, 517–531 (2016)
8. Lim, C.: Active vibration control of the linear structure with an active mass damper applying robust saturation controller. *Mechatronics* **18**, 391–399 (2008)
9. Shoeybi, M., Ghorashi, M.: Control of a nonlinear system using the saturation phenomenon. *Nonlinear Dyn.* **42**, 113–136 (2005)
10. Shoeybi, M., Ghorashi, M.: Nonlinear vibration control of a system with dry friction and viscous damping using the saturation phenomenon. *Nonlinear Dyn.* **45**, 249–272 (2006)
11. Pai, P.F., Schulz, M.J.: A refined nonlinear vibration absorber. *Int. J. Mech. Sci.* **42**, 537–560 (2000)
12. Xu, J., Chen, Y., Wai, K.: An improved time-delay saturation controller for suppression of nonlinear beam vibration. *Nonlinear Dyn.* **82**, 1691–1707 (2015)
13. El-Ganaini, W.A., Saeed, N.A., Eissa, M.: Positive position feedback (PPF) controller for suppression of nonlinear system vibration. *Nonlinear Dyn.* **72**, 517–537 (2013)
14. Abdelhafez, H.M., Nassar, M.E.: Suppression of vibrations of a forced and self-excited nonlinear beam by using positive position feedback controller PPF. *Br. J. Math. Comput. Sci.* **17**, 1–19 (2016)
15. Hristu-Varsakelis, D., Levine, W. S.: *Handbook of Networked and Embedded Control Systems*. Birkhäuser, Basel (2005)
16. Abdelhafez, H., Nassar, M.: Effects of time delay on an active vibration control of a forced and self-excited nonlinear beam. *Nonlinear Dyn.* **86** (2016)
17. Xu, L., Yu, Y., Cui, Y.: Active vibration control for seismic excited building structures under actuator saturation, measurement stochastic noise and quantisation. *Eng. Struct.* **156**, 1–11 (2018)
18. Zhao, Z., Ma, Y., Ren, Z., Tang, C., Wen, G.: Vibration boundary control for a one-dimensional flexible beam system with restricted input. *IEEE Access* **6**, 43336–43342 (2018)

Chapter 2

Use of the Modified Method of Parameter Continuation in Nonlinear Dynamics



Igor V. Andrianov, Viktor I. Olevskiy and Yuliia B. Olevska

Abstract The modified method of parameter continuation (MMPC) is an asymptotic technique for estimating the eigenfrequencies and eigenmodes of nonlinear oscillations of beams, plates and shells with complicated boundary conditions. Unlike the Bolotin method, which is usually used for such estimations, MMPC estimations depend on the shape of initial perturbation. When the frequency of perturbation coincides with the eigenfrequency of the structure, the vibration frequency is close to the corresponding eigenfrequency. In another case, it describes the real vibration shape of structure with different conditions on its edges. The comparison with numerical calculations confirms the advantages of proposed method and accuracy of it.

Keywords Linear oscillations · Nonlinear oscillations · Parameter continuation · Asymptotic technique · Boundary value problem · Eigenvalue problem

2.1 Introduction

Thin-walled structures are widely used in various branches of modern technology [1–3]. Plate and shell structures are subjected to various static and dynamic impacts, while demands to their strength and reliability are subject to ever-increasing. In real constructions, the boundary conditions for structures often have a complicated form [4]. Such conditions may be provided for constructive design decisions. It also exists the possibility of the appearance of mixed boundary conditions when joining elements of building structures with embedded parts, as well as intermittent welded

I. V. Andrianov (✉)

Institute of General Mechanics RWTH Aachen University, Templergraben 64, 52056 Aachen, Germany

V. I. Olevskiy

Mathematic Department of State Higher Educational Institution “Ukrainian State University of Chemical Technology”, 8 Gagarin Ave., Dnipro 49005, Ukraine

Yu. B. Olevska

Department of Mathematics, National Technical University “Dnipro Polytechnic”, 19 Dmytro Yavornytsky Ave., Dnipro 49600, Ukraine

© Springer Nature Switzerland AG 2020

H. Altenbach et al. (eds.), *Nonlinear Wave Dynamics of Materials and Structures*, Advanced Structured Materials 122, https://doi.org/10.1007/978-3-030-38708-2_2

seams. Finally, the calculation of structures with cracks or narrow cuts in some cases can be reduced to the calculation of structures with mixed boundary conditions. The design of the structure may change during operation under the influence of external environment (corrosion or fatigue cracks, destruction of a part of the supporting contour, etc.). In this case, the emergence of support of a mixed type is possible where it was not originally envisaged.

The calculation of plate vibrations can be reduced to integrating the F. Gehring equation of the parabolic type with various boundary conditions. An exact solution of this problem can be obtained only for several cases, when the boundary conditions allow complete separation of variables [5]. Otherwise, the problem has to be solved approximately, most often numerically [6]. The most developed of the approximate methods are the variational ones. These methods to some extent satisfy the requirements of practice, and their application allowed to solve a large number of problems. Unfortunately, the effectiveness of variational methods is significantly failed in problems with mixed boundary conditions, because of the difficulties in constructing coordinate functions that must satisfy different boundary conditions at different parts of the boundary.

One of the most useful ways of solving mixed boundary value problems in the theory of plates vibration is the method of multiple series [7]. A general solution of the differential equation containing a set of arbitrary constants is sought. In each individual section of mixed boundary conditions, these constants are chosen so that the boundary conditions are satisfied. In this case, if the solution is represented as a Fourier series, then there are as many different series as there are sections of change of boundary conditions. After this, a finite integral transformation is applied to the resulting system of series, which leads to an infinite system of linear algebraic or integral equations solved by known methods. This method can be used only in the case when the sizes of the sections of the boundary with different fixing conditions are commensurable with the linear sizes of the plate.

Another way is asymptotic approach [4, 8]. The most significant results in solving mixed boundary value problems in the theory of plates vibration were obtained by the asymptotic Bolotin method (BM), which can be applied to the calculation of eigenfrequencies and eigenmodes of natural vibration of rectangular plates with complex boundary conditions [9]. The main idea of the method is to represent the solution as a sum of two components: the main one in the inner region occupied by the plate and the corrective state of the dynamic edge effect localized in a small neighborhood of the contour. Corrective component rapidly decreases when propagating to the inner region. Unfortunately, the scope of the method is limited; for some problems, the method gives a significant error.

Therefore, it is very important to develop approximate analytical methods for calculating plates vibrations with complex boundary conditions, which make it possible to obtain solutions that are sufficiently accurate and give qualitative information on the behavior of the plate, and permit to investigate the influence of various factors on the structural behavior. The foundations of such a method are the modified method of parameter continuation (MMPC) [10–12] that has shown its effectiveness in solving the problems of the static of plates and shells with complex boundary conditions.

The task of this work is to create a technique that allows the calculation of nonlinear free vibrations of rectangular plates and cylindrical shells with complicated boundary conditions based on combining the advantages of BM and MMPC.

2.2 Asymptotic Method for Estimation of Free Vibrations of Beams and Rectangular Plates

2.2.1 Explanation of Main Ideas of the Method on the Base of Calculation of Beam Oscillations

Let us consider the natural linear oscillations of the uniform beam of length l , of area of cross section F , of Young's modulus E , of density ρ and of cross-sectional moment of inertia J . Governing equation is as follows:

$$\frac{\partial^4 w}{\partial x^4} + a^2 \frac{\partial^2 w}{\partial t^2} = 0, \quad a^2 = \frac{\rho F}{EJ} \quad (2.1)$$

Boundary conditions when $x = 0, l$ are in two variants:

(a) simply supported edges

$$w = 0, \quad \frac{\partial^2 w}{\partial x^2} = 0 \quad (2.2)$$

(b) clamped edges

$$w = 0, \quad \frac{\partial w}{\partial x} = 0 \quad (2.3)$$

According to the MMPC [10–12], we carry out a perturbation of the following form. We introduce an artificial parameter as follows

$$\frac{\partial^2 w}{\partial t^2} = -\frac{\varepsilon}{a^2} \frac{\partial^4 w}{\partial x^4} \quad (2.4)$$

We seek the solution in the form of a series in powers of the parameter ε

$$w = \sum_{i=0}^{\infty} w_i \varepsilon^i \quad (2.5)$$

We will consider problems with the initial shape perturbation. We consider two types of problems:

- (1) the initial perturbation $f_0(x)$ is known and we want to describe the oscillation of the beam;
- (2) the initial perturbation is unknown and we want to find the eigenfrequencies of the beam.

For the first case, zero-order approximation gives

$$w_0 = f_0 \quad (2.6)$$

first-order one is

$$w_1 = -\frac{t^2}{2a^2} f_0^{(IV)} \quad (2.7)$$

and the third-order approximation is

$$w_2 = \frac{t^4}{24a^4} f_0^{(VIII)} \quad (2.8)$$

Then one obtains

$$w \approx f_0 - \frac{t^2}{2a^2} \varepsilon f_0^{(IV)} + \frac{t^4}{24a^4} \varepsilon^2 f_0^{(VIII)} \quad (2.9)$$

Using Padé approximation gives

$$w \approx \left(f_0 + \frac{1}{2a^2} \left(\frac{f_0 f_0^{(VIII)}}{6 f_0^{(IV)}} - f_0^{(IV)} \right) t^2 \right) \left(1 + \frac{f_0^{(VIII)}}{12a^2 f_0^{(IV)}} t^2 \right)^{-1} \quad (2.10)$$

Both the series and the fractional-rational approximation describe only the initial motion of the beam. To describe motions for a longer time, it is necessary to carry out mandatory periodization or to increase the number of approximations. However, such an approximation makes it possible to obtain all the important characteristics of periodic motion for given initial and boundary conditions, and also corresponding eigenmodes and eigenfrequencies [13, 14].

For the second case, we also consider an initial shape function f with required variability, for which the solution is constructed easily but which does not completely satisfy the boundary conditions. In this case, we apply the technique, which is characteristic of BM. Zero-order approximation gives

$$w_0 = f \quad (2.11)$$

first-order one is

$$w_1 = -\frac{t^2}{2a^2} f^{(IV)} + f_0 - f \quad (2.12)$$

and the third-order approximation is

$$w_2 = \frac{t^4}{24a^4} f^{(VIII)} - \frac{t^2}{2a^2} (f_0^{(IV)} - f^{(IV)}) \quad (2.13)$$

Then one obtains

$$w \approx (f + \varepsilon(f_0 - f)) - \frac{t^2}{2a^2} (\varepsilon f^{(IV)} + \varepsilon^2 (f_0^{(IV)} - f^{(IV)})) + \frac{t^4}{24a^4} f^{(VIII)} \quad (2.14)$$

Using Padé approximation gives

$$w \approx \left(f_0 + \frac{1}{2a^2} \left(\frac{f_0 f^{(VIII)}}{6f_0^{(VIII)}} - f_0^{(IV)} \right) t^2 \right) \left(1 + \frac{f^{(VIII)}}{12a^2 f_0^{(VIII)}} t^2 \right)^{-1} \quad (2.15)$$

A quarter of the period T is obtained from the condition that the numerator of expression (2.15) is equal to zero

$$f_0 + \frac{1}{2a^2} \left(\frac{f_0 f^{(VIII)}}{6f_0^{(VIII)}} - f_0^{(IV)} \right) \left(\frac{T}{4} \right)^2 = 0 \quad (2.16)$$

$$T = 8a \sqrt{\frac{3f_0 f_0^{(IV)}}{6(f_0^{(IV)})^2 - f_0 f^{(VIII)}}} \quad (2.17)$$

The frequency is

$$\omega = 2\pi/T = \frac{\pi}{4a} \sqrt{2 \frac{f_0^{(IV)}}{f_0} - \frac{f^{(VIII)}}{3f_0^{(IV)}}} \quad (2.18)$$

Let us compare the results obtained by different methods. For BM, calculation results are well known [9, 13]. We get analogous results for proposed method. Thus, for simply supported edges, we suppose

$$\begin{aligned} f = f_0 &= A \sin \frac{m\pi x}{l}, & f^{IV} &= A \left(\frac{m\pi}{l} \right)^4 \sin \frac{m\pi x}{l}, \\ f^{VIII} &= A \left(\frac{m\pi}{l} \right)^8 \sin \frac{m\pi x}{l} \end{aligned} \quad (2.19)$$

Therefore, according to (2.18), the frequency is

$$\omega = \frac{\pi}{4a} \left(\frac{m\pi}{l} \right)^2 \sqrt{\frac{5}{3}} \quad (2.20)$$

Taking into account that

$$\frac{\pi}{4} \sqrt{\frac{5}{3}} \approx 1.0139 \quad (2.21)$$

we obtain an excellent agreement with the classical result [13] (up to 1.39%):

$$\omega \approx \frac{1}{a} \left(\frac{m\pi}{l} \right)^2, \quad T \approx 2\pi a \left(\frac{l}{m\pi} \right)^2 \quad (2.22)$$

For clamped edges, we suppose

$$f = f_0 = Ax^2(x-l)^2, \quad f^{IV} = 24A, \quad f^{VIII} = 0 \quad (2.23)$$

then

$$T = 2ax(l-x) \frac{\sqrt{3}}{3}, \quad \omega = \frac{\pi\sqrt{3}}{ax(l-x)} \quad (2.24)$$

For the middle point of the beam $x = l/2$, we get

$$\omega = \frac{4\pi\sqrt{3}}{al^2} \approx \left(\frac{4\sqrt{3}}{\pi} \right) \frac{\pi^2}{al^2} \approx (1 + 0.485)^2 \frac{\pi^2}{al^2} \quad (2.25)$$

We obtain an excellent agreement with the result of BM [13] (up to 1.99%) for $m = 1$:

$$\omega = (m + 0.5)^2 \frac{\pi^2}{al^2} \quad (2.26)$$

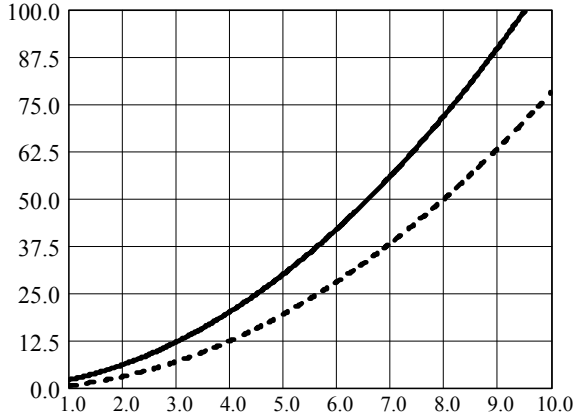
For a high-frequency vibration case, we suppose

$$f_0 = A \sin^2 \frac{m\pi x}{2l}, \quad f = A \sin \frac{m\pi x}{l} \quad (2.27)$$

then

$$f_0^{(IV)} = -\frac{A}{2} \left(\frac{m\pi}{l} \right)^4 \cos \frac{m\pi x}{l}, \quad f^{(VIII)} = A \left(\frac{m\pi}{l} \right)^8 \sin \frac{m\pi x}{l} \quad (2.28)$$

Fig. 2.1 Dependence of relevant frequency from number of waves for BM (2.26) (solid curve) and for presented method (dashed curve)



$$\omega = \frac{\pi}{4a} \left(\frac{m\pi}{l} \right)^2 \quad (2.29)$$

This result is in a good agreement with the result of BM (2.26) (Fig. 2.1).

2.2.2 Asymptotic Estimation of Free Vibrations of Nonlinear Plates

Let us investigate natural nonlinear oscillations of the uniform rectangular plate of length a , of width b , of thickness h , which is described by the Berger's equation [13]

$$D\nabla^4 w - J_1 \nabla^2 w \int_0^a \int_0^b \left((w_{,x})^2 + (w_{,y})^2 \right) dx dy + \rho w_{tt} = 0 \quad (2.30)$$

where

$$D = \frac{Eh^3}{12(1-\nu^2)}, \quad \bar{D} = \frac{Eh^2}{12(1-\nu^2)}, \quad J_1 = \frac{Eh}{2ab(1-\nu^2)} = \frac{6\bar{D}}{hab} \quad (2.31)$$

According to our method, we introduce an artificial parameter in the form

$$\frac{\partial^2 w}{\partial t^2} = -\frac{\varepsilon}{\rho} \left(\bar{D}\nabla^4 w - J_1 \nabla^2 w \int_0^a \int_0^b (w_x^2 + w_y^2) dx dy \right) \quad (2.32)$$

and seek the solution in the form (2.5). As a result, we get

$$\begin{aligned} \sum_{i=0}^{\infty} \frac{\partial^2 w_i}{\partial t^2} \varepsilon^i = & -\frac{\varepsilon}{\rho} \left(\bar{D} \sum_{i=0}^{\infty} \nabla^4 w_i \varepsilon^i \right. \\ & \left. - J_1 \left(\sum_{i=0}^{\infty} \nabla^2 w_i \varepsilon^i \right) \int_0^a \int_0^b \left(\left(\sum_{i=0}^{\infty} w_{i,x} \varepsilon^i \right)^2 + \left(\sum_{i=0}^{\infty} w_{i,y} \varepsilon^i \right)^2 \right) dx dy \right) \end{aligned} \quad (2.33)$$

After ε -splitting, we get

$$\begin{aligned} i = 0 : \frac{\partial^2 w_0}{\partial t^2} &= 0, \\ i = 1 : \frac{\partial^2 w_1}{\partial t^2} &= -\frac{1}{\rho} \left(\bar{D} w_0 - J_1 \nabla^2 w_0 \int_0^a \int_0^b \left((w_{0,x})^2 + (w_{0,y})^2 \right) dx dy \right), \\ i = 2 : \frac{\partial^2 w_2}{\partial t^2} &= -\frac{1}{\rho} \left(\bar{D} w_1 - J_1 \nabla^2 w_1 \times \int_0^a \int_0^b \left((w_{0,x})^2 + (w_{0,y})^2 \right) dx dy, \right. \\ & \quad \left. - 2J_1 \nabla^2 w_0 \int_0^a \int_0^b (w_{0,x} w_{1,x} + w_{0,y} w_{1,y}) dx dy \right) \end{aligned} \quad (2.34)$$

...

We also consider two types of problems with the initial shape perturbation:

- (1) the initial perturbation $f_0(x, y)$ is known and it is necessary to describe the oscillation of the plate;
- (2) the initial perturbation is unknown and it is necessary to find the eigenfrequencies of the plate.

For the first case, approximation is

$$w_0 = f_0, \quad w_1 = -\frac{1}{2\rho} t^2 J_0(f_0) f_0, \quad (2.35)$$

$$w_2 = \frac{t^4}{24\rho^2} \left((J_0(f_0))^2 f_0 - 2J_1 J_3(f_0) \int_0^a \int_0^b (\bar{\nabla} f_0 \cdot J_0(f_0) \bar{\nabla} f_0) dx dy \right) \quad (2.36)$$

$$J_2(f) = \int_0^a \int_0^b \left((f_{,x})^2 + (f_{,y})^2 \right) dx dy \quad (2.37)$$

$$J_0(f_0) = (\bar{D} \nabla^4 - J_1 J_2(f_0) \nabla^2) \quad (2.38)$$

Using Padé approximation, we obtain formula for displacement of the plate

$$w \approx \left(f_0 + \frac{1}{12\rho} t^2 A_1 \right) / \left(1 + \frac{1}{12} t^2 B_1 \right) \quad (2.39)$$

$$A_1 = \frac{f_0 \left(J_0^2(f_0) f_0 - 2J_1 \nabla^2 f_0 \int_0^a \int_0^b (\nabla f_0 \cdot J_0(f_0) \nabla f_0) dx dy \right) - 6(J_0(f_0) f_0)^2}{J_0(f_0) f_0} \quad (2.40)$$

$$B_1 = \left(J_0^2(f_0) f_0 - 2J_1 \nabla^2 f_0 \int_0^a \int_0^b (\nabla f_0 \cdot J_0(f_0) \nabla f_0) dx dy \right) / J_0(f_0) f_0 \quad (2.41)$$

For the second case, we consider an initial shape function $f(x, y)$ for which the solution is constructed easily, but boundary conditions are not completely satisfied, and initial function $f_0(x, y)$, which completely satisfied the boundary conditions. Thus, we get

$$w_0 = f, \quad w_1 = -\frac{t^2}{2\rho} J_0(f) f + f_0 - f \quad (2.42)$$

$$w_2 = \frac{t^4}{24\rho^2} \left[(J_0(f))^2 f - 2J_1 \nabla^2 f \right. \\ \left. \times \int_0^a \int_0^b (f_{,x} J_0(f) f_{,x} + f_{,y} J_0(f) f_{,y} - J_1 \nabla^2 f [J_2(f_{,x}) + J_2(f_{,y})]) dx dy \right] \\ - \frac{t^2}{2\rho} \left[J_0(f) (f_0 - f) - 2J_1 \nabla^2 f \int_0^a \int_0^b (f_{,x} (f_{0,x} - f_{,x}) + f_{,y} (f_{0,y} - f_{,y})) dx dy \right]. \quad (2.43)$$

So

$$w \approx f_0 - \frac{t^2}{2\rho} \left[J_0(f) f_0 - 2J_1 \nabla^2 f \int_0^a \int_0^b (f_{,x} (f_{0,x} - f_{,x}) + f_{,y} (f_{0,y} - f_{,y})) dx dy \right] \\ + \frac{t^4}{24\rho^2} \left[(J_0(f))^2 f - 2J_1 \nabla^2 f \right. \\ \left. \times \int_0^a \int_0^b (f_{,x} J_0(f) f_{,x} + f_{,y} J_0(f) f_{,y} - J_1 \nabla^2 f [J_2(f_{,x}) + J_2(f_{,y})]) dx dy \right]. \quad (2.44)$$

We introduce the notation

$$f_1 = J_0(f) f_0 - 2J_1 \nabla^2 f \int_0^a \int_0^b (f_{,x} (f_{0,x} - f_{,x}) + f_{,y} (f_{0,y} - f_{,y})) dx dy,$$

$$\begin{aligned}
f_2 &= J_0^2(f)f - 2J_1\nabla^2 f \\
&\times \int_0^a \int_0^b (f_{,x}J_0(f)f_{,x} + f_{,y}J_0(f)f_{,y} - J_1\nabla^2 f[J_2(f_{,x}) + J_2(f_{,y})])dxdy.
\end{aligned}
\tag{2.45}$$

Using Padé approximation, we get

$$w \approx \frac{f_0 + \frac{1}{12\rho}t^2 A_1}{1 + \frac{1}{12}t^2 B_1} \tag{2.46}$$

$$A_1 = \frac{f_0 f_2 - 6(f_1)^2}{f_1}, \quad B_1 = \frac{f_2}{f_1} \tag{2.47}$$

A quarter of the period T for both cases can be obtained from the condition

$$f_0 + \frac{A_1}{12\rho} \left(\frac{T}{4}\right)^2 = 0 \tag{2.48}$$

so

$$\begin{aligned}
T &= 8\sqrt{-\frac{3f_0\rho}{A_1}}, \\
\omega &= \frac{\pi}{4}\sqrt{-\frac{A_1}{3f_0\rho}}
\end{aligned}
\tag{2.49}$$

From (2.42), we can conclude that the frequency does not depend on the amplitude of initial perturbation f_0 .

For simply supported edges, we suppose

$$f = f_0 = A \sin \frac{m\pi x}{a} \sin \frac{n\pi y}{b} \tag{2.50}$$

The calculation is carried out for a point (x_0, y_0) with maximal amplitude of the initial deflection for which

$$\sin \frac{m\pi x_0}{a} = \sin \frac{n\pi y_0}{b} = 1 \tag{2.51}$$

According to (2.42), expression for frequency is

$$\omega = \frac{\pi}{4} \times \sqrt{\frac{2J_0(f_0)f_0}{f_0\rho} - \frac{f_0\left(J_0^2(f_0)f_0 - 2J_1\nabla^2 f_0 \int_0^a \int_0^b (\nabla f_0 \cdot J_0(f_0)\nabla f_0) dx dy\right)}{3\rho J_0(f_0)f_0}} \quad (2.52)$$

Substituting (2.51) to (2.52) gives

$$\omega = \frac{\pi^3}{4} \left[\left(\frac{m}{a}\right)^2 + \left(\frac{n}{b}\right)^2 \right] \sqrt{\frac{5\bar{D}}{3\rho} \left(1 + \frac{3}{2} \left(\frac{A}{h}\right)^2\right)} \quad (2.53)$$

Taking into account (2.21), we obtain

$$\omega \approx \pi^2 \left[\left(\frac{m}{a}\right)^2 + \left(\frac{n}{b}\right)^2 \right] \sqrt{\frac{\bar{D}}{\rho} \left(1 + \frac{3}{2} \left(\frac{A}{h}\right)^2\right)} \quad (2.54)$$

We can see that in general case the frequency is dependent on the amplitude of initial perturbation even for simply supported edges (Fig. 2.2). For linear case, we can represent real form by splitting initial perturbations in convergent Fourier series [15–17].

For clamped edges, we suppose

$$\begin{aligned} f_0 &= A \sin^2 \frac{m\pi x}{2a} \sin^2 \frac{n\pi y}{2b}, \\ f &= A \sin \frac{m\pi x}{a} \sin \frac{n\pi y}{b} \end{aligned} \quad (2.55)$$

Figure 2.3 shows good agreement results obtained by our method and BM [13].

2.3 Using Asymptotic Method for Estimation of Parameter-Dependent Vibrations of Beams and Rectangular Plates

Often asymptotic methods give possibility to calculate different types of boundary conditions in one calculation scheme. So we can obtain results for different boundary conditions only by changing parameter value. Such a scheme does not describe parametric vibrations, because parametric motion has to be caused by time-dependent change of parameter [4, 17]. This is very important at the stage of preliminary design

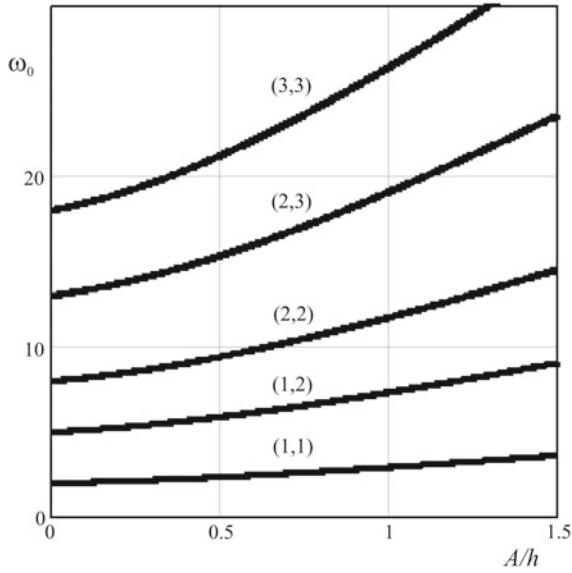
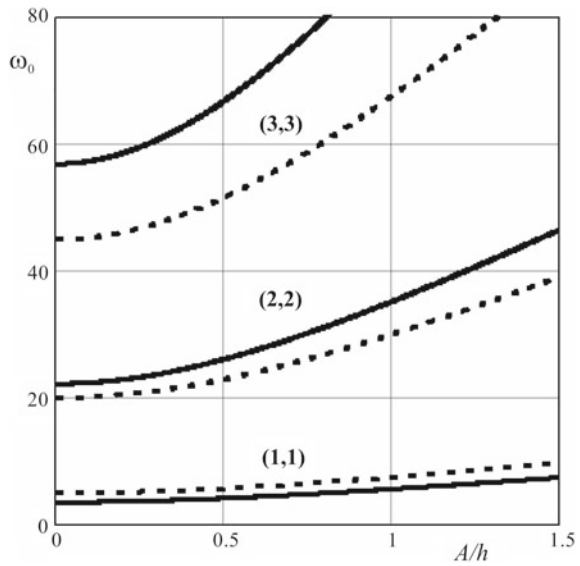


Fig. 2.2 Dependence of frequency $\omega_0 = (\omega/\pi^2 a^2)\sqrt{\rho/D}$ of square plate from amplitude A/h of initial perturbation for simply supported edges (numbers of waves in spatial directions are shown in above curves)

Fig. 2.3 Dependence of frequency from amplitude of initial perturbation for square plate according to BM [13] (solid curve) and to our method (dashed curve). Numbers of waves in spatial directions are shown in above curves



of structures, because it allows fast modification of possible boundary conditions in order to select the rational fastening of the edges. It is also important for solution of plate conjunction problems [18, 19].

2.3.1 Explanation of the Method on the Base of Parameter-Dependent Beam Oscillations

Let us consider the natural linear oscillations of the uniform beam under action of axes-directed compressive force N on its edges, described by the equation:

$$EJ \frac{\partial^4 w}{\partial x^4} + N \frac{\partial^2 w}{\partial x^2} + \rho F \frac{\partial^2 w}{\partial t^2} = 0 \quad (2.56)$$

Boundary conditions for simply supported edges at $x = 0, l$ are

$$w = 0, \quad \frac{\partial^2 w}{\partial x^2} = 0 \quad (2.57)$$

We introduce an artificial parameter according to MMPC in the form

$$\frac{\partial^2 w}{\partial t^2} = -\frac{\varepsilon}{\rho F} \left(EJ \frac{\partial^4 w}{\partial x^4} + N \frac{\partial^2 w}{\partial x^2} \right) \quad (2.58)$$

and represent as series

$$w = \sum_{i=0}^{\infty} w_i \varepsilon^i \quad (2.59)$$

We consider problems when the initial perturbation $f_0(x)$ is known [20]. After splitting, we get

$$\begin{aligned} w_0 &= f_0 \\ w_1 &= -\frac{t^2}{2\rho F} \left(N f_0'' + EJ f_0^{(IV)} \right) \\ w_2 &= \frac{t^4}{24\rho^2 F^2} \left(N^2 f_0^{(IV)} + 2NEJ f_0^{(VI)} + E^2 J^2 f_0^{(VIII)} \right) \end{aligned} \quad (2.60)$$

Then one obtains

$$w \approx f_0 - \frac{t^2}{2\rho F} \varepsilon \left(N f_0'' + EJ f_0^{(IV)} \right)$$

$$+ \frac{t^4}{24\rho^2 F^2} \varepsilon^2 \left(N^2 f_0^{(IV)} + 2NEJf_0^{(VI)} + E^2 J^2 f_0^{(VIII)} \right) \quad (2.61)$$

Using Padé approximation gives

$$w \approx \frac{f_0 + \frac{t^2}{2\rho F} \left(\frac{f_0(N^2 f_0^{(IV)} + 2NEJf_0^{(VI)} + E^2 J^2 f_0^{(VIII)})}{6(Nf_0'' + EJf_0^{(IV)})} - (Nf_0'' + EJf_0^{(IV)}) \right)}{1 + \frac{(N^2 f_0^{(IV)} + 2NEJf_0^{(VI)} + E^2 J^2 f_0^{(VIII)})}{(Nf_0'' + EJf_0^{(IV)})} \frac{t^2}{12\rho F}} \quad (2.62)$$

A quarter of the period T is obtained from the condition

$$f_0 + \frac{1}{2\rho F} \left(\frac{f_0(N^2 f_0^{(IV)} + 2NEJf_0^{(VI)} + E^2 J^2 f_0^{(VIII)})}{6(Nf_0'' + EJf_0^{(IV)})} - (Nf_0'' + EJf_0^{(IV)}) \right) \left(\frac{T}{4} \right)^2 = 0 \quad (2.63)$$

$$T = 8\sqrt{6\rho F} \sqrt{\frac{f_0(Nf_0'' + EJf_0^{(IV)})}{6(Nf_0'' + EJf_0^{(IV)})^2 - f_0(N^2 f_0^{(IV)} + 2NEJf_0^{(VI)} + E^2 J^2 f_0^{(VIII)})}} \quad (2.64)$$

For frequency ω , we get

$$\omega = \frac{2\pi}{T} = \frac{\pi}{4\sqrt{\rho F}} \sqrt{\frac{(N^2 f_0^{(IV)} + 2NEJf_0^{(VI)} + E^2 J^2 f_0^{(VIII)})}{6(Nf_0'' + EJf_0^{(IV)})} - \frac{(Nf_0'' + EJf_0^{(IV)})}{f_0}} \quad (2.65)$$

For eigenfrequency ω_e , we get

$$\omega_e = \omega(N = 0) = \frac{\pi}{4} \sqrt{\frac{EJ}{\rho F}} \sqrt{\frac{f_0^{(VIII)}}{6f_0^{(IV)}} - \frac{f_0^{(IV)}}{f_0}} \quad (2.66)$$

The value of buckling force N_c we get from condition of infinity of ω is:

$$N_c f_0'' + EJf_0^{(IV)} = 0 \Rightarrow N_c = -EJ \frac{f_0^{(IV)}}{f_0''} \quad (2.67)$$

Let us analyze results. For simply supported edges, we suppose

$$f = f_0 = A \sin \frac{m\pi x}{l}, \quad f^{IV} = A \left(\frac{m\pi}{l} \right)^4 \sin \frac{m\pi x}{l},$$

$$f^{\text{VIII}} = A \left(\frac{m\pi}{l} \right)^8 \sin \frac{m\pi x}{l} \quad (2.68)$$

So, according to (2.65), the frequency is

$$\omega = \frac{\pi^2 m}{4l} \sqrt{\frac{5 \left(EJ \left(\frac{\pi m}{l} \right)^2 - N \right)}{3 \rho F}} \quad (2.69)$$

Taking into account (2.21), we get an excellent agreement with the classical result [17] (up to 1.39%):

$$\omega \approx \frac{1}{\sqrt{\rho F}} \left(\frac{m\pi}{l} \right) \sqrt{EJ \left(\frac{m\pi}{l} \right)^2 - N} \quad (2.70)$$

For N_c , we get exact solution

$$N_c = -EJ \frac{f_0^{(\text{IV})}}{f_0''} = EJ \left(\frac{m\pi}{l} \right)^2 \quad (2.71)$$

and for eigenfrequency we get also agreement with the classical result up to 1.39%:

$$\omega_e \approx \sqrt{\frac{EJ}{\rho F}} \left(\frac{m\pi}{l} \right)^2 \quad (2.72)$$

2.3.2 Calculation of Parameter-Dependent Plates Vibrations

Let us investigate free nonlinear oscillations of the rectangular plate under action in-plane uniform compressive force N on its edges $x = 0, a$:

$$D\nabla^4 w + Nw_{xx} + \rho h w_{tt} = 0 \quad (2.73)$$

We consider simply supported boundary conditions on both edges:

$$w(x = 0, y) = w(x = a_1, y) = 0, \quad w(x, y = 0) = w(x, y = a_2) = 0 \quad (2.74)$$

$$\begin{aligned} \frac{\partial^2 w}{\partial x^2} \Big|_{x=0} &= \frac{\partial^2 w}{\partial x^2} \Big|_{x=a_1} = 0, \\ \frac{\partial^2 w}{\partial y^2} \Big|_{y=0} &= \frac{\partial^2 w}{\partial y^2} \Big|_{y=a_2} = 0 \end{aligned} \quad (2.75)$$

We carry out a perturbation of the following form

$$\begin{aligned}\frac{\partial^2 w}{\partial t^2} &= -\varepsilon \left(N w_{xx} + \frac{D}{\rho h} \nabla^4 w \right), \\ w &= \sum_{i=0}^{\infty} w_i \varepsilon^i\end{aligned}\quad (2.76)$$

After splitting, we get

$$\begin{aligned}w_0 &= f_0 \\ w_1 &= -\frac{t^2}{2\rho h} \left(N \frac{\partial^2 f_0}{\partial x^2} + D \nabla^4 f_0 \right) \\ w_2 &= \frac{t^4}{24\rho^2 h^2} \left(N^2 \frac{\partial^4 f_0}{\partial x^4} + 2ND \frac{\partial^2 f_0}{\partial x^2} \nabla^4 f_0 + D^2 \nabla^8 f_0 \right)\end{aligned}\quad (2.77)$$

Then one obtains

$$\begin{aligned}w &\approx f_0 - \frac{t^2 \varepsilon}{2\rho h} \left(N \frac{\partial^2 f_0}{\partial x^2} + D \nabla^4 f_0 \right) \\ &\quad + \frac{t^4 \varepsilon^2}{24\rho^2 h^2} \left(N^2 \frac{\partial^4 f_0}{\partial x^4} + 2ND \frac{\partial^2 f_0}{\partial x^2} \nabla^4 f_0 + D^2 \nabla^8 f_0 \right)\end{aligned}\quad (2.78)$$

Padé approximation for (2.78) is

$$w \approx \frac{f_0 + \frac{t^2}{2\rho h} \left(\frac{f_0}{6} \left(\frac{N^2 \frac{\partial^4 f_0}{\partial x^4} + 2ND \frac{\partial^2 f_0}{\partial x^2} \nabla^4 f_0 + D^2 \nabla^8 f_0 \right) - \left(N \frac{\partial^2 f_0}{\partial x^2} + D \nabla^4 f_0 \right) \right)}{1 + \frac{t^2}{12\rho h} \left(\frac{N^2 \frac{\partial^4 f_0}{\partial x^4} + 2ND \frac{\partial^2 f_0}{\partial x^2} \nabla^4 f_0 + D^2 \nabla^8 f_0 \right)}{\frac{N^2 \frac{\partial^4 f_0}{\partial x^4} + D \nabla^4 f_0}}}\quad (2.79)$$

We get formula for parameter-dependent motion of the plate.

Let us analyze results. For simply supported boundaries, we suppose

$$f_0 = A \sin \frac{m\pi x}{a_1} \sin \frac{m\pi y}{a_2}\quad (2.80)$$

After splitting, we get

$$w_0 = f_0, \quad w_1 = -\frac{t^2}{2\rho h} \left(\left(\frac{m\pi}{a_1} \right)^2 N + D \left(\left(\frac{m\pi}{a_1} \right)^2 + \left(\frac{n\pi}{a_2} \right)^2 \right) \right) f_0\quad (2.81)$$

$$w_2 = \frac{t^4}{24\rho^2 h^2} \left(\left(\frac{m\pi}{a_1} \right)^2 N + D \left(\left(\frac{m\pi}{a_1} \right)^2 + \left(\frac{n\pi}{a_2} \right)^2 \right)^2 \right)^2 f_0 \quad (2.82)$$

Padé approximation for (2.82) is

$$w \approx f_0 \frac{1 - \frac{5t^2}{12\rho h} \left(D \left(\left(\frac{m\pi}{a_1} \right)^2 + \left(\frac{n\pi}{a_2} \right)^2 \right)^2 - \left(\frac{m\pi}{a_1} \right)^2 N \right)}{1 + \frac{t^2}{12\rho h} \left(D \left(\left(\frac{m\pi}{a_1} \right)^2 + \left(\frac{n\pi}{a_2} \right)^2 \right)^2 - \left(\frac{m\pi}{a_1} \right)^2 N \right)} \quad (2.83)$$

Period and frequency are obtained from condition

$$w \left(\frac{T}{4}, x, y \right) = 0 \quad (2.84)$$

So

$$1 - \frac{5}{12\rho h} \left(D \left(\left(\frac{m\pi}{a_1} \right)^2 + \left(\frac{n\pi}{a_2} \right)^2 \right)^2 - \left(\frac{m\pi}{a_1} \right)^2 N \right) \left(\frac{T}{4} \right)^2 = 0 \quad (2.85)$$

$$T = 8\sqrt{\frac{3\rho h}{5}} \left(D \left(\left(\frac{m\pi}{a_1} \right)^2 + \left(\frac{n\pi}{a_2} \right)^2 \right)^2 - \left(\frac{m\pi}{a_1} \right)^2 N \right)^{-1/2} \quad (2.86)$$

$$\omega = \frac{\pi}{4} \sqrt{\frac{5}{3\rho h}} \sqrt{D \left(\left(\frac{m\pi}{a_1} \right)^2 + \left(\frac{n\pi}{a_2} \right)^2 \right)^2 - \left(\frac{m\pi}{a_1} \right)^2 N} \quad (2.87)$$

For N_c from condition of infinity of ω

$$\left(\frac{m\pi}{a_1} \right)^2 N_c - D \left(\left(\frac{m\pi}{a_1} \right)^2 + \left(\frac{n\pi}{a_2} \right)^2 \right)^2 = 0 \quad (2.88)$$

we obtain exact solution

$$N_c = D \left(\frac{m\pi}{a_1} \right)^2 \left(1 + \left(\frac{na_1}{ma_2} \right)^2 \right)^2 \quad (2.89)$$

and for eigenfrequency we get the value close to the result from [5] (up to 1.39%)

$$\omega_e = \frac{\pi}{4} \sqrt{\frac{5}{3\rho h}} \sqrt{D \left(\left(\frac{m\pi}{a_1} \right)^2 + \left(\frac{n\pi}{a_2} \right)^2 \right)^2} \approx \sqrt{\frac{D}{\rho h} \left[\left(\frac{m\pi}{a_1} \right)^2 + \left(\frac{n\pi}{a_2} \right)^2 \right]} \tag{2.90}$$

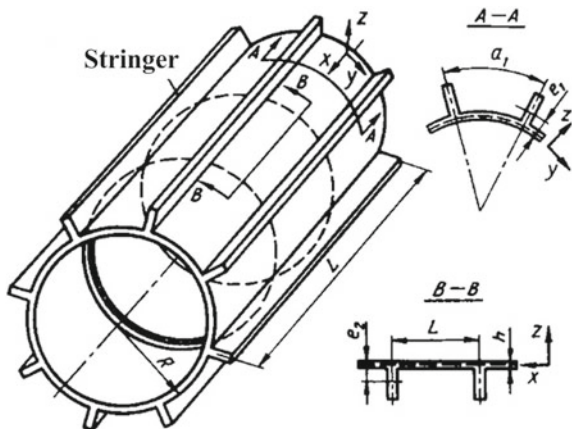
2.4 Nonlinear Vibration of Integrally Stiffened Cylindrical Shell

Now we use the proposed approach in combination with the known asymptotic methods. Consider the nonlinear vibration of a structurally inhomogeneous cylindrical shell [21–23]. We use Lagrangian (material) coordinates and assume that the coordinate system is a right-handed one, so that the x -axis is directed along the generatrix, y -axis is the circumferential coordinate and z -axis is directed toward the center of curvature. Shell is a right circular cylinder; stiffening consists of eccentrically attached circular rings and straight stringers (Fig. 2.4).

Suppose the shell has many closely spaced stiffeners, it gives possibility to use orthotropic theory in which the stiffener characteristics are smeared over the skin (“Smeared Stiffener Theory”). The mathematical justification for such a simplification is given by the asymptotic homogenization theory. We consider the governing equations of motion in the form [8]:

$$\begin{aligned} \frac{\partial N_{11}}{\partial x_1} + \frac{\partial N_{12}}{\partial x_2} + \frac{\partial M_{12}}{\partial x_2} - \frac{1}{2} \frac{\partial}{\partial x_2} [\phi(N_{11} + N_{22})] - \rho R^2 \frac{\partial^2 u_1}{\partial t^2} &= 0 \\ \frac{\partial N_{12}}{\partial x_1} + \frac{\partial N_{22}}{\partial x_2} - Q_2 - \frac{1}{2R} \frac{\partial M_{12}}{\partial x_2} + (\phi_1 N_{12} + \phi_2 N_{22}) & \end{aligned}$$

Fig. 2.4 Scheme of stiffened shell



$$\begin{aligned}
& + \frac{1}{2} \frac{\partial}{\partial x_1} [\phi(N_{11} + N_{22})] - \rho R^2 \frac{\partial^2 u_2}{\partial t^2} = 0 \\
& \frac{\partial Q_1}{\partial x_1} + \frac{\partial Q_2}{\partial x_2} + N_{22} - \frac{\partial}{\partial x_1} (\phi_1 N_{11} + \phi_2 N_{12}) \\
& - \frac{\partial}{\partial x_2} (\phi_1 N_{12} + \phi_2 N_{22}) - \rho R^2 \frac{\partial^2 w}{\partial t^2} = 0 \\
& \frac{\partial M_{11}}{\partial x_1} + \frac{\partial M_{12}}{\partial x_2} - R Q_1 = 0, \quad \frac{\partial M_{12}}{\partial x_1} + \frac{\partial M_{22}}{\partial x_2} - R Q_2 = 0
\end{aligned} \tag{2.91}$$

$$\phi_1 = -\frac{1}{R} \frac{\partial w}{\partial x_1}, \quad \phi_2 = -\frac{1}{R} \left(\frac{\partial w}{\partial x_2} + u_2 \right), \quad \phi_2 = \frac{1}{2R} \left(\frac{\partial u_1}{\partial x_2} + \frac{\partial u_2}{\partial x_1} \right), \tag{2.92}$$

where $u_1(u_2)$, w are the tangential and normal displacements in the middle point of the shell thickness,

$\rho_0, \rho_1(\rho_2)$ are the densities of the shell material and the stringer (ring) material, (ρ_0, ρ are mass per unit volume, ρ_1, ρ_2 are mass per unit area), $\rho = \rho_0 + (\rho_1/l_1) + (\rho_2/l_2)$

$x_1(x_2)$ are the axial and circumferential coordinates,

R, L are the radius and length of the shell,

$l_1(l_2)$ are the distances between stringers (rings).

Here N_{ij} are membrane stresses, M_{ij} are bending and torsion moments, Q_i are transverse shearing forces. Components of an elasticity tensor have the form [8]

$$\begin{aligned}
N_{11} &= B_{11}\varepsilon_{11} + B_{12}\varepsilon_{22} + K_{11}\kappa_{11}, & N_{22} &= B_{21}\varepsilon_{11} + B_{22}\varepsilon_{22} + K_{22}\kappa_{22}, \\
N_{12} &= B_{33}\varepsilon_{12}, & M_{11} &= D_{11}\kappa_{11} + D_{12}\kappa_{22} + K_{11}\varepsilon_{11}, \\
M_{22} &= D_{21}\kappa_{11} + D_{22}\kappa_{22} + K_{22}\varepsilon_{22}, & M_{12} &= D_{33}\kappa_{12}, \\
B_{11} &= B + E_s F_s/l_1, & B_{22} &= B + E_r F_r/l_2, \\
B &= Eh/(1 - \nu^2), & G &= Eh/(1 + \nu), \\
B_{21} &= B_{12} = \nu_{21} B_{11} = \nu_{12} B_{22}, & D_{11} &= D + E_s J_s/l_1, \\
D_{22} &= D + E_r J_r/l_2, & D_{21} &= D_{12} = \nu_{21} D_{11} = \nu_{12} D_{22} = D\nu, \\
D_{11} &= D/2 + E_s J_{ks}/l_1 + E_r J_{kr}/l_2, & K_{11} &= E_s S_s/l_1, & K_{22} &= E_r S_r/l_2
\end{aligned} \tag{2.93}$$

where $F_s(F_r)$, $J_s(J_r)$, $J_{ks}(J_{kr})$, $S_s(S_r)$ are the transverse section areas, moments of inertia, rotation moments of inertia, torsion moments of inertia and static moments of stringer (ring), respectively,

$E, E_s(E_r)$ are the Young's modulus of the shell material and stringer (ring) material, respectively,

ν is the Poisson's ratio of the shell material,

h is the shell thickness.

We accept the following geometrical relations

$$\varepsilon_{11} = \frac{1}{R} \frac{\partial u_1}{\partial x_1} + \frac{1}{2} \phi_1^2 + \phi^2, \quad \varepsilon_{22} = \frac{1}{R} \left(\frac{\partial u_2}{\partial x_2} - w \right) + \frac{1}{2} \phi_2^2 + \phi^2,$$

$$\begin{aligned}\varepsilon_{12} &= \frac{1}{2R} \left(\frac{\partial u_2}{\partial x_1} + \frac{\partial u_1}{\partial x_2} \right) + \frac{1}{2} \phi_1 \phi_2, & \kappa_{11} &= \frac{1}{R} \frac{\partial \phi_1}{\partial x_1}, & \kappa_{22} &= \frac{1}{R} \frac{\partial \phi_2}{\partial x_2}, \\ \kappa_{12} &= \frac{1}{2R} \left(\frac{\partial \phi_2}{\partial x_1} + \frac{\partial \phi_1}{\partial x_2} - \phi \right)\end{aligned}\quad (2.94)$$

We introduce a natural small parameter, $\varepsilon_1 = \sqrt{D_1/B_2 R^2}$, where $D_1 = D_{11} - K_{11}^2/B_1$ and $B_2 = B_{22}(1 - \nu_{12}\nu_{21})$. We also introduce the following dimensionless parameters:

$$\begin{aligned}\varepsilon_2 &= D_1/D_2, & \varepsilon_3 &= D_3/D_1, & \varepsilon_4 &= B_2/B_1, \\ \varepsilon_5 &= B_3/B_1, & \varepsilon_6 &= K_{11}/B_1 R, & \varepsilon_7 &= K_{22}/B_2 R, \\ B_1 &= B_{11}(1 - \nu_{21}\nu_{12}), & 1/B_3 &= 1/B_{33} - B_{21}/B_{11} B_{22}(1 - \nu_{21}\nu_{12}), \\ D_2 &= D_{22} - K_{22}^2/B_2, & D_3 &= D_{12} + D_{33} + (K_{11}K_{22}/B_1 B_2)B_{12}(1 - \nu_{21}\nu_{12})\end{aligned}\quad (2.95)$$

One can define three types of reinforced shells: stringer shells, ring-stiffened shells and integrally stiffened shells. For stringer shells, we can use the following estimations:

$$\varepsilon_1 \ll 1, \varepsilon_2 \sim \varepsilon_1^2, \varepsilon_3 \sim \varepsilon_1, \varepsilon_4 \sim \varepsilon_5 < 1, \varepsilon_6 \sim \varepsilon_1, \varepsilon_7 = 0$$

We introduce parameters of asymptotic estimations α_k :

$$\frac{\partial w}{\partial x_i} \sim \varepsilon_1^{-\alpha_i} w, \quad \frac{\partial w}{\partial t} \sim \varepsilon_1^{-\alpha_3}, \quad \frac{w}{R} \sim \varepsilon_1^{\alpha_4}, \quad u_i \sim \varepsilon_1^{\alpha_4+i}, \quad i = 1, 2 \quad (2.96)$$

We consider possible simplifications of the general relations of the stringer shells. For stringer shell, whose state is changing rapidly in the circumferential direction, we have the following simplified system [8]:

$$\begin{aligned}\alpha_1 &= 0, & \alpha_2 &= \alpha_6 = 1/2, & \alpha_3 &= -1, & \alpha_4 &= \alpha_5 = 1 \\ \frac{\partial N_{11}}{\partial x_1} + \frac{\partial N_{12}}{\partial x_2} &= 0, & \frac{\partial N_{12}}{\partial x_1} + \frac{\partial N_{22}}{\partial x_2} &= 0, \\ \frac{\partial^2 M_{11}}{\partial x_1^2} + 2 \frac{\partial^2 M_{12}}{\partial x_1 \partial x_2} + \frac{\partial^2 M_{22}}{\partial x_2^2} + RN_{22} + \frac{\partial}{\partial x_1} \left(\frac{\partial w}{\partial x_1} N_{11} + \frac{\partial w}{\partial x_2} N_{12} \right) \\ + \frac{\partial}{\partial x_2} \left(\frac{\partial w}{\partial x_1} N_{12} + \frac{\partial w}{\partial x_2} N_{22} \right) - \rho R^2 \frac{\partial^2 w}{\partial t^2} &= 0, \\ N_{11} &= B_{11}\varepsilon_{11} + B_{12}\varepsilon_{22} + K_{11}\kappa_{11}, & 0 &= B_{21}\varepsilon_{11} + B_{22}\varepsilon_{22}, & N_{12} &= B_{33}\varepsilon_{12}, \\ M_{11} &= D_{11}\kappa_{11} + K_{11}\varepsilon_{11}, & M_{22} &= D_{21}\kappa_{11} + D_{22}\kappa_{22}, & M_{12} &= D_{33}\kappa_{12}, \\ \varepsilon_{11} &= (1/R)\partial u_1/\partial x_1 + (1/2R^2)(\partial w/\partial x_1)^2, \\ 0 &= (1/R)(\partial u_2/\partial x_2 - w) + (1/2R^2)(\partial w/\partial x_2)^2,\end{aligned}$$

$$\begin{aligned}
0 &= (1/2R)(\partial u_2/\partial x_1 + \partial u_1/\partial x_2) + (1/2R^2)(\partial w/\partial x_1)(\partial w/\partial x_2), \\
\kappa_{11} &= -(1/R^2)\partial^2 w/\partial x_1^2, \quad \kappa_{22} = -(1/R^2)\partial^2 w/\partial x_2^2, \quad \kappa_{12} = -(1/R^2)\partial^2 w/\partial x_1 \partial x_2
\end{aligned} \tag{2.97}$$

Let us obtain the amplitude–frequency dependencies for the nonlinear vibrations of a simply supported stringer shell with following boundary conditions:

$$\begin{aligned}
w(0, y) = w(L, y) &= 0, \\
\frac{\partial^2 w}{\partial x^2} \Big|_{x=0} &= \frac{\partial^2 w}{\partial x^2} \Big|_{x=L} = 0,
\end{aligned} \tag{2.98}$$

We use for the radial displacement w the following Ansatz [8]

$$w = f_1(t) \sin(s_1 x_1) \cos(s_2 x_2) + f_2(t) \sin^2(s_1 x_1) \tag{2.99}$$

From the condition of continuity of circumferential displacement, one obtains [8]:

$$f_2 = 0.25R^{-1}s_2^2 f_1^2 \tag{2.100}$$

where $s_1 = \pi m l^{-1}$ and $s_2 = n$ are the parameters characterizing number of waves along the generatrix and directrix, respectively.

Taking into account (2.98), the Airy stress function has the form

$$\begin{aligned}
B_1^{-1} \Phi &= p^2 s_2^{-2} (1 - \varepsilon_6 \varepsilon_2^2) \xi \sin s_1 x_1 \cos s_2 x_2 - (5/16) p^2 \xi^2 \cos 2s_2 x_2 \\
&+ \frac{1}{2} s_1^2 \xi^3 \sin s_1 x_1 \cos 2s_1 x_1 \cos s_2 x_2, \quad p = s_1 s_2^{-1}, \quad \xi = f_1/R
\end{aligned} \tag{2.101}$$

Now one can use Bubnov–Galerkin procedure:

$$\int_0^{\tilde{\alpha}} \int_0^l L_1(w) \sin s_1 x_1 \cos s_2 x_2 dx_1 dx_2 = 0, \quad \int_0^{\tilde{\alpha}} \int_0^l L_1(w) \sin^2 s_1 x_1 dx_1 dx_2 = 0, \tag{2.102}$$

where

$$L_1(w) = \nabla^4 w - R(\partial^2/\partial x_1^2 - \nabla^4)\Phi - L(w, \Phi) + \rho R^2 \partial^2 w/\partial t^2 \tag{2.103}$$

Consider now a practically important case of steady-state periodic vibrations. As a result, one obtains the following ODE equation with constant coefficients for the time function ξ :

$$\frac{d^2 \xi}{dt_1^2} + \alpha \xi \left[\left(\frac{d\xi}{dt_1} \right)^2 + \xi \frac{d^2 \xi}{dt_1^2} \right] + A_1 \xi + A_2 \xi^3 + A_3 \xi^5 = 0,$$

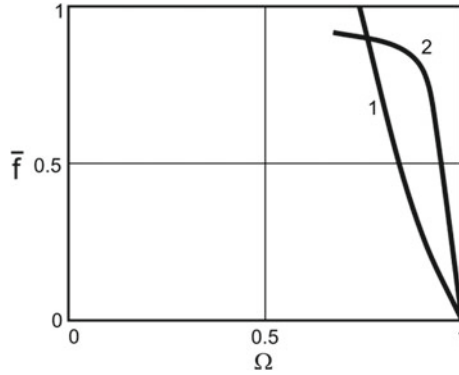


Fig. 2.5 Dependence of the frequency of stringer shell Ω from the amplitude of the initial disturbance $\bar{f} = fRh^{-1}$: curve 1—according to the proposed method; curve 2—data from [8]

$$t_1 = 0: \xi = f, \quad \frac{d\xi}{dt_1} = 0 \tag{2.104}$$

Here

$$t_1 = \sqrt{B_1/\rho R^2}t, \quad A_1 = \varepsilon_1^2\varepsilon_4 + 2\varepsilon_1^2\varepsilon_3\varepsilon_4p^{-2} + \varepsilon_1^2\varepsilon_2\varepsilon_4p^{-4} + s_2^{-4}(1 - \varepsilon_6^2s_2^2), \quad A_2 = \frac{1}{16} + \frac{1}{2}s_2^4\varepsilon_1^2\varepsilon_4 - \frac{3}{4}(1 - \varepsilon_6^2s_2^2), \quad A_3 = \frac{1}{4}s_2^4, \quad \alpha = \frac{3}{32}s_2^4 \tag{2.105}$$

The application of the proposed method of parameter continuation to the Cauchy problem (2.104) gives approximation of the second order for the artificial parameter for frequency Ω of nonlinear oscillations in the form

$$\Omega = \sqrt{\frac{1 + f^2(A_2/A_1) + f^4(A_3/A_1)}{1 + \alpha f}} \tag{2.106}$$

and represented in Fig. 2.5.

2.5 Using MMPC for Investigation of Systems with a Finite Number of Degrees of Freedom

For many problems of metrology [24, 25], technical [17, 26] and mining [27, 28] mechanics, finite-dimensional models are important.

2.5.1 Duffing Pendulum

Let us consider Duffing pendulum as a model example of nonlinear vibrations

$$\ddot{u} + u + \varepsilon u^3 = 0, \quad u(0) = a, \quad \dot{u}(0) = 0 \quad (2.107)$$

For small nonlinearity, it can be used Lindstedt–Poincaré method to construct appropriate approximate solution in terms of trigonometric series in form

$$u = a \cos(\omega t) + \frac{\varepsilon a^2}{32} \cos(3\omega t) + O(\varepsilon^2) \quad (2.108)$$

where circle frequency is

$$\omega = 1 + \frac{3}{8}\varepsilon a^2 - \frac{51}{256}(\varepsilon a^2)^2 + O(\varepsilon^3) \quad (2.109)$$

Thus period T is

$$T \approx 2\pi \left(1 + \frac{3}{8}\varepsilon a^2 - \frac{51}{256}(\varepsilon a^2)^2 \right)^{-1} \quad (2.110)$$

The same result can be found using extended parameters multi-scale asymptotic method or averaging method [13, 17]. MMPC solves this problem in the direct way [14]. We carry out a perturbation according to artificial parameter ε_1

$$\ddot{u} + \varepsilon_1 (u + \varepsilon u^3) = 0, \quad u = \sum_{i=0}^{\infty} u_i \varepsilon_1^i, \quad u_0(0) = a, \quad \dot{u}_0(0) = \dot{u}_1(0) = \dot{u}_i(0) = 0 \quad i = \overline{1, \infty} \quad (2.111)$$

We can get approximation in MMPC form

$$u \approx a - a \frac{(1 + \varepsilon a^2)}{2} \varepsilon_1 t^2 + a \frac{(1 + \varepsilon a^2)(1 + 3\varepsilon a^2)}{24} \varepsilon_1^2 t^4 \quad (2.112)$$

2D Padé approximation of (2.112) for $\varepsilon_1 = 1$ gives

$$u \approx a(12 - (5 + 3\varepsilon a^2)t^2)/(12 + (1 + 3\varepsilon a^2)t^2) \quad (2.113)$$

Period of oscillations is

$$T \approx \frac{8\sqrt{3}}{\sqrt{5+3\varepsilon a^2}} \quad (2.114)$$

Behavior of corresponding approximations for values of parameter ((2.109)—solid curves and (2.113)—dashed curves) is shown in Fig. 2.6. The numbers near curves correspond to values of parameter ϵa^2 . Comparison between Formulas (2.110) (solid curve) and (2.112) (dashed curve) is shown in Fig. 2.7. They demonstrate good agreement in the whole interval under consideration. It worse mentioned that near $\epsilon a^2 \approx 1.4889$ additional terms in (2.109) are equal to the circle frequency of linear pendulum and so cannot be treated as “small.”

Fig. 2.6 Dependence of $\bar{u} = u/a$ on time

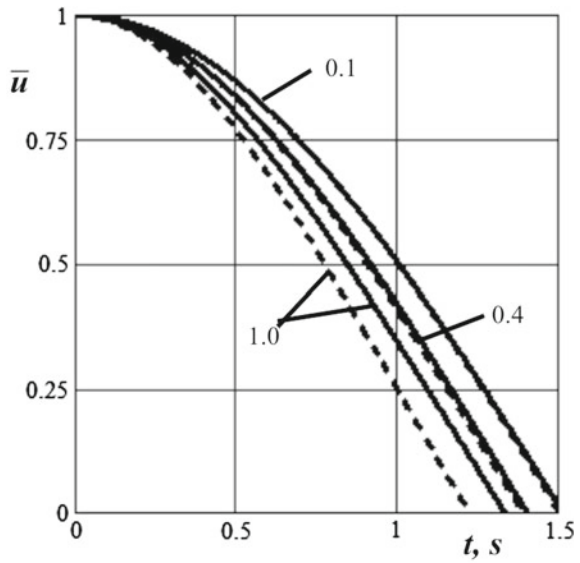
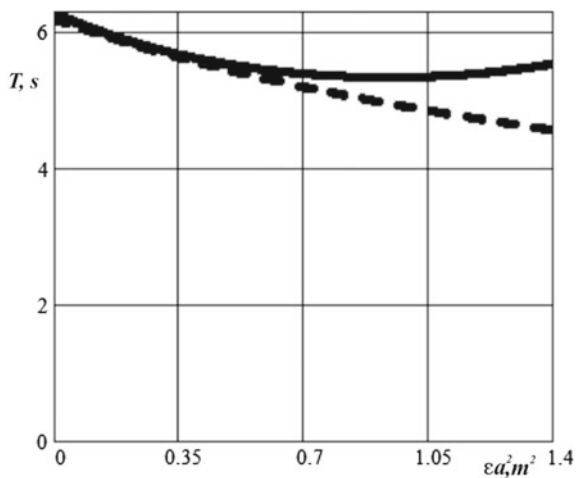


Fig. 2.7 Dependence of period on time



2.5.2 Application of MMPC for Two Coupled Oscillators

Coupled oscillators are one of the basic models both in physics [29] and in biology [30]. The equations describe the system of two identical coupled pendulums have the form

$$\ddot{x}_1 + \omega^2 x_1 - \lambda x_2 = 0 \quad (2.115)$$

$$\ddot{x}_2 + \omega^2 x_2 - \lambda x_1 = 0 \quad (2.116)$$

where x_1, x_2 are the deviations of the pendulums from the equilibrium position, ω is the frequency of natural oscillations of the pendulums (partial frequency), λ is the coupling constant.

The general solution of system (2.115), (2.116) has the form

$$x_1 = A \cos((\omega - \lambda)t + \psi_1) + B \sin((\omega + \lambda)t + \psi_2), \quad (2.117)$$

$$x_2 = A \cos((\omega - \lambda)t + \psi_1) - B \sin((\omega + \lambda)t + \psi_2), \quad (2.118)$$

where the amplitudes A, B and the phases ψ_1, ψ_2 are determined by the initial conditions.

For the initial deviation of the pendulums a and b with zero initial velocity, we obtain

$$A = 0.5(a + b), \quad B = 0.5(a - b), \quad (2.119)$$

$$\psi_1 = \psi_2 = 0. \quad (2.120)$$

Let us consider a case $a \neq 0, b = 0$. Then the exact solution has the form

$$x_1(t) = a \cdot \cos(\omega t) \cos(\lambda t), \quad (2.121)$$

$$x_2(t) = a \cdot \sin(\omega t) \sin(\lambda t). \quad (2.122)$$

For polynomial approximation of the system solution, we introduce an artificial parameter [10, 12, 20, 31]:

$$\ddot{x}_1 = \varepsilon(\lambda x_2 - \omega^2 x_1), \quad (2.123)$$

$$\ddot{x}_2 = \varepsilon(\lambda x_1 - \omega^2 x_2). \quad (2.124)$$

$$x_j = \sum_{i=0}^{\infty} x_{ij} \varepsilon^i, \quad j = 1, 2. \quad (2.125)$$

Solutions of recurrent systems after ε -splitting are

$$\varepsilon^0: \ddot{x}_{01} = \ddot{x}_{02} = 0, \quad x_{01} = a, \quad x_{02} = 0 \quad (2.126)$$

$$\varepsilon^1: \ddot{x}_{11} = -\omega^2 a, \quad \ddot{x}_{12} = \lambda a, \quad x_{11} = -0.5\omega^2 a t^2, \quad x_{12} = 0.5\lambda a t^2 \quad (2.127)$$

$$\begin{aligned} \varepsilon^2: \ddot{x}_{21} &= 0.5a(\omega^4 + \lambda^2)t^2, \quad \ddot{x}_{22} = -a\omega^2 \lambda t^2 \\ x_{21} &= \frac{1}{24}a(\omega^4 + \lambda^2)t^4, \quad x_{22} = -\frac{1}{12}a\omega^2 \lambda t^4 \end{aligned} \quad (2.128)$$

$$\begin{aligned} \varepsilon^3: \ddot{x}_{31} &= -\frac{a\omega^2}{24}(\omega^4 + 3\lambda^2)t^4, \quad \ddot{x}_{32} = \frac{a\lambda}{24}(3\omega^4 + \lambda^2)t^4 \\ x_{31} &= -\frac{a\omega^2}{6!}(\omega^4 + 3\lambda^2)t^6, \quad x_{32} = \frac{a\lambda}{6!}(3\omega^4 + \lambda^2)t^6 \end{aligned} \quad (2.129)$$

We introduce new variable $\xi = t^2$ and obtain an approximation in the form of truncated double series

$$\begin{aligned} x_1 &\approx a - \frac{1}{2}\omega^2 a \cdot \varepsilon \xi + \frac{1}{24}a(\omega^4 + \lambda^2) \cdot \varepsilon^2 \xi^2 - \frac{a\omega^2}{6!}(\omega^4 + 3\lambda^2) \cdot \varepsilon^3 \xi^3 \\ &= a \left(1 - \frac{\omega^2}{2} \cdot \varepsilon \xi + \frac{1}{4!}(\omega^4 + \lambda^2) \cdot \varepsilon^2 \xi^2 - \frac{\omega^2}{6!}(\omega^4 + 3\lambda^2) \cdot \varepsilon^3 \xi^3 \right) \end{aligned} \quad (2.130)$$

$$\begin{aligned} x_2 &\approx \frac{1}{2}\lambda a \cdot \varepsilon \xi - \frac{1}{12}a\omega^2 \lambda \cdot \varepsilon^2 \xi^2 + \frac{a\lambda}{6!}(3\omega^4 + \lambda^2) \cdot \varepsilon^3 \xi^3 \\ &= \lambda a \varepsilon \xi \left(\frac{1}{2} - \frac{2}{4!}\omega^2 \cdot \varepsilon \xi + \frac{1}{6!}(3\omega^4 + \lambda^2) \cdot \varepsilon^2 \xi^2 \right) \end{aligned} \quad (2.131)$$

Thus, we have two segments of double power series in parentheses. Using, for them, 2D Padé approximation, we obtain for $\varepsilon = 1$

$$x_1(t) \approx 2a \frac{6\omega^2 + (\lambda^2 - 2\omega^4)t^2}{12\omega^2 + (\omega^4 + \lambda^2)t^2}, \quad (2.132)$$

$$x_2(t) \approx \frac{\lambda a}{5} \frac{30\omega^2 + (\omega^4 + 2\lambda^2)t^2}{12\omega^2 + (\omega^4 + \lambda^2)t^2}. \quad (2.133)$$

For harmonic approximation of the solution, let us consider another scheme for introducing the artificial parameter:

$$\ddot{x}_1 + \omega^2 x_1 = \varepsilon \lambda x_2 \quad (2.134)$$

$$\ddot{x}_2 + \omega^2 x_2 = \varepsilon \lambda x_1. \quad (2.135)$$

Solution has the form (2.125). Solution of recurrent systems gives

$$\varepsilon^0: \ddot{x}_{01} + \omega^2 x_{01} = 0, \quad \ddot{x}_{02} + \omega^2 x_{02} = 0, \quad x_{01} = a \cdot \cos(\omega t), \quad x_{02} = 0 \quad (2.136)$$

$$\begin{aligned} \varepsilon^1: \ddot{x}_{11} + \omega^2 x_{11} = 0, \quad \ddot{x}_{12} + \omega^2 x_{12} = a\lambda \cdot \cos(\omega t) \\ x_{11} = 0, \quad x_{12} = -\frac{a\lambda}{2\omega} \cdot t \cdot \sin(\omega t) \end{aligned} \quad (2.137)$$

$$\begin{aligned} \varepsilon^2: \ddot{x}_{21} + \omega^2 x_{21} = -\frac{a\lambda^2}{2\omega} \cdot t \cdot \sin(\omega t), \quad \ddot{x}_{22} + \omega^2 x_{22} = 0 \\ x_{21} = \frac{a\lambda^2}{8\omega^2} \cdot t^2 \cdot \cos(\omega t) - \frac{a\lambda^2}{8\omega^3} \cdot t \cdot \sin(\omega t), \quad x_{22} = 0 \end{aligned} \quad (2.138)$$

$$\begin{aligned} \varepsilon^3: \ddot{x}_{31} + \omega^2 x_{31} = 0, \quad \ddot{x}_{32} + \omega^2 x_{32} = \frac{a\lambda^3}{8\omega^2} \cdot t^2 \cdot \cos(\omega t) - \frac{a\lambda^3}{8\omega^3} \cdot t \cdot \sin(\omega t) \\ x_{31} = 0, \quad x_{32} = \frac{a\lambda^3}{16\omega^3} t^2 \cos(\omega t) + \left(\frac{a\lambda^3}{48\omega^3} t^3 - \frac{a\lambda^3}{16\omega^4} t \right) \sin(\omega t) \end{aligned} \quad (2.139)$$

$$x_1 \approx a \cdot \cos(\omega t) + \frac{a\lambda^2}{8\omega^3} (\omega \cdot t^2 \cdot \cos(\omega t) - t \cdot \sin(\omega t)) \cdot \varepsilon^2 \quad (2.140)$$

$$x_2 \approx \varepsilon t \left[-\frac{a\lambda}{2\omega} \sin(\omega t) + \frac{a\lambda^3}{48\omega^4} (3\omega t \cdot \cos(\omega t) + (\omega t^2 - 3) \sin(\omega t)) \cdot \varepsilon^2 \right] \quad (2.141)$$

After expanding secular term in series of trigonometric functions on the interval $(-\pi/\omega, \pi/\omega)$

$$\omega \cdot t^2 \cdot \cos(\omega t) - t \cdot \sin(\omega t) \approx -\frac{6}{\omega} + \frac{\pi^2 + 3}{3\omega} \cos(\omega t) - \frac{7}{9\omega} \cos(2\omega t) \quad (2.142)$$

$$3\omega t \cdot \cos(\omega t) + \omega t^2 \cdot \sin(\omega t) = -\frac{27\omega - 2\pi^2 + 3}{6\omega} \sin(\omega t) + 2\frac{9\omega - 4}{9\omega} \sin(2\omega t) \quad (2.143)$$

we get 2D power series

$$x_1 \approx a \cdot \left(\cos(\omega t) - \frac{3\lambda^2}{4\omega^4} \varepsilon^2 + \frac{\lambda^2(\pi^2 + 3)}{24\omega^4} \varepsilon^2 \cos(\omega t) - \frac{7\lambda^2}{72\omega^4} \varepsilon^2 \cos(2\omega t) \right) \quad (2.144)$$

$$x_2 \approx -\frac{a\lambda}{2\omega} \varepsilon t \left[\sin(\omega t) - \frac{\lambda^2(27\omega - 2\pi^2 + 3)}{144\omega^4} \varepsilon^2 \sin(\omega t) + \frac{\lambda^2(9\omega - 4)}{108\omega^4} \varepsilon^2 \sin(2\omega t) \right] \quad (2.145)$$

We introduce complex quantities X_1, X_2 of form

$$X_1 = \frac{x_1}{a} = e^{i\omega t} - \frac{3\lambda^2}{4\omega^4} \varepsilon^2 + \frac{\lambda^2(\pi^2 + 3)}{24\omega^4} \varepsilon^2 e^{i\omega t} - \frac{7\lambda^2}{72\omega^4} \varepsilon^2 e^{2i\omega t} \quad (2.146)$$

$$X_2 = e^{i\omega t} - \frac{\lambda^2(27\omega - 2\pi^2 + 3)}{144\omega^4} \varepsilon^2 e^{i\omega t} + \frac{\lambda^2(9\omega - 4)}{108\omega^4} \varepsilon^2 e^{2i\omega t} \quad (2.147)$$

associated with approximated functions by dependencies

$$x_1 = a\text{Re}(X_1), x_2 = -a \frac{\lambda t}{2\omega} \varepsilon \text{Im}(X_2) \quad (2.148)$$

Using Padé approximation, one obtains

$$X_1(\varepsilon, t) \approx a \frac{-\frac{3\lambda^2}{4\omega^4} \varepsilon^2 + e^{i\omega t} + \frac{\lambda^2(\pi^2+3)}{24\omega^4} \varepsilon^2 e^{i\omega t}}{1 + \frac{3}{7(\pi^2+3)} e^{i\omega t}} \quad (2.149)$$

Function $X_1(\varepsilon, t)$ can be obtained analogously. The values of x_1 for $t \in (0, 2\pi/\omega)$ and different parameter values are shown in Fig. 2.8.

Number 1 corresponds to Formula (2.132), 2—(2.121), 3—(2.130), 7—(2.144), 8—(2.148) with accounting (2.149). Comparison of curves 1 and 3 shows the advantage of the Formula (2.132) in half period. Comparison of curves 7 and 8 shows good agreement of Formulas (2.121) and (2.148) with the exact result already on the

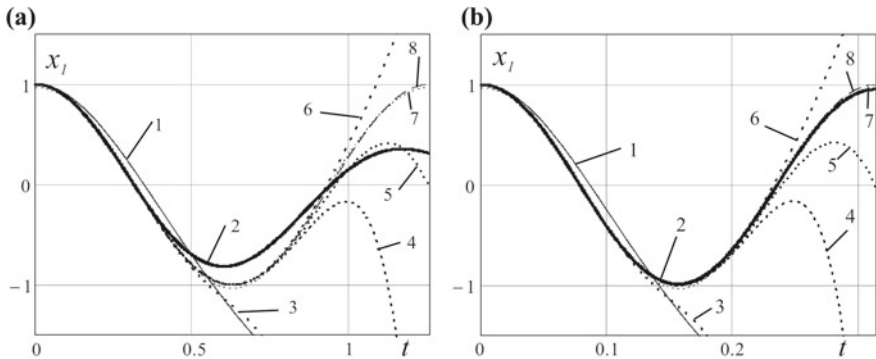


Fig. 2.8 Displacement x_1 as a function of time for $\omega = 5, \lambda = 1$ (a) and $\omega = 20, \lambda = 1$ (b)

period, although the process of constructing such an approximation is more cumbersome than (2.132). To analyze the convergence of the approximants, we also constructed power series segment of t of tenth order (curve 4) and its Padé approximations ($5-P_1[1, 3/1, 2](\varepsilon, \xi)$, $6-P_1[1, 4/1, 1](\varepsilon, \xi)$). It is seen that an increase in the order of the polynomial approximation extends its applicability area.

2.6 Conclusions

The modified method of parameter continuation can be successfully used for estimating the frequencies and modes of linear and nonlinear oscillations of plates and shells with complicated boundary conditions and of parameter-dependent oscillations of plates. MMPC estimations depend on the shape of initial perturbation. Proposed technique allows using it for estimation of the eigenfrequency of vibration and buckling loads. It describes real vibration shape with different conditions on the edges. The comparison with known results confirms the accuracy of proposed method.

References

1. Amabili, M.: *Nonlinear Vibrations and Stability of Shells and Plates*. Cambridge University Press, New York (2008)
2. Elishakoff, I.: Bolotin's dynamic edge-effect method. *Shock Vib. Digest*, **8**(1), 95–104 (1976)
3. Mossakovskii, V.I., Mil'tsyn, A.M., Olevskii, V.I.: Deformation and stability of technologically imperfect cylindrical shells in a nonuniform stress state. *Strength Mater.* **22**(12), 1745–1750 (1990)
4. Andrianov, I.V., Awrejcewicz, J., Danishevs'kyi, V.V., Ivankov, A.O.: *Asymptotic Methods in the Theory of Plates with Mixed Boundary Conditions*. Wiley, Chichester (2014)
5. Timoshenko, S.P., Woinowsky-Krieger, S.: *Theory of Plates and Shells*, 2nd edn. McGraw-Hill, New York (1959)
6. Filippi, P.J.T.: *Vibrations and Acoustic Radiation of Thin Structures: Physical Basis, Theoretical Analysis and Numerical Methods*. Wiley, London (2013)
7. Tseitlin, A.I.: *Applied Methods for Solving Boundary Value Problems of Structural Mechanics*. Stroyizdat, Moscow (1984). (in Russian)
8. Andrianov, I.V., Kholod, E.G., Olevsky, V.I.: Approximate non-linear boundary value problems of reinforced shell dynamics. *JSV* **194**(3), 369–387 (1996)
9. Bolotin, V.V.: An asymptotic method for the study of the problem of eigenvalue for rectangular regions. In: *Problems in Continuum Mechanics: Contributions in Honor of the Seventieth Birthday of Academician N. I. Muskhelishvili*, pp. 56–68. SIAM, Philadelphia (1961)
10. Andrianov, I.V., Olevskiy, V.I., Awrejcewicz, J.: Approximate boundary value problems of a deformed flexible closed torso shell with excited edges. *Int. J. Appl. Mech.* **08**(04), 1650051, 19 (2016)
11. Andrianov, I.V., Olevs'kyi, V.I., Awrejcewicz, J.: Application of 2-D Padé approximants in nonlinear shell theory: Stability calculation and experimental justification. In: Awrejcewicz, J., Hagedorn, P. (eds.) *Nonlinearity, Bifurcation and Chaos—Theory and Applications*, pp. 1–26. InTech., Rijeka (2012)

12. Andrianov, I., Olevs'kyy, V., Awrejcewicz, J.: Analytical perturbation method for calculation of shells based on 2-D Padé approximants. *Int. J. Struct. Stab. Dyn.* **13**(7), 1340003, 7 (2013)
13. Obraztsov, I.F., Nerubailo, B.V., Andrianov, I.V.: *Asymptotic Methods in the Structural Mechanics of Thin-Walled Structures*. Mashinostroyeniye, Moscow (1991). (in Russian)
14. Olevs'kyy, V.I., Andrianov, I.V.: Using 2-D Padé approximants in nonlinear dynamics of shells. In: *Proceedings of the 4th International Conference on Nonlinear Dynamics, ND-KhPI 2013, Sevastopol, 2013*
15. Yemel'yanov, T.V., Naumenko, A.V., Strelnikova, E.A., Sheludko, G.A.: Eigenoscillations of plates in a compressible fluid. *Bull. Kharkiv Natl. Univ.* **960**, 132–140 (2011). (in Russian)
16. Olevskiy, V.I., Olevska, Y.B.: Geometric aspects of multiple Fourier series convergence on the system of correctly counted sets. In: *Mladenov, I.M., Yoshioka, A. (eds.) Proceedings of the Nineteenth International Conference on Geometry, Integrability and Quantization*, pp. 159–167. Avangard Prima, Sofia (2018)
17. Chelomei, V.N., et al. (eds.): *Vibrations in Technology: Handbook in 6 vols. Mechanical Engineering, Moscow (1978)*. Bolotin, V.V. (ed.) *Oscillations of Linear Systems*, vol. 1. (in Russian)
18. Kolpakov, A.G., Rakin, S.I.: Estimation of stress concentration in a welded joint formed by explosive welding. *J. Appl. Mech. Tech. Phys.* **59**(03), 569–575 (2018)
19. Kolpakov, A.G., Andrianov, I.V., Rakin, S.I., Rogerson, G.A.: An asymptotic strategy to couple homogenized elastic structures. *Int. J. Eng. Sci.* **131**, 26–39 (2018)
20. Andrianov, I., Olevskiy, V., Olevska, Y.: Asymptotic estimation of free vibrations of nonlinear plates with complicated boundary conditions. In: *AIP Conference Proceedings*, vol. 1895, 080001, 10 p. American Institute of Physics, Melville (2017)
21. Altenbach, H., Maugin, G., Erofeev, V. (eds.): *Mechanics of Generalized Continua—From Micromechanical Basics to Engineering Applications*. Springer, New York (2011)
22. Gerasimov, S.N., Erofeev, V.N., Soldatov, I.N.: *Wave Processes in Continuous Media*. Publishing House RFNC-VNIIEF, Sarov (2012). (in Russian)
23. Andrianov, I., Olevskiy, V., Olevska, Y.: Analytic approximation of periodic Ateb functions via elementary functions in nonlinear dynamics. In: *AIP Conference Proceedings*, vol. 1773, 040001, 7 p. American Institute of Physics, Melville (2016)
24. Klepko, V.V., Slisenko, V.I., Sukhyy, K.M., Nesin, S.D., Kovalenko, V.L., Serhienko, Y.O., Sukha, I.V.: Structure, morphology, thermal and conductivity properties of gel electrolyte system based on polyvinyl chloride and LiClO₄. *Nucl. Phys. At. Energy* **19**(1), 43–47 (2018)
25. Levchuk, I., Shut, O.: Iterative-connectionist identification of mathematical models of chemical technology processes. *Metall. Min. Ind.* **7**(2), 282–286 (2015)
26. Drobakhin, O.O., Olevskiy, O.V.: Verification of applicability in space domain of the inverse filtering with evolution control for reconstruction of images obtained by radar scanning. In: *AIP Conference Proceedings*, vol. 2025, no. 1, 050002, 7 p. American Institute of Physics, Melville (2018)
27. Shashenko, A.N., Zhuravlev, V.N., Sdvizhkova, Y.A., Dubitska, M.S.: Forecast of disjunctives based on mathematical interpretation of acoustic signal phase characteristics. *Naukovyi Visnyk Natsionalnoho Hirnychoho Universytetu* **2**, 61–66 (2015). (in Russian)
28. Olevska, Y., Mishchenko, V., Olevskiy, V.: Mathematical models of magnetite desliming for automated quality control systems. In: *AIP Conference Proceedings*, vol. 1773, 040007, 6 p. American Institute of Physics, Melville (2016)
29. Olevskiy, V.I.: Asymptotic method of modeling of thin walled shells based on 2D Padé approximations. In: *AIP Conference Proceedings*, vol. 1629, pp. 110–126. American Institute of Physics, Melville (2014)

30. Brailove, A.A.: The dynamics of two pulse-coupled relaxation oscillators. *IJBC* **2**(2), 341–352 (1992)
31. Mirollo, R., Strogatz, S.: Synchronization of pulse-coupled biological oscillators. *J. Appl. Math.* **50**, 1645–1662 (1990)

Chapter 3

A Mathematically Consistent Vector-Matrix Representation of Generalized Hooke's Law for Shear-Rigid Plates



Marcus Aßmus and Holm Altenbach

Abstract The present contribution is dedicated to the mathematical consistent expression of constitutive relations needed for efficient computational treatment of thin-walled structural elements within a geometrically and physically linear framework, as usually used by engineers. Hereby, the direct approach for homogeneous plates is taken as a basis. We confine our research to shear-rigid plates. We further on do not restrict ourselves by material symmetry classes and consider an aelotropic material. Based on the fully coupled constitutive equations, we introduce an approach by applying normalized bases to decay into a vector-matrix representation. It is thus possible to formulate the tensorial quantities in form of vector-matrix equations which are mathematically consistent. The key advantages of this approach are disclosed.

Keywords Shear-rigid plate theory · Computational efficiency · Consistency

3.1 Introduction

3.1.1 Motivation

Many engineering materials exhibit an anisotropic behavior, i.e., a behavior deviating significantly from isotropy. In the most general case, this is called aelotropic (or triclinic). Thin-walled structural elements such as plates are increasingly made of such materials. In addition to inelasticity, anisotropy is therefore an important influence in the description of the structural behavior. Here, we limit our description to shear-rigid plates, often referred to the work of Kirchhoff [6], concerned with pure

M. Aßmus (✉) · H. Altenbach
Otto von Guericke University, Universitätsplatz 2, 39106 Magdeburg, Germany
e-mail: marcus.assmus@ovgu.de

H. Altenbach
e-mail: holm.altenbach@ovgu.de

© Springer Nature Switzerland AG 2020
H. Altenbach et al. (eds.), *Nonlinear Wave Dynamics of Materials and Structures*, Advanced Structured Materials 122,
https://doi.org/10.1007/978-3-030-38708-2_3

bending. In doing so, the interesting but at least at this point, problematic case of shear-deformable plates, i.e., the transverse shear-rigidity does not tend to infinity as presented by Mindlin [8], remains out of the sphere of present manuscript. To broaden the scope of present treatise, we include the in-plane loaded plate state what results in a description well known as classical laminate (or multi-layered) theory. However, we still limit ourselves to homogeneous plates, i.e., the different composite plies of a laminate result in a homogeneous substitute material for a single layer.

As usual in context of plate theories, all operations are referred to a reference surface $\mathfrak{S} \subset \mathbb{E}^2$ within or beyond the volume V occupied by the three-dimensional plate like body $\mathfrak{B} \subset \mathbb{E}^3$. Since we are interested in plates solely (in contrast to shells), the reference surface is a plane. In the best case, one chooses the plates mid-surface, i.e., the surface that halves the thickness of the plate at each point, since the plate states are decoupled but superposed eventually, even if this is not the case for all material symmetry classes. However, in a more general context, the choice of the position of \mathfrak{S} is arbitrary, i.e., the constitutive relations are coupled.

Following the seminal work of Rychlewski [10], we will find four distinct symmetry classes for the shear-rigid, planar two-dimensional body manifold, i.e., for the plane of elastic symmetries. These are

- full anisotropy (lack of any symmetry),
- symmetry of a rectangle (also known as square symmetry),
- symmetry of a square (also known as plane orthotropy), and
- plane isotropy,

while all classes condense out of material symmetries of elastic bulk [1]. However, restricting to physical reality, the number of elastic symmetries may increase since the reference plane does not necessarily have to be parallel to the outer surface of the plate, etc. To capture the most general description, we operate with a fully coupled set of constitutive equations, i.e., we derive such a representation in the absence of geometric symmetry and consider an aelotropic material, i.e., arbitrary material symmetry. Thereby, we are very much interested in the structure and the properties of such relations. The cognitions of such scrutinies enable us to reduce the tensorial description to a form appropriate for computer algebra systems. In contrast to classical procedures in this field, we introduce a mathematically consistent representation where calculations in the form introduced lead to identical results like the ones known from a tensorial description.

To conclude, we handle a topic relevant in anisotropic elasticity of small plate deformations with a focus on computational efficiency.

3.1.2 Organization of the Paper

In present context, we skip any derivation of stress-like, strain-like, or stiffness measures from a three-dimensional parent continuum and start with our description directly on \mathfrak{S} . In Sect. 3.2, we introduce constitutive relations of linear elastic shear-

rigid plates since they are necessary for the subsequent considerations. Subsequently, we determine the properties of the tensorial quantities for kinetic and kinematic measures as well as for stiffnesses and coupling stiffnesses introduced. In Sect. 3.3, an approach to determine components for an mathematically equivalent vector-matrix notation based on tensorial quantities is introduced. The advantages of this approach are named, and specific examples are given. Finally, we point on the importance and generality of this notation and refer to fields of application.

3.1.3 Preliminaries and Notation

In present work, we make use of the direct tensor notation and vector-matrix notation simultaneously. Due to reasons of clarity, we have introduced a special syntax for distinction. Tensors of zeroth-order (or scalars) are symbolized by italic letters (e.g., a), italic lowercase bold letters denote first-order tensors (e.g., $\mathbf{a} = a_\alpha \mathbf{e}_\alpha$), second-order tensors are designated by italic uppercase bold letters (e.g., $\mathbf{A} = A_{\alpha\beta} \mathbf{e}_\alpha \otimes \mathbf{e}_\beta$), and fourth-order tensors are symbolized by italic uppercase bold calligraphic letters (e.g., $\mathcal{A} = A_{\alpha\beta\gamma\delta} \mathbf{e}_\alpha \otimes \mathbf{e}_\beta \otimes \mathbf{e}_\gamma \otimes \mathbf{e}_\delta$), whereas Einstein's sum convention is applied. As becomes evident, we reduce our representation to an orthonormal basis, where the basis vectors are given as $\{\mathbf{e}_\alpha\}$ or $\{\mathbf{e}_\alpha, \mathbf{n}\}$, respectively. When lapse into vector-matrix notation, column vectors are symbolized by upright lowercase sans-serif bold letters (e.g., \mathbf{a})

$$\mathbf{a} = \begin{bmatrix} a_1 \\ a_2 \\ a_3 \end{bmatrix},$$

while matrices are designated by upright uppercase sans-serif bold letters (e.g.,

$$\mathbf{A} = \begin{bmatrix} A_{11} & A_{12} & A_{13} \\ A_{21} & A_{22} & A_{23} \\ A_{31} & A_{32} & A_{33} \end{bmatrix}.$$

Uppercase Greek indices run through the values 1, 2, and 3, while lowercase Greek indices run through the values 1 and 2 only.

While handling with tensors, some operations are essential which are introduced in the sequel. This is the dyadic product between two first-order tensors $\mathbf{a} \otimes \mathbf{b} = \mathbf{C}$, the dyadic product between two second-order tensors $\mathbf{A} \otimes \mathbf{B} = \mathbf{C}$, the double scalar product between two second-order tensors $\mathbf{A} : \mathbf{B} = c$, and the double scalar product between a fourth and a second-order tensor $\mathcal{A} : \mathbf{B} = \mathbf{C}$. The transposed of a second-order tensor is defined by $\mathbf{a} \cdot \mathbf{A}^\top \cdot \mathbf{b} = \mathbf{b} \cdot \mathbf{A} \cdot \mathbf{a}$. For detailed penetrations of these operations, we refer to e.g., [5].

3.2 Linear Elastic Shear-Rigid Plates

3.2.1 Generalized Hooke's Law

We directly enter the topic with the representation of fully coupled constitutive laws for shear-rigid plates. In general, the elastic energy is written in terms of second-order deformation measures. Approaching the elastic energy as a quadratic form results in following expression.

$$W = W(\mathbf{G}, \mathbf{K}) = \frac{1}{2} [\mathbf{G} : \mathcal{A} : \mathbf{G} + \mathbf{K} : \mathcal{D} : \mathbf{K}] + \mathbf{G} : \mathcal{B} : \mathbf{K} \quad (3.1)$$

On the right-hand side, we first can identify the deformation measures. Herein, $\mathbf{G} = G_{\gamma\delta} \mathbf{e}_\gamma \otimes \mathbf{e}_\delta$ denotes in-plane normal and shear strains and $\mathbf{K} = K_{\gamma\delta} \mathbf{e}_\gamma \otimes \mathbf{e}_\delta$ normal curvature changes due to bending and torsion. Next to the deformation measures exist some fourth-order tensors. This here involves stiffness and coupling stiffness tensors. Thereby, \mathcal{A} is the in-plane stiffness tensor, and \mathcal{D} is the out-of-plane stiffness tensor. Since in-plane and out-of-plane states shall be completely coupled, the (in-plane-out-of-plane) coupling stiffness tensor \mathcal{B} is introduced. In the spirit of Rychlewski [10], we will call this set of fourth-order constituents Hooke's tensors. In case of Hooke's law, the constitutive relations are given as linear mappings.

$$\mathbf{N} = \mathcal{A} : \mathbf{G} + \mathcal{B} : \mathbf{K} \quad (3.2a)$$

$$\mathbf{L} = \mathcal{B} : \mathbf{G} + \mathcal{D} : \mathbf{K} \quad (3.2b)$$

On the left-hand side appear the kinetic quantities. These are the in-plane forces $\mathbf{N} = N_{\alpha\beta} \mathbf{e}_\alpha \otimes \mathbf{e}_\beta$ and the polar tensor of moments $\mathbf{L} = L_{\alpha\beta} \mathbf{e}_\alpha \otimes \mathbf{e}_\beta$ (in contrast to the axial tensor of moments $\mathbf{M} = M_{\alpha\beta} \mathbf{e}_\alpha \otimes \mathbf{n} \times \mathbf{e}_\beta$, while both are correlated via $\mathbf{L} = \mathbf{M} \times \mathbf{n}$ with the surface normal $\mathbf{n} = \mathbf{e}_1 \times \mathbf{e}_2$). These quantities are derived by the differentiation of the elastic energy function, i.e., W serves as potential for the kinetic quantities.

$$\mathbf{N} = \frac{\partial W(\mathbf{G}, \mathbf{K})}{\partial \mathbf{G}} \quad \mathbf{L} = \frac{\partial W(\mathbf{G}, \mathbf{K})}{\partial \mathbf{K}} \quad (3.3)$$

As stated above, we will not introduce any further restrictions so that we can give Hooke's tensors in a general form.

$$\mathcal{A} = A_{\alpha\beta\gamma\delta} \mathbf{e}_\alpha \otimes \mathbf{e}_\beta \otimes \mathbf{e}_\gamma \otimes \mathbf{e}_\delta \quad (3.4a)$$

$$\mathcal{D} = D_{\alpha\beta\gamma\delta} \mathbf{e}_\alpha \otimes \mathbf{e}_\beta \otimes \mathbf{e}_\gamma \otimes \mathbf{e}_\delta \quad (3.4b)$$

$$\mathcal{B} = B_{\alpha\beta\gamma\delta} \mathbf{e}_\alpha \otimes \mathbf{e}_\beta \otimes \mathbf{e}_\gamma \otimes \mathbf{e}_\delta \quad (3.4c)$$

Alternative parametrizations of the tensors (3.4) as in the case of well-studied isotropy are not known for the anisotropic material. Clearly, \mathcal{A} and \mathcal{D} depend on material properties, while \mathcal{B} additionally depends on the position of the reference surface \mathfrak{S} .

3.2.2 Properties of Tensorial Quantities

The quantities introduced above have specific properties that can be useful when converting to vector-matrix notation. First of all, these are the symmetries of kinetic measures.

$$\mathbf{a} \cdot \mathbf{N} = \mathbf{N} \cdot \mathbf{a} \quad \mathbf{N} = \mathbf{N}^\top \quad N_{\alpha\beta} = N_{\beta\alpha} \quad (3.5a)$$

$$\mathbf{a} \cdot \mathbf{L} = \mathbf{L} \cdot \mathbf{a} \quad \mathbf{L} = \mathbf{L}^\top \quad L_{\alpha\beta} = L_{\beta\alpha} \quad (3.5b)$$

It is worth to mention that $\mathbf{M} \neq \mathbf{M}^\top$ holds. We furthermore work with symmetric kinematic measures.

$$\mathbf{a} \cdot \mathbf{G} = \mathbf{G} \cdot \mathbf{a} \quad \mathbf{G} = \mathbf{G}^\top \quad G_{\gamma\delta} = G_{\delta\gamma} \quad (3.6a)$$

$$\mathbf{a} \cdot \mathbf{K} = \mathbf{K} \cdot \mathbf{a} \quad \mathbf{K} = \mathbf{K}^\top \quad K_{\gamma\delta} = K_{\delta\gamma} \quad (3.6b)$$

Herein, \mathbf{a} is chosen arbitrary. The symmetries of the deformations measures are the result of purging the rigid-body rotations from the first gradient of the respective deformation measure. The symmetries of the kinetic measures originate from the balance of angular momentum which is locally fulfilled. However, each of these measures thus has only three independents.

The symmetries of fourth-order stiffness and coupling stiffness measures are of interest as well. These are the properties of the in-plane stiffness tensor

$$\mathbf{A} : \mathcal{A} : \mathbf{B} = \mathbf{B} : \mathcal{A}^\top : \mathbf{A} \quad A_{\alpha\beta\gamma\delta} = A_{\gamma\delta\alpha\beta} \quad \text{major symmetry} \quad (3.7a)$$

$$\mathbf{A} : \mathcal{A} = \mathbf{A}^\top : \mathcal{A} \quad A_{\alpha\beta\gamma\delta} = A_{\beta\alpha\gamma\delta} \quad \text{left subsymmetry} \quad (3.7b)$$

$$\mathcal{A} : \mathbf{A} = \mathcal{A} : \mathbf{A}^\top \quad A_{\alpha\beta\gamma\delta} = A_{\alpha\beta\delta\gamma} \quad \text{right subsymmetry} \quad (3.7c)$$

$$\mathbf{A} : \mathcal{A} : \mathbf{A} > 0 \quad \text{positive definiteness,} \quad (3.7d)$$

the out-of-plane stiffness tensor

$$\mathbf{A} : \mathcal{D} : \mathbf{B} = \mathbf{B} : \mathcal{D}^\top : \mathbf{A} \quad D_{\alpha\beta\gamma\delta} = D_{\gamma\delta\alpha\beta} \quad \text{major symmetry} \quad (3.8a)$$

$$\mathbf{A} : \mathcal{D} = \mathbf{A}^\top : \mathcal{D} \quad D_{\alpha\beta\gamma\delta} = D_{\beta\alpha\gamma\delta} \quad \text{left subsymmetry} \quad (3.8b)$$

$$\mathcal{D} : \mathbf{A} = \mathcal{D} : \mathbf{A}^\top \quad D_{\alpha\beta\gamma\delta} = D_{\alpha\beta\delta\gamma} \quad \text{right subsymmetry} \quad (3.8c)$$

$$\mathbf{A} : \mathcal{D} : \mathbf{A} > 0 \quad \text{positive definiteness,} \quad (3.8d)$$

and the coupling stiffness tensor

$$\mathbf{A} : \mathcal{B} : \mathbf{B} = \mathbf{B} : \mathcal{B}^\top : \mathbf{A} \quad B_{\alpha\beta\gamma\delta} = B_{\gamma\delta\alpha\beta} \quad \text{major symmetry} \quad (3.9a)$$

$$\mathbf{A} : \mathcal{B} = \mathbf{A}^\top : \mathcal{B} \quad B_{\alpha\beta\gamma\delta} = B_{\beta\alpha\gamma\delta} \quad \text{left subsymmetry} \quad (3.9b)$$

$$\mathcal{B} : \mathbf{A} = \mathcal{B} : \mathbf{A}^\top \quad B_{\alpha\beta\gamma\delta} = B_{\alpha\beta\delta\gamma} \quad \text{right subsymmetry} \quad (3.9c)$$

$$\mathbf{A} : \mathcal{B} : \mathbf{A} > 0 \quad \text{positive definiteness,} \quad (3.9d)$$

where $\mathbf{A} \neq \mathbf{0}$ and $\mathbf{B} \neq \mathbf{0}$ are chosen arbitrary. The left and right subsymmetries originate from the symmetries of kinetic and kinematic measures. The major symmetries arise from the existence theorem for the elastic energy.

To conclude, we have *six* independent parameters per stiffness or coupling stiffness tensor, i.e., we have 18 independent scalars in the general case. Fortunately, the coupling stiffness \mathcal{B} is dependent on \mathcal{A} and \mathcal{D} which may lead to a reduction in the number of independents. Dependencies between pure in-plane and out-of-plane state are also conceivable. However, all eigenvalues of these fourth-order tensors are positive due to their positive definiteness and major symmetry.

3.3 Vector-Matrix Notation

3.3.1 Derivation

Since deformation and kinetic measures are symmetric, significant simplifications are possible. This is also the case for the stiffness measures. This results in a representation using numerical vectors and matrices. The exploitation of the symmetries of the tensors described in the previous section allows a reduction to three independent parameters for second-order tensors and a reduction to six independent parameters for fourth-order tensors. One reason to transform the constitutive equations into vector-matrix form is the efficiency in calculations with computer algebra systems. Here, Voigt notation [12] is well established. However, it is known that Voigt notation is inconsistent, cf. Brannon [4]. We therefore make it our task to introduce an alternative way of representation. The origins of this alternative representation can be dated back well over 150 years, cf. Blinowski et al. [3].

We introduce a three-dimensional basis which often is referred to as Kelvin basis, cf. Thomson [11]. This is based on components of the orthonormal system introduced.

$$\mathbf{E}_\alpha = \mathbf{e}_\alpha \otimes \mathbf{e}_\alpha \quad \forall \alpha = \{1, 2\} \quad (3.10a)$$

$$\mathbf{E}_3 = \frac{\sqrt{2}}{2} [\mathbf{e}_1 \otimes \mathbf{e}_2 + \mathbf{e}_2 \otimes \mathbf{e}_1] \quad (3.10b)$$

Since the basis index is running from 1, ..., 3, we introduce Greek capitals so that $\mathbf{E}_\Gamma \forall \Gamma \in \{1, 2, 3\}$ holds. The Kelvin basis is orthonormal.

$$\mathbf{E}_\Gamma : \mathbf{E}_\Lambda = \delta_{\Gamma\Lambda} \quad \text{i.e.} \quad \mathbf{E}_\Gamma : \mathbf{E}_\Gamma = 1 \quad (3.11)$$

Note that this basis is Cartesian through the normalization with the square root $\sqrt{2}$ in Eq. (3.10b). This is not the case when simply introducing the symmetric part $\frac{1}{2}[\mathbf{e}_1 \otimes \mathbf{e}_2 + \mathbf{e}_2 \otimes \mathbf{e}_1]$, cf. Nye [9]. However, the normalization introduced is sometimes also referred to Mandel [7]. By the aid of the Kelvin bases, it is possible to determine the elements of kinematic and kinetic measures for a representation in three-dimensional vector space.

$$\mathbf{N}_\Gamma = \mathbf{G} : \mathbf{E}_\Gamma \quad \forall \Gamma = \{1, 2, 3\} \quad (3.12a)$$

$$\mathbf{L}_\Gamma = \mathbf{L} : \mathbf{E}_\Gamma \quad \forall \Gamma = \{1, 2, 3\} \quad (3.12b)$$

$$\mathbf{G}_\Lambda = \mathbf{G} : \mathbf{E}_\Lambda \quad \forall \Lambda = \{1, 2, 3\} \quad (3.12c)$$

$$\mathbf{K}_\Lambda = \mathbf{K} : \mathbf{E}_\Lambda \quad \forall \Lambda = \{1, 2, 3\} \quad (3.12d)$$

By the aid of this procedure, the tensorial representation with second-order quantities with originally 2×2 elements is reduced to three elements per quantity.

Furthermore, we can determine the elements of linear operator matrices based on stiffness and coupling stiffness tensors by the following calculation rule.

$$\mathbf{A}_{\Gamma\Lambda} = \mathbf{E}_\Gamma : \mathcal{A} : \mathbf{E}_\Lambda \quad \forall \Gamma, \Lambda = \{1, 2, 3\} \quad (3.13a)$$

$$\mathbf{D}_{\Gamma\Lambda} = \mathbf{E}_\Gamma : \mathcal{D} : \mathbf{E}_\Lambda \quad \forall \Gamma, \Lambda = \{1, 2, 3\} \quad (3.13b)$$

$$\mathbf{B}_{\Gamma\Lambda} = \mathbf{E}_\Gamma : \mathcal{B} : \mathbf{E}_\Lambda \quad \forall \Gamma, \Lambda = \{1, 2, 3\} \quad (3.13c)$$

In doing so, we can reduce the representation of the fourth-order tensors introduced with originally $2 \times 2 \times 2 \times 2$ elements, also.

Stepping back to tensor notation while keeping Eq. (3.13) in mind, we can now write tensorial quantities as follows.

$$\mathbf{N} = \mathbf{N}_\Gamma \mathbf{E}_\Gamma \quad (3.14a)$$

$$\mathbf{L} = \mathbf{L}_\Gamma \mathbf{E}_\Gamma \quad (3.14b)$$

$$\mathbf{G} = \mathbf{G}_\Lambda \mathbf{E}_\Lambda \quad (3.14c)$$

$$\mathbf{K} = \mathbf{K}_\Lambda \mathbf{E}_\Lambda \quad (3.14d)$$

$$\mathcal{A} = \mathbf{A}_{\Gamma\Lambda} \mathbf{E}_\Gamma \otimes \mathbf{E}_\Lambda \quad (3.14e)$$

$$\mathcal{D} = \mathbf{D}_{\Gamma\Lambda} \mathbf{E}_\Gamma \otimes \mathbf{E}_\Lambda \quad (3.14f)$$

$$\mathcal{B} = \mathbf{B}_{\Gamma\Lambda} \mathbf{E}_\Gamma \otimes \mathbf{E}_\Lambda \quad (3.14g)$$

However, by ordering the quantities derived in Eqs. (3.12) and (3.13), we can obtain an 3×1 array of ordinary vector components for the second-order tensors and an 3×3 array of matrix components for the fourth-order tensors.

$$\begin{bmatrix} N_1 \\ N_2 \\ N_3 \end{bmatrix} = \begin{bmatrix} A_{11} & A_{12} & A_{13} \\ & A_{22} & A_{23} \\ \text{sym} & & A_{33} \end{bmatrix} \begin{bmatrix} G_1 \\ G_2 \\ G_3 \end{bmatrix} + \begin{bmatrix} B_{11} & B_{12} & B_{13} \\ & B_{22} & B_{23} \\ \text{sym} & & B_{33} \end{bmatrix} \begin{bmatrix} K_1 \\ K_2 \\ K_3 \end{bmatrix} \quad (3.15a)$$

$$\begin{bmatrix} L_1 \\ L_2 \\ L_3 \end{bmatrix} = \begin{bmatrix} B_{11} & B_{12} & B_{13} \\ & B_{22} & B_{23} \\ \text{sym} & & B_{33} \end{bmatrix} \begin{bmatrix} G_1 \\ G_2 \\ G_3 \end{bmatrix} + \begin{bmatrix} D_{11} & D_{12} & D_{13} \\ & D_{22} & D_{23} \\ \text{sym} & & D_{33} \end{bmatrix} \begin{bmatrix} K_1 \\ K_2 \\ K_3 \end{bmatrix} \quad (3.15b)$$

We can also set these three-dimensional arrays in compact form if we introduce minuscule sans-serif bold letters for vectors and majuscule sans-serif bold letters for matrices. By the aid of this notation, we obtain following expressions.

$$\mathbf{n} = \mathbf{A} \mathbf{g} + \mathbf{B} \mathbf{k} \quad (3.16a)$$

$$\mathbf{l} = \mathbf{B} \mathbf{g} + \mathbf{D} \mathbf{k} \quad (3.16b)$$

The stiffness matrices \mathbf{A} , \mathbf{D} , and \mathbf{B} can be considered as linear symmetric operations, mapping the three-dimensional space (of originally second-order tensors) onto-itself. All three matrices are positive definite according to definitions (3.7d), (3.8d), and (3.9d).

In context of computer algebra systems, one may also define Eq. (3.16) as a single one.

$$\begin{bmatrix} \mathbf{n} \\ \mathbf{l} \end{bmatrix} = \begin{bmatrix} \mathbf{A} & \mathbf{B} \\ \mathbf{B} & \mathbf{D} \end{bmatrix} \begin{bmatrix} \mathbf{g} \\ \mathbf{k} \end{bmatrix} \quad (3.17)$$

For the sake of completeness, we state correlations of kinetic quantities

$$\begin{aligned} N_1 &= N_{11} & N_2 &= N_{22} & N_3 &= \sqrt{2} N_{12} \\ L_1 &= L_{11} & L_2 &= L_{22} & L_3 &= \sqrt{2} L_{12}, \end{aligned}$$

kinematic quantities

$$\begin{aligned} G_1 &= G_{11} & G_2 &= G_{22} & G_3 &= \sqrt{2} G_{12} \\ K_1 &= K_{11} & K_2 &= K_{22} & K_3 &= \sqrt{2} K_{12}, \end{aligned}$$

and the constitutive coefficients for an aelotropic material in context of in-plane stiffness

$$\begin{aligned} A_{11} &= A_{1111} & A_{12} &= A_{1122} & A_{13} &= \sqrt{2} A_{1112} \\ & & A_{22} &= A_{2222} & A_{23} &= \sqrt{2} A_{2212} \\ & & & & A_{33} &= 2 A_{1212}, \end{aligned}$$

out-of-plane stiffness

$$\begin{aligned} D_{11} &= D_{1111} & D_{12} &= D_{1122} & D_{13} &= \sqrt{2} D_{1112} \\ D_{22} &= D_{2222} & D_{23} &= \sqrt{2} D_{2212} \\ D_{33} &= 2 D_{1212}, \end{aligned}$$

and coupling stiffness

$$\begin{aligned} B_{11} &= B_{1111} & B_{12} &= B_{1122} & B_{13} &= \sqrt{2} B_{1112} \\ B_{22} &= B_{2222} & B_{23} &= \sqrt{2} B_{2212} \\ B_{33} &= 2 B_{1212}, \end{aligned}$$

while $A_{\Gamma\Lambda} = A_{\Lambda\Gamma}$, $D_{\Gamma\Lambda} = D_{\Lambda\Gamma}$, and $B_{\Gamma\Lambda} = B_{\Lambda\Gamma}$ hold true. Of course, we can also specify Eq. (3.15) in the context of the tensorial components.

$$\begin{bmatrix} N_{11} \\ N_{22} \\ \sqrt{2}N_{12} \end{bmatrix} = \begin{bmatrix} A_{1111} & A_{1122} & \sqrt{2}A_{1112} \\ & A_{2222} & \sqrt{2}A_{2212} \\ \text{sym} & & 2 A_{1212} \end{bmatrix} \begin{bmatrix} G_{11} \\ G_{22} \\ \sqrt{2}G_{12} \end{bmatrix} + \begin{bmatrix} B_{1111} & B_{1122} & \sqrt{2}B_{1112} \\ & B_{2222} & \sqrt{2}B_{2212} \\ \text{sym} & & 2 B_{1212} \end{bmatrix} \begin{bmatrix} K_{11} \\ K_{22} \\ \sqrt{2}K_{12} \end{bmatrix} \quad (3.18a)$$

$$\begin{bmatrix} L_{11} \\ L_{22} \\ \sqrt{2}L_{12} \end{bmatrix} = \begin{bmatrix} B_{1111} & B_{1122} & \sqrt{2}B_{1112} \\ & B_{2222} & \sqrt{2}B_{2212} \\ \text{sym} & & 2 B_{1212} \end{bmatrix} \begin{bmatrix} G_{11} \\ G_{22} \\ \sqrt{2}G_{12} \end{bmatrix} + \begin{bmatrix} D_{1111} & D_{1122} & \sqrt{2}D_{1112} \\ & D_{2222} & \sqrt{2}D_{2212} \\ \text{sym} & & 2 D_{1212} \end{bmatrix} \begin{bmatrix} K_{11} \\ K_{22} \\ \sqrt{2}K_{12} \end{bmatrix} \quad (3.18b)$$

This is, in absence of geometrical symmetry of the plate and material symmetry of the material considered as well, the most general form of a linear elastic mapping transferred consistently. Note that this notation differs from classical Voigt notation by the factor $\sqrt{2}$.

3.3.2 Mathematical Consistency

The normalization of the basis by $\sqrt{2}$ seems strange but is especially convenient for the equivalence of tensor operations. By the aid of this notation, we will derive an equivalence of mathematical operations both, in tensor and vector-matrix notation. With regard to Eq. (3.14), this modification allows to apply tensorial calculation rules for a reduced notation.

Vice versa, the equivalence allows to calculate parameters in vector-matrix notation which in context of computational efficiency is associated with some facilities (e.g., reduced number of loops). For example, we can state that components of the inverse tensors \mathcal{A}^{-1} , \mathcal{D}^{-1} , and \mathcal{B}^{-1} are found by simply inverting the matrices \mathbf{A} , \mathbf{D} , and \mathbf{B} . Furthermore, \mathbf{A} , \mathbf{D} , and \mathbf{B} feature the same invariants, eigenvalues, eigendirections as \mathcal{A} , \mathcal{D} , and \mathcal{B} . The positive definiteness of \mathcal{A} , \mathcal{D} , and \mathcal{B} is another property which was transferred to present matrix notation of these quantities. Fur-

thermore, there are vector and matrix calculations which are now equivalent with computations known from tensor notation/calculus. In particular, we can identify the following identities.

$$\mathbf{n}^\top \mathbf{n} = \mathbf{N} : \mathbf{N} \quad \mathbf{g}^\top \mathbf{g} = \mathbf{G} : \mathbf{G} \quad \mathbf{n}^\top \mathbf{g} = \mathbf{N} : \mathbf{G} \quad (3.19a)$$

$$\mathbf{l}^\top \mathbf{l} = \mathbf{L} : \mathbf{L} \quad \mathbf{k}^\top \mathbf{k} = \mathbf{K} : \mathbf{K} \quad \mathbf{l}^\top \mathbf{k} = \mathbf{L} : \mathbf{K} \quad (3.19b)$$

3.4 Conclusion

We have derived a mathematically consistent vector-matrix representation. Due to the normalization, the computation of significant properties like eigenvalues, eigendirections, etc., is significantly simplified. In the literature, such mathematical consistent vector-matrix representations are not widespread. In contrast, due to the many advantages named here, the application of present modified notation is of great interest, especially in finite element program systems. The application requires moderate efforts only, whereby mechanical problems at shear-rigid plates can be solved with significantly increased efficiency. This becomes particularly evident when inelastic material behavior is considered additionally.

A more general account would be the generalization to shear-deformable plates. In this process, however, the non-symmetric stress-force tensor and the non-symmetric surface strain tensor (cf. Aßmus et al. [2]) lead to a representation in nine-dimensional vector space, or when separately handling transverse shear, in an additional constitutive description with a dimension different to that presented in (3.15).

Since kinetic and kinematic measures introduced in the theories of plates are not necessarily symmetric, a representation in a nine-dimensional vector space would be more general, in context of present course, however, less efficient.

References

1. Ambartsumian, S.A.: Theory of Anisotropic Plates: Strength, Stability, Vibration. Progress in Materials Science Series. Technomic Pub. Co., Stamford (1970)
2. Aßmus, M., Naumenko, K., Altenbach, H.: Subclasses of mechanical problems arising from the direct approach for homogeneous plates. In: Altenbach, H., Chróścielewski, J., Eremeyev, V.A., Wiśniewski, K. (eds.) Recent Developments in the Theory of Shells, Advanced Structured Materials, vol. 110, pp. 43–63. Springer, Singapore (2019)
3. Blinowski, A., Ostrowska-Maciejewska, J., Rychlewski, J.: Two-dimensional Hooke's tensors—isotropic decomposition, effective symmetry criteria. Arch. Mech. **48**(2), 325–345 (1996)
4. Brannon, R.M.: Rotation, Reflection, and Frame Changes: Orthogonal tensors in Computational Engineering Mechanics. IOP Publishing, Philadelphia, PA (2018)
5. Eremeyev, V.A., Cloud, M.J., Lebedev, L.P.: Applications of Tensor Analysis in Continuum Mechanics. World Scientific, Singapore/Hackensack/London (2018)

6. Kirchhoff, G.R.: Über das Gleichgewicht und die Bewegung einer elastischen Scheibe. *J. Reine Angew. Math.* **40**, 51–88 (1850)
7. Mandel, J.: Generalisation de la theorie de plasticite de W. T. Koiter. *Int. J. Solids Struct.* **1**(3), 273–295 (1965)
8. Mindlin, R.D.: Influence of rotatory inertia and shear on flexural motions of isotropic, elastic plates. *J. Appl. Mech.* **18**, 31–38 (1951)
9. Nye, J.F.: *Physical Properties of Crystals: Their Representation by Tensors and Matrices.* Oxford University Press, Ely House, London (1957)
10. Rychlewski, J.: Unconventional approach to linear elasticity. *Arch. Mech.* **47**(2), 149–171 (1995)
11. Thomson, W.: Elements of a mathematical theory of elasticity. *Philos. Trans. R. Soc. Lond.* **146**, 481–498 (1856)
12. Voigt, W.: Theoretische Studien über die Elasticitätsverhältnisse der Krystalle. *Abhandlungen der Königl Gesellschaft der Wissenschaften in Göttingen* **34**, 3–52 (1887)

Chapter 4

Mathematical Simulation of the Plate–Beam Interaction Affected by Colored Noise



Valentin G. Bazhenov, Tatyana V. Yakovleva and Vadim A. Krysko

Abstract The article presents a mathematical simulation of interaction between a plate and a beam locally supporting the plate in its center. The system is exposed to an external transverse load and external additive colored noise (pink, red, white). The structure is located in a steady temperature field, accounted for in the Duhamel–Neumann theory by solving 3D (plate) and 2D (beam) heat conduction equations, using finite difference method (FDM). Heat transfer between the plate and the beam is disregarded. Kirchhoff simulation was used for the plate and the Euler–Bernoulli simulation was used for the beam. The mathematical simulation accounts for physical nonlinearity in elastically deformable materials. B. Y. Kantor’s theory is applied to simulate contact interaction. The differential equation set is reduced to the Cauchy problem, using the highest-approximation Bubnov–Galerkin methods or spatial-variable FDM. The Cauchy problem is solved using the fourth-order Runge–Kutta or Newmark method. I. A. Birger’s iterative procedure is used at each time step for analyzing a physically nonlinear problem. Numeric results are analyzed using the methods of nonlinear dynamics (signal patterning, phase portraits, Poincaré sections, Fourier and Wavelet power spectra, analysis of the Lyapunov exponents using the Wolf, Kantz, and Rosenstein methods). The convergence of the methods is studied. Different methods are used to obtain reliable results. Numerical results on the effect of colored noise on plate–beam interaction are presented. Additive red noise shows more significant effect on the vibrations and the plate–beam interaction than white and pink noises.

V. G. Bazhenov (✉) · T. V. Yakovleva
Research Institute for Mechanics, Lobachevsky State University of Nizhny Novgorod, 23 Gagarin Avenue, Nizhny Novgorod 603950, Russian Federation
e-mail: bazhenov@mech.unn.ru

T. V. Yakovleva
e-mail: yan-tan1987@mail.ru

T. V. Yakovleva · V. A. Krysko
Yuri Gagarin State Technical University of Saratov, 77 Politechnicheskaya St, Saratov 410054, Russian Federation
e-mail: tak@san.ru

Keywords Plate–beam interaction · Contact interaction · Kirchhoff and Euler–Bernoulli kinematic simulation · Physical nonlinearity · Additive colored noise · Temperature field · Highest-approximation Bubnov–Galerkin methods · Runge-Kutta method · I. A. Birger iterative procedure

4.1 Introduction

Modern technology involves various elements exposed to dynamic power- and noise-related effects. This fact shows the relevance and importance of a comprehensive study of the behavior of structures and the determination of their boundary conditions. Colored noise is suitable for simulating time-random environmental properties. The theory of noise-induced transitions in physics, chemistry, and biology is presented in [1]. In the field of mechanics of thin-walled structures, such studies are rather scarce. Colors refer to different types of noise signals using spectral density plots, i.e., signal power distribution over frequencies. Constant noise with uniform distribution of spectral components over the entire range of frequencies is considered white noise. Pink (flicker) noise occurs in electronic and mechanical devices. Following article [1], several publications have been dedicated to noise in nature and technology [2–4]. Noises in vacuum devices, transistors, and diodes [5–8] are mostly studied. Studies of the properties of statistical noise were carried out using physical [9] and mathematical [10] simulations and full-scale experiments [11]. The effect of noise on mechanical distributed structures is also considered, but without accounting for temperature fields [12, 13]. Articles [14, 15] consider the effect of the temperature field on mechanical structures. The present article is aimed at constructing a mathematical model of nonlinear vibrations and contact interaction of a plate–beam structure, where the effect of color noise, temperature field, and physical nonlinearity is accounted for.

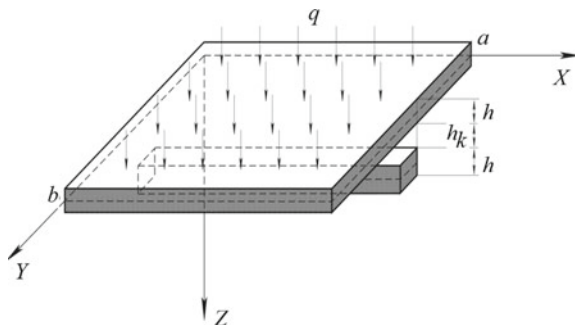
4.2 Problem Statement

The article presents a mathematical simulation of contact interaction in a mechanical two-layer plate–beam structure (Fig. 4.1), using kinematic simulations of the first approximation (Kirchhoff and Euler–Bernoulli for plate and beam, respectively). The mechanical structure is located in the field of external colored noise and subject to an external normally distributed alternating load applied to the plate. In this case, the structure is in a stationary temperature field.

The correlation between the load and plate ($\beta_1 = 1$) and beam ($\beta_1 = 0$) deformation is written as:

$$\varepsilon_1^z = \frac{1}{E}(\sigma_1 - \beta_1 \nu \sigma_2) + \alpha_T \theta, (\overleftrightarrow{1}, \overleftrightarrow{2}), \varepsilon_{12}^z = \beta_1 2 \frac{1 + \nu}{E} \sigma_{12}, (\overleftrightarrow{1}, \overleftrightarrow{2}), \quad (4.1)$$

Fig. 4.1 Plate–beam structure



where Young's modulus E and Poisson's ratio ν are not constants in the Hooke's law for two-dimensional stress state, but functions of $E = E(x, \beta_1 y, z, \varepsilon_0, \varepsilon_i, \theta)$, $\nu = \nu(x, \beta_1 y, z, \varepsilon_0, \varepsilon_i, \theta)$, where ε_0 is volumetric strain, ε_i is strain rate, α_T is linear thermal expansion coefficient, and $\theta(x, \beta_1 y, z)$ is temperature increment for the plate ($\beta_1 = 1$) and the beam ($\beta_1 = 0$). This representation is the basis of the I. A. Birger's method of the variable elasticity parameters.

Equations of motion of plate and beam elements as well boundary and initial conditions are obtained from the Hamilton–Ostrogradski variational principle (Hamilton principle). This principle allows comparison of near motions, leading a system of single mass points from the initial position at a time t_0 to the final position at a time t_1 . Actual motions shall meet the following condition:

$$\int_{t_0}^{t_1} (\delta K - \delta U + \delta W) dt = 0 \quad (4.2)$$

where K is kinetic energy, U is potential energy, W is total work of the external forces.

To simulate the contact interaction, Kantor's theory was used [16]. This theory introduces the following component in the equation of motion of the structural components: $q_k = (-1)^i K_1 (w_1 - h_k - w_2) \Psi$, where $i = 1, 2$ is element index (1 for the plate and 2 for the beam), function Ψ is determined from the formula $\Psi = \frac{1}{2} [1 + \text{sign}(w_1 - h_k - w_2)]$. Thus, if $w_1 > h_k + w_2$, the elements of the structure are in contact, and $\Psi = 1$; otherwise, $\Psi = 0$. K_1 is stiffness factor for transversal reduction in the contact area, h_k is plate–beam spacing. With the account of all the assumptions, the set of equations for the plate–beam structure is written as:

$$\begin{cases} \frac{\partial^2}{\partial x^2} [-C_{1x} - C_t] + \frac{\partial^2}{\partial y^2} [-C_{1y} - C_t] - 2 \frac{\partial^2}{\partial x \partial y} \left(\frac{\partial^2 w_1}{\partial x \partial y} C_{1xy} \right) + q_1 + q_{\text{noise}} + q_k \\ - \frac{\gamma}{g} h \frac{\partial^2 w_1}{\partial t^2} - \varepsilon \frac{\gamma}{g} h \frac{\partial w_1}{\partial t} = 0, \\ - \frac{\partial^2}{\partial x^2} \left(C_2 \frac{\partial^2 w_2}{\partial x^2} \right) - \frac{\partial^2 M_t}{\partial x^2} + q_2 - \frac{\gamma}{g} h \frac{\partial^2 w_2}{\partial t^2} - \varepsilon \frac{\gamma}{g} h \frac{\partial w_2}{\partial t} + q_k = 0, \end{cases} \quad (4.3)$$

$$\nabla^2(\theta_1) = 0, (\beta_1 = 1), \nabla^2(\theta_2) = 0, (\beta_1 = 0) \quad (4.4)$$

where $M_t = \alpha_2 \int_{-h/2}^{h/2} E_2 \theta_2 z dz$, $C_t = \alpha_1 \int_{-h/2}^{h/2} \theta z (1 + \nu) dz$, $C_{1x} = \frac{\partial^2 w_1}{\partial x^2} \int_{-h/2}^{h/2} \frac{E_1 z^2}{1-\nu^2} dz + \frac{\partial^2 w_1}{\partial y^2} \int_{-h/2}^{h/2} \frac{E_1 z^2 \nu}{1-\nu^2} dz$, $C_{1y} = \frac{\partial^2 w_1}{\partial y^2} \int_{-h/2}^{h/2} \frac{E_1 z^2}{1-\nu^2} dz + \frac{\partial^2 w_1}{\partial x^2} \int_{-h/2}^{h/2} \frac{E_1 z^2 \nu}{1-\nu^2} dz$, $C_{1xy} = \int_{-h/2}^{h/2} \frac{E_1 z^2}{1+\nu} dz$, $C_2 = \int_{-h/2}^{h/2} E_2 z^2 dz$, $e_1 = \varepsilon_{11}^z + \beta_1 \varepsilon_{22}^z$, $\nabla^2(\theta)$ is 3D Laplacian ($\beta_1 = 1$) and $\nabla^2(\theta)$ is 2D Laplacian ($\beta_1 = 0$), ε is dissipation coefficient. No limits are introduced for temperature distribution over the thickness of the plate and height of the beam. Various stress vs deformation/temperature plots $\sigma_i(\varepsilon_i, \theta)$ may be considered. The first-, second-, and third-type boundary conditions shall be applied to the heat equations for system (Eqs. 4.3–4.4).

The plate is exposed to the distributed external load of $q_1(x, y, t) = q_0 \sin(\omega_p t)$, where q_0 is its amplitude and ω_p is frequency. Additive colored noise is introduced into system (4.3) as a stochastic component of constant intensity q_{noise} [17, 18]. The colored noise is generated in MATHLAB. Power spectrum density of the excess (technical) noise obeys power law $S(\omega) = h_\gamma \omega^\gamma$, $-2 \leq \gamma \leq 2$, where h_γ is scaling factor to determine the noise level. Each integral value γ is conventionally associated with a definite color: $\gamma = 0$ for white noise, $\gamma = +2$ for Brownian (red) noise, $\gamma = +1$ for pink noise.

4.3 Solution Methods

The studied mechanical structure (Fig. 4.1) is located in a temperature field of constant intensity. The heating pattern in the plate–beam structure shall be determined by solving 3D (plate) and 2D (beam) heat equations with the respective first-, second-, and third-type boundary conditions. Steady-state heat equations are solved for plate and beam using the second- and fourth-order accuracy finite difference method. The convergence of the methods is studied. Equation set (4.3) is reduced to the Cauchy problem, using the Bubnov–Galerkin methods in the highest approximations and second- and fourth-order accuracy FDM. Functions w_1 and w_2 , the solutions of Equation set (4.3) are approximated by Bubnov–Galerkin as a product of time- and coordinate-dependent functions:

$$w_1 = \sum_{k=1}^N \sum_{j=1}^N A_{kj}(t) \phi_{kj}(x, y), \quad w_2 = \sum_{k=1}^N A_k(t) \phi_k(x) \quad (4.5)$$

Functions $\phi_{kj}(x, y)$ and $\phi_k(x)$ are selected so that they are continuous with their partial derivatives up to the fourth order, inclusively, linearly independent, and meet the boundary conditions. Cauchy problem is solved using either Newmark or Runge–Kutta-type method to obtain reliable results. The iterative procedure is formulated for each time step using the I. A. Birger’s method of variable elasticity parameters.

Thus, the study makes it possible to treat the problem in terms of a system with an « almost » unlimited number of degrees of freedom. The results are analyzed using the qualitative methods of the theory of differential equations and nonlinear dynamics involving signal patterning, phase portraits, Poincaré sections, Fourier and Wavelet power spectra, analysis of the Lyapunov exponents by Wolf [19], Rosenstein [20], and Kantz [21].

4.4 Numerical Experiment

Results of the numerical experiment for plate–beam interaction in colored noise are given as an example, without accounting for physical nonlinearity and temperature field. The pivoting support on the sides of the plate and on the ends of the beam was chosen as the boundary conditions in the numerical experiment:

$$\begin{aligned} w_1 = 0; \frac{\partial^2 w_1}{\partial x^2} = 0; w_2 = 0; \frac{\partial^2 w_2}{\partial x^2} = 0; \text{ with } x = 0; 1; \\ w_1 = 0; \frac{\partial^2 w_1}{\partial y^2} = 0; \text{ with } y = 0; 1 \end{aligned} \quad (4.6)$$

zero initial conditions are as follows:

$$w_i|_{t=0} = 0; \quad \dot{w}_i|_{t=0} = 0, \quad i = 1, 2 \quad (4.7)$$

The following control parameter values are chosen: dissipation factor $\varepsilon = 1$, external driving frequency $\omega_p = 5$, that is chosen close to the intrinsic frequency of the plate, external load amplitude $q_0 = 10$, plate–beam spacing $h_k = 0.01$. The effect of various (in terms of type and intensity) colored noise on the vibrations in the plate–beam structure was studied.

1. In the absence of the effect of noise field ($q_{\text{noise}} = 0$), the vibrations in the plate–beam structure are harmonic with external driving frequency $\omega_p = 5$. The beam in this case is quiescent, because of the absence of contact interaction (Fig. 4.2). Figure 4.2 shows the plot of the combined vibrations of the plate (solid red line) and the beam (blue dotted line) (a), Fourier power spectrum (b), 2D Morlet Wavelet spectrum (c).
2. With introducing additive pink noise ($\gamma = +1$) in the external load, starting with intensity $q_{\text{noise}} = 40$ the period triples: $\omega_p = 5$, $\omega_1 = \omega_p/3 = 1.6$ and $\omega_2 = 2\omega_p/3 = 3.3$. With $q_{\text{noise}} = 43$, the vibrations of the plate become chaotic.
3. After introducing additive red noise ($\gamma = +2$) in the external load, starting with the intensity $q_{\text{noise}} = 0.2$, vibrations of the plate occur with the period tripling. For $q_{\text{noise}} = 7$, initial plate–beam interaction occurs; the vibrations of the plate are chaotic.

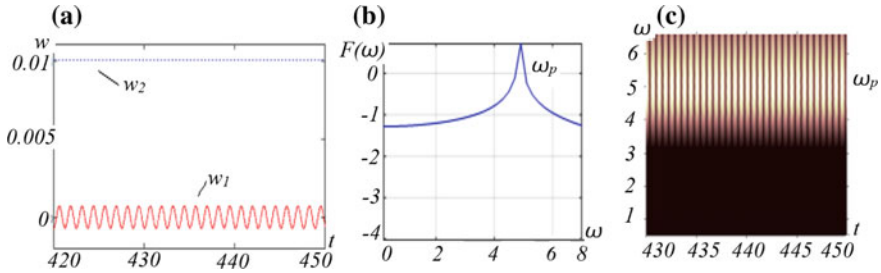


Fig. 4.2 Plate vibration for load $q_0 = 10$ and without noise $q_{\text{noise}} = 0$

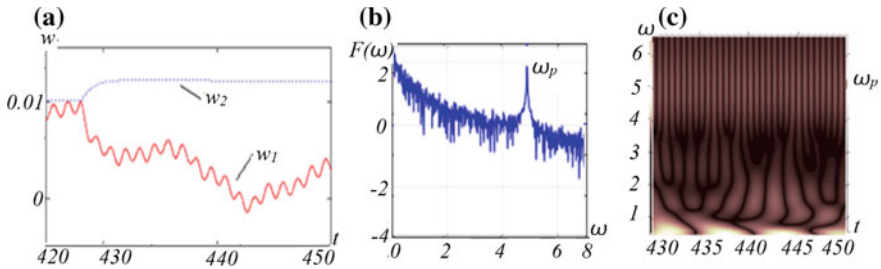


Fig. 4.3 Plate vibration for load $q_0 = 10$ and white noise ($\gamma = 0$) $q_{\text{noise}} = 244$

4. With introducing additive white noise ($\gamma = 0$) in the external load, for $q_{\text{noise}} = 1$, vibrations of the plate occur over two frequencies: $\omega_p = 5$ and $\omega_1 = \omega_p/3 = 1.6$. For $q_{\text{noise}} = 5$, vibrations of the plate occur with the period tripling. For $q_{\text{noise}} = 100$, plate vibrations are chaotic. The initial plate–beam interaction occurs at $q_{\text{pnois}} = 244$; the vibrations of the plate are chaotic (Fig. 4.3). The largest Lyapunov exponent, estimated by Kantz, Wolf, and Rosenstein, is positive.

4.5 Conclusion

The article presents a mathematical model of nonlinear vibrations and the contact interaction in the system of the plate, locally supported by a beam, affected by additive colored noise and a temperature field, accounting for physical nonlinearity. It follows from the analysis of colored (red, pink, and white) noise, that red noise shows more significant effect on vibrations and plate–beam interaction than white and pink noises.

Acknowledgements The Russian Science Foundation (project No. 15- 19-10039-P) financially supported this work.

References

1. Horsthemke, W., Lefever, R.: Noise-Induced transitions. In: Theory and Applications in Physics, Chemistry, and Biology. Springer, Berlin, Heidelberg, New York, Tokyo (1984)
2. Salmon, J., et al.: Poisson noise reduction with non-local PCA. *J. Math. Imaging Vis.* **48**(2), 279–294 (2014)
3. Chien, J.C., et al.: 2.8 A pulse-position-modulation phase-noise-reduction technique for a 2-to-16 GHz injection-locked ring oscillator in 20 nm CMOS. In: IEEE International Solid-State Circuits Conference Digest of Technical Papers (ISSCC), pp 52–53 (2014)
4. Galimullin, D.Z., Sibgatullin, M.E., Kamalova, D.I., Salahov, M.H.: Effect of color noise on the processing of optical signals using the swarm intellect algorithm. *Bull. Russ. Acad. Sci. Phys.* **80**(7), 855–858 (2016)
5. Noise and degradatsionny processes in semiconductor devices. Materials of Reports of the International Scientific and technical Seminars MEI. Moscow. MEI Publ. 1993–2000. (In Russian)
6. Santosa, H., et al.: Noise reduction in functional near-infrared spectroscopy signals by independent component analysis. *Rev. Sci. Instrum.* **84**(7), 073106 (2013)
7. Shapovalov, A.S., Lyashenko, A.V.: Modulation spectrums of the signal fluctuations of the multidiode microwave generator. *Heteromagnetic Microelectron.* **24**, 27–42 (2018). (In Russian)
8. Emel'yanov, A.M., Krutov, A.V., Rebrov, A.S.: Features of probe measurements of the noise coefficient of the transistor in the millimeter wavelength range. *Electron. Microelectron. Microw* **1**, 319–323 (2016). (In Russian)
9. Anisimov, M.P., Cherevko, A.G.: Fluctuation Phenomena in a Physicochemical Experiment. Nauka Publ, Novosibirsk (1986). (In Russian)
10. Potemkin, V.V., Stepanov, A.V.: On the stationary nature of $1/f$ noise in the low-frequency range of the experiment. *J. Commun. Technol. Electron.* **25**(6), 1269 (1980). (In Russian)
11. Restle, R.: Tests of Gaussian statistical properties of $1/f$ noise. *J. Appl. Phys.* **54**(10), 5844 (1983)
12. Awrejcewicz, J., Krysko, A.V., Erofeev, N.P., Dobriyan, V., Barulina, M.A., Krysko, V.A.: Quantifying chaos by various computational methods. Part 2: Vibrations of the Bernoulli-Euler beam subjected to periodic and colored noise. *Entropy* **20**(3), 170 (2018)
13. Awrejcewicz, J., Krysko, A.V., Papkova, I.V., Zakharov, V.M., Erofeev, N.P., Krylova, E.Y., et al.: Chaotic dynamics of flexible beams driven by external white noise. *Mech. Syst. Signal Process.* **79**, 225–253 (2016)
14. Yakovleva, T.V., Krys'ko, V.A.: Mathematical simulation of contact interaction of physically nonlinear three-layered plate-beam structure in temperature field. *Mech. deformation fract.* **6**, 9–14 (2017). (In Russian)
15. Krysko, A.V., Awrejcewicz, J., Kutepov, I.E., Krysko, V.A.: Stability of curvilinear Euler-Bernoulli beams in temperature fields. *Int. J. Non-Linear Mech.* **94**, 207–215 (2017)
16. Kantor, B.Ya.: Contact Problems of the Nonlinear Theory of Shells of Revolution. Dumka Publ, Kiev. Naukova (1990). (In Russian)
17. Bazhenov, V.G., Krylova, E.Yu., Yakovleva, T.V.: Nonlinear vibrations of a plate stiffened with a local set of ribs in the conditions of additive white noise. *Probl. Strength Plast.* **79**(3), 259–266 (2017). (In Russian)
18. Yakovleva, T.V., Bazhenov, V.G., Krysko, V.A., Krylova, C.Y.: Contact interaction plates, reinforced by ribs, with gaps under the influence of white noise. *PNRPU Mech. Bull.* **4**, 259–272 (2015). (In Russian)
19. Wolf, A., Swift, J.B., Swinney, H.L., Vastano, J.A.: Determining Lyapunov exponents from a time series. *Physica D: Nonlinear Phenomena.* **16**, 285–317 (1985)

20. Rosenstein, M.T., Collins, J.J., De Luca, C.J.: A practical method for calculating largest Lyapunov exponents from small data sets. *Physica D: Nonlinear Phenomena*. **65**, 117–134 (1993)
21. Kantz, H.: A robust method to estimate the maximal Lyapunov exponent of a time series. *Phys. Lett. A* **185**, 77–87 (1994)

Chapter 5

Dynamic Homogenization of a Chain with Bistable Springs. Statistical Approach



Charlotte Blake and Andrej Cherkaev

Abstract We study the problem of *dynamic homogenization*, replacing a high-frequency vibrating mass-spring chain with a single nonlinear spring and determine its time-averaged elastic characteristics. A mass-spring chain of n equal non-monotonic bistable springs that join equal small masses is considered. The potential energy of each spring is a nonconvex two-well function $V(U)$ with two local minima that correspond to equilibrium positions (a long and a short mode). The kinetic energy Q defines the intensity of the oscillations. Each spring may oscillate around either long or short equilibria; the total elongation U of the chain is not uniquely defined. The minimal potential energy of the homogenized static chain corresponds to the Maxwell line and is equal to the convex envelope $\mathcal{C}V(U)$ of the two-well potential energy $V(U)$ of a single spring. Here, we describe a family of homogenized energies $\mathcal{D}V(U, Q)$ of a vibrating chain; they depend on the kinetic energy Q . We treat the phase of each spring as a random variable; using the Central Limit Theorem, we find the homogenized behavior of the chain. We derive formulas for average elongation versus force dependence, and we show it is strictly monotonic and tends to the Maxwell line when kinetic energy is low. Numerical simulations validate our model. The results generalize the Maxwell rule to the dynamic chain.

Keywords Dynamic homogenization · Nonconvex energy · Bistable chain

5.1 Introduction

In this paper, we study the homogenized elastic response of a chain of vibrating masses joined with non-monotonic springs. We take into account the kinetic energy of the motion and obtain new homogenized force versus elongation dependence. Specifically, we study the average behavior of a mass-spring chain of n equal non-monotonic bistable springs that join similar masses. We assume that a force F applied

C. Blake · A. Cherkaev (✉)

Department of Mathematics, University of Utah, 155 1400 E, Salt Lake City, UT 84112, USA
e-mail: cherk@math.utah.edu

© Springer Nature Switzerland AG 2020
H. Altenbach et al. (eds.), *Nonlinear Wave Dynamics of Materials and Structures*, Advanced Structured Materials 122,
https://doi.org/10.1007/978-3-030-38708-2_5

to its end; the other end is fixed. The initial kinetic and potential energies of this conservative system of oscillating particles are given. The potential energy of each spring is a nonconvex two-well function $V(U)$; the force-elongation relation is non-monotonic. A spring may have two equilibrium positions (long and short equilibria). We find the homogenized behavior of the chain, assuming that the masses are small and the frequencies of their oscillations are high, replace the chain with a single nonlinear spring, and define the elastic characteristics of this equivalent spring.

In the transition zone, each spring may rest in either long or short phase. Therefore, the total elongation of the spring is not uniquely defined. The minimal energy of the static chain corresponds to the Maxwell line [10]: When F is smaller than a threshold F_T , $F < F_T$, all springs are in short phase; if $F > F_T$, all springs are in long phase; and if $F = F_T$, the chain length U is undetermined since springs can be either in the short or the long phase. For large n , the homogenized chain is described by an equivalent nonlinear spring that has discontinuous elongation vs. force dependence at $F = F_T$. The energy of the equivalent spring is proportional to the convex envelope $CV(U)$ of the two-well power $V(U)$ of a single spring. The dynamical homogenization (D-homogenization) is quite different. The conservative mass-spring system possesses kinetic energy Q that makes the masses oscillate. In the transition zone, the masses oscillate around one of the equilibria occasionally jumping from one equilibrium to the other. We compute the time average $\langle U \rangle$ of the deformation U of the chain, which depends on F and Q , $U = U(F, Q)$. The phase of each spring in a given time instance is assumed to be random; the probability of being in a short phase monotonically varies with F . For large n , the deformation is estimated using the Central Limit Theorem. The resulting homogenized behavior is expressed through error function *erf* of F ; the dispersion of the corresponding Gaussian process monotonically depends on the excitation energy Q . Unlike static homogenization, the D-homogenized dependence $U(F, Q)$ with a prescribed Q is continuous; it tends to static behavior (Maxwell line) when $Q \rightarrow 0$.

Integrating the force-elongation relation of this nonlinear spring yields a convex relaxation for the system energy. The D-homogenized energy $DV(U, Q)$ is strictly convex and $DV(U, Q) \geq CV(U, Q)$. We also show that $DV(U, Q) \rightarrow CV(L)$ when $Q \rightarrow 0$ and the jumps are rare. For piecewise linear spring, we find the lower bound of DV that corresponds to $Q \rightarrow \infty$. In this case, the function $U(F)$ is close to linear, and the D-homogenized energy is quadratic. The demonstrated numerical results confirm this model.

5.1.1 Some Previous Results

Propagation of transitions of bistable springs throughout a two-dimensional lattice has been used to approximate crack propagation in materials [6, 12, 14]. Bistable chains have also been found to be capable of absorbing higher amounts of energy than

linear chains due to their ability to delocalize damage and dissipate heat via high-frequency oscillations [1, 13]. The dynamics of transition waves in such systems is similar to models of material failure and energy absorption [2, 15]. The propagation of a phase transition wave in more complex models where masses are also connected to the next to nearest neighbors is studied in [16]. Transition waves in linear chains with bistable elements attached to the masses have been observed in several regimes depending on wave amplitude [8]. An addition of bistable elements allows control over energy transport in linear chains [4]. Chains of bistable elements have been found to have chaotic behavior Nekorkin and Makarov [9]. These chains also exhibit stochastic resonances [7]. Kinetic relations of impacts on chains in a heated bath have been studied [17] as well as chains where the springs can twist [18].

A similar problem of dynamics of a chain with bistable springs has been studied in Efendiev and Truskinovsky [3] using a physical model of thermalization of the motion. The high-frequency oscillations of the bistable springs were identified as a thermal component of the elongation, the statistical approach used assumptions about the probability of the “micro-states.”

Here, we use a more straightforward and rough approach to the problem. Namely, we state that the total elongation of the chain, being the sum of uncorrelated or weakly correlated elongations of the springs, is Gaussian by the Central Limit theorem. The universality of this approach allows us to obtain the average force vs. elongation dependence similar to those found in Efendiev and Truskinovsky [3].

5.1.2 Structure of the Paper

The structure of the paper is the following. In Sect. 5.3, we describe the vibration of a single mass attached to a non-monotonic spring. We describe regimes of vibrations and the time average of the homogenizing force. In Sect. 5.3, we show the result of simulation of the chain dynamics. In Sect. 5.4, we suggest a statistical approach to the *dynamic homogenization*—that is, computing an average stiffness which is based on the Central Limit Theorem and describe the formulas for dynamic homogenization. In Sect. 5.5.1 we discuss the details of the numerical procedure and validate the model, and in Sect. 5.5.2, we study the dependence of the relaxation on the kinetic energy of the system.

5.2 Preliminaries: Single-Spring Dynamics

Consider a unit mass joined to a base with a bistable spring with normalized piecewise linear force-elongation relation:

$$f(u) = u + v(u), \quad v(u) = \begin{cases} (k+1)a, & u \leq -a \\ -(k+1)u, & -a < u < a \\ -(k+1)a, & u \geq a \end{cases} \quad (5.1)$$

Here, u is the spring elongation, $f = f(u)$ is the force; $a > 0$ and $k > 0$ are given parameters. The stiffness of the linear part of spring is scaled to be one. The force-elongation relation has three equilibria positions where $f(u) = 0$: the unstable equilibrium at $u = 0$, and two stable equilibria at $u = \pm q$ where $q = (k + 1)a$. We say that the spring is in *short phase* if $u < -a$ and in *long phase* if $u > a$. The region where $-a \leq u \leq a$ is called the *unstable phase*.

Also, we consider the asymptotic case that we call a bistable discontinuous spring

$$f_A(u) = u - q \operatorname{sign}(u). \quad (5.2)$$

It corresponds to $(k + 1)a = q$ and $a \rightarrow 0$.

The potential energy V of the spring is

$$V(u) = \begin{cases} \frac{1}{2}(u + q)^2, & u \leq -a \\ \frac{k}{2}(-u^2 + qa), & -a < u < a \\ \frac{1}{2}(u - q)^2, & u \geq a \end{cases} \quad (5.3)$$

The energy is defined so that $V = 0$ at the stable equilibrium $u = \pm q$.

The differential equation of the motion of the bistable spring (5.3) is

$$\ddot{x} = -f(x); \quad (5.4)$$

and its solution is

$$x(t) = \begin{cases} A \sinh(\sqrt{k}t) + B \cosh(\sqrt{k}t), & x \in [-a, a] \\ A' \sin(t) + B' \cos(t) + x_0, & x \notin [-a, a] \end{cases} \quad (5.5)$$

where $x_0 = \pm q$ is one of the positions of the stable equilibria.

The total energy $V_0 = V + Q$ of the motion is constant. Initially, the kinetic energy Q is zero.

To pass from the short to long phase, V_0 must be greater than the energy barrier V_B . This energy barrier is equal to the energy of the unstable equilibrium at the $u = 0$.

$$V_B = \frac{k}{2}qa \quad (5.6)$$

5.2.1 Regimes

Vibration of the mass depends on its initial energy as it is illustrated in Fig. 5.1. The time average elongation of the spring is shown in Fig. 5.2.

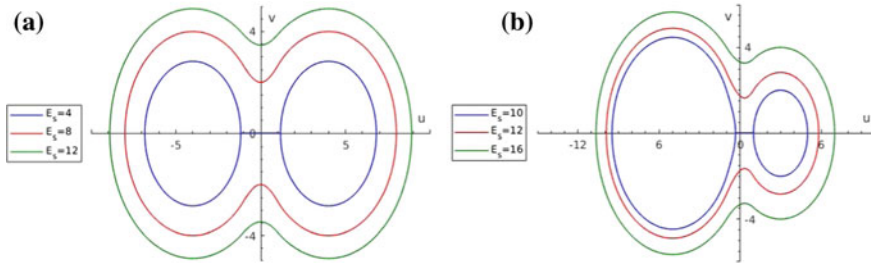
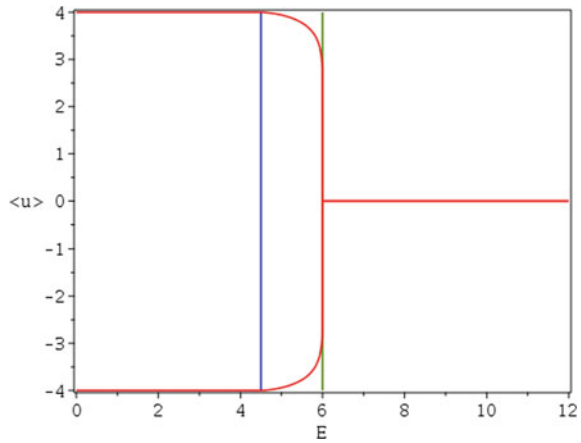


Fig. 5.1 Phase portrait for different total energy of the spring. Adding a prestress to the spring makes the profile asymmetric: **a** Phase portrait for $f_0 = 0$, **b** Phase portrait of the dynamics with prestress

Fig. 5.2 Time-averaged spring elongation versus energy for the spring. The part left of the blue line corresponds to the linear regime (i). The part between blue and green lines corresponds to regime (ii). The critical transitional regime (iii) lies at the bifurcation $\bar{u} = 0$ on the green line. The part right of the green line corresponds to the transitional regime



- (i) If $V_0 < \frac{1}{2}(q - a)^2$, the mass oscillates in a linear regime of either short or long phase. The time average $\langle u \rangle$ of its position is $\langle u \rangle = \pm q$, where

$$\langle u \rangle = \frac{1}{\tau} \int_0^\tau u(t) dt, \tau \rightarrow \infty \tag{5.7}$$

and the period T is $T = 2\pi$.

- (ii) When $\frac{1}{2}(q - a)^2 < V_0 < V_B$, (the unstable non-transitional regime), the elongation of the spring reaches the unstable region, but its energy is insufficient to overcome the repulsive force in the region and reach the critical point $u = 0$. The motion is periodic; as $V_0 \rightarrow V_B$, the period T tends to infinity and the average $\langle u \rangle$ tends to zero because the spring stays close to $u = 0$ for the most time:

$$\text{When } V_0 \rightarrow V_B, \quad \langle u \rangle \rightarrow 0; \quad T \rightarrow \infty$$

- (iii) The critical regime corresponds to the energy given by (5.6). The mass moves toward the point of unstable equilibrium but cannot reach it in the finite time. Indeed, at that point $u = 0$ and $\dot{u} = 0$ which contradicts (5.5). In this regime, the motion is non-periodic.
- (iv) In the transitional regime, where $V_0 > V_B$, the spring has sufficient energy to reach $u = 0$ with nonzero velocity, $|\dot{u}| > 0$, and it transits between short and long phases. By symmetry, the mass spends exactly half of its period in each phase. We have

$$\text{When } V_0 > V_B, \quad \langle u \rangle = 0$$

When $V_0 \rightarrow \infty$, the period decreases and tends to 2π , $T \rightarrow 2\pi$ when $V_0 \rightarrow \infty$.

5.3 Dynamics of a Multi-spring Chain

5.3.1 Differential Equations and Numerics

5.3.1.1 Differential Equations

Consider a chain of n bistable springs as described in Sect. 5.2 and $n - 1$ unit masses, where the first spring is anchored to a point $x_0 = 0$. The last spring is attached to a large mass of M , $M \gg n$, and the springs are connected by unit masses. Let x_i be the position of the i th mass. The masses are separated by the distance c , so that force f defined in (5.1) is becomes

$$f(u_i), \quad u_i = x_{i+1} - x_i - c$$

The dynamics of the chain are governed by a system of differential equations

$$\ddot{x}_i = \begin{cases} f(u_i) - f(u_{i+1}), & 0 < i < n \\ \frac{1}{M}f(u_n) + F, & i = n \end{cases} \quad (5.8)$$

where f is the bistable spring force function in Eq. (5.1), and F is the applied force.

The equation of for x_i , $i = 1, \dots, n - 1$ is rewritten as

$$\ddot{x}_i = u_u - u_{i-1} + v(u_i) - v(u_{i-1}) \quad 0 < i < n \quad (5.9)$$

where v is as in (5.1); initial conditions are assigned.

The system is complemented by the initial conditions

$$x_i = X_i, \quad \dot{x}_i = 0 \quad \text{if } t = 0.$$

Here, X_i are given data that specify the initial mode (short or long) of each mass; the initial speed is zero. Initially, the masses of the chain are in off equilibrium positions, which causes their oscillation. The kinetic energy of oscillation Q measures the intensity of the oscillation of the whole chain.

Below, we discuss the results of the numerical simulation of the dynamics of the chain. The numerical procedure is described below in Sect. 5.5.1. The system is conservative; its behavior depends on the amount of Q .

5.3.2 Results of Numerical Simulation

For a better visibility, the results of the simulations are shown for a very short chain of four mass. The actual simulation was performed on a longer chain, see Sect. 5.5.1. The system shows several types of behavior, depending on Q .

5.3.2.1 The Non-transitional Phase

Small excitation energy $Q < V_B$ corresponds to the case where there are no phase transitions because the energy is not enough to jump over the barrier between stable equilibria; all springs oscillate in their initial long or short phase. The dynamics are identical to a chain of linear springs. An example of such motion is shown in Fig. 5.3. The springs linearly oscillate around the equilibria in either the short or long phase. The total elongation of the chain is defined by the number of springs that initially are in either phase. The average system has multiple equilibria.

5.3.2.2 The Rare Transition State

This regime occurs when the total energy of the system is sufficient for a small percentage of springs to transition between short and long phases but little more than that. The chain undergoes rare transitions because sufficient energy is rarely concentrated in one spring.

We observe that the system tends toward the lowest potential energy so that the percentage of the long and short springs tends to those predicted by Maxwell's rule.

Figure 5.4 represents the oscillations of the same system as in Fig. 5.3, but with increased energy Q . The springs infrequently transition between long and short phases; the time between transitions is much greater than the average period of oscillations of a spring. The springs spend virtually all of their time linearly oscillating about the stable configuration.

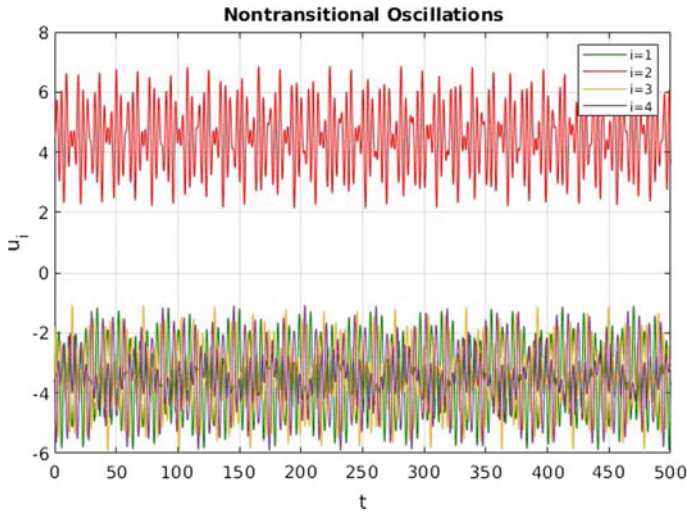


Fig. 5.3 The elongation versus time of a four-spring chain

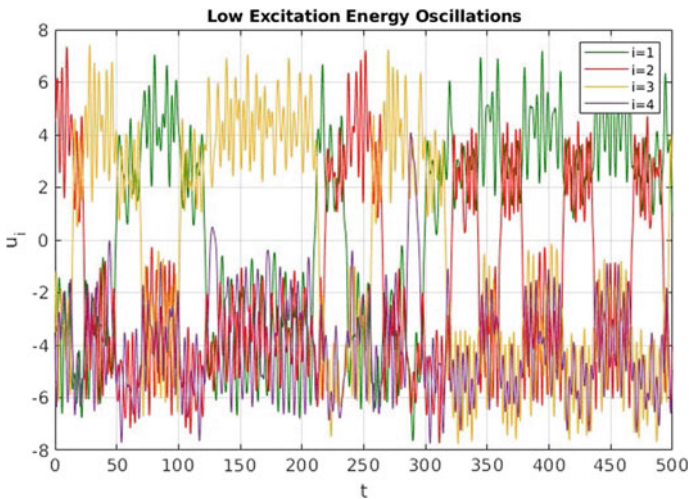


Fig. 5.4 Low excitation energy oscillations for the system in Fig. 5.3

5.3.2.3 Moderate Excitation Energy

With even greater kinetic energy, the average time between transitions in the system decreases as in Fig. 5.5. The frequency of phase shift becomes comparable with the average period T of oscillation of a single spring. In this regime, each spring spends a significant fraction of time in the unstable region.

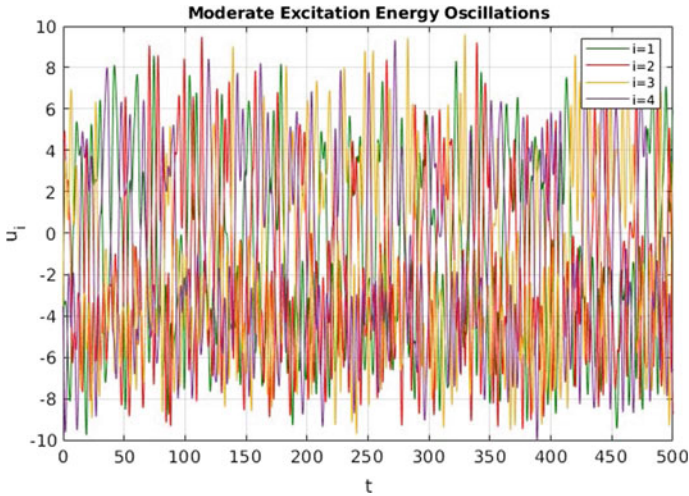


Fig. 5.5 Moderate excitation energy oscillations for the system in Fig. 5.3

As the excitation energy increases further, phase changes become increasingly frequent, one or two periods of the small mass oscillations. The masses frequently oscillate around both equilibria rather than switching between linear oscillations around stable points.

Large Excitation Energy

In this case, the excitation energy is much larger than the energy barrier, and an amplitude of oscillation is much larger than the span of the unstable region. Each spring spends most of the time in stable regions $|u_i| > a$. Also, the asymmetry of the starting conditions is negligible. The time average of the motion of an individual spring is similar to the motion of linear spring, $f = u$ because the springs spend approximately equal time in the long and short phases. Figure 5.6 represents the oscillations of the same system as in Fig. 5.3, but with high energy: the amplitude is forty units, and the length of the unstable region is two units.

5.4 Model for Dynamic Homogenization

5.4.1 Ansatz: Random Transitions

Here, we suggest a homogenized constitutive equation $F = \Phi(U_N)$ that connects the forces acting at the last mass of the chain F with the time average of the deformation of the chain

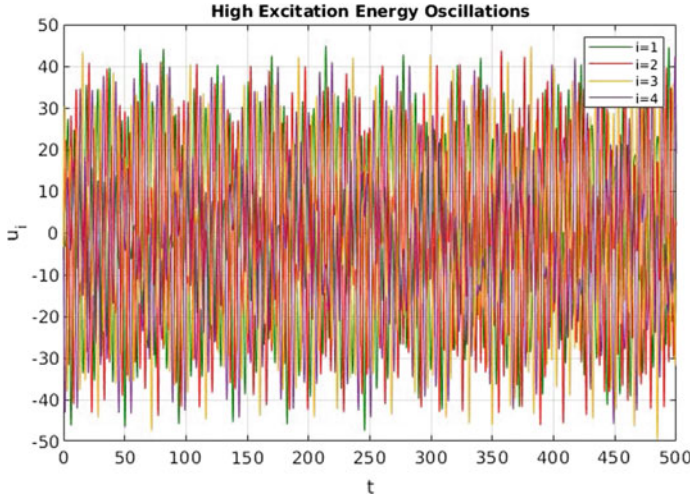


Fig. 5.6 High excitation energy oscillations for the system in Fig. 5.3

$$U_N = \frac{1}{n} \sum_{i=1}^n \bar{u}_i, \quad \bar{u}_i = \langle u_i(t) \rangle. \tag{5.10}$$

Here, $\langle z(t) \rangle$ is the time average of $z(t)$ defined in (5.7). The deformation U_N is the normalized elongation of the chain.

Consider a chain of vibrating spring, assume that a constant force F is applied to its end. The time average of the acceleration of each mass is zero, and the time average of the force $f_i(t)$ applied to each spring is F

$$\langle f_i(t) \rangle = F \quad \forall i.$$

Each spring oscillates around its equilibrium position, its average length $\langle u_i(t) \rangle$ is

$$\langle u_i(t) \rangle = F + qv_i$$

where the normalized variable $v_i \in [-1, 1]$ depends on the mode of the spring. Namely, for the springs that oscillate about stable equilibria in linear modes, v_i are, respectively,

$$v_i = 1 \quad \text{in the long mode,} \quad v_i = -1 \quad \text{in short long mode} \tag{5.11}$$

In the transitional mode, the masses at its ends spend equal time decelerating before reaching the point of unstable equilibrium and accelerating after passing this point. This symmetry implies that in average elongation is the same as in the linear spring with $v = 0$.

$$v_i = 0 \quad \text{in the transitional mode} \quad (5.12)$$

The remaining mode corresponds to the springs that enter the deceleration zone but does not reach the point of unstable equilibrium and is rejected, returning back and continue the oscillations around a stable equilibrium. This process is symmetrically applied for spring entering the unstable zone from both long and short mode. The spring spends more time in the unstable zone where the speed is slow; therefore, the time average of its length corresponds to

$$|v_i| < 1 \quad \text{in the nonlinear non-transitional mode} \quad (5.13)$$

The percentage of springs in each mode depends on the applied force F .

The deformation U_N of the chain is

$$U_N = F + q W_N, \quad W_N = \frac{1}{N} \sum_{i=1}^N v_i$$

We do not attempt to determine the exact value of $v_i(F, t)$. Instead, we assume that $v_i(F, t)$ is a random variable $\bar{v}_i(F)$ that takes values in $[-1, 1]$ with some probabilities; The probabilities depend only on the applied force F but not on the states of neighboring springs. In other words, we assume that modes $\bar{v}_i(F)$ are uncorrelated or only weakly correlated.

Consider the limit

$$W(F) = \lim_{N \rightarrow \infty} W_N.$$

Using the Central Limit Theorem Rosenblatt [11], we find that sum $U(F)$ of uncorrelated variables v_i is Gaussian or

$$W(F) = C_* \operatorname{erf} \left(\frac{F - F_*}{\sigma} \right), \quad (5.14)$$

where

$$\operatorname{erf}(z) = \frac{1}{\sqrt{2\pi}\sigma} \int_{-\infty}^z \exp(-\phi^2) d\phi$$

and C_* , F_* , and σ are a priori unknown parameters.

The asymptotics and the symmetry of the model imply the relations

$$\langle v(\infty) \rangle = 1, \quad \langle v(F) \rangle = -\langle v(-F) \rangle, \quad \langle v(0) \rangle = 0.$$

We conclude that in (5.14) $C_* = 1$ and $F_* = 0$, and $\langle v(F) \rangle$ becomes

$$W(F) = \operatorname{erf}\left(\frac{F}{\sigma}\right). \quad (5.15)$$

The remaining unknown standard deviation σ depends on the kinetic energy of vibration, $\sigma = \sigma(Q)$; we discuss this dependence below in Sect. 5.5.2.

In summary, the dependence $U(F)$ is

$$U(F) = F + qW = F + \frac{q}{\sqrt{2\pi}\sigma} \int_{-\infty}^F \exp\left(-\frac{\phi^2}{2\sigma^2}\right) d\phi \quad (5.16)$$

The deformation versus force relation depends on the remaining parameter σ . We call this dependence $\Psi_\sigma(F)$,

$$U(F) = \Psi_\sigma(F), \quad \Psi(F) = F + q \operatorname{erf}\left(\frac{F}{\sigma}\right) \quad (5.17)$$

Comment Here, we follow the approach of Slepyan [12] to describe nonlinear oscillations, assuming the type of motion of masses in the chain. In Slepyan [12], Slepyan et al. [15], Mishuris et al. [6] a nonlinear chain that experiences a phase transition was considered. The solution was sought in the form of a wave of transition that propagates with constant a priori unknown speed θ , which implied the ansatz, $v_i(t) = v_{i+1}(t + \theta)$. In Cherkhev et al. [1], a periodic solution of a nonlinear chain with phase transitions was sought using a similar ansatz. Here we use an ansatz by postulating a random Gaussian distribution of v_i . This assumption is numerically verified, as it is described in the next section.

5.4.2 Properties

5.4.2.1 Properties of $\Psi_\sigma(F)$

We state several immediate properties:

- (i) For $\sigma > 0$, $\Psi_\sigma(F)$ is a strictly monotonic analytic even function. Its Taylor series is

$$\Psi_\sigma(F) = \left(1 + 2 \frac{q}{\sqrt{\pi}s}\right) F - \frac{2q}{3\sqrt{\pi}s^3} F^3 + \frac{q}{5\sqrt{\pi}s^5} F^5 - \frac{q}{21\sqrt{\pi}s^7} F^7 + \dots \quad (5.18)$$

- (ii) $\Psi_\sigma(F)$ should be compared with the Maxwell rule $\Psi_M(F)$:

$$\Psi_M(F) = F + q \operatorname{sign} F \quad (5.19)$$

Maxwell rule assumes that all springs instantly change the mode when F reaches the threshold, which corresponds to minimum of potential energy of the

whole system. Maxwell rule corresponds to the limit of $\Psi_\sigma(F)$ when $\sigma \rightarrow 0$,

$$\Psi_M(F) = \Psi_0(F) = \lim_{\sigma \rightarrow 0} \Psi_\sigma(F) \quad (5.20)$$

(iii) When $\sigma \rightarrow \infty$, $\Psi_\sigma(F)$ becomes a linear function

$$\Psi_\infty(F) = \lim_{\sigma \rightarrow \infty} \Psi_\sigma(F) = F \quad (5.21)$$

This case corresponds to large kinetic energy and to magnitude of the vibrations that is much larger than the interval of non-convexity.

(iv) Function $\Psi_\sigma(F)$ monotonically depends of σ for a fixed F ,

$$\frac{\partial}{\partial \sigma} (\Psi_\sigma(F)) = -2 \frac{qF}{\sqrt{\pi} s^2} e^{-\frac{F^2}{\sigma^2}} < 0$$

In next section, we numerically find the relation between the energy V of a vibrating chain and standard deviation σ .

5.4.2.2 Properties of $\mathcal{D}F(U)$

The conventionally used force versus elongation relation corresponds to the inverted function $\Psi_\sigma^{-1}(U)$; we call it dynamical homogenized relation and denote

$$\mathcal{D}F(U) = \Psi_\sigma^{-1}(U)$$

- (i) This dependence is a continuous, infinitely differentiable, monotonic function.
- (ii) Derivative $(\mathcal{D}F)'(U)$ is uniformly bounded from above $(\mathcal{D}F)'(U) < 1$ for all U . The minimal value of derivative $(\mathcal{D}F)'(U)$ is reached at $U = 0$; the minimal value is computed using the theorem of inverse function is equal

$$\mathcal{D}F'(U) > \mathcal{D}F'(0) = \frac{\sqrt{\pi}\sigma}{\sqrt{\pi}\sigma + 2q} > 0$$

(iii) Using the Lagrange–Bürmann formula, we invert the power series (5.18) of $U = \Psi_\sigma(F)$ and obtain

$$\mathcal{D}F(U) = \sum_{i=1}^{\infty} A_i U^i \quad (5.22)$$

where $A_i = 0$ if i is even, and

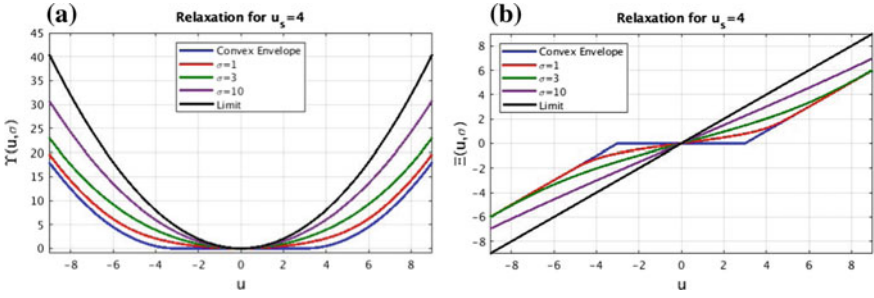


Fig. 5.7 Examples of relaxation of $\mathcal{D}W(u, \sigma)$ with $q = 1$: (a) Relaxation for different values of σ , (b) Corresponding force for (a)

$$A_1 = \frac{\sqrt{\pi}\sigma}{\sqrt{\pi}\sigma + 2k}, \quad A_3 = \frac{2k\pi^{3/2}\sigma}{3(\sqrt{\pi}\sigma + 2k)^4}, \quad A_5 = -\frac{(10\sigma^2 + 1)k\sigma^3\pi^{7/2}}{5(\sqrt{\pi}\sigma + 2k)^8},$$

$$A_7 = \frac{\pi^{7/2}(15\pi\sigma^2 - 276k\sigma\sqrt{\pi} + 508k^2)k\sigma}{315(\sqrt{\pi}\sigma + 2k)^{10}}$$

etc.

- (iv) The potential energy of the dynamically homogenized chain is obtained by integration of (5.22)

$$\mathcal{D}V(U, \sigma) = \int_0^U \mathcal{D}F(x, \sigma)dx = \sum_{n=2}^{\infty} \frac{A_{n-1}}{n} F^n$$

Fig. 5.7 illustrates the dynamically relaxed force-elongation dependence.

5.5 Validation of the Model

5.5.1 Numerical Issues

5.5.1.1 Remarks on the Numerical Procedure

Numerics were gathered with MATLAB’s `ode45` Inc. [5] as the primary solver. However, the solver could not reliably conserve energy. This was compensated for by rescaling the velocities of the masses. Given initial system energy E , and time-averaged system potential, and kinetic energies \bar{V} and \bar{K} over the correction time interval $[t_0 - T, t_0]$ of length T , the following formula was used to alter the velocities v_i of the small masses $i = 1, \dots, n - 1$ to new velocities \hat{v}_i :

$$\bar{V} = \frac{1}{T} \int_{t_0-T}^{t_0} V(\tau) d\tau, \quad \bar{K} = \frac{1}{T} \int_{t_0-T}^{t_0} K(\tau) d\tau,$$

$$K_{\text{exp}} = E - \bar{V}, \quad \hat{v}_i := \sqrt{\frac{K_{\text{exp}}}{\bar{K}}} v_i$$

This correction maintains the system energy within acceptable bounds.

5.5.1.2 Data

The simulation shows an agreement with the model, as is evident from Figs. 5.8 and 5.9. Figure 5.8 is numerical data for force versus elongation with a normalized kinetic energy $Q_N = \frac{E_I}{2}$. The blue line represents the force function for a single spring, the red is the numerical data for time-averaged force, and the green is the erf-approximation. Figure 5.9 contains the same curve fitting as Fig. 5.8, but for different energies. The numerical results are close to $DF(F)$, with consistent error dependent on dispersion.

5.5.1.3 Errors

Figure 5.10 shows the error of the prediction. The magnitude of the error decreases as the excitation energy increases. The noise in the error increases along with the excitation energy likely due to increasing errors in the ODE solver as the velocity through the unstable region increases. The errors follow a consistent shape for the varying values of Q_N ; the primary differences between different Q_N values are the broader dispersion and decreasing amplitude.

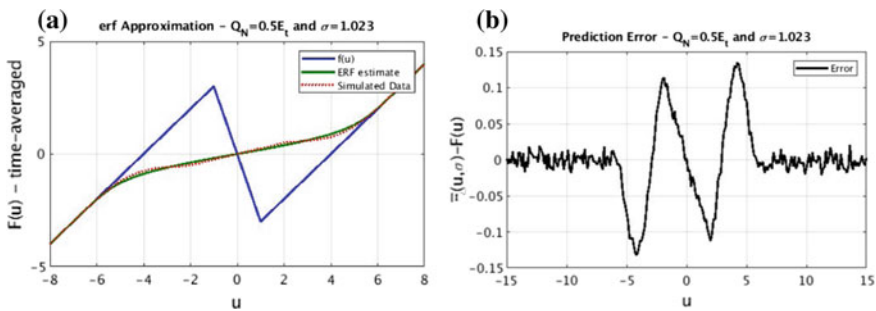


Fig. 5.8 Numerical results and the prediction for $Q_N = \frac{1}{2}E_I$: **a** Fit for $Q_N = \frac{E_I}{2}$, **b** Error of fit

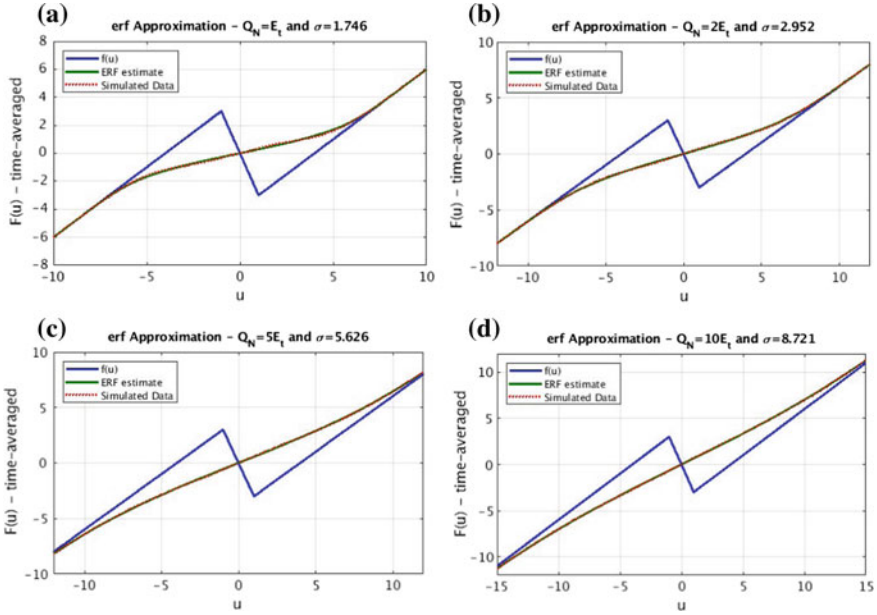


Fig. 5.9 a Fit for $Q_N = E_t$, b Fit for $Q_N = 2E_t$, c Fit for $Q_N = 5E_t$, d Fit for $Q_N = 10E_t$

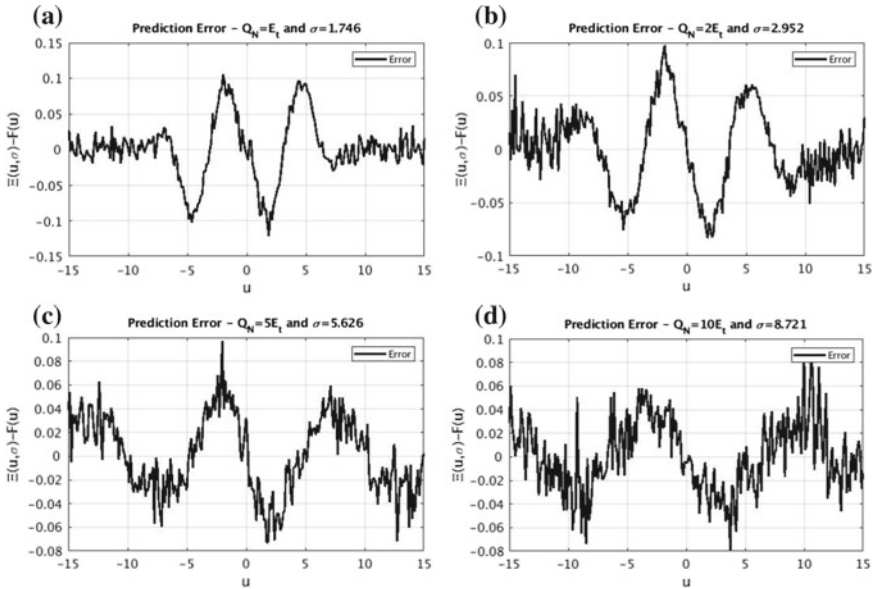


Fig. 5.10 Approximation errors for various energies: a Error for $Q_N = E_t$, b Error for $Q_N = 2E_t$, c Error for $Q_N = 5E_t$, d Error for $Q_N = 10E_t$

5.5.1.4 Stickiness

Lower values of excitation energy Q_N resulted in a more significant inconsistency in the data due to simulating over a fixed time interval. For $Q_N \ll V_B$, the data tended to “stick” the spring’s force graph between the stable equilibria—a region where analytics suggest that the force should be near zero—as illustrated in Fig. 5.11. At such energy level, the average time interval between transitions of the springs is large ($\bar{\tau} \gg \bar{T}$). The system is biased to the initial conditions rather than show the long-term average, explaining the observed “sticking” of the data.

However, for the larger excitation energy values of $Q_N \geq E_t$, no such “sticking” was visible, and the approximation was monotonic.

5.5.2 Relationship of Excitation Energy and Dispersion

The relationship between the excitation energy Q_N and the dispersion parameter σ of Ξ and Υ is determined only numerically. The data shown in Table 5.1 and Fig. 5.12 suggest a slightly sublinear trend on a log–log comparison for the interval examined. We postulated the dependence of type

$$\sigma \approx \beta \left(\frac{Q_N}{E_t} \right)^\alpha$$

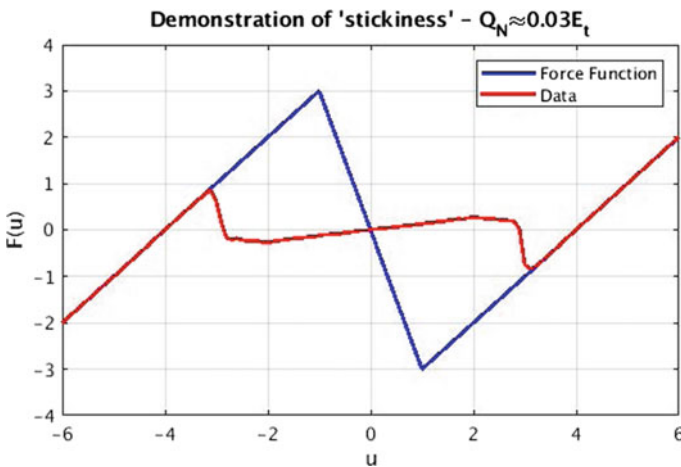


Fig. 5.11 Example of “stickiness.” The time-averaged force curve is deflected away from the nearly quasistatic prediction and toward the single-spring force curve

Table 5.1 Table comparing Q_N and σ

Q_N/E_t	σ
0.5	1.023
1	1.746
2	2.952
5	5.626
10	8.721
20	13.13
100	32.56

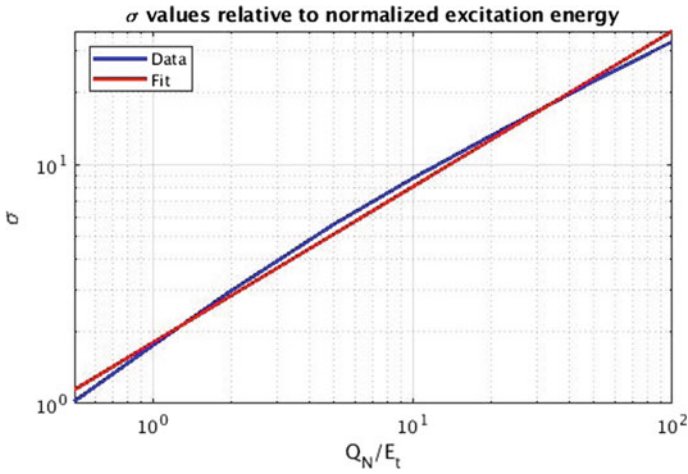


Fig. 5.12 Correspondence between Q_N and σ on a log-log chart. Fit is $\sigma_p = 1.793 \left(\frac{Q_N}{E_t}\right)^{0.6513}$

and found α, β to fit the data. The best fit for the above data yields $\alpha = 0.6513$, $\beta = 1.793$; however, we do not generalize this dependence to values of Q_N , not in the interval.

The asymptotic cases of Q_N can be established from the analytic solutions in Sect. 5.3. As $Q_N \rightarrow 0$, the system approaches the quasistatic mode. One observes that this corresponds with $\sigma = 0$. Furthermore, as $Q_N \rightarrow \infty$, the approximation of the system becomes increasingly linear. Similar behavior only occurs in Ξ as σ approaches infinity. We can thus conclude

$$\lim_{Q_N \rightarrow 0} \sigma = 0, \quad \lim_{Q_N \rightarrow \infty} \sigma = \infty \tag{5.23}$$

Finally, we observe that σ is a monotonic function of Q_N . In the interval investigated, the relation can be approximated with the power function

$$\sigma \approx 1.793 \left(\frac{Q_N}{E_t} \right)^{0.6513}$$

5.6 Conclusions

The relaxed energy of a spring depends on both elongation and system energy, rather than on just the elongation. The value of σ measures how relaxed Υ is toward the parabolic limit; greater values of σ correspond to greater relaxation toward that limit.

We model uncertain dynamics by introducing random mode change and the Central Limit Theorem for homogenization that replaces the mass-spring chain with a single nonlinear spring. The replacement with Ξ is numerically validated, particularly at higher energies. Increasing the excitation energy of the system decreases the error $|F(u) - \Xi(u, \sigma)|$ when the optimal dispersion σ is chosen.

Acknowledgements The research was supported by NSF DMS Grant 1515125 and by Office of Undergraduate Research, University of Utah.

References

1. Cherkaev, A., Cherkaev, E., Slepyan, L.: Transition waves in bistable structures. I. Delocalization of damage. *J. Mech. Phys. Solids* **53**(2):383–405 (2005a)
2. Cherkaev, A., Vinogradov, V., Leelavanishkul, S.: The waves of damage in elastic-plastic lattices with waiting links: design and simulation. *Mech. Mater.* **38**, 748–756 (2005b)
3. Efendiev, Y.R., Truskinovsky, L.: Thermalization of a driven bi-stable FPU chain. *Continuum. Mech. Thermodyn.* **22**, 679–698 (2010)
4. Frazier, M.J., Kochmann, D.M.: Band gap transmission in periodic bistable mechanical systems. *J. Sound Vib.* **388**, 315–326 (2017)
5. Inc TM: ode45 documentation. <https://www.mathworks.com/help/matlab/ref/ode45.html>, accessed: 2019-4-23 (2018)
6. Mishuris, G., Movchan, A., Slepyan, L.: Dynamics of a bridged crack in a discrete lattice. *Q. J. Mech. Appl. Math.* **61**, 151–160 (2008)
7. Morillo, M., Gómez-Ordóñez, J., Casado, J.M.: Equilibrium and stochastic resonance in finite chains of noisy bistable elements. *Chem. Phys.* **375**(2–3), 416–423 (2010)
8. Nadkarni, N., Daraio, C., Kochmann, D.M.: Dynamics of periodic mechanical structures containing bistable elastic elements: from elastic to solitary wave propagation. *Phys. Rev. E Stat. Nonlinear Soft Matter Phys.* **90**(2) (2014)
9. Nekorkin, V.I., Makarov, V.A.: Spatial chaos in a chain of coupled bistable oscillators. *Phys. Rev. Lett.* **74**(24) (1995)
10. Puglisi, G., Truskinovsky, L.: Mechanics of a discrete chain with bi-stable elements. *J. Mech. Phys. Solids* **48**, 1–27 (2000)
11. Rosenblatt, M.: A central limit theorem and a strong mixing condition. *Proc. Natl. Acad. Sci. U.S.A.* **42**(1) (1956)

12. Slepyan, L.: *Models and Phenomena in Fracture Mechanics*. Springer, Berlin (2002)
13. Slepyan, L.: Structural discontinuity as generalized strain and Fourier transform for discrete-continuous systems. *Int. J. Eng. Sci.* **130**, 199–214 (2018)
14. Slepyan, L., Ayzenberg-Stepanenko, M.V.: Localized transition waves in bistable-bond lattices. *J. Mech. Phys. Solids* **52**(7), 1447–1479 (2004)
15. Slepyan, L., Cherkaev, A., Cherkaev, E.: Transition waves in bistable structures. II. Analytical solution: wave speed and energy dissipation. *J. Mech. Phys. Solids* **53**(2), 407 – 436 (2005)
16. Vainchtein, A., Vleck, E.S.V.: Nucleation and propagation of phase mixtures in a bistable chain. *Phys. Rev. B* **79**(14) (2009)
17. Zhao, Q., Purohit, P.K.: Extracting a kinetic relation from the dynamics of a bistable chain. *Model. Simul. Mater. Sci. Eng.* **22**(4), 045004 (2014). URL <http://stacks.iop.org/0965-0393/22/i=4/a=045004>
18. Zhao, Q., Purohit, P.K.: (Adiabatic) phase boundaries in a bistable chain with twist and stretch. *J. Mech. Phys. Solids* **92**, 176–194 (2016)

Chapter 6

Analysis of Resistance to Penetration of a Cone into Frozen Sand Based on Data from Inverted Experiments



Anatoliy Bragov, Vladimir V. Balandin, Vladimir VI. Balandin,
Leonid Igumnov and Vasiliy Kotov

Abstract The laws of contact interaction between rigid and deformable strikers with dry and water-saturated soils in a wide range of temperatures were studied experimentally. Studies of the processes of impact and penetration of a steel conical striker into frozen sandy soil were carried out on the basis of the inverse experiment employing methodology of measuring bars. The dependences of the maximal values of the resistance force to penetration into soil of cones as a function of impact velocity ranging from 100 to 400 m/s are presented. The condition of sandy soil samples before freezing at a temperature of $-18\text{ }^{\circ}\text{C}$ is characterized by almost complete water saturation. A comparative analysis of the forces resisting to penetration of a striker into compacted dry, water-saturated and frozen sandy soil has been carried out. The resistance of frozen soil to penetration at low impact velocities significantly exceeds the resistance of dry and water-saturated soils. According to the results of the present experiments, at impact velocities over 300 m/s, the resistance curves of frozen and water-saturated soil tend to approach each other.

Keywords Impact · Penetration · Inverse experiment · Conical striker · Frozen sandy soil

A. Bragov · V. V. Balandin · V. VI. Balandin · L. Igumnov · V. Kotov (✉)
Research Institute of Mechanics, National Research Lobachevsky State University of Nizhny
Novgorod, Nizhny Novgorod 603950, Russian Federation
e-mail: vkotov@inbox.ru

A. Bragov
e-mail: bragov@mech.unn.ru

V. V. Balandin
e-mail: balandin@mech.unn.ru

V. VI. Balandin
e-mail: rustydog2007@yandex.ru

L. Igumnov
e-mail: igumnov@mech.unn.ru

6.1 Introduction

The behavior of frozen soil is well studied in the experiments on uniaxial and triaxial compression at pressures up to 20 MPa and strain rates up to 10^{-2} s^{-1} [1–3]. Higher strain rates of the order of $10^2\text{--}10^3 \text{ s}^{-1}$ were realized in the experiments using the SHPB system [4, 5], in which the deformation diagrams of frozen sand were obtained at a temperature of $-28 \text{ }^\circ\text{C}$. The experimental data are used to equip mathematical models of the elastic–plastic behavior of soil with various approximations of yield and failure surfaces [1–5]. Models that are more complex explicitly take into account the dependence on temperature [6] or the influence of incompletely frozen water [7]. The elastic properties of frozen sand, characterized by the velocities of propagation of compression and shear waves, were determined in [8–11]. It was found that the velocity of a longitudinal wave in a water-saturated frozen soil at temperatures below $-10 \text{ }^\circ\text{C}$ could amount to 3–4 km/s.

An experimental complex for determining the main parameters of the process of impact and penetration of solid deformable bodies into soft soil media, based on the methodology of the inverse experiment with a measuring bar, was presented earlier in [12–17]. The forces resisting penetration of flat-ended strikers with hemispherical heads into compacted dry sandy soil are determined. Peculiar features of determining the maximal resistance force and the force values at quasi-stationary state of penetration of a flat-ended striker into a water-saturated soil, associated with dispersion during the propagation of short pulses of force in a measuring bar, were demonstrated. The maximal values of the force resisting to penetration of a hemispherical striker into dry, wet and water-saturated sandy soils were determined [17].

However, the results of impact experiments with frozen soil are not presented well enough in the available literature, though they could be used for numerical verification of mathematical models. The paper presents new results of inverse experiments, in which time histories of the resistance force and the dependences of the maximum values of the resistance to penetration of a conical striker into frozen sand were determined.

6.2 Measuring Bars Methodology in Inverse Experiment

Measuring bars methodology in inverse experiment was used to determine the resistance forces acting on heads during penetration into frozen sand. In the inverse experiment, a resistance force was measured at an initial stage of penetration. The technique of measuring the force resisting the penetration of a striker into the sand using a measuring bar is as follows [12]. A container filled with sand is accelerated up to the required velocities and impacted against a stationary striker fixed on a measuring bar. The impact velocity and material properties of the bar are to be such that no plastic strains should occur in the bar. In this case, an elastic strain pulse $\varepsilon(t)$ is formed in the bar. Registering this pulse makes it possible to determine

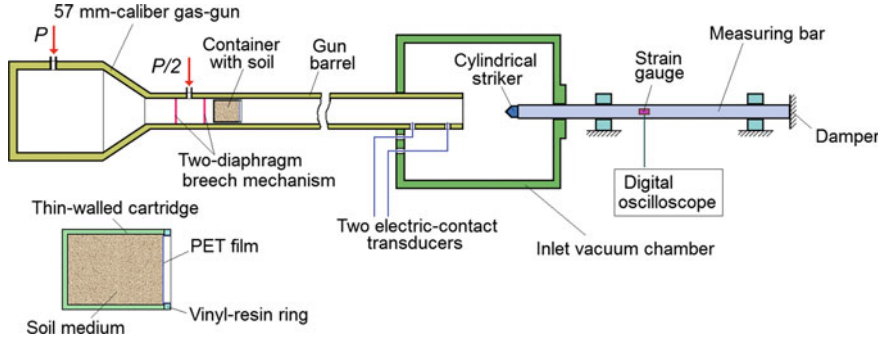


Fig. 6.1 Schematic representation of the setup for measuring forces resisting to penetration in the inverse experiment

force F , acting on the striker upon its interaction with the medium, according to the well-known relation $F(t) = E\varepsilon(t) S$, where E is elastic modulus of the bar, S is its cross-sectional area. Thus, in this method, the task of measuring forces is greatly simplified and reduced to registering an elastic strain pulse in the bar, using strain gages. The setup implementing this method is schematically depicted in Fig. 6.1. In the present version of the inverse experiment, a soil container is accelerated using a 57 mm—caliber gas-gun with a two-diaphragm breech mechanism, which makes it possible to provide stable and easily controlled impact velocities in the range of 50–500 m/s.

The container is a thin-walled cartridge, made of D16T aluminum alloy and filled with soil medium. To prevent soil from spilling in the process of preparation of the experiment and during the acceleration of the container, the front part of the container is sealed with 0.01-mm-thick PET film. The film is fixed and secured against the soil surface with a vinyl-plastic ring.

The impact velocity of the container was determined using two electric-contact transducers located in the orifices of the barrel drilled in front of its muzzle. A 1.5-m-long and 20-mm-diameter steel rod with a yield strength of over 2000 MPa was used as a measuring bar. One of the ends of the measuring bar has a threaded orifice (M10) housing a cylindrical striker with a head of appropriate geometry. The bar is located at a certain distance from the barrel muzzle, so that the impact occurs immediately after the container entirely leaves the barrel. The stand, on which the bar is located, has adjusting supports, which ensure the axisymmetric nature of the interaction. The rear end of the bar rests against a special damper, preventing it from displacement and damping the impact energy. Impact takes place inside the vacuum chamber, to which the gun barrel is connected and into which the measuring bar with the striker is inserted. The cylindrical parts of the striker heads were 19.8 mm in diameter, with a hemisphere radius of 10 mm, and were made of 45 steel ($\sigma \geq 600$ MPa) and EP638 steel ($\sigma \geq 1800$ MPa).

The measuring bar was made of 03N18K9M5T steel with the density of 8050 kg/m³, Young's modulus of 186 GPa and yield strength of 2 GPa. The bar



Fig. 6.2 Heads of measuring bars used in the inverse experiments

was 20.5 mm in diameter and 1.5 m in length. At one end, the bar had a threaded orifice (M10) for screwing in heads of required geometries. The conical heads with a cone angle of 60° were used in the experiments. There were two types of the heads with a base diameter of 19.8 mm and 10 mm, respectively. The heads were made of 03N18K9M5T steel.

Besides, the effect on the experimental results of the threaded connections and joints between the head and the bar was evaluated using a 12-mm-diameter 30HGSA steel with a yield strength of 700 MPa. One of the ends of the bar was in the form of a cone with an angle of 60° (Fig. 6.2).

The experiments were carried out with a sand mixture of natural composition, from which particles larger than 1 mm and smaller than 0.1 mm had been removed. The accelerated containers were filled with dry sand, which was then compacted to an average density of about 1750 kg/m^3 . The containers were made of D16T alloy in the form of a thin-walled 70 mm high cylindrical cartridge with a wall thickness of 1.4 mm, an outer diameter of 56.8 mm and a bottom thickness of 2 mm. The containers were weighed to find the mass and density of the dry sand, and then gradually filled with water until the sand was fully saturated. Further humidification resulted in the formation of a water layer over the surface of the sand, so the excess water was poured off. The containers were weighed again to determine the density of the water-saturated sand and its moisture content relative to its initial density. The average density of the water-saturated natural mixture was respectively $2090 \pm 2050 \text{ kg/m}^3$. Since sand mainly consists of quartz particles, the density of which is 2650 kg/m^3 , thus, the porosity of sand is 0.34. When all the cavities are completely filled with water, the density of the humid sand should increase by 340 kg/m^3 , and the density of the water-saturated sand should be equal to 2090 kg/m^3 , which actually



Fig. 6.3 Container with frozen sand used in the inverse experiments

was the case during the preparation of the experiments. The moisture content of water-saturated sand was 18–19%. Then, the container with water-saturated soil was frozen at $-18\text{ }^{\circ}\text{C}$ in a freezer for at least 2 days.

When freezing, some of the water was displaced from the sand (since the density of ice is somewhat lower than that of water). The surface of the container got covered with a layer of ice which was removed before the experiment. After that, the container (Fig. 6.3) was weighed to find the density of the frozen sand. The average density of the frozen sand was $2050 \pm 50\text{ kg/m}^3$.

6.3 Mathematical Formulation of the Impact and Penetration Problem

To get a better insight into the processes taking place during the impact of solid bodies against soil and to choose the conditions for inverse experiments, numerical methods evaluating the influence of geometric dimensions of the containers on the integral loads at the initial, nonstationary state of penetration into frozen soil were used in the present study. The computations were done using Grigoryan's model of soil media, which contains a system of differential equations expressing laws of conservation of mass, pulse and constant maximal attained in the process of actively loading the soil, as well as equations of the theory of plastic flow with plasticity condition of Mises-Schleicher. The system of differential equations is closed with finite relations determining pressure and a fractional-rational function in the condition of plasticity of the soil medium. The applied Grigoryan's model of soil media describes failure

of the structure of frozen soil under compression and the increase in shear resistance with increasing pressure [15, 16].

The system of equations of soil dynamics is complemented by initial and boundary conditions. A contact algorithm of “impermeability” along the normal line with “sliding along the tangent with dry friction” is used on the head of a conical striker contacting with soil medium, in accordance with Coulomb’s friction model with a constant friction coefficient. The normal and shear stresses on the free surfaces of the soil and the striker were set equal to zero. The outer boundaries of the computed soil region correspond to the geometric dimensions of the container used in the inverse experiment. The deformation of the container is not accounted; the effect of the container walls is modeled by two versions of imposing the boundary conditions: “impermeability” along the normal and free sliding in the tangential direction and “free surface,” corresponding to the absence of any walls. Stresses and velocity of the soil particles are equal to zero at an initial time. The striker is assumed to be rigid, moving at a constant speed equal to the impact velocity.

6.4 The Data from Inverted Experiments and Calculations

Figure 6.4 presents the pulses of resistance force obtained in inverse experiments acting on the cones with different basis diameters: 10 mm, 12 mm and 20 mm, at impact velocities of 356 m/s, 354 m/s and 339 m/s, respectively. The maximum is reached when the cone is completely immersed into the soil. Until the maximum is reached, a time interval is noted, which is characterized by an increase in force close to a parabolic one and practically coincides for all used strikers. No signs of

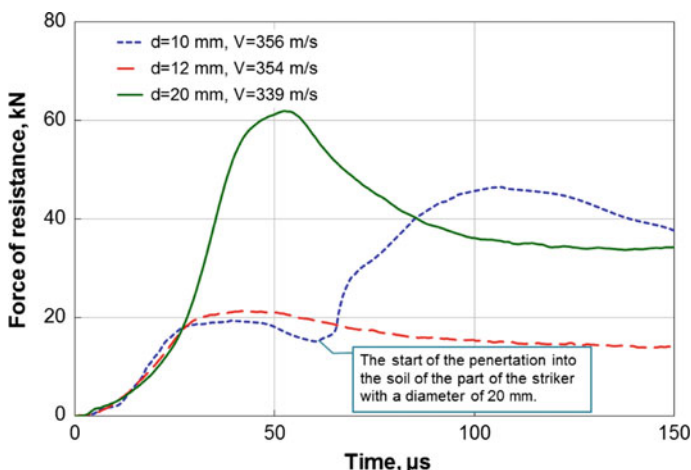


Fig. 6.4 Dependences of the force resisting to the penetration cones into frozen soil obtained during inverse experiments

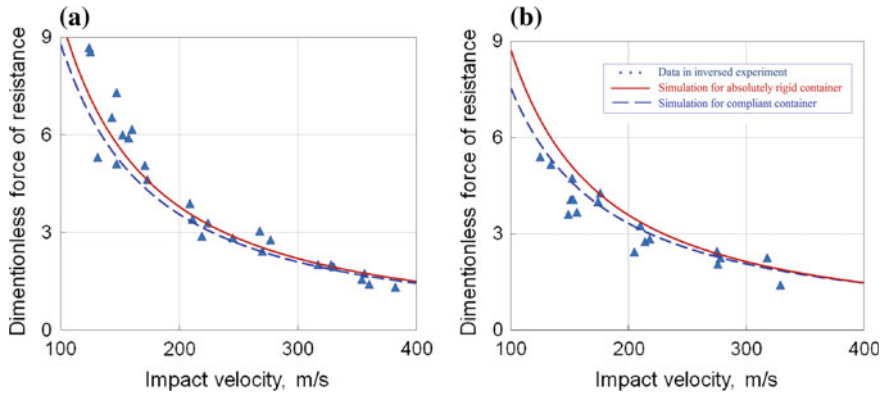


Fig. 6.5 Dimensionless dependences of the maximal values of the force resisting penetration of cones with a base diameter of $d = 10$ (a) and 12 (b) as a function of impact velocity, obtained in inverse experiments and numerical results

the effect of the joints on the pulse shape were revealed on the dependences of the force on time.

Figure 6.5 presents dimensionless dependences of the maximal values of the force resisting penetration of cones with a base diameter of $d = 10$ (a) and 12 (b) as a function of impact velocity. The data presented in Fig. 6.5 were obtained in inverse experiments (dark triangles); the solid and dashed lines correspond to the results of numerical calculations with boundary conditions that simulate absolutely rigid and compliance containers. Good agreement between the experimental data and numerical results is evident. The containers in the experiments were assumed to be compliant for all considered diameters of conical strikers. The proximity (taking into account the variability of experimental data) of the maximal values of the forces resisting penetration of conical strikers of 10 and 12 mm in diameter at impact velocities of more than 150 m/s is to be noted. All dimensionless resistance forces exhibit a similar change from 3 to 1.5 at velocities from 200 to 400 m/s.

Figure 6.6 shows the dimensionless dependences of the maximal values of the force resisting penetration of the cone into the frozen (dark triangles and solid line), compacted dry (oblique crosses and dashed lines) and water-saturated soil (light triangles and dash-dotted lines). The markers correspond to the data of the inverse experiment; the lines show the results of axisymmetric numerical computations of the cone penetration into half-space of the soil.

6.5 Conclusion

For the problems of penetration of conical strikers into frozen and water-saturated soil, a good agreement between experimental data and numerical results can be

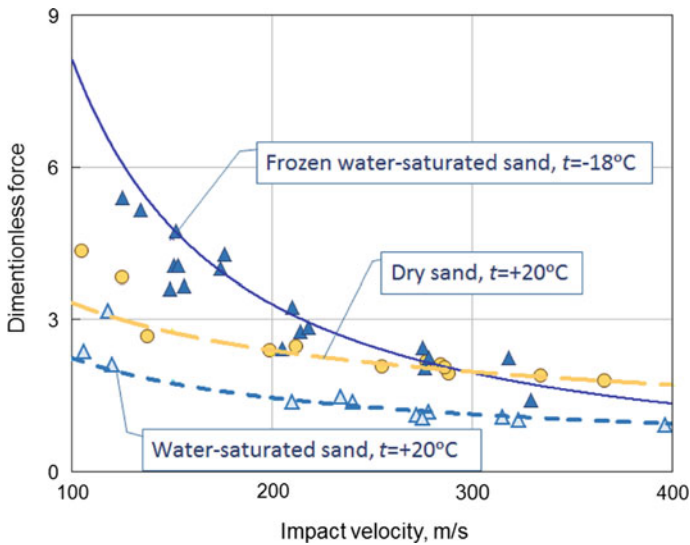


Fig. 6.6 Dimensionless dependences of the maximal values of the force resisting penetration of cones into frozen, dry and water-saturated soil as a function of impact velocity, obtained in inverse experiments and numerical results

obtained with the help of Grigoryan's model accounting for the pressure-dependent parameters. No significant effect of the threaded connection and joints between the head and the bar on the experimental results was found. This widens the scope of the inverse experiment methodology and the measuring bars technique by way of using changeable heads of required geometries. Resistance of frozen soil to penetration at low impact velocities is significantly higher than that of dry and especially water-saturated soils. According to the present experimental results, at impact velocities over 300 m/s, the resistance diagrams for the frozen and water-saturated soils tend to approach each other.

Acknowledgements The work is financially supported by the Federal Targeted Program for Research and Development in Priority Areas of Development of the Russian Scientific and Technological Complex for 2014–2020 under the contract No. 14.578.21.0246 (unique identifier RFMEFI57817X0246) in part of modeling and by the Russian Science Foundation (Grant No. 16-19-10237-P) in part of experiments

References

1. Shujuan, Z., Yuanming, L., Zhizhong, S., Zhihua, G.: Volumetric strain and strength behavior of frozen soils under confinement. *Cold Reg. Sci. Technol.* **47** (2007)
2. Yuanming, L., Long, J., Xiaoxiao, C.: Yield criterion and elasto-plastic damage constitutive model for frozen sandy soil. *Int. J. Plast.* **25** (2009)

3. Yugui, Y., Yuanming, L., Jingbo, L.: Laboratory investigation on the strength characteristic of frozen sand considering effect of confining pressure. *Cold Reg. Sci. Technol.* **60** (2010)
4. Haimin, D., Wei, M., Shujuan, Z., Zhiwei, Z., Enlong, L.: Strength properties of ice-rich frozen silty sands under uniaxial compression for a wide range of strain rates and moisture contents. *Cold Reg. Sci. Technol.* **123** (2016)
5. Qin-Yong, M.: Experimental analysis of dynamic mechanical properties for artificially frozen clay by the split Hopkinson pressure bar. *J. Appl. Mech. Tech. Phys.* **51**, 3 (2010)
6. Qijun, X., Zhiwu, Z., Guozheng, K.: Dynamic stress–strain behavior of frozen soil: Experiments and modeling. *Cold Reg. Sci. Technol.* 106–107, (2014)
7. Yang, R., Lemarchand, E., Fen-Chong, T., Azouni, A.: A micromechanics model for partial freezing in porous media. *Int. J. Solids Struct.* 75–76, (2015)
8. Zhiwu, Z., Guozheng, K., Yue, M., Qijun, X., Dan, Z., Jianguo, N.: Temperature damage and constitutive model of frozen soil under dynamic loading. *Mech. Mat.* **102** (2016)
9. Christ, M., Park, J.: Ultrasonic technique as tool for determining physical and mechanical properties of frozen soils. *Cold Reg. Sci. Technol.* **58** (2009)
10. Park, J., Lee, J.: Characteristics of elastic waves in sand–silt mixtures due to freezing. *Cold Reg. Sci. Technol.* **9** (2014)
11. Ling, X.Z., Zhang, F., Li, Q.L., An, L.S., Wang, J.H.: Dynamic shear modulus and damping ratio of frozen compacted sand subjected to freeze–thaw cycle under multi-stage cyclic loading. *Soil Dyn. Earthq. Eng.* **76** (2015)
12. Balandin, V.V., Bragov, A.M., Igumnov, L.A., Konstantinov, A.Yu., Kotov, V.L., Lomunov, A.K.: Dynamic deformation of soft soil media: experimental studies and mathematical modeling. *Mech. of Solids* **50**, 3 (2015)
13. Balandin, V.I., Balandin, V.I., Bragov, A.M., Kotov, V.L.: Experimental study of the dynamics of penetration of a solid body into a soil medium. *Tech. Phys.* **61**(6) (2016)
14. Kotov, V.L., Balandin, V.V., Bragov, A.M., Balandin, V.I.: Investigation of dynamic resistance to the shear of water-saturated sand according to the results of the inverse experiment technique. *Tech. Phys. Let.* **43**(9) (2017)
15. Kotov, V.L., Balandin, V.I., Balandin, V.I. et al.: Application of the reverse experiment to study the resistance of a conical shocker during penetration in frozen sand. *Probl. Strength Plast.* **79**(2) (2017) [In Russian]
16. Bragov, A.M., Balandin, V.I., Kotov, V.L., Balandin, V.I.: Investigation of the dynamic properties of water-saturated sand by the results of inverted experiments. *Tech. Phys.* **63**(4) (2018)
17. Bragov, A.M., Balandin, V.V., Igumnov, L.A., Kotov, V.L., Kruszka, L., Lomunov, A.K.: Impact and penetration of cylindrical bodies into dry and water-saturated sand. *Int. J. Impact Eng.* **122** (2018)

Chapter 7

Some Solutions of Dynamic and Static Nonlinear Nonautonomous Klein-Fock-Gordon Equation



Anatolii N. Bulygin and Yuri V. Pavlov

Abstract Methods of constructing exact analytical solutions of dynamic and static nonlinear nonautonomous Klein-Fock-Gordon (NKFG) equations are developed. Solutions are given in the form of a composite function $U = f(W)$. For dynamic equations, the function $W(x, y, z, t)$ (ansatz) is constructed so that the function $f(W)$ is explicitly found. For static equations, the ansatz $\theta(x, y, z)$ is chosen as a root of equations of algebraic surface families that are used to transition to the curved coordinates. It is shown that such ansatzes allow us to construct exact analytical solutions of some static nonautonomous NKFG equations.

Keywords Klein-Fock-Gordon equation · Nonautonomous equation · Exact solution · Ansatz

7.1 Introduction

A large amount of papers are devoted to the study of the dynamic

$$U_{xx} + U_{yy} + U_{zz} - \frac{U_{tt}}{v^2} = p(x, y, z, t) F(U) \quad (7.1)$$

and static

$$U_{xx} + U_{yy} + U_{zz} = p(x, y, z) F(U) \quad (7.2)$$

nonautonomous Klein-Fock-Gordon (NKFG) equations. Here, $p(x, y, z, t)$ and $F(U)$ are arbitrary functions of their arguments, v is a constant, and the subscript means the derivative with respect to the corresponding variable. Equation (7.1) appears in many

A. N. Bulygin (✉) · Y. V. Pavlov
Institute for Problems in Mechanical Engineering of Russian Academy of Sciences,
61 Bol'shoy, V.O., Saint Petersburg 199178, Russia

branches of modern applied and theoretical physics, mechanics, and mathematics; it describes dislocations in solids [1], the deformation of a nonlinear crystal lattice [2, 3], properties of ferromagnets [4], the orientation of liquid crystals (LC) [5], and many other phenomena and processes. Most of studied concern the autonomous NKFG equations at ($p = \text{const}$). However, this condition imposes strict restrictions on the physical properties of the media under study and external influences on them. For example, when describing the deformation of a nonlinear crystal lattice, the value of p makes sense of half of the height of the energy barrier for the crystal lattice atoms. The condition $p = \text{const}$ requires that the crystal lattice should be perfect and contains no defects. In the LC physics, the value p is equal to the moment M of the external forces that change the orientation structure of LC. For the case when the orientation of the LC medium is changed by the electromagnetic field (E, H), the moment is $M = M(E, H, \varepsilon_{ik}, \chi_{ik})$. Apart from (E, H), the moment depends on the dielectric constant ε_{ik} and diamagnetic susceptibility χ_{ik} . The case of $p = \text{const}$ requires that the medium is uniform, $(\varepsilon_{ik}, \chi_{ik}) = \text{const}$, the orientation structure contains no defects, and the electromagnetic field (E, H) is constant. The NKFG equations, ($p \neq \text{const}$), describe the physical processes more adequately. There are practically no analytical methods of solutions to these equations in the literature. Methods of finding exact analytical solutions of some nonautonomous dynamic and static NKFG equations will be described below. The methods are based on the ideas and methods of finding functional invariant solutions of the wave equation. They develop the methods that have been proposed earlier [6–10].

7.2 Methods of Construction of Exact Analytical Solutions of Dynamic and Static Nonautonomous Nonlinear Klein-Fock-Gordon Equations

The solutions of Eq. (7.1) are sought in the form of a composite function,

$$U = f(W). \quad (7.3)$$

The function $W(x, y, z, t)$ is called ansatz. Then, Eq. (7.1) takes the form

$$f_{WW} \left[W_x^2 + W_y^2 + W_z^2 - \frac{W_t^2}{v^2} \right] + f_W \left[W_{xx} + W_{yy} + W_{zz} - \frac{W_{tt}}{v^2} \right] = p F[f]. \quad (7.4)$$

Suppose that the ansatz $W(x, y, z, t)$ is the solution of one of the following differential equations,

$$1. \quad W_x^2 + W_y^2 + W_z^2 - \frac{W_t^2}{v^2} = 0, \quad W_{xx} + W_{yy} + W_{zz} - \frac{W_{tt}}{v^2} = p(x, y, z, t), \quad (7.5)$$

$$2. W_x^2 + W_y^2 + W_z^2 - \frac{W_t^2}{v^2} = p(x, y, z, t), \quad W_{xx} + W_{yy} + W_{zz} - \frac{W_{tt}}{v^2} = 0, \quad (7.6)$$

$$3. \begin{aligned} W_x^2 + W_y^2 + W_z^2 - \frac{W_t^2}{v^2} &= q(x, y, z, t)P(W), \\ W_{xx} + W_{yy} + W_{zz} - \frac{W_{tt}}{v^2} &= q(x, y, z, t)Q(W). \end{aligned} \quad (7.7)$$

Here, $q(x, y, z, t)$, $P(W)$, and $Q(W)$ are arbitrary functions of their arguments. From Eqs. (7.4–7.6), it can be seen that if the ansatz W satisfies Eqs. (7.5) or (7.6), then the problem of finding the function $f(W)$ is reduced to obtain the solution of ordinary differential equations of the first and second orders,

$$1. f_W = F(f), \quad \int \frac{df}{F(f)} = W + C, \quad (7.8)$$

$$2. f_{WW} = F(f), \quad \int \frac{df}{\sqrt{E + V(f)}} = \pm\sqrt{2}(W + C), \quad (7.9)$$

Here, (E, C) are the integration constants and $V_f = F(f)$.

If the ansatz $W(x, y, z, t)$ satisfies Eqs. (7.7), then we get an ordinary second-order differential equation to find the function $f(W)$

$$f_{WW}P(W) + f_WQ(W) = \frac{p(x, y, z, t)}{q(x, y, z, t)}F(f). \quad (7.10)$$

Let us multiply Eq. (7.10) by the arbitrary function $R(W)$ and apply the following conditions

$$(PR)_W = 2QR, \quad p(x, y, z, t) = \frac{q(x, y, z, t)}{R(W)}. \quad (7.11)$$

From the first equation in (7.11), we find

$$R(W) = \frac{A}{P(W)} \exp\left(2 \int \frac{Q(W)}{P(W)} dW\right). \quad (7.12)$$

Here, A is an integration constant. The second equation in (7.11) defines the function $p(x, y, z, t)$, for which the described method allows us to construct exact analytical solutions of the dynamic nonautonomous NKFG equation. In other words, this condition defines a class of nonautonomous NKFG equations that admit exact analytical solutions by this method.

Taking into account Eq. (7.12), we find

$$p(x, y, z, t) = \frac{q(x, y, z, t)}{A} P(W) \exp\left(-2 \int \frac{Q}{P} dW\right). \quad (7.13)$$

If the first condition in (7.11) is satisfied, then Eq. (7.10) is written as

$$\frac{d}{dW} \left[\frac{f_W^2}{2} RP - V(f) \right] = 0. \quad (7.14)$$

Equation (7.14) is solved in quadratures,

$$\int \frac{df}{\sqrt{E + V(f)}} = G(W), \quad G(W) = \pm \sqrt{2} \int \frac{dW}{\sqrt{P(W)Q(W)}}. \quad (7.15)$$

From Eqs. (7.8), (7.9), and (7.15), one can see that the proposed method of solving the equation allows us to find a solution $f(W)$ of Eq. (7.1) for arbitrary function $F(U)$ provided that the corresponding integrals exist. If they allow inversion, the solution $f(W)$ can be found in an explicit form. Thus, the proposed method reduces obtaining the solution of Eq. (7.1) to find the ansatz $W(x, y, z, t)$ from the Eqs. (7.5–7.7).

The proposed method of constructing exact analytical solutions of dynamic equation (7.1) is also fully applicable for finding solutions of the static equation (7.2) in the form of a composite function

$$U = f(\theta) \quad (7.16)$$

provided that the ansatz $\theta(x, y, z)$ is independent on time.

7.3 Ansatzes for Solution of Dynamic Equation

Ansatzes for finding solutions of Eq. (7.1) can be constructed by using the methods of finding functional invariant solutions of the wave equation [11]–[13]. Let us introduce the function $\tau(x, y, z, t)$, which is the root of the algebraic equation,

$$[x - \xi(\tau)]^2 + [y - \eta(\tau)]^2 + [z - \zeta(\tau)]^2 = v^2(t - \tau)^2. \quad (7.17)$$

Here, $\xi(\tau), \eta(\tau), \zeta(\tau)$ are the arbitrary functions. They define the function $\tau(x, y, z, t)$. Let us consider a simple case,

$$\xi = vx_1\tau, \quad \eta = vx_2\tau, \quad \zeta = vx_3\tau. \quad (7.18)$$

Then, we find from Eq. (7.17),

$$\tau = -\frac{X \pm \beta}{vR_0}, \quad \beta = \sqrt{X^2 + R_0s^2}, \quad R_0 \neq 0, \quad (7.19)$$

$$X = x_1x + x_2y + x_3z - vt, \quad s^2 = x^2 + y^2 + z^2 - v^2t^2, \quad R_0 = 1 - (x_1^2 + x_2^2 + x_3^2).$$

The function $\beta(x, y, z, t)$ contains the square root. Radicand is a quadratic form of four variables (x, y, z, t) . One can show that it is non-negative if $x_1^2 + x_2^2 + x_3^2 \leq 1$. Hence, the function $\beta(x, y, z, t)$ is real. We will choose the following functions for the ansatzes,

$$W = [\beta(x, y, z, t), \lambda(x, y, z, t), \chi(x, y, z, t)], \tag{7.20}$$

$$\lambda(x, y, z, t) = vw(\tau)\beta, \quad \chi(x, y, z, t) = \xi_\tau(x - \xi) + \eta_\tau(y - \eta) + \zeta_\tau(z - \zeta).$$

Here, $w(\tau)$ is an arbitrary function of τ . Obtaining the partial derivatives of the first and second orders, one can prove that

$$\beta_x^2 + \beta_y^2 + \beta_z^2 - \frac{\beta_t^2}{v^2} = R_0, \quad \beta_{xx} + \beta_{yy} + \beta_{zz} - \frac{\beta_{tt}}{v^2} = \frac{2R_0}{\beta}, \tag{7.21}$$

$$\lambda_x^2 + \lambda_y^2 + \lambda_z^2 - \frac{\lambda_t^2}{v^2} = \lambda\sigma, \quad \lambda_{xx} + \lambda_{yy} + \lambda_{zz} - \frac{\lambda_{tt}}{v^2} = 2\sigma, \tag{7.22}$$

$$\chi_x^2 + \chi_y^2 + \chi_z^2 - \frac{\chi_t^2}{v^2} = v^2R_0, \quad \chi_{xx} + \chi_{yy} + \chi_{zz} - \frac{\chi_{tt}}{v^2} = \frac{2v^2R_0}{\chi}. \tag{7.23}$$

Here

$$\sigma = 2w_\tau \left(\frac{vwR_0}{2\beta w_\tau} - 1 \right). \tag{7.24}$$

Taking into account Eqs. (7.21–7.23), Eq. (7.1) can be solved by the third way. Finally, we obtain

$$\int \frac{df}{\sqrt{E + V(f)}} = G(W), \quad G(W) = \pm\sqrt{2} \left[\left(c + \frac{1}{\beta} \right), \left(c + \frac{1}{\lambda} \right), \left(c + \frac{1}{\chi} \right) \right]. \tag{7.25}$$

Here, c is an integration constant. For the considered ansatzes, we have

$$p(x, y, z, t) = \left[\frac{R_0}{\beta^4}, \frac{\sigma}{\lambda^3}, \frac{v^2R_0}{\chi^4} \right]. \tag{7.26}$$

Ansatz $W(x, y, z, t)$ can be also a function of two variables. Let us consider the following cases,

$$W = \left[\frac{\Phi(\tau)}{\beta}, \frac{\Phi(\tau)}{\lambda}, \frac{\Phi(\lambda/\beta)}{\lambda} \right]. \tag{7.27}$$

Here, $\Phi(u)$ is an arbitrary function. One can show that ansatzes (7.27) are the wave functions. Therefore, their utilization allows us to solve Eq. (7.1) by the second way. For these solutions, the function $p(x, y, z, t)$ is

$$p(x, y, z, t) = \left[\frac{2\Phi^2(\tau)}{v\beta^3} \left(\frac{vR_0}{2\beta} + \frac{\Phi_\tau}{\Phi} \right), \frac{2\Phi^2(\tau)w}{\lambda^3} \left(\frac{\sigma}{2w} + \frac{\Phi_\tau}{\Phi} \right), \right. \\ \left. 2w_\tau \Psi^2 \left(\frac{R_0}{2w_\tau \beta^2} + \frac{\Psi_\lambda}{\Psi} \right) \right]. \quad (7.28)$$

In the last expression $\Psi = \Phi(\lambda/\beta)/\lambda$.

The number of the wave functions can be increased if one uses new coordinates that allow us to find the other wave functions from one function. So, if $f(x, y, z, t)$ is a wave function, then

$$\frac{1}{s^2} f \left(\frac{x}{s^2}, \frac{y}{s^2}, \frac{z}{s^2}, \frac{t}{s^2} \right), \quad (7.29)$$

and

$$\frac{1}{z - vt} f \left(\frac{x}{z - vt}, \frac{y}{z - vt}, \frac{s^2 - 1}{2(z - vt)}, \frac{s^2 + 1}{2v(z - vt)} \right) \quad (7.30)$$

will be also the wave functions [12].

Let us

$$W = [\Psi(\tau), \Psi(u), \Psi(v)]. \quad (7.31)$$

Here

$$u = \ln \lambda - \sigma \frac{\tau}{2w(\tau)}, \quad v = \frac{2\beta}{vR_0} + \tau.$$

The ansatzes (7.31) satisfy the equation

$$W_x^2 + W_y^2 + W_z^2 - \frac{W_t^2}{v^2} = 0 \quad (7.32)$$

and hence Eq. (7.1) can be solved by the first way. For these ansatzes, we have

$$p(x, y, z, t) = \left[\frac{2}{\chi} \Psi_\tau, \frac{\sigma}{\lambda} ((1 + \lambda)\Psi'' + 2\Psi'), \frac{2}{v\beta} \Psi' \right]. \quad (7.33)$$

Here, the prime denotes a derivative of a function with respect to its argument. Let us illustrate general methods for solving Eq. (7.1) by some particular examples.

7.4 Particular Solutions

Consider the cases where

$$F(U) = \{\sin U, \sinh U, \exp(mU)\}. \quad (7.34)$$

The integrals (7.8) and (7.9) exist and can be inverted for such functions. Finally, we find

$$F(U) = \left\{ 2 \tan^{-1} e^W, 2 \tanh^{-1} e^W, \frac{-1}{m} \log(E - mW) \right\}, \quad (7.35)$$

$$U = \begin{cases} 2 \tan^{-1} \left[\sqrt{1 - r^2} \operatorname{tn} \left(\frac{W}{r}, r \right) \right], \\ 2 \tanh^{-1} \left[\operatorname{sn} \left(\frac{W}{\sqrt{1 - r^2}}, r \right) \right], \\ \frac{2}{m} \log \left[\frac{\sqrt{Em}}{\sinh \left(W \frac{m\sqrt{E}}{\sqrt{2}} \right)} \right]. \end{cases} \quad (7.36)$$

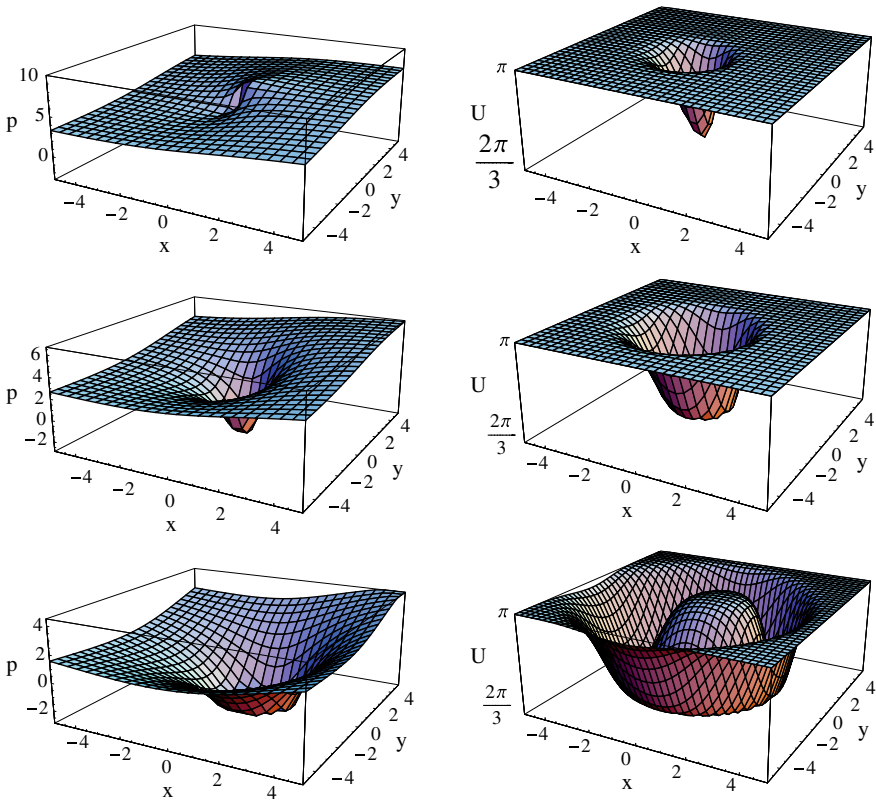


Fig. 7.1 Function p and solution U for $z = 0, t = 0$ (at the top), $t = 1$ (at the middle), $t = 3$ (at the bottom)

Here, E is an integration constant, $\operatorname{tn}(u, r) = \operatorname{sn}(u, r) / \operatorname{cn}(u, r)$, $\operatorname{sn}(u, r)$, $\operatorname{cn}(u, r)$ are the Jacobi elliptic functions ($0 \leq r \leq 1$).

In Fig. 7.1, the spatial plots of the amplitude $p(x, y, z, t)$ and the solution $U(x, y, z, t)$ are given for different times ($t = 0, 1, 3$) and for the case $F(U) = \sin U$, $W = \Psi(\tau)$, $w(\tau) = \tau^2$, $\tau = -(X + \beta) / (vR_0)$, $R_0 \neq 0$ (see (7.19)). One can see that $p(x, y, z, t)$ and $U(x, y, z, t)$ have the form of localized waves that change both their shape and size in time. The same forms of the functions $p(x, y, z, t)$ and $U(x, y, z, t)$ are shown in Fig. 7.2 for solution (7.27) with $F(U) = \exp U$, $W = \Phi(\tau) / \lambda$, $w(\tau) = \tau$, $\tau = -(X + \beta) / (vR_0)$, $R_0 \neq 0$.

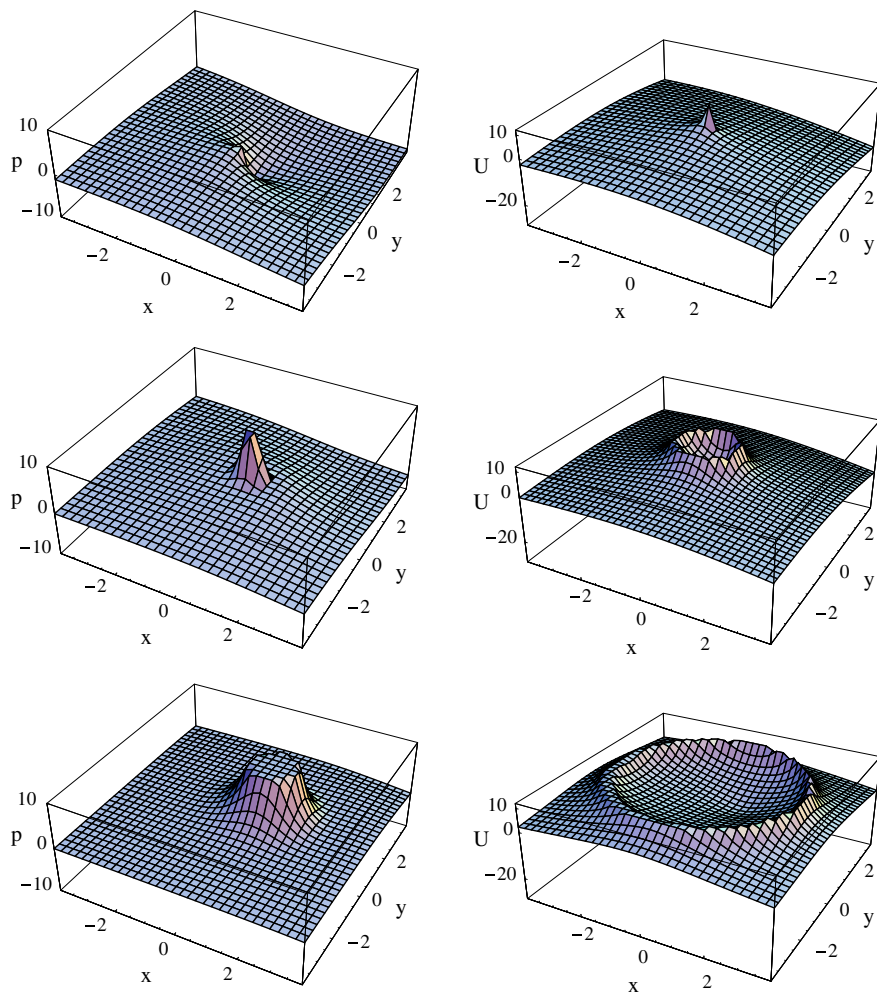


Fig. 7.2 Function p and solution U for $z = 0$, $t = 0$ (at the top), $t = 1$ (at the middle), $t = 3$ (at the bottom)

7.5 Ansatzes for Solution of Static Equation

We find a solution of static equation (7.2) in the form (7.16). It will be proven that an ansatz $\theta(x, y, z)$ can be obtained in the forms that express curved coordinates $(\theta_1, \theta_2, \theta_3)$ through the Cartesian coordinates (x, y, z) . This result is important as it allows us to construct a solution of the NKFG equation satisfying the boundary conditions imposed on such surfaces.

Let us consider the curvilinear coordinates that are the most studied in mathematical physics [14]. The general elliptic coordinates are defined by the family of surfaces

$$\frac{x^2}{a^2 + \theta} + \frac{y^2}{b^2 + \theta} + \frac{z^2}{c^2 + \theta} = 1. \quad (7.37)$$

For definiteness, we assume that $c > b > a$. The geometrical form of the surface (7.37) depends on the parameters θ, a, b, c . If $-a^2 < \theta < \infty$, then (7.37) is a family of three-axis spheroids, if $-b^2 < \theta < -a^2$, then (7.37) is a family of hyperboloids with one sheet, if $-c^2 < \theta < -b^2$, then (7.37) is a family of hyperboloids with two sheets. From Eq. (7.37), one can see that θ is the solution of the cubic equation. Any root θ_1, θ_2 , and θ_3 of this equation can be chosen for the anzates. It should satisfy the system of the equations,

$$\theta_x^2 + \theta_y^2 + \theta_z^2 = q(x, y, z)P(\theta), \quad (7.38)$$

$$\theta_{xx} + \theta_{yy} + \theta_{zz} = q(x, y, z)Q(\theta). \quad (7.39)$$

Equation (7.37) implicitly defines $\theta(x, y, z)$. By the method of differentiation of implicit functions, we find

$$\theta_x^2 + \theta_y^2 + \theta_z^2 = \frac{4}{M}, \quad M = \frac{x^2}{(a^2 + \theta)^2} + \frac{y^2}{(b^2 + \theta)^2} + \frac{z^2}{(c^2 + \theta)^2}, \quad (7.40)$$

$$\theta_{xx} + \theta_{yy} + \theta_{zz} = \frac{2N}{M}, \quad N = \frac{1}{a^2 + \theta} + \frac{1}{b^2 + \theta} + \frac{1}{c^2 + \theta}. \quad (7.41)$$

From Eqs. (7.40) and (7.41), we can see that θ satisfies the system of Eqs. (7.38), (7.39) and

$$q(x, y, z) = \frac{2}{M}, \quad P(\theta) = 2, \quad Q(\theta) = N, \quad (7.42)$$

$$R(\theta) = \frac{A}{2}(a^2 + \theta)(b^2 + \theta)(c^2 + \theta), \quad (7.43)$$

$$G(\theta) = \frac{1}{\sqrt{A}} \int_0^\theta \frac{d\theta}{\sqrt{(a^2 + \theta)(b^2 + \theta)(c^2 + \theta)}}, \quad (7.44)$$

$$p(x, y, z) = \frac{2}{A(a^2 + \theta)(b^2 + \theta)(c^2 + \theta)M}. \quad (7.45)$$

Therefore, any root of Eq. (7.37) can be chosen as an ansatz for the solution of Eq. (7.2).

Parabolic coordinates are defined by crossing of the elliptic and hyperbolic paraboloids. This family of coordinate surfaces is described by the equation,

$$\frac{x^2}{\theta - a} + \frac{y^2}{\theta - b} - 2z - \theta = 0. \quad (7.46)$$

It implicitly defines the function $\theta(x, y, z)$. From Eq. (7.46), we find

$$\theta_x^2 + \theta_y^2 + \theta_z^2 = \frac{4}{M}, \quad M = 1 + \frac{x^2}{(\theta - a)^2} + \frac{y^2}{(\theta - b)^2}, \quad (7.47)$$

$$\theta_{xx} + \theta_{yy} + \theta_{zz} = \frac{2N}{M}, \quad N = \frac{1}{\theta - a} + \frac{1}{\theta - b}. \quad (7.48)$$

From Eqs.(7.47) and (7.48), it follows that θ satisfies the system of Eqs. (7.38), (7.39) and

$$q(x, y, z) = \frac{2}{M}, \quad P(\theta) = 2, \quad Q(\theta) = N, \quad (7.49)$$

$$R(\theta) = \frac{C}{2}(\theta - a)(\theta - b), \quad C = \text{const}, \quad (7.50)$$

$$p(x, y, z) = \frac{2}{CM(\theta - a)(\theta - b)}. \quad (7.51)$$

Thus, the roots of the equations of the surfaces determining parabolic coordinates are the ansatzes for the solution of Eq. (7.2).

It is possible to prove by direct calculations that the roots of the equations of other coordinate surfaces also satisfy Eqs. (7.37), (7.38); that is, they can be applied to finding the solutions of Eq. (7.2). Let us give the final results for the following coordinate surfaces:

1. Cones

$$\frac{x^2}{\theta} + \frac{y^2}{\theta - b^2} + \frac{z^2}{\theta - c^2} = 0, \quad (7.52)$$

$$q(x, y, z) = \frac{2}{L}, \quad L = \frac{x^2}{\theta^2} + \frac{y^2}{(\theta - b^2)^2} + \frac{z^2}{(\theta - c^2)^2}, \quad P(\theta) = 2,$$

$$Q(\theta) = \frac{1}{\theta} + \frac{1}{\theta - b^2} + \frac{1}{\theta - c^2}.$$

2. Oblate spheroids of rotation

$$\frac{x^2 + y^2}{1 + \theta} + \frac{z^2}{\theta} = a^2, \quad (7.53)$$

$$q(x, y, z) = \frac{2}{L}, \quad L = \frac{x^2 + y^2}{(1 + \theta)^2} + \frac{z^2}{\theta^2}, \quad P(\theta) = 2, \quad Q(\theta) = \frac{1}{\theta} + \frac{2}{1 + \theta},$$

$$R(\theta) = \frac{A}{2}\theta(1 + \theta)^2, \quad p = \frac{2}{A\theta(1 + \theta)^2L}.$$

3. Hyperboloids of revolution with two sheets

$$\frac{x^2 + y^2}{1 - \theta} - \frac{z^2}{\theta} = a^2, \quad (7.54)$$

$$q(x, y, z) = \frac{2}{L}, \quad L = \frac{x^2 + y^2}{(1 - \theta)^2} + \frac{z^2}{\theta^2}, \quad P(\theta) = 2, \quad Q(\theta) = \frac{1}{\theta} - \frac{2}{1 - \theta},$$

$$R(\theta) = \frac{A}{2}\theta(1 - \theta)^2, \quad p = \frac{2}{A\theta(1 - \theta)^2L}.$$

4. Hyperboloids of revolution with two sheets

$$\frac{x^2 + y^2}{\theta} = 2z + \theta, \quad (7.55)$$

$$q(x, y, z) = \frac{2}{L}, \quad L = \sqrt{x^2 + y^2 + z^2}, \quad P(\theta) = 2, \quad Q(\theta) = \theta.$$

Static Eq. (7.2) is solved by the third way using the given ansatzes. It can be solved by the second way if one converts the function $\theta(x, y, z, t)$ to a harmonic function. It is easy to show that $\phi[\theta(x, y, z)]$ satisfies Laplace's equation if

$$\frac{\theta_{xx} + \theta_{yy} + \theta_{zz}}{\theta_x^2 + \theta_y^2 + \theta_z^2} = -\frac{\phi_{\theta\theta}}{\phi_\theta} = \chi(\theta). \quad (7.56)$$

Here, $\chi(\theta)$ is an arbitrary function of θ . From Eq. (7.56), we find

$$\phi(\theta) = A \int e^{-\int \chi(\theta) d\theta} d\theta + B, \quad (7.57)$$

where A and B are the constants of integration. The harmonic function $\phi(\theta)$ can be used for construction of the solution of the nonautonomous NKFG equation.

Let us write the solution of Eq. (7.2) in form

$$U = f[\phi(\theta)] \quad (7.58)$$

and accept that

$$p(x, y, z) = \phi_x^2 + \phi_y^2 + \phi_z^2. \quad (7.59)$$

Then, the solution of Eq. (7.2) is reduced to the solution of the ordinary nonlinear differential equation of the second order,

$$f_{\phi\phi} = F(f). \quad (7.60)$$

It is integrated in quadratures,

$$\int \frac{df}{\sqrt{E + V(f)}} = \sqrt{2}(\phi + C). \quad (7.61)$$

Here, E and C are the arbitrary constants and $F(f) = V_f$.

Let us define the function $\phi(\theta)$ for the ansatzes which are the roots of the equations of some families of coordinate surfaces:

1. Three-axis spheroids

$$\begin{aligned} \chi(\theta) &= \frac{1}{2} \left[\frac{1}{\theta + a^2} + \frac{1}{\theta + b^2} + \frac{1}{\theta + c^2} \right], \\ \phi(\theta) &= A \int \frac{d\theta}{\sqrt{(\theta + a^2)(\theta + b^2)(\theta + c^2)}} + B. \end{aligned} \quad (7.62)$$

2. Cones with axes coinciding with coordinates axes

$$\chi(\theta) = \frac{1}{2} \left[\frac{1}{\theta} + \frac{1}{\theta - b^2} + \frac{1}{\theta - c^2} \right], \quad \phi(\theta) = A \int \frac{d\theta}{\sqrt{\theta(\theta - b^2)(\theta - c^2)}} + B. \quad (7.63)$$

3. Elliptic paraboloids

$$\chi(\theta) = \frac{1}{2} \left[\frac{1}{\theta - a} + \frac{1}{\theta - b} \right], \quad \phi(\theta) = 2A \ln \left[\sqrt{\theta - a} + \sqrt{\theta - b} \right] + B. \quad (7.64)$$

4. Oblate spheroids of rotation

$$\chi(\theta) = \frac{1}{2} \left[\frac{1}{\theta} + \frac{2}{1 + \theta} \right], \quad \phi(\theta) = 2A \tan^{-1} \sqrt{\theta} + B. \quad (7.65)$$

5. Hyperboloids of revolution with two sheets

$$\chi(\theta) = \frac{1}{2} \left[\frac{1}{\theta} - \frac{2}{1 - \theta} \right], \quad \phi(\theta) = A \ln \frac{1 + \sqrt{\theta}}{1 - \sqrt{\theta}} + B. \quad (7.66)$$

6. Confocal paraboloids of revolution

$$\chi(\theta) = \theta, \quad \phi(\theta) = A \ln \theta + B. \quad (7.67)$$

Functions $\phi(\theta)$ determined by Eqs. (7.62) and (7.63) are expressed through the elliptic integral of the first kind.

7.6 Conclusion

Methods of finding exact analytical solutions of the dynamic and static nonautonomous NKFG equations are proposed. The most important step in the implementation of the proposed methods is the calculation of the ansatz. For dynamic equations, it is found from special equations by the methods developed in the theory of constructing the functionally invariant wave equation solutions.

It is proven for the static equations that the algebraic expressions of orthogonal curvilinear coordinates through the Cartesian coordinates can be taken as an ansatz. This result seems important, as it allows us to solve the static nonautonomous NKFG equations in orthogonal curved coordinates.

Acknowledgements This work was supported by the Russian Foundation for Basic Researches, Grant No. 17-01-00230-a.

References

1. Frenkel, J., Kontorova, T.: On the theory of plastic deformation and twinning. *Acad. Sci. U.S.S.R. J. Phys.* **1**, 137–149 (1939)
2. Aero, E.L.: Micromechanics of a double continuum in a model of a medium with variable periodic structure. *J. Eng. Math.* **55**, 81–95 (2006)
3. Aero, E.L., Bulygin, A.N.: Strongly nonlinear theory of nanostructure formation owing to elastic and nonelastic strains in crystalline solids. *Mech. Solids.* **42**, 807–822 (2007)
4. Dodd, R.K., Eilbeck, J.C., Gibbon, J.D., Morris, H.C.: *Solitons and Nonlinear Wave Equations*. Academic Press, New York (1982)
5. De Gennes, P.G.: *The Physics of Liquid Crystals*. Clarendon Press, Oxford (1974)
6. Aero, E.L., Bulygin, A.N., Pavlov, Y.V.: Functionally invariant solutions of nonlinear Klein-Fock-Gordon equation. *Appl. Math. Comput.* **223**, 160–166 (2013)
7. Aero, E.L., Bulygin, A.N., Pavlov, Y.V.: Solutions of the sine-Gordon equation with a variable amplitude. *Theor. Math. Phys.* **184**, 961–972 (2015)
8. Aero, E.L., Bulygin, A.N., Pavlov, Yu.V.: Exact analytical solutions for nonautonomic nonlinear Klein-Fock-Gordon equation. In: dell’Isola F., Eremeyev V., Porubov A. (eds.) *Advances in Mechanics of Microstructured Media and Structures*. Advanced Structured Materials, vol. 87. Springer, Cham, pp. 21–33 (2018)
9. Bulygin, A.N., Pavlov, Yu.V.: Solutions of nonlinear non-autonomous Klein-Fock-Gordon equation. In: *Proceedings of XLVI Summer School—Conference “Advanced Problems in Mechanics”*, APM 2018, St. Petersburg, pp. 33–43 (2018)

10. Bulygin, A.N., Pavlov, Yu.V.: Methods of finding of exact analytical solutions of nonautonomous nonlinear Klein-Fock-Gordon equation. In: Altenbach, H., Belyaev, A., Eremeyev, V., Krivtsov, A., Porubov, A. (eds.) *Dynamical Processes in Generalized Continua and Structures*. *Advanced Structured Materials*, vol. 103. Springer, Cham, pp. 147–161 (2019)
11. Forsyth, A.R.: New solutions of some of the partial differential equations of mathematical physics. *Messenger Math.* **27**, 99–118 (1898)
12. Bateman, H.: *The Mathematical Analysis of Electrical and Optical Wave-Motion on the Basis of Maxwell's Equations*. Cambridge University Press, Cambridge (1915)
13. Smirnov, V., Sobolev, S.: Sur une méthode nouvelle dans le problème plan des vibrations élastiques. *Tr. Seism. Inst.* **20**, 1–37 (1932) [English transl.: On a new method in the plane problem on elastic vibrations. In: *Selected Works of S.L. Sobolev*, vol. I, pp. 45–80. Springer, New York (2006)]
14. Korn, G.A., Korn, T.M.: *Mathematical Handbook for Scientists and Engineers. Theorems and Formulas for Reference and Review*. McGraw-Hill Inc, New York, Definitions (1968)

Chapter 8

A Comparison Between Heterogeneous and Homogeneous Layers for Nonlinear Bright Solitary SH Waves in Terms of Heterogeneous Effect



Dilek Demirkuş

Abstract In this chapter, we compare the nonlinear bright solitary shear horizontal (SH) waves in heterogeneous and homogeneous layers in terms of the heterogeneous effect. Each layer has finite thickness overlying a rigid substratum. We assume that the layers are made up of isotropic, hyper-elastic and generalized neo-Hookean (similarly, compressible or incompressible) materials. Moreover, one layer contains heterogeneous materials and another contains homogeneous materials. The existence of nonlinear bright solitary SH waves in such layers can be found in the literature. Therefore, we aim to overcome the difficulty of a comparison of two nonlinear analyzes for this paper. Besides a comparison part, we add a discussion on some materials in homogeneous media.

Keywords Nonlinear SH waves · Bright solitary waves · Heterogeneous layer

8.1 Introduction

Phase velocities of elastic waves propagating in an unbounded homogeneous medium are constant. In other words, the wave propagation is nondispersive. Nondispersive medium is not useful for constructing a continuous wave propagation. Therefore, in such a situation, one of the required aims is to get dispersive elastic waves. This aim can be achieved using some waveguides such as a layer, plate, half-space, layered plate, and layered half-space. Dispersive elastic waves have found many important applications in some areas such as seismology, geophysics, nondestructive inspection of material surfaces, and electronic signal processing devices. For further information about applications and reviews, we refer to Achenbach [2], Ewing [18], Farnell [19],

D. Demirkuş (✉)

Department of Mathematics, Beykent University, Istanbul, Turkey
e-mail: dilekdemirkus@beykent.edu.tr

© Springer Nature Switzerland AG 2020
H. Altenbach et al. (eds.), *Nonlinear Wave Dynamics of Materials and Structures*, Advanced Structured Materials 122,
https://doi.org/10.1007/978-3-030-38708-2_8

Graff [22], and Maugin [27]. Moreover, for a modern theory of propagation and interaction of elastic waves in solids with microstructure, we refer to Erofeev [17].

Elastic waves are called seismic waves in seismology and they have some known types. That is to say, they can divide into two categories known as body waves and surface waves. P and S waves are two types of body waves to measure pressure and shear, respectively. Furthermore, Love and Rayleigh waves are two types of surface waves. As earthquakes waves, body waves and surface waves come from to the interior and surface of the Earth, respectively. We know that body waves move faster than surface waves; whereas, surface waves are more dangerous than body waves. Besides parallel to the damage, understanding the mathematical behavior of surface waves is more difficult than others because they use more than one displacement.

The dispersive effect (or linear behavior) of the elastic waves is a well-worked topic in the literature. We want to give some examples of them with different properties such as Hudson [23], Kaplunov and Nobili [25], Kaplunov et al. [26], Prikazchikova et al. [31], Sahu et al. [34], and Vardoulakis and Georgiadiis [39]. In addition to understanding the dispersive effect, some researchers think that the nonlinear effect of the elastic waves is also to be considerable. For such works, we refer to Ahmetolan and Teymur [3, 4], Deliktas and Teymur [6], Demirkus and Teymur [13], Destrade et al. [14], Ferreira and Boulanger [20], Fu [21], Maugin and Hadouaj [28], Mayer [29], Porubov and Samsonov [32], Pucci and Saccomandi [33], Teymur [36, 37], and Teymur et al. [38]. Moreover, for an example of the anti-plane surface wave propagation in lattice structures, we refer to Eremeyev and Sharma [35].

From recent developments, we see that a few works exist for the propagation of the nonlinear SH waves in heterogeneous media. We are willing to complete the literature in this direction. Therefore, we show the existence of the nonlinear bright and dark solitary SH waves in a heterogeneous layer in [7, 12], respectively. Similarly, besides the existence of the nonlinear antisymmetric and symmetric bright solitary SH waves in a heterogeneous plate, we also show the existence of the nonlinear antisymmetric and symmetric dark solitary SH waves in [8–11]. In this paper, we give a review part for some materials in homogeneous media and compare a heterogeneous layer with a homogeneous one, in terms of heterogeneous effect. The comparison of the nonlinear effect is also possible, but we will see it elsewhere. Moreover, similar comparisons are valid for a plate case; however, they are out of this work.

8.2 A Review Part for Some Materials in Homogeneous Media

Before a comparison part, we will start with a review part for the nonlinear SH waves or surface SH waves in homogeneous media given materials such as compressible, incompressible, and generalized neo-Hookean. In this discussion, the spatial and material coordinates of a point referred to the same fixed rectangular Cartesian system of axes are x_k and X_K , respectively. Latin and Greek indices have the respective ranges

(1, 2, 3) and (1, 2), and also the summation convention on repeated indices is implied in this text. Subscripts preceded by a comma also indicate the partial differentiation with respect to material or spatial coordinates in the sequel.

If the constituent materials of a bounded medium are hyper-elastic, then there exists a strain energy function Σ characterizing the mechanical properties of the materials and stress constitutive equation [16] can be given by

$$T_{Kk} = \frac{\partial \Sigma}{\partial x_{k,K}}. \quad (8.1)$$

Here, T_{Kk} indicates the components of the first Piola–Kirchhoff stress tensor and anti-plane shear motion can be described by the equation below

$$x_k = X_K \delta_{kK} + u_3(X_\Delta, t) \delta_{k3} \quad (8.2)$$

where $u_3 = u_3(X_\Delta, t)$ is the displacement in the X_3 -direction, t is the time, and δ_{kK} is the usual Kronecker symbol. We assume that an SH wave described by (8.2) is to propagate along X_1 -axis in this medium. Because of SH waves, the displacements in the X_1 - and X_2 -directions are zero.

For an isotropic solid, Σ is an isotropic function of the principal invariants of the Finger deformation tensor \mathbf{c}^{-1} , and invariants [16] are defined by

$$I_1 = \text{tr} \mathbf{c}^{-1}, \quad 2I_2 = (\text{tr} \mathbf{c}^{-1})^2 - \text{tr}(\mathbf{c}^{-2}), \quad I_3 = \det \mathbf{c}^{-1} \quad (8.3)$$

and also calculated for deformation field (8.2) as follows:

$$I_1 = I_2 = 3 + K^2, \quad I_3 = 1 \quad (8.4)$$

where $K^2 = u_{3,\Delta} u_{3,\Delta}$. Moreover, if the motion takes place for homogeneous materials, then three possibilities on dependency of Σ come up as follows:

- For compressible materials, i.e., $\Sigma = \Sigma(I_1, I_2, I_3)$,
- For incompressible materials, i.e., $\Sigma = \Sigma(I_1, I_2)$,
- For generalized neo-Hookean materials, i.e., $\Sigma = \Sigma(I_1)$.

The components of the deformation gradient tensors $x_{k,K}$ and $X_{K,k}$ for deformation fields (8.2) are calculated as follows:

$$\begin{aligned} x_{\alpha,\Delta} &= \delta_{\alpha\Delta}, & x_{\alpha,3} &= 0, & x_{3,\Delta} &= u_{3,\Delta}, & x_{3,3} &= 1, \\ X_{\Delta,\alpha} &= \delta_{\Delta\alpha}, & X_{\Delta,3} &= 0, & X_{3,\alpha} &= -u_{3,\Delta} \delta_{\Delta\alpha}, & X_{3,3} &= 1. \end{aligned} \quad (8.5)$$

Note that deformation field (8.2) is isochoric, i.e., $j = \det x_{k,K} = 1$. Similarly, the components of $c_{kl}^{-1} = x_{k,K} x_{l,K}$ and $c_{km}^{-1} c_{ml}^{-1}$ are as follows, respectively:

$$\begin{aligned} c_{\alpha\beta}^{-1} &= \delta_{\alpha\Delta}\delta_{\beta\Delta}, & c_{\alpha 3}^{-1} &= \delta_{\alpha\Delta}u_{3,\Delta}, \\ c_{3\beta}^{-1} &= u_{3,\Delta}\delta_{\beta\Delta}, & c_{33}^{-1} &= 1 + K^2, \end{aligned} \quad (8.6)$$

and

$$\begin{aligned} c_{\alpha m}^{-1}c_{m\beta}^{-1} &= (\delta_{\alpha\Delta}\delta_{\gamma\Delta})(\delta_{\gamma\Delta}\delta_{\beta\Delta}) + (\delta_{\alpha\Delta}u_{3,\Delta})(u_{3,\Delta}\delta_{\beta\Delta}), \\ c_{\alpha m}^{-1}c_{m3}^{-1} &= (\delta_{\alpha\Delta}\delta_{\gamma\Delta})(\delta_{\gamma\Delta}u_{3,\Delta}) + (\delta_{\alpha\Delta}u_{3,\Delta})(1 + K^2), \\ c_{3m}^{-1}c_{m\beta}^{-1} &= (u_{3,\Delta}\delta_{\gamma\Delta})(\delta_{\gamma\Delta}\delta_{\beta\Delta}) + (1 + K^2)(u_{3,\Delta}\delta_{\beta\Delta}), \\ c_{3m}^{-1}c_{m3}^{-1} &= (u_{3,\Delta}\delta_{\gamma\Delta})(\delta_{\gamma\Delta}u_{3,\Delta}) + (1 + K^2)^2. \end{aligned} \quad (8.7)$$

Without the body forces, the equations of the motion [16] in the reference state can be written as

$$\begin{aligned} T_{\Delta\beta,\Delta} + T_{3\beta,3} &= 0, \\ T_{\Delta 3,\Delta} + T_{33,3} &= \rho_0\ddot{u}_3. \end{aligned} \quad (8.8)$$

Here, ρ_0 is the density of the medium. Using components (8.5) with the relation $T_{Kl} = jX_{K,k}t_{kl}$ between the Cauchy stress tensor t_{kl} and the first Piola-Kirchhoff stress tensor T_{Kl} , we obtain

$$\begin{aligned} T_{\Delta\beta} &= \delta_{\Delta\alpha}t_{\alpha\beta}, & T_{\Delta 3} &= \delta_{\Delta\alpha}t_{\alpha 3}, \\ T_{3\beta} &= -u_{3,\Delta}\delta_{\Delta\alpha}t_{\alpha\beta} + t_{3\beta}, & T_{33} &= -u_{3,\Delta}\delta_{\Delta\alpha}t_{\alpha 3} + t_{33}. \end{aligned} \quad (8.9)$$

Therefore, the equations of the motion are expressed in terms of t_{kl} as below

$$\begin{aligned} (\delta_{\Delta\alpha}t_{\alpha\beta})_{,\Delta} + (-u_{3,\Delta}\delta_{\Delta\alpha}t_{\alpha\beta} + t_{3\beta})_{,3} &= 0, \\ (\delta_{\Delta\alpha}t_{\alpha 3})_{,\Delta} + (-u_{3,\Delta}\delta_{\Delta\alpha}t_{\alpha 3} + t_{33})_{,3} &= \rho_0\ddot{u}_3. \end{aligned} \quad (8.10)$$

To express Eq. (8.10) well, we need to calculate the components of t_{kl} . For this reason, it is necessary to determine types of materials. Therefore, the following discussion is for this aim.

8.2.1 Compressible Materials

In this case, if we assume that materials of the medium are not only hyper-elastic, homogeneous and isotropic, but also compressible, then the strain energy function Σ has the following form as stated above

$$\Sigma = \Sigma(I_1, I_2, I_3). \quad (8.11)$$

If we take into consideration such materials, then the stress constitutive equation [16] is given by

$$t_{kl} = 2\sqrt{I_3} \frac{\partial \Sigma}{\partial I_3} \delta_{kl} + \frac{2}{\sqrt{I_3}} \left(\frac{\partial \Sigma}{\partial I_1} + I_1 \frac{\partial \Sigma}{\partial I_2} \right) c_{kl}^{-1} - \frac{2}{\sqrt{I_3}} \frac{\partial \Sigma}{\partial I_2} c_{km}^{-1} c_{ml}^{-1}. \quad (8.12)$$

For finding the components of the stress constitutive equation (8.12), we need to use components (8.6) and (8.7), then listed as:

$$\begin{aligned} t_{11} &= 2 \frac{\partial \Sigma}{\partial I_1} + 2(2 + u_{3,2}^2) \frac{\partial \Sigma}{\partial I_2} + 2 \frac{\partial \Sigma}{\partial I_3}, \\ t_{12} &= t_{21} = -2 \frac{\partial \Sigma}{\partial I_2} u_{3,1} u_{3,2}, \\ t_{22} &= 2 \frac{\partial \Sigma}{\partial I_1} + 2(2 + u_{3,1}^2) \frac{\partial \Sigma}{\partial I_2} + 2 \frac{\partial \Sigma}{\partial I_3}, \\ t_{13} &= t_{31} = 2 \left(\frac{\partial \Sigma}{\partial I_1} + \frac{\partial \Sigma}{\partial I_2} \right) u_{3,1}, \\ t_{23} &= t_{32} = 2 \left(\frac{\partial \Sigma}{\partial I_1} + \frac{\partial \Sigma}{\partial I_2} \right) u_{3,2}, \\ t_{33} &= 2(1 + K^2) \frac{\partial \Sigma}{\partial I_1} + 2(2 + K^2) \frac{\partial \Sigma}{\partial I_2} + 2 \frac{\partial \Sigma}{\partial I_3}. \end{aligned} \quad (8.13)$$

Here, we aim to calculate the components of the stress constitutive equation, explicitly. If we assume that Σ is an analytic function of I_1, I_2, I_3 around $(3, 3, 1)$, then we can expand the function Σ to a Taylor series as

$$\Sigma(I_1, I_2, I_3) = \sum_{p=0}^{\infty} \sum_{q=0}^{\infty} \sum_{r=0}^{\infty} c_{pqr} (I_1 - 3)^p (I_2 - 3)^q (I_3 - 1)^r \quad (8.14)$$

where the coefficients c_{pqr} are defined by

$$c_{pqr} = \frac{1}{(p+q+r)!} \frac{\partial^{p+q+r} \Sigma(3, 3, 1)}{\partial I_1^p \partial I_2^q \partial I_3^r} \quad (8.15)$$

and $\Sigma(3, 3, 1) = 0$. Moreover, at the initial state we assume that the energy is zero and the medium has no stress. Using series expansion (8.14), the following partial derivatives can be found

$$\begin{aligned} \frac{\partial \Sigma}{\partial I_1} &= c_{100} + (2c_{200} + c_{110})K^2 + \mathcal{O}(K^4), \\ \frac{\partial \Sigma}{\partial I_2} &= c_{010} + (2c_{020} + c_{110})K^2 + \mathcal{O}(K^4), \\ \frac{\partial \Sigma}{\partial I_3} &= c_{001} + (c_{101} + c_{011})K^2 + \mathcal{O}(K^4). \end{aligned} \quad (8.16)$$

Under the following conditions

$$\begin{aligned} c_{010} &= 0, \\ c_{100} + c_{001} &= 0, \\ 2c_{200} + c_{110} + c_{101} + c_{011} &= 0, \\ 2c_{020} + c_{110} &= 0, \end{aligned} \tag{8.17}$$

and using derivatives (8.16), we get the relations as follows:

$$\begin{aligned} \frac{\partial \Sigma}{\partial I_2} &= \mathcal{O}(K^4), \\ \frac{\partial \Sigma}{\partial I_1} + \frac{\partial \Sigma}{\partial I_3} &= \mathcal{O}(K^4). \end{aligned} \tag{8.18}$$

Such assumptions (8.17) are helpful for reducing the number of equations that comes from such a medium. We see that this medium can be expressed by three equations. But, all equations contain the nonlinearity and it is known that the area of science suffers from the lack of the general theory about the system of nonlinear partial differential equations. Therefore, the components of the stress constitutive equation can be expressed as given in the list below

$$\begin{aligned} t_{\alpha\beta} &= \mathcal{O}(K^4), \\ t_{\alpha 3} = t_{3\alpha} &= 2[c_{100} + 2(c_{200} + c_{020} + c_{110})K^2]u_{3,\alpha} + \mathcal{O}(K^4), \\ t_{33} &= 2c_{100}K^2 + \mathcal{O}(K^4). \end{aligned} \tag{8.19}$$

In (8.19), we can omit the terms that contain K^4 and higher than K^4 . Consequently, the first two equations in (8.10) are satisfied identically, and the third equation becomes

$$\ddot{u}_3 - c_{0r}^2 u_{3,\Delta\Delta} = n_{0r} (u_{3,\Delta} K^2)_{,\Delta} \tag{8.20}$$

where

$$\begin{aligned} n_{0r} &= 4(c_{200} + c_{020} + c_{110})/\rho_0, \\ c_{0r}^2 &= 2c_{100}/\rho_0 = \mu_0/\rho_0. \end{aligned} \tag{8.21}$$

8.2.2 Incompressible Materials

In this case, if we assume that materials of the medium are not only hyper-elastic, homogeneous and isotropic, and but also incompressible, then the strain energy function Σ has the following form as stated above

$$\Sigma = \Sigma(I_1, I_2). \tag{8.22}$$

If we take into consideration such materials, then the stress constitutive equation [16] is given by

$$t_{kl} = -p\delta_{kl} + 2 \left(\frac{\partial \Sigma}{\partial I_1} + I_1 \frac{\partial \Sigma}{\partial I_2} \right) c_{kl}^{-1} - 2 \frac{\partial \Sigma}{\partial I_2} c_{km}^{-1} c_{ml}^{-1} \quad (8.23)$$

where $p(X_K, t)$ is an arbitrary hydrostatic pressure function. Using (8.6) and (8.7), we get the following components of the stress constitutive equation (8.23)

$$\begin{aligned} t_{11} &= -p + 2 \frac{\partial \Sigma}{\partial I_1} + 2(2 + u_{3,2}^2) \frac{\partial \Sigma}{\partial I_2}, \\ t_{12} &= t_{21} = -2 \frac{\partial \Sigma}{\partial I_2} u_{3,1} u_{3,2}, \\ t_{22} &= -p + 2 \frac{\partial \Sigma}{\partial I_1} + 2(2 + u_{3,1}^2) \frac{\partial \Sigma}{\partial I_2}, \\ t_{\alpha 3} &= t_{3\alpha} = 2 \left(\frac{\partial \Sigma}{\partial I_1} + \frac{\partial \Sigma}{\partial I_2} \right) u_{3,\alpha}, \\ t_{33} &= -p + 2(1 + K^2) \frac{\partial \Sigma}{\partial I_1} + 2(2 + K^2) \frac{\partial \Sigma}{\partial I_2}. \end{aligned} \quad (8.24)$$

Therefore, the equations of motion (8.10) take the following forms

$$\begin{aligned} \left[-p + 2 \frac{\partial \Sigma}{\partial I_1} + 4 \frac{\partial \Sigma}{\partial I_2} \right]_{,1} + \left[2 \left(u_{3,2} \frac{\partial \Sigma}{\partial I_2} \right)_{,1} u_{3,2} - 2 \left(u_{3,2} \frac{\partial \Sigma}{\partial I_2} \right)_{,2} u_{3,1} \right] + u_{3,1} p_{,3} &= 0, \\ \left[-p + 2 \frac{\partial \Sigma}{\partial I_1} + 4 \frac{\partial \Sigma}{\partial I_2} \right]_{,2} + \left[2 \left(u_{3,1} \frac{\partial \Sigma}{\partial I_2} \right)_{,2} u_{3,1} - 2 \left(u_{3,1} \frac{\partial \Sigma}{\partial I_2} \right)_{,1} u_{3,2} \right] + u_{3,2} p_{,3} &= 0, \\ \left[2 \left(\frac{\partial \Sigma}{\partial I_1} + \frac{\partial \Sigma}{\partial I_2} \right) u_{3,1} \right]_{,1} + \left[2 \left(\frac{\partial \Sigma}{\partial I_1} + \frac{\partial \Sigma}{\partial I_2} \right) u_{3,2} \right]_{,2} - \rho_0 \ddot{u}_3 &= p_{,3}. \end{aligned} \quad (8.25)$$

From the last equation of (8.25), we get

$$p_{,3} = \kappa_0(X_1, X_2, t) \quad (8.26)$$

and hence

$$p = \kappa_0(X_1, X_2, t) X_3 + \kappa_1(X_1, X_2, t) \quad (8.27)$$

where κ_0 and κ_1 are arbitrary functions. Then, the use of (8.27) in the first two equations of (8.25) yields

$$\kappa_{0,1} = 0, \quad \kappa_{0,2} = 0. \quad (8.28)$$

Therefore, we have

$$\kappa_0 = f(t) \quad (8.29)$$

where f is an arbitrary function. Moreover, the first two equations of (8.25) can be written as

$$\begin{aligned} \left[-\kappa_1 + 2\frac{\partial \Sigma}{\partial I_1} + 4\frac{\partial \Sigma}{\partial I_2} + u_3 f(t) \right]_{,1} + 2 \left[\left(u_{3,2} \frac{\partial \Sigma}{\partial I_2} \right)_{,1} u_{3,2} - \left(u_{3,2} \frac{\partial \Sigma}{\partial I_2} \right)_{,2} u_{3,1} \right] &= 0, \\ \left[-\kappa_1 + 2\frac{\partial \Sigma}{\partial I_1} + 4\frac{\partial \Sigma}{\partial I_2} + u_3 f(t) \right]_{,2} + 2 \left[\left(u_{3,1} \frac{\partial \Sigma}{\partial I_2} \right)_{,2} u_{3,1} - \left(u_{3,1} \frac{\partial \Sigma}{\partial I_2} \right)_{,1} u_{3,2} \right] &= 0. \end{aligned} \quad (8.30)$$

Using (8.30) with differentiation, we get the following compatibility condition

$$\left[\left(u_{3,2} \frac{\partial \Sigma}{\partial I_2} \right)_{,1} u_{3,2} - \left(u_{3,2} \frac{\partial \Sigma}{\partial I_2} \right)_{,2} u_{3,1} \right]_{,2} - \left[\left(u_{3,1} \frac{\partial \Sigma}{\partial I_2} \right)_{,2} u_{3,1} - \left(u_{3,1} \frac{\partial \Sigma}{\partial I_2} \right)_{,1} u_{3,2} \right]_{,1} = 0. \quad (8.31)$$

Using this compatibility condition, then Eq.(8.30) becomes such that

$$\begin{aligned} \left[-\kappa_1 + 2\frac{\partial \Sigma}{\partial I_1} + u_3 f(t) \right]_{,1} &= 0, \\ \left[-\kappa_1 + 2\frac{\partial \Sigma}{\partial I_1} + u_3 f(t) \right]_{,2} &= 0. \end{aligned} \quad (8.32)$$

By integrating Eq. (8.32), we obtain that

$$\kappa_1 = 2\frac{\partial \Sigma}{\partial I_1} + u_3 f(t) + g(t) \quad (8.33)$$

where g is an arbitrary function. Therefore, the pressure function can be written as

$$p = f(t)X_3 + 2\frac{\partial \Sigma}{\partial I_1} + u_3 f(t) + g(t). \quad (8.34)$$

Using Eq. (8.34) in (8.24), then we find that

$$\begin{aligned} t_{11} = t_{22} &= -f(t)X_3 - u_3 f(t) - g(t), \\ t_{12} = t_{21} &= 0, \\ t_{\alpha 3} = t_{3\alpha} &= 2\frac{\partial \Sigma}{\partial I_1} u_{3,\alpha}, \\ t_{33} &= -f(t)X_3 - u_3 f(t) - g(t) + 2K^2 \frac{\partial \Sigma}{\partial I_1}. \end{aligned} \quad (8.35)$$

Here, we assume that the natural states of the materials are stress-free. Hence,

$$g(t) = 0. \quad (8.36)$$

In a similar manner, all stress components must be bounded at $X_3 = \pm\infty$. Therefore, we have

$$f(t) = 0. \quad (8.37)$$

As a result, stress components (8.35) can be given as listed:

$$\begin{aligned} t_{\alpha\beta} &= 0, \\ t_{\alpha 3} &= t_{3\alpha} = 2 \frac{\partial \Sigma}{\partial I_1} u_{3,\alpha}, \\ t_{33} &= 2K^2 \frac{\partial \Sigma}{\partial I_1}, \end{aligned} \quad (8.38)$$

and the pressure function can be written as

$$p = 2 \frac{\partial \Sigma}{\partial I_1}. \quad (8.39)$$

For calculating the components of the stress constitutive equation, we assume that Σ is an analytic function of I_1, I_2 around $(3, 3)$, then we can expand the function Σ to a Taylor series as

$$\Sigma(I_1, I_2) = \sum_{p=0}^{\infty} \sum_{q=0}^{\infty} c_{pq0} (I_1 - 3)^p (I_2 - 3)^q \quad (8.40)$$

where the coefficients c_{pq0} are defined by

$$c_{pq0} = \frac{1}{(p+q)!} \frac{\partial^{p+q} \Sigma(3, 3)}{\partial I_1^p \partial I_2^q} \quad (8.41)$$

and $\Sigma(3, 3) = 0$. Partial derivatives can be found as

$$\begin{aligned} \frac{\partial \Sigma}{\partial I_1} &= c_{100} + (c_{110} + 2c_{200})K^2 + \mathcal{O}(K^4), \\ \frac{\partial \Sigma}{\partial I_2} &= c_{010} + (c_{110} + 2c_{020})K^2 + \mathcal{O}(K^4). \end{aligned} \quad (8.42)$$

Under the following condition

$$\begin{aligned} c_{010} &= 0, \\ c_{110} + 2c_{020} &= 0, \end{aligned} \quad (8.43)$$

we get

$$\frac{\partial \Sigma}{\partial I_2} = \mathcal{O}(K^4). \quad (8.44)$$

Therefore, stress components (8.38) can be expressed as given in the list below

$$\begin{aligned} t_{\alpha\beta} &= 0, \\ t_{\alpha 3} &= t_{3\alpha} = 2[c_{100} + (c_{110} + 2c_{200})K^2]u_{3,\alpha} + \mathcal{O}(K^4), \\ t_{33} &= 2c_{100}K^2 + \mathcal{O}(K^4). \end{aligned} \quad (8.45)$$

Consequently, the first two equations in (8.10) are satisfied identically, and the third equation becomes Eq.(8.20) with

$$n_{0r} = 2(c_{110} + 2c_{200})/\rho_0. \quad (8.46)$$

8.2.3 Generalized Neo-Hookean Materials

In this case, if we assume that materials of the medium are not only hyper-elastic, homogeneous and isotropic, but also generalized neo-Hookean, then the strain energy function Σ has the following form as stated above

$$\Sigma = \Sigma(I_1). \quad (8.47)$$

If we take into consideration such materials, then the stress constitutive equation [16] is given by

$$t_{kl} = -p\delta_{kl} + 2\frac{d\Sigma}{dI_1}c_{kl}^{-1}. \quad (8.48)$$

In a similar manner, we have $p = 2\frac{d\Sigma}{dI_1}$. Using (8.6), the components of stress constitutive equation (8.48) are found to be

$$\begin{aligned} t_{\alpha\beta} &= 0, \\ t_{\alpha 3} &= t_{3\alpha} = 2\frac{d\Sigma}{dI_1}u_{3,\alpha}, \\ t_{33} &= 2K^2\frac{d\Sigma}{dI_1}. \end{aligned} \quad (8.49)$$

Similarly, if we assume that Σ is an analytic function of I_1 around 3, then the following Taylor series can be written as

$$\Sigma(I_1) = \sum_{p=0}^{\infty} c_{p00}(I_1 - 3)^p \quad (8.50)$$

where the coefficients c_{p00} are defined by

$$c_{p00} = \frac{1}{p!} \frac{d^p \Sigma(3)}{dI_1^p} \quad (8.51)$$

and $\Sigma(3) = 0$. Hence, we have

$$\frac{d\Sigma}{dI_1} = c_{100} + 2c_{200}K^2 + \mathcal{O}(K^4). \quad (8.52)$$

Therefore, the components of the stress constitutive equation (8.48) can be expressed as given in the list below

$$\begin{aligned} t_{\alpha\beta} &= 0, \\ t_{\alpha 3} &= t_{3\alpha} = 2(c_{100} + 2c_{200}K^2)u_{3,\alpha} + \mathcal{O}(K^4), \\ t_{33} &= 2c_{100}K^2 + \mathcal{O}(K^4). \end{aligned} \quad (8.53)$$

Consequently, the first two equations in (8.10) are satisfied identically, and the third equation becomes Eq. (8.20) with

$$n_{0r} = 4c_{200}/\rho_0. \quad (8.54)$$

From the discussion above for some materials used in homogeneous media, we see that one of the required aims is to reduce the number of nonlinear equations since the lack of a general theory of nonlinear partial differential equations. In each case, the number of equations reduces from three to one as wanted. Therefore, as a review, we observe that except for some assumptions on the mechanical properties of the materials, three types of materials are very similar to each other. In other words, the same equation occurs as a governing equation for measuring the medium with a small difference in the material constant n_{0r} . Consequently, we state that the existence or the stability of solutions are not affected by using compressible, incompressible or neo-Hookean materials. For a similar discussion, we refer to [5, 36, 37]. Furthermore, we see some works in homogeneous media that include this discussion such as [3, 4, 6, 13, 36–38]. Under this review, we can say that mentioned works in homogeneous media for nonlinear SH waves or nonlinear surface SH waves are different from each other in view of the geometries, i.e., using different boundary conditions. After this observation and showing the importance of heterogeneity in [7–12], our main aim is to improve some works about nonlinear SH waves or nonlinear surface SH waves from homogeneity to heterogeneity. Since the importance of heterogeneous materials is known, we hope that such works will make sense in terms of materials science and geophysics.

8.3 Comparison of Nonlinear Shear Horizontal Waves

In this part, we consider the comparison of nonlinear SH waves between a heterogeneous, isotropic, and generalized neo-Hookean layer overlying a rigid substratum and a homogeneous, isotropic, and generalized neo-Hookean layer overlying a rigid substratum. From the previous review part, we know that the difference between the neo-Hookean and compressible materials is small as seen in the material expression n_{0_T} . Therefore, the work [13] can be thought the homogeneous case of the work [7, 12]. After this review, it is clear that the main difference can be seen in the materials being heterogeneous or homogeneous. This difference may give us the opportunity to this comparison part.

In [7, 13], we see the existence of nonlinear bright solitary SH waves in heterogeneous and homogeneous layers, using the method of multiple scales [24] and known solutions of the nonlinear Schrödinger (NLS) equation. Because of these works, two possible comparisons come up for given bright solitary SH waves. One of them, i.e., heterogeneous effect, is the subject of this paper. It is clear that there are also some comparisons for the dark solitary SH waves, but they are not considered here.

Needless to emphasize the importance of this work, it is clear that this paper deals with the propagation of nonlinear SH waves as a comparative study between two layers. So, it includes the comparison of two nonlinear analyzes which base on asymptotic analyzes and numerical analyzes. Moreover, the present work can be considered as a good connection between homogeneous and heterogeneous materials in view of materials science and engineering. In the literature, it is very rare to consider nonlinear SH waves in a heterogeneous medium in more detail see for a plate case [8–11] and a layer case [7, 12]. It is necessary to be aware of that the half of the deformation field [8–11] gives rise to the deformation field [7, 12]. Because this work includes nonlinearity, heterogeneity, and comparability, it gives us a rich source about SH waves for the other researchers who work for interdisciplinary science. In more detail such as the anti-plane shear motion of this problem, the method of multiple scales [24] and the main analysis of this problem, we refer to [7, 13].

From the review part, let $X = X_1$, $Y = X_2$, $Z = X_3$ and $u = u_3$ be and let us define the problem well. We consider a layer from $Y = 0$ to $Y = h$ with two models. The first model is about being homogeneous and the second one is about being heterogeneous. Moreover, the free surface is $Y = h$ and the rigid surface is $Y = 0$. As boundary conditions, we assume that the free surface is free of traction and the rigid surface is fixed. Since our aim is to deal with the small but finite amplitude wave motions, proceeding with the approximate equations, rather than the exact ones, will be more convenient, then the following approximate governing equations and boundary conditions involving terms not higher than the third degree in the deformation gradients are written as for a homogeneous layer

$$\begin{aligned} \frac{\partial^2 u}{\partial t^2} - c_{0r}^2 \left(\frac{\partial^2 u}{\partial X^2} + \frac{\partial^2 u}{\partial Y^2} \right) &= n_{0r} \left[\frac{\partial}{\partial X} \left(\frac{\partial u}{\partial X} \mathcal{K}(u) \right) + \frac{\partial}{\partial Y} \left(\frac{\partial u}{\partial Y} \mathcal{K}(u) \right) \right], \\ \frac{\partial u}{\partial Y} + \frac{n_{0r}}{c_{0r}^2} \mathcal{K}(u) \frac{\partial u}{\partial Y} &= 0 \quad \text{on } Y = h, \\ u &= 0 \quad \text{on } Y = 0, \end{aligned} \tag{8.55}$$

where the linear shear wave velocity c_{0r} , the nonlinear material constant n_{0r} , and \mathcal{K} are defined by

$$\begin{aligned} c_{0r}^2 &= \frac{\mu_0}{\rho_0} = \frac{2\Sigma'(3)}{\rho_0}, \\ n_{0r} &= \frac{2\Sigma''(3)}{\rho_0}, \\ \mathcal{K}(u) &= \left(\frac{\partial u}{\partial X} \right)^2 + \left(\frac{\partial u}{\partial Y} \right)^2, \end{aligned} \tag{8.56}$$

respectively, and similarly for a heterogeneous layer

$$\begin{aligned} \frac{\partial^2 u}{\partial t^2} - c_T^2 \left(\frac{\partial^2 u}{\partial X^2} + \frac{\partial^2 u}{\partial Y^2} \right) - \frac{1}{\rho} \frac{\partial(\rho c_T^2)}{\partial Y} \frac{\partial u}{\partial Y} &= \\ n_T \left[\frac{\partial}{\partial X} \left(\frac{\partial u}{\partial X} \mathcal{K}(u) \right) + \frac{\partial}{\partial Y} \left(\frac{\partial u}{\partial Y} \mathcal{K}(u) \right) \right] + \frac{\mathcal{K}(u)}{\rho} \frac{\partial(\rho n_T)}{\partial Y} \frac{\partial u}{\partial Y}, & \tag{8.57} \\ \frac{\partial u}{\partial Y} + \frac{n_T}{c_T^2} \mathcal{K}(u) \frac{\partial u}{\partial Y} &= 0 \quad \text{on } Y = h, \\ u &= 0 \quad \text{on } Y = 0, \end{aligned}$$

where the linear shear wave velocity c_T , the nonlinear material function n_T , and \mathcal{K} are defined by

$$\begin{aligned} c_T^2 &= \frac{\mu}{\rho} = \frac{2\Sigma'(3, Y)}{\rho}, \\ n_T &= \frac{2\Sigma''(3, Y)}{\rho}, \\ \mathcal{K}(u) &= \left(\frac{\partial u}{\partial X} \right)^2 + \left(\frac{\partial u}{\partial Y} \right)^2, \end{aligned} \tag{8.58}$$

respectively. It can be seen that the functions μ , ρ , and n_T are not constants as a homogeneous case in (8.55)–(8.56). In the absence of the nonlinearity, i.e., $n_T = 0$ in (8.57)–(8.58) or $n_{0r} = 0$ in (8.55)–(8.56), the governing equations with the boundary conditions for the linear SH waves in a heterogeneous or homogeneous layer are found, respectively. Moreover, the constituent materials of a heterogeneous or homogeneous layer soften in shear if $n_T < 0$ or if $n_{0r} < 0$, but if $n_T > 0$ or if $n_{0r} > 0$ they harden, respectively. In our analysis, for a heterogeneous layer, n_T is a differentiable function of Y , and the following suitable choices in [7] on the functions μ and ρ ,

$$\mu = \mu_0 \cosh^2(\alpha Y), \quad \rho = \rho_0 \cosh^2(\alpha Y) \quad (8.59)$$

are considered where μ_0 and ρ_0 are constants, and α is a parameter that measures the heterogeneous effect. Moreover, for a numerical calculation, we choose as

$$n_T = n_{0_T} \cosh^2(\gamma Y) \quad (8.60)$$

where γ is a parameter that measures the nonlinear effect. For further information, we refer to [7, 13] for heterogeneous and homogeneous layers, respectively.

8.4 Conclusions with Some New Results

From (8.55)–(8.56) and (8.57)–(8.58), we observe some additional terms there. In other words, under $\alpha \rightarrow 0$ and $\gamma \rightarrow 0$, the heterogeneous case (8.57)–(8.58) can be reducible to the homogeneous case (8.55)–(8.56). Let us continue with the given analyzes of considered problems [7, 13], we see that there are three possibilities for n_{0_T} as follows:

Case 1: If $n_{0_T} = 0$, then we obtain the linear SH waves that are easy to consider, so it is not the case.

Case 2: If $n_{0_T} > 0$, then we show the existence of nonlinear dark solitary SH waves in a heterogeneous layer with heterogeneous and nonlinear effects and a homogeneous layer for details see [12, 13], respectively. We observe that, in this case, there are some possible comparisons, but they are out of this work.

Case 3: If $n_{0_T} < 0$, then we show the existence of nonlinear bright solitary SH waves in a heterogeneous layer with heterogeneous and nonlinear effects and a homogeneous layer for details see [7, 13], respectively. We observe that, in this case, there are also some possible comparisons. One possible comparison can be given as follows:

$$n = 0; \quad A \neq 0, \Lambda \rightarrow 0 \Leftrightarrow A \rightarrow 0, \Lambda \rightarrow 0 \quad (8.61)$$

where $A = \alpha h$ and $\Lambda = \gamma h$ in a non-dimensional sense. Moreover, n indicates a branch of the dispersion relation in [7].

Here, we need to remember some physically important functions in our analysis. Phase velocity, shear wave velocity, group velocity, wavenumber, and angular frequency can be denoted by c , c_{0_T} , V_g , k , and w , respectively. Moreover, it is possible to define some non-dimensional expressions such as $C = c/c_{0_T}$ for phase velocity, $V_G = V_g/c_{0_T}$ for group velocity, $K = kh$ for wavenumber, and $W = wh/c_{0_T}$ for angular frequency. Using non-dimensional expressions, we can rewrite the dispersion relation of the considered problem from [7] for another result also see [12] as follows:

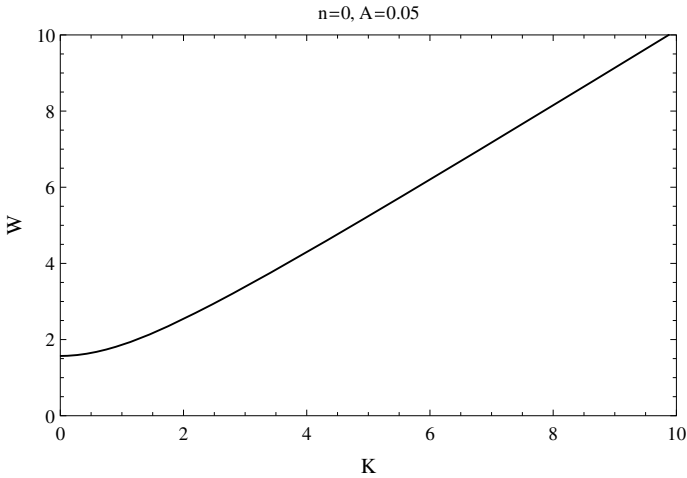


Fig. 8.1 Variation of W versus K

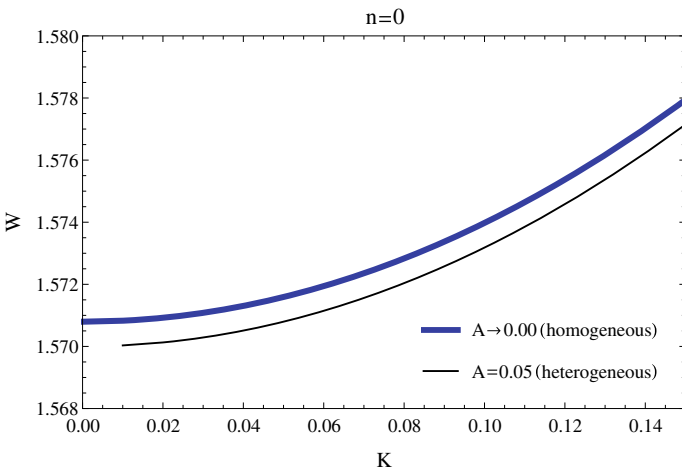


Fig. 8.2 Comparison of the heterogeneous effects of W versus K

$$KP = \arctan[KP/(A \tanh A)] + n\pi \tag{8.62}$$

where $P = \sqrt{C^2 - 1 - (A^2/K^2)}$.

For all branches, i.e., $n = 0, 1, 2, \dots$, of dispersion relation (8.62), the following limits exist

$$\begin{aligned} C \rightarrow \infty, \quad V_G \rightarrow 0, \quad \Gamma \rightarrow 0 \quad \text{as } K \rightarrow 0, \\ C \rightarrow 1, \quad V_G \rightarrow 1, \quad \Gamma \rightarrow 0 \quad \text{as } K \rightarrow \infty. \end{aligned} \tag{8.63}$$

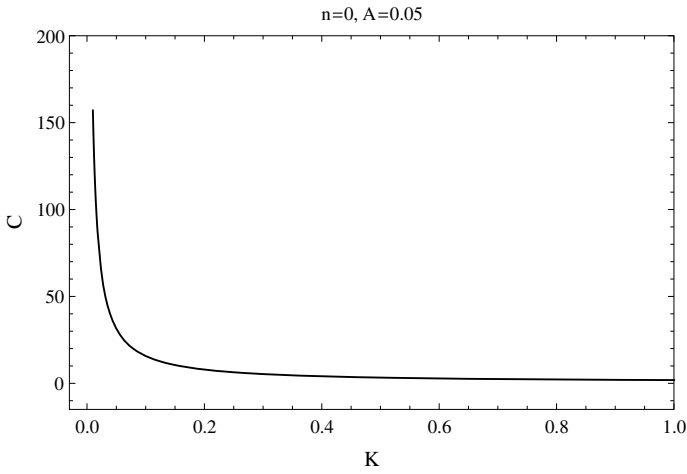


Fig. 8.3 Variation of C versus K

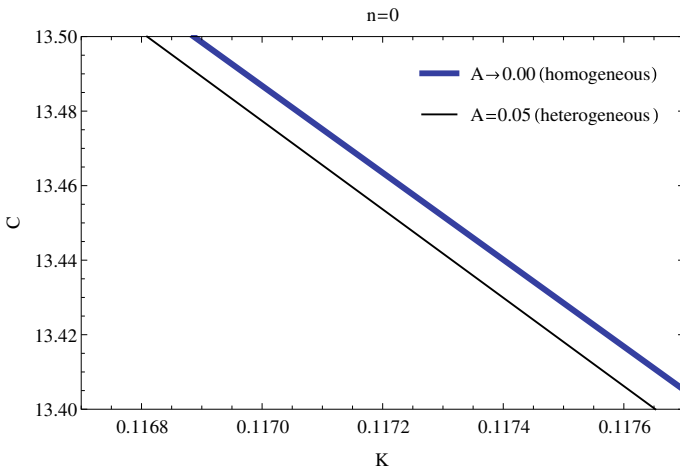


Fig. 8.4 Comparison of the heterogeneous effects of C versus K

Such limits are also valid in [23]. We see the existence of nonlinear bright solitary SH waves in this layer for homogeneous materials in [13] and for heterogeneous materials in [7] with heterogeneous effects. In both works, the self-modulation of nonlinear SH waves is given via the following nonlinear partial differential equation

$$i \frac{\partial \mathcal{A}}{\partial \tau} + \Gamma \frac{\partial^2 \mathcal{A}}{\partial \xi^2} + \Delta |\mathcal{A}|^2 \mathcal{A} = 0 \tag{8.64}$$

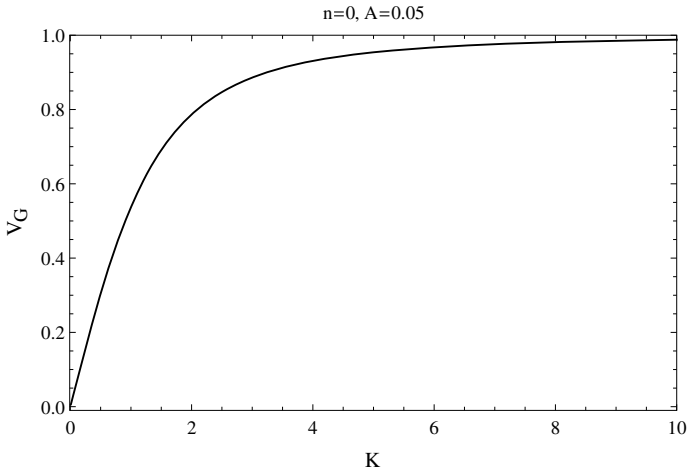


Fig. 8.5 Variation of V_G versus K

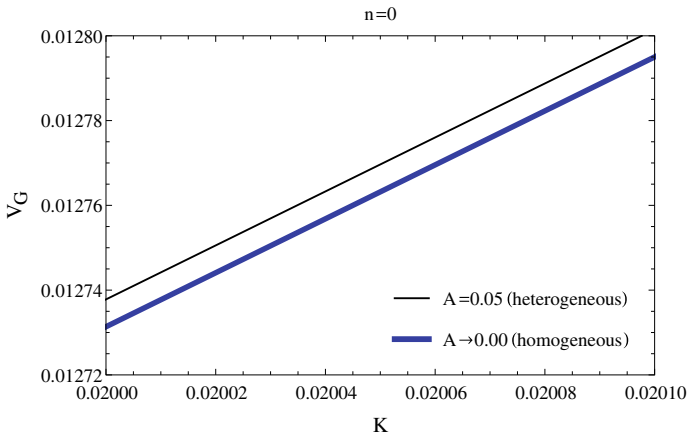


Fig. 8.6 Comparison of the heterogeneous effects of V_G versus K

which is known as an NLS equation, but with different coefficients. The NLS equation is an important prototypical equation for nonlinear modulation of elastic waves. We need to emphasize the importance of the sign of product $\Gamma \Delta$ for the existence of solitary wave solutions. For known solitary wave solutions to (8.64), we refer to [1, 15, 30, 40]. Needless to say, as $A \rightarrow 0$ and $\Lambda \rightarrow 0$ (in dimensional case $\alpha \rightarrow 0$ and $\gamma \rightarrow 0$, respectively) the coefficients of the NLS equation obtained in [7], for another result also see [12], reduce to the coefficients of the NLS equation given in [13]. Therefore, the works in [7, 12] are an improved version of the work [13]. Improvement is from homogeneity to heterogeneity. Here, our goal is to emphasize the comparison of heterogeneous material with homogeneous one for nonlinear bright

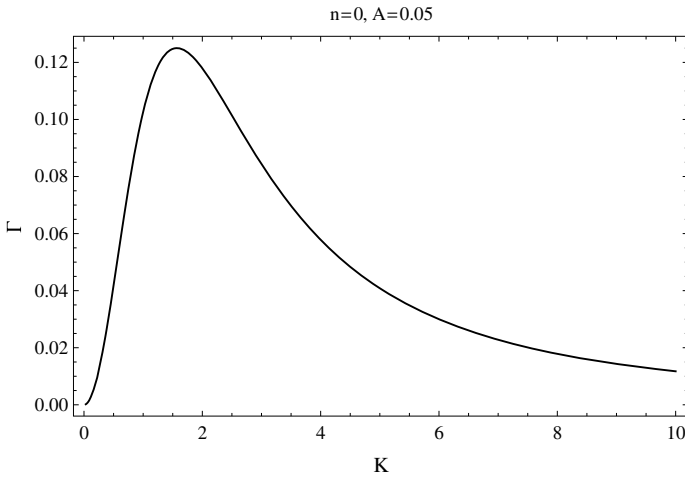


Fig. 8.7 Variation of Γ versus K

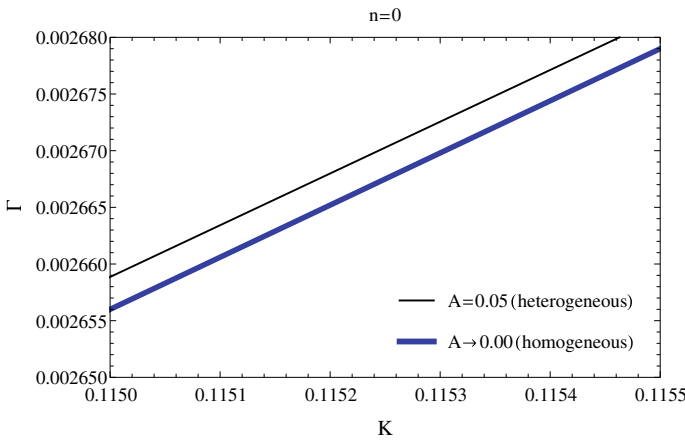


Fig. 8.8 Comparison of the heterogeneous effects of Γ versus K

solitary SH waves in terms of heterogeneous effect, i.e., the comparison of [7, 13] in terms of heterogeneous effect for this paper.

It is necessary to emphasize, we know that, in such an analysis, Γ carries the dispersion and Δ carries the nonlinearity. In limits above, we see that Γ approaches to zero as K approaches to zero at where V_G has a minimum there. Namely, the dispersion vanishes at $K = 0$. And also, for the lowest branch of the dispersion relation, we see that Δ approaches to ∞ as K approaches to zero for nonlinear bright solitary SH waves. Namely, Δ grows unboundedly at $K = 0$. At such critical points, it is not possible to balance the nonlinearity and the dispersion with the given analysis. The analyzes in [7, 13] for another result also see [12] do not work well

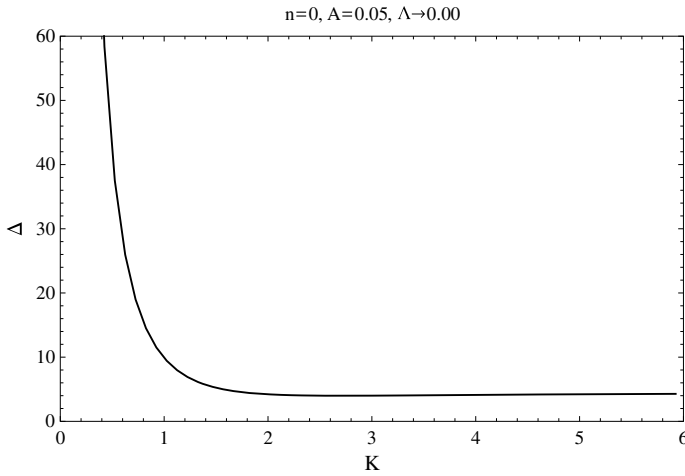


Fig. 8.9 Variation of Δ versus K

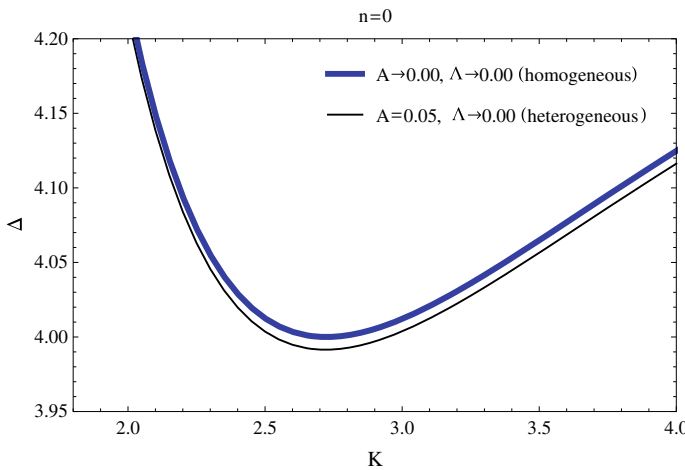


Fig. 8.10 Comparison of the heterogeneous effects of Δ versus K

for such cases. Maybe, some researchers can try to improve the analysis at this point for a future job. Moreover, for the stability of solutions of such problems [7, 13], for another result also see [12], and other types of solutions of the NLS equation, we refer to [36], which is a good and scientifically valuable paper for this area.

Let us talk about the related comparison part in view of existence of solutions. The existence of the traveling wave solutions of the NLS equation of the form

$$\mathcal{A}(\xi, \tau) = \phi(\eta)\text{Exp}[i(K_0\xi - \Omega\tau)]; \quad \eta = \xi - V_0\tau, \tag{8.65}$$

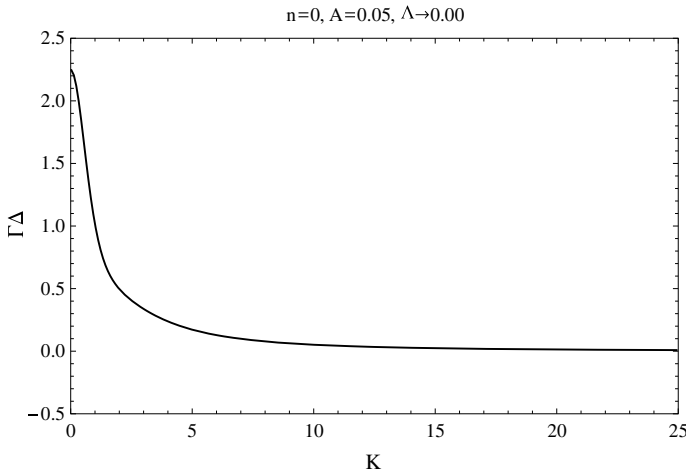


Fig. 8.11 Variation of $\Gamma \Delta$ versus K

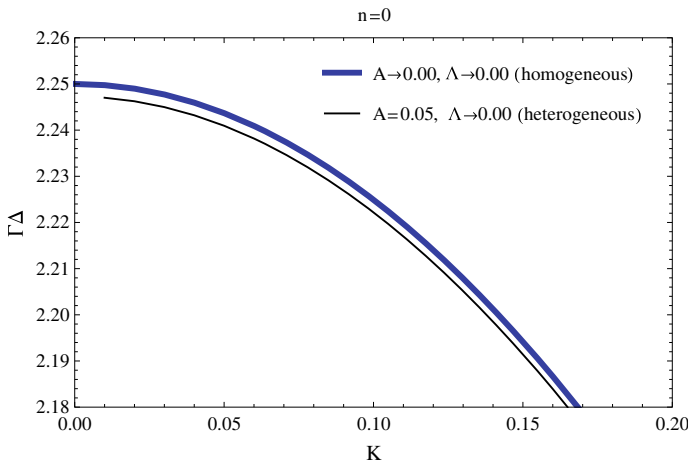


Fig. 8.12 Comparison of the heterogeneous effects of $\Gamma \Delta$ versus K

bases on the sign of $\Gamma \Delta$, where V_0 and K_0 are constants. For $\Gamma \Delta > 0$, if $\phi \rightarrow 0$ and $d\phi/d\eta \rightarrow 0$ as $|\eta| \rightarrow \infty$, the solution \mathcal{A} is

$$\mathcal{A}(\xi, \tau) = \phi_0 \operatorname{sech}[(\Delta/2\Gamma)^{1/2} \phi_0 \eta] \operatorname{Exp}[i(K_0 \xi - \Omega \tau)]. \tag{8.66}$$

Here, $(\Gamma K_0^2 - \Omega)/\Delta \phi_0^2 = 1/2$ and $V_0 = 2K_0 \Gamma$. This solution is called a bright solitary wave solution [1, 15, 30, 40]. In [7, 13], we claim that if the layers are made up of a softening material (S), i.e., $n_{0r} < 0$, then $\Gamma \Delta > 0$ for all $K > 0$. Therefore, the bright solitary SH waves exist in such layers using a short review of the solution of

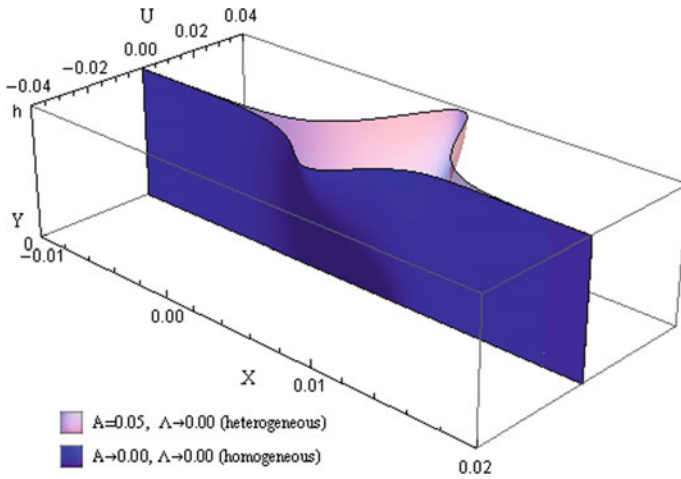


Fig. 8.13 Comparison of the heterogeneous effects for deformation fields of the planes $Z = 0$ of the layers

the NLS equation. In terms of the heterogeneous effect, we compare the nonlinear bright solitary SH waves via the NLS equation considering the material model S as follows:

$$S : \quad \mu_0 = \rho_0 = 1, \quad n_{0r} = -1, \quad K = K_0 = \phi_0 = 0.01. \quad (8.67)$$

For the mentioned comparison, using the material model (8.67), fixing the nonlinear effect (i.e. $\Lambda \rightarrow 0.00$) and changing the heterogeneous effect from $A = 0.00$ to $A = 0.05$, all numerical results for the lowest branch of both dispersion relations are graphically presented as follows:

- the variation of W versus K and the comparison between heterogeneous and homogeneous materials for the variation of W versus K in Figs. 8.1 and 8.2, respectively,
- the variation of C versus K and the comparison between heterogeneous and homogeneous materials for the variation of C versus K in Figs. 8.3 and 8.4, respectively,
- the variation of V_G versus K and the comparison between heterogeneous and homogeneous materials for the variation of V_G versus K in Figs. 8.5 and 8.6, respectively,
- the variation of Γ versus K and the comparison between heterogeneous and homogeneous materials for the variation of Γ versus K in Figs. 8.7 and 8.8, respectively,
- the variation of Δ versus K and the comparison between heterogeneous and homogeneous materials for the variation of Δ versus K in Figs. 8.9 and 8.10, respectively,
- the variation of $\Gamma \Delta$ versus K and the comparison between heterogeneous and homogeneous materials for the variation of $\Gamma \Delta$ versus K in Figs. 8.11 and 8.12, respectively,

and also, the comparison of heterogeneous and homogeneous materials for the deformation fields of the planes $Z = 0$ of the layers in Fig. 8.13.

Acknowledgements We would like to thank the editor and the referees for their useful suggestions.

References

1. Ablowitz, M.J., Clarkson, P.A.: Solitons, Nonlinear Evolution Equations, and Inverse Scattering. Cambridge University Press, Cambridge (1991)
2. Achenbach, J.D.: Wave Propagation in Elastic Solids. North-Holland Publishing Co., Amsterdam (1973)
3. Ahmetolan, S., Teymur, M.: Nonlinear modulation of SH waves in a two-layered plate and formation of surface SH waves. *Int. J. Non-linear Mech.* **38**, 1237–1250 (2003)
4. Ahmetolan, S., Teymur, M.: Nonlinear modulation of SH waves in an incompressible hyperelastic plate. *Z. Angew. Math. Phys.* **58**, 457–474 (2007)
5. Carroll, M.M.: Some results on finite-amplitude elastic waves. *Acta Mech.* **3**, 167 (1967)
6. Deliktas, E., Teymur, M.: Surface shear horizontal waves in a double-layered nonlinear elastic half-space. *IMA J. Appl. Math.* **83**(3), 471–495 (2018)
7. Demirkuş, D.: Nonlinear bright solitary SH waves in a hyperbolically heterogeneous layer. *Int. J. Nonlinear Mech.* **102**, 53–61 (2018)
8. Demirkuş, D.: Antisymmetric bright solitary SH waves in a nonlinear heterogeneous plate. *Z. Angew. Math. Phys.* **69**(5), 128 (2018)
9. Demirkuş, D.: Symmetric bright solitary SH waves in a nonlinear heterogeneous plate. *Z. Angew. Math. Phys.* **70**(2), 63 (2019)
10. Demirkuş, D.: Symmetric dark solitary SH waves in a nonlinear heterogeneous plate. *Z. Angew. Math. Phys.* **70**(4), 108 (2019)
11. Demirkuş, D.: Antisymmetric dark solitary SH waves in a nonlinear heterogeneous plate. *Z. Angew. Math. Phys.* **70**(6), 173 (2019)
12. Demirkuş, D.: Nonlinear dark solitary SH waves in a heterogeneous layer, *TWMS J. Appl. & Eng. Math.* <https://doi.org/10.26837/jaem.627563> (2020)
13. Demirkuş, D., Teymur, M.: Shear horizontal waves in a nonlinear elastic layer overlying a rigid substratum. *Hacettepe J. Math. Stat.* **46**(5), 801–815 (2017)
14. Destrade, M., Goriely, M.A., Saccomandi, G.: Scalar evolution equations for shear waves in incompressible solids: a simple derivation of the Z, ZK, KZK and KP equations. *Proc. R. Soc. A* **467**, 1823–1834 (2011)
15. Dodd, R.K., Eilbeck, J.C., Gibbon, J.D., Morris, H.C.: Solitons and Nonlinear Wave Equations. Academic Press, London (1982)
16. Eringen, A.C., Şuhubi, E.S.: *Elastodynamics*, vol. 1. Academic Press, New York (1974)
17. Erofeev, V.I.: *Wave Processes in Solids with Microstructure*. World Scientific, Singapore (2002)
18. Ewing, W.M., Jardetsky, W.S., Press, F.: *Elastic Waves in Layered Media*. McGraw-Hill, New York (1957)
19. Farnell, G.W.: Types and properties of surface waves. In: A.A. Oliner (ed.) *Acoustic Surface Waves*, pp. 13–60. Springer, Berlin (1978)
20. Ferreira, E.R., Boulanger, Ph., Destrade, M.: Large amplitude Love waves. *Q. Jl. Mech. Appl. Math.* **61**(3), 353–371 (2008)
21. Fu, Y.: On the propagation of non-linear traveling waves in an incompressible elastic plate. *Wave Motion* **19**, 271–292 (1994)
22. Graff, K.F.: *Wave Motion in Elastic Solids*. Clarendon Press, Oxford (1975)
23. Hudson, J.A.: Love waves in a heterogeneous medium. *R. Astr. Soc. Geophys. J.* **6**, 131–147 (1962)
24. Jeffrey, A., Kawahara, T.: *Asymptotic Methods in Non-linear Wave Theory*. Pitman, Boston (1981)
25. Kaplunov, J., Nobili, A.: Multi-parametric analysis of strongly inhomogeneous periodic waveguides with internal cut-off frequencies. *Math. Meth. App. Sci.* **40**(9), 3381–3392 (2017)

26. Kaplunov, J., Prikazchikov, D.A., Prikazchikova, L.A.: Dispersion of elastic waves in a strongly inhomogeneous three-layered plate. *Int. J. Solids Struct.* **113**, 169–179 (2017)
27. Maugin, G.A.: Elastic surface waves with transverse horizontal polarization. In: Hutchinson, J.W. (ed.) *Advances in Applied Mechanics*, vol. 23, pp. 373–434. Academic Press, New York (1983)
28. Maugin, G.A., Hadouaj, H.: Solitary surface transverse waves on an elastic substrate coated with a thin film. *Phy. Rev. B.* **44**(3), 1266–1280 (1991)
29. Mayer, A.P.: Surface acoustic waves in nonlinear elastic media. *Phys. Reports* **256**, 4–5 (1995)
30. Peregrine, D.H.: Water waves, nonlinear Schrödinger equations, and their solutions. *J. Aust. Math. Soc. Ser. B.* **25**, 16–43 (1983)
31. Prikazchikova, L., Aydın, Y.E., Erbaş, B., Kaplunov, J.: Asymptotic analysis of an anti-plane dynamic problem for a three-layered strongly inhomogeneous laminate. *Math. Mech. Solids* (2018). <https://doi.org/10.1177/1081286518790804>
32. Porubov, A.V., Samsonov, A.M.: Long nonlinear strain waves in layered elastic half-space. *Int. J. Nonlinear Mech.* **30**(6), 861–877 (1995)
33. Pucci, E., Saccomandi, G.: Secondary motions associated with anti-plane shear in nonlinear isotropic elasticity. *Q. Jl. Mech. Appl. Math.* **66**, 221–239 (2013)
34. Sahu, S.A., Saroj, P.K., Dewangan, N.: SH-waves in viscoelastic heterogeneous layer over half-space with self-weight. *Arch. Appl. Mech.* **84**, 235–245 (2014)
35. Sharma, B.L., Eremeyev, V.A.: Wave transmission across surface interfaces in lattice structures. *Int. J. Eng. Sci.* **145**, 103173 (2019)
36. Teymur, M.: Nonlinear modulation of Love waves in a compressible hyper-elastic layered half-space. *Int. J. Eng. Sci.* **26**, 907–927 (1988)
37. Teymur, M.: Small but finite amplitude waves in a two-layered incompressible elastic medium. *Int. J. Eng. Sci.* **34**, 227–241 (1996)
38. Teymur, M., Var, H., Deliktas, E.: Nonlinear modulation of surface SH waves in a double-layered elastic half-space. In: *Dynamical Processes in Generalized Continua and Structures* vol. 103, pp. 465–483 (2019)
39. Vardoulakis, I., Georgiadis, H.G.: SH surface waves in a homogeneous gradient-elastic half-space with surface energy. *J. Elast.* **47**, 147–165 (1997)
40. Zakharov, V.E., Shabat, A.B.: Interaction between solitons in a stable medium. *Sov. Phys. JETP* **37**, 823–828 (1973)

Chapter 9

On Surface Kinetic Constitutive Relations



Victor A. Eremeyev  and Leonid P. Lebedev

Abstract In the framework of the strain gradient surface elasticity we discuss a consistent form of surface kinetic energy. This kinetic constitutive equation completes the statement of initial–boundary value problems. The proposed surface kinetic energy density is the most general function consistent with the constitutive relations in bulk. As the surface strain energy depends on the surface deformation gradient and its gradient, the kinetic energy is a quadratic function of the velocity and its surface gradient.

9.1 Introduction

Nowadays it is well established that nanostructured materials may demonstrate quite unusual and very promising properties due to high surface-to-volume ratio with respect to a characteristic size of nano-objects. The size-dependence observed in nanoscale results in certain enhancements of the models is used for such materials. It is worth to mention here the strain gradient elasticity and surface elasticity, see [1, 2, 7, 9, 10, 21, 27, 28, 45], respectively. The both approaches may describe surface-related phenomena such as the size-effect. Within the framework of the surface elasticity we introduce additional surface constitutive relations that are a surface strain energy density and surface stresses. This changes the corresponding boundary

V. A. Eremeyev (✉)

Faculty of Civil and Environmental Engineering, Gdańsk University of Technology,
ul. Gabriela Narutowicza 11/12, 80-233 Gdańsk, Poland

Southern Federal University, Milchakova str. 8a, 344090 Rostov on Don, Russia

Southern Scientific Center of RASci, Chekhova str. 41, 344006 Rostov on Don, Russian Federation

e-mail: victor.eremeev@pg.edu.pl

L. P. Lebedev

Universidad Nacional de Colombia, Cr. 45, # 26–85, Bogotá, D.C., Colombia

e-mail: llebedev@unal.edu.co

© Springer Nature Switzerland AG 2020

H. Altenbach et al. (eds.), *Nonlinear Wave Dynamics of Materials and Structures*, Advanced Structured Materials 122,
https://doi.org/10.1007/978-3-030-38708-2_9

conditions which affect the solutions, see, e.g., the analysis of stress concentration near a crack tip [23, 29, 46].

Let us note that for dynamics problems we have to introduce also an additional surface kinetic energy density. The simplest form of the surface kinetic energy was proposed by Gurtin and Murdoch [26]. As a result, in the dynamics of solids with surface stresses we get also inertia terms in the boundary conditions. These inertia terms affect the propagation of surface waves. In particular, in the media with surface stresses there exists anti-plane surface waves [16, 47]. Similar waves exist also for other models possessing surface energy such as the strain gradient elasticity, see [8, 22, 24, 30, 35–37, 44, 48]. A straightforward comparison of the Toupin–Mindlin strain gradient elasticity with Gurtin–Murdoch’s elasticity was performed by Eremeyev et al. [18]. As the form of the strain energy in bulk, the form of surface kinetic energy plays an important role in dynamics of solids with surface stresses. From the lattice dynamics point of view, the surface kinetic energy can be interpreted as a kinetic energy of a surface row of atoms [14] but for more complex surface structures as discussed by Eremeyev [10, 12] it can be a more complex function.

The aim of this paper is to discuss the most general form of the surface kinetic energy consistent with the strain energy density. Here we consider the surface strain energy as an objective function of the surface deformation gradient and its surface gradient. So the surface kinetic energy depends on the velocity and its surface gradient. Using the least action principle we derive the generalized Young–Laplace equation which contains inertia terms.

The paper is organized as follows. In Sect. 9.2 we briefly introduce the basic equations for large deformations of solids with surface stresses and surface hyperstresses. In Sect. 9.3 we discuss possible forms of kinetic equations that is the forms of surface kinetic energy. Using the least action principle we derive the generalized Young–Laplace equation in Sect. 9.4.

9.2 Kinematics and Surface Strain Energy

Let us consider an elastic solid body B with surface stresses. Deformation of B is described as a mapping from a reference placement \varkappa into a current placement χ

$$\mathbf{x} = \mathbf{x}(\mathbf{X}, t), \quad (9.1)$$

where \mathbf{x} and \mathbf{X} are the position vectors of the same material particle in the current and reference placements, respectively, and t is time. For a hyperelastic solid there exists a strain energy density W given by

$$W = W(\mathbf{F}), \quad (9.2)$$

where $\mathbf{F} = \nabla \mathbf{x}$ is the deformation gradient defined as in [17, 39], and ∇ is the 3D nabla-operator.

In addition to (9.2) we introduce the surface strain energy as a function of the surface deformation gradient $\mathbf{F}_s = \nabla_s \mathbf{x}$ and its surface gradient $\nabla_s \mathbf{F}_s = \nabla_s \nabla_s \mathbf{x}$. Here $\nabla_s = \mathbf{A} \cdot \nabla$, where $\mathbf{A} = \mathbf{I} - \mathbf{N} \otimes \mathbf{N}$, \mathbf{I} is the 3D unit tensor, \mathbf{N} is the unit vector of outward normal to the boundary of B in \varkappa , and \otimes is the dyadic product. So we have the surface constitutive relation in the form

$$U = U(\mathbf{F}_s, \nabla_s \mathbf{F}_s). \quad (9.3)$$

Equation (9.3) includes constitutive relations of the surface elasticity by Gurtin and Murdoch [25] and by Steigmann and Ogden [40, 41] as the special cases. The strongly anisotropic surface elasticity proposed by Eremeyev [12] is also a particular case of (9.3).

The principle of the material frame indifference [43] states that W and U should be objective functions of their arguments, that is the following relations are fulfilled

$$W = W(\mathbf{F}) = W(\mathbf{F} \cdot \mathbf{O}), \quad (9.4)$$

$$U = U(\mathbf{F}_s, \nabla_s \mathbf{F}_s) = U(\mathbf{F}_s \cdot \mathbf{O}, \nabla_s \mathbf{F}_s \cdot \mathbf{O}) \quad (9.5)$$

for any orthogonal tensor \mathbf{O} , $\mathbf{O} \cdot \mathbf{O}^T = \mathbf{I}$. Here the centered dot denotes the dot product.

Relations (9.2) and (9.3) can be simplified if we take into account the material symmetry. In particular, knowing a priori a material symmetry one can significantly reduce the number of arguments used in (9.2) and (9.3), see, e.g., [13, 33] for 2D structures.

9.3 Kinetic Constitutive Equation

For dynamic problems, we also should introduce a surface kinetic energy K_s . A simple form of the surface kinetic energy density was proposed by Gurtin and Murdoch [26] as follows

$$K_s = \frac{1}{2} m \mathbf{v} \cdot \dot{\mathbf{v}}, \quad (9.6)$$

where m is the referential surface mass density, $\mathbf{v} = \dot{\mathbf{x}}$ is the velocity, and overdot stands for the derivative with respect to t . Obviously, Eq. (9.6) is a surface analog of the kinetic energy in the bulk given by

$$K = \frac{1}{2} \rho \mathbf{v} \cdot \dot{\mathbf{v}}, \quad (9.7)$$

where ρ is the referential mass density.

Let us note that the form of (9.6) is similar to the form of the kinetic energy for an elastic membrane. The discussion of comparison of the Gurtin–Murdoch surface elasticity with other models of thin interfaces and surface structures was

performed in many works, see, e.g., [19, 38]. Even for (9.6) we have new behaviour in dynamics of solids with surface stresses such as anti-plane surface waves, see [16, 47]. Considering other 2D models used in mechanics of structures such as plates and shells we have to note that there are more general forms of kinetic energy. Indeed, it is worth to mention the seminal papers by Timoshenko [42] and by Mindlin [32], where rotatory inertia was introduced and discussed, see also [6, 15, 31]. In the framework of six-parameter shell theory the general form of a kinetic equation was discussed by Pietraszkiewicz [34]. So in the case of surface elasticity we may also have a rather complex form of kinetic energy, especially if we consider nonhomogeneous microstructured and anisotropic thin coatings.

It is natural to assume K_s to be of a quadratic function with respect to \mathbf{v} and $\nabla_s \mathbf{v}$

$$K_s = \frac{1}{2} \mathbf{v} \cdot \mathbf{J}_0 \cdot \mathbf{v} + \mathbf{v} \cdot \mathbf{J}_1 : \nabla_s \mathbf{v} + \frac{1}{2} \nabla_s \mathbf{v} : \mathbf{J}_2 : \nabla_s \mathbf{v}, \quad (9.8)$$

where \mathbf{J}_0 , \mathbf{J}_1 , and \mathbf{J}_2 are inertia tensors of second, third and fourth-order, respectively, and $:$ is the double dot product. They have the following properties

$$\mathbf{J}_0 = \mathbf{J}_0^T, \quad \mathbf{J}_1 : \mathbf{N} \otimes \mathbf{a} = \mathbf{0}, \quad \mathbf{N} \otimes \mathbf{a} : \mathbf{J}_2 : \mathbf{N} \otimes \mathbf{b} = 0, \quad \forall \mathbf{a}, \mathbf{b}.$$

Taking $\mathbf{J}_0 = m\mathbf{I}$, $\mathbf{J}_1 = \mathbf{0}$, $\mathbf{J}_2 = \mathbf{0}$ we get (9.6). \mathbf{J}_2 is similar to the inertia tensors in the theory of shells which describe rotatory inertia whereas \mathbf{J}_1 describes coupling between rotatory and translational inertia, see e.g. [3, 31, 34]. Tensors \mathbf{J}_0 , \mathbf{J}_1 , and \mathbf{J}_2 are 2D analogs of the ones used in 3D strain gradient elasticity, see [18, 35]. In general, \mathbf{J}_0 , \mathbf{J}_1 , and \mathbf{J}_2 may depend on t , \mathbf{x} , \mathbf{X} , and \mathbf{F}_s .

Considering possible a priori restrictions imposed on K_s , let us note that a kinetic energy is not invariant under rigid body motions, so we cannot apply the same technique as the invariance arguments followed from the material frame indifference principle, as for W and U . In general, K_s may possess the same material symmetry as U but this is not so obvious as dynamic properties may differ from static ones. So in the following we leave the general form of K_s .

9.4 Generalized Young–Laplace Equation

In order to derive the equation of motion and corresponding natural boundary conditions we apply the least action principle [5]. The least action functional is

$$\mathcal{H} = \int_{t_1}^{t_2} \iiint_V (K - W) dV dt + \int_{t_1}^{t_2} \iint_S (K_s - U) dS dt, \quad (9.9)$$

where V is the volume occupied by B in the reference placement, $S \subset \partial V$ is a part of ∂V , the boundary of V , where the surface energy is defined, and t_1 and t_2 are two time instants. Here for brevity we omit external loadings.

Considering the variational equation for all kinematically admissible variations $\delta \mathbf{x}$, that is

$$\delta \mathcal{H} = 0, \quad (9.10)$$

where δ is the symbol of variation, we derive the governing equations of dynamics of solids with surface stresses.

The first variation of \mathcal{H} takes the form

$$\begin{aligned} \delta \mathcal{H} &= \int_{t_1}^{t_2} \iiint_V (\rho \mathbf{v} \cdot \delta \mathbf{v} - \delta W) \, dV \, dt \\ &\quad + \int_{t_1}^{t_2} \iint_S (\mathbf{v} \cdot \mathbf{J}_0 \cdot \delta \mathbf{v} + \delta \mathbf{v} \cdot \mathbf{J}_1 : \nabla_s \mathbf{v} + \mathbf{v} \cdot \mathbf{J}_1 : \nabla_s \delta \mathbf{v} + \nabla_s \mathbf{v} : \mathbf{J}_2 : \nabla_s \delta \mathbf{v} \\ &\quad - \delta U) \, dS \, dt \\ &= \int_{t_1}^{t_2} \iiint_V (\rho \mathbf{v} \cdot \delta \mathbf{v} - \mathbf{P} : \nabla_s \delta \mathbf{x}) \, dV \, dt \\ &\quad + \int_{t_1}^{t_2} \iint_S (\mathbf{v} \cdot \mathbf{J}_0 \cdot \delta \mathbf{v} + \delta \mathbf{v} \cdot \mathbf{J}_1 : \nabla_s \mathbf{v} + \mathbf{v} \cdot \mathbf{J}_1 : \nabla_s \delta \mathbf{v} + \nabla_s \mathbf{v} : \mathbf{J}_2 : \nabla_s \delta \mathbf{v} \\ &\quad - \mathbf{M} : \nabla_s \nabla_s \delta \mathbf{x} - \mathbf{T} : \nabla_s \delta \mathbf{x}) \, dS \, dt, \end{aligned} \quad (9.11)$$

where \mathbf{P} is the Piola–Kirchhoff stress tensor of first kind, \mathbf{T} , is the first Piola–Kirchhoff surface stress tensor, and \mathbf{M} is the first Piola–Kirchhoff surface hyper stress tensor, which are defined as follows

$$\mathbf{P} = \frac{\partial W}{\partial \mathbf{F}}, \quad \mathbf{T} = \frac{\partial U}{\partial \mathbf{F}_s}, \quad \mathbf{M} = \frac{\partial U}{\partial \nabla_s \mathbf{F}_s}. \quad (9.12)$$

\mathbf{T} and \mathbf{M} have the following properties

$$\mathbf{N} \cdot \mathbf{T} = \mathbf{0}, \quad \mathbf{N} \cdot \mathbf{M} = \mathbf{0}, \quad (\mathbf{a} \otimes \mathbf{N}) : \mathbf{M} = \mathbf{0}, \quad \forall \mathbf{a}.$$

Integrating by parts we transform $\delta \mathcal{H}$ into

$$\begin{aligned}
\delta \mathcal{H} = & \int_{t_1}^{t_2} \iiint_V (-\rho \dot{\mathbf{v}} + \nabla \cdot \mathbf{P}) \cdot \delta \mathbf{v} \, dV \, dt \\
& + \int_{t_1}^{t_2} \iint_S [-\mathbf{N} \cdot \mathbf{P} + \nabla_s \cdot (\mathbf{T} - \nabla_s \cdot \mathbf{M}) \\
& - (\mathbf{v} \cdot \mathbf{J}_0) - (\mathbf{J}_1 : \dot{\nabla}_s \mathbf{v})^T + \nabla_s \cdot (\mathbf{v} \cdot \mathbf{J}_1) + \nabla_s \cdot (\nabla_s \dot{\mathbf{v}} : \mathbf{J}_2)] \cdot \delta \mathbf{v} \, dS \, dt, \quad (9.13)
\end{aligned}$$

For brevity we omit here the analysis of the natural boundary conditions at edge ∂S which will be performed similar to Eremeyev [11] in the forthcoming papers. Using standard calculus of variations from (9.10) and (9.13) we get the Lagrangian equation of motion

$$\nabla \cdot \mathbf{P} = \rho \dot{\mathbf{v}}, \quad \mathbf{X} \in V, \quad (9.14)$$

and the natural boundary condition at S

$$\begin{aligned}
\mathbf{N} \cdot \mathbf{P} = & \nabla_s \cdot (\mathbf{T} - \nabla_s \cdot \mathbf{M}) \\
& - (\mathbf{v} \cdot \mathbf{J}_0) - (\mathbf{J}_1 : \dot{\nabla}_s \mathbf{v})^T + \nabla_s \cdot (\mathbf{v} \cdot \mathbf{J}_1) + \nabla_s \cdot (\nabla_s \dot{\mathbf{v}} : \mathbf{J}_2), \quad \mathbf{X} \in S. \quad (9.15)
\end{aligned}$$

Following Duan et al. [9] we call (9.15) the generalized Young–Laplace equation. From the physical point of view it describes the motions of a 2D strain gradient medium attached to an elastic solid. Mathematically it represents nonlinear PDE with partial derivatives up to fourth order including mixed spatial and time derivatives as for the Timoshenko beams [42]. Let us note that nonlinearity here appears due to common nonlinearity of constitutive equations for \mathbf{P} , \mathbf{T} , and \mathbf{M} , as well as due to nonlinearity of the kinetic constitutive relation (9.8).

9.5 Conclusions

In the framework of the strain gradient surface elasticity we have discussed the surface kinetic constitutive equation. This equation introduces the surface kinetic energy as a quadratic function of velocity. The presented form is the most general which is consistent to the surface strain density. The corresponding natural boundary conditions are derived using the least action principle. Let us note that the presented results on the statement of the initial–boundary value problems of nonlinear media with microstructure lies in the fields of interests of Prof. Erofeev, to whom this paper is devoted, see, e.g., the books [4, 20] and references therein.

Acknowledgements VAE acknowledges the support of the Ministry of Education and Science of the Russian Federation, Project No. 9.1001.2017/4.6.

References

1. Aifantis, E.: Chapter one - internal length gradient (ilg) material mechanics across scales and disciplines. In: Bordas, S.P.A., Balint, D.S. (eds.) *Advances in Applied Mechanics*, vol. 49, pp. 1–110. Elsevier (2016)
2. Aifantis, E.C.: Gradient deformation models at nano, micro, and macro scales. *J. Eng. Mater. Technol.* **121**(2), 189–202 (1999)
3. Altenbach, H., Eremeyev, V.A.: Eigen-vibrations of plates made of functionally graded material. *CMC Comput. Mater. Continua* **9**(2), 153–178 (2009)
4. Bagdoev, A.G., Erofeev, V.I., Shekoyan, A.V.: *Wave Dynamics of Generalized Continua, Advanced Structured Materials*, vol. 24. Springer, Berlin, Heidelberg (2016)
5. Berdichevsky, V.: *Variational Principles of Continuum Mechanics: I. Fundamentals*. Springer, Heidelberg (2009)
6. Chróścielewski, J., Makowski, J., Pietraszkiewicz, W.: *Statyka i dynamika powłok wielopłatkowych. Nieliniowa teoria i metoda elementów skończonych* (in Polish), Wydawnictwo IPPT PAN, Warszawa (2004)
7. Cordero, N.M., Forest, S., Busso, E.P.: Second strain gradient elasticity of nano-objects. *J. Mech. Phys. Solids* **97**, 92–124 (2016)
8. dell'Isola, F., Madeo, A., Placidi, L.: Linear plane wave propagation and normal transmission and reflection at discontinuity surfaces in second gradient 3d continua. *ZAMM* **92**(1), 52–71 (2012)
9. Duan, H.L., Wang, J., Karihaloo, B.L.: Theory of elasticity at the nanoscale. In: Aref, H., van der Giessen, E. (eds.) *Advances in Applied Mechanics*, vol. 42, pp. 1–68. Elsevier (2009)
10. Eremeyev, V.A.: On effective properties of materials at the nano- and microscales considering surface effects. *Acta Mech.* **227**(1), 29–42 (2016)
11. Eremeyev, V.A.: On equilibrium of a second-gradient fluid near edges and corner points. In: Naumenko, K., Aßmus, M. (eds.) *Advanced Methods of Continuum Mechanics for Materials and Structures, Advanced Structured Materials*, vol. 60, pp. 547–556. Springer (2016)
12. Eremeyev, V.A.: Strongly anisotropic surface elasticity and antiplane surface waves. *Philos. Trans. R. Soc. A.* **378**(2162), 20190100 (2020). <https://doi.org/10.1098/rsta.2019.0100>
13. Eremeyev, V.A., Pietraszkiewicz, W.: Local symmetry group in the general theory of elastic shells. *J. Elast.* **85**(2), 125–152 (2006)
14. Eremeyev, V.A., Sharma, B.L.: Anti-plane surface waves in media with surface structure: discrete vs. continuum model. *Int. J. Eng. Sci.* **143**, 33–38 (2019)
15. Eremeyev, V.A., Lebedev, L.P., Altenbach, H.: *Foundations of Micropolar Mechanics*. Springer-Briefs in Applied Sciences and Technologies, Springer, Heidelberg (2013)
16. Eremeyev, V.A., Rosi, G., Naili, S.: Surface/interfacial anti-plane waves in solids with surface energy. *Mech. Res. Commun.* **74**, 8–13 (2016)
17. Eremeyev, V.A., Cloud, M.J., Lebedev, L.P.: *Applications of Tensor Analysis in Continuum Mechanics*. World Scientific, New Jersey (2018)
18. Eremeyev, V.A., Rosi, G., Naili, S.: Comparison of anti-plane surface waves in strain-gradient materials and materials with surface stresses. *Math. Mech. Solids* **24**, 2526–2535 (2019)
19. Eremeyev, V.A., Rosi, G., Naili, S.: Transverse surface waves on a cylindrical surface with coating. *Int. J. Eng. Sci.* 103188 (2020). <https://doi.org/10.1016/j.jengsci.2019.103188>
20. Erofeev, V.I.: *Wave Processes in Solids with Microstructure*. World Scientific, Singapore (2003)
21. Forest, S., Cordero, N.M., Busso, E.P.: First vs. second gradient of strain theory for capillarity effects in an elastic fluid at small length scales. *Comput. Mater. Sci.* **50**(4), 1299–1304 (2011)
22. Georgiadis, H., Vardoulakis, I., Lykotraftis, G.: Torsional surface waves in a gradient-elastic half-space. *Wave Motion* **31**(4), 333–348 (2000)
23. Gorbushin, N., Eremeyev, V.A., Mishuris, G.: On stress singularity near the tip of a crack with surface stresses. *Int. J. Eng. Sci.* **146**:103183 (2020)

24. Gourgiotis, P., Georgiadis, H.: Torsional and SH surface waves in an isotropic and homogenous elastic half-space characterized by the Toupin-Mindlin gradient theory. *Int. J. Solids Struct.* **62**, 217–228 (2015)
25. Gurtin, M.E., Murdoch, A.I.: A continuum theory of elastic material surfaces. *Arch. Ration. Mech. Anal.* **57**(4), 291–323 (1975)
26. Gurtin, M.E., Murdoch, A.I.: Surface stress in solids. *Int. J. Solids Struct.* **14**(6), 431–440 (1978)
27. Javili, A., dell’Isola, F., Steinmann, P.: Geometrically nonlinear higher-gradient elasticity with energetic boundaries. *J. Mech. Phys. Solids* **61**(12), 2381–2401 (2013)
28. Javili, A., McBride, A., Steinmann, P.: Thermomechanics of solids with lower-dimensional energetics: on the importance of surface, interface, and curve structures at the nanoscale. A unifying review. *Appl. Mech. Rev.* **65**(1), 010802 (2013)
29. Kim, C.I., Ru, C.Q., Schiavone, P.: A clarification of the role of crack-tip conditions in linear elasticity with surface effects. *Math. Mech. Solids* **18**(1), 59–66 (2013)
30. Li, Y., Wei, P.J., Tang, Q.: Reflection and transmission of elastic waves at the interface between two gradient-elastic solids with surface energy. *Eur. J. Mech. A Solids* **52**(C):54–71 (2015)
31. Libai, A., Simmonds, J.G.: *The Nonlinear Theory of Elastic Shells*, 2nd edn. Cambridge University Press, Cambridge (1998)
32. Mindlin, R.D.: Influence of rotatory inertia and shear on flexural motions of isotropic elastic plates. *Trans. ASME J. Appl. Mech.* **18**, 31–38 (1951)
33. Murdoch, A.I., Cohen, H.: Symmetry considerations for material surfaces. *Arch. Ration. Mech. Anal.* **72**(1), 61–98 (1979)
34. Pietraszkiewicz, W.: Refined resultant thermomechanics of shells. *Int. J. Eng. Sci.* **49**(10), 1112–1124 (2011)
35. Placidi, L., Rosi, G., Giorgio, I., Madeo, A.: Reflection and transmission of plane waves at surfaces carrying material properties and embedded in second-gradient materials. *Math. Mech. Solids* **19**(5), 555–578 (2014)
36. Rosi, G., Auffray, N.: Anisotropic and dispersive wave propagation within strain-gradient framework. *Wave Motion* **63**, 120–134 (2016)
37. Rosi, G., Nguyen, V.H., Naili, S.: Surface waves at the interface between an inviscid fluid and a dipolar gradient solid. *Wave Motion* **53**, 51–65 (2015)
38. Ru, C.Q.: Simple geometrical explanation of Gurtin-Murdoch model of surface elasticity with clarification of its related versions. *Sci. China Phys. Mech. Astron.* **53**(3), 536–544 (2010)
39. Simmonds, J.G.: *A Brief on Tensor Analysis*, 2nd edn. Springer, New York (1994)
40. Steigmann, D.J., Ogden, R.W.: Plane deformations of elastic solids with intrinsic boundary elasticity. *Proc. R. Soc. A* **453**(1959), 853–877 (1997)
41. Steigmann, D.J., Ogden, R.W.: Elastic surface-substrate interactions. *Proc. R. Soc. A* **455**(1982), 437–474 (1999)
42. Timoshenko, S.P.: LXVI. On the correction for shear of the differential equation for transverse vibrations of prismatic bars. *Philos. Mag.* **41**(245):744–746 (1921)
43. Truesdell, C., Noll, W.: *The Non-linear Field Theories of Mechanics*, 3rd edn. Springer, Berlin (2004)
44. Vardoulakis, I., Georgiadis, H.G.: SH surface waves in a homogeneous gradient-elastic half-space with surface energy. *J. Elast.* **47**(2), 147–165 (1997)
45. Wang, J., Huang, Z., Duan, H., Yu, S., Feng, X., Wang, G., Zhang, W., Wang, T.: Surface stress effect in mechanics of nanostructured materials. *Acta Mech. Solida Sin.* **24**, 52–82 (2011)
46. Wang, X., Schiavone, P.: A mode-III crack with variable surface effects. *J. Theor. Appl. Mech.* **54**(4), 1319–1327 (2016)
47. Xu, L., Wang, X., Fan, H.: Anti-plane waves near an interface between two piezoelectric half-spaces. *Mech. Res. Commun.* **67**, 8–12 (2015)
48. Yerofeyev, V.I., Sheshenina, O.A.: Waves in a gradient-elastic medium with surface energy. *J. Appl. Math. Mech.* **69**(1), 57–69 (2005)

Chapter 10

Reduced Linear Viscoelastic Isotropic Cosserat Medium with Translational Viscosity: A Double Negative Acoustic Metamaterial



Elena F. Grekova and Aleksandra P. Piatysheva

Abstract We investigate here the influence of translational viscosity on the plane shear-rotational wave propagation in the linear isotropic reduced Cosserat medium. In such a medium, body points possess independent rotational and translational degrees of freedom, but the medium does not resist to the gradient of microrotation. Stress tensor is asymmetric, but the couple stress is zero. In the purely elastic case, a band gap is present. It was shown before that introducing viscoelasticity we may qualitatively change dispersion behaviour. In this work, we investigate in detail the case of viscosity related to the translational strain. We show that in this case the band gap disappears. We investigate asymptotically the case of infinitesimal viscosity and show that the band gap in the elastic material becomes in our case a decreasing part of the dispersion curve, i.e. the medium transforms from a single negative acoustic metamaterial to the double one. The most interesting fact is that the dissipation makes the wave pass. Dispersion curve has some other peculiarities, for instance, a point where $\text{Re } k(\omega)$ has a maximum, situated somewhat below the former boundary frequency.

Keywords Reduced Cosserat media · Waves in micropolar continua · Acoustic metamaterials · Viscoelasticity

E. F. Grekova (✉)

Institute of Problems in Mechanical Engineering, Russian Academy of Sciences,
St. Petersburg, Russian Federation
e-mail: elgreco@pdmi.ras.ru

A. P. Piatysheva

Peter the Great St. Petersburg Polytechnic University, St. Petersburg, Russian Federation

© Springer Nature Switzerland AG 2020

H. Altenbach et al. (eds.), *Nonlinear Wave Dynamics of Materials and Structures*, Advanced Structured Materials 122,
https://doi.org/10.1007/978-3-030-38708-2_10

10.1 Introduction

In this chapter, we continue our work on the reduced Cosserat continua started several years ago. The interest to the continua with rotational degrees of freedom is increasing during last decades, since such media are necessary to describe several microstructured media. Without doubt, all real media have microstructure, but while the deformation processes do not make it manifest itself, we can neglect it. The technical progress makes possible to make more fine experiments with shorter waves (ultrasound, coupled magnetoelastic waves etc.) and also make some complex materials with desired properties artificially. Therefore, the theory of generalised continua developed very actively in the last decades.

The first work on 3D continua with rotational degrees of freedom belongs to Cosserat brothers [6]. In particular, they introduced the Cosserat deformation tensor to characterise the strain in the medium, whose linear term looks as $\nabla \mathbf{u} + \boldsymbol{\theta} \times \mathbf{E}$, where \mathbf{u} is the vector of translational displacement, and $\boldsymbol{\theta}$ is the microrotation vector. Later on, Kafadar and Eringen [19] obtained the equations of the Cosserat media, preceded by various works, for instance, Palmov [24], Aero and Kuvshinski [2]. A seminal contribution was made in Altenbach and Zhilin [3], since in this work they suggested a rigorous and universal way to obtain the constitutive theory of micropolar media. Many works are devoted to the micropolar continua of various types, e.g. Eremeyev et al. [7], Ivanova and Vilchevskaya [18], Müller and Vilchevskaya [23] and others.

Granular materials and blocky media, in particular, geomedium, are often modelled taking into account rotational degrees of freedom, especially when we need to consider wave propagation, and there are various experimental evidences that this can be important [1, 21, 22, 26, 28, 29]. Wave propagation in Cosserat media is considered also, for instance, in Maugin and Miled [20], Porubov et al. [25], Altenbach et al. [4], Erofeev et al. [11].

Reduced isotropic linear elastic Cosserat continuum was introduced in Schwartz et al. [27] as a model for granular materials. Later on wave propagation in such a continua or its modifications (anisotropic, with non-spherical inertia tensor, in the vicinity of a nonlinear prestressed state) was investigated in Grekova et al. [17], Grekova [14, 15] and other works. These media have a band gap (or band gaps) for various types of waves, i.e. they are single negative acoustic metamaterials in these domains of frequencies. In Grekova and Abreu [16], it was found out that if we use viscoelastic model [8] instead of elastic one, the type of metamaterial may change. In examples considered in the mentioned band gaps disappeared, and sometimes the graphs presented decreasing parts of dispersion curves (i.e. the medium was a double-negative acoustic metamaterial in this domain). In this work, we investigate in detail a particular case of infinitesimal viscosity related to the translational strain rate in the isotropic reduced Cosserat medium and study its effect on the wave propagation.

10.2 Dynamic Equations and Dispersion Relation

Let \mathbf{u} be the vector of translational displacement of a body point, \mathbf{P} the microrotation tensor. We consider the linear theory: $\mathbf{u} = o(1)$, $\mathbf{P} = \mathbf{E} + \boldsymbol{\theta} \times \mathbf{E}$, where $\boldsymbol{\theta}$ is the infinitesimal microrotation vector, \mathbf{E} is the identity tensor. As it was done also in Grekova and Abreu [16], we consider an isotropic-reduced viscoelastic model (suggested for the full variant of the Cosserat continuum in Grekova and Abreu [8]). We denote by $(\dot{})$ the material derivative with respect to time t , by \mathbf{r} the position vector. In the reduced theory, the couple stress is zero since no stresses work on $\nabla\boldsymbol{\theta}$. Let $\boldsymbol{\tau}$ be the Cauchy stress tensor. We will consider the case of the spherical inertia tensor $I\mathbf{E}$.

For any second rank tensor $\boldsymbol{\Lambda} = \lambda_{mn}\mathbf{e}_m\mathbf{e}_n$, we denote $\boldsymbol{\Lambda}^\top = \lambda_{nm}\mathbf{e}_m\mathbf{e}_n$, symmetric part of $\boldsymbol{\Lambda}$ as $\boldsymbol{\Lambda}^S = (\boldsymbol{\Lambda} + \boldsymbol{\Lambda}^\top)/2$, its antisymmetric part as $\boldsymbol{\Lambda}^A = (\boldsymbol{\Lambda} - \boldsymbol{\Lambda}^\top)/2$, and its vectorial invariant (accompanying vector of $\boldsymbol{\Lambda}^A$) as $\boldsymbol{\Lambda}_\times = \lambda_{mn}\mathbf{e}_m \times \mathbf{e}_n$. Note that $\boldsymbol{\Lambda}^A = -(\boldsymbol{\Lambda}_\times \times \mathbf{E})/2$.

The balance of force and moment, and the constitutive equations take form [16]

$$\nabla \cdot \boldsymbol{\tau} = \rho \ddot{\mathbf{u}}, \quad (10.1)$$

$$\boldsymbol{\tau}_\times = I \ddot{\boldsymbol{\theta}}, \quad (10.2)$$

$$\begin{aligned} \boldsymbol{\tau} = & \lambda \nabla \cdot \mathbf{u} \mathbf{E} + 2\mu (\nabla \mathbf{u})^S + 2\alpha (\nabla \mathbf{u} + \boldsymbol{\theta} \times \mathbf{E})^A \\ & + \lambda \kappa \nabla \cdot \dot{\mathbf{u}} \mathbf{E} + \mu \nu (\nabla \dot{\mathbf{u}})^S + \alpha \beta (\nabla \mathbf{u}^A + \boldsymbol{\theta} \times \mathbf{E}). \end{aligned} \quad (10.3)$$

where coefficients κ , ν , β characterise the dissipation in the medium. We will consider only the case of translational viscosity: $\nu \neq 0$, but $\beta = 0$. The equations of motion in displacements for this particular case take form

$$\begin{aligned} (\lambda + 2\mu) \nabla \nabla \cdot \mathbf{u} - \mu \nabla \times (\nabla \times \mathbf{u}) + 2\alpha \nabla \times (\boldsymbol{\theta} - \nabla \times \mathbf{u}/2) \\ + (\lambda \kappa + 2\mu \nu) \nabla \nabla \cdot \dot{\mathbf{u}} - \mu \nu \nabla \times (\nabla \times \dot{\mathbf{u}}) = \rho \ddot{\mathbf{u}}, \quad (10.4) \\ -4\alpha (\boldsymbol{\theta} - \nabla \times \mathbf{u}/2) = I \ddot{\boldsymbol{\theta}}. \end{aligned}$$

We limit ourselves to the investigation of the shear–rotational wave, since the compression wave is the same as in the classical medium. The dispersion relation obtained in Grekova and Abreu [16] for $\beta = 0$ takes form

$$k^2 = \frac{\rho \omega^2}{\mu(1 + i\nu\omega) + \alpha} \frac{\omega^2 - 4\alpha/I}{\omega^2 - \frac{4\mu(1 + i\nu\omega)\alpha}{[\mu(1 + i\nu\omega) + \alpha]I}}. \quad (10.5)$$

Let us introduce the following notation:

$$c_s^2 = \frac{\mu}{\rho}, \quad c_{s\alpha}^2 = \frac{\mu + \alpha}{\rho}, \quad \omega_0^2 = \frac{4\alpha}{I}, \quad \omega_{1d}^2 = \frac{c_s^2}{c_{s\alpha}^2} \omega_0^2. \quad (10.6)$$

Note that ω_{1d} and ω_0 in this particular case of only translational viscosity represent the boundary and the cut-off frequency, respectively, for the elastic case, where $(\omega_{1d}; \omega_0)$ is a band gap.

Let us use dimensionless parameters

$$n = \omega_0 \nu, \quad \Omega = \frac{\omega}{\omega_0}, \quad \Omega_{1d}^2 = \frac{\omega_{1d}^2}{\omega_0^2} = \frac{1}{1 + \alpha/\mu}. \quad (10.7)$$

Thus, for k^2 we have the next expression:

$$k^2 = \frac{\omega_0^2 \Omega^2 (\Omega^2 - 1)}{c_{s\alpha}^2 ((\Omega^2 - \Omega_{1d}^2)^2 + \Omega_{1d}^4 n^2 \Omega^2 (\Omega^2 - 1)^2)} (\Omega^2 - \Omega_{1d}^2 - i \Omega \Omega_{1d}^2 n (\Omega^2 - 1)) \quad (10.8)$$

A typical graph of dispersion relation, obtained numerically, is shown in Fig. 10.1.

In this graph, we can see that the band gap present in the purely elastic case, has disappeared, and instead we have a decreasing part of the dispersion curve, which continues a little below the boundary frequency for the elastic case. Let us investigate this dispersion relation.

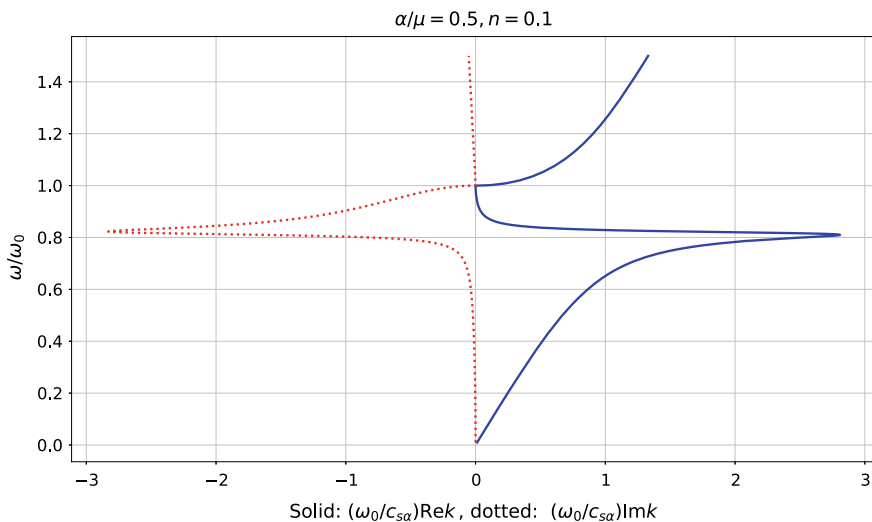


Fig. 10.1 A typical dispersion graph, numerical solution

10.3 Absence of the Band Gap for an Arbitrary Translational Dissipation n

Let us denote

$$\zeta = n\Omega_{1d}^2 \frac{\Omega(\Omega^2 - 1)}{\Omega^2 - \Omega_{1d}^2}. \quad (10.9)$$

Note that up to the multiplying by a positive constant ζ is equal to Ωk_e^2 , where $k_e(\omega) = 0$ is the dispersive relation for the purely elastic case, it has qualitatively the same behaviour, and that at $n = o(1)$ the order of ζ is the same ($\zeta = o(1)$) if $|\Omega - \Omega_{1d}| \gg n$. When we approach Ω_{1d} , ζ becomes finite or infinitely large. Then we have from Eq. (10.8)

$$\left(\frac{\Omega_{1d} c_{s\alpha}}{\omega_0} k \right)^2 = \frac{\Omega}{n} \frac{\zeta}{1 + \zeta^2} (1 - i\zeta). \quad (10.10)$$

Separating real and imaginary part of this equation, we obtain

$$\text{Im } k = - \frac{\omega_0^2}{\Omega_{1d}^2 c_{s\alpha}^2} \frac{\Omega}{2n} \frac{\zeta^2}{1 + \zeta^2} \frac{1}{\text{Re } k} \quad (10.11)$$

and the biquadratic equation for $\text{Re } k$

$$\left(\text{Re } \frac{\Omega_{1d} c_{s\alpha}}{\omega_0} k \right)^4 - \frac{\Omega}{n} \frac{\zeta}{1 + \zeta^2} \left(\text{Re } \frac{\Omega_{1d} c_{s\alpha}}{\omega_0} k \right)^2 - \frac{\Omega^2}{4n^2} \frac{\zeta^4}{(1 + \zeta^2)^2} = 0. \quad (10.12)$$

As we see, the signs of $\text{Re } k$ and $\text{Im } k$ are opposite. Solving this equation and choosing the branch giving us the positive value of $(\text{Re } k)^2$, we obtain

$$\left(\frac{\Omega_{1d} c_{s\alpha}}{\omega_0} \right)^2 (\text{Re } k)^2 = \frac{\Omega \zeta}{2n} \frac{1}{1 + \zeta^2} (1 + (\text{sgn } \zeta) \sqrt{1 + \zeta^2}), \quad (10.13)$$

or, which is the same,

$$(\text{Re } k)^2 = \frac{\omega_0^2 \Omega^2 (\Omega^2 - 1) (\Omega^2 - \Omega_{1d}^2)}{2c_{s\alpha}^2 ((\Omega^2 - \Omega_{1d}^2)^2 + \Omega_{1d}^4 n^2 \Omega^2 (\Omega^2 - 1)^2)} \left[1 + \text{sgn}((\Omega^2 - \Omega_{1d}^2)(\Omega^2 - 1)) \sqrt{1 + \frac{n^2 \Omega_{1d}^4 \Omega^2 (\Omega^2 - 1)^2}{(\Omega^2 - \Omega_{1d}^2)^2}} \right] \quad (10.14)$$

We see here that contrary to the purely elastic case, the dispersion relation has no band gap. The viscosity makes it disappear. This phenomenon seems to be a paradox,

but we can understand it if we remember that the band gap in the elastic case was related to the localisation and not to the damping. The expressions for the imaginary part are

$$\left(\frac{\Omega_{1d}c_{s\alpha}}{\omega_0}\right)^2 (\text{Im } k)^2 = \frac{\Omega\zeta^3}{2n(1+\zeta^2)[1+(\text{sgn } \zeta)\sqrt{1+\zeta^2}]} \quad (10.15)$$

or, which is the same,

$$(\text{Im } k)^2 = \left(\frac{\omega_0}{\Omega_{1d}c_{s\alpha}}\right)^2 \frac{n^2\Omega_{1d}^6\Omega^4(\Omega^2-1)^3}{2(\Omega^2-\Omega_{1d}^2)^3\left(1+\frac{n^2\Omega_{1d}^4\Omega^2(\Omega^2-1)^2}{(\Omega^2-\Omega_{1d}^2)^2}\right)} \frac{1}{1+\text{sgn}[(\Omega^2-\Omega_{1d}^2)(\Omega^2-1)]\sqrt{1+\frac{n^2\Omega_{1d}^4\Omega^2(\Omega^2-1)^2}{(\Omega^2-\Omega_{1d}^2)^2}}} \quad (10.16)$$

10.4 Asymptotical Approximation for Infinitesimal n

The behaviour of the dispersion relation at infinitesimal n depends on the behaviour of ζ , which, in its turn, depends on how Ω is close to Ω_{1d} . We have to consider three cases: $(\Omega^2 - \Omega_{1d}^2)$ and n are of the same order, or one of them is much less than another one.

10.4.1 Case $|\Omega^2 - \Omega_{1d}^2| \gg n$

In this case $\zeta = O(n) = o(1)$, and we can approximate (10.13) as

$$\begin{aligned} \left(\frac{\Omega_{1d}c_{s\alpha}}{\omega_0}\right)^2 (\text{Re } k)^2 &= \frac{\Omega\zeta}{2n} \{(1-\zeta^2)[1+(\text{sgn } \zeta)(1+\zeta^2/2)] + O(\zeta^4)\} \\ &= \begin{cases} \Omega\zeta(1-\frac{3}{4}\zeta^2)/n, & \zeta > 0 \\ -\Omega\zeta^3/(4n), & \zeta < 0 \end{cases} + O(n^4), \end{aligned} \quad (10.17)$$

which gives us the following result for the real part of k up to the orders of $O(n^4)$ (if $n\Omega \ll 1$):

$$|\operatorname{Re} k| \approx \begin{cases} \frac{\omega_0 \Omega}{c_{s\alpha}} \left(\frac{\Omega^2 - 1}{\Omega^2 - \Omega_{1d}^2} \right)^{1/2} \left(1 - \frac{3}{8} n^2 \frac{\Omega^2 \Omega_{1d}^4 (\Omega^2 - 1)^2}{(\Omega^2 - \Omega_{1d}^2)^2} \right), & \Omega \notin [\Omega_{1d}; 1) \\ \frac{n \omega_0 \Omega^2 \Omega_{1d}^2}{2c_{s\alpha}} \left(-\frac{\Omega^2 - 1}{\Omega^2 - \Omega_{1d}^2} \right)^{3/2}, & \Omega_{1d} < \Omega \leq 1. \end{cases} \quad (10.18)$$

It can be also rewritten as:

$$|\operatorname{Re} k| \approx \begin{cases} \frac{\omega}{c_{s\alpha}} \left(\frac{\omega^2 - \omega_0^2}{\omega^2 - \omega_{1d}^2} \right)^{1/2} \left(1 - \frac{3}{8} v^2 \frac{\omega_{1d}^4}{\omega_0^4} \frac{\omega^2 (\omega^2 - \omega_0^2)^2}{(\omega^2 - \omega_{1d}^2)^2} \right), & \omega \notin [\omega_{1d}; \omega_0) \\ \frac{v \omega_{1d}^2}{2c_{s\alpha} \omega_0^2} \omega^2 \left(-\frac{\omega^2 - \omega_0^2}{\omega^2 - \omega_{1d}^2} \right)^{3/2}, & \omega_{1d} < \omega \leq \omega_0. \end{cases} \quad (10.19)$$

Recall that these expressions are obtained for $|\omega - \omega_{1d}| \gg v\omega_0$.

If $n\Omega = O(1)$, then we have from (10.8)

$$\operatorname{Re} k = \frac{\omega}{c_{s\alpha}} \sqrt{\frac{1 + \sqrt{1 + v^2 \Omega_{1d}^4 \omega^2}}{2(1 + v^2 \Omega_{1d}^4 \omega^2)}}. \quad (10.20)$$

At very large Ω such that $n\Omega \rightarrow \infty$, the dissipation prevails and we obtain

$$\operatorname{Re} k \approx \frac{1}{\omega_{1d}} \sqrt{\frac{\omega}{2v}}. \quad (10.21)$$

We also need to see the behaviour of imaginary part:

$$\begin{aligned} \left(\frac{\Omega_{1d} c_{s\alpha}}{\omega_0} \right)^2 (\operatorname{Im} k)^2 &= \frac{\Omega \zeta^3}{2n(1 + \zeta^2)[1 + (\operatorname{sgn} \zeta) \sqrt{1 + \zeta^2}]} \\ &= \begin{cases} \frac{\Omega \zeta^3 (1 - \zeta^2) (1 - \frac{\zeta^2}{8})}{4n}, & \zeta \geq 0 \\ -\frac{\Omega \zeta (1 - \zeta^2)}{n}, & \zeta < 0 \end{cases} + O(n^4), \quad (10.22) \\ &= \begin{cases} \frac{\Omega \zeta^3}{4n}, & \zeta \geq 0 \\ -\frac{\Omega \zeta (1 - \zeta^2)}{n}, & \zeta < 0 \end{cases} \end{aligned}$$

This gives us:

$$\frac{c_{s\alpha}}{\omega_0} \operatorname{Im} k \approx \begin{cases} -n \frac{\Omega_{1d}^2}{2} \Omega^2 \left(\frac{\Omega^2 - 1}{\Omega^2 - \Omega_{1d}^2} \right)^{3/2}, & \Omega \notin [\Omega_{1d}; 1) \\ -\Omega \left(\frac{1 - \Omega^2}{\Omega^2 - \Omega_{1d}^2} \right)^{1/2} \left(1 - n^2 \frac{\Omega_{1d}^4}{2} \Omega^2 \frac{(\Omega^2 - 1)^2}{(\Omega^2 - \Omega_{1d}^2)^2} \right), & \Omega_{1d} < \Omega \leq 1, \end{cases} \quad (10.23)$$

or

$$\operatorname{Im} k \approx \begin{cases} -\frac{\nu}{c_{s\alpha}} \frac{\omega_{1d}^2}{2\omega_0^2} \omega^2 \left(\frac{\omega^2 - \omega_0^2}{\omega^2 - \omega_{1d}^2} \right)^{3/2}, & \omega \notin [\omega_{1d}; \omega_0) \\ -\frac{\omega}{c_{s\alpha}} \left(\frac{\omega_0^2 - \omega^2}{\omega^2 - \omega_{1d}^2} \right)^{1/2} \left[1 - \nu^2 \frac{\omega_{1d}^4}{2} \omega^2 \frac{(\omega^2 - \omega_0^2)^2}{(\omega^2 - \omega_{1d}^2)^2} \right], & \omega_{1d} < \omega \leq \omega_0. \end{cases} \quad (10.24)$$

We see that in the second case the main term is the same as in the purely elastic case:

$$(\operatorname{Im} k)^2 = -\frac{\omega^2}{c_{s\alpha}^2} \frac{\omega^2 - \omega_0^2}{\omega^2 - \omega_{1d}^2} + O(n^2), \quad \omega_{1d} < \omega \leq \omega_0. \quad (10.25)$$

The viscosity somewhat reduces the absolute value of the imaginary part in the band gap for the elastic case, and the real part becomes different from zero. We see that in the domain $(\omega_{1d}; \omega_0)$, which corresponds to the band gap in the elastic case, the logarithmic decrement equals

$$2\pi \left| \frac{\operatorname{Im} k}{\operatorname{Re} k} \right| = \frac{4\pi}{|\zeta|} = \frac{4\pi \omega_0^2}{\nu \omega_{1d}^2} \frac{\omega^2 - \omega_{1d}^2}{\omega(\omega_0^2 - \omega^2)} \quad (10.26)$$

Therefore, we see that in this case a small translational dissipation favours the wave propagation. This is, probably, related to the fact that dissipation breaks the conditions for localisation due to the presence of microstructure. At $\omega_0 - 0$, the logarithmic decrement tends to infinity.

It is easy to see that out of the $[\omega_{1d}; \omega_0)$ the logarithmic decrement can be approximated as

$$\pi \frac{n \Omega_{1d}^2}{2} \Omega \frac{\Omega^2 - 1}{\Omega^2 - \Omega_{1d}^2} = \pi \frac{\nu \omega_{1d}^2}{2\omega_0^2} \omega \frac{\omega^2 - \omega_0^2}{\omega^2 - \omega_{1d}^2} = \pi \zeta. \quad (10.27)$$

At $\omega_0 + 0$ it is zero.

10.4.2 Case $|\Omega^2 - \Omega_{1D}^2| \ll n$

In this case $\zeta \rightarrow \pm\infty$, $h = 1/\zeta \rightarrow 0$. Equation (10.13) gives us

$$\left(\frac{\Omega_{1d}c_{s\alpha}}{\omega_0}\right)^2 (\operatorname{Re} k)^2 = \frac{\Omega}{2n} \frac{h + \sqrt{1+h^2}}{1+h^2} = \frac{\Omega}{2n} \left[\frac{h + (1+h^2/2)}{1+h^2} + o(h^2) \right]$$

$$\stackrel{(\operatorname{Re} k)^2 > 0}{=} \frac{\Omega_{1d}}{2n} [1 + h + o(h)]. \quad (10.28)$$

The last approximation can be done since we consider $\Omega^2 - \Omega_{1d}^2 = nhO(1) \ll h$. Using the expression for

$$h = \frac{\Omega^2 - \Omega_{1d}^2}{n} \frac{1}{\Omega_{1d}^2 \Omega (\Omega^2 - 1)},$$

we obtain

$$|\operatorname{Re} k| \approx \frac{\omega_0}{c_{s\alpha}} \frac{1}{\sqrt{2n\Omega_{1d}}} \left[1 + \frac{\Omega - \Omega_{1d}}{n\Omega_{1d}^2(\Omega_{1d}^2 - 1)} \right]. \quad (10.29)$$

It can be also rewritten as:

$$|\operatorname{Re} k| \approx \frac{\omega_0}{c_{s\alpha}\sqrt{2\nu\omega_{1d}}} \left[1 + \frac{(\omega - \omega_{1d})\omega_0^2}{\nu\omega_{1d}^2(\omega_{1d}^2 - \omega_0^2)} \right] \quad (10.30)$$

We see that at ω_{1d} we have $\operatorname{Re} k = \omega_0^{3/2}/\sqrt{2n c_{s\alpha} \omega_{1d}}$, as it also follows from (10.8). Now let us obtain the approximation for the imaginary part using (10.15).

$$\left(\frac{\Omega_{1d}c_{s\alpha}}{\omega_0}\right)^2 (\operatorname{Im} k)^2 = \frac{\Omega}{2n} \frac{h^{-3}}{(1+h^{-2})[1+(\operatorname{sgn} h)\sqrt{1+h^{-2}}]}$$

$$= \frac{\Omega}{2n} \frac{1}{(1+h^2)(h+\sqrt{1+h^2})} \stackrel{h=O(1)}{=} \frac{\Omega}{2n} [1 - h - 3h^2/2 + O(h^4)]$$

$$= \frac{\Omega_{1d} + nhO(1)}{2n} [1 - h + O(h^2)] = \frac{\Omega_{1d}[1 - h + o(h)]}{2n} \approx \frac{\Omega_{1d}}{2n} \left[1 - \frac{2(\Omega - \Omega_{1d})}{n\Omega_{1d}^2(\Omega_{1d}^2 - 1)} \right]. \quad (10.31)$$

The main term is

$$\frac{\Omega_{1d}c_{s\alpha}}{\omega_0} \operatorname{Im} k = -\sqrt{\frac{\Omega_{1d}}{2n}} \left[1 - \frac{\Omega - \Omega_{1d}}{n\Omega_{1d}^2(\Omega_{1d}^2 - 1)} \right], \quad (10.32)$$

or

$$\operatorname{Im} k = -\frac{\omega_0}{c_{s\alpha}\sqrt{2\nu\omega_{1d}}} \left[1 + \frac{\omega - \omega_{1d}}{\nu} \frac{\omega_0^2}{\omega_{1d}^2(\omega_0^2 - \omega_{1d}^2)} \right]. \quad (10.33)$$

The logarithmic decrement in this case is very high and close to 2π , larger above ω_{1d} than below it:

$$\begin{aligned}
2\pi \left| \frac{\operatorname{Im} k}{\operatorname{Re} k} \right| &\approx 2\pi \sqrt{\frac{1-h}{1+h}} = 2\pi(1-h) = 2\pi \left[1 + 2(\Omega - \Omega_{1d}) \frac{1 - \Omega_{1d}^2}{n\Omega_{1d}^2} \right] \\
&= 2\pi \left[1 + 2(\omega - \omega_{1d}) \frac{\omega_0^2 - \omega_{1d}^2}{v\omega_0^2\omega_{1d}^2} \right].
\end{aligned} \tag{10.34}$$

10.4.3 Case $(\Omega^2 - \Omega_{1d}^2)/n = O(1)$

Here we have to keep all the combinations $n/(\Omega - \Omega_{1d})$ but we can use the fact that $\varepsilon \stackrel{\text{def}}{=} \Omega - \Omega_{1d} \ll 1$. After some calculations, we have from (10.14):

$$(\operatorname{Re} k)^2 = \frac{\omega_0^2}{c_{s\alpha}^2} \frac{\Omega_{1d}(\Omega_{1d}^2 - 1)}{4(\Omega - \Omega_{1d})} \left\{ \frac{1}{1 + \left[\frac{n}{\Omega - \Omega_{1d}} \frac{\Omega_{1d}^2}{2} (\Omega_{1d}^2 - 1) \right]^2} - \frac{\operatorname{sgn}(\Omega - \Omega_{1d})}{\sqrt{1 + \left[\frac{n}{\Omega - \Omega_{1d}} \frac{\Omega_{1d}^2}{2} (\Omega_{1d}^2 - 1) \right]^2}} \right\} \tag{10.35}$$

Let us denote

$$A = n^2 \Omega_{1d}^4 (1 - \Omega_{1d}^2)^2 / 4 > 0, \quad \varkappa = \frac{4c_{s\alpha}^2 (\operatorname{Re} k)^2}{\omega_0^2 (1 - \Omega_{1d}^2) \Omega_{1d}}. \tag{10.36}$$

Then equation (10.35) can be rewritten as

$$\varkappa = \varepsilon^{-1} [(\operatorname{sgn} \varepsilon)(1 + A\varepsilon^{-2})^{1/2} - (1 + A\varepsilon^{-2})^{-1}] \tag{10.37}$$

Investigating function $\varkappa(\varepsilon)$, we find that it has maximum point at

$$\varepsilon = -\sqrt{A \frac{\sqrt{5} + 1}{2}}.$$

It means that $\operatorname{Re} k$ reaches its maximal value at

$$\Omega_{\max} = \Omega_{1d} \left[1 - \frac{n\Omega_{1d}(1 - \Omega_{1d}^2)}{2\sqrt{\Phi}} \right], \tag{10.38}$$

$\Phi = (\sqrt{5} + 1)/2$ being the golden ratio. We see that this point of maximum corresponds to the asymptotical case under consideration, since $\Omega_{\max}^2 - \Omega_{1d}^2 = O(n)$.

The maximal value is

$$(\operatorname{Re} k)^2 = \frac{1}{2n} \frac{\omega_0^2}{c_{s\alpha}^2} \sqrt{\Phi} [(1 + \Omega_{1d}^2 \Phi)^{-1} + (1 + \Omega_{1d}^2 \Phi)^{-1/2}]. \quad (10.39)$$

The values of $(\operatorname{Re} k)^2$ at Ω_{max} , calculated by exact Formula (10.14) and by approximated Formula (10.35), coincide. However, since (10.38) gives us only an approximated value for the maximum point, Eq. (10.39) is an estimation from below of the true maximal value for $(\operatorname{Re} k)^2$. Numerical results show that this estimation is good enough (for instance, at $\mu/\alpha = 1.1$, $n = 0.01$ it gives approximately 0.97 of the true maximal value of $\operatorname{Re} k$). In some cases, the asymptotics for another domain of Ω , very close to Ω_{1d} , considered in the previous section, gives us larger values than this maximum, but this is not a valid result, since maximum point does not belong to that domain. In fact, the asymptotics obtained in this section works often better even for the very small neighbourhood of Ω_{1d} .

Imaginary part (10.16) can be approximated as

$$(\operatorname{Im} k)^2 = -\frac{\omega_0^2 n^2}{c_{s\alpha}^2 \varepsilon^2} \frac{\Omega_{1d}^5 (1 - \Omega_{1d}^2)^3}{16|\varepsilon| \left[\sqrt{1 + \frac{n^2}{\varepsilon^2} \frac{\Omega_{1d}^2 (\Omega_{1d}^2 - 1)^2}{4}} - \operatorname{sgn} \varepsilon \right] \left[1 + \frac{n^2}{\varepsilon^2} \frac{\Omega_{1d}^2 (\Omega_{1d}^2 - 1)^2}{4} \right]} \quad (10.40)$$

We have to choose negative sign for $\operatorname{Im} k$ (opposite to the sign of $\operatorname{Re} k$). This can be written also as

$$(\operatorname{Im} k)^2 = -\frac{1}{\omega_0^9 c_{s\alpha}^2} \frac{\omega_{1d}^5 (\omega_0^2 - \omega_{1d}^2)^3}{16|\varepsilon| \left[\sqrt{1 + \frac{v^2}{\varepsilon^2} \frac{\omega_{1d}^2 (\omega_{1d}^2 - \omega_0^2)^2}{4\omega_0^4}} - \operatorname{sgn} \varepsilon \right] \left[1 + \frac{v^2}{\varepsilon^2} \frac{\omega_{1d}^2 (\omega_{1d}^2 - \omega_0^2)^2}{4\omega_0^4} \right]} \quad (10.41)$$

The logarithmic decrement in this case can be calculated as

$$2\pi \left| \frac{\operatorname{Im} k}{\operatorname{Re} k} \right| = \pi \frac{n}{|\varepsilon|} \frac{\Omega_{1d}^2 (1 - \Omega_{1d}^2)}{\sqrt{1 + \left[\frac{n}{\varepsilon} \frac{\Omega_{1d}^2 (1 - \Omega_{1d}^2)}{2} \right]^2} - \operatorname{sgn} \varepsilon}, \quad (10.42)$$

or, in terms of ω ,

$$2\pi \left| \frac{\operatorname{Im} k}{\operatorname{Re} k} \right| = \frac{\pi v}{|\omega - \omega_{1d}|} \frac{\omega_{1d}^2}{\omega_0^2} \frac{\omega_0^2 - \omega_{1d}^2}{\sqrt{1 + \left[\frac{v}{\omega - \omega_{1d}} \frac{\omega_{1d}^2 (\omega_0^2 - \omega_{1d}^2)}{2\omega_0^2} \right]^2} - \operatorname{sgn}(\omega - \omega_{1d})}. \quad (10.43)$$

We see that below ω_{1d} the attenuation is smaller than above it.

10.5 Comparison of Analytical and Numerical Results and Discussion

We have compared the numerical solution for the dispersion relation, based on (10.8), and the asymptotical approximation for $\text{Re } k(\omega)$ and $\text{Im } k(\omega)$ (for finite ω). We combined three asymptotical solutions: approximation calculated in Sect. 10.4.1 for $\omega > \omega_{1d} + n\omega_0$ and for $\omega < \omega_{1d} - n\omega_0$, approximation calculated in Sect. 10.4.2 for $\omega_{1d} - 0.04n\omega_0 < \omega < \omega_{1d} + 0.04n\omega_0$, and approximation obtained in Sect. 10.4.3 for $\omega_{1d} - n\omega_0 < \omega < \omega_{1d} - 0.04n\omega_0$ and $\omega_{1d} + 0.04n\omega_0 < \omega < \omega_{1d} + n\omega_0$. The results are in excellent agreement even for $n = 0.1$ which is not very small, if ω is not too large (see Figs. 10.2 and 10.3). We see that there is a small mismatch near ω_{1d} . For some reason, the asymptotics for $\text{Re } k$ considered in Sect. 10.4.3 fits better the numerical curve even very close to ω_{1d} than the solution in Sect. 10.4.2, but for $\text{Im } k$ it is not so. Anyway the advantage of asymptotics for ω very close to ω_{1d} is that we can see in a clear way the influence of the infinitesimal dissipation.

Performing numerical calculation, we have found out that the larger α/μ is, the smaller we have to choose n to make the asymptotical solution coincide with the numerical one. For instance, at $\alpha/\mu = 5$ asymptotical approximation fits well the numerical solution at $n \leq 0.07$, and $\alpha/\mu = 15$ they coincide almost exactly at $n \leq 0.04$. Asymptotics obtained in Sect. 10.4.2 gives us somewhat overestimated values of $\text{Re } k$ when α/μ increases, and fits worse the numerical curve than the asymptotics obtained in Sect. 10.4.3. Asymptotics for $\text{Re } k$ at large ω and infinitesimal ν was

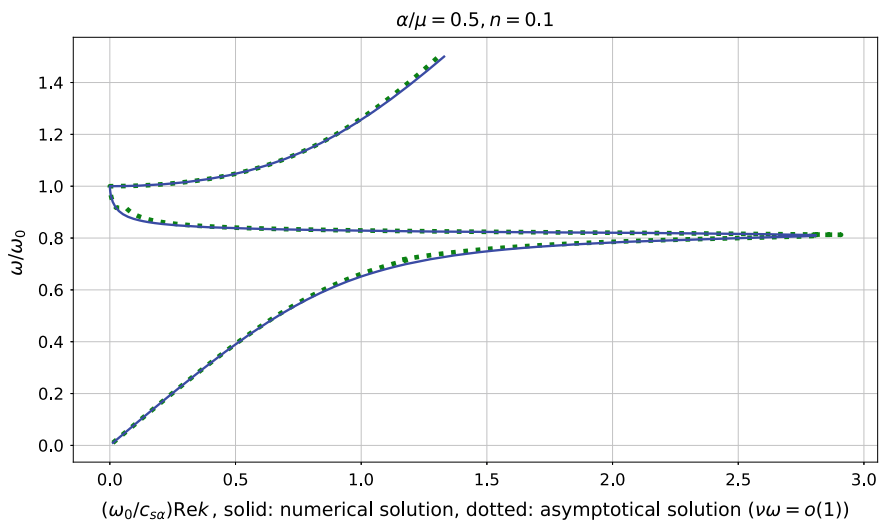


Fig. 10.2 Comparison of numerical and asymptotical results for the dispersion relation (real part of the wave number) at finite ω . Asymptotics obtained in Sect. 10.4.2 overestimates $\text{Re } k$

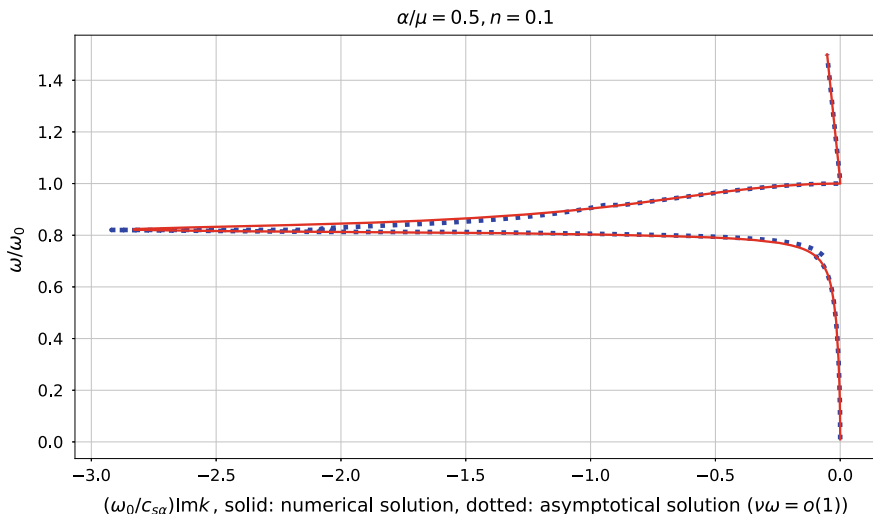


Fig. 10.3 Comparison of numerical and asymptotical results for the dispersion relation (imaginary part of the wave number) at finite ω

also numerically verified and the results practically coincide. We do not put here the graphs since they do not bring any principal new information.

The main result of this work is that we have verified that small viscosity related to the translational strain rate favours the wave propagation in the reduced Cosserat medium. The band gap which existed in the elastic case disappears and converts into the decreasing part of the dispersion curve. Thus, this kind of viscosity changes the type of the acoustic metamaterial from single negative to the double negative one.

In the former band gap, we have logarithmic decrement inverse proportional to the small viscosity parameter $n = \nu\omega_0$, if we do not approach the low boundary ω_{1d} . Near it the dependence becomes more sophisticated but anyway decreasing when n increases, at least in the case under consideration (for small n).

We have seen also that there $\text{Re } k(\omega)$ has a maximum point somewhat below this zone (the former boundary frequency ω_{1d}) and we have found this value. It is an open question for us, what does happen in this point. The group velocity there is infinite. We see in numerical examples that starting from this point, the logarithmic decrement drastically increases with increasing frequency (and reaches infinity at ω_0 , suffering a jump to 0 at $\omega_0 + 0$, as it was shown asymptotically). However, it is not infinite in this maximum point for $\text{Re } k(\omega)$. We see in numerical examples that $\text{Im } k(\omega)$ also has a maximum point not far from it, but these points do not coincide. To answer this question, we have to investigate in details analytically the behaviour of $\text{Im } k$ and logarithmic decrement, which is one of directions of our future research.

Acknowledgements We are very happy to dedicate this work to Prof. Vladimir Erofejev on the occasion of his 60th anniversary. Prof. Erofejev made a big contribution to the development of generalised continua (see, for instance [5, 9, 10, 12, 13]). The authors had a pleasure to discuss

Cosserat continua with Prof. Erofeev over many years, which was very fruitful also due to his open-minded nature and great erudition.

In addition, the authors are grateful to Dr. Rafael Abreu who brought their attention to the topic of wave propagation in reduced viscoelastic Cosserat media.

Elena F. Grekova thanks the Russian Foundation for Basic Research (grant 17-01-00230) for partial support of this work.

References

1. Abreu, R., Thomas, C., Durand, S.: Effect of observed micropolar motions on wave propagation in deep Earth minerals. *Phys. Earth Planet. Inter.* **276**, 215–225 (2018)
2. Aero, E.L., Kuvshinski, E.V.: Fundamental equations of the theory of elasticity with rotational particle interactions [in Russ.]. *Phiz. Tverd. Tela* **2**(7), 1399 (1969)
3. Altenbach, H., Zhilin, P.A.: A general theory of elastic simple shells [in Russ.]. *Uspekhi Mekhaniki* **11**(4), 107–148 (1988)
4. Altenbach, H., Eremeyev, V.A., Lebedev, L.P., Rendón, L.A.: Acceleration waves and ellipticity in thermoelastic micropolar media. *Arch. Appl. Mech.* **80**(3), 217–227 (2010)
5. Bagdoev, A.G., Erofeev, V.I., Shekoyan, A.V.: *Wave Dynamics of Generalized Continua*. Springer, Berlin (2016)
6. Cosserat, E., Cosserat, F.: *Théorie des Corps Déformables*. A. Hermann et fils (in French) (1909)
7. Eremeyev, V.A., Lebedev, L.P., Altenbach, H.: *Foundations of Micropolar Mechanics*. Springer, Berlin (2013)
8. Eringen, A.C.: Linear theory of micropolar viscoelasticity. *Int. J. Eng. Sci.* **5**(2), 191–204 (1967)
9. Erofeev, V.I., Zemlyanukhin, A.I., Catson, V.M., Sheshenin, S.F.: Nonlinear waves in the Cosserat continuum with constrained rotation. In: *Mechanics of Generalized Continua*, pp 221–230. Springer, Berlin (2011)
10. Erofeev, V.I., Leontyeva, A.V., Pavlov, I.S.: Propagation of rotational waves in a block geomedium. *J. Vibroeng.* **19**(8) (2017)
11. Erofeev, V.I., Pavlov, I.S., Porubov, A.V., Vasiliev, A.A.: Dispersion properties of a closed-packed lattice consisting of round particles. In: *Generalized Models and Non-classical Approaches in Complex Materials 2*, pp 101–117. Springer, Berlin (2018)
12. Erofeev, V.I.: Propagation and interaction of waves in nonlinear-elastic solids with microstructure. In: *Acoustic Interactions With Submerged Elastic Structures: Part II: Propagation, Ocean Acoustics and Scattering*, pp. 41–83. World Scientific (2001)
13. Erofeev, V.I.: *Wave Processes in Solids with Microstructure*. World Scientific (2003)
14. Grekova, E.F.: Plane waves in the linear elastic reduced Cosserat medium with a finite axially symmetric coupling between volumetric and rotational strains. *Math. Mech. Solids* **21**(1), 73–93 (2016)
15. Grekova, E.F.: Nonlinear isotropic elastic reduced and full Cosserat media: waves and instabilities. In: *Continuum Mechanics and Thermodynamics*, pp. 1–20 (2019)
16. Grekova, E.F., Abreu, R.: Isotropic linear viscoelastic reduced Cosserat medium: an acoustic metamaterial and a first step to model geomedium. In: *New Achievements in Continuum Mechanics and Thermodynamics*, pp 165–185. Springer, Berlin (2019)
17. Grekova, E.F., Kulesh, M.A., Herman, G.C.: Waves in linear elastic media with microrotations, Part 2: Isotropic reduced Cosserat model. *Bull. Seismol. Soc. Am.* **99**(2B), 1423–1428 (2009)
18. Ivanova, E.A., Vilchevskaya, E.N.: Micropolar continuum in spatial description. In: *Continuum Mechanics and Thermodynamics*, vol. 28(6), pp. 1759–1780 (2016)
19. Kafadar, C.B., Eringen, A.C.: Micropolar media—I: The classical theory. *Int. J. Eng. Sci.* **9**(3), 271–305 (1971)

20. Maugin, G.A., Miled, A.: Solitary waves in micropolar elastic crystals. *Int. J. Eng. Sci.* **24**(9), 1477–1499 (1986)
21. Merkel, A., Tournat, V., Gusev, V.: Dispersion of elastic waves in three-dimensional noncohesive granular phononic crystals: properties of rotational modes. *Phys. Rev. E* **82**(3), 031305 (2010)
22. Merkel, A., Tournat, V., Gusev, V.: Experimental evidence of rotational elastic waves in granular phononic crystals. *Phys. Rev. Lett.* **107**(22), 225502 (2011)
23. Müller, W.H., Vilchevskaya, E.N.: Micropolar theory with production of rotational inertia: a rational mechanics approach. In: *Generalized Models and Non-classical Approaches in Complex Materials* vol. 1, pp. 581–606. Springer, Berlin (2018)
24. Palmov, V.A.: Fundamental equations of the theory of asymmetric elasticity. *J. Appl. Math. Mech.* **28**(3), 496–505 (1964)
25. Porubov, A.V., Aero, E.L., Maugin, G.A.: Two approaches to study essentially nonlinear and dispersive properties of the internal structure of materials. *Phys. Rev. E* **79**(4), 046608 (2009)
26. Sadovskii, V.M., Sadovskaya, O.V.: Modeling of elastic waves in a blocky medium based on equations of the Cosserat continuum. *Wave Motion* **52**, 138–150 (2015)
27. Schwartz, L.M., Johnson, D.L., Feng, S.: Vibrational modes in granular materials. *Phys. Rev. Lett.* **52**(10), 831 (1984)
28. Turco, E.: In-plane shear loading of granular membranes modeled as a Lagrangian assembly of rotating elastic particles. *Mech. Res. Commun.* **92**, 61–66 (2018)
29. Twiss, R.J.: An asymmetric micropolar moment tensor derived from a discrete-block model for a rotating granular substructure. *Bull. Seismol. Soc. Am.* **99**(2B), 1103–1131 (2009)

Chapter 11

On Dynamic Model of Structural Transformations in Solids



Dmitry A. Indeitsev, Boris N. Semenov, Dmitry Yu. Skubov
and Dmitry S. Vavilov

Abstract A two-component model of material with a nonlinear internal interaction force is proposed for describing its structural transformations. An analogy between the equations of a continuous medium and their discrete representation allows demonstrating the effect of quenching of a non-stationary wave, caused by the transfer of energy to internal degrees of freedom. The parameters of the external impact at which the transformation of crystalline lattice takes place are determined. Analytical results are compared with numerical calculations, performed by using the finite difference method.

Keywords Structural transformations · Two-component model · Nonlinear interaction force

D. A. Indeitsev · B. N. Semenov · D. Yu. Skubov · D. S. Vavilov
Institute for Problems in Mechanical Engineering, V.O., Bolshoi pr., 61, St. Petersburg 199178,
Russian Federation
e-mail: dmitry.indeitsev@gmail.com

B. N. Semenov
e-mail: semenov@bs1892.spb.edu

D. Yu. Skubov
e-mail: skubov.dsk@yandex.ru

D. A. Indeitsev · B. N. Semenov
St. Petersburg University, Universitetskaya Naberezhnaya, 13B, St. Petersburg 199034, Russian
Federation

D. A. Indeitsev · B. N. Semenov · D. Yu. Skubov
St. Petersburg Polytechnic University Peter the Great, Polytechnicheskaya, 29, St. Petersburg
195251, Russian Federation

D. S. Vavilov (✉)
Mozhaisky Military Space Academy, Zhdanovskaya 13, St. Petersburg 197198, Russian
Federation
e-mail: londr@yandex.ru

11.1 Introduction

The classical equations of continuum mechanics do not take into account a complex internal structure of material, including various defects (vacancies, dislocations, interfaces, inclusions of another phase). Meanwhile, such important properties as electrical conductivity, strength, and ductility substantially depend on the defects of the structure, which itself may undergo drastic transformations under external impact. For example, in a series of experimental works on high-speed deformation, it was found that in a certain range of the projectile speeds new stable mesh formations $0.1 - 0.3 \mu\text{m}$ in diameter are generated because of the passage of the shock wave through the matter [1]. In further investigations, it was demonstrated that grains with such structure have a higher microhardness compared to the original material, improving its spall strength. At the macrolevel, the transformation processes of the crystalline lattice are manifested in the form of energy losses or in the shift of parameters included in the equations of continuum mechanics.

Development of theories allowing to describe the influence of the internal microstructure on macroparameters entails the introduction of additional degrees of freedom corresponding to its dynamics. There are several approaches for implementing this procedure. One of them consists in bringing qualitative changes to the constitutive equation, which would allow taking into account the possibility of transition to a new equilibrium configuration. In the articles on phase transitions [2–5], it is often accepted that the relationship between stress and strain is a non-monotonic function, which results in non-convexity of potential energy. The main feature of such diagrams is the inability to determine uniquely the deformation at a given static load. The presence of an unstable branch on the constitutive curve means that when the critical value of the deformation is reached, a local loss of stability in the crystal lattice takes place, i.e., the material loses its ability to resist an external load. With further deformation, this ability is restored. In such material, the interphase boundary is considered to be a new degree of freedom, the motion of which is described by a kinetic equation connecting the velocity of the boundary with the energy dissipation on it [6].

Another approach to the problem of describing structural conversions consists in considering a model of multicomponent medium with several interacting continua. It is assumed that at each point of the volume, the functions of densities $\rho_i(\mathbf{x}, t)$ and velocities $\mathbf{v}_i(\mathbf{x}, t)$ ($i = 1, 2, \dots, N$) are specified [7–10]. Then, the equations of mass and momentum balance for each of the components are given by:

$$\begin{aligned} \frac{\partial \rho_i}{\partial t} + \nabla \cdot (\rho_i \mathbf{v}_i) &= \sum_{j=1, i \neq j}^N J_{ij} \\ \nabla \cdot \boldsymbol{\sigma}_i + \sum_{j=1, i \neq j}^N \mathbf{R}_{ij} &= \rho_i \frac{d\mathbf{v}_i}{dt} + \sum_{j=1, i \neq j}^N J_{ij} \mathbf{v}_i, \end{aligned} \quad (11.1.1)$$

where \mathbf{R}_{ij} is the interaction force between i and j components. The Cauchy stress tensor is indicated as $\boldsymbol{\sigma}$ and the operator $\frac{d}{dt} = \frac{\partial}{\partial t} + \mathbf{v} \cdot \nabla$ stands for taking the material derivative. The functions J_{ij} characterize the intensity of the mass exchange between the components, which can be used, for example, in case of chemical reactions in the medium. From the law of mass conservation for the whole medium, it follows that $J_{ij} = -J_{ji}$, similarly, from the law of conservation of momentum— $\mathbf{R}_{ij} = -\mathbf{R}_{ji}$.

Such approach, when a deformable body is considered as a multicomponent medium, significantly enhanced the methods of continuous mechanics allowing to describe processes that occur at different scale levels. Multicomponent models cover a wide range of problems from describing the interaction of the electron gas with the lattice to the problem of creating composite materials. In the most general case, each of the media is characterized not only by density and velocity, but also by its temperature. Then, the system of equations should be supplemented with the heat equations for each of the components and taken into account the energy exchange between them. Two-temperature models, which are often used for considering problems of laser irradiation of thin films, are analyzed in [11–13]. The great advantage of the multicomponent approach over the hypothesis of a non-monotonic constitutive curve is that the interphase boundary is not introduced explicitly, but arises in a natural way, as a result of solving the problem. The phase of the material at a fixed point can be defined as the concentration of the corresponding component. The main difficulty lies in determining the source terms and the interaction forces between the components, which, like the specifying of kinetic equation, is a difficult question with an ambiguous answer.

11.2 Basic Equations of Two-Component Medium

In the present article, we restrict ourselves by considering only two-component model, when a complex crystalline structure of material consists of two almost similar lattices connected by nonlinear interaction force. In the case of small strains, we assume that the Hooke law is satisfied for both components. Then, in the framework of the one-dimensional model, in the absence of source terms, the momentum balance equations take the form

$$\begin{aligned} E_1 \frac{\partial^2 u_1}{\partial x^2} - \rho_{10} \frac{\partial^2 u_1}{\partial t^2} - R &= 0 \\ E_2 \frac{\partial^2 u_2}{\partial x^2} - \rho_{20} \frac{\partial^2 u_2}{\partial t^2} + R &= 0. \end{aligned} \quad (11.2.1)$$

Here, u_i ($i = 1, 2$) denotes the displacement of each of the components, E_i is Young's modulus, and ρ_{i0} is the density in the equilibrium state. For convenience, the notation $R_{12} = R$ is introduced. When choosing an analytical expression for the interaction force, we will proceed from a general assumption that it consists of

two terms. The first one is determined by the nonlinear elastic coupling between the components, and the second one describes the dissipation

$$R = R_1(u_1 - u_2) + R_2(\dot{u}_1 - \dot{u}_2). \quad (11.2.2)$$

Determining the functions R_1 and R_2 , one has to consider the possibility of the transition of material from one state to another. This means that a nonlinear elastic bond is obliged to have a non-trivial stable equilibrium position. In addition, it should take into account the periodicity of the complex lattice, the structure of which does not change when the components are mutually displaced at the distance multiple of the period. Thus, one of the simplest expressions for the interaction force may be written as

$$R = K \sin \lambda z + \nu \dot{z}, \quad (11.2.3)$$

where $z = u_1 - u_2$ signifies the relative displacement. The parameter K defines the maximum value of the interaction, and ν characterizes the viscous friction. The coefficient $\lambda = \frac{2\pi}{d}$ is inversely proportional to the period of the lattice d .

Equations (11.2.1) are formulated for both lattices, but the experimentally measured parameter is not the displacement of each component, but some average value. We assume this quantity containing information about the physical state of the system to be the center of mass displacement $U = \frac{\rho_{10}u_1 + \rho_{20}u_2}{\rho_{10} + \rho_{20}}$. Then, it is convenient to rewrite the equations of the two-component medium with respect to the center of mass and the relative displacement [14]

$$\begin{aligned} \frac{\partial^2 U}{\partial x^2} - \frac{1}{c_u^2} \frac{\partial^2 U}{\partial t^2} &= \alpha \frac{\partial^2 z}{\partial x^2} \\ \frac{\partial^2 z}{\partial x^2} - \frac{1}{c_z^2} \frac{\partial^2 z}{\partial t^2} &= \beta R(z, \dot{z}) + \gamma \frac{\partial^2 U}{\partial t^2}, \end{aligned} \quad (11.2.4)$$

where the following notation is introduced: $c_u^2 = \frac{E_1 + E_2}{\rho_{10} + \rho_{20}}$, $c_z^2 = \frac{E_1 E_2 (\rho_{10} + \rho_{20})}{(E_1 + E_2) \rho_{10} \rho_{20}}$. The parameters α , β and γ are determined by the physical properties of material: $\alpha = \frac{E_2 \rho_{10} - E_1 \rho_{20}}{(E_1 + E_2)(\rho_{10} + \rho_{20})}$, $\beta = \frac{E_1 + E_2}{E_1 E_2}$, $\gamma = \frac{E_2 \rho_{10} - E_1 \rho_{20}}{E_1 E_2}$.

As a result, we obtain a system of Eq. (11.2.4) for the material with two scales. The first one corresponds to the displacement on macrolevel measured during the experiment, whereas the second one describes microstructural transformations. In fact, relative displacement plays the role of an internal degree of freedom, which can be excited by energy transfer from the center of mass in a certain range of external impact. In this model, the process of rearrangement in crystalline structure is associated with the dynamics of the internal variable, and under the term ‘‘new phase,’’ we imply the domain of material with the function z occupying a new equilibrium state. Finally, it is necessary to say that here we consider only mechanical impact as the cause of structural transformations. The influence of other factors is excluded.

11.3 Statement of the Problem. Dispersion Curves

After introducing dimensionless variables $\tilde{x} = \frac{x\omega}{c_1}$, $\tilde{t} = \omega t$, $\tilde{U} = U\lambda$, $\tilde{z} = z\lambda$, $\tilde{v} = \frac{v\omega^*}{K\lambda}$, where $\omega^* = c_1\sqrt{\frac{(1-\chi)\delta K\lambda}{(1-\chi)E_1}}$, one can write governing Eq. (11.2.4) as

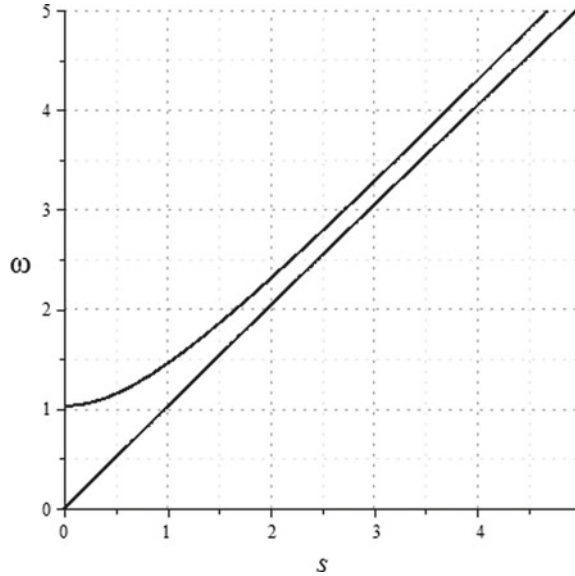
$$\begin{aligned}\frac{\partial^2 \tilde{U}}{\partial \tilde{x}^2} - \frac{1}{c_u^2} \frac{\partial^2 \tilde{U}}{\partial \tilde{t}^2} &= \alpha \frac{\partial^2 \tilde{z}}{\partial \tilde{x}^2} \\ \frac{\partial^2 \tilde{z}}{\partial \tilde{x}^2} - \frac{1}{c_z^2} \frac{\partial^2 \tilde{z}}{\partial \tilde{t}^2} &= \widetilde{\sin z} + \tilde{v} \dot{\tilde{z}} + \delta \frac{\partial^2 \tilde{U}}{\partial \tilde{t}^2}.\end{aligned}\quad (11.3.1)$$

Here, the following notation is used: $c_u^2 = \frac{(1-\chi)\delta}{1-\delta}$, $c_z^2 = \frac{1}{1-\chi\delta}$, $\alpha = \frac{(1-\chi)\chi\delta}{1-\chi\delta}$. The sound velocity of the first component is signified as $c_1 = \sqrt{\frac{E_1}{\rho_1}}$, the coefficient $\chi = \frac{\rho_1}{\rho_1 + \rho_2}$ denotes its mass fraction, and the small parameter $\delta = 1 - \frac{c_1^2}{c_2^2} \ll 1$ characterizes the difference in physical properties of the lattices. Hereinafter, for definiteness, we assume that $\chi = \frac{1}{2}$ and $\delta = 0.1$. Equations (11.3.1) with zero initial conditions are considered in the semi-finite region $0 \leq \tilde{x} < \infty$. The stress on the boundary $\tilde{x} = 0$ is given in the form of the short rectangular pulse $\sigma_{\text{imp}}(t) = \sigma_0(H(t) - H(t - t_0))$ of t_0 duration. Here, $H(t)$ is the unit step function. If we suppose that the stress on the boundary is distributed proportionally to the density of the components, then the boundary conditions for Eq. (11.3.1) have the form

$$\begin{aligned}\left. \frac{\partial \tilde{U}}{\partial \tilde{x}} \right|_{\tilde{x}=0} &= \tilde{\sigma}_{\text{imp}}(\tilde{t}) \left(1 + \frac{\chi(1-\chi)\delta^2}{1-\delta} \right) \\ \left. \frac{\partial \tilde{z}}{\partial \tilde{x}} \right|_{\tilde{x}=0} &= \frac{\tilde{\sigma}_{\text{imp}}(\tilde{t})\delta}{1-\delta},\end{aligned}\quad (11.3.2)$$

where $\tilde{\sigma} = \frac{c_1\lambda\sigma}{\omega^*(E_1+E_2)}$ and $\sigma = \sigma_1 + \sigma_2$. The standard type of boundary conditions is applied at infinity: $\tilde{U}|_{\tilde{x} \rightarrow \infty} = 0$, $\tilde{z}|_{\tilde{x} \rightarrow \infty} = 0$. Neglecting the terms of order δ^2 , it is possible to present the initial-boundary value problem as

$$\begin{aligned}\frac{\partial^2 \tilde{U}}{\partial \tilde{x}^2} - \frac{\partial^2 \tilde{U}}{\partial \tilde{t}^2} &= \frac{\delta}{4} \frac{\partial^2 \tilde{z}}{\partial \tilde{x}^2} \\ \frac{\partial^2 \tilde{z}}{\partial \tilde{x}^2} - \frac{\partial^2 \tilde{z}}{\partial \tilde{t}^2} &= \widetilde{\sin z} + \tilde{v} \dot{\tilde{z}} + \delta \frac{\partial^2 \tilde{U}}{\partial \tilde{t}^2} \\ \left. \frac{\partial \tilde{U}}{\partial \tilde{x}} \right|_{\tilde{x}=0} &= \tilde{\sigma}_{\text{imp}}(\tilde{t}) \\ \left. \frac{\partial \tilde{z}}{\partial \tilde{x}} \right|_{\tilde{x}=0} &= \tilde{\sigma}_{\text{imp}}(\tilde{t})\delta.\end{aligned}\quad (11.3.3)$$

Fig. 11.1 Dispersion curves

The graph of dispersion curves for system (11.3.3) described by the equation

$$(1 - \delta)\omega^4 - \omega^2\left((2 - \delta)s^2 + 1 - \frac{\delta}{2}\right) + s^4 + s^2 = 0, \quad (11.3.4)$$

where s is the wave number and ω signifies the frequency, as presented in Fig. 11.1.

It consists of two branches. The lower one corresponds to the center of mass displacement, and the upper one—to the relative motion. Its dynamics is described with the second equation of system (11.3.3). It is represented by the nonlinear Klein–Gordon equation complemented by the additional term, which expresses the influence of inertia forces. This equation plays an important role in the theory of nonlinear waves since it is very often used in different types of applications [15–17], such as physics of dislocations, simulation of seismic phenomena, and the description of Josephson junctions. Its exact solution can be obtained in the form of stationary waves, but here we deal with the Cauchy problem and, therefore, it seems reasonable to think about applying numeric methods. However, a considerable difficulty exists in defining the values of parameters for numeric solution and providing the estimation of time required for the system to reach the desired state. In this regard, we need a reliable procedure for constructing an approximate analytical expression to be able at least qualitatively to predict the dynamics of the model and to separate the physical phenomena from the effects brought by applying numerical integration.

11.4 On the Method of Variable Interval

For many non-stationary problems, a quite good approximation can be obtained by applying the method of searching the solution on a variable interval, proposed by Slepian [18]. Similarly to the Galerkin procedure, the solution of the differential equation is sought in the form of eigenfunction expansion, and however, the length of the interval $l(t)$, in contrast to the classical approach, is an unknown function of time. In case of hyperbolic equations, this function usually is taken as

$$l(t) = c_0 t, \quad (11.4.1)$$

where c_0 is a phase velocity of a wave. As a more general criterion, the minimum of the standard deviation of the approximate solution $\tilde{u}(x, t)$ from the exact solution of the differential equation $u(x, t)$ can be used

$$\frac{\partial}{\partial l} \int_0^l (\tilde{u} - u)^2 dx = 0, \quad (11.4.2)$$

Let us show the essence of this approach using the simplest example. For this purpose, we consider the semi-finite region described by d'Alembert operator

$$\frac{\partial^2 u}{\partial x^2} - \frac{\partial^2 u}{\partial t^2} = 0, \quad (11.4.3)$$

and satisfying the following boundary conditions

$$\begin{aligned} \left. \frac{\partial u}{\partial x} \right|_{x=0} &= F(t) = F_0 H(t) \\ u|_{x \rightarrow \infty} &= 0, \end{aligned} \quad (11.4.4)$$

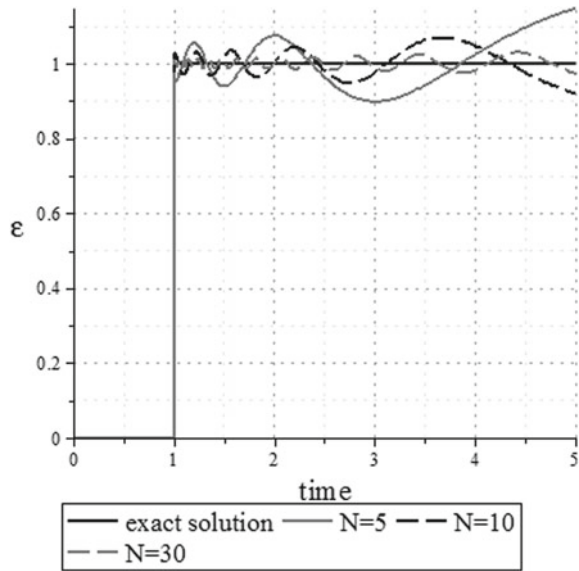
where F_0 is an arbitrary constant. Initial conditions are assumed to be zero. The exact solution of Eq. (11.3.3) is obvious

$$\varepsilon = \frac{\partial u}{\partial x} = F_0 H(t - x). \quad (11.4.5)$$

Now we are going to find the solution of the same problem in the form of the series $u(x, t) = \sum_{n=0}^N q_n(t) f_n(x)$, where $f_n(x) = \cos \frac{\pi(2n+1)x}{2l} H(l-x)$. After multiplying Eq. (11.4.3) by the form and integrating it the interval from 0 to $l(t)$ we obtain the ordinary differential equation for $q_n(t)$

$$\ddot{q}_n + \Omega_n^2 q_n = -\frac{2F(t)}{l}, \quad (11.4.6)$$

Fig. 11.2 Convergence of approximate solution



where $\Omega_n = \frac{\pi(2n+1)}{2l}$. Its solution is given by

$$q_n(t) = -\frac{2F_0}{l} \frac{(1 - \cos \Omega_n t)H(t)}{\Omega_n^2}. \tag{11.4.7}$$

Then, the derivative of the function $u(x, t)$ takes the form

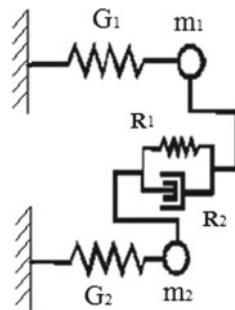
$$\frac{\partial u}{\partial x} = \frac{4F_0}{\pi} \sum_{n=0}^N \frac{(1 - \cos \Omega t)}{(2n + 1)} \sin \frac{\pi(2n + 1)x}{2l} H(l - x). \tag{11.4.8}$$

Its convergence to the exact solution (11.4.5) at $x = 1$ is demonstrated in Fig. 11.2.

11.5 Discrete Model

As a result of applying the Galerkin procedure on a variable interval, a continuous problem is reduced to the ordinary equations describing dynamics of a single element from the rheological model of material. For one-component medium, a spring pendulum represents this element. For the two-component material, it turns to be a nonlinear system of the coupled oscillators (Fig. 11.3) with close natural frequencies.

Denoting their displacements as x_1 and x_2 , it is possible to describe its dynamics analogously to continuous problem, taking for unknown functions the center of mass displacement $x = \frac{1}{2}(x_1 + x_2)$ and the relative displacement $z = x_1 - x_2$. If their

Fig. 11.3 Coupled oscillators

masses are equal, their behavior is described with the following system of equations:

$$\begin{aligned} \ddot{x} + x &= \frac{\delta z}{4} \\ \ddot{z} + 2n\dot{z} + z + \kappa \sin z &= \delta x. \end{aligned} \quad (11.5.1)$$

Differentiating in (11.5.1) is performed by the dimensionless time $\tau = \omega_1 t$, where $\omega_1 = \sqrt{\frac{G_1}{m_1}}$ is one of the partial frequencies. Small parameter $\delta = \frac{\omega_2^2 - \omega_1^2}{\omega_1^2}$ is given by their relative difference. The coefficient κ describes the nonlinear interaction between the masses. Subsequently, it is assumed that it is equal to the minimum value ($\kappa = 1$), providing non-convexity for potential energy of z . At the same time, the following relations establish the correspondence between continuous and discrete systems

$$\kappa = \frac{4\pi K d}{E_1}, \quad n = \frac{\omega^{*2} d^2 \nu}{4\pi c_1 K}. \quad (11.5.2)$$

In the linear system ($\kappa = 0$), we obtain beat oscillations with the period $T = \frac{4\pi}{\delta}$ depending on the difference between physical properties of the lattices (Fig. 11.4).

The appearance of nonlinear term makes the system very sensible to initial velocity V_0 . If it does not exceed the critical value $V_0 \approx \frac{\kappa}{\delta}$, there is no interaction between two degrees of freedom. They oscillate independently from each other (Fig. 11.5).

However, when the threshold is broken, the dynamics of the system changes dramatically. The oscillations of x , obtained by numerical integration at $n = 0.011$, are depicted in Fig. 11.6 by dashed line.

The specific feature of the process for sufficiently large value of V_0 is the time point separating two different regimes. Note that the amplitude of oscillations at the second one is reduced in comparison with initial value. To realize the energy transfer, it is important that its duration $\tau_e = \frac{2\pi}{\delta}$ will not exceed the relaxation time $\tau_r = \frac{1}{n}$ of the partial system. Otherwise, the oscillations of the relative displacement will be damped before the center of mass displacement has enough time to be excited. This implies that $n \leq \frac{\delta}{2\pi}$.

In order to obtain an analytical expression demonstrating this effect, let us suppose that the process of switching happens immediately at the point τ_* . Then, the nonlinear

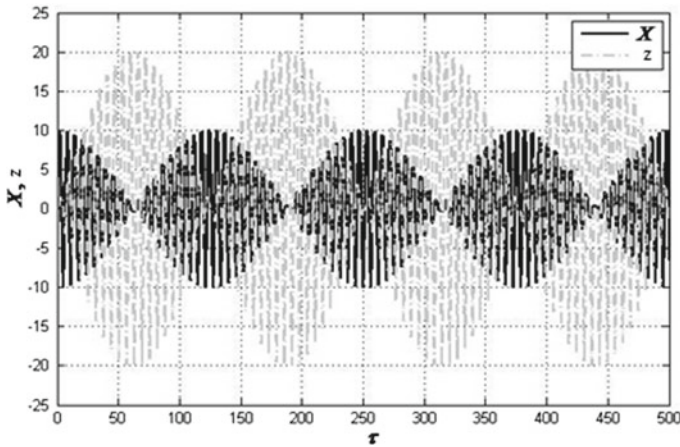


Fig. 11.4 Beats, $\delta = 0.1, n = 0$

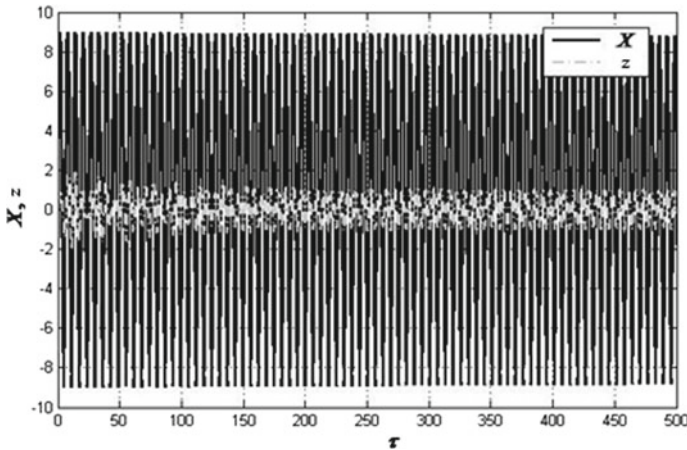


Fig. 11.5 Oscillations X и $z, V_0 = 9, n = 0.011$

term in Eq. (11.5.1) can be written as $\kappa_0 \sin z \delta_0(\tau - \tau_*)$, where $\delta_0(\tau)$ signifies delta function. The parameters τ_* and κ_0 are found by means of Laplace transform. Under the accepted assumptions, the solution of system (11.5.1) in the image space has the form

$$\begin{aligned}
 x^L(p) &= \frac{(p^2 + 1)V_0 - \frac{\delta}{4}\kappa_0 \sin z(\tau_*)e^{-p\tau_*}}{(p^2 + 1)^2 - \frac{\delta^2}{4}} \\
 z^L(p) &= \frac{V_0\delta - (p^2 + 1)\kappa_0 \sin z(\tau_*)e^{-p\tau_*}}{(p^2 + 1)^2 - \frac{\delta^2}{4}}.
 \end{aligned}
 \tag{11.5.3}$$

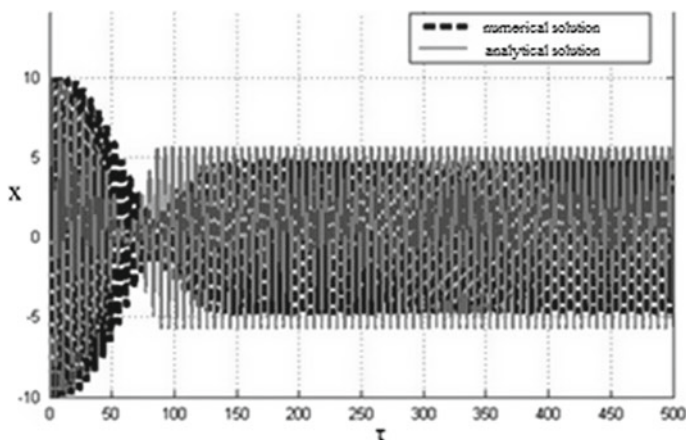


Fig. 11.6 Center of mass oscillations

The only way to cease beats is to eliminate one of the natural frequencies. Such situation is possible if the pole of the function $x^L(p)$ coincides with the root of the numerator. This requirement leads to the following expressions for unknown parameters:

$$\tau_* = \frac{\pi k}{1 - \frac{\delta}{4}} \quad (11.5.4)$$

$$\kappa_0 \sin z(\tau_*) = (-1)^{k+1} 2V_0, \quad (11.5.5)$$

where k is integer. After taking the inverse transform, one can obtain

$$\begin{aligned} X(\tau) &= V_0 \left(\cos \frac{\delta \tau}{4} \sin \tau + (-1)^k \sin \frac{\delta(\tau - \tau_*)}{4} \cos(\tau - \tau_*) H(\tau - \tau_*) \right) \\ \varphi(\tau) &= -2V_0 \left(\sin \frac{\delta \tau}{4} \cos \tau + (-1)^k \cos \frac{\delta(\tau - \tau_*)}{4} \sin(\tau - \tau_*) H(\tau - \tau_*) \right) \end{aligned} \quad (11.5.6)$$

Substituting relations (11.5.4) and (11.5.5) in (11.5.6) allows to show that after passing the point τ_* , the system switches to the regime of harmonic oscillations

$$\begin{aligned} X_+(\tau) &= \frac{V_0}{2} \left(\left(1 + \cos \frac{\pi k \delta}{2} \right) \sin \left(1 + \frac{\delta}{4} \right) \tau - \sin \frac{\pi k \delta}{2} \cos \left(1 + \frac{\delta}{4} \right) \tau \right) \\ z_+(\tau) &= V_0 \left(\left(1 + \cos \frac{\pi k \delta}{2} \right) \sin \left(1 + \frac{\delta}{4} \right) \tau - \sin \frac{\pi k \delta}{2} \cos \left(1 + \frac{\delta}{4} \right) \tau \right) \end{aligned} \quad (11.5.7)$$

The value of k can be determined from energy balance if we equate the work of the viscous friction on the time interval $[0, \tau_*]$ to the energy jump at τ_* in the model with a delta function. This requirement results in the following equation

$$2V_0^2 \cos \frac{\pi k \delta}{2} = -n \int_0^{\tau_*} \dot{\phi}^2(\tau) d\tau. \quad (11.5.8)$$

With the selected values of parameters, one can find that $k = 27$. The analytical solution obtained from (11.5.3) is presented in Fig. 11.6 by solid line. It correlates well with the result of numeric integration.

11.6 Continuous Model

After the process of energy transition was demonstrated in the oscillator, we return to the original continuous problem given by Eq. (11.3.3) considered in the half space $0 < \tilde{x} < \infty$. It is quite reasonable to expect the same effect in continuous model. However, talking about continuum immediately raises a number of additional issues. The primarily is the determination of the distance, at which the structural transformation takes place. The evaluation of this parameter is a problem of great importance for both experimental and numeric simulation. Let us apply the method of variable interval for Eq. (11.3.3), seeking their solution as $\tilde{U} = \sum_{n=1}^N Q_n(\tilde{t}) \cos \frac{\pi(2n+1)\tilde{x}}{2l} H(l - \tilde{x})$, $\tilde{z} = \sum_{n=1}^N q_n(\tilde{t}) \cos \frac{\pi(2n+1)\tilde{x}}{2l} H(l - \tilde{x})$. After multiplying them by the form and integrating between 0 and $l = \tilde{l}$, we obtain the system of equations for the functions $Q(t)$ and $q(t)$

$$\begin{aligned} \ddot{Q} + \Omega^2 Q &= \frac{\Omega^2 \delta q}{4} - \frac{2\sigma_{\text{imp}}(\tilde{t})}{l} \\ \ddot{q} + \nu \dot{q} + \Omega^2 q + 2J_1(q) &= -\delta \ddot{Q} - \frac{2\sigma_{\text{imp}} \delta}{l}, \end{aligned} \quad (11.6.1)$$

where $\Omega = \frac{\pi(2n+1)}{2l}$ is the frequency of the corresponding form. Here, $J_1(q)$ denotes the Bessel function of the first kind. After excluding \ddot{Q} from the second equation and introducing dimensionless time $\tau = \Omega \tilde{t}$, the system (11.4.1) can be written as

$$\begin{aligned} \ddot{Q} + Q &= \frac{\delta q}{4} - \frac{2\sigma_{\text{imp}}\left(\frac{\tau}{\Omega}\right)}{\Omega^2 l} \\ \ddot{q} + \frac{\nu}{\Omega} \dot{q} + q + \frac{2}{\Omega^2} J_1(q) &= \delta Q. \end{aligned} \quad (11.6.2)$$

These equations resemble Eq. (11.5.1). This gives us the idea to apply the same procedure, which was carried out for the discrete model. The same arguments turn

out to be applicable to system (11.6.2). Using delta function $\delta_0(t)$ instead of the pulse of finite duration in the right part of the first equation, we obtain

$$\begin{aligned}\ddot{Q}_n + Q_n &= \frac{\delta q_n}{4} - \frac{2\tilde{\sigma}_0\delta_0(\tau)}{\Omega_n l} \\ \ddot{q}_n + q_n + \frac{2}{\Omega_n^2} J_1(q_n)\delta_0(\tau - \tau_*) &= \delta Q_n.\end{aligned}\quad (11.6.3)$$

The analogy between (11.6.3) and equations describing the coupled oscillators (11.5.6) immediately allows writing the dependencies for $Q_n(\tau)$ and $q_n(\tau)$ using (11.5.6)

$$\begin{aligned}Q_n(\tau) &= -\frac{2\tilde{\sigma}_0}{\Omega_n l} \left(\cos \frac{\delta\tau}{4} \sin \tau + (-1)^k \sin \frac{\delta(\tau - \tau_*)}{4} \cos(\tau - \tau_*) H(\tau - \tau_*) \right) \\ q_n(\tau) &= \frac{4\tilde{\sigma}_0}{\Omega_n l} \left(\sin \frac{\delta\tau}{4} \cos \tau + (-1)^k \cos \frac{\delta(\tau - \tau_*)}{4} \sin(\tau - \tau_*) H(\tau - \tau_*) \right)\end{aligned}\quad (11.6.4)$$

The parameter τ_* in the discrete model has been found by using condition (11.5.4) of leaving only one natural frequency in the system of coupled oscillators. This condition for Eq. (11.6.2) is preserved, whereas the analog of expression (11.5.5) has the form

$$-\frac{2\tilde{\sigma}_0}{l} = \frac{(-1)^k J_1(q(\tau_*))}{\Omega}, \quad k = 1, 2, \dots \quad (11.6.5)$$

Here, the role of parameter that determines the magnitude of momentum, required for switching the system from one regime to another, is carried out by the distance at which the structural transformation starts. To estimate this distance, let us multiply Eq. (11.6.5) by $\frac{1}{t_*}$, assuming the existence of the parameter similar to τ_* in the discrete model. Taking into account the introduction of the new variable $\tau = \Omega_n t$ and the length of the interval $l = \tilde{l}$, it follows from (11.6.5) that

$$t_*^2 = -\frac{2\tilde{\sigma}_0\tau_*(-1)^k}{J_1\left(\frac{4\tilde{\sigma}_0}{\tau_*} \sin \frac{\delta\tau_*}{4} \cos \tau_*\right)}.\quad (11.6.6)$$

If $4\tilde{\sigma}_0 \ll \tau_*$, relation (11.6.6) can be simplified

$$t_* = \tau_* \sqrt{-\frac{(-1)^k}{\sin \frac{\delta\tau_*}{4} \cos \tau_*}}.\quad (11.6.7)$$

Again, the unknown integer k is determined based on energy balance represented by Eq. (11.5.8), where the role of coefficient for viscous friction is performed by the

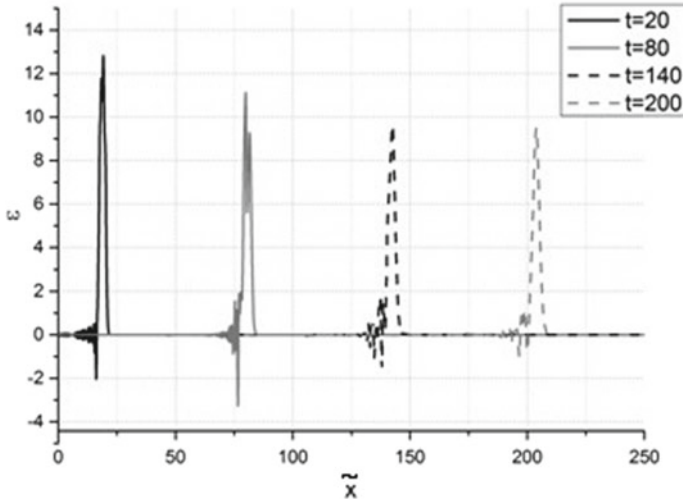


Fig. 11.7 Strain distribution, $\tilde{\sigma}_0 = 11$, $\tilde{t}_0 = 3$

term $\frac{v}{\Omega_n}$. Using (11.6.7) and (11.5.2) and substituting in (11.5.8) $\delta = 0.1$, we obtain $k = 27$ and $\tilde{t}_* \approx 127$.

After the necessary estimates of parameters are provided, we move on to numerical integration. The obtained analytical results are confirmed by solving initial nonlinear problem (11.3.3) by applying finite difference method. The strain distribution, demonstrating the quenching of non-stationary wave due to the internal dissipation of energy, is depicted in Fig. 11.7.

At the same time following the dynamics of the relative displacement, we observe the process of transition to the new equilibrium, which is treated in the model as a structural conversion of material. It is shown in Fig. 11.8. Note that the region occupied by material with the rearranged crystalline structure slowly expands.

Last question left for discussion is the duration of the external pulse, which can be estimated using the dispersion curve (Fig. 11.1). The dimensionless cutoff frequency characterizing the spectral properties of the system is approximately equal to 1, and in order to awaken the internal degree of freedom, the spectral composition of the signal should contain frequencies lying above the given frequency. Otherwise, the relative displacement will not be manifested during the dynamic impact on the medium. The spectral characteristic of a rectangular pulse, referred to its area, is shown in Fig. 11.9.

Since the main part of the pulse energy is concentrated in the first lobe, the energy transfer to the internal degree of freedom takes place, when the first zero of spectral density exceeds the cutoff frequency, which implies that $\tilde{t}_0 < 2\pi$. The examples of strain distribution with the violation of this inequality and the corresponding relative displacement are depicted in Figs. 11.10 and 11.11.

Naturally, the effect of the initial pulse reduction is lost and the area of new phase of material does not change in time. Finally, it should be noted that the numeric

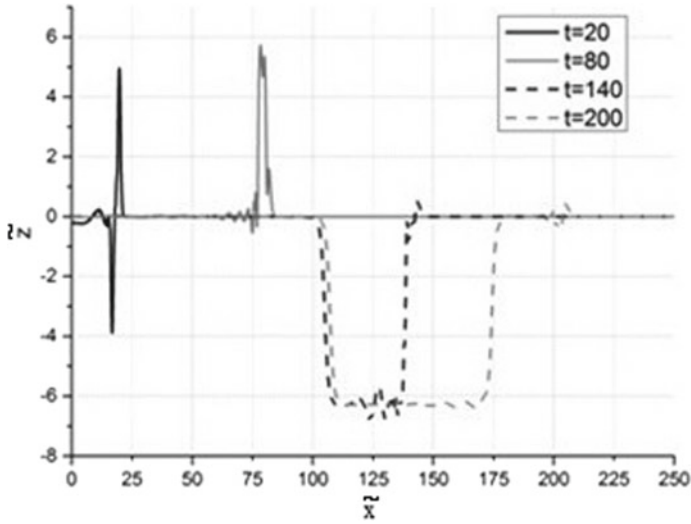
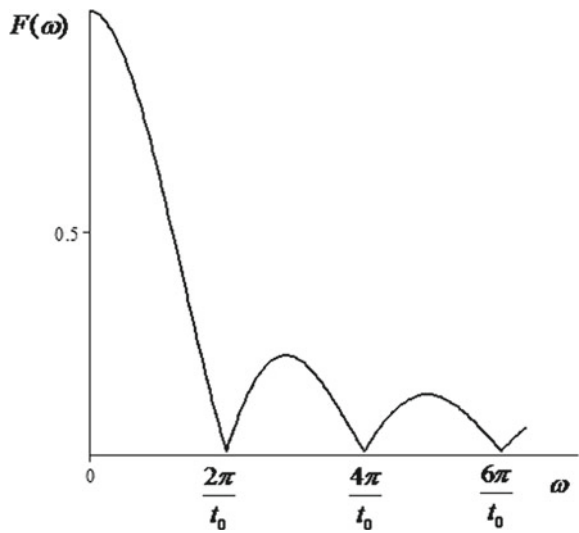


Fig. 11.8 Relative displacement, $\tilde{\sigma}_0 = 11$, $\tilde{t}_0 = 3$

Fig. 11.9 Spectral characteristic of the pulse



solution in this case is worthless without preliminary analytical investigation, as the nonlinear system turns to be very sensitive to small changes of parameters.

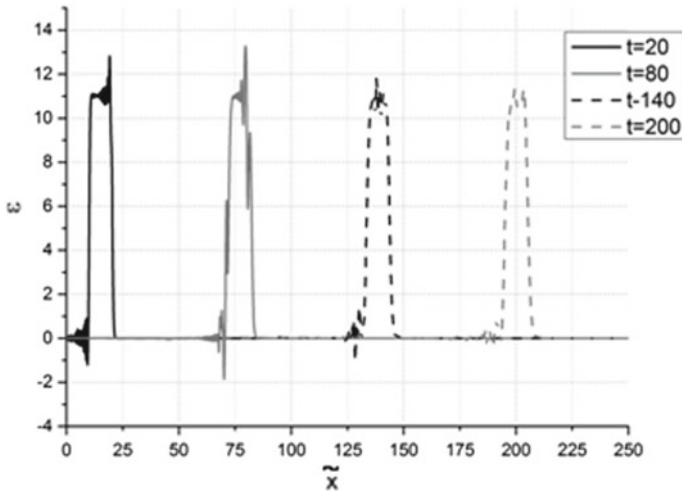


Fig. 11.10 Strain distribution, $\tilde{\sigma}_0 = 11$, $\tilde{t}_0 = 10$

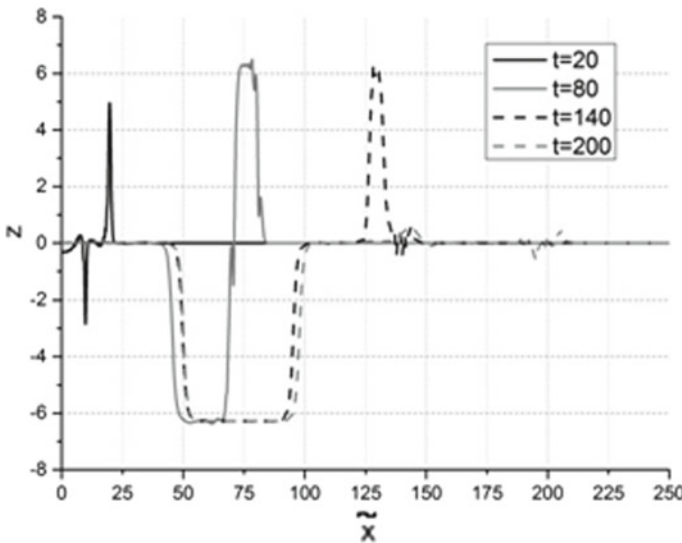


Fig. 11.11 Relative displacement, $\tilde{\sigma}_0 = 11$, $\tilde{t}_0 = 10$

11.7 Conclusion

In the present article, one-dimensional dynamic model of structural transformations in solids under pure mechanical impact is proposed. It is based on the equations of two-component medium with similar crystalline lattices coupled by nonlinear

interaction force. Their relative displacement possessing several equilibrium states plays the role of the additional degree of freedom responsible for rearrangement of internal structure. The dispersion curve of the system consists of two branches, and the main goal is to determine the conditions for energy exchange between them. For this purpose after the statement of the continuous problem, we start our investigation from analyzing the dynamics of a single element from the rheological model of material. Thus, the problem is reduced to consideration of nonlinear oscillator with two masses, described by the system of ordinary differential equations. We apply the method of variable interval in order to discover the analogy between discrete and continuous systems. Such approach gives the possibility to demonstrate the process of energy transfer to internal degree of freedom and to estimate its duration. On macrolevel, it is revealed through the quenching of non-stationary wave leading to reduction of the amplitude of the initial signal. All analytical results are confirmed by numeric integration fulfilled by using finite difference method.

Despite the extremely simplified description of structural changes in material, still many unresolved issues remain within the framework of the proposed model. This primarily refers to the problem of parameters identifying. The evaluation of cutoff frequency may be performed based on experiments on high-speed deformation. In several works, it has been shown that the structural changes caused by shock-wave loading are accompanied by rapid oscillations on the plastic front [19]. They indicate that the transformation of the structure is a complex dynamic process involving several scale levels. The frequency of these oscillations, equal to several gigahertz, can be taken as an estimation for this parameter. If we also know Young's modulus and the period of the structure, then we are able to estimate the coefficient of nonlinear bond. The analogous question on parameter of viscous friction seems to be more complicated.

References

1. Meshcheryakov, Y.I., et al.: Dynamic structures in shock-loaded copper. *Phys. Rev. B.* **78**(6) (2008)
2. Truskinovsky, L., Zanzotto, G.: Ericksen's bar revisited: energy wiggles. *J. Mech. Phys. Solids* **44**(8), 1371–1408 (1996)
3. Rosakis, P., Knowles, J.K.: Unstable kinetic relations and the dynamics of solid-solid phase transitions. *J. Mech. Phys. Solids* **45**(11), 2055–2081 (1997)
4. Ngan, S.C., Truskinovsky, L.: Thermo-elastic aspects of dynamic nucleation. *J. Mech. Phys. Solids* **50**(6), 1193–1229 (2002)
5. Truskinovsky, L., Vainchtein, A.: Kinetics of martensitic phase transitions: Lattice model. *SIAM J. Appl. Math.* **66**(2), 533–553 (2005)
6. Knowles, J.K.: Stress-induced phase transitions in elastic solids. *Comput. Mech.* **22**(6), 429–436 (1999)
7. Nigmatulin, R.I.: *Dynamics of Multiphase Media*, vol. 2. CRC Press (1990)
8. Zhilin, P.A.: *Advanced problems in mechanics*. St. Petersburg **2**, 271 (2006)
9. Vilchevskaya, E.N., Ivanova, E.A., Altenbach, H.: Description of liquid–gas phase transition in the frame of continuum mechanics. *Continuum Mech. Thermodyn.* **26**(2), 221–245 (2014)

10. Indeitsev, D., Mochalova, Y.: Mechanics of multi-component media with exchange of mass and non-classical supplies. In: *Dynamics of Mechanical Systems with Variable Mass*. pp. 165–194. Springer, Vienna (2014)
11. Jiang, L., Tsai, H.L.: Improved two-temperature model and its application in ultrashort laser heating of metal films. *J. Heat Transfer* **127**(10), 1167–1173 (2005)
12. Chen, J.K., et al.: Modeling of femtosecond laser-induced non-equilibrium deformation in metal films. *Int. J. Solids Struct.* **39**(12), 3199–3216 (2002)
13. Chowdhury, I.H., Xu, X.: Heat transfer in femtosecond laser processing of metal. *Numer. Heat Transfer: Part A: Appl.* **44**(3), 219–232 (2003)
14. Aero, E.L., Bulygin, A.N., Pavlov, Y.V.: The nonlinear theory of reorganization of structure of superthin crystal layers at intensive loadings. *Mater. Phys. Mech.* **15**, 126–134 (2012)
15. Braun, O.M., Kivshar, Y.: *The Frenkel-Kontorova Model: Concepts, Methods, and Applications*. Springer Science & Business Media (2013)
16. Erofeev, V.I., Klyueva, N.V.: Solitons and nonlinear periodic strain waves in rods, plates, and shells (a review). *Acoust. Phys.* **48**(6), 643–655 (2002)
17. Dehghan, M., Shokri, A.: Numerical solution of the nonlinear Klein-Gordon equation using radial basis functions. *J. Comput. Appl. Math.* **230**(2), 400–410 (2009)
18. Slepian, L.I.: *Non-stationary elastic waves* (1972)
19. Barakhtin, B.K., Meshcheryakov, Y.I., Savenkov, G.G.: Dynamic and fractal properties of sp-28 steel under high-rate loading. *Zh. Tekh. Fiz.* **68**(10), 43–49 (1998)

Chapter 12

Dynamic Penetration into Water Saturated and Frozen Sand: Numerical Analysis of the Inverse Experimental Methodology



Vasiliy Kotov, Vladimir V. Balandin, Vladimir Vl. Balandin, Anatoliy Bragov, Andrey Lomunov and Svetlana Litvinchuk

Abstract The present paper numerically analyzes the applicability of the inverse experiment methodology for determining the force resisting penetration of a conical striker into frozen sand soil at a temperature of $-18\text{ }^{\circ}\text{C}$. The condition of the soil specimen prior to freezing is characterized as fully water saturated. The deformational behavior of the soil is described in the framework of the model of compressible elastic-plastic media with the plasticity condition depending on pressure. The dynamic compressibility diagram of the frozen soil includes the initial linearly elastic part. The errors in determining the force resisting penetration of a conical striker into frozen soil in the inverse experiment due to the effect of the waves reflected from the container walls were analyzed. The difference between maximal values of the force resisting penetration, obtained in the numerical calculations with the two versions of the boundary conditions, was used as a measure of the effect. For the problems of penetration of conical strikers into frozen and water-saturated soil, a good agreement between the experimental data and numerical results can be obtained with the help of Grigoryan's model accounting for the pressure-dependent parameters.

V. Kotov (✉) · V. V. Balandin · V. Vl. Balandin · A. Bragov · A. Lomunov · S. Litvinchuk
Research Institute of Mechanics, National Research Lobachevsky State University of Nizhny
Novgorod, 603950 Nizhny Novgorod, Russian Federation
e-mail: vkotov@inbox.ru

V. V. Balandin
e-mail: balandin@mech.unn.ru

V. Vl. Balandin
e-mail: rustydog2007@yandex.ru

A. Bragov
e-mail: bragov@mech.unn.ru

A. Lomunov
e-mail: lomunov@mech.unn.ru

S. Litvinchuk
e-mail: litvinchuk@mech.unn.ru

Keywords Grigoryan's soil model · Inverse experiment · Conical striker · Frozen sand · Water-saturated soil

12.1 Introduction

Determining the parameters of the laws of dynamic deformation for dry and water-saturated soils under varied parameters of temperature is of great scientific and applied importance. In the middle of the last century, the stress and velocity fields were determined in field experiments as a result of spherical explosion of blasting charges in frozen soil. A substantial dependence of the wave parameters on temperature and soil characteristics in the initial non-frozen condition: humidity, porosity, fractional and component composition and others, was determined.

The inverse experiment methodology [1–3] with measuring bar has proved very effective in determining the force characteristics of penetration of rigid cylindrical strikers with heads of various geometries. It allows to measure integral loads at the initial nonstationary stage of penetration. Earlier, experimental data were obtained on strain-rate dependences of dynamic penetration of cylindrical solids with flat, hemispherical and conical heads into dry and water-saturated sand at positive temperatures [4–7].

A significant disadvantage of the inverse techniques is the necessity to accelerate soil containers of considerable mass and small geometrical dimensions that leads to the effect of the container walls on the integral loads and final penetration depths [8]. Earlier, the effect of the boundaries on the maximal and quasi-stationary values of the force resisting penetration of a 20 mm-diameter hemispherical striker into dry sand, determined in inverse experiments, was studied. It was found that, if a boundary condition modeling the effect of a rigid container was used in computations, the quasi-stationary value of the force resisting penetration exceeds the analogous value calculated for penetration into a half-space by 20% at impact velocities over 100 m/s and then decreases with the increasing impact velocity. The computations of the process of penetration into dry soil conducted without a container showed lower values of the resistance force.

A qualitatively similar picture is observed when analyzing the process of penetration into frozen soil. The quantitative differences are explained by the fact that the longitudinal wave velocity in frozen soil (3000–4000 m/s) is an order of magnitude higher than the propagation velocity of small-amplitude waves in dry sand, which is 300–400 m/s.

In this paper, the process of penetration of a conical striker along the normal line to the free surface was numerically analyzed in an axisymmetric formulation, using software package *Dinamika-2* of the Research Institute for Mechanics of Nizhny Novgorod Lobachevsky State University, and in a 3D formulation in the framework of software product *LS-DYNA*. The relations of the soil media model were numerically realized in the framework of the modified Godunov scheme, implemented in the applied software package *Dinamika-2* of the Research Institute for Mechanics

of Nizhny Novgorod Lobachevsky State University. The earlier computations of the processes of impact and penetration of axisymmetric strikers into soft soil media showed good agreement between the numerical results and experimental data. The impact and penetration velocities are varied during the calculations from 150 to 300 m/s, with the cone basis diameters of 10, 12 and 20 mm. Computational geometry is determined by the size of the container used in the inverse experiment. The deformation of the container was neglected; the effect of the container walls was modeled by two choices of the boundary conditions: free surface (the absence of the walls) and “impermeability” along the normal line and free sliding in the tangential direction.

12.2 Grigoryan’s Mathematical Model of the Dynamics of Soil Media

Grigoryan’s mathematical model of the dynamics of soil media [9] can be written in the cylindrical coordinate system rOz (where Oz is the symmetry axis) as the system of differential equations. They express the laws of conservation of mass, pulse and maximal density attained in the process of actively loading the soil, as well as equations of plastic flow theory with the von Mises–Schleicher plasticity condition

$$\begin{aligned}
 d\rho/dt + \rho(u_{r,r} + u_{z,z}) &= -(\rho u_r)/r, \\
 \rho du_r/dt - \sigma_{rr,r} - \sigma_{rz,z} &= (\sigma_{rr} - \sigma_{\theta\theta})/r, \\
 \rho du_z/dt - \sigma_{rz,r} - \sigma_{zz,z} &= (\sigma_{rz})/r, \\
 d\rho_*/dt &= d\rho/dt H(\rho - \rho_*) H(d\rho/dt), \\
 D_J s_{ij} + \lambda s_{ij} &= 2G e_{ij}, \quad (i, j = r, z), \\
 s_{ij} s^{ij} &\leq \frac{2}{3} \sigma_Y^2,
 \end{aligned} \tag{12.1}$$

where the following notation is used: t is time, ρ_0 , ρ and ρ_* are the initial, current and maximal density attained in the loading process, u_i , σ_{ij} , s_{ij} , e_{ij} are the components of the velocity vector, Cauchy stress tensor, and deviators of the stress and strain-rate tensors, respectively, H is the Heaviside function, D_J is the Jaumann derivative, d/dt is the total derivative with respect to time, G is the shear modulus, σ_Y is the yield strength and sums are taken over repeated indices. Parameter $\lambda = 0$ in case of elastic strain and $\lambda > 0$ if the von Mises–Schleicher plasticity condition is satisfied.

The system of differential Eq. (12.1) is closed with finite relations, determining pressure p and plasticity condition of the soil

$$\begin{aligned}
 p &= f_1(\rho, \rho_*) H(\rho_* - \rho) H(\rho_0 - \rho) \\
 \sigma_T &= f_2(p).
 \end{aligned} \tag{12.2}$$

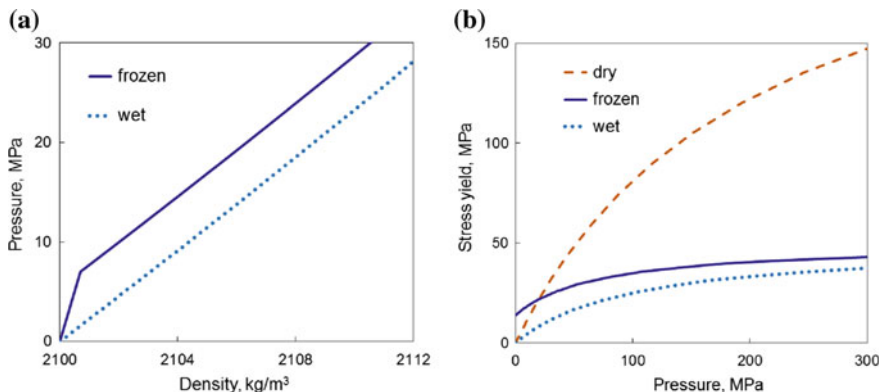


Fig. 12.1 Volume compressibility (a) and yield stress condition (b) dependencies

The system of Eqs. (12.1) and (12.2) of soil dynamics is complemented with initial and boundary conditions. On the head part of the striker, contacting with the soil medium, a contact algorithm of “impermeability” is used along the normal line with “sliding in the tangential direction with dry friction” in accordance with the Coulomb friction model with a constant friction coefficient k_f . Over the free surfaces of the soil and the striker, normal and tangential stresses were set to be equal to zero. The outer boundaries of the analyzed region of the soil corresponded to the geometry of the container used in the inverse experiment. Deformation of the container was neglected, and the effect of the container walls was modeled by two versions of the boundary conditions: (1) “impermeability” along the normal line and free sliding in the tangential direction (boundary condition 1) and (2) free surface, corresponding to the absence of walls (boundary condition 2). At an initial time, the stresses and velocity of the soil particles are equal to zero. The striker was assumed to be rigid, moving at a constant speed, equal to the impact velocity.

Let us concretize the assignment of functions f_1 and f_2 in Grigoryan’s model of soil media (1) and (2) schematically shown in Fig. 12.1.

The dynamic compressibility of the soil, as well as some other compressible materials, is characterized by shock adiabat, represented by the linear dependence of the shock wave velocity D as a function of the mass velocity U :

$$D = A + Bu \tag{12.3}$$

Here, the value of the constant A is approximately equal to the propagation velocity of the plane compression wave in soil under small pressures; B characterizes the ultimate compressibility of soil. The shock adiabat represented in the form of a linear dependence (3), and the Hugoniot conditions for a shock wave $\sigma = \rho_0 Du$, $\theta = u/D$ imply the well-known relation between the stress $\sigma(\theta)$ and the bulk strain θ .

$$\sigma(\theta) = \frac{\rho_0 A^2 \theta}{(1 - B\theta)^2}, \quad \theta = 1 - \frac{\rho_0}{\rho}, \quad (12.4)$$

The shear resistance of the medium is determined by the fractional-rational dependence of the yield strength as a function of pressure

$$f_2(p) \equiv \sigma_0 + kp/(1 + kp/\Delta\sigma), \quad \Delta\sigma = \sigma_M - \sigma_0 \quad (12.5)$$

The coefficients σ_0 , σ_M and k characterize adhesion, maximal value of yield strength and the internal friction of the soil.

The pressure is described with the following equation

$$p(\theta) = f_1(\theta) \equiv \begin{cases} K\theta, & -\theta_e < \theta < \theta_e \\ K\theta_e + \frac{\rho_0 a^2 \theta}{(1-b\theta)^2}, & \theta \geq \theta_e \end{cases} \quad (12.6)$$

Here, K , a and b are constant coefficients, the value θ_e limits an elastic behavior of the soil. The method for determining the coefficients a and b based on the known dependency parameters (3)–(5) is given in [10].

Unloading the medium from a state characterized by pressure and density values p_* and ρ_* is assumed to be linear

$$p - p_* = \frac{K}{\rho_0}(\rho - \rho_*)$$

12.3 Formulation of Numerical Modeling Problems

The relations (1) and (2) were realized within the framework of the methodology [11], based on the modified Godunov scheme, implemented in the applied software package Dynamika 2 of the Research Institute for Mechanics, Nizhny Novgorod Lobachevsky State University [12]. The earlier computations of the processes of impact and penetration of axisymmetric strikers into soft soil media [4] showed good agreement between the numerical results and experimental data.

To increase the reliability of the results of numerical analyses, the problem of penetration of a conical striker into an elastic-plastic medium modeling frozen soil was analyzed in a fully 3D formulation, using commercial software product LS-DYNA. The striker was modeled by a non-deformable rigid body (*MAT_RIGID), the soil was modeled by an elastic-plastic medium and the behavior of which is described in the framework of the model *MAT_SOIL_AND_FOAM.

The problem was analyzed in fluid–structure interaction (FSI) formulation, where the equations of motion of the striker were integrated in Lagrangian coordinates, while the equations for the soil were solved on the Eulerian grid. The interaction between the striker and an elastic-plastic medium was realized using a special

type of contact (CONSTRAINED_LAGRANGE_IN_SOLID). The formulation and solution of the problem of penetration correspond to the one given earlier [13].

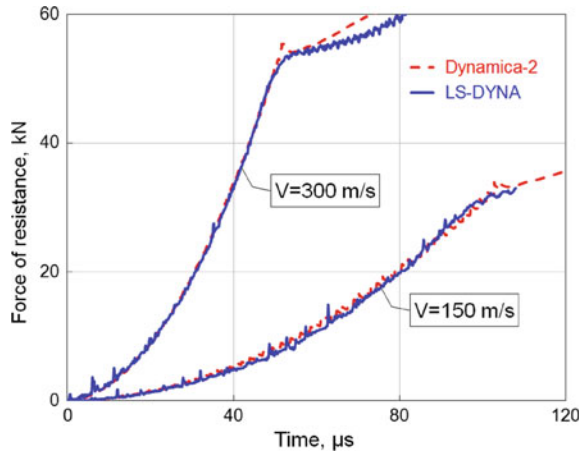
The parameters of the soil model (5) and (6) are the following: $\rho_0 = 2100 \text{ kg/m}^3$, $p_e = 6 \text{ MPa}$, $K = 21,000 \text{ MPa}$, $G = 7875 \text{ MPa}$ (determined by the value of Poisson's ratio $1/3$), $a = 1400 \text{ m/s}$, $b = 4$, $\sigma_0 = 15 \text{ MPa}$, $k = 0.5$, $\sigma_M = 50 \text{ MPa}$ and $k_f = 0.2$.

The choice of values of the parameters is determined by the following reasons. Up to stress values of $\sigma^* = 15 - 21 \text{ MPa}$, which correspond to compressive strength of the frozen soil, the soil behaves like a linearly elastic medium. Under conditions of uniaxial stress, we have $p_e = \sigma^* / 3$; at pressure $p_e \ll \sigma_M$, $\sigma^* = \sigma_0 + k p_e$ is also correct, whence it follows that $\sigma_0 = (1 - k/3)\sigma^*$. The results of dynamic tests [14–16] also indicate stress-rate dependence of the deformation diagrams of frozen soil, resulting in the approximately 1.5-fold increase of compressive strength in the strain-rate range from 300 to 1000 1/s. It is to be noted that the strength values of the frozen soil obtained in both static and dynamic tests are characterized by considerable scatter. In the present paper, the average strength value $\sigma^* = 18 \text{ MPa}$ was assumed. Strain-rate dependence was not accounted for in the first approximation. At pressures of about 200 MPa and a temperature of $-18 \text{ }^\circ\text{C}$, ice-water transition takes place, and the behavior of the frozen soil becomes similar to that of water-saturated soil, the parameters of the equation of state for which were determined by us earlier [10]. The longitudinal wave velocity c , determined by the inclination of the deformation diagram (6) at its initial part, amounts $\sqrt{(K + 4G/3)/\rho_0} = 3.8 \text{ km/s}$, while the shear wave velocity is $\sqrt{G/\rho_0} = 1.9 \text{ km/s}$. When the compression strength is exceeded, the longitudinal wave velocity drops to the value of 1.5 km/s, which corresponds to failure of the skeleton of the frozen soil.

The rectangular section of the cylindrical area of the soil is divided by a difference grid into square cells with the side size of d/n , where n is the number of cells. The convergence of the used Godunov scheme [11] was analyzed by a series of numerical computations on condensing grids. The change in quasi-stationary force depending on the cell size d/n appeared to be close to linear one with a reliability of at least 0.95, whereas the difference in values of the forces at $n = 200$ from the predicted values was 10–15%.

Figure 12.2 presents the forces resisting to penetration into the frozen soil of the conical striker with an apex angle of 60° and basis diameter of $d = 20 \text{ mm}$ in a rigid jacket at velocities of 150 m/s and 300 m/s. The red dotted curves represent the results obtained in calculations employing the applied software package Dynamika 2, while the solid blue curves represent the results obtained within the framework of software product LS-DYNA. The soil occupied a cylindrical area with a diameter of 54 mm and a height of 65 mm. It is to be noted that, the curves are coincident at the stage of penetration of the conical part of the striker and the numerical results after separation of the flow are in good agreement.

Fig. 12.2 Forces resisting to the penetration into the frozen soil of the conical striker with an apex angle of 60° and basis diameter of $d = 20$ mm in a rigid jacket at velocities of 150 m/s and 300 m/s



12.4 Results of Numerical Computations

The results of numerical calculations of penetration of conical strikers with an apex angle of 60° and basis diameters of $d = 10, 12$ and 20 mm at penetration velocities of $V_0 = 150$ and 300 m/s are given onwards. Two versions of the boundary conditions modeling absolutely elastic and absolutely rigid containers are analyzed.

Figure 12.3 presents the forces resisting to penetration of a conical striker with basis diameters of $d = 10$ (a), 12 (b) and 20 mm (c) into frozen soil at velocities of 150 and 300 m/s. Curves marked BC-1 show the results, obtained in computations using the boundary condition 1 modeling the effect of a rigid container, whereas curves marked BC-2 show the results of computations without a container (boundary condition 2).

Let us consider the value of the resistance force at the moment of penetration of a conical part of the striker $t^* = \frac{\sqrt{3}}{2} \frac{d}{V_0}$. Further, the growth of the contact surface area does not occur, and the observed changes in the resistance force to penetration are associated with the action of the boundary conditions caused by compressional-dilatational waves reflected from the borders of the region (container walls). The value of the resistance force at the moment of t^* is considered the maximal value of the force resisting to penetration.

It can be seen from Fig. 12.3b that the influence of the boundary conditions on the maximal value of the force resisting penetration of a striker with a $d = 12$ mm basis does not exceed 10% at penetration velocities of 150 m/s and then decreases with the increasing velocity. The force resisting penetration of a striker with a $d = 10$ mm basis is practically independent of the type of the boundary conditions until the $t < t^*$. The boundary conditions have a significant effect on the force resisting penetration of a striker with a basis diameter of $d = 20$ mm: when penetration velocities are varied from 150 to 300 m/s the difference in maximal values decreases from 60 to 15%.

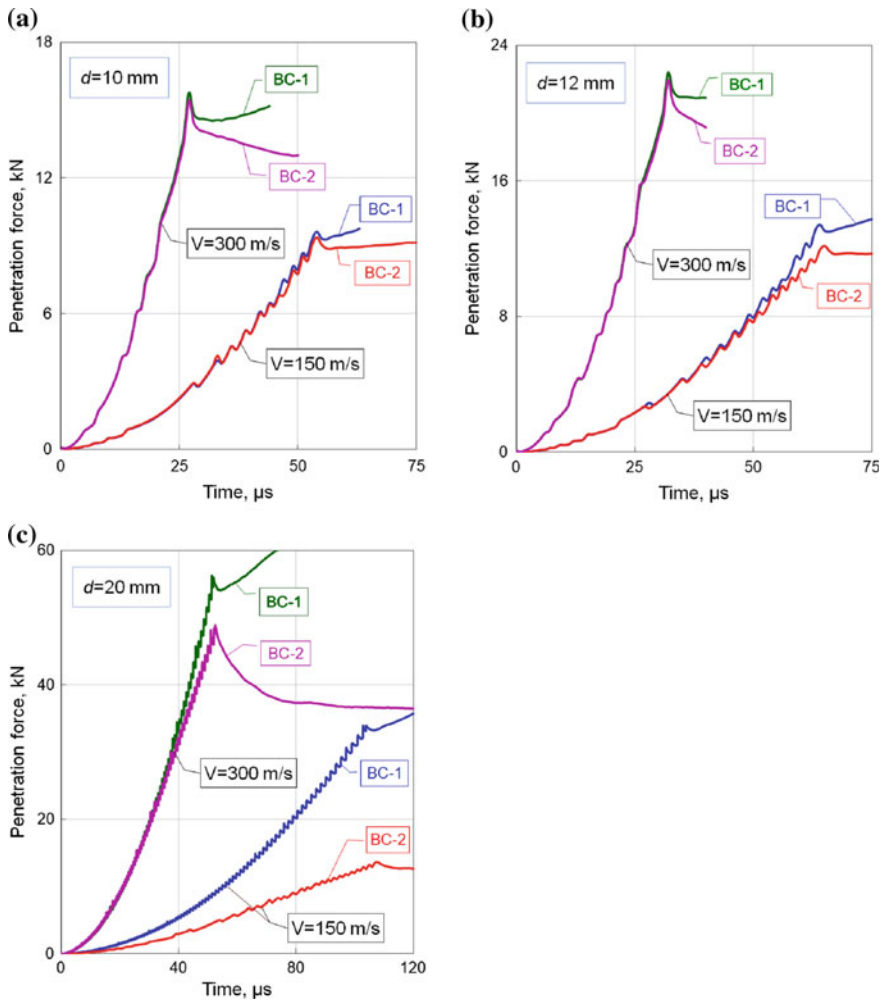
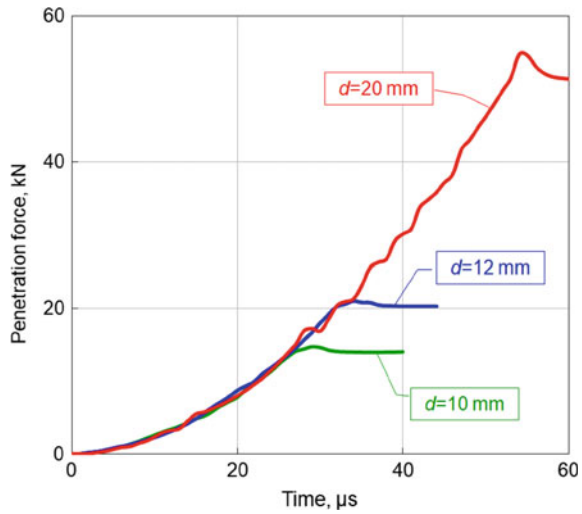


Fig. 12.3 Forces resisting to penetration of a conical striker with basis diameters of $d = 10$ (a), 12 (b) and 20 mm (c) into frozen soil at velocities of 150 m/s and 300 m/s

The problems of penetration of a striker into frozen soil at a penetration velocity of 300 m/s, within the time interval of $0 < t < 1.5t^*$, equivalent to the problems of penetration into a half-space, were also considered.

Figure 12.4 presents the results of computations in the form of time history of the force resisting penetration. Curves show the computational results of penetration into frozen soil of cones with basis diameters $d = 10, 12$ and 20 mm. Practically constant (quasi-stationary) level of the force resisting penetration is observed upon reaching its maximal value. It is to be noted that, the maximal value practically coincides with

Fig. 12.4 Penetration into a half-space of frozen sand (impact velocity 300 m/s)

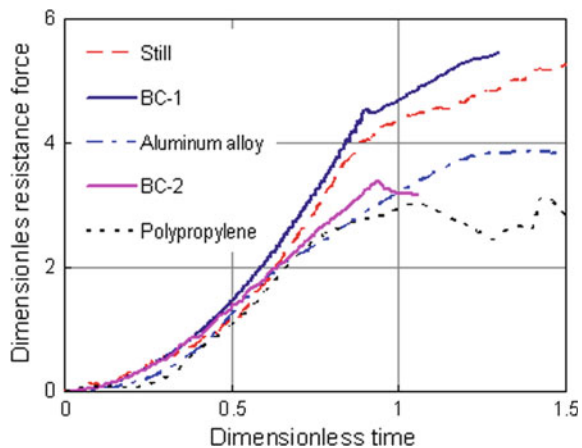


the value, obtained in computations using boundary condition 1, which simulates an absolutely rigid container (see also Fig. 12.3).

Figure 12.5 shows the dimensionless dependences of the resistance to penetration of a cone with a base diameter = 20 mm obtained in inverted experiments and numerical calculations. The values of resistance force and time are assigned, respectively, to $F^* = \frac{1}{2} \rho_0 S_0 V_0^2$ and t^* .

Dashed, dashed-dotted and dotted curves show the results of experiments using the following container materials: steel, aluminum alloy and polypropylene; the penetration rate was 133, 135 and 150 m/s, respectively. Solid curves correspond to the results of numerical calculations of cone penetration at a speed of 150 m/s using boundary conditions BC-1 and BC-2.

Fig. 12.5 Penetration into the frozen sand: experiment and calculations (impact velocities are about 150 m/s)



From Fig. 12.5, it can be seen that the maximum value is reached at, which may be due to the faster growth of the wetted surface due to the formation of a spray jet and the rise of the free surface of the soil toward the impactor upon impact. Note that the resistance to penetration of a projectile into frozen soil obtained because of calculations using boundary condition 1 (absolutely rigid container) is close to the results of an inverted experiment using a steel container. The influence of waves reflected from the walls of the container of aluminum alloy and polypropylene is close to the simulation results in the absence of the container. Up to the point in time, all results are close to each other.

12.5 Conclusion

It is shown that, in problems of penetration of conical strikers into frozen and water-saturated soils, a fairly good agreement between the experimental data and numerical results can be achieved using Grigoryan's model of elastic-plastic soil medium, accounting for the dependence of the yield criterion on pressure (the Mohr-Coulomb-Tresca limit yield criterion).

The error in determining the force resisting penetration of a conical striker into frozen soil in the inverse experiment due to the effect of the waves, reflected from the container walls, was analyzed. The difference between maximal values of the force resisting penetration, obtained in the numerical calculations with two versions of the boundary conditions, was used as a measure of the effect.

It is shown that, for a striker with 20 mm-diameter basis, the error amounts 15% at velocities over 300 m/s and then decreases with the increasing velocity. For conical strikers with 10 and 12 mm-diameter bases, at impact velocities over 150 m/s, the effect of the container walls can be neglected.

Acknowledgements This work was supported by a grant from the Government of the Russian Federation (contract No. 14.Y26.31.0031).

References

1. Forrestal, M.J., Grady, D.E.: Penetration experiments for normal impact into geological targets. *Int. J. Solids Struct.* **1**, 18 (1982)
2. Forrestal, M.J., Lee, L.M., Jenrette, B.D.: Laboratory-scale penetration experiments into geological targets to impact velocities of 2.1 km/s. *J. Appl. Mech.* **53**(2) (1986)
3. Balandin, V.I., Balandin, V.I., Bragov, A.M., Kotov, V.L.: Experimental study of the dynamics of penetration of a solid body into a soil medium. *Tech. Phys.* **61**(6) (2016)
4. Bazhenov, V.G., Bragov, A.M., Kotov, V.L., Kochetkov, A.V.: An investigation of the impact and penetration of solids of revolution into soft earth. *J. Appl. Math. Mech.* **67**, 4 (2003)
5. Balandin, V.V., Bragov, A.M., Igumnov, L.A., Konstantinov, A.Yu., Kotov, V.L., Lomunov, A.K.: Dynamic deformation of soft soil media: experimental studies and mathematical modeling. *Mech. Solids* **50**, 3 (2015)

6. Kotov, V.L., Balandin, V.V., Bragov, A.M., Balandin, V.I.: Investigation of dynamic resistance to the shear of water-saturated sand according to the results of the inverse experiment technique. *Tech. Phys. Lett.* **43**(9) (2017)
7. Bragov, A.M., Balandin, V.I., Kotov, V.L., Balandin, V.I.: Investigation of the dynamic properties of water-saturated sand by the results of inverted experiments. *Tech. Phys.* **63**(4) (2018)
8. Bazhenov, V.G., Kotov, V.L., Krylov, S.V., Balandin, V.V., Bragov, A.M., Tsvetkova, E.V.: Experimental-theoretical analysis of non-stationary interaction of deformable impactors with soil. *J. Appl. Mech. Tech. Phys.* **6**, 42 (2001)
9. Grigoryan, S.S.: On basic concepts of soil dynamics. *J. Appl. Math. Mech.* **24**, 6 (1960)
10. Bragov, A.M., Balandin, V.V., Igumnov, L.A., Kotov, V.L., Kruszka, L., Lomunov, A.K.: Impact and penetration of cylindrical bodies into dry and water-saturated sand. *Int. J. Impact Eng.* **122** (2018)
11. Abouziarov, M., Bazhenov, V.G., Kotov, V.L., Kochetkov, A.V., Krylov, S.V., Fel'dgun, V.R.: A Godunov-type method in dynamics of elastoplastic media. *Comput. Math. Math. Phys.* **40**, 6 (2000)
12. Bazhenov, V.G., Zefirov, S.V., Kochetkov, A.V., Krylov, S.V., Feldgun, V.R.: The dynamica-2 software package for analyzing plane and axisymmetric nonlinear problems of non-stationary interaction of structures with compressible media. *Matem. Mod.* **12**, 6 (2000)
13. Kotov, V.L., Balandin, V.I., Balandin, V.I., et al.: Application of the reverse experiment to study the resistance of a conical shocker during penetration in frozen sand. *Probl. Strength Plast.* **79**(2) (2017) (In Russian)
14. Haimin, D., Wei, M., Shujuan, Z., Zhiwei, Z., Enlong, L.: Strength properties of ice-rich frozen silty sands under uniaxial compression for a wide range of strain rates and moisture contents. *Cold Reg. Sci. Technol.* **123** (2016)
15. Qin-Yong, M.: Experimental analysis of dynamic mechanical properties for artificially frozen clay by the split Hopkinson pressure bar. *J. Appl. Mech. Tech. Phys.* **51**(3) (2010)
16. Qijun, X., Zhiwu, Z., Guozheng, K.: Dynamic stress-strain behavior of frozen soil: experiments and modeling. *Cold Reg. Sci. Technol.*, 106–107 (2014)

Chapter 13

Extended Model of Surface-Related Effects in Second-Gradient Elasticity. Surface Waves Related to the Nature of Adhesion



Sergey Lurie, Petr Belov and Elena Lykosova

Abstract It is considered a continuum theory of the adhesion properties of the surface of elastic bodies, which can be considered as theory of surface elasticity. We consider the surface of the body as the set of all the boundary points of the elastic body and believe that upon deformation, this surface is endowed with its own density of surface energy in the case of an adhesion-active surface. The definition of the “ideal” and gradient theory of elasticity of surface interactions is given, and it is shown that the ideal adhesion theory constructed by Gurtin and Murdoch, taking into account the properties of symmetry and material indifference, is far from complete. The work gives a fairly broad generalization of the surface-related theory of elastic bodies. The statements of the problems of propagation of surface waves on the adhesion-active surface of the classical elastic half-space are considered. We considered five types of surface waves that are attractive from the point of view of experimental determination of the characteristics of adhesive interactions and found that these types of surface waves could not be existed for the classical theory of elasticity with adhesion-passive surfaces, where moduli of the adhesion interactions are equal zero. The first three of these types of waves are associated separately with each of the three components of the surface displacement vector. The fourth and fifth types of surface waves are associated, respectively, with the field of local changes in the surface area and with the field of its local rotations with a vector that coincides with the normal to the surface.

Keywords Generalized adhesion model · Classical elasticity · Symmetry conditions · Frame-indifference conditions · Surface waves

S. Lurie (✉) · P. Belov · E. Lykosova
Institute of Applied Mechanics of Russian Academy of Science, Leningradskii pr.7 build.1,
Moscow 125040, Russian Federation
e-mail: salurie@mail.ru

P. Belov
e-mail: belovpa@yandex.ru

E. Lykosova
e-mail: elykosova@mail.ru

13.1 Introduction

The special properties of the surface of bodies have been studied for a long time, starting with the works of Young, Laplace, and Poisson [1–3], which introduced the concept of surface tension. Undoubtedly, the fundamental contribution to the development of continuous adhesion interactions was made by the fundamental works [4, 5] and then in the works [6, 7]. In works [4, 5], the governing relations of the surface properties of elastic bodies and a modern understanding of superficial interactions were proposed. Further generalizations of this model were considered in [6–9]. Classification of the surface-related models was proposed in [10, 11] which may be useful to describe effects associated with special intrinsic surface properties of bodies in various problems (wettability, capillarity, surface tension, etc.), contact problems and in modeling of the materials properties of a micro- and nanostructures with a high density of phase-contact zones. Variants of variational models of adhesion interactions for the gradient elasticity and the model of media with defect fields were considered in [12–14]. The works [15–21] made a significant impact on the development of continuum adhesion models, the understanding of physical processes in surface-related mechanics, and in the interpretation of physical modules of surface elasticity and their role in applied problems. In the works [20–26], the applied variants of the adhesion interactions were proposed based on the variants of classical and gradient theories of elasticity.

The history of the development of mathematical models of surface phenomena was briefly but sufficiently fully discussed in [27, 28]. In these interesting works, it was indicated the importance of attracting models of surface interactions in the problems of the propagation of surface waves. This remark is very important and fully corresponds to the Gurtin–Murdoch model, since the adhesion model gives additional terms in the boundary conditions with greater variability on the coordinates compared to the classical terms.

In the work [20], it was defined the difference between perfect and non-perfect surfaces. It was defined that if the boundaries of solids can be modeled as mathematical smooth enough surfaces with additional physical surface-related properties then such surfaces are adhesion-active surfaces. Correspondingly, the boundaries of elastic bodies for which the boundary conditions have a classical form without additional physical properties will be called as adhesion passive.

In the present work, we do not take into account the phenomena associated with the formation of the boundary of an elastic body and restrict ourselves considering elastic bodies in the framework of the linear theory of elasticity, assuming that the boundaries of elastic bodies have their own spectrum of mechanical properties. We consider classical theory of elasticity and show that the continuum theory of the surface elasticity constructed in [4, 5], which can be considered as classical, is not absolutely complete. A generalized model of surface interactions with an extended spectrum of properties is presented. It is shown that for the case of classical linear elasticity with a symmetric stress tensor, the tensor properties of the generalized

elastic moduli of the surface properties (and, therefore, adhesive interactions) are determined by three independent modules.

13.2 Formulation of Boundary Value Problems for Elastic Bodies with Adhesion-Active Surfaces

We consider the classical theory of elasticity for elastic bodies with additional properties of an adhesion-active surface. We formulate the variational model and believe that the properties of an elastic body and the properties of the body surface are formally completely determined by the accepted kinematics and the existence of elastic potentials of the body and its surface.

For the general case under consideration, we should write the following equations for the potentials energy in the volume V and on the surface F of the elastic body:

$$2U_V = C_{ijmn} R_{i,j} R_{m,n}, \quad 2U_F = A_{ijmn} R_{i,j} R_{m,n} \quad (13.1)$$

In this case, the Lagrange functional is written as

$$\begin{aligned} L &= A - \iiint U_V dV - \oint U_F dF \\ &= A - \frac{1}{2} \iiint C_{ijmn} R_{i,j} R_{m,n} dV - \frac{1}{2} \oint A_{ijmn} R_{i,j} R_{m,n} dF \end{aligned} \quad (13.2)$$

where $A = \iiint P_i^V R_i dV + \oint P_i^F R_i dF$ is the work of predetermined forces distributed in the volume and on the surface of the body, R_i are displacement vector components, $R_{i,j}$ are distortion tensor components, C_{ijmn} , A_{ijmn} are tensors of elastic moduli in volume and on the surface of the body.

The physical relationships for the stresses defined in the body volume σ_{ij} and on the body surface a_{ij} are obviously determined by the extended Green formulas. Given (13.1) and (13.2), we get

$$\sigma_{ij} = \frac{\partial U_V}{\partial R_{i,j}} = C_{ijmn} R_{m,n}, \quad a_{ij} = \frac{\partial U_F}{\partial R_{i,j}} = A_{ijmn} R_{m,n} \quad (13.3)$$

Obviously, for elastic tensors C_{ijmn} , A_{ijmn} in (13.3), it is imperative that the symmetry conditions are satisfied

$$C_{ijmn} = C_{mnij}, \quad A_{ijmn} = A_{mnij} \quad (13.4)$$

In the volume of an elastic isotropic body, the elastic modulus tensor C_{ijmn} satisfying the symmetry conditions (13.4) is determined by two modules and has a classical form, $C_{ijmn} = \lambda \delta_{ij} \delta_{mn} + \mu (\delta_{im} \delta_{jn} + \delta_{in} \delta_{jm})$, where λ , μ are Lamé coefficients. The

tensor of the elastic moduli of a body surface A_{ijmn} is defined on the surface and has a more general form, since the surface properties should obviously be considered different in the normal direction n_i and in the direction tangent to the body surface. Therefore, the surface of the body cannot be considered isotropic, and the structure of the tensor of elasticity moduli of surface interactions A_{ijmn} should be studied additionally.

Indeed, we select the normal to the surface n_i and the “flat” delta Kronecker tensor δ_{mn}^* , which is an isotropic tensor of the second rank, in a tangent plane at every point on the surface, $\delta_{mn}^* = \delta_{mn} - n_m n_n$, $\delta_{mn}^* n_m \equiv 0$. It is easy to see that the transversely isotropic tensor of the elastic moduli of the body surface A_{ijmn} , satisfying the fundamental conditions of symmetry (13.4), can be represented as an expansion in the following basic tensors of the fourth rank. Moreover, in the general case, there are only eight basic tensors of the fourth rank composed of tensors of the second rank of the form δ_{mn}^* and $(n_i n_j)$, ensuring the fulfillment of symmetry conditions (13.4):

$$\begin{aligned} & \delta_{ij}^* \delta_{mn}^*, \delta_{im}^* \delta_{jn}^*, \delta_{ij}^* \delta_{mn}^*, (n_i n_j \delta_{mn}^* + n_m n_n \delta_{ij}^*), (n_i n_n \delta_{jm}^* + n_m n_j \delta_{in}^*), \\ & n_i n_m \delta_{jn}^*, \delta_{im}^* n_j n_n, n_i n_j n_m n_n \end{aligned}$$

As a result, in the general case, the tensor A_{ijmn} is determined with an accuracy of eight constants

$$\begin{aligned} A_{ijmn} = & \lambda^F \delta_{ij}^* \delta_{mn}^* + (\mu^F + \chi^F) \delta_{im}^* \delta_{jn}^* + (\mu^F - \chi^F) \delta_{in}^* \delta_{jm}^* \\ & + \alpha^F (n_i n_j \delta_{mn}^* + n_m n_n \delta_{ij}^*) + \beta^F (n_i n_n \delta_{jm}^* + n_m n_j \delta_{in}^*) \\ & + \delta^F n_i n_m \delta_{jn}^* + B^F \delta_{im}^* n_j n_n + A^F n_i n_j n_m n_n \end{aligned} \quad (13.5)$$

Note that the structure and general form of the tensor of adhesion interaction moduli in the gradient theory of elasticity for bodies with a smooth surface A_{ijmn} is completely determined by the structure of the basic tensors of the fourth rank composed of tensors of the second rank of the form δ_{mn}^* and $(n_i n_j)$. Therefore, the problem of constructing a complete sequence of such basic tensors is important. In the fundamental work [8], a system of basic tensors is constructed for the general case of higher-gradient surface elasticity theory for bodies with a non-smooth surface.

Suppose, for simplicity, that a body with a smooth surface is considered, and no restrictions are imposed on adhesion stresses and adhesion elastic moduli. Then, in accordance with the Lagrange principle, a mathematical model of the theory of elasticity with an adhesion-active surface (boundary value problem) in the general case is completely determined by the following variational equality obtained based on the relations (13.1)–(13.4):

$$\delta L = \delta A - \iiint \sigma_{ij} \delta R_{i,j} dV - \oint a_{ij} \delta R_{i,j} dF$$

$$\begin{aligned}
&= \iiint (\sigma_{ij,j} + P_i^V) \delta R_i dV \\
&+ \oint [(P_i^F - \sigma_{ij} n_j + a_{ij,p} \delta_{pj}^*) \delta R_i + (-a_{ij} n_j) \delta (R_{i,p} n_p)] dF = 0 \quad (13.6)
\end{aligned}$$

An analysis of variational Eq. (13.6) shows that the boundary value problem contains six boundary conditions at each non-singular point on the surface, three of which are associated only with adhesion stresses a_{ij} that perform work on normal derivatives of displacements. At the same time, in the classical theory of elasticity, boundary conditions are determined only by the work of stresses and only at possible displacements R_i .

Therefore, the boundary value problem for the classical theory of elasticity is redefined, since for it a correctly formulated system of boundary conditions contains only three boundary conditions at each non-singular point on the surface.

In addition, we note that even if, for some reason, the last term in (13.5) is excluded, the boundary value problem resulting from the variational Eq. (13.5) and the governing relations (13.3) lead to an incorrect boundary value problem from the point of view of the classical solution [15, 29]. Indeed, following (13.6) and (13.3), we obtain that the boundary condition contains the second derivatives of the displacements, while the Lamé operator (the resolving equation) is also a second-order operator.

There are two ways to remove this contradiction. First, in order to remove this contradiction, one can require that on the surface of classical elastic bodies force factors with variations $\delta \dot{R}_i$, ($\dot{R}_i = R_{i,p} n_p$) always be zero. This requirement is equivalent to the following conditions on the tensor of adhesion modules (13.5):

$$A_{ijmn} n_j = \alpha^F n_m \delta_{in}^* + \beta^F n_i \delta_{mn}^* + B^F \delta_{im}^* n_n + A^F n_i n_m n_n \equiv 0 \quad (13.7)$$

Then, the adhesion module tensor (13.5) has the following most general structure for the surface bounding the classical medium:

$$\begin{aligned}
A_{ijmn} &= \lambda^F \delta_{ij}^* \delta_{mn}^* + \mu^F (\delta_{im}^* \delta_{jn}^* + \delta_{in}^* \delta_{jm}^*) \\
&+ \chi^F (\delta_{im}^* \delta_{jn}^* - \delta_{in}^* \delta_{jm}^*) + \delta^F n_i n_m \delta_{jn}^* \quad (13.8)
\end{aligned}$$

Based on (13.5)–(13.8), we can say that the “classical surface” of a body generally has four adhesion moduli λ^F , μ^F , χ^F , δ^F .

The second way is connected with the introduction of the gradient theory of elasticity in the body volume with potential energy of the form

$$2U_V = C_{ijmn} R_{i,j} R_{m,n} + C_{ijkml} R_{i,jk} R_{m,nl}$$

where C_{ijkml} is the tensor of the elastic moduli.

In the gradient theory of elasticity, the force model is determined by Cauchy stresses σ_{ij} and moment stresses μ_{ijk} —double stresses. For gradient elasticity, the constitutive equations have the form

$$\sigma_{ij} = \frac{\partial U_V}{\partial R_{i,j}} = C_{ijmn} R_{m,n}, \mu_{ijk} = \frac{\partial U_V}{\partial R_{i,jk}} = C_{ijkmnl} R_{m,nl} \quad (13.9)$$

For gradient elasticity, the correct variational formulation for bodies with an adhesion-active surface is written based on the Lagrange principle taking into account relations (13.9) and has the form:

$$\begin{aligned} \delta L &= \delta A - \iiint (\sigma_{ij} \delta R_{i,j} + \mu_{ijk} \delta R_{i,jk}) dV - \oint a_{ij} \delta R_{i,j} dF \\ &= \iiint [(\sigma_{ij} - \mu_{ijk,k})_{,j} + P_i^V] \delta R_i dV \\ &\quad + \oint \{ [P_i^F - (\sigma_{ij} - \mu_{ijk,k}) n_j + (\mu_{ijk} n_k + a_{ij})_{,p} \delta_{pj}^*] \delta R_i \\ &\quad - (\mu_{ijk} n_k + a_{ij}) n_j \delta (R_{i,p} n_p) \} dF = 0 \end{aligned} \quad (13.10)$$

Obviously, the variational model of the gradient theory of elasticity for bodies with an adhesion-active surface (13.10) and the boundary value problem as a whole is consistent and mathematically correct for gradient elasticity in the body volume.

Note that the formulated theory is not completely gradient, because the density of potential energy of the surface (1) is a quadratic form only of distortions, defined on the surface, and does not contain the quadratic form of the second derivatives (curvatures). A surface which properties are determined by the conventionally classical density of potential energy, which depends only on distortions with a tensor of adhesion elastic moduli of the fourth rank, will be called ideal. On the other hand, the surface determined by the density of the gradient potential energy, which is the quadratic form of the terms of distortions and derivatives of distortions with the tensor of adhesion modules of the fourth and sixth ranks, will be called the gradient surface. An example of a gradient model of adhesion is the Steinberg–Ogden model [6, 7].

13.3 Qualitative Analysis of the Elastic Moduli of Surface Interactions

An analysis of variational Eq. (13.6) shows that the boundary value problem for gradient elasticity is correct, since the formulated system of boundary conditions contains six pairs of alternative boundary conditions at each non-singular point on the surface. We note that constants in condition (13.7), which determine the structure of adhesion tensors moduli for surfaces, distinguish a group of adhesion modules that can appear only on surfaces of gradient media in Mindlin–Toupin models. Therefore, the following lemma is proved: “Adhesion modules α^F , β^F , B^F , A^F are adhesion modules specific only to gradient theories of elasticity”.

Let us consider in more detail the structure of the potential energy of adhesion on the surface in gradient elasticity. We represent the vector of displacements R_i on the surface of the body in the form of decomposition into the tangent $r_i = R_j \delta_{ij}^*$ and normal components $R = R_j n_j$:

$$R_i = r_i + R n_i \quad (13.11)$$

Then, the potential energy of adhesion can be represented as:

$$\begin{aligned} & \frac{1}{2} \oint\!\!\!\oint A_{ijmn} R_{i,j} R_{m,n} dF \\ &= \frac{1}{2} \oint\!\!\!\oint [\lambda^F r_{i,i} r_{j,j} + 2\alpha^F \dot{R} r_{m,m} + A^F \dot{R} \dot{R} \\ & \quad + 2\mu^F (r_{i,j} + r_{j,i})(r_{i,j} + r_{j,i}) + 2\chi^F (r_{i,j} - r_{j,i})(r_{i,j} - r_{j,i}) \\ & \quad + \delta^F R_{,i} R_{,i} + 2\beta^F R_{,i} \dot{r}_i + B^F \dot{r}_i \dot{r}_i] dF \end{aligned} \quad (13.12)$$

It follows from (13.12) that the potential adhesion energy determined by the normal derivatives \dot{R} , ($\dot{R} = R_{,p} n_p$), and \dot{r}_i in (13.12) depends on the adhesion modules A^F and B^F . Adhesion modules α^F and β^F in bilinear terms in the potential adhesion energy determine the couple interaction energy.

Let us conditionally define “the surface of a gradient body” as the surface on which the quadratic form of the normal derivatives of the surface of the displacement vector determines its gradient adhesion properties. Then, the surface on which the considered potential adhesion energy is determined can be represented as two surfaces immersed one in another. The first surface is the “surface of the classical body.” Its adhesion properties are generally determined through four adhesion moduli λ^F , μ^F , χ^F , δ^F . The second surface is the “surface of the gradient body.” Its adhesion properties are determined in the general case through two adhesion moduli A^F , B^F . In addition, these two surfaces interact with each other. This interaction is determined by the adhesion modules α^F and β^F , as well as the corresponding interaction energy.

Indeed, we bring the potential adhesion energy to the canonical form:

$$\begin{aligned} & \frac{1}{2} \oint\!\!\!\oint A_{ijmn} R_{i,j} R_{m,n} dF \\ &= \frac{1}{2} \oint\!\!\!\oint \left\{ \left(\lambda^F - \frac{\alpha^F \alpha^F}{A^F} \right) r_{i,i} r_{j,j} + A^F \left(\dot{R} + \frac{\alpha^F}{A^F} r_{i,i} \right) \left(\dot{R} + \frac{\alpha^F}{A^F} r_{j,j} \right) \right. \\ & \quad + 2\mu^F (r_{i,j} + r_{j,i})(r_{i,j} + r_{j,i}) + 2\chi^F (r_{i,j} - r_{j,i})(r_{i,j} - r_{j,i}) \\ & \quad \left. + \left(\delta^F - \frac{\beta^F \beta^F}{B^F} \right) R_{,i} R_{,i} + B^F \left(\dot{r}_i + \frac{\beta^F}{B^F} R_{,i} \right) \left(\dot{r}_i + \frac{\beta^F}{B^F} R_{,i} \right) \right\} dF \end{aligned} \quad (13.13)$$

From (13.13), it follows that if there is no interaction energy between the surfaces of a classical and gradient body, the potential adhesion energy can be represented as

a direct sum of the potential energies of each surface:

$$\begin{aligned}
 & \frac{1}{2} \iint A_{ijmn} R_{i,j} R_{m,n} dF \\
 &= \frac{1}{2} \iint \{ \lambda^F r_{i,i} r_{j,j} + 2\mu^F (r_{i,j} + r_{j,i})(r_{i,j} + r_{j,i}) \\
 & \quad + 2\chi^F (r_{i,j} - r_{j,i})(r_{i,j} - r_{j,i}) + \delta^F R_{,i} R_{,i} \\
 & \quad + A^F \dot{R}\dot{R} + B^F \dot{r}_i \dot{r}_i \} dF \tag{13.14}
 \end{aligned}$$

The right part of (13.14) contains the sum of the four terms of the potential adhesion energy of the classical surface and the sum of two terms of the potential adhesion energy of the surface of the gradient body. Comparing (13.13) and (13.14), it can be noted that in the presence of adhesion interaction between the surfaces of a classical and gradient body, the potential energy of the surface of a classical body is always less than the same potential energy in the presence of interaction. At the same time, the potential adhesion energy of the gradient body can be either greater or less than the corresponding energy in the absence of adhesion interaction between the surfaces. With positive α^F and β^F , potential energy of the surface of the gradient body is greater, and with negative α^F and β^F , it is less than in the case adhesion-passive surfaces.

We give a physical interpretation of all adhesion elasticity moduli. The physical meaning of each term in the expression of the potential adhesion energy (13.12) is obvious. The term $\lambda^F r_{i,i} r_{j,j}$ determines the energy of the surface tension of the surface of a classical body, since deformations $r_{i,i}$ determine a local change in the surface area, and the corresponding force factor in the presence of interaction with the surface of the gradient body $\lambda^F r_{i,i} + \alpha^F \dot{R}$ determines the generalized surface tension. The term $A^F \dot{R}\dot{R}$ determines the strain energy of the normal to the surface of the gradient body, and the corresponding force factor $\alpha^F r_{i,i} + A^F \dot{R}$ determines the generalized adhesion pressure.

The bilinear term $2\alpha^F \dot{R} r_{m,m}$ determines the adhesion interaction energy of the surfaces of the classical and gradient medium through normal force factors, the kinematic variables of which are the local change in area $r_{i,i}$ and the deformation \dot{R} of the tensile/compression normal to the surface. The term $2\mu^F (r_{i,j} + r_{j,i})(r_{i,j} + r_{j,i})$ determines the shear strain energy in the tangent plane to the surface of a classical body. The term $2\chi^F (r_{i,j} - r_{j,i})(r_{i,j} - r_{j,i})$ determines the energy of local rotations in a tangent plane to the surface of a classical body. The term $\delta^F R_{,i} R_{,i}$ determines the energy of local surface bends (rotation of a linear surface element from a tangent plane to the surface). In [10, 20], the adhesion module δ^F for liquids was treated as the Laplace constant for capillary pressure. The corresponding force factor determines the generalized adhesion shear stress $\delta^F R_i + \beta^F \dot{r}_i$. The term $B^F \dot{r}_i \dot{r}_i$ determines the energy of rotation of the normal to the surface (the elementary shift of the normal relative to the linear surface element of the classical body). The corresponding force factor $\delta^F \dot{r}_i + B^F R_i$ determines the generalized adhesion shear stress in the presence of adhesion interaction between the surfaces of a classical and gradient body. The

bilinear term $2\beta^F R_i \dot{r}_i$ determines the adhesion interaction energy of the surfaces of the classical and gradient medium through tangential force factors whose kinematic variables are elementary rotations of the normal \dot{r}_i and the linear surface element R_i .

Further, in this paper, we consider an elastic body with a smooth surface and restrict ourselves to a consideration of the “ideal” theory of surface elasticity for the classical (first-order) continuum theory of elasticity in the bulk.

13.4 Extended Continual Adhesion Models of Classical Body

Properties of symmetry and material indifference are important when we discuss the governing equations for the model of surface elasticity [5]. Indeed, the requirements for satisfying the conditions of symmetry and material-indifference conditions can lead to significant restrictions for the physical model of surface elasticity. The properties of a classical linearly elastic body with a symmetric stress tensor in the volume are completely determined by the potential energy density $2U_V = C_{ijmn} R_{i,j} R_{m,n}$, $C_{ijmn} = \lambda \delta_{ij} \delta_{mn} + \mu (\delta_{im} \delta_{jn} + \delta_{in} \delta_{jm})$. It is obvious that in classical elastic bodies, where the surface of the body does not have any additional properties, the symmetry conditions and material-indifference conditions are satisfied. We consider a model of adhesive interactions of classical elastic bodies with a symmetric stress tensor, for which the general form of the elastic modulus tensor has the form (13.8) and in the general case is determined through four physical parameters λ^F , μ^F , χ^F , δ^F . For linear elastic bodies with an adhesive-active surface, the problem of symmetry and material indifference should be considered taking into account the fact that the surface of the body has its own properties different from the properties of an elastic body in the bulk. In the following sections of the paper, we will consider the question of whether the symmetry conditions of the stress tensor of an elastic body and the material indifference of an elastic body with an adhesion-active surface lead to additional restrictions for the tensor of adhesion interaction moduli (13.8).

We consider classical bodies, which are described by the classical theory of elasticity and propose that their additional surface adhesion properties are defined by the common model (13.8). The model (13.8) follows directly from tensor properties of transversely isotropic tensor of adhesion interactions A_{ijmn} and gives the classical Gurtin–Murdoch theory of adhesion interaction if $\chi^F \neq 0$, $\delta^F \neq 0$. Let us discuss possibility and conditions of existence of such generalization. In the fundamental work, it was noted that the symmetry conditions frame-indifference symmetry must be considered when formulate the theory of adhesion. We will consider both of these problems, symmetry and material objectivity, in connection with the discussion of the generalized adhesion model.

13.4.1 Symmetry Conditions

Let us consider the tensor A_{ijmn} (13.8). It is easy to see that this tensor becomes fully symmetric tensor if the following conditions are satisfied

$$\begin{aligned} (A_{ijmn} + A_{jimn} - A_{ijnm} - A_{jinm})/4 &= 0 \\ (A_{ijmn} - A_{jimn} + A_{ijnm} - A_{jinm})/4 &= 0 \\ (A_{ijmn} - A_{jimn} - A_{ijnm} + A_{jinm})/4 &= 0 \end{aligned} \quad (13.15)$$

Using the definition of the tensor A_{ijmn} for the classical media (13.8), it can be checked that conditions (13.15) are satisfied only when

$$\chi^F = 0, \delta^F = 0 \quad (13.16)$$

In other words for Gurtin–Murdoch adhesion theory, the tensor A_{ijmn} is fully symmetric. First, it seems that in symmetric theory of elasticity, all tensors in constitutive equations must be also symmetric. But for adhesion model, the full symmetry conditions (13.15) are redundant conditions. Indeed if we introduce weak symmetry conditions

$$a_{ij} \partial_{ijk} n_k = 0 \quad (13.17)$$

then we will require stress symmetry only in the tangent plane in the elastic body, which is sufficient for the model of adhesion from a physical point of view.

The symmetry of the stress tensor in the volume is determined by the tensor of elastic moduli $C_{ijmn} = \lambda \delta_{ij} \delta_{mn} + \mu (\delta_{im} \delta_{jn} + \delta_{in} \delta_{jm})$. Condition (13.17) written using equality (13.8) obviously leads only to the following condition

$$\chi^F = 0$$

and does not give any restriction on the physical constant δ^F [see Eq. (13.16)].

13.4.2 Frame-Indifference Condition

Let us consider the frame-indifference condition. The following theorem holds.

Theorem Necessary and sufficient conditions for physical objectivity are

– the condition of global equilibrium:

$$\begin{aligned}
 P_i &= \int_V P_i^V dV + \int_F P_i^F dF = 0 \\
 M_m &= \int_V P_i^V (x_n - x_n^0) \partial_{mni} dV + \int_F P_i^F (x_n - x_n^0) \partial_{mni} dF = 0
 \end{aligned} \tag{13.18}$$

– equality to zero of the global torsional stiffness tensor:

$$E_{pq} = \int_V (C_{ijmn} \partial_{pji} \partial_{qnm}) dV + \int_F (A_{ijmn} \partial_{pji} \partial_{qnm}) dF = 0 \tag{13.19}$$

– and isoperimetric conditions:

$$\begin{aligned}
 &\int_V C_{ijmn} (r_{m,n} \partial_{pji} + r_{i,j} \partial_{pnm}) dV \\
 &+ \int_F A_{ijmn} (r_{m,n} \partial_{pji} + r_{i,j} \partial_{pnm}) dF
 \end{aligned} \tag{13.20}$$

Proof Let us write the generalized Cesaro's formulas as the following:

$$R_i = R_i^0 + \omega_m^0 (x_n - x_n^0) \partial_{mni} + r_i \tag{13.21}$$

Substituting displacements R_i into Lagrangian (13.2) with the aid of (13.21) we receive after some transformation:

$$\begin{aligned}
 L &= \tilde{L} + P_i R_i^0 + M_m \omega_m^0 \\
 &- \frac{1}{2} \left[\int_V (C_{ijmn} \partial_{pji} \partial_{qnm}) dV + \int_F (A_{ijmn} \partial_{pji} \partial_{qnm}) dF \right] \omega_p^0 \omega_q^0 \\
 &+ \left[\int_V C_{ijmn} (r_{m,n} \partial_{pji} + r_{i,j} \partial_{pnm}) dV + \int_F A_{ijmn} (r_{m,n} \partial_{pji} + r_{i,j} \partial_{pnm}) dF \right] \omega_q^0
 \end{aligned} \tag{13.22}$$

Thus, we can see from (13.22) that the sufficient conditions for the invariance of the Lagrangian with respect to translations R_i^0 and rotations ω_m^0 of rigid body lead to the conditions:

$$P_i = 0, M_m = 0 \tag{13.23}$$

$$E_{pq} = \int_V (C_{ijmn} \partial_{pji} \partial_{qnm}) + \int_F (A_{ijmn} \partial_{pji} \partial_{qnm}) dF = 0 \quad (13.24)$$

$$\int_V C_{ijmn} (r_{m,n} \partial_{pji} + r_{i,j} \partial_{pnm}) dV = + \int_F (A_{ijmn} (r_{m,n} \partial_{pji} + r_{i,j} \partial_{pnm})) dF = 0 \quad (13.25)$$

The necessary conditions for the invariance of the Lagrangian are defined by the following variational equation:

$$P_i \delta R_i^0 + [M_q - E_{pq} \omega_p^0 + \int_V C_{ijmn} (r_{m,n} \partial_{pji} + r_{i,j} \partial_{pnm}) dV + \int_F A_{ijmn} (r_{m,n} \partial_{pji} + r_{i,j} \partial_{pnm}) dF] \delta \omega_q^0 = 0$$

The last equations show that the necessary conditions coincide with Eqs. (13.23)–(13.25). The theorem is proved.

Let us consider (13.24). For the symmetric classical theory of elasticity, this equation can be written in the form

$$\int_F (A_{ijmn} \partial_{mnq}) dF = 0 \quad (13.26)$$

Taking into account the definition of adhesion moduli (13.8), we can write

$$\begin{aligned} & \int_F A_{ijmn} \partial_{qnm} \partial_{pji} dF \\ &= \int_F [\chi^F (\delta_{im}^* \delta_{jn}^* - \delta_{in}^* \delta_{jm}^*) + \delta^F n_i n_m \delta_{jn}^*] \partial_{qnm} \partial_{pji} dF \\ &= -4 \int_F \chi^F n_p n_q dF + \int_F \delta^F \delta_{pq}^* dF \end{aligned} \quad (13.27)$$

Similarly, we consider Eq. (13.25) for the symmetric classical theory of elasticity. Assuming $M_i = 0$, we can transform one to the following view

$$\begin{aligned} & \int_V C_{ijmn} (r_{m,n} \partial_{pji} + r_{i,j} \partial_{pnm}) dV + \int_F A_{ijmn} (r_{m,n} \partial_{pji} + r_{i,j} \partial_{pnm}) dF \\ &= 8 \int_F \chi^F (-r_{i,j} \partial_{ija} n_a / 2) n_p dF + 2 \int_F \delta^F (n_m r_{m,n} \partial_{pni} n_i) dF \end{aligned} \quad (13.28)$$

Thus, we can conclude that following Eqs. (13.23)–(13.25) and (13.27)–(13.28), the necessary and sufficient conditions for the invariance of the Lagrangian are:

$$P_i = 0, M_i = 0, \chi^F = 0, \delta^F = 0$$

It seems now that symmetry conditions (13.17) and frame-indifference conditions lead to the only Gurtin–Murdoch continuum model [see Eq. (13.16)].

13.4.3 Weak Frame-Indifference Condition

The dependence of stresses on translations R_i^0 and rotations ω_k^0 of the coordinate system follows from the existence of a bilinear term containing local $\omega_k = -r_{i,j} \partial_{ijk}/2$ and global rotations ω_k^0 in the potential energy (13.22):

$$\begin{aligned} & -\frac{1}{2} \left[\int_V C_{ijmn} (r_{m,n} \partial_{pji} + r_{i,j} \partial_{pnm}) dV + \int_F A_{ijmn} (r_{m,n} \partial_{pji} + r_{i,j} \partial_{pnm}) dF \right] \omega_p^0 \\ & = - \left[4 \int_F \chi^F (-r_{i,j} \partial_{ija} n_a / 2) n_p dF + \int_F \delta^F (n_m r_{m,n} \partial_{pni} n_i) dF \right] \omega_p^0 \end{aligned} \quad (13.29)$$

Note that the term $-\frac{1}{2} E_{pq} \omega_p^0 \omega_q^0$ in (13.22) does not change the constitutive equations for the stresses (Green's relations) and can be omitted.

Let us consider separately the bilinear term from local and global rotations (see (13.22) and (13.29) $[L_{ijp} r_{i,j}] \omega_p^0$ where

$$[L_{ijp} r_{i,j}] = 4 \int_F \chi^F (-r_{i,j} \partial_{ija} n_a / 2) n_p dF + \int_F \delta^F (n_i r_{i,j} \partial_{pjb} n_b) dF \quad (13.30)$$

Then, let us introduce the “weak” criterion of physical objectivity as a condition under which this bilinear term in potential energy is equal to zero.

$$[L_{ijp} r_{i,j}] = 0 \quad (13.31)$$

Note that, on the one hand, equality to zero of a linear combination of surface integrals (13.30) and (13.31) can be represented as a condition on the elastic moduli $\chi^F = 0, \delta^F = 0$. On the other hand, the equality (13.31) can be considered as an integral requirement for the desired field of displacements (isoperimetric conditions). In a linear statement, isoperimetric conditions can always be satisfied both before and after solving the boundary value problem with respect to the desired displacement

field. For this, one should pay attention to the fact that an arbitrary displacement field can always be represented as a direct sum of a displacement field \tilde{r}_i satisfying the condition (13.31) and a displacement field of an absolutely rigid body R_i^0, ω_m^0 :

$$r_i = R_i^0 + \omega_m^0 (x_n - x_n^0) \varepsilon_{mni} + \tilde{r}_i \quad (13.32)$$

Let us act on Eq. (13.32) by the integro-differential operator L_{ijp} and take into account that by definition $L_{ijp}(\tilde{r}_{i,j}) = 0$. Then, we get

$$[L_{ijp}r_{i,j}] = G_{pq}\omega_q^0 \quad (13.33)$$

where $G_{pq} = \delta^F F \delta_{pq} - (4\chi^F + \delta^F) \int_F n_p n_q dF$.

Let us find ω_q^0 from the Eq. (13.33) and substitute them to (13.32). As a the result, we obtain that

$$\tilde{r}_i = (r_i - R_i^0) - G_{mp}^{-1} [L_{abp}r_{a,b}] (x_n - x_n^0) \varepsilon_{mni}, R_i^0 = \text{constant} \quad (13.34)$$

and

$$\tilde{r}_{i,j} = r_{i,j} - G_{kp}^{-1} [L_{ijp}r_{i,j}] \varepsilon_{kji}$$

The last equation shows that we can always separate from any field of deformations the part $\tilde{r}_{i,j}$ that does not depend on the rotation ω_q^0 of the coordinate system.

Note that if $G_{pq} = 0$ (when $\chi^F = 0, \delta^F = 0$), the weak frame-indifference condition satisfies automatically. But on the other side, the weak frame-indifference condition can be satisfied for any values of χ^F, δ^F ($G_{pq} \neq 0$).

In other words, if the conditions of global equilibrium are satisfied $P_i = 0, M_m = 0$ and solution of the boundary value problem of the elasticity is considered in the subspace (13.34), then the weak frame-indifference conditions are satisfied.

As a result, the condition of material objectivity does not introduce any restrictions on the values of adhesion elasticity moduli $\lambda^F, \mu^F, \delta^F$:

$$\begin{aligned} A_{ijmn} &= \lambda^F \delta_{ij}^* \delta_{mn}^* + \mu^F (\delta_{im}^* \delta_{jn}^* + \delta_{in}^* \delta_{jm}^*) + \delta^F n_i n_m \delta_{jn}^*, \\ a_{ij} &= \partial U_F / \partial R_{i,j} = (\lambda^F + \mu^F) \cdot R_{n,m} \delta_{nm}^* \delta_{ij}^* \\ &\quad + 2\mu^F \cdot (R_{n,m} \delta_{in}^* \delta_{jm}^* - (1/2) R_{n,m} \delta_{ij}^* \delta_{nm}^*) + \delta^F \cdot R_{n,m} n_n \delta_{mj}^* n_i \end{aligned}$$

13.5 Surface Waves Related to the Nature of Adhesion

We consider a classical elastic body with an adhesion-active surface characterized by adhesion modules $\lambda^F, \mu^F, \delta^F$ and briefly study the five types of surface waves.

The first three of these types of waves are associated separately with each of the three components of the surface displacement vector. The fourth and fifth types of surface waves are associated, respectively, with the field of local changes in the surface area and with the field of its local rotations with a vector that coincides with the normal to the surface.

Note that this work does not take into account the phenomena associated with the formation of the interface between bodies and the boundary of an elastic body. This non-trivial problem may turn out to be important during the modeling of surface interactions in dynamic and coupled thermodynamic processes. These questions were studied in an interesting paper [9].

13.5.1 Longitudinal Surface U-waves

Let the displacement vector in the equation of motion has only one component directed parallel to the half-space surface in the direction of the unit vector X_i of the OX-axis: $R_i = U(x, z, t)X_i$. Then, the system of motion equations is reduced to a single equation:

$$(2\mu + \lambda)\frac{\partial^2 U}{\partial x^2} + \mu\frac{\partial^2 U}{\partial z^2} - \rho\frac{\partial^2 U}{\partial t^2} = 0 \quad (13.35)$$

For this particular case, we consider a surface wave, setting

$$U = e^{-az+i(kx-\omega t)} \quad (13.36)$$

Here, as accepted, k is the wave number, $k = 1/l$, l is the wave length, ω is the circular frequency, a is the attenuation coefficient along the normal to the surface, t is time, and z is the coordinate counted in the direction of the normal to the half-surface $z \in [0, \infty)$.

The corresponding surface wave (13.35) and (13.36) will be called the surface U-wave. The characteristic equation for this type of wave immediately follows from Eqs. (13.35) and (13.36):

$$-(2\mu + \lambda)k^2 + \mu a^2 + \rho\omega^2 = 0 \quad (13.37)$$

Equality (13.37) gives the definition of the circular frequency ω in terms of the wave number k and attenuation coefficient a :

$$\omega^2 = \frac{(2\mu + \lambda)}{\rho}k^2 - \frac{\mu}{\rho}a^2 \quad (13.38)$$

Consider the boundary condition on the flat surface of a semi-infinite medium. Taking into account (13.6), we have

$$(P_i^F - \sigma_{ij}n_j + a_{ij,j})X_i = -\mu \frac{\partial U}{\partial z} + (2\mu^F + \lambda^F) \frac{\partial^2 U}{\partial x^2} = 0 \quad (13.39)$$

Taking into account (13.36), from the boundary condition (13.39), we obtain the relation for determining the coefficient of wave attenuation in depth:

$$a = \frac{(2\mu^F + \lambda^F)}{\mu} k^2 \quad (13.40)$$

Note that in the absence of adhesion, it immediately follows from (13.40) that $a = 0$, and the dispersion relation (13.37) formally reduces into the dispersion law for longitudinal waves.

Substituting (13.40) into (13.37), we obtain the following expression for the circular frequency ω of the U -wave:

$$\omega = c_L k \sqrt{1 - \frac{(2\mu^F + \lambda^F)^2}{\mu(2\mu + \lambda)} k^2} = c_L k \sqrt{1 - (kl_U)^2} \quad (13.41)$$

Here the following notation is introduced:

$$l_U = \frac{(2\mu^F + \lambda^F)}{\sqrt{\mu(2\mu + \lambda)}} \quad (13.42)$$

The parameter l_U [see (13.42)] depends only on the physical characteristics of the continuum under consideration with an adhesion-active surface, and therefore is a characteristic U -wave length. It is important to note that if $(2\mu^F + \lambda^F) = 0$, then only the trivial solution of Eqs. (13.37) and (13.39) takes place. Therefore, in the absence of adhesion, surface U -waves do not exist. This type of wave is predicted only if there are adhesion properties of the surface such as surface tension, when $(2\mu^F + \lambda^F) \neq 0$.

13.5.2 Transverse Surface V-Waves

Similarly, we consider the case of transverse surface V -waves. Indeed, suppose that in the equations of motion, it is kept only one component of displacements, directed along the unit vector Y_i of the OY -axis: $R_i = V(x, z, t)Y_i$, and the corresponding type of surface waves is considered

$$V = e^{-az+i(kx-\omega t)} \quad (13.43)$$

Then, there remains the only equation of motion that determines the V -wave:

$$\mu(V_{,xx} + V_{,zz}) - \rho \ddot{V} = 0 \quad (13.44)$$

In this case, the boundary condition on the flat surface of a semi-infinite medium is written using (13.6) and has the form

$$(P_i^F - \sigma_{ij}n_j + a_{ij,j})Y_i = -\mu \frac{\partial V}{\partial z} + \mu^F \frac{\partial^2 V}{\partial x^2} = 0 \quad (13.45)$$

Given the Eqs. (13.43)–(13.45), we write the characteristic equation:

$$\mu(-k^2 + a^2) + \rho\omega^2 = 0 \quad (13.46)$$

and the equation relating the wave attenuation parameter from the boundary a and the wave number k

$$\mu a - \mu^F k^2 = 0 \quad (13.47)$$

Excluding the parameter a from (13.46) using (13.47), we get:

$$\omega = k \sqrt{\frac{\mu}{\rho}} \sqrt{1 - k^2 \left(\frac{\mu^F}{\mu}\right)^2} = c_T k \sqrt{1 - (l_V k)^2}, \quad a = k^2 \frac{\mu^F}{\mu} \quad (13.48)$$

In expression (13.48), l_V is the characteristic V -wavelength,

$$l_V = \frac{\mu^F}{\mu} \quad (13.49)$$

13.5.3 Transverse Surface W -Waves

Now let the displacement vector has only one component directed along the unit vector Z_i , parallel to the OZ -axis: $R_i = W(x, z, t)Z_i$. The OZ -axis is parallel to the normal to the half-surface. Assume that

$$W = e^{-az+i(kx-\omega t)} \quad (13.50)$$

This case corresponds to transverse surface W -waves. The motion equation and the boundary condition on the half-space surface for W -waves are written in the form

$$\mu \frac{\partial^2 W}{\partial x^2} + (2\mu + \lambda) \frac{\partial^2 W}{\partial z^2} - \rho \frac{\partial^2 W}{\partial t^2} = 0$$

$$(P_i^F - \sigma_{ij}n_j + a_{ij,j})Z_i = -(2\mu + \lambda)\frac{\partial W}{\partial z} + \delta^F\frac{\partial^2 W}{\partial x^2} = 0$$

It is easy to verify that for the transverse surface W -waves under consideration (13.50), the last equations lead to the dispersion law in the form

$$a = k^2 \frac{\delta^F}{(2\mu + \lambda)}$$

$$\omega = c_T k \sqrt{\left[1 - \frac{(\delta^F)^2}{\mu(2\mu + \lambda)} k^2\right]} = c_T k \sqrt{[1 - (l_W k)^2]}$$

The characteristic length l_W of the adhesion W -wave has following view:

$$l_W = \frac{\delta^F}{\sqrt{\mu(2\mu + \lambda)}}$$

13.5.4 Surface Θ -Waves and Plane Surface Ω -Waves

Finally, we consider two more types of surface waves corresponding to a relative change in volume in the plane parallel to the surface of the half-space and rotation in this plane, i.e., wave with a pseudorotation vector having a projection only on the OZ -axis. We call plane surface waves Θ -waves if they are characterized by two components of displacements lying in a plane parallel to the surface of the half-space:

$$R_i = \varphi_{,j}(\delta_{ij} - Z_i Z_j) \quad (13.51)$$

where φ is scalar potential. In this case, as follows from (13.51), the motion equation can be written only with respect to the change in volume $\Theta(x, z, t) = R_{i,i} = \varphi_{,ij}(\delta_{ij} - Z_i Z_j) = \nabla^2 \varphi$:

$$(2\mu + \lambda)\nabla^2 \Theta - \rho \ddot{\Theta} = 0 \quad (13.52)$$

The boundary condition on the flat surface of a semi-infinite continuum for Θ -wave with kinematics (13.51) has the form:

$$(P_i^F - \sigma_{ij}n_j + a_{ij,j})_k \delta_{ki}^* = -\mu \frac{\partial \Theta}{\partial z} + (2\mu^F + \lambda^F) \frac{\partial^2 \Theta}{\partial x^2} = 0 \quad (13.53)$$

The solution to the problem (13.51)–(13.53) is constructed in the form of a plane wave:

$$\Theta = e^{-az+i(kx-\omega t)}$$

Using the procedure described above, we obtain the following dispersion law for the surface Θ -wave

$$\begin{aligned} a &= \frac{(2\mu^F + \lambda^F)}{\mu} k^2 \\ \omega &= c_L k \sqrt{1 - \frac{(2\mu^F + \lambda^F)^2}{\mu^2} k^2} = c_L k \sqrt{1 - (l_\Theta k)^2} \end{aligned} \quad (13.54)$$

In a dispersion law (13.54), the characteristic length of the adhesion Θ -wave is equal to:

$$l_\Theta = \frac{2\mu^F + \lambda^F}{\mu}$$

We also consider plane surface Ω waves whose kinematics is determined for the projection of the pseudovector of rotations on the OZ-axis

$$\begin{aligned} \Omega(x, z, t) &= -R_{i,j} \vartheta_{ijk} Z_k / 2 = -\psi_{,mj} Z_n \vartheta_{mni} \vartheta_{ijk} Z_k / 2 \\ &= -\psi_{,mj} (\delta_{mj} - Z_m Z_j) / 2 \end{aligned}$$

which are described by the equation

$$\Omega = e^{-az+i(kx-\omega t)} \quad (13.55)$$

In this case, the motion equation and the boundary condition on the surface of the half-space have the form

$$\begin{aligned} \mu \left(\frac{\partial^2 \Omega}{\partial x^2} + \frac{\partial^2 \Omega}{\partial z^2} \right) - \rho \frac{\partial^2 \Omega}{\partial t^2} &= 0 \\ (P_m^F - \sigma_{mj} n_j + a_{mj,j})_{,n} \vartheta_{mnk} n_k &= -\mu \frac{\partial \Omega}{\partial z} + \mu^F \frac{\partial^2 \Omega}{\partial x^2} = 0 \end{aligned}$$

Taking into account (13.55), it easy to find that the last equations gave the dispersion law in the following form:

$$\omega = c_T k \sqrt{1 - (l_\Omega k)^2}, \quad a = \frac{\mu^F}{\mu} k^2, \quad l_\Omega = \frac{\mu^F}{\mu}$$

Note that for all types of considered plane waves for adhesion-active media, the waves exist only in the presence of the corresponding adhesion properties: The presence of surface tension $(2\mu^F + \lambda^F) \neq 0$ determines the existence of U -waves

and Θ -waves, and shear adhesion properties $\mu^F \neq 0$ determine the existence of V -waves and Θ -waves. Finally, transverse surface W -waves exist only if $\delta^F \neq 0$.

13.6 Conclusion

The paper considers media with adhesion-active properties. The structure of adhesion modules that determine the mechanical adhesion properties of surfaces in the framework of continuum adhesion models has been studied. It is shown that classical adhesion media models are modeled using a wider set of physical constants than it is prescribed by the Gurtin–Murdoch model. The surface waves on the adhesion-active surface. There are predicted five types of adhesion waves, which cannot be determined for adhesion-passive surfaces of classical media, and dispersion laws for each type are constructed.

Acknowledgements The authors are deeply grateful to Professor Holm Altenbach and Victor Eremeyev for useful discussions of our research. This work was carried out with the support from the Russian Government Foundation of Institute of Applied Mechanics of RAS, Project-AAAA-A-19-119012290177-0 and particularly supported by the Russian Foundation for Basic Research grant 18-01-00553-A.

References

1. Young, T.: An essay on the cohesion of fluids. *Philos. Trans. R. Soc. Lond.* **95**, 65–87 (1805)
2. Laplace, P.S.: Sur l'action capillaire. supplément à la théorie de l'action capillaire. *Traité de mécanique céleste.* **4**, 771–777 (1805)
3. Poisson, S.D.: Nouvelle théorie de l'action capillaire. Bachelier Père et Fils, Paris (1831)
4. Gurtin, M.E., Murdoch, A.I.: A continuum theory of elastic material surfaces. *Arch. Ration. Mech. An.* **57**, 291–323 (1975)
5. Gurtin, M.E., Murdoch, A.I.: Surface stress in solids. *Int. J. Solids Struct.* **14**, 431–440 (1978)
6. Steigmann, D.J., Ogden, R.W.: Plane deformations of elastic solids with intrinsic boundary elasticity. *Proc. Roy. Soc. A: Math. Phys. Eng. Sci.* **453**, 853–877 (1997)
7. Steigmann, D.J., Ogden, R.W.: Elastic surface-substrate interactions. *Proc. Roy. Soc. A: Math., Phys. Eng. Sci.* **455**, 437–474 (1999)
8. Javili, A., dell'Isola, F., Steinmann, P.: Geometrically nonlinear higher-gradient elasticity with energetic boundaries. *J. Mech. Phys. Solids* **61**(12), 2381–2401 (2013)
9. dell'Isola, F., Romano, A.: On the derivation of thermomechanical balance equations for continuous systems with a nonmaterial interface. *Int. J. Eng. Sci.* **25**(11–12), 1459–1468 (1987)
10. Lurie, S., Belov, P., Altenbach, H.: Classification of gradient adhesion theories across length scale. In: Altenbach, H., Forest, S. (eds.) *Generalized Continua as Models for Classical and Advanced Materials*, *Advanced Structured Materials* 42, pp. 261–277. Springer, New York (2016)
11. Belov, P.A., Lurie, S.A., Golovina, N.Y.: Classifying the existing continuum theories of ideal-surface adhesion. In: *Adhesions and Adhesion Joints in Industry Applications* (2019)
12. Belov, P.A., Lurie, S.A.: Theory of ideal adhesion interactions. *J Compos Mech Des* **14**, 545–561 (2007)

13. Belov, P.A., Lurie, S.A.: Continual theory of adhesion interactions of damaged media. *J Compos Mech Des* **15**(4), 610–629 (2009)
14. Lurie, S.A., Belov, P.A., Rabinskiy, L.N.: Model of media with conserved dislocation. special cases: cosserat model, aero-kuvshinskii media model, porous media model. In: *Advanced Structured Materials*, pp. 215–249. Springer, New York (2017)
15. Altenbach, H., Eremeev, V., Morozov, N.F.: On equations of the linear theory of shells with surface stresses taken into account. *Mech. Solids* **45**, 331–342 (2010)
16. Altenbach, H., Eremeyev, V.A.: On the shell theory on the nanoscale with surface stresses. *Int. J. Eng. Sci.* **49**, 1294–1301 (2011)
17. Altenbach, H., Eremeyev, V.A., Lebedev, L.P.: On the existence of solution in the linear elasticity with surface stresses. *ZAMM* **90**, 231–240 (2010)
18. dell’Isola, F., Madeo, A., Seppecher, P.: Boundary conditions at fluid-permeable interfaces in porous media: a variational approach. *Int. J. Solids Struct.* **46**, 3150–3164 (2009)
19. Wang, J., Huang, Z., Duan, H., Yu, S., Feng, X., Wang, G., Zhang, W., Wang, T.: Surface stress effect in mechanics of nanostructured materials. *Acta Mech. Solida Sin.* **24**(1), 52–82 (2011)
20. Eremeyev, V.A.: On effective properties of materials at the nano- and microscales considering surface effects. *Acta Mech.* **227**, 29–42 (2016)
21. Murdoch, A.I.: Some fundamental aspects of surface modelling. *J. Elast.* **80**, 33–52 (2005)
22. Lurie, S.A., Belov, P.A.: Cohesion field: barenblatt’s hypothesis as formal corollary of theory of continuous media with conserved dislocations. *Int. J. Fract.* **50**(1–2), 181–194 (2008)
23. Lurie, S.A., Volkov-Bogorodsky, D.B., Zubov, V.I., Tuchkova, N.P.: Advanced theoretical and numerical multiscale modeling of cohesion/adhesion interactions in continuum mechanics and its applications for filled nanocomposites. *Int J Compos Mater Sci* **45**(3), 709–741 (2009)
24. Lurie, S., Belov, P.: Gradient effects in fracture mechanics for nano-structured materials. In: *Engineering Fracture Mechanics*, vol. 130, pp. 3–11. Pergamon Press Ltd, Oxford (2014)
25. Lurie, S.A., Belov, P.A., Tuchkova, N.P.: Adhesion model of hyperfine shells (SWNT). In: *Book of Shell Structures: Theory and Applications*, vol. 4, pp. 121–124 (2017)
26. Yerofeyev, V.I., Sheshenina, O.A.: Waves in a gradient-elastic medium with surface energy. *J. Appl. Math. Mech.* **69**(1), 57–69 (2005)
27. Eremeyev, V.A.: Strongly anisotropic surface elasticity and antiplane surface waves. *Philos. Trans. R. Soc. A.* 1–14 (2019)
28. Eremeyev, V.A., Sharma B.L.: Anti-plane surface waves in media with surface structure: Discrete vs. continuum model. *Int. J. Eng. Sci.* **143**, 33–38 (2019)
29. Moiseev, E.I., Lurie, S.A., Korzuk, V.I., Nefedov, P.V.: On solvability and uniqueness of solutions of problems of deformation of homogeneous and heterogeneous structure in response adhesion interaction. *Compos. Nanostructures* **4**, 6–22 (2013)

Chapter 14

Generalized Space–Time Fractional Dynamics in Networks and Lattices



Thomas M. Michelitsch, Alejandro P. Riascos, Bernard A. Collet,
Andrzej F. Nowakowski and Franck C. G. A. Nicolleau

Abstract We analyze generalized space–time fractional motions on undirected networks and lattices. The continuous-time random walk (CTRW) approach of Montroll and Weiss is employed to subordinate a space fractional walk to a generalization of the time fractional Poisson renewal process. This process introduces a non-Markovian walk with long-time memory effects and fat-tailed characteristics in the waiting time density. We analyze ‘generalized space–time fractional diffusion’ in the infinite d -dimensional integer lattice \mathbb{Z}^d . We obtain in the diffusion limit a ‘macroscopic’ space–time fractional diffusion equation. Classical CTRW models such as with Laskin’s fractional Poisson process and standard Poisson process which occur as special cases are also analyzed. The developed generalized space–time fractional CTRW model contains a four-dimensional parameter space and offers therefore a great flexibility to describe real-world situations in complex systems.

T. M. Michelitsch (✉) · B. A. Collet
Institut Jean le Rond d’Alembert, Sorbonne Université,
CNRS UMR 7190, 4 place Jussieu, 75252 Paris cedex 05, France
e-mail: michel@lmm.jussieu.fr

B. A. Collet
e-mail: bernard.collet@upmc.fr

A. P. Riascos
Instituto de Física, Universidad Nacional Autónoma de México,
Apartado Postal 20-364, 01000 Ciudad de México, Mexico
e-mail: aperezr@fisica.unam.mx

A. F. Nowakowski · F. C. G. A. Nicolleau
Department of Mechanical Engineering, University of Sheffield,
Mappin Street, Sheffield S1 3JD, UK
e-mail: a.f.nowakowski@sheffield.ac.uk

F. C. G. A. Nicolleau
e-mail: f.nicolleau@sheffield.ac.uk

Keywords Renewal process · Continuous-time random walk · Fractional Poisson process · Generalized fractional Poisson process · Fractional dynamics · Networks and lattices · Space–time fractional diffusion · Fractional calculus · Fat-tailed waiting time density · Power laws · Diffusion limit

14.1 Introduction

Random walk models are considered to be the most fundamental approaches to describe stochastic processes in nature. Hence, applications of random walks cover a very wide area in fields as various as random search strategies, the proliferation of plant seeds, the spreading phenomena of pandemics or pollution, chemical reactions, finance, population dynamics, properties of public transportation networks, anomalous diffusion and generally such approaches are able to capture empirically observed power law features in ‘complex systems’ [1–7]. On the other hand, the emergence of ‘network science’ and especially the study of random walks on networks have become a major subject for the description of dynamical properties in complex systems [8–10].

In classical random walks in networks, the so-called normal random walks, the walker in one step can reach only connected next neighbor sites [11, 12]. To the class of classical Markovian walks refers continuous-time random walks (CTRWs) where the walker undertakes jumps from one node to another where the waiting time between successive jumps is exponentially distributed leading to Poisson distributed numbers of jumps. The classical CTRW models with Poisson renewal process are able to capture normal diffusive properties such as the linear increase of the variance of a diffusing particle [6]. However, these classical walks are unable to describe power law features exhibited by many complex systems such as the sublinear time characteristics of the mean-square displacement in anomalous diffusion [5]. It has been demonstrated that such anomalous diffusive behavior is well described by a random walk subordinated to the fractional generalization of the Poisson process. This process which was to our knowledge first introduced by Repin and Saichev [13] was developed and analyzed by Laskin who called this process the fractional Poisson process [14, 15]. Laskin’s fractional Poisson process was further generalized in order to obtain greater flexibility to adopt real-world situations [16–18]. We refer this renewal process to as ‘generalized fractional Poisson process’ (GFPP). Recently, we developed a CTRW model of a normal random walk subordinated to a GFPP [17, 18].

The purpose of the present paper is to explore space fractional random walks that are subordinated to a GFPP. We analyze such motions in undirected networks and as a special application in the multidimensional infinite integer lattice \mathbb{Z}^d .

14.2 Renewal Process and Continuous-Time Random Walk

In the present section, our aim is to give a brief outline of renewal processes (or also referred to as ‘compound processes’) and closely related to the ‘continuous-time

random walk (CTRW)’ approach which was introduced by Montroll and Weiss [19]. For further outline of renewal theory and related subjects, we refer to the references [2, 4, 19–22]. It is mention worthy that we deal in this paper with causal generalized functions and distributions in the sense of Gelfand and Shilov [23].

We consider a sequence of randomly occurring ‘events’. Such events can be for instance the jumps of a diffusing particle or failure events in technical systems. We assume that the events occur at nonnegative random times $0 \leq t_1, t_2, \dots, t_n, \dots, \infty$ where $t = 0$ represents the start of the observation. The random times t_k when events occur are called ‘arrival times.’ The time intervals between successive events $\Delta t_k = t_k - t_{k-1} \geq 0$ are called ‘waiting times’ or ‘interarrival times’ [20]. The random event stream is referred to as a *renewal process* if the waiting time Δt between successive events is an ‘independent and identically distributed’ (IID) random variable which may take any nonnegative continuous value. This means in a renewal process the waiting time Δt_k between successive events is drawn $\forall k$ from the same waiting probability density function (PDF) $\chi(t)$. This distribution function is called *waiting time distribution function* (waiting time PDF) or short *waiting time density*.¹ The quantity $\chi(t)dt$ indicates the probability that an event occurs at time t (within $[t, t + dt]$).

We can then write the probability $\Psi(t)$ that the waiting time for the first event is $\Delta t \leq t$ or equivalently that *at least one event occurs* in the time interval $[0, t]$ as

$$\Psi(t) = \int_0^t \chi(\tau)d\tau, \quad t \geq 0, \quad \lim_{t \rightarrow \infty} \Psi(t) = 1 - 0 \tag{14.1}$$

with the obvious initial condition $\Psi(t = 0) = 0$. The distribution (14.1) in the context of lifetime models often is also called ‘failure probability’ [20]. From this relation follows that the waiting time density $\chi(t)$ is a normalized PDF. In classical renewal theory, the waiting time PDF was assumed to be exponential $\chi(t) = \xi e^{-\xi t}$ ($\xi > 0$) which leads as we will see later to Markovian memoryless Poisson-type processes.

The waiting time PDF has physical dimension sec^{-1} , and the cumulative distribution (14.1) indicates a dimensionless probability. Another quantity of interest is the so-called survival probability $\Phi^{(0)}(t)$ defined as

$$\Phi^{(0)}(t) = 1 - \Psi(t) = \int_t^\infty \chi(\tau)d\tau \tag{14.2}$$

which indicates the (dimensionless) probability that no event has occurred within $[0, t]$, i.e., in a random walk the probability that the walker at time t still is waiting on its departure site. Of further interest is the PDF of the arrival of n jump events which we denote by $\chi^{(n)}(t)$ ($\chi^{(n)}(t)dt$ being the probability that the n th jump is performed at time t). Since the events are IID, we can establish the recursion

¹In the context of random walks where the events indicate random jumps, we also utilize the notion ‘jump density’ [17].

$$\chi^{(n)}(t) = \int_0^t \chi^{(n-1)}(\tau)\chi(t - \tau)d\tau, \quad \chi^{(0)}(t) = \delta(t) \tag{14.3}$$

and with $\chi^{(1)}(t) = \chi(t)$. Thus, the PDF for the arrival of the n th event is given by the $n - 1$ -fold convolution of $\chi(t)$ with itself, namely

$$\chi^{(n)}(t) = \int_0^\infty \dots \int_0^\infty \chi(\tau_1) \dots \chi(\tau_n) \delta\left(t - \sum_{j=1}^n \tau_j\right) d\tau_1 \dots d\tau_n, \quad t > 0, \quad n = 1, 2, \dots \tag{14.4}$$

In this relation, we have assumed that the waiting time PDF is *causal*; i.e., $\chi(t)$ is nonzero only for $t \geq 0$. For an outline of causal distributions and some of their properties especially Laplace transforms, see Appendix. The probability that n events happen within time interval $[0, t]$ then can be written as

$$\begin{aligned} \Phi^{(n)}(t) &= \int_0^t (1 - \Psi(t - \tau))\chi^{(n)}(\tau)d\tau = \int_0^t \Phi^{(0)}(t - \tau)\chi^{(n)}(\tau)d\tau, \quad n = 0, 1, 2, \dots \\ &= \int_0^t \Phi^{(n-1)}(t - \tau)\chi(\tau)d\tau. \end{aligned} \tag{14.5}$$

This convolution takes into account that the n th event may happen at a time $\tau < t$ and no further event is taking place during $t - \tau$ with survival probability $\Phi^{(0)}(t)$ where $0 \leq \tau \leq t$. The probabilities $\Phi^{(n)}(t)$ are dimensionless, whereas the PDFs $\chi^{(n)}(t)$ have physical dimension of sec^{-1} . It is especially instructive to consider all these convolution relations in the Laplace domain. We then obtain with (14.4) the convolution relation

$$\begin{aligned} \tilde{\chi}^{(n)}(s) &= \int_0^\infty \dots \int_0^\infty \chi(\tau_1) \dots \chi(\tau_n) e^{-st} \delta\left(t - \sum_{j=1}^n \tau_j\right) d\tau_1 \dots d\tau_n \\ &= \left\{ \int_0^\infty \chi(t) e^{-st} dt \right\}^n = (\tilde{\chi}(s))^n, \quad n = 0, 1, 2, \dots \end{aligned} \tag{14.6}$$

where $\tilde{\chi}^{(0)}(s) = 1$ indeed recovers $\chi^{(0)}(t) = \delta(t)$ for $n = 0$. This relation also shows that the density of n events $\chi^{(n)}(t)$ is normalized, namely

$$\tilde{\chi}^{(n)}(s)|_{s=0} = 1 \tag{14.7}$$

as a consequence of the normalization of the waiting time PDF $\chi(t)$. Now in view of (14.1) and (14.2), it is straightforward to obtain the Laplace transforms

$$\tilde{\psi}(s) = \frac{\tilde{\chi}(s)}{s}, \quad \tilde{\Phi}^{(0)}(s) = \frac{1}{s} - \tilde{\psi}(s) = \frac{1 - \tilde{\chi}(s)}{s} \tag{14.8}$$

thus, the Laplace transform of the probability distribution (14.5) for n events is given by

$$\tilde{\Phi}^{(n)}(s) = \tilde{\Phi}^{(0)}(s)(\tilde{\chi}(s))^n = \frac{1 - \tilde{\chi}(s)}{s} (\tilde{\chi}(s))^n, \quad n = 0, 1, 2, \dots \tag{14.9}$$

For a brief demonstration of further general properties of renewal processes, it is convenient to introduce the following generating function

$$G(t, v) = \sum_{n=0}^{\infty} v^n \Phi^{(n)}(t) \tag{14.10}$$

and its Laplace transform²

$$\tilde{G}(s, v) = \mathcal{L}\{G(t, v)\} = \sum_{n=0}^{\infty} v^n \tilde{\Phi}^{(n)}(s). \tag{14.11}$$

Taking into account (14.9) together with the obvious property $|\tilde{\chi}(s)| \leq |\tilde{\chi}(s = 0)| = 1$ we get for (14.11), a geometric series

$$\tilde{G}(s, v) = \frac{1 - \tilde{\chi}(s)}{s} \sum_{n=0}^{\infty} v^n (\tilde{\chi}(s))^n = \frac{1 - \tilde{\chi}(s)}{s} \frac{1}{1 - v\tilde{\chi}(s)} \tag{14.12}$$

converging for $|v\tilde{\chi}(s)| < 1$, i.e., for $|v| \leq 1$ if $s \neq 0$ and $|v| < 1$ for $s = 0$. We directly observe in this relation the normalization condition

$$\mathcal{L}^{-1}\{\tilde{G}(s, v)|_{v=1}\} = \mathcal{L}^{-1}\left\{\frac{1}{s}\right\} = G(t, 1) = \sum_{n=0}^{\infty} \Phi^{(n)}(t) = 1, \quad t > 0. \tag{14.13}$$

The generating function is often useful for the explicit determination of the $\Phi^{(n)}(t)$, namely

$$\Phi^{(n)}(t) = \frac{1}{n!} \frac{d^n}{dv^n} G(t, v) \Big|_{v=0} = \mathcal{L}^{-1}\left\{\frac{1 - \tilde{\chi}(s)}{s} (\tilde{\chi}(s))^n\right\} \tag{14.14}$$

where the Laplace transform of this relation recovers by accounting for (14.12) again the expression (14.9).

Of further interest is the expected number of events $\bar{n}(t)$ that are taking place within the time interval $[0, t]$. This quantity can be obtained from the relation

$$\begin{aligned} \bar{n}(t) &= \sum_{n=0}^{\infty} n \Phi^{(n)}(t) = \frac{d}{dv} G(t, v) \Big|_{v=1} = \mathcal{L}^{-1}\left\{\frac{d}{dv} \tilde{G}(s, v) \Big|_{v=1}\right\} \\ &= \mathcal{L}^{-1}\left\{\frac{\tilde{\chi}(s)}{s(1 - \tilde{\chi}(s))}\right\}. \end{aligned} \tag{14.15}$$

²We denote $\tilde{f}(s) = \mathcal{L}\{f(t)\}$ the Laplace transform of $f(t)$, and by $\mathcal{L}^{-1}\{...\}$ Laplace inversion, see Appendix for further details.

14.3 Poisson Process

Before we pass on to non-classical generalizations, it appears instructive to recall some properties of the classical variant which is the ‘Poisson renewal process’ (compound Poisson process) [24]. In this process, the waiting time PDF has exponential form

$$\chi_P(t) = \xi e^{-\xi t} \Theta(t), \quad \xi > 0 \tag{14.16}$$

where ξ is a characteristic constant with physical dimension sec^{-1} where ξ^{-1} defines a characteristic timescale in the process. With the Heaviside $\Theta(t)$ -function, we indicate here that (14.16) is a causal distribution.³ We see that (14.16) is a normalized PDF which has the Laplace transform

$$\tilde{\chi}_P(s) = \xi \int_0^\infty e^{-st} e^{-\xi t} dt = \frac{\xi}{\xi + s} \tag{14.17}$$

where $\tilde{\chi}_P(s = 0) = 1$ reflects normalization of waiting time PDF (14.16). Then, we get straightforwardly the failure and survival probabilities, respectively

$$\Psi_P(t) = 1 - e^{-\xi t}, \quad \Phi_P^{(0)}(t) = 1 - \Psi_P(t) = e^{-\xi t}. \tag{14.18}$$

Also, the generating function can be written down directly as

$$\tilde{G}_P(s, v) = \frac{1}{\xi + s} \sum_{n=0}^\infty \frac{(\xi v)^n}{(\xi + s)^n} = \frac{1}{\xi(1 - v) + s} \quad \Re\{s\} > \xi, \tag{14.19}$$

thus

$$G_P(t, v) = e^{-\xi(1-v)t}. \tag{14.20}$$

By using (14.14), we obtain then for the probability of n events

$$\Phi_P^{(n)}(t) = \frac{1}{n!} \frac{d^n}{dv^n} e^{(v-1)\xi t} \Big|_{v=0} = \frac{(\xi t)^n}{n!} e^{-\xi t}, \quad n = 0, 1, 2, \dots, \quad t \geq 0 \tag{14.21}$$

which is the *Poisson distribution*. Therefore, the renewal process generated by an IID exponential waiting time PDF (14.16) is referred to as *Poisson renewal process* or also *compound Poisson process*. This process is the classical proto-example of renewal process [20, 24] (and see the references therein). We further mention in view of Eq. (14.15) that the average number of events $\bar{n}(t)$ taking place within $[0, t]$ is obtained as

$$\bar{n}_P(t) = \frac{d}{dv} G_P(t, v) \Big|_{v=1} = \frac{d}{dv} e^{(v-1)\xi t} \Big|_{v=1} = \xi t, \quad t \geq 0. \tag{14.22}$$

³We often skip $\Theta(t)$ when there is no time derivative involved.

In a Poisson renewal process, the expected number of arrivals increases linearly in time. The exponential decay in the distributions related to the Poisson process makes this process memoryless with the Markovian property [17, 20].

14.4 Fractional Poisson Process

In anomalous diffusion, one has for the average number of arrivals instead of the linear behavior (14.22) a power law $\sim t^\beta$ with $0 < \beta < 1$ [5, 17, 18], among others. To describe such anomalous power law behavior, a ‘fractional generalization’ of the classical Poisson renewal process was introduced and analyzed by Laskin [14, 15] and others [13, 20, 25]. The *fractional Poisson renewal process* can be defined by a waiting time PDF with the Laplace transform

$$\tilde{\chi}_\beta(s) = \frac{\xi}{s^\beta + \xi}, \quad \xi > 0, \quad 0 < \beta \leq 1. \tag{14.23}$$

The fractional Poisson process introduces long-time memory effects with non-Markovian features. We will come back to these issues later. The constant ξ has here physical dimension $\text{sec}^{-\beta}$ defining a characteristic timescale in the fractional Poisson process. For $\beta = 1$, the fractional Poisson process recovers the standard Poisson process outlined in the previous section. The waiting time density of the fractional Poisson process is then defined by

$$\chi_\beta(t) = \mathcal{L}^{-1}\left\{\frac{\xi}{s^\beta + \xi}\right\} = \mathcal{L}^{-1}\left\{\xi s^{-\beta} \frac{1}{1 + \xi s^{-\beta}}\right\}. \tag{14.24}$$

In order to evaluate the inverse Laplace transform, it is useful to expand $(1 + \xi s^{-\beta})^{-1}$ into a geometric series with respect to $\xi s^{-\beta}$ which converges for $s = \sigma + i\omega$ with $\sigma = \Re\{s\} > \xi^{\frac{1}{\beta}}$ for all ω . Doing so, we obtain

$$\chi_\beta(t) = \sum_{m=0}^{\infty} (-1)^m \xi^{m+1} \mathcal{L}^{-1}\{s^{-\beta(m+1)}\}, \quad 0 < \beta \leq 1, \quad \Re\{s\} > \xi^{\frac{1}{\beta}}. \tag{14.25}$$

Taking into account, the inverse Laplace transform⁴ $\mathcal{L}^{-1}\{s^{-\mu}\} = \Theta(t) \frac{t^{\mu-1}}{\Gamma(\mu)}$ where $\mu > 0$ (see also Appendix for the discussion of some properties). We obtain then for (14.25) [14, 17, 20]

⁴In this relation in the sense of generalized functions, we can include the value $\mu = 0$ as the limit $\lim_{\mu \rightarrow 0+} \frac{t^{\mu-1}}{\Gamma(\mu)} = \delta(t)$ [23].

$$\begin{aligned} \chi_\beta(t) &= \xi t^{\beta-1} \sum_{m=0}^{\infty} \frac{(-\xi t^\beta)^m}{\Gamma(\beta m + \beta)}, \quad 0 < \beta \leq 1, \quad t > 0 \\ &= \xi t^{\beta-1} E_{\beta,\beta}(-\xi t^\beta) = \frac{d}{dt}(1 - E_\beta(-\xi t^\beta)) \end{aligned} \tag{14.26}$$

where in this relation we introduced the generalized Mittag-Leffler function $E_{\beta,\gamma}(z)$ and the standard Mittag-Leffler function $E_\beta(z)$ defined in the Appendix by Eqs. (14.99) and (14.100), respectively. The waiting time PDF of the fractional Poisson process also is referred to as Mittag-Leffler density and was introduced first by Hilfer and Anton [26]. It is now straightforward to obtain in the same way the survival probability for the fractional Poisson process, namely [see also Eq. (14.8)]

$$\Phi_\beta^{(0)}(t) = \mathcal{L}^{-1} \left\{ \frac{s^{\beta-1}}{s^\beta + \xi} \right\} = E_\beta(-\xi t^\beta), \quad 0 < \beta \leq 1. \tag{14.27}$$

The generating function (14.10) is then by accounting for (14.27) obtained as

$$G_\beta(t, v) = \mathcal{L}^{-1} \left\{ \frac{s^{\beta-1}}{\xi(1-v) + s^\beta} \right\} = E_\beta(-\xi(1-v)t^\beta), \quad t \geq 0. \tag{14.28}$$

For $v = 1$, this relation takes $G(t, 1) = \Theta(t) = 1$ ($t \geq 0$), and for $\beta = 1$, the Poisson exponential (14.20) is recovered. The probability for n arrivals within $[0, t]$ is then with relation (14.14) obtained as

$$\begin{aligned} \Phi_\beta^{(n)}(t) &= \frac{1}{n!} \frac{d^n}{dv^n} E_\beta((v-1)\xi t^\beta) \Big|_{v=0} \\ &= \frac{(\xi t^\beta)^n}{n!} \sum_{m=0}^{\infty} \frac{(m+n)!}{m!} \frac{(-\xi t^\beta)^m}{\Gamma(\beta(m+n)+1)}, \quad 0 < \beta \leq 1. \end{aligned} \tag{14.29}$$

This distribution is called the *fractional Poisson distribution* and is of utmost importance in fractional dynamics, generalizing the Poisson distribution (14.21) [14, 15]. For $\beta = 1$, the fractional Poisson distribution (14.29) turns into the classical Poisson distribution (14.21). We directly confirm the normalization of the fractional Poisson distribution by the relation

$$\sum_{n=0}^{\infty} \Phi_\beta^{(n)}(t) = \sum_{n=0}^{\infty} \frac{1}{n!} \frac{d^n}{dv^n} E_\beta((v-1)\xi t^\beta) \Big|_{v=0} = E_\beta((-1+1)\xi t^\beta) = E_\beta(0) = 1. \tag{14.30}$$

We notice that for $\beta = 1$, the Mittag-Leffler function becomes the exponential $E_1(-\xi t) = e^{-\xi t}$; thus, the distributions of the standard Poisson process of last section are then reproduced. It is worthy to consider the distinct behavior of the

fractional Poisson process for large observation times. To this end, let us expand Laplace transform (14.23) for $|s|$ small which governs the asymptotic behavior for large times

$$\tilde{\chi}_\beta(s) = \left(1 + \frac{s^\beta}{\xi}\right)^{-1} = \sum_{m=0}^{\infty} (-1)^m \xi^{(-m)} s^{m\beta} = 1 - \frac{1}{\xi} s^\beta + \dots \quad (14.31)$$

which yields as asymptotically for large observation times for $0 < \beta < 1$ fat-tailed behavior⁵

$$\chi_\beta(t) \approx -\frac{1}{\xi \Gamma(-\beta)} t^{-\beta-1}, \quad 0 < \beta < 1, \quad t \rightarrow \infty. \quad (14.32)$$

The fat-tailed behavior $\chi_\beta(t) \sim t^{-\beta-1}$ is a characteristic power law feature of the fractional Poisson renewal process reflecting the non-locality in time that produces Laplace transform (14.31) within the fractional index range $0 < \beta < 1$. As a consequence of the fat-tailed behavior for $0 < \beta < 1$, extremely long waiting times occur; thus, the fractional Poisson process is non-Markovian exhibiting long-time memory effects [17, 20].

Further of interest is the power law tail in the fractional Poisson distribution. We obtain this behavior by considering the lowest power in their Laplace transform, namely

$$\begin{aligned} \Phi_\beta^{(n)}(t) &= \mathcal{L}^{-1} \left\{ \frac{1}{s} \left((1 + \xi^{-1} s^\beta)^{-n} - (1 + \xi^{-1} s^\beta)^{-n-1} \right) \right\} \approx \mathcal{L}^{-1} \left\{ \frac{s^{\beta-1}}{\xi} \right\} \\ &\approx \frac{(t\xi^{\frac{1}{\beta}})^{-\beta}}{\Gamma(1-\beta)} \quad 0 < \beta < 1, \quad n = 0, 1, \dots, \quad t\xi^{\frac{1}{\beta}} \rightarrow \infty. \end{aligned} \quad (14.33)$$

The fractional Poisson distribution exhibits for large (dimensionless) observation times $t\xi^{\frac{1}{\beta}} \rightarrow \infty$ universal $t^{-\beta}$ power law behavior independent of the arrival number n . We will come back subsequently to this important issue.

14.5 Generalization of the Fractional Poisson Process

In this section, our aim is to develop a renewal process which is a generalization of the fractional Poisson process of previous section. The waiting time PDF of this process has the Laplace transform

$$\tilde{\chi}_{\beta,\alpha}(s) = \frac{\xi^\alpha}{(s^\beta + \xi)^\alpha}, \quad 0 < \beta \leq 1, \quad \alpha > 0, \quad \xi > 0. \quad (14.34)$$

⁵Note that $-\Gamma(-\beta) = \beta^{-1} \Gamma(1-\beta) > 0$.

This process was first introduced by Cahoy and Polito [16]. We referred the renewal process defined by (14.34) to as the *generalized fractional Poisson process* (GFPP) [17, 18]. The characteristic dimensional constant ξ in (14.34) has as in the fractional Poisson process physical dimension $\text{sec}^{-\beta}$ and defines a characteristic timescale. The GFPP contains further two index parameters $\alpha > 0$ and $0 < \beta \leq 1$. The advantage of generalizations such as the GFPP is that they offer a larger parameter space allowing to greater flexibility in adapting to real-world situations. The GFPP recovers for $\alpha = 1, 0 < \beta < 1$ the above-described fractional Poisson process and for $\alpha = 1, \beta = 1$ the standard Poisson process and for $\beta = 1, \alpha > 0$ the so-called (generalized) Erlang process where α is allowed to take positive integer or non-integer values [17]. The waiting time density of the GFPP is then obtained as (see also Ref. [16])

$$\begin{aligned} \chi_{\beta,\alpha}(t) &= \xi^\alpha \sum_{m=0}^{\infty} (-1)^m \frac{(\alpha)_m}{m!} \xi^m \mathcal{L}^{-1}\{s^{-\beta(m+\alpha)}\} \\ &= \xi^\alpha t^{\beta\alpha-1} \sum_{m=0}^{\infty} \frac{(\alpha)_m}{m!} \frac{(-\xi t^\beta)^m}{\Gamma(\beta m + \alpha\beta)} = \xi^\alpha t^{\beta\alpha-1} E_{\beta,\alpha\beta}^\alpha(-\xi t^\beta) \end{aligned} \quad (14.35)$$

$t > 0, \sigma = \Re\{s\} > \xi^{\frac{1}{\beta}}, 0 < \beta \leq 1, \alpha > 0$

In this expression is introduced a generalization of the Mittag-Leffler function which was first described by Prabhakar [27] and is defined by

$$E_{a,b}^c(z) = \sum_{m=0}^{\infty} \frac{(c)_m}{m!} \frac{z^m}{\Gamma(am + b)}, \quad \Re\{a\} > 0, \quad \Re\{b\} > 0, \quad c, z \in \mathbb{C}. \quad (14.36)$$

In the Prabhakar’s Mittag-Leffler function (14.36) and in the expansion (14.35), we introduced the Pochhammer symbol $(c)_m$ which is defined as [28]

$$(c)_m = \frac{\Gamma(c + m)}{\Gamma(c)} = \begin{cases} 1, & m = 0 \\ c(c + 1) \dots (c + m - 1), & m = 1, 2, \dots \end{cases} \quad (14.37)$$

Despite $\Gamma(c)$ is singular at $c = 0$, the Pochhammer symbol can be defined also for $c = 0$ by the limit $(0)_m = \lim_{c \rightarrow 0^+} (c)_m = \delta_{m0}$ which is also fulfilled by the right-hand side of (14.37). Then, $(c)_m$ is defined for all $c \in \mathbb{C}$; thus, we have $E_{a,b}^0(z) = 1$. The series (14.36) converges absolutely in the entire complex z -plane. The Prabhakar’s Mittag-Leffler function (14.36) and related problems were analyzed by several authors [28–32].

In Fig. 14.1 a is drawn the waiting time PDF of Eq. (14.35) for a fixed value of $\alpha = 2$ and variable β in the admissible range $0 < \beta \leq 1$. The waiting time PDF exhibits for t small the power law behavior $\chi_{\beta,\alpha}(t) \approx \frac{\xi^\alpha}{\Gamma(\alpha\beta)} t^{\alpha\beta-1}$ [corresponding to the zero order in the expansion (14.35)] with two distinct regimes: For $\alpha\beta < 1$, the waiting time PDF becomes singular at $t = 0$ corresponding to ‘immediate’ arrivals of the first event. For $\alpha\beta = 1$, the jump density takes the constant value $\chi_{\alpha^{-1},\alpha}(t = 0) = \xi^\alpha$ whereas for

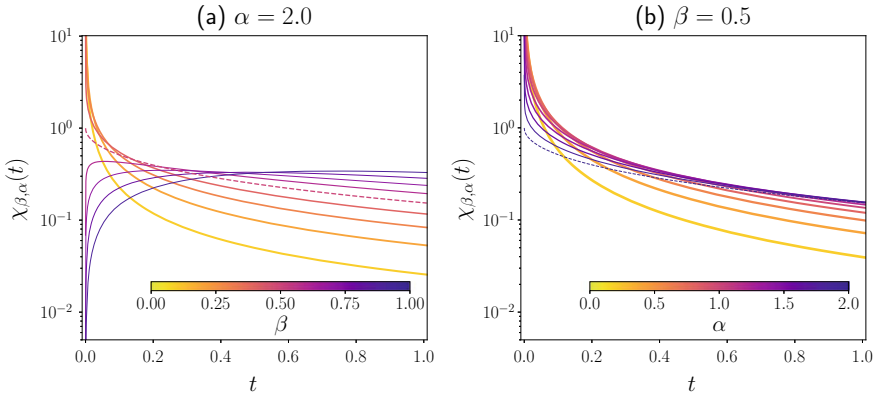


Fig. 14.1 Waiting time density $\chi_{\beta,\alpha}(t)$ as a function of t . We explore the results for **a** $\alpha = 2.0$ for different values $0 < \beta \leq 1$ and **b** $\beta = 0.5$ for $0 < \alpha \leq 2$ (in each case, the parameters are codified in the color bar). Results were obtained numerically using $\xi = 1$ and Eqs. (14.35) and (14.36). We depict with dashed lines the case when $\alpha\beta = 1$

$\alpha\beta > 0$ the waiting time density $\chi_{\beta,\alpha}(t = 0) = 0$ tends to zero as $t \rightarrow 0$ where the waiting times become longer the larger $\alpha\beta$.

In Fig. 14.1b, we depict the behavior of the waiting time PDF for fixed $\beta = 0.5$ and $0 < \alpha \leq 2$ thus $\alpha\beta \leq 1$. It can be seen that the smaller $\alpha\beta$ the more narrowly the waiting time PDF is concentrated at small t -values close to $t = 0$. This behavior can also be identified in view of Laplace transform (14.34) which takes in the limit $\alpha \rightarrow 0$ the value $\lim_{\alpha \rightarrow 0} \tilde{\chi}_{\beta,\alpha}(s) = 1$ thus $\chi_{\beta,0+}(t) = \mathcal{L}^{-1}(1) = \lim_{\alpha \rightarrow 0} \frac{\xi^\alpha}{\Gamma(\alpha\beta)} t^{\alpha\beta-1} = \delta(t)$ exhibits the shape of a Dirac δ -distribution peak.

Now, our goal is to determine the generalization of the fractional Poisson distribution (14.29) which is determined by Eq. (14.9) with (14.34), namely

$$\begin{aligned} \Phi_{\beta,\alpha}^{(n)}(t) &= \mathcal{L}^{-1} \left\{ \frac{1}{s} \left(\tilde{\chi}_{\beta,\alpha}^n(s) - \tilde{\chi}_{\beta,\alpha}^{n+1}(s) \right) \right\} \\ &= \mathcal{L}^{-1} \left\{ \frac{1}{s} \left(\tilde{\chi}_{\beta,n\alpha}(s) - \tilde{\chi}_{\beta,(n+1)\alpha}(s) \right) \right\}, \quad n = 0, 1, 2, \dots \end{aligned} \tag{14.38}$$

where it is convenient to utilize $\tilde{\chi}_{\beta,\alpha}^n(s) = \tilde{\chi}_{\beta,n\alpha}(s) = \frac{\xi^{n\alpha}}{(\xi + s^\beta)^{n\alpha}}$, i.e., to replace $\alpha \rightarrow n\alpha$ in the expression (14.35). We then obtain for the probability for n arrivals within $[0, t]$ the expression

$$\Phi_{\beta,\alpha}^{(n)}(t) = \xi^{n\alpha} t^{n\alpha\beta} \left(E_{\beta,(n\alpha\beta+1)}^{n\alpha}(-\xi t^\beta) - \xi^\alpha t^{\alpha\beta} E_{\beta,(n+1)\alpha\beta+1}^{(n+1)\alpha}(-\xi t^\beta) \right). \tag{14.39}$$

We refer this distribution to as the ‘generalized fractional Poisson distribution (GFPPD)’ [17, 18]. This distribution was also obtained by Cahoy and Polito [16]. For $\alpha = 1$ and $0 < \beta < 1$, the GFPP (14.39) recovers the fractional Poisson distribution (14.29) and for $\alpha = 1, \beta = 1$ the standard Poisson distribution (14.21), and

finally for $\alpha > 0$ and $\beta = 1$ the Erlang distribution [17, 18]. For applications in the dynamics in complex systems, the asymptotic properties of the GFPD are of interest. For small (dimensionless) times, the GFPD behaves as

$$\Phi_{\beta,\alpha}^{(n)}(t) \approx \frac{(\xi t^\beta)^{n\alpha}}{\Gamma(n\alpha\beta + 1)}, \quad t\xi^{\frac{1}{\beta}} \rightarrow 0, \quad n = 0, 1, 2, \dots \quad (14.40)$$

representing the lowest nonvanishing order in (14.39). It follows that the GFPD fulfills the initial condition

$$\Phi_{\beta,\alpha}^{(n)}(t) \Big|_{t=0} = \delta_{n0}, \quad (14.41)$$

reflecting that per construction at $t = 0$ no event has arrived. Further of interest is the asymptotic behavior for large (dimensionless) times $t\xi^{\frac{1}{\beta}}$. To this end, let us expand the Laplace transform for small $s \rightarrow 0$ in (14.38) up to the lowest nonvanishing order in $\frac{s^\beta}{\xi}$ to arrive at

$$\Phi_{\beta,\alpha}^{(n)}(t) \approx \frac{\alpha}{\xi} \mathcal{L}^{-1}\{s^{\beta-1}\} = \frac{\alpha}{\Gamma(1-\beta)} \left(t\xi^{\frac{1}{\beta}}\right)^{-\beta}, \quad t\xi^{\frac{1}{\beta}} \rightarrow \infty, \quad n = 0, 1, \dots, \infty \quad (14.42)$$

where this inverse power law holds universally for all $\alpha > 0$ for $0 < \beta < 1$ and is independent of the number of arrivals n recovering the fractional Poisson distribution for $\alpha = 1$ of Eq. (14.33). We notice that for large (dimensionless) observation times, an universal $(t\xi^{\frac{1}{\beta}})^{-\beta}$ power law decay occurs which is *independent* of the arrival number n where α occurs only as a scaling parameter in relation (14.42). We interpret this behavior as quasi-ergodicity property, i.e., quasi-equal distribution of all ‘states’ n for $t\xi^{\frac{1}{\beta}}$ large [17]. The fractional exponent $-\beta$ further is independent of α ; thus, the power law is of the same type as in the fractional Poisson process.

In Fig. 14.2a, we have plotted the probabilities $\Phi_{\beta,\alpha}^{(n)}(t)$ of Eq. (14.39) for fixed α and β for different arrival numbers n . One can see that for large times, the $\Phi_{\beta,\alpha}^{(n)}(t)$ converge to the same universal behavior independent of n which reflects the asymptotic power law relation (14.42). On the other hand, the asymptotic power law behavior for small t is shown in Fig. 14.2b [see also relation (14.40)]. The decay to zero $\lim_{t \rightarrow 0} \Phi_{\beta,\alpha}^{(n)}(t) \Big|_{t=0} \sim (\xi t^\beta)^{n\alpha} \rightarrow 0$ ($n > 0$) becomes the more pronounced the larger n . This behavior also can be interpreted that the higher n , the less likely are n arrivals to happen within a small time interval of observation.

The GFPP and the fractional Poisson process for large observation times exhibit the same power law asymptotic feature [see again asymptotic relation (14.42)]. This behavior reflects the ‘asymptotic universality’ of the fractional Poisson dynamics, and the latter was demonstrated in Ref. [33]. The inverse power law decay occurring for $0 < \beta < 1$ with fat-tailed waiting time PDF indeed is the source of non-Markovian behavior with long-time memory. We mention that for simultaneously $0 < \beta \leq 1$ and

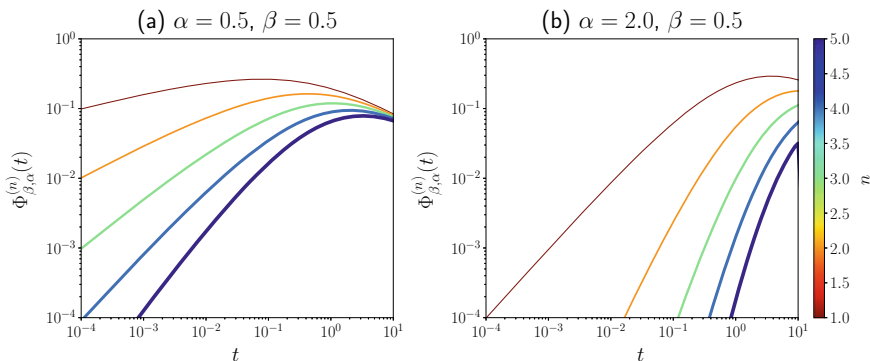


Fig. 14.2 Probability $\Phi_{\beta,\alpha}^{(n)}(t)$ as a function of t for different n . **a** $\alpha = 0.5$ and $\beta = 0.5$, **b** $\alpha = 2.0$ and $\beta = 0.5$. In the color bar, we represent $n = 1, 2, \dots, 5$. The values were obtained numerically using $\xi = 1$ with Eq. (14.38). The results for $t \ll 1$ show the power law relation $\Phi_{\beta,\alpha}^{(n)}(t) \propto t^{n\alpha\beta}$ in Eq. (14.40)

$0 < \alpha \leq 1$ with $0 < \alpha\beta \leq 1$ the waiting time PDF $\chi_{\beta,\alpha}(t)$ and survival probability $\Phi_{\beta,\alpha}^{(0)}(t)$ both are *completely monotonic functions*, i.e. they fulfill the condition⁶

$$(-1)^n \frac{d^n}{dt^n} f(t) \geq 0, \quad n = 0, 1, 2, \dots, \quad t > 0. \quad (14.43)$$

An analysis of various aspects of completely monotonic functions is performed in our recent works [8, 34], and see the references therein.

14.6 Continuous-Time Random Walk on Networks

Having recalled above basic properties of renewal theory⁷ our goal is now to analyze stochastic motions on undirected networks and lattices that are governed by the GFPP renewal process. To develop our model, we employ the continuous-time random walk (CTRW) approach by Montroll and Weiss [19] (and see also Refs. [2, 21, 22]). In the present section, our aim is to develop a CTRW model for undirected networks in order to apply the theory to infinite d -dimensional integer lattices \mathbb{Z}^d .

We consider an undirected connected network with N nodes which we denote with $p = 1, \dots, N$. The topology of the network is described by the positive-semidefinite $N \times N$ Laplacian matrix which is defined by [8, 12, 36–40]

$$L_{pq} = K_p \delta_{pq} - A_{pq} \quad (14.44)$$

⁶See Ref. [20] for a discussion of this issue for the fractional Poisson process.

⁷For further details on renewal theory, see, e.g., [35].

where $\mathbf{A} = (A_{pq})$ denotes the adjacency matrix having elements $A_{pq} = 1$ if a pair pq of nodes is connected and $A_{pq} = 0$ if a pair pq is disconnected. Further, we forbid that nodes are connected with themselves; thus, $A_{pp} = 0$. In an undirected network adjacency and Laplacian matrices are symmetric. The diagonal elements $L_{pp} = K_p$ of the Laplacian matrix are referred to as the degrees of the nodes p counting the number of neighbor nodes of a node p with $K_p = \sum_{q=1}^N A_{pq}$. In order to relate the network topology with random walk features, we introduce the one-step transition matrix $\mathbf{W} = (W_{pq})$ which is defined by [8, 12]

$$W_{pq} = \frac{1}{K_p} A_{pq} = \delta_{pq} - \frac{1}{K_p} L_{pq}. \quad (14.45)$$

Generally, the transition matrix is non-symmetric for networks with variable degrees $K_i \neq K_j$ ($i \neq j$). The one-step transition matrix W_{pq} defines the conditional probability that a random walker which is on node p jumps in one step to node q where in one step only neighbor nodes with equal probability $\frac{1}{K_p}$ can be reached.

We see in definition (14.45) that the one-step transition matrix $\sum_{q=1}^N W_{pq} = 1$ and $0 \leq W_{pq} \leq 1$ and also the n -step transition matrices \mathbf{W}^n are (row-)stochastic [8].

Now, let us assume that each step of the walker from one to another node is associated with a jump event or arrival in a CTRW with identical transition probability (W_{pq}) for a step from node p to node q . We assume the random walker performs IID random steps at random times $0 \leq t_1, t_2, \dots, t_n, \dots, \infty$ in a renewal process with IID waiting times Δt_k where the observation starts at $t = 0$. To this end, let us recall some basic relations holding generally, and then, we specify the renewal process to be a GFPP.

Introducing the transition matrix $\mathbf{P}(t) = (P_{ij}(t))$ indicating the probability to find the walker at time t on node j under the condition that the walker at $t = 0$ initially was sitting at node i , we can write [35, 41]

$$\mathbf{P}(t) = \mathbf{P}(0) \sum_{n=0}^{\infty} \Phi^{(n)}(t) \mathbf{W}^n \quad (14.46)$$

where we assume here a general initial condition $\mathbf{P}(t)|_{t=0} = \mathbf{P}(0)$ which is fulfilled by accounting for the initial conditions $\Phi^{(n)}(t)|_{t=0} = \delta_{n0}$. In this series, the $\Phi^{(n)}(t)$ indicate the probabilities of n (jump-) events in the renewal process, i.e., the probability that the walker performs n steps within $[0, t]$ [see Eq. (14.5)], and $(\mathbf{W}^n)_{ij}$ indicates the probability that the walker in n jumps moves from the initial node i to node j . We observe in view of relation (14.13) together with $\sum_{j=1}^N (\mathbf{W}^n)_{ij} = 1$ that the normalization condition $\sum_{j=1}^N P_{ij}(t) = \sum_{n=0}^{\infty} \Phi^{(n)}(t) = 1$ is fulfilled. The convergence of series (14.46) can be easily proved by using that \mathbf{W} has uniquely eigenvalues $|\lambda_m| \leq 1$ and with $|\tilde{\chi}(s)| \leq 1$ [8, 17]. Let us assume that at $t = 0$, the walker is

sitting on departure node i ; thus, the initial condition is given by $P_{ij}(0) = (\delta_{ij})$, and then, the Laplace transform of (14.46) writes [17]

$$\tilde{\mathbf{P}}(s) = \frac{(1 - \tilde{\chi}(s))}{s} \{\mathbf{1} - \tilde{\chi}(s)\mathbf{W}\}^{-1} \tag{14.47}$$

where $\tilde{\mathbf{P}}(s)$ has the eigenvalues [17]

$$\tilde{P}(m, s) = \frac{(1 - \tilde{\chi}(s))}{s} \frac{1}{(1 - \lambda_m \tilde{\chi}(s))}, \quad m = 1, \dots, N. \tag{14.48}$$

The λ_m indicate the eigenvalues of the one-step transition matrix \mathbf{W} . This expression is the celebrated *Montroll–Weiss formula* [19] and occurs in various contexts of physics.

14.7 Generalized Space–Time Fractional Diffusion in \mathbb{Z}^d

In this section, our aim is to develop a CTRW which is a random walk subordinated to a GFPP. For the random walk on the network, we allow long-range jumps which can be described when we replace the Laplacian matrix by its fractional power in the one-step transition matrix (14.45). In this way, the walker cannot only jump to connected neighbor nodes, but also to far distant nodes in the network [5, 6, 8, 34, 36–39, 42, 43]. The model to be developed in this section involves both space- and time fractional calculus. As an example, we consider the infinite d -dimensional integer lattice \mathbb{Z}^d . The lattice points $\mathbf{p} = (p_1, \dots, p_d)$ ($p_j \in \mathbb{Z}_0$) represent the nodes where we assume each node is connected to any of its $2d$ neighbor nodes. The \mathbb{Z}^d is an infinite cubic primitive d -dimensional lattice with lattice constant one. In this network, any node has identical degree $2d$. The one-step transition matrix with the elements $W^{(\mu)}(\mathbf{p} - \mathbf{q})$ has then the canonic representation [8, 38]

$$W^{(\mu)}(\mathbf{p} - \mathbf{q}) = \frac{1}{(2\pi)^d} \int_{-\pi}^{\pi} dk_1 \dots \int_{-\pi}^{\pi} dk_d e^{i\mathbf{k} \cdot (\mathbf{p} - \mathbf{q})} \lambda^{(\mu)}(\mathbf{k}) \tag{14.49}$$

with the eigenvalues

$$\lambda^{(\mu)}(\mathbf{k}) = 1 - \frac{1}{\mathcal{K}^{(\mu)}} \eta^{\frac{\mu}{2}}(\mathbf{k}), \quad \eta(\mathbf{k}) = 2d - 2 \sum_{j=1}^d \cos(k_j), \quad 0 < \mu \leq 2 \tag{14.50}$$

where $\mathbf{k} = (k_1, \dots, k_d)$ denotes the wave vector with $-\pi \leq k_j \leq \pi$. One can show that the fractional index μ is restricted to the interval $0 < \mu \leq 2$ as a requirement

for stochasticity of the one-step transition matrix [8, 34, 38]. In (14.50), the constant $\mathcal{K}^{(\mu)}$ can be conceived as a fractional generalization of the degree and is given by the trace of the fractional power of Laplacian matrix, namely [8, 34]

$$\mathcal{K}^{(\mu)} = \frac{1}{N} \text{tr}(\mathbf{L}^{\frac{\mu}{2}}) = \frac{1}{N} \sum_{m=1}^N (\eta_m)^{\frac{\mu}{2}} \tag{14.51}$$

where η_m denote the eigenvalues of the Laplacian matrix (14.44) and in an infinite network the sum in (14.51) has to be performed in the limit $N \rightarrow \infty$. In the \mathbb{Z}^d , the fractional degree with Eq. (14.51) is then determined from [8, 34]

$$\mathcal{K}^{(\mu)} = \frac{1}{(2\pi)^d} \int_{-\pi}^{\pi} dk_1 \dots \int_{-\pi}^{\pi} dk_d (\eta(\mathbf{k}))^{\frac{\mu}{2}} \tag{14.52}$$

with the eigenvalues given in Eq. (14.50). It is necessary to account for the fractional degree since it plays the role of a normalization factor in the one-step transition matrix [see Eq. (14.45)].

For the present analysis, it is sufficient to consider $\mathcal{K}^{(\mu)}$ as a (positive) constant where for $\mu = 2$ recovers $\mathcal{K}^{(\mu=2)} = 2d$ the degree of any node. The transition matrix (14.46) is then determined by its Laplace transform (14.47) which writes in the \mathbb{Z}^d as

$$\tilde{P}^{(\mu)}(\mathbf{p} - \mathbf{q}, s) = \frac{(1 - \tilde{\chi}(s))}{s} \frac{1}{(2\pi)^d} \int_{-\pi}^{\pi} dk_1 \dots \int_{-\pi}^{\pi} dk_d \tilde{P}(\mathbf{k}, 0) \frac{e^{i\mathbf{k} \cdot (\mathbf{p} - \mathbf{q})}}{(1 - \lambda^{(\mu)}(\mathbf{k}) \tilde{\chi}(s))} \tag{14.53}$$

where $\tilde{P}(\mathbf{k}, 0)$ indicates the Fourier transform of the initial condition which has the Fourier representation

$$P^{(\mu)}(\mathbf{p} - \mathbf{q}, t = 0) = P_0(\mathbf{p} - \mathbf{q}) = \frac{1}{(2\pi)^d} \int_{-\pi}^{\pi} dk_1 \dots \int_{-\pi}^{\pi} dk_d e^{i\mathbf{k} \cdot (\mathbf{p} - \mathbf{q})} \tilde{P}(\mathbf{k}, 0). \tag{14.54}$$

In order to analyze the diffusive limit of (14.53), i.e., its long-wave approximation, it will be sufficient to account for the eigenvalues (14.50) for $k \rightarrow 0$ (where $k = |\mathbf{k}|$). Then, we have with $\eta^{\frac{\mu}{2}}(\mathbf{k}) \approx k^\mu$ the behavior

$$\lambda^{(\mu)}(\mathbf{k}) \approx 1 - \frac{1}{\mathcal{K}^{(\mu)}} k^\mu, \quad 0 < \mu \leq 2, \quad k \rightarrow 0. \tag{14.55}$$

These equations hold so far for space fractional walks for an arbitrary renewal process with waiting time PDF $\chi(t) = \mathcal{L}^{-1}\{\tilde{\chi}(s)\}$.

Now let us consider a space fractional walk subordinated to a GFPP with $\tilde{\chi}(s) = \tilde{\chi}_{\beta,\alpha}(s)$ of Eq. (14.34). We denote the corresponding transition matrix of this stochastic motion as $\mathbf{P}_{\beta,\alpha}^{(\mu)}(t)$ which contains three index parameters $0 < \mu \leq 2$,

$0 < \beta \leq 1$ and $\alpha > 0$ and one timescale parameter ξ (of units $\text{sec}^{-\beta}$). In order to derive the generalized space–time fractional diffusion equation, it is convenient to proceed in the Fourier–Laplace domain. The Fourier–Laplace transform of the $\mathbf{P}_{\beta,\alpha}^{(\mu)}(t)$ is then with Eq. (14.53) given by the Montroll–Weiss equation

$$\begin{aligned} \tilde{\mathbf{P}}_{\beta,\alpha}^{(\mu)}(k, s) &= \tilde{\mathbf{P}}(\mathbf{k}, 0) \frac{(1 - \tilde{\chi}_{\beta,\alpha}(s))}{s} \frac{1}{(1 - \tilde{\chi}_{\beta,\alpha}(s)\lambda^{(\mu)}(\mathbf{k}))} \\ &= \tilde{\mathbf{P}}(\mathbf{k}, 0) \frac{s^{-1}}{\left(1 + \frac{\tilde{\chi}_{\beta,\alpha}(s)}{(1 - \tilde{\chi}_{\beta,\alpha}(s))} \eta^{\frac{\mu}{2}}(\mathbf{k})\right)} \end{aligned} \quad (14.56)$$

$$\approx \tilde{\mathbf{P}}(\mathbf{k}, 0) \frac{s^{-1}}{\left(1 + \frac{\tilde{\chi}_{\beta,\alpha}(s)}{(1 - \tilde{\chi}_{\beta,\alpha}(s))} \frac{k^\mu}{\mathcal{K}^{(\mu)}}\right)}, \quad k \rightarrow 0 \quad (14.57)$$

containing also the Fourier transform $\tilde{\mathbf{P}}(\mathbf{k}, 0)$ of the initial condition (14.54). The exact equation (14.56) can be rewritten as

$$\begin{aligned} -\frac{\xi^\alpha \eta^{\frac{\mu}{2}}(\mathbf{k})}{\mathcal{K}^{(\mu)}} \tilde{\mathbf{P}}_{\beta,\alpha}^{(\mu)}(k, s) &= (s^\beta + \xi)^\alpha \tilde{\mathbf{P}}_{\beta,\alpha}^{(\mu)}(k, s) - \xi^\alpha \tilde{\mathbf{P}}_{\beta,\alpha}^{(\mu)}(k, s) \\ &+ \frac{\xi^\alpha - (s^\beta + \xi)^\alpha}{s} \tilde{\mathbf{P}}(\mathbf{k}, 0), \quad k_j \in [-\pi, \pi]. \end{aligned} \quad (14.58)$$

Transforming back this equation into the causal time domain and by using Eqs. (14.54) and (14.53) yields the generalized time fractional matrix equation

$$-\frac{\xi^\alpha}{\mathcal{K}^{(\mu)}} \mathbf{L}^{\frac{\mu}{2}} \cdot \mathbf{P}_{(\beta,\alpha)}^{(\mu)}(t) = {}_0\mathcal{D}_t^{\beta,\alpha} \cdot \mathbf{P}_{\beta,\alpha}^{(\mu)}(t) - \xi^\alpha \mathbf{P}_{\beta,\alpha}^{(\mu)}(t) + \mathbf{P}_0 \left\{ \xi^\alpha \Theta(t) - K_{\beta,\alpha}^{(0)}(t) \right\}, \quad t \geq 0 \quad (14.59)$$

which we refer to as ‘generalized space–time fractional Kolmogorov–Feller equation’ where $0 < \mu \leq 2$ with $0 < \beta \leq 1$ and $\alpha > 0$. This equation was obtained and analyzed recently for normal walks ($\mu = 2$) subordinated to a GFPP [17, 18]. Equations of the type (14.59) generally describe the generalized space–time fractional diffusion on undirected networks connecting the network topology (contained in Laplacian matrix \mathbf{L}) with the GFPP-governed stochastic motion on the network. We used notation $\mathbf{L}^{\frac{\mu}{2}}$ which denotes the fractional power of Laplacian matrix \mathbf{L} , and $\mathbf{P}_{(\beta,\alpha)}^{(\mu)}(t)$ the transition matrix with the initial condition $\mathbf{P}_{(\beta,\alpha)}^{(\mu)}(t = 0) = \mathbf{P}_0$ where all these matrices are defined in \mathbb{Z}^d . Since the \mathbb{Z}^d is an infinite network, these are symmetric and circulant $\infty \times \infty$ matrices with elements $L^{(\mu)}(\mathbf{p} - \mathbf{q})$, $P_{(\beta,\alpha)}^{(\mu)}(\mathbf{p} - \mathbf{q}, t)$, $\mathbf{P}_0(\mathbf{p} - \mathbf{q})$,

respectively, where $\mathbf{p}, \mathbf{q} \in \mathbb{Z}^d$. In Eq. (14.59), we have introduced the causal convolution operator ${}_0\mathcal{D}_t^{\beta,\alpha}$ and the causal function $K_{\beta,\alpha}^{(0)}(t)$ which were obtained in explicit forms [17, 18]

$$\begin{aligned} \mathcal{D}^{\beta,\alpha}(t) &= \mathcal{L}^{-1}\{(s^\beta + \xi)^\alpha\} = \frac{d^{[\alpha\beta]}}{dt^{[\alpha\beta]}}(\Theta(t)d^{\beta,\alpha}(t)) \\ &= \frac{d^{[\alpha\beta]}}{dt^{[\alpha\beta]}}(\Theta(t)d^{\beta,\alpha}(t - \tau)) \\ &= \begin{cases} \frac{d^{[\alpha\beta]}}{dt^{[\alpha\beta]}}\left(\Theta(t)t^{[\alpha\beta]-\beta\alpha-1}\sum_{m=0}^\infty \frac{\alpha!}{(\alpha-m)!m!} \frac{(\xi t^\beta)^m}{\Gamma(\beta m + [\alpha\beta] - \beta\alpha)}\right), & \alpha\beta \notin \mathbb{N} \\ \frac{d^{\alpha\beta}}{dt^{\alpha\beta}}\left(\delta(t) + \Theta(t)\frac{d}{dt}\sum_{m=0}^\infty \frac{\alpha!}{(\alpha-m)!m!} \frac{(\xi t^\beta)^m}{\Gamma(m\beta + 1)}\right), & \alpha\beta \in \mathbb{N} \end{cases} \\ &= \begin{cases} \frac{d^{[\alpha\beta]}}{dt^{[\alpha\beta]}}(\Theta(t)t^{[\alpha\beta]-\beta\alpha-1}E_{\alpha,\beta,([\alpha\beta]-\alpha\beta)}(\xi t^\beta)), & \alpha\beta \notin \mathbb{N} \\ \frac{d^{\alpha\beta}}{dt^{\alpha\beta}}(\delta(t) + \Theta(t)\frac{d}{dt}E_{\alpha,\beta,1}(\xi t^\beta)), & \alpha\beta \in \mathbb{N}. \end{cases} \end{aligned} \tag{14.60}$$

In these expressions, we introduced the *ceiling function* $[\gamma]$ indicating the smallest integer greater or equal to γ and the function $E_{c,a,b}(z) = E_{a,b}^{-c}(-z)$ where $E_{v,w}^u(\zeta)$ indicating the Prabhakar’s Mittag-Leffler function (14.36). The operator ${}_0\mathcal{D}_t^{\beta,\alpha}$ acts on a causal distribution $P(t)$ such as in Eq. (14.59) in the following way

$${}_0\mathcal{D}_t^{\beta,\alpha} \cdot P(t) = \frac{d^{[\alpha\beta]}}{dt^{[\alpha\beta]}} \int_0^t d^{\beta,\alpha}(t - \tau)P(\tau)d\tau. \tag{14.61}$$

The function $K_{\beta,\alpha}^{(0)}(t)$ of equation (14.59) was obtained as

$$\begin{aligned} K_{\beta,\alpha}^{(0)}(t) &= \mathcal{L}^{-1}\left\{\frac{(s^\beta + \xi)^\alpha}{s}\right\} \\ &= \begin{cases} \Theta(t)t^{-\alpha\beta}E_{\alpha,\beta,1-\alpha\beta}(\xi t^\beta), & 0 < \alpha\beta < 1 \\ \frac{d^{[\alpha\beta]-1}}{dt^{[\alpha\beta]-1}}(\Theta(t)t^{[\alpha\beta]-\beta\alpha-1}E_{\alpha,\beta,([\alpha\beta]-\alpha\beta)}(\xi t^\beta)) & \alpha\beta > 1, \quad \alpha\beta \notin \mathbb{N} \\ \frac{d^{\alpha\beta-1}}{dt^{\alpha\beta-1}}\left(\delta(t) + \Theta(t)\frac{d}{dt}E_{\alpha,\beta,1}(\xi t^\beta)\right), & \alpha\beta \geq 1 \in \mathbb{N}. \end{cases} \end{aligned} \tag{14.62}$$

Equation (14.59) governs the ‘microscopic’ stochastic motions of the space fractional walk subordinated to a GFPP.

14.8 Diffusion Limit

Our goal now is to determine the ‘diffusion limit’ of above stochastic motion to obtain a ‘macroscopic picture’ on spatial scales large compared to the lattice constant 1 of the \mathbb{Z}^d . To this end, it is sufficient to consider Montroll–Weiss equation (14.56) for k small. Then, Eq. (14.58) can be rewritten as

$$\begin{aligned}
 -\frac{\xi^\alpha k^\mu}{\mathcal{K}(\mu)} \tilde{P}_{\beta,\alpha}^{(\mu)}(\mathbf{k}, s) &\approx (s^\beta + \xi)^\alpha \tilde{P}_{\beta,\alpha}^{(\mu)}(\mathbf{k}, s) - \xi^\alpha \tilde{P}_{\beta,\alpha}^{(\mu)}(\mathbf{k}, s) \\
 &+ \frac{\xi^\alpha - (s^\beta + \xi)^\alpha}{s} \tilde{P}(\mathbf{k}, 0), \quad k \rightarrow 0.
 \end{aligned}
 \tag{14.63}$$

In order to derive the ‘diffusive limit’ which corresponds to the space–time representation of this equation, it appears instructive to consider the long-wave contribution of some kernels such as the fractional power of the Laplacian matrix in \mathbb{Z}^d . The fractional Laplacian matrix in \mathbb{Z}^d has the canonic form [8, 38]

$$[\mathbf{L}^{\frac{\mu}{2}}]_{\mathbf{p}-\mathbf{q}} = \frac{1}{(2\pi)^d} \int_{-\pi}^{\pi} dk_1 \dots \int_{-\pi}^{\pi} dk_d e^{i\mathbf{k}\cdot(\mathbf{p}-\mathbf{q})} \eta^{\frac{\mu}{2}}(\mathbf{k}), \quad 0 < \mu \leq 2 \tag{14.64}$$

where $\eta(\mathbf{k})$ are the eigenvalues of the Laplacian matrix in \mathbb{Z}^d defined by Eq. (14.50). Let us consider the contribution generated by small $k \rightarrow 0$ by integrating over a small d -cube $|k_j| \leq k_c \ll 1$ around the origin (corresponding to very large wavelengths), namely

$$\begin{aligned}
 [\mathbf{L}'^{\frac{\mu}{2}}]_{\mathbf{p}-\mathbf{q}} &\approx \frac{1}{(2\pi)^d} \int_{-k_c}^{k_c} dk_1 \dots \int_{-k_c}^{k_c} dk_d e^{i\mathbf{k}\cdot(\mathbf{p}-\mathbf{q})} \eta^{\frac{\mu}{2}}(\mathbf{k}) \\
 &= \frac{h^d}{(2\pi)^d} \int_{-\pi h^{-\frac{1}{2}}}^{\pi h^{-\frac{1}{2}}} d\bar{k}_1 \dots \int_{-\pi h^{-\frac{1}{2}}}^{\pi h^{-\frac{1}{2}}} d\bar{k}_d e^{i\bar{\mathbf{k}}\cdot(\mathbf{p}-\mathbf{q})h} \eta^{\frac{\mu}{2}}(h\bar{\mathbf{k}}).
 \end{aligned}
 \tag{14.65}$$

In the second line, we have introduced a new wave vector $\bar{\mathbf{k}}$ with $k_j = \bar{k}_j h \leq k_c$ with $k_c(h) = \pi h^{\frac{1}{2}} \rightarrow 0$ small; thus, $0 \leq |\bar{k}_j| \leq \pi h^{-\frac{1}{2}} \rightarrow \infty$ (where any exponent $0 < \delta < 1$ could be used with $|\bar{k}_j| \leq \pi h^{-\delta} \rightarrow \infty$ and $h\bar{k}_j \leq \pi h^{1-\delta} \rightarrow 0$). In this way, the integral (14.65) (rescaled h^{-d}) over small k becomes an integral over the complete infinite $\bar{\mathbf{k}}$ -space where in this integration $k = \bar{k}h$ is small. Hence, $(\eta(h\bar{k}))^{\frac{\mu}{2}} \approx h^\mu \bar{k}^\mu \leq \pi^\mu h^{\frac{\mu}{2}} \ll 1$ remains valid in the entire region of integration in (14.65)₂. Introducing the rescaled quasi-continuous very slowly varying ‘macroscopic’ coordinates $(\mathbf{p} - \mathbf{q})h = \mathbf{r} - \mathbf{r}' \in h\mathbb{Z}^d$ of the nodes, we arrive at⁸

⁸This picture corresponds to the introduction of a lattice constant $h \rightarrow 0$.

$$[\mathbf{L}'^{\frac{\mu}{2}}]_{\mathbf{p}-\mathbf{q}} \approx h^{\mu+d} \frac{1}{(2\pi)^d} \int_{-\infty}^{\infty} d\bar{k}_1 \dots \int_{-\infty}^{\infty} d\bar{k}_d e^{i\bar{\mathbf{k}} \cdot (\mathbf{r}-\mathbf{r}')} \bar{k}^\mu = h^{\mu+d} (-\Delta)^{\frac{\mu}{2}} \delta^d(\mathbf{r}-\mathbf{r}'). \quad (14.66)$$

The new macroscopic coordinates $\mathbf{r} = h\mathbf{p}$, $\mathbf{r}' = h\mathbf{q} \in \mathbb{R}^d$ are nonzero only for very large values of the integer values $p_j \sim h^{-1} \gg 1$, $q_j \sim h^{-1} \gg 1$; i.e., the representation (14.66) captures the far-field contribution $|\mathbf{p}-\mathbf{q}| \gg 1$. In Eq. (14.66), $\Delta = \sum_{j=1}^d \frac{\partial^2}{\partial x_j^2}$ denotes the standard Laplacian with respect to the macroscopic coordinates \mathbf{r} . The Fourier integral coincides up to the sign with the kernel of the Riesz fractional derivative $-(-\Delta)^{\frac{\mu}{2}} \delta^d(\mathbf{r}-\mathbf{r}')$ of the \mathbb{R}^d (which has the eigenvalues $-k^{-\mu}$ and also is referred to as fractional Laplacian recovering for $\mu = 2$ the standard Laplacian Δ) [8]. It follows that Eq. (14.63) can be transformed into the spatial (long-wave) representation by

$$P^{(\mu)}(\mathbf{p}-\mathbf{q}, t) \approx h^d \bar{P}^{(\mu)}(h(\mathbf{p}-\mathbf{q}), t), \quad h \rightarrow 0 \quad (14.67)$$

where we denote $h(\mathbf{p}-\mathbf{q}) = \mathbf{r}-\mathbf{r}' \in \mathbb{Z}^d h \rightarrow \mathbb{R}^d$. The smooth field $\bar{P}^{(\mu)}(\mathbf{r}-\mathbf{r}', t)$ introduced in asymptotic relation (14.67) indicates the macroscopic transition probability *density* kernel having physical units cm^{-d} . By using Eqs. (14.53)–(14.56) and $\lambda^{(\mu)}(h\bar{k}) \approx 1 - \frac{h^\mu \bar{k}^\mu}{\mathcal{K}^{(\mu)}}$, we arrive at

$$\bar{P}^{(\mu)}(\mathbf{r}-\mathbf{r}', t) \approx \mathcal{L}^{-1} \left\{ \frac{s^{-1}}{(2\pi)^d} \int_{-\infty}^{\infty} dk_1 \dots \int_{-\infty}^{\infty} dk_d e^{i\bar{\mathbf{k}} \cdot (\mathbf{r}-\mathbf{r}')} \frac{\bar{P}(h\bar{k}, 0)}{\left(1 + \frac{\tilde{\chi}_{\beta,\alpha}(s)}{1 - \tilde{\chi}_{\beta,\alpha}(s)} \frac{h^\mu \bar{k}^\mu}{\mathcal{K}^{(\mu)}}\right)} \right\} \quad (14.68)$$

where the integration limits here can be thought to be generated by a limiting process $\pm \lim_{h \rightarrow 0} \pi h^{-\frac{1}{2}} \rightarrow \pm \infty$ in the same way as in integral (14.65); thus, only small $h\bar{k} \leq \pi h^{\frac{1}{2}}$ in the integrand of (14.68) is relevant. Then, let us rewrite Eq. (14.63) in the Fourier–Laplace domain in the form

$$\begin{aligned} -\frac{h^\mu \bar{k}^\mu}{\mathcal{K}^{(\mu)}} \tilde{P}_{\beta,\alpha}^{(\mu)}(h\bar{k}, s) &\approx \left[\left(1 + \frac{s^\beta}{\xi}\right)^\alpha - 1 \right] \tilde{P}_{\beta,\alpha}^{(\mu)}(h\bar{k}, s) \\ &+ \frac{\tilde{P}(h\bar{k}, 0)}{s} \left[1 - \left(1 + \frac{s^\beta}{\xi}\right)^\alpha \right], \quad h \rightarrow 0. \end{aligned} \quad (14.69)$$

We observe that $h \rightarrow 0$ makes left-hand side converging to zero (as within the integration limits of integral (14.65) $k^\mu = h^\mu \bar{k}^\mu \leq \pi^\mu h^{\mu/2} \rightarrow 0$, i.e., only small $k = h\bar{k}$ are captured). In order to maintain the equality for $h \rightarrow 0$, it is required that on the right-hand side of Eq. (14.69) $h \rightarrow 0$ thus we can expand $(1 + \frac{s^\beta}{\xi})^\alpha \approx 1 + \frac{\alpha}{\xi} s^\beta$ and obtain

$$-\frac{\xi h^\mu \bar{k}^\mu}{\alpha \mathcal{K}^{(\mu)}} \tilde{P}_{\beta,\alpha}^{(\mu)}(h\bar{k}, s) \approx s^\beta \tilde{P}_{\beta,\alpha}^{(\mu)}(h\bar{k}, s) - \tilde{P}(h\bar{k}, 0) s^{\beta-1}. \quad (14.70)$$

The existence of the diffusive limit requires the left-hand side of this equation to remain finite, i.e., $\xi h^\mu = \text{const}$ when $h \rightarrow 0$. It follows that ξ then scales as $\xi \sim h^{-\mu}$ leading to the new generalized diffusion constant

$$\mathcal{A} = \frac{\xi h^\mu}{\alpha \mathcal{K}^{(\mu)}} > 0, \quad \alpha > 0, \quad 0 < \mu \leq 2, \tag{14.71}$$

having physical dimension $cm^\mu \text{sec}^{-\beta}$. We obtain hence the *universal diffusion limit* in the form of a *space–time fractional diffusion equation* of the form

$$-\mathcal{A}(-\Delta)^{\frac{\mu}{2}} \cdot \bar{P}_{(\beta,\alpha)}^{(\mu)}(r, t) = {}_0D_t^\beta \cdot \bar{P}_{\beta,\alpha}^{(\mu)}(\mathbf{r}, t) - \bar{P}_0(\mathbf{r}) \frac{t^{-\beta}}{\Gamma(1-\beta)} \quad 0 < \beta < 1. \tag{14.72}$$

In this equation, ${}_0D_t^\beta \cdot (\dots)$ denotes the Riemann–Liouville fractional derivative of order β [see Appendix, Eq. (14.104)], and $-(-\Delta)^{\frac{\mu}{2}}$ indicates the Riesz fractional derivative convolution operator (fractional Laplacian) in the d -dimensional infinite space.⁹ The diffusion limit Eq. (14.72) is coinciding with a space–time fractional diffusion equation given by several authors [3, 6] in various contexts (among others). This equation is of the same type as the equation that occurs in the purely fractional Poisson process, i.e., for $\alpha = 1$. We notice in view of the diffusion constant (14.71) that index α appears in Eq. (14.72) only as a scaling parameter. The universal space–time fractional behavior of the diffusive limit reflects the *asymptotic universality* of the Mittag-Leffler waiting time PDF which was demonstrated by Gorenflo and Mainardi [33]. We emphasize the non-Markovian characteristics of this time fractional diffusion process in the range $0 < \beta < 1$, i.e., when the waiting time PDF is fat-tailed. The non-Markovianity is reflected by the occurrence of the slowly decaying memory term $-\bar{P}_0(\mathbf{r}) \frac{t^{-\beta}}{\Gamma(1-\beta)}$ in Eq. (14.72) exhibiting a long-time memory of the initial condition $\bar{P}_{\beta,\alpha}^\mu(\mathbf{r}, t = 0) = \bar{P}_0(\mathbf{r})$.

Let us briefly consider the case when the walker at $t = 0$ is in the origin. The initial condition then is given by $\bar{P}_0(\mathbf{r}) = \delta^d(\mathbf{r})$ and from Eqs. (14.70)–(14.72) follows that

$$\tilde{P}_{\beta,\alpha}^{(\mu)}(h\bar{k}, s) = \frac{s^{\beta-1}}{\mathcal{A}\bar{k}^\mu + s^\beta}. \tag{14.73}$$

In view of Eq. (14.27), we obtain for the causal Fourier time domain the solution

$$\hat{P}_{\beta,\alpha}^{(\mu)}(h\bar{k}, t) = \mathcal{L}^{-1} \left\{ \frac{s^{\beta-1}}{\mathcal{A}\bar{k}^\mu + s^\beta} \right\} = \Theta(t) E_\beta(-\mathcal{A}\bar{k}^\mu t^\beta), \quad 0 < \beta \leq 1 \tag{14.74}$$

⁹For explicit representations and evaluations, see, e.g., [8].

where $E_\beta(z)$ denotes the Mittag-Leffler function defined in Eq. (14.100) and for later convenience we included the Heaviside step function $\Theta(t)$. In the space–time domain, the transition probability kernel is given by the Fourier inversion

$$\bar{P}_{\beta,\alpha}^{(\mu)}(\mathbf{r}, t) = \frac{\Theta(t)}{(2\pi)^d} \int_{-\infty}^{\infty} \bar{d}k_1 \dots \int_{-\infty}^{\infty} \bar{d}k_d e^{i\bar{\mathbf{k}} \cdot \mathbf{r}} E_\beta(-\mathcal{A}\bar{k}^\mu t^\beta) \tag{14.75}$$

where by accounting for $E_\beta(0) = 1$ the initial condition $\bar{P}_{\beta,\alpha}^{(\mu)}(\mathbf{r}, 0) = \delta^d(\mathbf{r})$ is directly confirmed. For $0 < \beta < 1$ the Mittag-Leffler function exhibits for $\mathcal{A}\bar{k}^\mu t^\beta \gg 1$ inverse power law behavior, namely

$$\hat{P}_{\beta,\alpha}^{(\mu)}(h\bar{k}, t) \approx \mathcal{L}^{-1}\{\mathcal{A}^{-1}\bar{k}^{-\mu} s^{\beta-1}\} = \mathcal{A}^{-1}\bar{k}^{-\mu} \frac{t^{-\beta}}{\Gamma(1-\beta)}. \tag{14.76}$$

In the limit $\beta \rightarrow 1 - 0$, Eq. (14.72) with $P_0(\mathbf{r}) = \delta^d(\mathbf{r})$ takes for $0 < \mu < 2$ the form of a standard space fractional Lévy flight diffusion equation¹⁰

$$-\mathcal{A}(-\Delta)^{\frac{\mu}{2}} \bar{P}_{(1,\alpha)}^{(\mu)}(r, t) = \frac{\partial}{\partial t} \bar{P}_{(1,\alpha)}^{(\mu)}(r, t) - \delta^d(\mathbf{r})\delta(t) \tag{14.77}$$

where $0 < \mu \leq 2$ is admissible. This walk is Markovian and hence memoryless due to the immediate vanishing of the memory term $-\delta^{(d)}(\mathbf{r})\delta(t)$ for $t > 0$. For $\mu = 2$, this equation recovers Fick’s second law of normal diffusion. For $\beta = 1$, the Mittag-Leffler function in (14.74) turns into the form of exponential $E_1(-\mathcal{A}\bar{k}^\mu t) = e^{-\mathcal{A}\bar{k}^\mu t}$; thus, the Fourier integral (14.75) becomes

$$\bar{P}_{(1,\alpha)}^{(\mu)}(r, t) = \frac{\Theta(t)}{(2\pi)^d} \int_{-\infty}^{\infty} \bar{d}k_1 \dots \int_{-\infty}^{\infty} \bar{d}k_d e^{i\bar{\mathbf{k}} \cdot \mathbf{r}} e^{-\mathcal{A}\bar{k}^\mu t}, \quad 0 < \mu \leq 2. \tag{14.78}$$

One directly confirms that (14.78) solves (14.77)¹¹ and is indeed the well-known expression for a symmetric Lévy distribution in \mathbb{R}^d [5, 6, 8] (and many others). Further mention worthy is the case $\beta = 1$ and $\mu = 2$ for which Eq. (14.77) recovers the form of a normal diffusion equation (Fick’s second law) where (14.78) turns into the Gaussian distribution

$$\bar{P}_{(1,\alpha)}^{(2)}(r, t) = \Theta(t) \frac{e^{-\frac{r^2}{4\mathcal{A}t}}}{(4\pi\mathcal{A}t)^{\frac{d}{2}}} \tag{14.79}$$

which indeed is the well-known causal solution of Fick’s second law in \mathbb{R}^d .

¹⁰See also Laplace transform (14.73) for $\beta = 1$ and Appendix.

¹¹Where we take into account with $\delta(t) = \frac{d}{dt}\Theta(t)$ that $\frac{d}{dt}(\Theta(t)f(t)) = \delta(t)f(0) + \Theta(t)\frac{d}{dt}f(t)$, and further properties are outlined in the Appendix.

14.9 Conclusions

We developed a Montroll–Weiss CTRW model for space fractional walks subordinated to a generalization of Laskin’s fractional Poisson process; i.e., the fractional (long-range) jumps are performed with waiting time PDF according to a ‘generalized fractional Poisson process’ (GFPP). We obtained a space–time fractional diffusion equation by defining a ‘well-scaled’ diffusion limit in the infinite d -dimensional integer lattice \mathbb{Z}^d with a combined rescaling of space- and timescales. The index $\alpha > 0$ of the GFPP appears in this space–time fractional diffusion equation only as a scaling parameter. This diffusion equation is of the same type as for $\alpha = 1$ when the GFPP coincides with the pure Laskin’s fractional Poisson process and exhibits for $0 < \beta < 1$ non-Markovian features (long-time memory) and for $\beta = 1$ becomes a Markovian memoryless (Lévy flight) diffusion equation of standard Poisson.

The GFPP contains three parameters, two index parameters $0 < \beta \leq 1$ and $\alpha > 1$ and parameter ξ defining a timescale. For $\alpha = 1$ and $0 < \beta < 1$, the equations of Laskin’s fractional Poisson process, and for $\alpha = 1, \beta = 1$, the classical equations of the standard Poisson process are recovered, respectively. Some of the discussed results were obtained in recent papers [17, 18]. Generalizations of fractional diffusion as analyzed in the present paper are interesting models for a better understanding of the stochastic dynamics in complex systems. Since these models offer more parameters, they are susceptible to be adopted to describe real-world situations.

Appendix: Laplace Transforms and Fractional Operators

Here, we derive briefly some basic mathematical apparatus used in the paper in the context of causal functions and distributions involving fractional operators and Heaviside calculus. All functions and distributions considered are to be conceived as generalized functions and distributions in the Gelfand–Shilov sense [23]. Let us first introduce the Heaviside step function

$$\Theta(t) = \begin{cases} 1, & t \geq 0 \\ 0, & t < 0. \end{cases} \tag{14.80}$$

A function is causal if it has the form $\Theta(t)f(t)$, i.e., is null for $t < 0$ and nonvanishing only for nonnegative times t . We introduce the Laplace transform of $\Theta(t)f(t)$ by

$$\tilde{f}(s) = \mathcal{L}(f(t)) = \int_{-\infty}^{\infty} e^{-st} \Theta(t) f(t) dt = \int_0^{\infty} f(t) e^{-st} dt, \quad s = \sigma + i\omega \tag{14.81}$$

with suitably chosen $\sigma > \sigma_0$ in order to guarantee convergence of (14.81). In view of the fact that (14.81) can be read as Fourier transform of the causal function $e^{-\sigma t} f(t)\Theta(t)$, it is straightforward to see that the Laplace inversion corresponds to

the representation of this function as Fourier integral, namely

$$e^{-\sigma t} f(t)\Theta(t) = \frac{1}{2\pi} \int_{-\infty}^{\infty} e^{i\omega t} \tilde{f}(\sigma + i\omega) d\omega \tag{14.82}$$

which can be rewritten as

$$f(t)\Theta(t) = \frac{e^{\sigma t}}{2\pi} \int_{-\infty}^{\infty} e^{i\omega t} \tilde{f}(\sigma + i\omega) d\omega = \frac{1}{2\pi i} \int_{-i\infty}^{+i\infty} e^{st} \tilde{f}(s) ds. \tag{14.83}$$

Sometimes when there is no time derivative involved, we skip the Heaviside $\Theta(t)$ -function implying that all expressions are written for $t \geq 0$. Then, we mention that

$$\Theta(t)f(t) = \int_{-\infty}^{\infty} \delta(t - \tau)\Theta(\tau)f(\tau)d\tau \tag{14.84}$$

and introduce the shift operator $e^{-\tau \frac{d}{dt}}$ acting on a function $g(t)$ as $e^{-\tau \frac{d}{dt}} g(t) = g(t - \tau)$ thus

$$e^{-\tau \frac{d}{dt}} \delta(t) = \delta(t - \tau). \tag{14.85}$$

Substituting this relation into (14.84) yields

$$\Theta(t)f(t) = \left\{ \int_{-\infty}^{\infty} e^{-\tau \frac{d}{dt}} \Theta(\tau)f(\tau)d\tau \right\} \delta(t) = \mathcal{L}^{-1}\{\tilde{f}(s)\} = \tilde{f}\left(\frac{d}{dt}\right) \delta(t) \tag{14.86}$$

where the operator $\tilde{f}\left(\frac{d}{dt}\right)$ is related with the Laplace transform (14.81) by replacing $s \rightarrow \frac{d}{dt}$. Equation (14.86) is the operator representation of the causal function $\Theta(t)f(t)$. A convolution of two causal functions $\Theta(t)f(t)$, $g(t)\Theta(t)$ then can be represented by

$$\begin{aligned} & \int_0^t g(t - \tau)f(\tau)d\tau \\ &= \int_{-\infty}^{\infty} \int_{-\infty}^{\infty} \delta(t - \tau_1 - \tau_2)g(\tau_1)\Theta(\tau_1)f(\tau_2)\Theta(\tau_2)d\tau_1d\tau_2, \quad t > 0 \\ & \left(\int_{-\infty}^{\infty} e^{-\tau_1 \frac{d}{dt}} \Theta(\tau_1)f(\tau_1)d\tau_1 \right) \left(\int_{-\infty}^{\infty} e^{-\tau_2 \frac{d}{dt}} \Theta(\tau_2)f(\tau_2)d\tau_2 \right) \delta(t) \\ &= \mathcal{L}^{-1}\{\tilde{g}(s)\tilde{f}(s)\} = \tilde{f}\left(\frac{d}{dt}\right)\tilde{g}\left(\frac{d}{dt}\right) \delta(t) = \tilde{g}\left(\frac{d}{dt}\right)\tilde{f}\left(\frac{d}{dt}\right) \delta(t) \end{aligned} \tag{14.87}$$

where it has been used $\delta(t - \tau_1 - \tau_2) = e^{-(\tau_1+\tau_2) \frac{d}{dt}} \delta(t)$. We observe that in (14.86) and (14.87), the Laplace variable is replaced $s \rightarrow \frac{d}{dt}$ in the causal time domain. By considering $\tilde{f}(t)\Theta(t) = f(t)\Theta(t)e^{-\lambda t}$, we observe that

$$f(t)\Theta(t)e^{-\lambda t} = \left\{ \int_{-\infty}^{\infty} e^{-\tau(\lambda + \frac{d}{dt})} f(\tau)\Theta(\tau)d\tau \right\} \delta(t) = \tilde{f}\left(\lambda + \frac{d}{dt}\right)\delta(t) \quad (14.88)$$

where $\tilde{f}(s) = \mathcal{L}\{f(t)\}$. We are especially dealing with normalized (probability) distributions

$$\tilde{f}(s = 0) = 1 = \int_{-\infty}^{\infty} \Theta(t)f(t)dt. \quad (14.89)$$

A very important consequence of relations (14.86) and (14.87) is that they can be used to solve differential equations and to determine causal Green’s functions. As a simple example, consider the trivial algebraic equation in the Laplace domain

$$(s + \xi) \frac{\xi}{(s + \xi)} = \xi, \quad \xi > 0 \quad (14.90)$$

takes with $\mathcal{L}^{-1}\{s + \xi\} = \frac{d}{dt} + \xi$ and $\mathcal{L}^{-1}\left\{\frac{\xi}{s + \xi}\right\} = \Theta(t)\xi e^{-\xi t}$ where on the right-hand side is used that $\mathcal{L}^{-1}\{1\} = \delta(t)$. In the causal time domain (14.90) then gives the representation

$$\left(\frac{d}{dt} + \xi\right) (\xi\Theta(t)e^{-\xi t}) = \xi\delta(t), \quad (14.91)$$

result which is straightforwardly confirmed, i.e., the normalized causal Green’s function of $\frac{d}{dt} + \xi$ is directly obtained as $(\frac{d}{dt} + \xi)^{-1}\xi\delta(t) = \Theta(t)\xi e^{-\xi t}$ where it is important that the $\Theta(t)$ -function is taken into account in the Laplace inversion.

A less trivial example is obtained when considering fractional powers of operators. For instance, let us consider in the Laplace domain the equation

$$(s^\beta + \xi) \frac{\xi}{(s^\beta + \xi)} = \xi, \quad \xi > 0, \quad 0 < \beta \leq 1 \quad (14.92)$$

which writes in the time domain

$$\left\{ \left(\frac{d}{dt}\right)^\beta + \xi \right\} \Theta(t)g_{\beta,\xi}(t) = \xi\delta(t) \quad (14.93)$$

where the fractional derivative $(\frac{d}{dt})^\beta$ is determined subsequently. The causal Green’s function $\Theta(t)g_{\beta,\xi}(t)$ is obtained from the Laplace inversion

$$g_{\beta,\xi}(t) = \mathcal{L}^{-1}\left\{\frac{\xi}{s^\beta + \xi}\right\}. \quad (14.94)$$

The inversion is performed directly when taking into account

$$\frac{\xi}{(s^\beta + \xi)} = s^{-\beta} \frac{\xi}{(1 + \xi s^{-\beta})} = \xi \sum_{n=0}^{\infty} (-1)^n \xi^n s^{-\beta(n+1)}, \quad \sigma = \Re\{s\} > \xi^{\frac{1}{\beta}} \quad (14.95)$$

where $\sigma = \Re\{s\} > \xi^{\frac{1}{\beta}}$ guarantees convergence of this geometric series $\forall \omega = \Im\{s\}$, i.e., for the entire interval of integration of the corresponding Laplace inversion integral (14.88). On the other hand, we have

$$s^{-\mu} = \mathcal{L}\left\{ \Theta(t) \frac{t^{\mu-1}}{\Gamma(\mu)} \right\}, \quad \mu > 0, \quad \sigma > 0, \quad (14.96)$$

where we use the notation $\Gamma(\xi + 1) = \xi!$ for the gamma function. We then arrive at

$$\begin{aligned} \Theta(t)g_{\beta,\xi}(t) &= \mathcal{L}^{-1}\left\{ \frac{\xi}{\xi + s^\beta} \right\} \\ &= \sum_{n=0}^{\infty} (-1)^n \xi^{n+1} \mathcal{L}^{-1}\{s^{-\beta(n+1)}\} = \Theta(t) \sum_{n=0}^{\infty} (-1)^n \xi^{n+1} \frac{t^{n\beta+\beta-1}}{\Gamma(n\beta + \beta)} \end{aligned} \quad (14.97)$$

with

$$g_{\beta,\xi}(t) = \xi t^{\beta-1} \sum_{n=0}^{\infty} \frac{(-\xi t^\beta)^n}{\Gamma(n\beta + \beta)} = \xi t^{\beta-1} E_{\beta,\beta}(-\xi t^\beta). \quad (14.98)$$

Here, we have introduced the generalized Mittag-Leffler function, e.g., [4, 30, 44]

$$E_{\beta,\gamma}(z) = \sum_{n=0}^{\infty} \frac{z^n}{\Gamma(\beta n + \gamma)}, \quad \beta, \gamma > 0, \quad z \in \mathbb{C} \quad (14.99)$$

It follows that ξ is a dimensional constant having units $\text{sec}^{-\beta}$ so that (14.98) has physical dimension of sec^{-1} of a density. The result (14.98) also is referred to as *Mittag-Leffler density* and represents the waiting time density of Eq. (14.26) of the fractional Poisson renewal process introduced by Laskin [14]. Generally, Mittag-Leffler type functions play a major role in time fractional dynamics. We further often use the Mittag-Leffler function which is defined as, e.g., [4, 30, 44]

$$E_\beta(z) = \sum_{n=0}^{\infty} \frac{z^n}{\Gamma(\beta n + 1)}, \quad \beta > 0, \quad z \in \mathbb{C} \quad (14.100)$$

where with (14.99) we have $E_\beta(z) = E_{\beta,1}(z)$. The Mittag-Leffler function has the important property that for $\beta = 1$ it recovers the exponential $E_1(z) = e^z$.

Riemann–Liouville fractional integral and derivative

Now let us derive the kernel of the fractional power of time-derivative operator of Eq. (14.93) where we consider now exponents $\gamma > 0$. This kernel is then obtained with above-introduced methods in the following short way

$$\begin{aligned}
 \mathcal{L}^{-1}\{s^\gamma\} &= \mathcal{L}^{-1}\{s^{[\gamma]}s^{\gamma-[\gamma]}\} = e^{\sigma t} \left(\sigma + \frac{d}{dt}\right)^{[\gamma]} \left(\sigma + \frac{d}{dt}\right)^{\gamma-[\gamma]} \delta(t) \\
 &= e^{\sigma t} \left(\sigma + \frac{d}{dt}\right)^{[\gamma]} \int_{-\infty}^{\infty} \frac{d\omega}{(2\pi)} e^{i\omega t} (\sigma + i\omega)^{\gamma-[\gamma]} \\
 &= e^{\sigma t} \left(\sigma + \frac{d}{dt}\right)^{[\gamma]} \left\{ e^{-\sigma t} \Theta(t) \frac{t^{[\gamma]-\gamma-1}}{([\gamma] - \gamma - 1)!} \right\} = \frac{d^{[\gamma]}}{dt^{[\gamma]}} \left(\Theta(t) \frac{t^{[\gamma]-\gamma-1}}{\Gamma([\gamma] - \gamma)} \right).
 \end{aligned}
 \tag{14.101}$$

with $\gamma > 0, \gamma \notin \mathbb{N}$. Here, we introduced the *ceiling function* $[\gamma]$ indicating the smallest integer greater or equal to γ . In this way, the Fourier integral in the second line is integrable around $\omega = 0 \forall \sigma \geq 0$ since $\gamma - [\gamma] > -1$. We then obtain for the Laplace inversion

$$\mathcal{L}^{-1}\{s^{-\gamma}\} = \Theta(t) \frac{t^{\gamma-1}}{\Gamma(\gamma)}, \quad \gamma > 0
 \tag{14.102}$$

as a fractional generalization of integration operator. This kernel indeed can be identified with the kernel of the *Riemann–Liouville fractional integral* operator of order γ [45–47] which recovers for $\gamma \in \mathbb{N}$ the multiple integer-order integrations.

On the other hand, the kernel (14.101) with explicit representation in (14.101)₃ can be conceived as the ‘fractional derivative’ operator $(\frac{d}{dt})^\gamma$. The fractional derivative acts on causal functions $\Theta(t)f(t)$ as

$$\begin{aligned}
 \mathcal{L}^{-1}\{s^\gamma\} \cdot f(t)\Theta(t) &=: {}_0D_t^\gamma f(t) = \frac{d^{[\gamma]}}{dt^{[\gamma]}} \int_{-\infty}^{\infty} \left\{ \Theta(t - \tau) \frac{(t - \tau)^{[\gamma]-\gamma-1}}{\Gamma([\gamma] - \gamma)} \right\} f(\tau)\Theta(\tau)d\tau, \\
 {}_0D_t^\gamma f(t) &= \frac{1}{\Gamma([\gamma] - \gamma)} \frac{d^{[\gamma]}}{dt^{[\gamma]}} \int_0^t (t - \tau)^{[\gamma]-\gamma-1} f(\tau)d\tau.
 \end{aligned}
 \tag{14.103}$$

with $\gamma > 0$. We identify in the last line this operator with the *Riemann–Liouville fractional derivative* [45–47] which recovers for $\gamma \in \mathbb{N}$ integer-order standard derivatives. We emphasize that (14.101) requires causality, i.e., a distribution of the form $f(t)\Theta(t)$; thus, the Laplace transform captures the entire nonzero contributions of the causal distribution. In the diffusion equation (14.72), the Riemann–Liouville fractional derivative is of order $0 < \beta < 1$ with $[\beta] = 1$. In this case (14.103) then has representation

$${}_0D_t^\beta f(t) = \frac{1}{\Gamma(1 - \beta)} \frac{d}{dt} \int_0^t (t - \tau)^{-\beta} f(\tau)d\tau, \quad 0 < \beta < 1, \quad t > 0.
 \tag{14.104}$$

References

1. Zaslavsky, G.M.: Chaos, fractional kinetics, and anomalous transport. *Phys. Rep.* **371**(6), 461–580 (2002)
2. Shlesinger, M.: Origins and applications of the Montroll-Weiss continuous time random walk. *Eur. Phys. J. B* **90**, 93 (2017)
3. Saichev, A.I., Zaslavsky, G.M.: Fractional kinetic equations: solutions and applications. *Chaos* **7**, 753–764 (1997)
4. Gorenflo, R., Abdel Rehim, E.A.A.: From power laws to fractional diffusion: the direct way. *Vietnam J. Math.* **32**(SI), 65–75 (2004)
5. Metzler, R., Klafter, J.: The random walk's guide to anomalous diffusion: a fractional dynamics approach. *Phys. Rep.* **339**, 1–77 (2000)
6. Metzler, R., Klafter, J.: The restaurant at the end of the random walk: recent developments in the description of anomalous transport by fractional dynamics. *J. Phys. A: Math. Gen.* **37**, R161–R208 (2004)
7. Barkai, E., Metzler, R., Klafter, J.: From continuous time random walks to the fractional Fokker-Planck equation. *Phys. Rev. E* **61**(1) (2000)
8. Michelitsch, T., Riascos, A.P., Collet, B.A., Nowakowski, A., Nicolleau, F.: *Fractional Dynamics on Networks and Lattices*. Wiley, United States (2019)
9. Masuda, N., Porter, M.A., Lambiotte, R.: Random walks and diffusion on networks. *Phys. Rep.* **716–717**, 1–58 (2017)
10. Riascos, A.P., Wang-Michelitsch, J., Michelitsch, T.M.: Aging in transport processes on networks with stochastic cumulative damage. *Phys. Rev. E* **100**, 022312 (2019)
11. Polya, G.: Über eine Aufgabe der Wahrscheinlichkeitsrechnung betreffend die Irrfahrt im Strassennetz. *Math. Ann.* **83**, 149–160 (1921)
12. Noh, J.D., Rieger, H.: Random walks on complex networks. *Phys. Rev. Lett.* **92**(11) (2004)
13. Repin, O.N., Saichev, A.I.: Fractional Poisson law. *Radiophys. Quantum Electron.* **43**, 738–741 (2000)
14. Laskin, N.: Fractional Poisson process. *Commun. Nonlinear Sci. Numer. Simul.* **8**(3–4), 201–213 (2003)
15. Laskin, N.: Some applications of the fractional Poisson probability distribution. *J. Math. Phys.* **50**, 113513 (2009)
16. Cahoy, D.O., Polito, F.: Renewal processes based on generalized Mittag-Leffler waiting times. *Commun. Nonlinear Sci. Numer. Simul.* **18**(3), 639–650 (2013)
17. Michelitsch, T., Riascos, A.P.: Continuous time random walk and diffusion with generalized fractional Poisson process. *Physica A* (in press). <https://doi.org/10.1016/j.physa.2019.123294>. Preprint: [arXiv:1907.03830v2](https://arxiv.org/abs/1907.03830v2) [cond-mat.stat-mech]
18. Michelitsch, T.M., Riascos, A.P.: Generalized fractional Poisson process and related stochastic dynamics (submitted for publication). Preprint: [arXiv:1906.09704](https://arxiv.org/abs/1906.09704) [cond-mat.stat-mech]
19. Montroll, E.W., Weiss, G.H.: Random walks on lattices II. *J. Math. Phys.* **6**(2), 167–181 (1965)
20. Mainardi, F., Gorenflo, R., Scalas, E.: A fractional generalization of the Poisson processes. *Vietnam J. Math.* **32**, 53–64 (2004). MR2120631
21. Scher, H., Lax, M.: Stochastic transport in a disordered solid. I. Theory. *Phys. Rev. B* **7**, 4491 (1973)
22. Kutner, R., Masoliver, J.: The continuous time random walk, still trendy: fifty-year history, state of art and outlook. *Eur. Phys. J. B* **90**, 50 (2017)
23. Gelfand, I.M., Shilov, G.E.: *Generalized Functions*, vols. I–III. Academic Press, New York (1968) (reprinted by the AMS, 2016)
24. Feller, W.: *An Introduction to Probability Theory and its Applications*, vol. I, 3rd edn. Wiley, New York (1968)
25. Beghin, L., Orsingher, E.: Fractional Poisson processes and related random motions. *Electron. J. Probab.* **14**(61), 1790–1826 (2009)
26. Hilfer, R., Anton, L.: Fractional master equation and fractal time random walks. *Phys. Rev. E* **51**, R848–R851 (1995)

27. Prabhakar, T.R.: A singular integral equation with a generalized Mittag-Leffler function in the kernel. *Yokohama Math. J.* **19**, 7–15 (1971)
28. Mathai, A.M.: Some properties of Mittag-Leffler functions and matrix variant analogues: a statistical perspective. *Fract. Calc. Appl. Anal.* **13**(2) (2010)
29. Shukla, A.K., Prajapati, J.C.: On a generalization of Mittag-Leffler function and its properties. *J. Math. Anal. Appl.* **336**, 797–811 (2007)
30. Haubold, H.J., Mathai, A.M., Saxena, R.K.: Mittag-Leffler functions and their applications. *J. Appl. Math.* **2011**(298628), 51 (2011)
31. Gara, R., Garrappa, R.: The Prabhakar or three parameter Mittag-Leffler function: theory and application. *Commun. Nonlinear Sci. Numer. Simul.* **56**, 314–329 (2018)
32. Garra, R., Gorenflo, R., Polito, F., Tomovski, Z.: Hilfer-Prabhakar derivatives and some applications. *Appl. Math. Comput.* **242**, 576–589 (2014)
33. Gorenflo, R., Mainardi, F.: The asymptotic universality of the Mittag-Leffler waiting time law in continuous time random walks. In: *Invited Lecture at the 373. WE-Heraeus-Seminar on Anomalous Transport: Experimental Results and Theoretical Challenges*, Physikzentrum Bad-Honnef (Germany), 12–16 July 2006
34. Riascos, A.P., Michelitsch, T.M., Collet, B.A., Nowakowski, A.F., Nicolleau, F.C.G.A.: Random walks with long-range steps generated by functions of Laplacian matrices. *J. Stat. Mech. Stat. Mech.* **2018**, 043404 (2018)
35. Cox, D.R.: *Renewal Theory*, 2nd edn. Methuen, London (1967)
36. Riascos, A.P., Mateos, J.L.: Fractional dynamics on networks: emergence of anomalous diffusion and Lévy flights. *Phys. Rev. E* **90**, 032809 (2014)
37. Riascos, A.P., Mateos, J.L.: Fractional diffusion on circulant networks: emergence of a dynamical small world. *J. Stat. Mech.* **2015**, P07015 (2015)
38. Michelitsch, T.M., Collet, B.A., Riascos, A.P., Nowakowski, A.F., Nicolleau, F.C.G.A.: On recurrence of random walks with long-range steps generated by fractional Laplacian matrices on regular networks and simple cubic lattices. *J. Phys. A: Math. Theor.* **50**, 505004 (2017)
39. Michelitsch, T., Collet, B., Riascos, A.P., Nowakowski, A., Nicolleau, F.: On recurrence and transience of fractional random walks in lattices. In: *Altenbach, H., Pouget, J., Rousseau, M., Collet, B., Michelitsch, T. (eds.) Generalized Models and Non-classical Approaches in Complex Materials*, vol. 1, pp. 555–580. Springer, Cham (2018)
40. Michelitsch, T.M., Collet, B.A., Nowakowski, A.F., Nicolleau, F.C.G.A.: Fractional Laplacian matrix on the finite periodic linear chain and its periodic Riesz fractional derivative continuum limit. *J. Phys. A: Math. Theor.* **48**, 295202 (2015)
41. Gorenflo, R.: Mittag-Leffler Waiting Time, Power Laws, Rarefaction, Continuous Time Random Walk, Diffusion Limit. [arXiv:1004.4413](https://arxiv.org/abs/1004.4413) [math.PR] (2010)
42. Riascos, A.P., Mateos, J.L.: Long-range navigation on complex networks using Lévy random walks. *Phys. Rev. E* **86**, 056110 (2012)
43. Michelitsch, T.M., Collet, B.A., Riascos, A.P., Nowakowski, A.F., Nicolleau, F.C.G.A.: Fractional random walk lattice dynamics. *Phys. A: Math. Theor.* **50**, 055003 (2017)
44. Gorenflo, R., Kilbas, A.A., Mainardi, F., Rogosin, S.V.: *Mittag-Leffler Functions, Related Topics and Applications*. Springer, New York (2014)
45. Oldham, K.B., Spanier, J.: *The Fractional Calculus*. Academic Press, New York (1974)
46. Miller, K.S., Ross, B.: *An Introduction to the Fractional Calculus and Fractional Differential Equations*. Wiley, New York (1993)
47. Samko, S.G., Kilbas, A.A., Marichev, O.I.: *Fractional Integrals and Derivatives: Theory and Applications*. Gordon and Breach Science Publishers, Switzerland (1993)

Chapter 15

Analytical Method for Describing the Dynamics of Mechanical Systems in Variable Time Intervals



Andrey N. Morozov and Andrey L. Nazolin

Abstract Within the framework of the linear model of the fluctuating time interval, there has been developed an analytical method for the statistical description of the dynamics of mechanical systems in variable time intervals of passing the fixed coordinates by the systems' elements. We obtained the linear relations between the displacement variations and variations of time intervals for rotational, vibrational, and reciprocating motion in different coordinate systems. We also analytically assessed the influence of the type of motion and coordinates of fixed positions on the variations of time intervals. The research shows the possibility of restoring the true values of the displacement variations from the variations of the current oscillation period by multiplying each period variation value by the appropriate scale factor, which takes into account the coordinate of the fixed angular position. We found the system correlation functions and the frequency characteristics of transformations of the displacement variations in variations of the time intervals. On their basis, we analyzed the transformation features in the time and frequency domains. The advantages and disadvantages of measuring the current period, the current time interval and the current time for the experimental study of the dynamics of mechanical systems are determined. The study shows that the scope of linear relations depends on the type of motion and the choice of coordinates of the fixed positions and is limited to the level of relative variations of the period of no more than 10%.

Keywords Mechanical system · Fixed coordinate · Displacement fluctuations · Time interval fluctuations

A. N. Morozov (✉) · A. L. Nazolin
Bauman Moscow State Technical University, Moscow, Russian Federation

A. L. Nazolin
Mechanical Engineering Research Institute of the Russian Academy of Sciences,
Moscow, Russian Federation

15.1 Introduction

In the steady operating conditions, most of the mechanical systems of cyclic action, hereinafter referred to as mechanical systems (MS), perform rotational or quasi-periodic oscillatory motions close to uniform. The cyclical motion is manifested in the fact that after a certain constant time T , called a period, all the details of the ideal mechanical systems return to their original position.

Projected on the fixed axes of Cartesian coordinate system, the law of motion $x(t)$ of links of non-ideal mechanical systems satisfies the inequality [1–3].

$$|x(t) - x(t + T)| \leq \varepsilon, \quad (15.1)$$

where T and ε are constant values. The smallest number T satisfying the condition (15.1) is called the period.

The traditional description of the MS dynamics consists of compiling the differential equations of motion and obtaining their solutions in the form of the dependence of the current displacement x , describing the state of the system, on time t . With time discretization of the continuous law of motion $x(t)$, the flow of time is assumed to be uniform, and the time intervals Δt between successive moments of determining the displacement value are assumed to be constant (Fig. 15.1a). Such a discrete model provides a fairly sufficient description of the MS dynamics in the case if the sampling frequency satisfies the sampling theorem [4] and does not take into account the errors of real-time measurement, i.e., when approaching time as a purely geometric parameter.

The principal feature of describing the MS dynamics in variable time intervals of passing the fixed angular or linear positions, i.e., coordinates, by the systems' elements is the need to find the time points t , corresponding to certain discrete values of the displacement x_n , i.e., obtaining the dependence (Fig. 15.1b). In this case, the

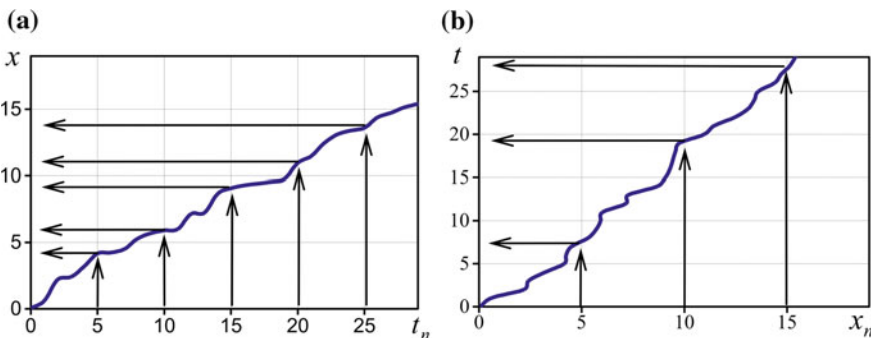


Fig. 15.1 Displacement dependence x on discrete time t_n (a) and dependence of time points t on discrete displacement x_n (b)

discretization of information retrieval is carried out by moving the elements of the MS itself.

From discrete values $t_n = t(x_n)$, it is possible to form various sequences of values of time intervals of the form

$$\tau_n = t_n - t_{n-k}, \quad n = 1, 2, \dots, k < n, \quad (15.2)$$

and their variations

$$\delta\tau_n = \tau_n - \tau_0, \quad (15.3)$$

where τ_0 is the mean value of time intervals, t_n are the time points, corresponding to the passage of coordinates of the fixed positions x_n .

In practice, the coordinate discretization interval depends on the measurement design and, in general, is non-uniform. The restrictions imposed by the sampling theorem on the discrete analogue of the continuous process $t(x)$ remain valid and determine the required number of discrete coordinates of the fixed positions to reconstruct the spectrum of the continuous process. So, if the upper frequency of the studied frequency range or the highest expected frequency of oscillations is N -fold higher than the frequency of rotation or oscillation, then the number of discrete positions should be no less than $2N$. Otherwise, part of the information contained in the high frequency part of the spectrum will be lost, and part of the spectrum will be distorted by the components due to the effect of frequency overlap [4].

Relations (15.2) and (15.3) are fundamental for studying the MS dynamics by the method of time intervals. To apply them in practice, it is necessary to study the features of transforming displacement fluctuations into fluctuations of time intervals with various types of motion and methods of recording. This paper is devoted to solving the problem of the analytical description of the MS dynamics in variable time intervals within the linear model of the fluctuating time interval.

15.2 Problem of Analytical Description of the Dynamics of Mechanical Systems in Variable Time Intervals

In an explicit form, the continuous law of motion $t(x)$ can only be obtained from the differential equation of free vibrations of a conservative system with one degree of freedom [5]

$$m\ddot{x} + F(x) = 0, \quad (15.4)$$

$$t(x) = \int_0^x \frac{dx}{\pm \sqrt{\frac{2}{m} \left[C - \int_0^x F(x) dx \right]}}, \quad (15.5)$$

where $F(x)$ is the quasi-elastic characteristic in the form of a smooth, piecewise smooth, or piecewise linear restoring force. In the case of a symmetric restoring force, the period of free oscillations is calculated by the formula

$$T = 2\sqrt{2m} \int_0^A \left[\int_0^A F(x) dx \right]^{-1/2} dx, \quad (15.6)$$

where A is the oscillation amplitude. The formula (15.6), in particular, implies an important property of the non-isochronism of nonlinear systems, expressed in the dependence of the period of free oscillations on the amplitude.

For linear systems $F(x) = p^2x$, the calculation by the formula (15.6) gives a well-known solution $T = 2\pi/p$. For nonlinear systems, calculations using the formula (15.6) are difficult and the result cannot be represented in the final form through elementary functions. Despite the fact that the formula (15.5) is fundamentally accurate, in practical applications it requires cumbersome calculations, usually not feasible in closed form. Therefore, various methods of approximate solutions of nonlinear differential equations of motion in the form $x(t)$ are used.

It is known from the theory of oscillations that in autonomous conservative, auto-oscillating systems, as well as non-autonomous conservative and dissipative systems, under the influence of a periodic perturbing force, strictly periodic motion modes are implemented, for which at any time point t the following relation is fulfilled.

$$x(t + T) = x(t). \quad (15.7)$$

The description of the dynamics of such idealized mechanical systems in variations of a period, for example, does not make sense, since $T = \text{const}$.

In mechanical engineering, idealized dynamic models of MS that describe periodic motion modes, where the period T is a constant, are most prevalent. Such models are based on the assumption of the existence of ideal constraints and that the kinematic chain of an ideal mechanism is always closed, i.e., the movement of all points of the mechanism is always reversible. To simplify the calculations, dynamic replacement schemes for machines and mechanisms are attempted to bring to a system with one degree of freedom, less often with two or a finite number of degrees of freedom. Possible deviations from periodicity are usually neglected, which greatly simplifies the obtaining of analytical solutions of the equations of motion, and, in particular, it makes it possible to find closed solutions to the problem of the action of an arbitrary periodic force.

Ideal models have proven themselves to be good in solving practical problems of mechanical engineering. They make it possible to explore the dynamic stability and are the basis for strength calculations, and in the first approximation, they describe the dynamics of real systems in good condition and are used to determine the norms for the output motion parameters, including kinematic ones.

Real machines and mechanisms differ from idealized models in more diverse properties. Due to defects in fabrication and installation, wear, gaps and slippage, the number of degrees of freedom of the system increases, the closure condition of the kinematic scheme is not observed—the positions occupied by the elements at some time point are never repeated again, and the movement is irreversible. In addition, there are always perturbing forces that depend on the structural and operating parameters of the machine, which excite oscillations of its elements at different frequencies, including those that are not multiple of the fundamental frequency of rotation or oscillation. All this excludes the possibility of an ideal periodicity. Therefore, in practice, one always has to deal with quasi-periodic processes, for which the condition of periodicity (15.7) is satisfied approximately (15.1).

Quasi-periodic processes are much more diverse than periodic ones. An example of deterministic quasi-periodic processes is damped oscillations

$$x(t) = Ae^{-\beta t} \cos(\omega t + \varphi_0), \quad (15.8)$$

with a sufficiently small β . Here, A , β , and ω , φ_0 are constant values, $T = 2\pi/\omega$. Another example is the sum of two or several oscillations with incommensurable frequencies

$$x(t) = \cos(\omega_1 t) + \cos(\omega_2 t), \quad (15.9)$$

where ω_2/ω_1 is an irrational number, in general.

Stationary random oscillations, described by differential equations in which the coefficients and (or) free terms are random functions of time, are also quasi-periodic. An analogue of such equations in the classical theory does not exist. For them, a special theory of stochastic differential equations of K. Ito [6] type has been developed. When the solutions of these equations are Markov processes, there are effective methods for determining the finite dimensional distributions of the solution. For non-Markov processes such methods have not yet been found.

In the absence of an analytical description of the process of transforming linear and angular displacements into time intervals, it is not possible to find the law of motion $t(x)$ explicitly. Therefore, in practice, the solution is sought numerically. For example, period variations $\delta T(t)$ are calculated not from the solution of the differential equations of motion, where $\delta T(t)$ acts as a variable, but numerically from the solution of implicit equations of the form

$$x(t_n) = x(t_n + T_0 + \delta T_n), \quad (15.10)$$

where T_0 is a mean period and δT_n are variations (fluctuations) of the period at time points t_n obtained by displacement coordinates $x(t_n) = x_n$. In this case, it is necessary to take into account the features arising from the use of the formula (15.10) both in calculations and measurements of the period variations.

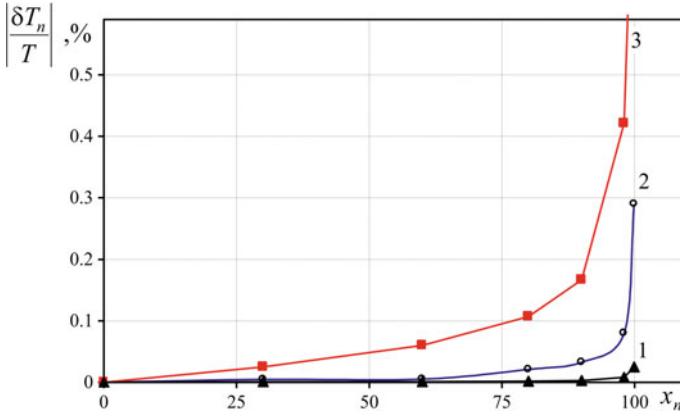


Fig. 15.2 Dependence of the period deviation δT_n of the oscillatory process (15.8) on the coordinates of the fixed positions x_n . Here, $A = 100$, $1 - \beta = 0.1$, $T = 0.001$; $2 - \beta = 0.1$, $T = 0.01$; $3 - \beta = 0.5$, $T = 0.01$

For example, from the graphs in Fig. 15.2, one can see that the period deviations δT_n calculated by the formula (15.10) for the case of the simplest quasi-harmonic oscillatory process of the form (15.8), depend not only on the parameters of the oscillatory process A , β , T but also on the coordinates of the fixed positions x_n . When these deviations are commensurate with variations in the time intervals of a real object, it is necessary to take into consideration the influence of the coordinates of the fixed positions.

The fundamentals of the analytical description of the dynamics of high-quality oscillatory systems in variations and fluctuations of the period were laid in the monograph by Morozov [7]. In this work, for the high-quality torque balance as a measuring system that implements the procedure for measuring period variations (15.10), an approximate analytical relation was obtained for the first time, which relates variations in the angle of torsion of the torque balance arm $\delta\varphi(t_n)$, caused by seismic and gravitational disturbances, with period variations

$$\delta T_n(t) = \frac{1}{\Omega_{0\beta} \sqrt{\varphi_0^2 - \varphi_n^2}} [\delta\varphi(t_n + T_{0\beta}) - \delta\varphi(t_n)], \tag{15.11}$$

where $T_{0\beta}$ is the period of free torsional oscillations of the balance, $\Omega_{0\beta} = 2\pi/T_{0\beta}$ is the frequency of free oscillations, which is much higher than the characteristic frequency of external influences, φ_0 is the initial angle of torsion of the balance arm, and t_n are time points, defined by angular coordinates of the fixed positions, i.e., $\varphi(t_n) = \varphi_n$.

15.3 Method of Time Intervals

The rotational and oscillatory motion of MS elements is traditionally described either in the polar coordinate system $\bar{r}(\varphi)$, associated with the axis of rotation, i.e., the origin of the coordinate system during oscillations, or in projections onto the fixed axes of coordinates:

$$x(t) = |\bar{r}(\varphi)| \sin \varphi(t), \tag{15.12}$$

where: $x(t)$ is the current projection displacement; $|\bar{r}(\varphi)|$, $\varphi(t)$ are the amplitude and phase of the cyclic motion, respectively.

The choice of the coordinate system is largely determined by the convenience of the mathematical description of the MS dynamics. Such a description in the general case includes a set of parameters on the left side of the differential equation, i.e., structural parameters of the system which determine the transfer function of the mechanical system, and the external influences on the right side of the equation, where $M(t)$ is the external moment, $F(t)$ is the external force. The influences determine the conditions and its operating conditions, and the law of control, if there is one. The dynamic analysis is carried out at given initial and boundary conditions. According to the formula (15.12), information about the MS dynamics is contained in the changes in the amplitude $|\bar{r}(\varphi)|$ and the phase $\varphi(t)$ of the law of motion $x(t)$, as well as in the inverse function $t(x)$ (Fig. 15.3).

The discrete process of receiving information about the time of passing the fixed positions by MS elements allows us to form different sequences of values of time intervals that form the basis of the time interval method.

We will distinguish the sequences that are obtained when implementing the procedures for measuring the following quantities:

1. The current period T_n in the polar and Cartesian coordinate systems, respectively:

$$T_n = t(\varphi_n) - t(\varphi_{n-N_0}), \tag{15.13}$$

$$x(t_n) = x(t_n - T_n), \tag{15.14}$$

where φ_n are the fixed angular positions of the MS element, $n = 1, 2, \dots$; N_0 is the number of the fixed positions in the cycle, and t_n is the moment of passing of the fixed position by the MS element x_n , $n = 1, 2, \dots, N_0$;

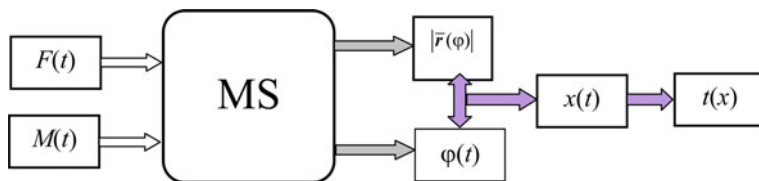


Fig. 15.3 Parameters that carry information about the dynamics of the mechanical system

2. The current time interval τ_n for the passage of the adjacent fixed positions in the polar and Cartesian coordinate systems, respectively:

$$\tau_n = t(\varphi_n) - t(\varphi_{n-1}), \quad (15.15)$$

$$\tau_n = t(x_n) - t(x_{n-1}). \quad (15.16)$$

3. The current time t_n for the passage of the fixed positions in the polar and Cartesian coordinate systems, respectively:

$$t_n = t(\varphi_n), \quad (15.17)$$

$$t_n = t(x_n). \quad (15.18)$$

The development of the analytical description of the MS dynamics in variable time intervals involves finding dependencies that uniquely associate variations of displacements with variations of time intervals. The construction of these dependencies will make it possible to determine the time and spectral windows for the transformation of displacement parameters into time intervals, to have the possibility of studying the MS dynamics by the method of time intervals.

15.4 Relationship of Time Intervals with the Angle of Rotation During Rotational Motion

Let us find the relationship between the time intervals T_n , τ_n and t_n with the angle of shaft rotation during rotational motion. Further, the index n , which corresponds to the passage of φ_n th angular position by the shaft, will not be indicated without disturbing the generality of reasoning.

Assuming the number of the fixed angular positions of the shaft to be equal and neglecting the error of the interval of their location, we write down the relationship between the mean period T_0 and the mean time of passing the neighboring positions τ_0 in the form

$$T_0 = N_0 \tau_0. \quad (15.19)$$

To determine the current period $T(t)$ of the shaft rotation, we use the following relation [8]:

$$2\pi = \int_{t-T(t)}^t \dot{\varphi}(\tau) d\tau, \quad (15.20)$$

where $\varphi(t)$ is the time dependence of the angle of shaft rotation. The solution of the integral relation (15.20) is sought within the linear model of the fluctuating time interval, considering that

$$T(t) = T_0 + \delta T(t), \quad (15.21)$$

$$|\delta T(t)| \ll T_0, \quad (15.22)$$

where $\delta T(t)$ is the period fluctuation.

Assuming that the shaft rotates according to the near-to-uniform law close, the equation of the shaft motion in the polar coordinate system is written in the form

$$\varphi(t) = \omega_0 t + \delta\varphi(t), \quad (15.23)$$

$$|\delta\varphi(t)| \ll 1, \quad (15.24)$$

where $\omega_0 = 2\pi/T_0$ is the mean angular frequency of shaft rotation; $\delta\varphi(t)$ are the small fluctuations of the angle of shaft rotation.

Further, unless otherwise specified, we will analyze the stochastic connectivity of the rotation angle with time intervals. Taking into account the assumptions made, the expression (15.20) in the first approximation takes the form

$$2\pi = \omega_0 T(t) + \int_{t-T_0}^t \delta\dot{\varphi}(\tau) d\tau. \quad (15.25)$$

Let us introduce the notation

$$\langle \delta\dot{\varphi}(t, T_0) \rangle = \frac{1}{T_0} \int_{t-T_0}^t \delta\dot{\varphi}(\tau) d\tau = \frac{1}{T_0} [\delta\varphi(t) - \delta\varphi(t - T_0)], \quad (15.26)$$

which is the mean velocity of fluctuations of the angle of shaft rotation of in the interval $[t - T_0, t]$.

The formula (15.25) makes it possible to write a linear relation connecting fluctuations of the current period $\delta T(t)$ with fluctuations of the angle $\delta\varphi(t)$:

$$\delta T(t) = -\frac{T_0}{2\pi} [\delta\varphi(t) - \delta\varphi(t - T_0)], \quad (15.27)$$

or, taking into account (15.26),

$$\frac{\delta T(t)}{T_0} = -\frac{\langle \delta\dot{\varphi}(t, T_0) \rangle}{\omega_0}. \quad (15.28)$$

Analysis of the expression (15.28) shows that within the linear model of the fluctuating time interval, the relative period fluctuations with an accuracy of the sign are equal to the ratio of the mean velocity of fluctuations of the angle of shaft rotation over the period T_0 to the mean angular frequency of its rotation. From (15.28), in particular, it follows that with rotational motion, the condition for the smallness of period fluctuations (15.22) is satisfied if

$$\left| \frac{\langle \delta \dot{\varphi}(t, T_0) \rangle}{\omega_0} \right| \ll 1. \quad (15.29)$$

The condition (15.29) clarifies (15.24), and as well as (15.22), it limits the scope of the linear relations (15.27) and (15.28).

After similar transformations, we obtain a relation connecting fluctuations of the current time interval for the passage of the adjacent fixed positions $\delta \tau(t)$ with angle fluctuations $\delta \varphi(t)$:

$$\delta \tau(t) = -\frac{T_0}{2\pi} [\delta \varphi(t) - \delta \varphi(t - \tau_0)]. \quad (15.30)$$

By analogy with the formula (15.23), we present the dependence of the current time on the angle of shaft rotation and fluctuations of the current time in the form

$$t(\varphi) = \frac{T_0}{2\pi} \varphi + \delta t(\varphi). \quad (15.31)$$

Simultaneously solving (15.23) and (15.31) and taking into account that $t = t(\varphi)$ and $\varphi = \varphi(t)$, we find the connection between fluctuations of the current time $\delta t(t)$ and fluctuations of the angle $\delta \varphi(t)$:

$$\delta t(t) = -\frac{T_0}{2\pi} \delta \varphi(t). \quad (15.32)$$

Note that the time t in formulas (15.27), (15.28), (15.30), and (15.32) is not arbitrary, but corresponds to the moments at which the shaft passes through the fixed angular positions φ_n .

The analysis of expressions (15.27) and (15.30) shows that fluctuations of the current period and time intervals contain information about the change in fluctuations of the angle of shaft rotation during the current time interval. This does not directly determine the current angle. Therefore, the restoration of the dependence $\varphi(t)$ after performing transformations (15.27) and (15.30) or according to the results of measurements of time intervals $T(t)$ and $\tau(t)$ is not possible.

Another situation occurs when measuring the current time and describing the MS dynamics in variations of the current time, calculated by the formula (15.32). Fluctuations of the current angle of rotation $\delta \varphi(t)$ and the current time $\delta t(t)$ are in antiphase, differing only in the scale factor $-T_0/(2\pi)$. In the case of small fluctuations of the angle of rotation, the linear single-valued relation (15.32) allows us to first

recover fluctuations of the angle of rotation $\delta\varphi(t)$ from fluctuations of the current time $\delta t(t)$ and then restore the dependence $\varphi(t)$ using the formula (15.23).

Despite the simplicity of the expression (15.32), its use in practice to restore the dependence (15.23) from the results of temporary measurements is fraught with a number of difficulties. This is both a non-uniform interval of the fixed angular coordinates and a non-uniform in time discretization interval of determining the angular positions of the shaft. The algorithm for recovering the dependence $\varphi(t)$ from measurements of time intervals $T(t)$, $\tau(t)$, and $\delta t(t)$ is presented in [9].

In this paper, we confine ourselves to considering the features of analytical description of the MS dynamics in fluctuations of the current period and time intervals. Despite certain shortcomings in the completeness of the description and study of the MS dynamics, this approach, as will be shown below, has in some cases advantages over the algorithm [9], since it is insensitive to the fixed coordinates interval error.

We study the spectral correlation characteristics of transformations of fluctuations of the angle of rotation into fluctuations of time intervals. Taking into account the similarity of relations (15.27) and (15.30), we first define the form of the spectral window transformation into fluctuations of the current period, and then, based on the obtained expression, we make a formula describing the spectral window of transformation in the fluctuations of the current time interval.

Let the expression (15.27) describe an ideal system with one input and one output, then the time window of the transformation can be represented as

$$h_{\delta T}(t) = -\frac{T_0}{2\pi} [\delta(t) - \delta(t - T_0)], \quad (15.33)$$

where $\delta(t)$ is the delta function. The system correlation function of transforming angle fluctuations into fluctuations of the current period takes the form

$$R_{h,\delta T}(\tau) = \int_{-\infty}^{\infty} h_{\delta T}(t) h_{\delta T}(t + \tau) dt = \frac{T_0^2}{(2\pi)^2} [2\delta(\tau) - \delta(\tau - T_0) - \delta(\tau + T_0)]. \quad (15.34)$$

In this case, the correlation functions of period fluctuations $R_{\delta T}(\tau)$ and angle fluctuations $R_{\delta\varphi}(\tau)$ will be related by the dependence

$$R_{\delta T}(\tau) = \int_{-\infty}^{\infty} R_{h,\delta T}(t) R_{\delta\varphi}(t + \tau) dt. \quad (15.35)$$

Applying the direct Fourier transform to the expression (15.34), we obtain the spectral window (Fig. 15.4) of transforming angle fluctuations into fluctuations of the current period

$$G_{h,\delta T}(\omega) = \frac{T_0^2}{\pi^2} \sin^2\left(\frac{\omega T_0}{2}\right). \quad (15.36)$$

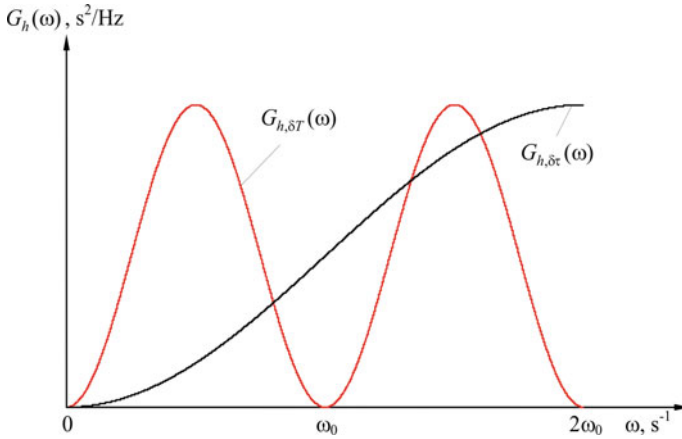


Fig. 15.4 Spectral window of transforming angle fluctuations into fluctuations of the current period $G_{h,\delta T}(\omega)$ and current time interval $G_{h,\delta\tau}(\omega)$ ($N_0 = 4$)

Similarly, the spectral window of transforming angle fluctuations into fluctuations of the current time interval has the form

$$G_{h,\delta\tau}(\omega) = \frac{T_0^2}{\pi^2} \sin^2\left(\frac{\omega\tau_0}{2}\right). \tag{15.37}$$

When applying formulas (15.36) and (15.37), it is necessary to take into account the relation (15.19). As follows from the expression (15.36), when the condition

$$\omega T_0 = 2\pi k, \tag{15.38}$$

where k is any integer, is met, the amplitude of period fluctuations tends to zero. This means that when measuring the current period, processes that have frequencies close to $\omega = 2\pi k/T_0$ are not recorded. In particular, when measuring the current period, there is no possibility of recording processes at frequencies that are integer multiples of the mean frequency of shaft rotation. Due to this circumstance, the accuracy of measurement of the current period does not depend on the location of the fixed angular positions, but is determined only by the accuracy of measurements of time intervals. Similarly, it follows from (15.37) that when measuring the current time interval for the passage of the adjacent fixed angular positions, the above limitations, related to the impossibility of describing processes at frequencies which are integer multiple of the mean rotation frequency, are shifted to a higher frequency domain and take the form

$$\omega T_0 = 2\pi k N_0. \tag{15.39}$$

The frequency extension leads to the fact that in current time intervals there is information both about the processes occurring in the MS and the interval error

of the fixed angular positions. Thus, the uneven arrangement of the fixed angular positions contributes to the intensity of the spectral lines at frequencies that are integer multiples of the mean rotation frequency. For this reason, when putting into practice the procedure of measuring time intervals for a MS moving element to pass the fixed angular positions, the problem of their precise task arises, which in most cases is rather complicated or completely unsolvable.

From expressions (15.36) and (15.37), we can conclude that the intensity of fluctuations of time intervals with the same fluctuations of the angle of rotation is determined by the term T_0^2/π^2 . Therefore, with an increase in the mean frequency of shaft rotation, more precise means of measuring time intervals are required for recording the same angle fluctuations.

15.5 Relationship of the Period with the Displacement During Oscillatory Motion

The above statistical description of fluctuations of time intervals during rotational motion cannot be directly transferred to the MS whose links make oscillatory movements. This is due to the fact that the speed of movement of the oscillatory links during the passage of various fixed positions changes significantly depending on the displacement from the equilibrium position. For this reason, the description of fluctuations of the oscillation period of devices such as a torque balance or clock mechanisms is associated with the problem of finding the instrument functions of transforming fluctuations of linear and angular displacements of oscillating links into fluctuations of the oscillation period.

In the most general formulation, we consider the problem of transforming fluctuations of the variable $x(t)$, which describes a linear displacement of a link performing rectilinear oscillations, from an equilibrium position in period fluctuations. The condition for determining the current oscillation period can be written as (15.14):

$$x(t) = x(t - T(t)), \quad (15.40)$$

where $T(t)$ is the current period of oscillation.

Assuming that oscillations occur according to a near-to-harmonic law, we write the equation of motion in Cartesian coordinate system in the form

$$x(t) = x_0 \sin(\omega_0 t + \alpha_0) + \delta x(t), \quad (15.41)$$

$$|\delta x(t)| \ll 1, \quad (15.42)$$

where x_0 is the oscillation amplitude; $\omega_0 = 2\pi/T_0$ is the mean angular frequency of oscillations; α_0 is the initial phase; $\delta x(t)$ are small fluctuations, i.e., variations, of the oscillation link displacement with zero expectation. In addition, we believe

that the velocity of fluctuations $\delta\dot{x}(t)$ is small compared to the velocity of harmonic oscillations

$$\left| \frac{\delta\dot{x}(t)}{x_0\omega_0 \cos(\omega_0 t + \alpha_0)} \right| \ll 1. \tag{15.43}$$

Under these conditions, the oscillation period can be represented within the linear model of the fluctuating time interval, i.e. in the form of (15.21) and (15.22). Then, the expression (15.40) in the first approximation can be represented as

$$x(t) = x(t - T_0) - \dot{x}(t - T_0) \delta T(t). \tag{15.44}$$

Solving simultaneously (15.41) and (15.44) and neglecting terms of a higher order of smallness, we obtain a relation connecting period fluctuations $\delta T(t)$ with fluctuations of displacement $\delta x(t)$ of the oscillatory link

$$\delta T(t) = -\frac{T_0}{2\pi} \frac{1}{\sqrt{x_0^2 - x_n^2}} (\delta x(t) - \delta x(t - T_0)) \tag{15.45}$$

or

$$\frac{\delta T(t)}{T_0} = -\frac{\langle \delta\dot{x}(t, T_0) \rangle}{\omega_0 \sqrt{x_0^2 - x_n^2}}, \tag{15.46}$$

where x_n are coordinates of the fixed positions in which time points $t_n = t(x_n)$ of passing the specified displacements are recorded, $\langle \delta\dot{x}(t, T_0) \rangle$ is the mean velocity of displacement fluctuations for the period T_0 calculated by the formula (15.26). In (15.46), it is taken into account that, under the condition (15.43), the velocity of the oscillatory link in the first approximation is

$$\dot{x}(t) = x_0\omega_0 \cos(\omega_0 t + \alpha) = \text{sign}(\dot{x}(t))\omega_0\sqrt{x_0^2 - x^2(t)}, \tag{15.47}$$

where

$$\text{sign}(A) = \begin{cases} 1, & \text{if } A > 0, \\ 0, & \text{if } A = 0, \\ -1, & \text{if } A < 0, \end{cases} \tag{15.48}$$

is the piecewise constant function of the argument A . Note that in (15.45) and (15.46), time points t are not arbitrary but correspond to the moments of passing the fixed positions x_n by the oscillatory link.

From the comparison of expressions (15.45) and (15.27), it follows that fluctuations of the period of oscillatory links depend on coordinates of the fixed positions. The scope of the expression (15.45) is substantially limited by conditions (15.42), (15.43) and the condition (15.22), which, as it can be seen from the expression (15.46), can be represented as

$$\left| \frac{\langle \delta \dot{x}(t, T_0) \rangle}{\omega_0 \sqrt{x_0^2 - x_n^2}} \right| \ll 1. \quad (15.49)$$

At the same time, the condition (15.43) is decisive, since its non-fulfillment leads to a change in the transformation function and calculation errors by the formula (15.45).

The description of fluctuations of the current time interval $\delta\tau(t)$ or fluctuations of the current time $\delta t(t)$ of passing the fixed positions by the oscillatory link is impossible within the linear model of the fluctuating time interval due to large changes in the motion speed. There is a need to use a nonlinear transformation with a time variable coefficient.

Performing similar transformations allows us to obtain a relation connecting the fluctuations of the period $\delta T(t)$ and the angle of rotation $\delta\varphi(t)$ for the link performing angular oscillations. For example, for the torque balance or the clockwork mechanism, in the polar coordinate system

$$\delta T(t) = -\frac{T_0}{2\pi} \frac{1}{\sqrt{\varphi_0^2 - \varphi_n^2}} (\delta\varphi(t) - \delta\varphi(t - T_0)), \quad (15.50)$$

where φ_0 is the amplitude of angular oscillations of the link; φ_n are the fixed position angular coordinates.

The expression (15.50) can be reduced to the form (15.27) by multiplying the values $\delta T(t)$ by a scale factor $\sqrt{\varphi_0^2 - \varphi_n^2}$. Moreover, each measured value $\delta T(t)$ should be scaled, taking into account the angular coordinate of the fixed position. Similarly, to bring (15.45) to the form (15.27), it is necessary to multiply the measurement results by a scale factor $\sqrt{x_0^2 - x_n^2}$. Note that the direct use of measured period fluctuations $\delta T(t)$ of the form (15.45) or (15.50) without performing the scaling described above causes certain difficulties in interpreting the data, due to the dependence $\delta T(t)$ on the linear, that is angular, coordinates of the fixed positions, and not on the MS dynamics.

In accordance with the method described above, the relation (15.45) allows us to obtain an expression for the spectral window of transforming displacement fluctuations into fluctuations of the current period of oscillations during translational motion of the MS link. In the first approximation, with $x_n \ll x_0$, up to a constant factor, it will coincide with the formula (15.36)

$$G_{h,\delta T}(\omega) = \frac{T_0^2}{\pi^2} \frac{1}{x_0^2 - x_n^2} \sin^2\left(\frac{\omega T_0}{2}\right). \quad (15.51)$$

Replacing the linear coordinate x with the angular coordinate φ in the formula (15.51) gives an expression for the spectral window of the current period in the case of angular oscillations of the MS link:

$$G_{h,\delta T}(\omega) = \frac{T_0^2}{\pi^2} \frac{1}{\varphi_0^2 - \varphi_n^2} \sin^2\left(\frac{\omega T_0}{2}\right). \quad (15.52)$$

Thus, in the study of fluctuations of the oscillation period, expressions (15.36) and (15.37) can be used for rotational motion. In this case, one only needs to enter the appropriate scale factor.

The equation of the form (15.41) also reduces the problem of transforming the fluctuations of the shaft point projection displacement, the shaft making a near uniform rotational motion, into period fluctuations. The projection displacement equation in Cartesian coordinate system takes the form of

$$x(t) = x_0 \sin(\omega_0 t + \alpha_0 + \delta\varphi(t)), \quad (15.53)$$

where $\delta\varphi(t)$ are small fluctuations of the angle of shaft rotation. Using the trigonometric formula, we represent the expression (15.53) in the form

$$x(t) = x_0 \sin(\omega_0 t + \alpha_0) \cos(\delta\varphi(t)) + x_0 \cos(\omega_0 t + \alpha_0) \sin(\delta\varphi(t)). \quad (15.54)$$

When the condition (15.24) is satisfied, as well as the smallness of the velocity of fluctuations of the angle $\delta\dot{\varphi}(t)$ compared with the mean angular frequency ω_0 , i.e.,

$$\left| \frac{\delta\dot{\varphi}(t)}{\omega_0} \right| \ll 1, \quad (15.55)$$

Equation (15.54) in the first approximation takes the form (15.41), and the displacement $\delta x(t)$ and the angle $\delta\varphi(t)$ fluctuations will be related by

$$\delta x(t) = \frac{\dot{x}(t)}{\omega_0} \delta\varphi(t), \quad (15.56)$$

where $\dot{x}(t)$ is the displacement velocity determined by the formula (15.47).

Using expressions (15.44) and (15.47), we obtain the relation connecting period fluctuations $\delta T(t)$ and projection displacement fluctuations $\delta x(t)$ of a point of the shaft making a rotational motion, in Cartesian coordinate system in the form (15.45).

Substitution of the formula (15.56) into the expression (15.45) allows the transition from Cartesian coordinate system to the polar one and to obtain the connection between fluctuations of the period $\delta T(t)$ and the angle of shaft rotation $\delta\varphi(t)$ in the form (15.27). However, it should be borne in mind that, unlike (15.27), the scope of the linear relation (15.45) and expression (15.56) is limited by the additional condition (15.55). As a result, the level of relative fluctuations of the current period, for which the linear relation (15.45) is satisfied, must be less than for the relation (15.27).

Thus, the instrument function of transforming displacement fluctuations into fluctuations of the current period and the level of relative fluctuations of the current period, which allows using a linear model of fluctuating time to study the MS dynamics, depend on the type of motion and the choice of the coordinate system.

15.6 Relationship of Time Intervals with Displacement During Reciprocating Motion

Changing the direction during the reciprocating motion of the MS moving element is usually accompanied by the excitation of transients. Therefore, the description of fluctuations of time intervals on these parts of motion within the linear model of the fluctuating time interval in the general case is not possible. However, if after the damping of transients the motion of the moving element is close to harmonic (15.41), then to describe small fluctuations of the current period, one can use the linear relation (15.45). If the movement is close to uniform

$$x(t) = V_0 t + \delta x(t), \quad (15.57)$$

where V_0 is the mean velocity, $\delta x(t)$ are the small fluctuations of the moving element displacement, then the description of fluctuations of time intervals for rotational motion can be fully transferred to fluctuations of time intervals during reciprocating motion.

Let us show this by describing the fluctuations of the current time interval. We believe that the recording of the current time interval $\tau(t)$ for the passage of the adjacent fixed positions allows us to determine the current velocity of the moving element

$$\dot{x}(t) = \Delta x / \tau(t), \quad (15.58)$$

where Δx is the distance between the adjacent fixed positions.

At a constant velocity of movement V_0 , the time interval for the passage of the adjacent fixed positions will be constant

$$\tau_0 = \Delta x / V_0, \quad (15.59)$$

The formula for finding the current time interval can be written in general [10]:

$$\Delta x = \int_{t-\tau(t)}^t \dot{x}(t) dt. \quad (15.60)$$

The solution of the integral relation (15.60) in the framework of the linear model of the fluctuating time interval suggests that

$$\tau(t) = \tau_0 + \delta\tau(t); \quad (15.61)$$

$$|\delta\tau(t)| \ll \tau_0, \quad (15.62)$$

where $\delta\tau(t)$ are fluctuations of the current time interval.

According to the method outlined above, we obtain a relation connecting fluctuations of the current time interval $\delta\tau(t)$ with displacement fluctuations $\delta x(t)$:

$$\delta\tau(t) = -\frac{1}{V_0} [\delta x(t) - \delta x(t - \tau_0)] \quad (15.63)$$

or

$$\frac{\delta\tau(t)}{\tau_0} = -\frac{\langle \delta\dot{x}(t, \tau_0) \rangle}{V_0}, \quad (15.64)$$

where $\langle \delta\dot{x}(t, \tau_0) \rangle$ is the mean velocity of displacement fluctuations in the interval $[t - \tau_0, t]$, determined by the formula (15.26).

Substituting (15.57) and (15.59) into expression (15.63) allows us to write a linear relation connecting fluctuations of the current time interval $\delta\tau(t)$ with the displacement $x(t)$:

$$\delta\tau(t) = -\{[x(t) - x(t - T_0)] - \Delta x\}/V_0. \quad (15.65)$$

In accordance with the method described above, from the formula (15.63), it is possible to obtain an expression for the spectral window for transformation of displacement fluctuations into fluctuations of the current time interval

$$G_{h,\delta\tau}(\omega) = \frac{1}{V_0^2} \sin^2\left(\frac{\omega\tau_0}{2}\right). \quad (15.66)$$

Having compared expressions (15.37) and (15.66), we found that the features and limitations inherent in fluctuations of the current time interval during rotational motion fully relate to fluctuations in the current time interval during reciprocating motion.

Let us consider the special features of the description of fluctuations that intersect in time of the current time intervals. In this case, the time and spectral transformation windows take the form

$$h_{\delta T}(t) = -\frac{1}{V_0} [\delta(t) - \delta(t - T_0)], \quad (15.67)$$

$$G_{h,\delta T}(\omega) = \frac{1}{V_0^2} \sin^2\left(\frac{\omega T_0}{2}\right). \quad (15.68)$$

Here, N_0 is the number of intersecting time intervals and T_0 is the mean time of passing N_0 of the fixed positions, which is equal to (15.19). The upper frequency in the fluctuation spectrum of the current time interval will be equal to $N_0/(2\tau_0)$, and at frequencies defined by the formula (15.38), the amplitude of fluctuations of the current time intervals will tend to zero. The system of “hills,” which is typical for time measurements, appears (see Fig. 15.4).

15.7 Estimation of the Scope of Linear Relations

In the framework of the linear model of the fluctuating time interval, in the first approximation, solutions of integral relations (15.20), (15.40), and Eq. (15.60) for various types of MS motions were obtained. The scope of linear relations (15.27), (15.30), and (15.32) is limited by conditions (15.24) and (15.29), and the scope of relations (15.45) and (15.50) is limited by conditions (15.42), (15.43), and (15.49).

To determine the scope of relations (15.27), (15.30), and (15.32), it is necessary to estimate the level of relative fluctuations of the period, which allows using inequality (15.22) when making the transition from the formula (15.20) to the expression (15.25). To do this, we conduct a numerical calculation of the dependence of the angle of shaft rotation on the current time in the polar coordinate system:

$$\varphi(t_k) = \frac{2\pi}{T_0} t_k + \delta\varphi(t_k), \quad (15.69)$$

where $T_0 = 1$ s, $t_k = k \Delta t$; $k = 1, 2, \dots$; $\Delta t = 10^{-6}$ s; $\delta\varphi(t_k)$ is the white Gaussian variance noise $\sigma_{\delta\varphi}^2$. The values of the current period by $N_0 = 12$ fixed positions are calculated by the formula (15.13): $T_n = t_{k(n)} - t_{k(n-1)}$, where $t_{k(n)}$ is the current time of passing the n th fixed position, determined from the condition

$$2\pi n = \frac{2\pi}{T_0} t_{k(n)} + \delta\varphi(t_{k(n)}), \quad (15.70)$$

where $n = 1, 2, \dots$. The formula (15.28) was used to calculate the maximum value of relative fluctuations of the current period and the maximum value of relative fluctuations of the mean velocity of fluctuations of the angle of shaft rotation according to 12,000 values. The result of calculation is shown in Fig. 15.5.

Analysis of the numerical simulation results in Figs. 15.5 and 15.6 shows that the first approximation for solving the integral relation (15.20) quite well describes the relationship between angle fluctuations and fluctuations of time intervals in the steady-state mode of MS operation with a relative level of fluctuations of time intervals of no more than 10%. An increase in the intensity of angle fluctuations leads to a nonlinear transformation of angle fluctuations into period fluctuations, which is expressed in changes in the distribution function (Fig. 15.5) and low-frequency filtration in the spectral region (Fig. 15.6).

Thus, the application of the obtained spectral and time windows of transformations of angle fluctuations into fluctuations of time intervals is possible only for studying the dynamics of mechanical systems, whose elements make a near-to-uniform motion. In the study of the dynamics of mechanical systems, whose period of shaft rotation changes greatly, one must directly analyze the formula (15.20).

The scope of linear relations (15.45) and (15.50) is limited not only by the level of fluctuations of the current period of 10%, but also by the stronger conditions (15.43) and (15.55), respectively. Failure to meet these conditions is easily detected by changing the shape of the spectral transformation window. Such situation is most

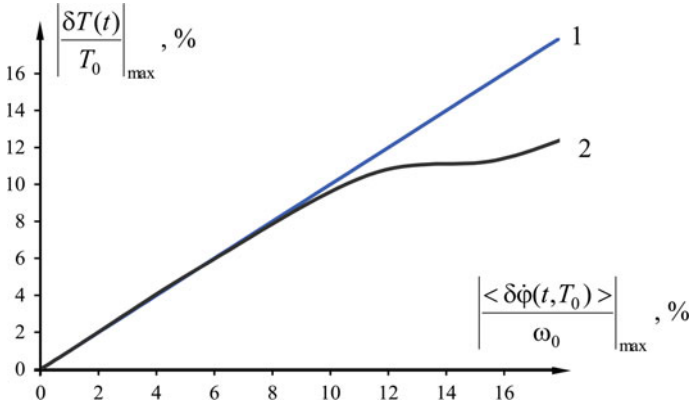


Fig. 15.5 The ideal linear (1) and real nonlinear (2) transformation of fluctuations of the angle of rotation in the period fluctuations during rotational motion

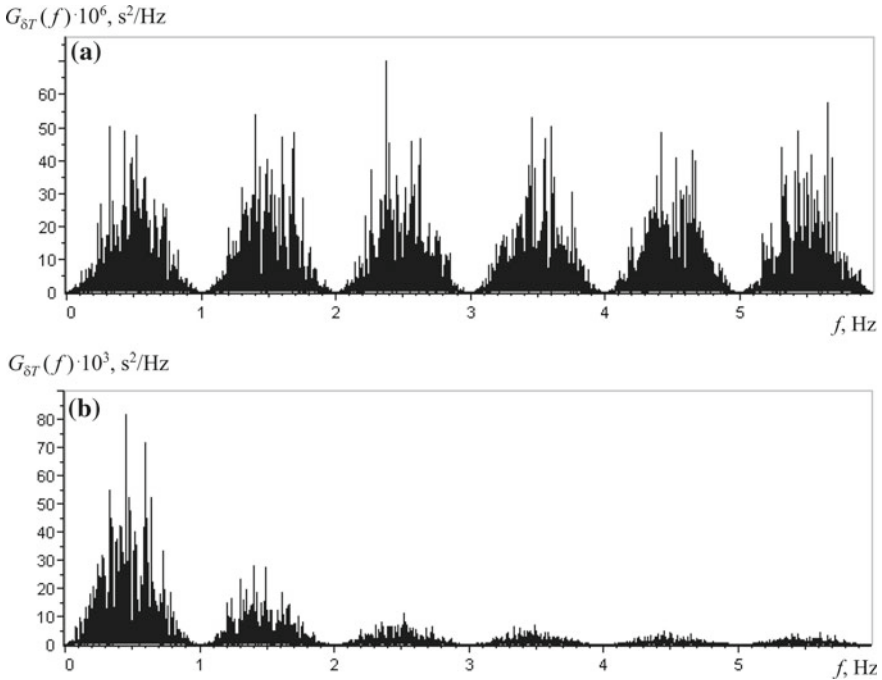


Fig. 15.6 Power spectral density of rotation period fluctuations at 12 angular positions: **a** $|\delta T/T_0|_{\max} = 1.5\%$; **b** $|\delta T/T_0|_{\max} = 16\%$

likely to occur at large displacements of the moving element from the equilibrium position. In this case, the scope of linear relations (15.45) and (15.50) should be limited to $x_n \ll x_0$ or $\varphi_n \ll \varphi_0$.

15.8 Conclusion

The developed method of analytic description of the dynamics of cyclic mechanical systems is an approximate method, whose scope of applicability is limited to stationary modes of operation of machines and mechanisms. This is due to the fact that when considering models of systems with randomly varying time intervals, only the case of minor fluctuations of these intervals was considered. Such an assumption made it possible to obtain linear relations and, on their basis, to construct an analytical method for describing dynamical systems with fluctuating time intervals. Moreover, the simultaneous solution of linear and nonlinear differential equations of motion of mechanical systems with these relations allows us to find complete solutions in both time and frequency domains in variable time intervals. Examples of solving such problems are presented in [8, 10].

Application of the obtained relations is not only theoretical. They make it possible to properly interpret and process the results of experimental measurements of variations in time intervals of motion of mechanical systems elements, taking into account the influence of the type of motion and the coordinate system. Examples of solving problems of diagnosing machines and mechanisms by variations in time intervals are presented in [10, 11].

References

1. Il'in, M.M., Kolesnikov, K.S., Saratov, Yu.S.: Vibration theory. In: Kolesnikov, K.S. (ed.) Textbook for Universities. Bauman Moscow State Technical University, Moscow (2003) (in Russian)
2. Verichev, N.N., Verichev, S.N., Gerasimov, S.I., Erofeev, V.I.: Chaos, Synchronization and Structures in the Dynamics of Rotators. RFNC-VNIIEF, Sarov (2016). (in Russian)
3. Verichev, N.N., Gerasimov, S.I., Erofeev, V.I.: Additional Chapters of Vibration Theory. RFNC-VNIIEF, Sarov (2018). (in Russian)
4. Ifeachor, E.C., Jervis, B.W.: Digital Signal Processing: A Practical Approach, 2nd edn. Pearson Education, Harlow, UK (2002)
5. Biderman, V.L.: Applied Theory of Mechanical Vibrations. Manual for Technical Universities. Moscow, Vysshaya shkola (1972). (in Russian)
6. Blekhman, I.I. (ed.): Vibrations in Engineering: Reference Book in 6 vols., vol. 2. Oscillations of nonlinear mechanical systems. Mashinostroenie, Moscow (1979) (in Russian)
7. Morozov, A.N.: Irreversible Processes and Brownian Movement: Physical and Technical Problems. Bauman Moscow State Technical University, Moscow (1997). (in Russian)
8. Morozov, A.N., Nazolin, A.L.: Determinate and random processes in cyclic and dynamic systems. J. Eng. Math. **55**(1–4), 277–298 (2006)

9. Resor, B.R., Trethewey, M.W., Maynard, K.P.: Compensation for encoder geometry and shaft speed variation in time interval torsional vibration measurement. *J. Sound Vib.* textbf286(4–5), 897–920 (2005)
10. Morozov, A.N., Nazolin, A.L.: *Dynamic Systems with Fluctuating Time*. Bauman Moscow State Technical University, Moscow (2001). (in Russian)
11. Morozov, A.N., Nazolin, A.L., Polyakov, V.I.: A precision optoelectronic system for monitoring torsional vibrations of turbine drive shafts. *Doklady Phys.* **62**(1), 20–23 (2017)

Chapter 16

Propagation of Non-stationary Axisymmetric Perturbations from a Spherical Cavity in Cosserat Medium



Lam V. Nguyen and Dmitry V. Tarlakovskii

Abstract We consider the space filled with the Cosserat medium with a spherical cavity on which unsteady axisymmetric displacements are specified and there is no rotation angle. The equations of axisymmetric motion are written in a spherical coordinate system associated with the cavity with respect to non-trivial components of the displacement potentials and the angle of rotation. To them are added the displacement relation with potentials and physical relationships. The initial conditions are zero, and there are no disturbances at infinity. To solve this we expand the desired functions in the series in the Legendre and Gegenbauer polynomials, as well as transform Laplace over time. When defining originals in linear approximation, the method of a small parameter is used, coefficient, that relates the fields of displacement and rotation, as well as the relationship of the Bessel functions of a half-integer index with elementary functions. Examples of calculations are presented for a granular composite of aluminum fraction in an epoxy matrix, and a comparison with a classical elastic medium is given.

Keywords Cosserat medium · Space · Spherical cavity · Axial symmetry · Non-stationary perturbations · Spherical functions · Laplace transform · Analytical solution · Small parameter · Linear approximation · Two wave fronts

16.1 Introduction

Currently, the development of modern science and technology requires accurate knowledge of the deformation processes not only for “traditional” materials, but also for materials with a complicated structure, including deformation of the medium

L. V. Nguyen (✉) · D. V. Tarlakovskii
Moscow Aviation Institute, Moscow, Russian Federation

D. V. Tarlakovskii
Institute of Mechanics, Lomonosov Moscow State University, Moscow, Russian Federation

which is described not only by the displacement vector, but also by the rotation vector. The general theory of such an asymmetric theory of elasticity was first developed by the Cosserat brothers [1].

The number of publications devoted to non-stationary problems of the moment theory of elasticity is limited. These include works [2–9]. In [2], the dynamic problem of the moment theory of elasticity on a crack of finite length under normal load on the banks by the method of integral transforms is reduced to a system of singular integral equations for displacements and rotations, which is solved numerically. In [3], in the three-dimensional region of a thin plate, the initial-boundary value problem of the general three-dimensional asymmetric theory of elasticity is taken into consideration. In [4], solutions of a dynamic system of equations were obtained for an unbounded body, isotropic and centrally symmetric, within which a concentrated mass force acts, which changes in time spasmodically or periodically. In [5], the dynamic problem for micropolar elastic bodies was studied by the eigenvalue method. In [6], a dynamical coupled axisymmetric problem of the micropolar theory of elasticity for an isotropic medium that is infinite in the radial direction is taken into consideration. In [7], based on the one-dimensional dynamic equations of micropolar elastic thin beams with free rotation, with constrained rotation and low shear stiffness, in which all rotational shear deformations are taken into account, the free vibrations of beams when pivotally supported at the ends are studied. The work [9], where axisymmetric unsteady processes are studied in bodies bounded by spherical surfaces modeled by the Cosserat pseudocontinuum, is closest to the problem considered below.

In [10, 11], solutions of two-dimensional non-stationary problems for half-spaces of elastic moment and half-planes were constructed. Axisymmetric problems for elastic bodies with spherical boundaries were studied in [12, 13].

The aim of this work is the formulation and construction of analytical solutions to problems on the propagation of unsteady axisymmetric perturbations from a spherical cavity in the Cosserat medium.

16.2 Statement of the Problem

On a spherical cavity of radius R in a space filled with medium [14], unsteady surface perturbations are specified. We use a spherical coordinate system r, θ, ϑ , where $r \geq 0, 0 \leq \theta \leq \pi, 0 \leq \vartheta < 2\pi$, with the origin in the center of the cavity and the normalized basis $\mathbf{e}_r, \mathbf{e}_\theta, \mathbf{e}_\vartheta$.

Limitations are given to axisymmetric (symmetric with respect to the half-line $\theta = 0$) perturbations, as well as to the fields of displacements \mathbf{u} and rotation $\boldsymbol{\omega}$, which is equivalent to the equalities

$$\mathbf{u} = w(r, \theta, t) \mathbf{e}_r + v(r, \theta, t) \mathbf{e}_\theta, \quad \boldsymbol{\omega} = \omega(r, \theta, t) \mathbf{e}_\vartheta. \quad (16.1)$$

We express the displacement through the scalar φ and vector $\boldsymbol{\psi}$ displacement potentials:

$$\mathbf{u} = \text{grad } \varphi + \text{rot } \boldsymbol{\psi}, \quad \text{div } \boldsymbol{\psi} = 0, \quad \boldsymbol{\psi} = \boldsymbol{\psi}(r, \theta, t) \mathbf{e}_\vartheta.$$

which is equivalent to scalar equalities [15]

$$w = \frac{\partial \varphi}{\partial r} + \frac{1}{r} \left(\frac{\partial \psi}{\partial \theta} + \psi \text{ctg} \theta \right), \quad v = \frac{1}{r} \left(\frac{\partial \varphi}{\partial \theta} - \psi \right) - \frac{\partial \psi}{\partial r}. \quad (16.2)$$

To describe the motion of the medium, we use the equations for the potentials and the rotation vector [14]:

$$\begin{aligned} \frac{\partial^2 \varphi}{\partial t^2} &= c_1^2 \Delta \varphi, \quad \frac{\partial^2 \boldsymbol{\psi}}{\partial t^2} = \left(c_2^2 + \frac{\alpha}{\rho} \right) \Delta \boldsymbol{\psi} + 2 \frac{\alpha}{\rho} \boldsymbol{\omega}, \quad c_1 = \sqrt{\frac{\lambda + 2\mu}{\rho}}, \quad c_2 = \sqrt{\frac{\mu}{\rho}}, \\ \frac{\partial^2 \boldsymbol{\omega}}{\partial t^2} &= c_3^2 \Delta \boldsymbol{\omega} + \frac{\beta + \gamma - \varepsilon}{J} \text{grad div } \boldsymbol{\omega} - 2 \frac{\alpha}{J} (\Delta \boldsymbol{\psi} + 2\boldsymbol{\omega}), \quad c_3 = \sqrt{\frac{\gamma + \varepsilon}{J}}, \end{aligned}$$

where λ, μ —the Lamé constants; J —a measure of the inertia of the medium during rotation (the density of the moment of inertia); $\alpha, \beta, \gamma, \varepsilon$ —additional physical parameters of the medium characterizing the presence of moment effects; c_1, c_2 , and c_3 —the propagation velocity of the waves of tensile-compression, shaping, and torsion, respectively; Δ —Laplace operator.

Given the axisymmetric nature of motion (16.1) and the type of operators in a spherical coordinate system [15], these equations are reduced to the following scalar form:

$$\begin{aligned} \frac{\partial^2 \varphi}{\partial t^2} &= c_1^2 \Delta \varphi, \\ \frac{\partial^2 \psi}{\partial t^2} &= \left(c_2^2 + \frac{\alpha}{\rho} \right) L(\psi) + 2 \frac{\alpha}{\rho} \omega, \quad \frac{\partial^2 \omega}{\partial t^2} = c_3^2 L(\omega) - 2 \frac{\alpha}{J} [L(\psi) + 2\omega], \\ \Delta \varphi &= \frac{\partial^2 \varphi}{\partial r^2} + \frac{2}{r} \frac{\partial \varphi}{\partial r} + \frac{1}{r^2} \left(\frac{\partial^2 \varphi}{\partial \theta^2} + \frac{\partial \varphi}{\partial \theta} \text{ctg} \theta \right), \quad L(\psi) = \Delta \psi - \frac{\psi}{r^2 \sin^2 \theta}. \end{aligned} \quad (16.3)$$

In this case, the physical components $\gamma_{\xi\zeta}$ and $\chi_{\xi\zeta}$, where $\{\xi, \zeta\} = \{r, \vartheta, \theta\}$, of strain tensors $\boldsymbol{\gamma}$ bending torsion $\boldsymbol{\chi}$ related to movement and rotation angle ω so:

$$\begin{aligned} \gamma_{rr} &= \frac{\partial w}{\partial r}, \quad \gamma_{\theta\theta} = \frac{1}{r} \left(\frac{\partial v}{\partial \theta} + w \right), \quad \gamma_{\vartheta\vartheta} = \frac{1}{r} (v \text{ctg} \theta + w), \quad \gamma_{r\theta} = \frac{\partial v}{\partial r} - \omega, \\ \gamma_{\theta r} &= \frac{1}{r} \left(\frac{\partial w}{\partial \theta} - v \right) + \omega, \quad \gamma_{r\vartheta} = \gamma_{\vartheta r} = \gamma_{\theta\vartheta} = \gamma_{\vartheta\theta} = 0; \end{aligned} \quad (16.4)$$

$$\begin{aligned} \chi_{r\vartheta} &= \frac{\partial \omega}{\partial r}, \quad \chi_{\vartheta r} = -\frac{\omega}{r}, \quad \chi_{\theta\vartheta} = \frac{1}{r} \frac{\partial \omega}{\partial \theta}, \quad \chi_{\vartheta\theta} = -\frac{\omega}{r} \text{ctg} \theta, \\ \chi_{rr} &= \chi_{\theta\theta} = \chi_{\vartheta\vartheta} = \chi_{r\theta} = \chi_{\theta r} \equiv 0. \end{aligned} \quad (16.5)$$

The physical components $\sigma_{\xi\zeta}$ and $\mu_{\xi\zeta}$ of stresses σ and moment stresses μ are expressed through deformations as follows:

$$\begin{aligned} \sigma_{rr} &= (\lambda + 2\mu)\gamma_{rr} + \lambda(\gamma_{\theta\theta} + \gamma_{\vartheta\vartheta}), \quad \sigma_{\theta\theta} = (\lambda + 2\mu)\gamma_{\theta\theta} + \lambda(\gamma_{rr} + \gamma_{\vartheta\vartheta}), \\ \sigma_{\vartheta\vartheta} &= (\lambda + 2\mu)\gamma_{\vartheta\vartheta} + \lambda(\gamma_{rr} + \gamma_{\theta\theta}), \quad \sigma_{r\theta} = (\mu + \alpha)\gamma_{r\theta} + (\mu - \alpha)\gamma_{\theta r}, \\ \sigma_{\theta r} &= (\mu + \alpha)\gamma_{\theta r} + (\mu - \alpha)\gamma_{r\theta}, \quad \sigma_{r\vartheta} = \sigma_{\vartheta r} = \sigma_{\theta\vartheta} = \sigma_{\vartheta\theta} \equiv 0; \\ \mu_{r\vartheta} &= (\gamma + \varepsilon)\chi_{r\vartheta} + (\gamma - \varepsilon)\chi_{\vartheta r}, \quad \mu_{\theta\vartheta} = (\gamma + \varepsilon)\chi_{\theta\vartheta} + (\gamma - \varepsilon)\chi_{\vartheta\theta}, \\ \mu_{\vartheta r} &= (\gamma + \varepsilon)\chi_{\vartheta r} + (\gamma - \varepsilon)\chi_{r\vartheta}, \quad \mu_{\vartheta\theta} = (\gamma + \varepsilon)\chi_{\vartheta\theta} + (\gamma - \varepsilon)\chi_{\theta\vartheta}, \\ \mu_{rr} &= \mu_{\theta\theta} = \mu_{r\theta} = \mu_{\vartheta r} = \mu_{\vartheta\theta} \equiv 0. \end{aligned} \tag{16.6}$$

We suppose that at the initial moment of time $t = 0$ disturbances are absent:

$$\varphi|_{t=0} = \psi|_{t=0} = 0, \quad \omega|_{t=0} = 0, \quad \frac{\partial\varphi}{\partial t}\Big|_{t=0} = \frac{\partial\psi}{\partial t}\Big|_{t=0} = 0, \quad \frac{\partial\omega}{\partial t}\Big|_{t=0} = 0.$$

Among all possible perturbations on the surface of the cavity, we restrict ourselves to setting the kinematic conditions of the following form:

$$w|_{r=R} = W_0(\theta, \tau), \quad v|_{r=R} = V_0(\theta, \tau), \quad \omega|_{r=R} = 0, \tag{16.7}$$

Ratios (16.2), (16.3)–(16.7), together with the condition for the boundedness of the desired functions, form an initial-boundary value problem.

Further, we will use dimensionless quantities (for the same style they are indicated by hatches, which are omitted in the following statement):

$$\begin{aligned} r' &= \frac{r}{R}, \quad \tau = \frac{c_1 t}{R}, \quad w' = \frac{w}{R}, \quad v' = \frac{v}{R}, \quad W'_0 = \frac{W_0}{R}, \quad V'_0 = \frac{v}{R}, \quad \varphi' = \frac{\varphi}{R^2}, \quad \psi' = \frac{\psi}{R^2}, \\ \sigma'_{\xi\zeta} &= \frac{\sigma_{\xi\zeta}}{\lambda + 2\mu}, \quad \chi'_{\xi\zeta} = L\chi_{\xi\zeta}, \quad \mu'_{\xi\zeta} = \frac{L\mu_{\xi\zeta}}{\gamma + \varepsilon} \quad \{\xi, \zeta\} = \{r, \theta, \vartheta\}, \\ \alpha' &= \frac{\alpha}{\rho c_1^2} = \frac{\alpha}{\lambda + 2\mu}, \quad \gamma_1^2 = \frac{c_1^2}{c_2^2}, \quad \gamma_2^2 = \frac{c_1^2}{c_3^2}, \quad \eta = \frac{\gamma - \varepsilon}{\gamma + \varepsilon}, \quad \delta = \frac{\rho L^2}{J}, \quad \kappa = \frac{\lambda}{\lambda + 2\mu}. \end{aligned} \tag{16.8}$$

In these quantities, the kinematic relations (16.2), (16.4), and (16.5) retain their form, and formulas (16.3), (16.6), and (16.7) take the following form (the points hereinafter marked with dimensionless time derivatives τ):

$$\begin{aligned} \ddot{\varphi} &= \Delta\varphi, \quad \gamma_1^2 \ddot{\psi} = (1 + \gamma_1^2 \alpha) L(\psi) + 2\alpha\gamma_1^2 \omega, \\ \gamma_2^2 \ddot{\omega} &= L(\omega) - 2\alpha\gamma_2^2 \delta [L(\psi) + 2\omega]; \end{aligned} \tag{16.9}$$

$$\begin{aligned}
\sigma_{rr} &= \frac{\partial w}{\partial r} + \frac{\kappa}{r} \left(\frac{\partial v}{\partial \theta} + v \operatorname{ctg} \theta + 2w \right), \\
\sigma_{\theta\theta} &= \kappa \frac{\partial w}{\partial r} + \frac{1}{r} \left[(1 + \kappa) w + \frac{\partial v}{\partial \theta} + \kappa v \operatorname{ctg} \theta \right], \\
\sigma_{\vartheta\vartheta} &= \kappa \frac{\partial w}{\partial r} + \frac{1}{r} \left[(1 + \kappa) w + \kappa \frac{\partial v}{\partial \theta} + v \operatorname{ctg} \theta \right], \\
\sigma_{r\theta} &= (\gamma_1^{-2} + \alpha) \frac{\partial v}{\partial r} + (\gamma_1^{-2} - \alpha) \frac{1}{r} \left(\frac{\partial w}{\partial \theta} - v \right) - 2\alpha\omega, \\
\sigma_{\theta r} &= (\gamma_1^{-2} + \alpha) \frac{1}{r} \left(\frac{\partial w}{\partial \theta} - v \right) + (\gamma_1^{-2} - \alpha) \frac{\partial v}{\partial r} + 2\alpha\omega, \\
\mu_{r\vartheta} &= \chi_{r\vartheta} + \eta \chi_{\vartheta r}, \quad \mu_{\vartheta r} = \chi_{\vartheta r} + \eta \chi_{r\vartheta}, \quad \mu_{\theta\vartheta} = \chi_{\theta\vartheta} + \eta \chi_{\vartheta\theta}, \quad \mu_{\vartheta\theta} = \chi_{\vartheta\theta} + \eta \chi_{\theta\vartheta}; \\
\varphi|_{\tau=0} &= \psi|_{\tau=0} = \omega|_{\tau=0} = \dot{\varphi}|_{\tau=0} = \dot{\psi}|_{\tau=0} = \dot{\omega}|_{\tau=0} = 0; \\
w|_{r=1} &= W_0(\theta, \tau), \quad v|_{r=1} = V_0(\theta, \tau), \quad \omega|_{r=1} = 0.
\end{aligned} \tag{16.10}$$

$$w|_{r=1} = W_0(\theta, \tau), \quad v|_{r=1} = V_0(\theta, \tau), \quad \omega|_{r=1} = 0. \tag{16.11}$$

16.3 Presentation of the Solution in the Form of Series

We represent potentials, displacements, and stress state components within the form of series of Legendre $P_n(x)$ and Gegenbauer polynomials $C_{n-1}^{3/2}(x)$ [16]:

$$\begin{pmatrix} \varphi \\ w \end{pmatrix} = \sum_{n=0}^{\infty} \begin{pmatrix} \varphi_n \\ w_n \end{pmatrix} P_n(\cos \theta), \quad \begin{pmatrix} \psi \\ v \\ \omega \end{pmatrix} = -\sin \theta \sum_{n=1}^{\infty} \begin{pmatrix} \psi_n \\ v_n \\ \omega_n \end{pmatrix} C_{n-1}^{3/2}(\cos \theta). \tag{16.12}$$

Substituting them in (16.2), we obtain

$$w_n = \frac{\partial \varphi_n}{\partial r} - n(n+1) \frac{\psi_n}{r}, \quad (n \geq 0), \quad v_n = \frac{\varphi_n - \psi_n}{r} - \frac{\partial \psi_n}{\partial r}, \quad (n \geq 1). \tag{16.13}$$

Next, using the series (16.12) and formulas (16.4) and (16.5), we find the decompositions of the components of the strain and bending torsion tensors:

$$\begin{aligned}
\gamma_{rr} &= \sum_{n=0}^{\infty} \gamma_{rm} P_n(\cos \theta), \quad \begin{pmatrix} \gamma_{r\theta} \\ \gamma_{\theta r} \end{pmatrix} = -\sin \theta \sum_{n=1}^{\infty} \begin{pmatrix} \gamma_{r\theta n} \\ \gamma_{\theta r n} \end{pmatrix} C_{n-1}^{3/2}(\cos \theta), \\
\begin{pmatrix} \gamma_{\theta\theta} \\ \gamma_{\vartheta\vartheta} \end{pmatrix} &= \sum_{n=0}^{\infty} \begin{pmatrix} \gamma_{\theta\theta n} \\ \gamma_{\vartheta\vartheta n} \end{pmatrix} P_n(\cos \theta) + \frac{1}{r} \cos \theta \sum_{n=1}^{\infty} \begin{pmatrix} 1 \\ -1 \end{pmatrix} v_n C_{n-1}^{3/2}(\cos \theta),
\end{aligned}$$

where

$$\begin{aligned} \gamma_{rm} &= \frac{\partial w_n}{\partial r}, \quad \gamma_{\theta\theta n} = \frac{w_n - N v_n}{r}, \quad \gamma_{\vartheta\vartheta n} = \frac{w_n}{r}, \quad \gamma_{r\theta n} = \frac{\partial v_n}{\partial r} - \omega_n, \\ \gamma_{\theta m} &= \frac{w_n - v_n}{r} + \omega_n, \quad N = n(n+1). \end{aligned}$$

$$\begin{pmatrix} \chi_{r\vartheta} \\ \chi_{\vartheta r} \end{pmatrix} = -\sin\theta \sum_{n=1}^{\infty} \begin{pmatrix} \chi_{r\vartheta n} \\ \chi_{\vartheta m} \end{pmatrix} C_{n-1}^{3/2}(\cos\theta),$$

$$\chi_{\theta\theta} = \cos\theta \sum_{n=1}^{\infty} \chi_{\vartheta\theta n}(r, \tau) C_{n-1}^{3/2}(\cos\theta),$$

$$\chi_{\theta\vartheta} = \sum_{n=0}^{\infty} \chi_{\theta\vartheta n} P_n(\cos\theta) + \frac{\cos\theta}{r} \sum_{n=1}^{\infty} \omega_n C_{n-1}^{3/2}(\cos\theta),$$

and

$$\chi_{r\vartheta n} = \frac{\partial \omega_n}{\partial r}, \quad \chi_{\vartheta m} = -\frac{\omega_n}{r}, \quad \chi_{\theta\vartheta n} = N \chi_{\vartheta m}, \quad \chi_{\vartheta\theta n} = -\chi_{\vartheta m}.$$

Similarly, we build the expansion into series of components of the tensors of stresses and moment stresses:

$$\sigma_{rr} = \sum_{n=0}^{\infty} \sigma_{rm} P_n(\cos\theta), \quad \begin{pmatrix} \sigma_{r\theta} \\ \sigma_{\theta r} \end{pmatrix} = -\sin\theta \sum_{n=1}^{\infty} \begin{pmatrix} \sigma_{r\theta n} \\ \sigma_{\theta m} \end{pmatrix} C_{n-1}^{3/2}(\cos\theta),$$

$$\begin{pmatrix} \sigma_{\theta\theta} \\ \sigma_{\vartheta\vartheta} \end{pmatrix} = \sum_{n=0}^{\infty} \begin{pmatrix} \sigma_{\theta\theta n} \\ \sigma_{\vartheta\vartheta n} \end{pmatrix} P_n(\cos\theta) + \frac{1-\kappa}{r} \cos\theta \sum_{n=1}^{\infty} \begin{pmatrix} 1 \\ -1 \end{pmatrix} v_n C_{n-1}^{3/2}(\cos\theta),$$

where

$$\sigma_{rm} = \frac{\partial w_n}{\partial r} + \frac{\kappa}{r} (2w_n - N v_n), \quad \sigma_{\theta\theta n} = \kappa \frac{\partial w_n}{\partial r} + (\kappa + 1) \frac{w_n}{r} - N \frac{v_n}{r},$$

$$\sigma_{\vartheta\vartheta n} = \kappa \frac{\partial w_n}{\partial r} + (\kappa + 1) \frac{w_n}{r} - N \kappa \frac{v_n}{r},$$

$$\sigma_{r\theta n} = (\gamma_1^{-2} + \alpha) \frac{\partial v_n}{\partial r} + (\gamma_1^{-2} - \alpha) \frac{w_n - v_n}{r} - 2\alpha \omega_n,$$

$$\sigma_{\theta m} = (\gamma_1^{-2} - \alpha) \frac{\partial v_n}{\partial r} - (\gamma_1^{-2} + \alpha) \frac{v_n - w_n}{r} + 2\alpha \omega_n;$$

$$\begin{pmatrix} \mu_{r\vartheta} \\ \mu_{\vartheta r} \end{pmatrix} = -\sin\theta \sum_{n=1}^{\infty} \begin{pmatrix} \mu_{r\vartheta n} \\ \mu_{\vartheta m} \end{pmatrix} C_{n-1}^{3/2}(\cos\theta),$$

$$\begin{pmatrix} \mu_{\theta\vartheta} \\ \mu_{\vartheta\theta} \end{pmatrix} = \sum_{n=0}^{\infty} \begin{pmatrix} \mu_{\theta\vartheta n} \\ \mu_{\vartheta\theta n} \end{pmatrix} P_n(\cos\theta) + \frac{2\eta \cos\theta}{r} \sum_{n=1}^{\infty} \begin{pmatrix} 1 \\ 1 \end{pmatrix} \omega_n C_{n-1}^{3/2}(\cos\theta),$$

(16.14)

and

$$\mu_{r\vartheta n} = \frac{\partial \omega_n}{\partial r} - \eta \frac{\omega_n}{r}, \quad \mu_{\vartheta r n} = \eta \frac{\partial \omega_n}{\partial r} - \frac{\omega_n}{r}, \quad \mu_{\theta\vartheta n} = -N \frac{\omega_n}{r}, \quad \mu_{\vartheta\theta n} = \eta \mu_{\theta\vartheta n}$$

In this case, Eq. (16.9) and additional conditions (16.10) and (16.11) pass into the following equalities:

$$\begin{aligned} \ddot{\varphi}_n &= \Delta_n \varphi_n \quad (n \geq 0), \quad \Delta_n = \frac{\partial^2 \varphi_n}{\partial r^2} + \frac{2}{r} \frac{\partial \varphi_n}{\partial r} - \frac{N}{r^2}, \\ \gamma_1^2 \ddot{\psi}_n &= (1 + \alpha \gamma_1^2) \Delta_n \psi_n + 2\alpha \gamma_1^2 \omega_n, \\ \gamma_2^2 \ddot{\omega}_n &= \Delta_n \omega_n - 2\alpha \delta \gamma_2^2 (\Delta_n \psi_n + 2\omega_n) \quad (n \geq 1); \end{aligned} \quad (16.15)$$

$$\begin{aligned} \varphi_n|_{\tau=0} &= \dot{\varphi}_n|_{\tau=0} = 0 \quad (n \geq 0), \\ \psi_n|_{\tau=0} &= \dot{\psi}_n|_{\tau=0} = \omega_n|_{\tau=0} = \dot{\omega}_n|_{\tau=0} = 0 \quad (n \geq 1); \\ w_n|_{r=1} &= w_{0n}(\tau) \quad (n \geq 0), \quad v_n|_{r=1} = v_{0n}(\tau), \quad \omega_n|_{r=1} = 0 \quad (n \geq 1). \end{aligned} \quad (16.16)$$

Here, decompositions into the series of the right parts of the conditions (16.11) are used:

$$W_0(\theta, \tau) = \sum_{n=0}^{\infty} w_{0n}(\tau) P_n(\cos \theta), \quad V_0(\theta, \tau) = -\sin \theta \sum_{n=1}^{\infty} v_{0n}(\tau) C_{n-1}^{3/2}(\cos \theta). \quad (16.17)$$

Ratios (16.15), (16.16), and (16.13) together with the requirement of boundedness form independent initial-boundary value problems.

16.4 General Solution Images

To solve these problems, we use the representations of the desired functions in the form of the series constructed above and apply the Laplace transform in time domain to Eq. (16.15) and relations (16.13) and (16.14) (s -parameter; index « L » denotes the transform). As a result, we obtain equations for images

$$s^2 \varphi_n^L = \Delta_n \varphi_n^L \quad (n \geq 0) \quad (16.18)$$

$$\begin{aligned} \gamma_1^2 s^2 \psi_n^L &= (1 + \alpha \gamma_1^2) \Delta_n \psi_n^L + 2\alpha \gamma_1^2 \omega_n^L, \\ \gamma_2^2 s^2 \omega_n^L &= \Delta_n \omega_n^L - 2\alpha \delta \gamma_2^2 (\Delta_n \psi_n^L + 2\omega_n^L) \quad (n \geq 1). \end{aligned} \quad (16.19)$$

and additional ratios

$$w_n^L = \frac{\partial \varphi_n^L}{\partial r} - N \frac{\psi_n^L}{r} \quad (n \geq 0), \quad v_n^L = \frac{\varphi_n^L - \psi_n^L}{r} - \frac{\partial \psi_n^L}{\partial r} \quad (n \geq 1); \quad (16.20)$$

$$\begin{aligned} \sigma_{rm}^L &= \frac{\partial w_n^L}{\partial r} + \kappa \frac{2w_n^L - Nv_n^L}{r}, \quad \sigma_{\theta\theta n}^L = \kappa \frac{\partial w_n^L}{\partial r} + (\kappa + 1) \frac{w_n^L}{r} - N \frac{v_n^L}{r}, \\ \sigma_{\vartheta\vartheta n}^L &= \kappa \frac{\partial w_n^L}{\partial r} + (\kappa + 1) \frac{w_n^L}{r} - N\kappa \frac{v_n^L}{r}, \end{aligned} \tag{16.21}$$

$$\begin{aligned} \sigma_{r\theta n}^L &= (\gamma_1^{-2} + \alpha) \frac{\partial v_n^L}{\partial r} + (\gamma_1^{-2} - \alpha) \frac{w_n^L - v_n^L}{r} - 2\alpha\omega_n^L, \\ \sigma_{\theta m}^L &= (\gamma_1^{-2} - \alpha) \frac{\partial v_n^L}{\partial r} - (\gamma_1^{-2} + \alpha) \frac{v_n^L - w_n^L}{r} + 2\alpha\omega_n^L; \end{aligned}$$

$$\mu_{r\vartheta n}^L = \frac{\partial \omega_n^L}{\partial r} - \eta \frac{\omega_n^L}{r}, \quad \mu_{\vartheta m}^L = \eta \frac{\partial \omega_n^L}{\partial r} - \frac{\omega_n^L}{r}, \quad \mu_{\theta\vartheta n}^L = -N \frac{\omega_n^L}{r}, \quad \mu_{\vartheta\theta n}^L = \eta \mu_{\theta\vartheta n}^L. \tag{16.22}$$

The general solution of Eq. (16.18) has the form [16–18]:

$$\begin{aligned} \varphi_n^L &= C_{n1}^{(0)}(s) Z_{1n}(rs) + C_{n2}^{(0)}(s) Z_{2n}(rs), \\ Z_{1n}(z) &= z^{-1/2} K_{n+1/2}(z), \quad Z_{2n}(z) = z^{-1/2} I_{n+1/2}(z), \end{aligned} \tag{16.23}$$

where $C_{n1}^{(0)}(s)$ and $C_{n2}^{(0)}(s)$ are the integration constants, and $I_\nu(z)$ and $K_\nu(z)$ are modified Bessel functions of the first kind and second kind of order ν . To construct a general solution to the system of Eq. (16.19), we use a rather simply proved statement.

Let the matrix of a system of ordinary differential equations

$$L(\mathbf{y}) = \mathbf{A}\mathbf{y}, \quad \mathbf{y} = (y_1(x), y_2(x), \dots, y_n(x))^T, \quad \mathbf{A} = (a_{ij})_{n \times n} \quad (x, a_{ij} \in \mathbb{R}),$$

$$L(y) = \sum_{k=0}^m b_{m-k}(x) y^{(k)}(x), \tag{16.24}$$

where a_{ij} is independent of x and has a simple spectrum with eigenvalues λ_k and eigenvectors \mathbf{Y}_k ($k = 1, 2, \dots, n$). Then, its general solution has the form

$$\mathbf{y} = \mathbf{Tz}, \quad \mathbf{T} = (\mathbf{Y}_1, \dots, \mathbf{Y}_n), \quad \mathbf{z} = (z_1(x), z_2(x), \dots, z_n(x))^T, \quad z_k = \sum_{l=1}^m C_{kl} F_{kl}(x) \tag{16.25}$$

where $\{F_{kl}(x)\}$ ($l = 1, 2, \dots, m$) are the fundamental systems of solutions of equations $L(z_k) = \lambda_k z_k$, and C_{kl} are arbitrary constants.

In light of this statement, we write the system of equations in matrix form

$$\begin{aligned} C\Delta_n \begin{pmatrix} \psi_n^L \\ \omega_n^L \end{pmatrix} &= \mathbf{B} \begin{pmatrix} \psi_n^L \\ \omega_n^L \end{pmatrix}, \quad \mathbf{B} = \begin{pmatrix} \gamma_1^2 s^2 & -2\alpha\gamma_1^2 \\ 0 & \gamma_2^2 (s^2 + 4\alpha\delta) \end{pmatrix}, \\ \mathbf{C} &= \begin{pmatrix} (1 + \alpha\gamma_1^2) & 0 \\ -2\alpha\delta\gamma_2^2 & 1 \end{pmatrix}. \end{aligned}$$

and reduce it to canonical form (16.24):

$$\Delta_n \begin{pmatrix} \psi_n^L \\ \omega_n^L \end{pmatrix} = \mathbf{A} \begin{pmatrix} \psi_n^L \\ \omega_n^L \end{pmatrix}, \quad L = \Delta_n,$$

$$\mathbf{A} = \mathbf{C}^{-1}\mathbf{B} = \frac{1}{1 + \alpha\gamma_1^2} \begin{pmatrix} \gamma_1^2 s^2 & -2\alpha\gamma_1^2 \\ 2\alpha\delta\gamma_1^2\gamma_2^2 s^2 & \gamma_2^2 [(1 + \alpha\gamma_1^2)s^2 + 4\alpha\delta] \end{pmatrix}.$$

Next, we construct the characteristic equation of the matrix \mathbf{A} regarding to the eigenvalues λ^2 :

$$|\mathbf{A} - \lambda^2 \mathbf{E}| = \frac{1}{1 + \alpha\gamma_1^2} (A\lambda^4 - B\lambda^2 + C) = 0, \quad \text{Re}\lambda > 0,$$

$$A = 1 + \alpha\gamma_1^2, \quad B = B_0 + B_1\alpha, \quad B_0 = (\gamma_1^2 + \gamma_2^2)s^2, \quad B_1 = \gamma_2^2(\gamma_1^2 s^2 + 4\delta),$$

$$C = \frac{\gamma_1^2\gamma_2^2 s^2}{1 + \alpha\gamma_1^2} [(1 + \alpha\gamma_1^2)s^2 + 4\alpha\delta + 4\alpha^2\delta\gamma_1^2].$$

Its roots are defined as follows:

$$\lambda_{1,2}^2 = \frac{B \pm \sqrt{D}}{2A}, \quad D = D_0 - 2\alpha D_1 + \alpha^2 D_2, \quad D_0 = (\gamma_1^2 - \gamma_2^2)^2 s^4,$$

$$D_1 = \gamma_2^2(\gamma_1^2 - \gamma_2^2)s^2(\gamma_1^2 s^2 + 4\delta), \quad D_2 = \gamma_2^2[\gamma_2^2(\gamma_1^2 s^2 + 4\delta)^2 - 16\delta\gamma_1^4 s^2].$$

Note that whence $\alpha = 0$, the equalities

$$\lambda_{1,2}^2|_{\alpha=0} = \frac{(\gamma_2^2 + \gamma_1^2)s^2 \pm (\gamma_1^2 - \gamma_2^2)s^2}{2} = s^2 \begin{cases} \gamma_1^2, \\ \gamma_2^2, \end{cases}$$

which corresponds to system (16.19). Here, it is taken into account that for many materials, including the composite in the form of an aluminum fraction in an epoxy matrix, the characteristic velocities obey the inequality $c_2 < c_1 < c_3$ [19], which implies the following relationship between dimensionless coefficients in (16.8): $\gamma_2 < 1 < \gamma_1$.

The λ_k^2 corresponding eigenvectors are solutions of systems of linear algebraic equations

$$(\mathbf{A} - \lambda_k^2 \mathbf{E}) \mathbf{Y}_k = \mathbf{0}, \quad \mathbf{Y}_k = (y_{1k}, y_{2k})^T$$

We choose them so that linear independence takes place even when $\alpha = 0$:

$$y_{11} = \gamma_2^2 [(1 + \alpha\gamma_1^2)s^2 + 4\alpha\delta] - \lambda_1^2 (1 + \alpha\gamma_1^2), \quad y_{21} = -2\alpha\delta\gamma_1^2\gamma_2^2 s^2,$$

$$y_{12} = 2\alpha\gamma_1^2, \quad y_{22} = \gamma_1^2 s^2 - \lambda_2^2 (1 + \alpha\gamma_1^2). \quad (16.26)$$

Independence is confirmed by the nonzero determinant of the matrix \mathbf{T} in (16.25):

$$\det \mathbf{T}|_{\alpha=0} = (\gamma_2^2 s^2 - \lambda_1^2) (\gamma_1^2 s^2 - \lambda_2^2)|_{\alpha=0} = -(\gamma_1^2 - \gamma_2^2)^2 s^4.$$

The fundamental system of solutions is actually constructed in (16.21):

$$F_{k1}(r, s) = Z_{1n}(\lambda_k r), \quad F_{k2}(r, s) = Z_{2n}(\lambda_k r).$$

Therefore, in accordance with (16.25), the general solution of the system of equations (16.17) has the form:

$$\begin{pmatrix} \psi_n^L \\ \omega_n^L \end{pmatrix} = \sum_{k=1}^2 \begin{pmatrix} y_{1k} \\ y_{2k} \end{pmatrix} \left[C_{n1}^{(k)}(s) Z_{1n}(\lambda_k r) + C_{n2}^{(k)}(s) Z_{2n}(\lambda_k r) \right]. \tag{16.27}$$

Further, substituting (16.23) and (16.27) in (16.20)–(16.22), taking into function properties of Bessel functions, we obtain the following results:

$$\begin{aligned} w_n^L &= s \sum_{l=1}^2 C_{nl}^{(0)}(s) X_{ln}(rs) + N \sum_{k,l=1}^2 y_{1k} \lambda_k C_{nl}^{(k)}(s) Y_{ln}(\lambda_k r), \\ v_n^L &= \sum_{k,l=1}^2 y_{1k} \lambda_k C_{nl}^{(k)}(s) Y_{l+2,n}(\lambda_k r) - s \sum_{l=1}^2 C_{nl}^{(0)}(s) Y_{ln}(rs), \\ \omega_n^L &= \sum_{k,l=1}^2 y_{2k} \lambda_k C_{nl}^{(k)}(s) Z_{ln}(\lambda_k r); \end{aligned} \tag{16.28}$$

$$\begin{aligned} \sigma_{\xi n}^L &= s^2 T_{\xi n}^{(0)} + N T_{\xi n}^{(1)} \quad (\xi = rr, \theta\theta, \vartheta\vartheta), \\ \sigma_{r\theta n}^L &= s^2 T_{r\theta n}^{(0)} + T_{r\theta n}^{(1)} - 2\alpha \omega_n^L, \quad \sigma_{\theta r n}^L = s^2 T_{\theta r n}^{(0)} + T_{\theta r n}^{(1)} + 2\alpha \omega_n^L, \\ T_{\xi n}^{(0)} &= \sum_{l=1}^2 C_{nl}^{(0)}(s) S_{\xi ln}^{(0)}(rs), \quad T_{\xi n}^{(1)} = \sum_{k,l=1}^2 y_{1k} \lambda_k^2 C_{nl}^{(k)}(s) S_{\xi ln}^{(1)}(\lambda_k r), \\ & \quad (\xi = rr, \theta\theta, \vartheta\vartheta, r\theta, \theta r), \end{aligned} \tag{16.29}$$

where

$$\begin{aligned} S_{rrln}^{(0)}(z) &= c_n(z) Z_{ln}(z) - 2 \frac{1-\kappa}{z} \left(1 + N \frac{1-\kappa}{z^2} \right) X_{ln}(z), \\ S_{rrln}^{(1)}(z) &= -\frac{1-\kappa}{z} [X_{ln}(z) + Y_{ln}(z)], \quad S_{\theta\theta ln}^{(1)}(z) = \frac{1-\kappa}{z} X_{ln}(z), \\ S_{\theta\theta ln}^{(0)}(z) &= \frac{1-\kappa}{z} X_{ln}(z) + \left(\kappa - N \frac{1-\kappa}{z^2} \right) Z_{ln}(z), \\ S_{\vartheta\vartheta ln}^{(0)}(z) &= \frac{1-\kappa}{z} X_{ln}(z) + \kappa Z_{ln}(z), \quad S_{\vartheta\vartheta ln}^{(1)}(z) = \frac{1-\kappa}{z} Y_{ln}(z), \end{aligned}$$

$$\begin{aligned}
 S_{r\theta ln}^{(0)}(z) &= S_{\theta rln}^{(0)}(z) = -\frac{2}{(1-\kappa)\gamma_1^2} S_{rrln}^{(1)}(z), \\
 S_{r\theta ln}^{(1)}(z) &= \frac{2}{z\gamma_1^2} X_{ln}(z) - \left[\gamma_1^{-2} \left(1 + 2\frac{N-1}{z^2} \right) + \alpha \right] Z_{ln}(z), \\
 S_{\theta rln}^{(1)}(z) &= \frac{2}{z\gamma_1^2} X_{ln}(z) - \left[\gamma_1^{-2} \left(1 + 2\frac{N-1}{z^2} \right) - \alpha \right] Z_{ln}(z); \\
 \mu_{r\vartheta n}^L &= \sum_{k,l=1}^2 y_{2k} C_{nl}^{(k)}(s) \lambda_k^2 [X_{ln}(\lambda_k r) + \eta Y_{ln}(\lambda_k r)], \quad \mu_{\vartheta\vartheta n}^L = -N \frac{\omega_n^L}{r}, \\
 \mu_{\vartheta m}^L &= \sum_{k,l=1}^2 y_{2k} C_{nl}^{(k)}(s) \lambda_k^2 [\eta X_{ln}(\lambda_k r) + Y_{ln}(\lambda_k r)], \quad \mu_{\vartheta\theta n}^L = \eta \mu_{\vartheta\vartheta n}^L.
 \end{aligned}
 \tag{16.30}$$

Notation used here

$$\begin{aligned}
 X_{ln}(z) &= Z'_{ln}(z) = \frac{1}{z} [nZ_{ln}(z) + (-1)^l z Z_{l,n+1}(z)], \\
 Y_{ln}(z) &= -\frac{1}{z} Z_{ln}(z), \quad Y_{l+2,n}(z) = Y_{ln}(z) - X_{ln}(z).
 \end{aligned}
 \tag{16.31}$$

16.5 Problem-Solving Images

Since the Bessel function $I_{n+1/2}(z)$ is unbounded in a neighborhood of an infinitely distant point [16], by power of (16.23) and (16.31), these are also such functions $Z_{2n}(z)$, $X_{2n}(z)$, $Y_{2n}(z)$, and $U_{2n}(z)$. Therefore, in (16.23), (16.27)–(16.29), (16.30) it is necessary to put:

$$C_{n2}^{(0)}(s) = C_{n2}^{(1)}(s) = C_{n2}^{(2)}(s) = 0.$$

Substituting now (16.28) into the images of the boundary conditions (16.16), we obtain algebraic equations for the integration constants:

$$\begin{aligned}
 sC_{01}^{(0)}(s) X_{10}(s) &= w_{00}^L(s); \\
 \mathbf{A}_n \mathbf{C}_n &= \mathbf{B}_n \quad (n \geq 1), \quad \mathbf{C}_n = \begin{pmatrix} C_{n1}^{(0)}(s) \\ C_{n1}^{(1)}(s) \\ C_{n1}^{(2)}(s) \end{pmatrix}, \quad \mathbf{B}_n = \begin{pmatrix} w_{0n}^L(s) \\ v_{0n}^L(s) \\ 0 \end{pmatrix}, \\
 \mathbf{A}_n &= \begin{pmatrix} sX_{1n}(s) & Ny_{11}\lambda_1 Y_{1n}(\lambda_1) & Ny_{12}\lambda_2 Y_{1n}(\lambda_2) \\ -sY_{1n}(s) & y_{11}\lambda_1 Y_{3n}(\lambda_1) & y_{12}\lambda_2 Y_{3n}(\lambda_2) \\ 0 & y_{21}Z_{1n}(\lambda_1) & y_{22}Z_{1n}(\lambda_2) \end{pmatrix}.
 \end{aligned}
 \tag{16.32}$$

Substituting the solutions of the last system in (16.20)–(16.22), we obtain images of the desired functions:

$$\begin{aligned} w_n^L(r, s) &= G_{wvn}^L(r, s) w_{0n}^L(s) + G_{vvn}^L(r, s) v_{0n}^L(s), \\ v_n^L(r, s) &= G_{vvn}^L(r, s) w_{0n}^L(s) + G_{vvn}^L(r, s) v_{0n}^L(s), \\ \omega_n^L(r, s) &= G_{\omega vn}^L(r, s) w_{0n}^L(s) + G_{\omega vn}^L(r, s) v_{0n}^L(s); \end{aligned} \tag{16.33}$$

$$\begin{aligned} \sigma_{\xi n}^L &= G_{\sigma \xi wn}^L(r, s) w_{0n}^L(s) + G_{\sigma \xi vn}^L(r, s) v_{0n}^L(s) \quad (\xi = rr, \theta\theta, \vartheta\vartheta, r\theta, \theta r) \\ \mu_{\xi n}^L &= G_{\mu \xi wn}^L(r, s) w_{0n}^L(s) + G_{\mu \xi vn}^L(r, s) v_{0n}^L(s) \quad (\xi = r\vartheta, \vartheta r, \theta\vartheta, \vartheta\theta); \end{aligned} \tag{16.34}$$

Here $G_{wvn}^L(r, s)$, $G_{vvn}^L(r, s)$, \dots , $G_{\sigma \vartheta \theta vn}^L(r, s)$ are images of surface influence functions, which are defined as follows:

$$\begin{aligned} D_n G_{wvn}^L &= sA_{n11}X_{1n}(rs) + N \sum_{k=1}^2 y_{1k} \lambda_k A_{n1,k+1} Y_{1n}(\lambda_k r), \\ D_n G_{vvn}^L &= sA_{n21}X_{1n}(rs) + N \sum_{k=1}^2 y_{1k} \lambda_k A_{n2,k+1} Y_{1n}(\lambda_k r), \\ D_n G_{\omega vn}^L &= \sum_{k=1}^2 y_{1k} \lambda_k A_{n1,k+1} Y_{3n}(\lambda_k r) - sA_{n11}Y_{1n}(rs), \\ D_n G_{\sigma \xi wn}^L &= \sum_{k=1}^2 y_{1k} \lambda_k A_{n2,k+1} Y_{3n}(\lambda_k r) - sA_{n21}Y_{1n}(rs), \\ D_n G_{\omega wn}^L &= \sum_{k=1}^2 y_{2k} \lambda_k A_{n1,k+1} Z_{1n}(\lambda_k r), \\ D_n G_{\omega vn}^L &= \sum_{k=1}^2 y_{2k} \lambda_k A_{n2,k+1} Z_{1n}(\lambda_k r); \\ D_n(s) &= s[X_{1n}(s)A_{n11}(s) - Y_{1n}(s)A_{n21}(s)]; \\ D_n G_{\sigma \xi \zeta rwn}^L &= s^2 A_{n11} S_{\xi \zeta 1n}^{(0)}(rs) + N \sum_{k=1}^2 y_{1k} \lambda_k^2 A_{n1,k+1} S_{\xi \zeta 1n}^{(1)}(\lambda_k r), \\ D_n G_{\sigma \xi \zeta rvn}^L &= s^2 A_{n21} S_{\xi \zeta 1n}^{(0)}(rs) + N \sum_{k=1}^2 y_{1k} \lambda_k^2 A_{n2,k+1} S_{\xi \zeta 1n}^{(1)}(\lambda_k r) \\ & \quad (\xi \zeta = rr, \theta\theta, \vartheta\vartheta), \end{aligned} \tag{16.35}$$

$$\begin{aligned}
D_n G_{\sigma r \theta r w n}^L &= s^2 A_{n11} S_{r \theta 1 n}^{(0)}(rs) + \sum_{k=1}^2 y_{1k} \lambda_k^2 A_{n1,k+1} S_{r \theta 1 n}^{(1)}(\lambda_k r) - 2\alpha D_n G_{\omega w n}^L, \\
D_n G_{\sigma r \theta r v n}^L &= s^2 A_{n21} S_{r \theta 1 n}^{(0)}(rs) + \sum_{k=1}^2 y_{1k} \lambda_k^2 A_{n2,k+1} S_{r \theta 1 n}^{(1)}(\lambda_k r) - 2\alpha D_n G_{\omega w n}^L, \\
D_n G_{\sigma \theta r r w n}^L &= s^2 A_{n11} S_{\theta r 1 n}^{(0)}(rs) + \sum_{k=1}^2 y_{1k} \lambda_k^2 A_{n1,k+1} S_{\theta r 1 n}^{(1)}(\lambda_k r) + 2\alpha D_n G_{\omega w n}^L, \\
D_n G_{\sigma \theta r r v n}^L &= s^2 A_{n21} S_{\theta r 1 n}^{(0)}(rs) + \sum_{k=1}^2 y_{1k} \lambda_k^2 A_{n2,k+1} S_{\theta r 1 n}^{(1)}(\lambda_k r) + 2\alpha D_n G_{\omega w n}^L,
\end{aligned} \tag{16.36}$$

$$\begin{aligned}
D_n G_{\mu r \vartheta w n}^L &= \sum_{k=1}^2 y_{2k} \lambda_k^2 [X_{1n}(\lambda_k r) + \eta Y_{1n}(\lambda_k r)] A_{n1,k+1}, \\
D_n G_{\mu r \vartheta v n}^L &= \sum_{k=1}^2 y_{2k} \lambda_k^2 [X_{1n}(\lambda_k r) + \eta Y_{1n}(\lambda_k r)] A_{n2,k+1}, \\
D_n G_{\mu \vartheta r w n}^L &= \sum_{k=1}^2 y_{2k} \lambda_k^2 [\eta X_{1n}(\lambda_k r) + Y_{1n}(\lambda_k r)] A_{n1,k+1}, \\
D_n G_{\mu \vartheta r v n}^L &= \sum_{k=1}^2 y_{2k} \lambda_k^2 [\eta X_{1n}(\lambda_k r) + Y_{1n}(\lambda_k r)] A_{n2,k+1}, \\
G_{\mu \theta \vartheta w n}^L &= -\frac{N}{r} G_{\omega w n}^L, \quad G_{\mu \theta \vartheta v n}^L = -\frac{N}{r} G_{\omega w n}^L, \\
G_{\mu \vartheta \theta w n}^L &= \eta G_{\mu \theta \vartheta w n}^L, \quad G_{\mu \vartheta \theta v n}^L = \eta G_{\mu \theta \vartheta v n}^L.
\end{aligned}$$

In these equalities and hereinafter, $A_{nij}(s)$ is the algebraic complement located in the i th row and j -m column of the matrix element \mathbf{A}_n .

16.6 Linear Approximation of the Solution

Get analytically originals of functions of influence when $n \geq 1$ it is not possible. Therefore, we use expansions in exponential series in a small parameter α , with limitation of linear terms only. Wherein, replace approximate equalities with exact ones.

The corresponding equalities for $\lambda_{1,2}$ and coordinates (16.26) of the eigenvectors have the form:

$$\lambda_1 = \gamma_{1\alpha} s, \quad \lambda_2 = \gamma_2 \left(s + \frac{2\alpha\delta}{s} \right), \quad \gamma_{1\alpha} = \gamma_1 \sqrt{1 - \alpha\gamma_1^2};$$

$$y_{22} = -y_{11} = (\gamma_1^2 - \gamma_2^2) s^2 - \gamma_2^2 (\gamma_1^2 s^2 + 4\delta) \alpha,$$

$$y_{12} = 2\alpha\gamma_1^2, \quad y_{21} = -2\alpha\delta\gamma_1^2\gamma_2^2 s^2.$$

From this, taking into account (16.32), it follows that only for two of all the complements $A_{nij}(i = 1, 2; i = 1, 2, 3)$ the relations are:

$$A_{n13} = -sy_{21} Y_{1n}(s) Z_{1n}(\lambda_1) = O(\alpha),$$

$$A_{n23} = -sy_{21} X_{1n}(s) Z_{1n}(\lambda_1) = O(\alpha), \quad \alpha \rightarrow 0.$$

These formulas allow, with the accepted accuracy, to reduce equalities (16.35)–(16.36) to the following form:

$$G_{\xi\zeta n}^L = \frac{F_{\xi\zeta n}(r, s)}{\Pi_n(s, \gamma_{1\alpha s})}, \quad \Pi_n(x, y) = X_{1n}(x) Y_{3n}(y) + N Y_{1n}(x) Y_{1n}(y);$$

$$(\xi = w, v, \omega, \sigma rr, \sigma \theta \theta, \sigma \vartheta \vartheta, \sigma r \theta, \sigma \theta r, \mu r \vartheta, \mu \vartheta r, \mu \theta \vartheta, \mu \vartheta \theta; \zeta = w, v).$$

(16.37)

where

$$F_{wvn}(r, s) = Y_{3n}(\gamma_{1\alpha s}) X_{1n}(rs) + N Y_{1n}(s) Y_{1n}(\gamma_{1\alpha sr}),$$

$$F_{vvn}(r, s) = N [X_{1n}(s) Y_{1n}(\gamma_{1\alpha rs}) - Y_{1n}(\gamma_{1\alpha s}) X_{1n}(rs)],$$

$$F_{\omega vn}(r, s) = Y_{1n}(s) Y_{3n}(\gamma_{1\alpha rs}) - Y_{3n}(\gamma_{1\alpha s}) Y_{1n}(rs),$$

$$F_{\sigma rr vn}(r, s) = N Y_{1n}(\gamma_{1\alpha s}) Y_{1n}(rs) + X_{1n}(s) Y_{3n}(\gamma_{1\alpha sr}),$$

$$F_{\sigma \theta \theta vn}(r, s) = \alpha k_\omega s^{-1} Y_{1n}(s) Z_{1n}(\gamma_{1\alpha rs}),$$

$$F_{\sigma \vartheta \vartheta vn}(r, s) = \alpha k_\omega s^{-1} X_{1n}(s) Z_{1n}(\gamma_{1\alpha rs});$$

$$F_{\sigma rr wn} = s \left[Y_{3n}(\gamma_{1\alpha s}) S_{rr1n}^{(0)}(rs) + N \gamma_{1\alpha} Y_{1n}(s) S_{rr1n}^{(1)}(\gamma_{1\alpha rs}) \right],$$

$$F_{\sigma rr vn} = N s \left[-Y_{1n}(\lambda_1) S_{rr1n}^{(0)}(rs) + \gamma_{1\alpha} X_{1n}(s) S_{rr1n}^{(1)}(\gamma_{1\alpha rs}) \right],$$

$$F_{\sigma \xi wn} = s \left[Y_{3n}(\gamma_{1\alpha s}) S_{\xi 1n}^{(0)}(rs) + N \gamma_{1\alpha} Y_{1n}(s) S_{\xi 1n}^{(1)}(\gamma_{1\alpha rs}) \right],$$

$$F_{\sigma \xi vn} = s \left[-N Y_{1n}(\gamma_{1\alpha s}) S_{\xi 1n}^{(0)}(rs) + N \gamma_{1\alpha} X_{1n}(s) S_{\xi 1n}^{(1)}(\gamma_{1\alpha rs}) \right], \quad (\xi = \theta \theta, \vartheta \vartheta)$$

$$F_{\sigma \xi wn} = s \left[Y_{3n}(\gamma_{1\alpha s}) S_{\xi 1n}^{(0)}(rs) + \gamma_{1\alpha} Y_{1n}(s) S_{\xi 1n}^{(1)}(\gamma_{1\alpha rs}) \right],$$

$$F_{\sigma \xi vn} = s \left[-N Y_{1n}(\gamma_{1\alpha s}) S_{\xi 1n}^{(0)}(rs) + \gamma_{1\alpha} X_{1n}(s) S_{\xi 1n}^{(1)}(\gamma_{1\alpha rs}) \right], \quad (\xi = r \theta, \theta r)$$

$$F_{\mu r \vartheta wn} = s \alpha \gamma_1^2 k_\omega [X_{1n}(\lambda_1 r) + \eta Y_{1n}(\lambda_1 r)] Y_{1n}(s), \quad k_\omega = \frac{2\delta \gamma_1 \gamma_2^2}{\gamma_1^2 - \gamma_2^2}$$

$$F_{\mu r \vartheta vn} = s \alpha \gamma_1^2 k_\omega [X_{1n}(\lambda_1 r) + \eta Y_{1n}(\lambda_1 r)] X_{1n}(s),$$

$$F_{\mu \vartheta r wn} = s \alpha \gamma_1^2 k_\omega [\eta X_{1n}(\lambda_1 r) + Y_{1n}(\lambda_1 r)] Y_{1n}(s),$$

$$F_{\mu \vartheta r vn} = s \alpha \gamma_1^2 k_\omega [\eta X_{1n}(\lambda_1 r) + Y_{1n}(\lambda_1 r)] X_{1n}(s),$$

$$F_{\mu \theta \vartheta wn} = s N \alpha \gamma_1^2 k_\omega Y_{1n}(\gamma_{1\alpha sr}) Y_{1n}(s), \quad F_{\mu \theta \vartheta vn} = s N \alpha \gamma_1^2 k_\omega Y_{1n}(\gamma_{1\alpha sr}) X_{1n}(s),$$

$$F_{\mu \vartheta \theta wn} = \eta F_{\mu \theta \vartheta wn}, \quad F_{\mu \vartheta \theta vn} = \eta F_{\mu \theta \vartheta vn}(r, s).$$

Fractions in (16.37), taking into account the relationship between the modified Bessel functions with elementary [16], are conveniently represented as ($\zeta = w, v$):

$$\begin{aligned}
 G_{\xi\zeta n}^L &= \sum_{k=0}^1 H_{\xi\zeta n}^{(k)L}(r, s) e^{-\rho_k s}, \quad \rho_0 = r - 1, \quad \rho_1 = \gamma_{1\alpha}(r - 1), \\
 H_{\xi\zeta n}^{(k)L}(r, s) &= \frac{F_{\xi\zeta n}^{(k)}(r, s)}{r^{n+2} P_n(s)} \quad (\xi = w, v), \quad H_{\omega\zeta n}^{(1)L}(r, s) = \frac{F_{\omega\zeta n}^{(1)}(r, s)}{r^{n+1} P_n(s)}, \\
 H_{\xi\zeta n}^{(k)L}(r, s) &= \frac{F_{\xi\zeta n}^{(k)}(r, s)}{r^{n+3} P_n(s)} \quad (\xi = \sigma rr, \sigma\theta\theta, \sigma\vartheta\vartheta, \sigma r\theta, \sigma\theta r), \\
 H_{\xi\zeta n}^{(k)L}(r, s) &= \frac{F_{\xi\zeta n}^{(k)}(r, s)}{r^{n+2} P_n(s)} \quad (\xi = \mu r\vartheta, \mu\vartheta r, \mu\theta\vartheta, \mu\vartheta\theta), \\
 P_n(s) &= R_{n1}(s) R_{n3}(\gamma_{1\alpha}s) - N R_{n0}(s) R_{n0}(\gamma_{1\alpha}s).
 \end{aligned} \tag{16.38}$$

where

$$\begin{aligned}
 F_{wwn}^{(0)}(r, s) &= R_{n3}(\gamma_{1\alpha}s) R_{n1}(rs), \quad F_{wwn}^{(1)}(r, s) = -N R_{n0}(s) R_{n0}(\gamma_{1\alpha}sr), \\
 F_{wvn}^{(0)}(r, s) &= N R_{n0}(\gamma_{1\alpha}s) R_{n1}(rs), \quad F_{wvn}^{(1)}(r, s) = -N R_{n1}(s) R_{n0}(\gamma_{1\alpha}rs), \\
 F_{vwn}^{(0)}(r, s) &= -R_{n3}(\gamma_{1\alpha}s) R_{n0}(rs), \quad F_{vwn}^{(1)}(r, s) = R_{n0}(s) R_{n3}(\gamma_{1\alpha}rs), \\
 F_{vvn}^{(0)}(r, s) &= -N R_{n0}(\gamma_{1\alpha}s) R_{n0}(rs), \quad F_{vvn}^{(1)}(r, s) = R_{n1}(s) R_{n3}(\gamma_{1\alpha}rs), \\
 F_{own}^{(1)}(r, s) &= \alpha k_{\omega} \gamma_{1\alpha} R_{n0}(s) R_{n0}(\gamma_{1\alpha}sr), \\
 F_{ovn}^{(1)}(r, s) &= \alpha k_{\omega} \gamma_{1\alpha} R_{n1}(s) R_{n0}(\gamma_{1\alpha}sr), \\
 F_{\sigma rrw}^{(0)}(r, s) &= -s Q_n(rs) R_{n3}(\gamma_{1\alpha}s), \\
 F_{\sigma rrw}^{(1)}(r, s) &= sN(1 - \kappa) R_{n4}(\gamma_{1\alpha}rs) R_{n0}(s), \\
 F_{\sigma rrv}^{(0)}(r, s) &= -sN Q_n(rs) R_{n0}(\gamma_{1\alpha}s), \\
 F_{\sigma rrv}^{(1)}(r, s) &= sN(1 - \kappa) R_{n4}(\gamma_{1\alpha}rs) R_{n1}(s), \\
 F_{\sigma\theta\theta wn}^{(0)}(r, s) &= -s K_n(rs) R_{n3}(\gamma_{1\alpha}s), \\
 F_{\sigma\theta\theta wn}^{(1)}(r, s) &= -sN(1 - \kappa) R_{n1}(\gamma_{1\alpha}rs) R_{n0}(s), \\
 F_{\sigma\theta\theta vn}^{(0)}(r, s) &= -sN K_n(rs) R_{n0}(\gamma_{1\alpha}s), \\
 F_{\sigma\theta\theta vn}^{(1)}(r, s) &= -sN(1 - \kappa) R_{n1}(\gamma_{1\alpha}rs) R_{n1}(s), \\
 F_{\sigma\vartheta\vartheta wn}^{(0)}(r, s) &= -s [(\kappa - 1) R_{n1}(\gamma_{1\alpha}rs) + \kappa(rs)^2 R_{n0}(rs)] R_{n3}(\gamma_{1\alpha}s), \\
 F_{\sigma\vartheta\vartheta wn}^{(1)}(r, s) &= -sN(1 - \kappa) R_{n0}(s) R_{n0}(\gamma_{1\alpha}rs), \\
 F_{\sigma\vartheta\vartheta vn}^{(0)}(r, s) &= -sN [(\kappa - 1) R_{n1}(\gamma_{1\alpha}rs) + \kappa(rs)^2 R_{n0}(rs)] R_{n0}(\gamma_{1\alpha}s), \\
 F_{\sigma\vartheta\vartheta vn}^{(1)}(r, s) &= -sN(1 - \kappa) R_{n1}(s) R_{n0}(\gamma_{1\alpha}rs),
 \end{aligned} \tag{16.39}$$

$$\begin{aligned}
F_{\sigma r \theta w n}^{(0)}(r, s) &= F_{\sigma \theta r w n}^{(0)}(r, s) = 2s\gamma_1^{-2}R_{n4}(rs)R_{n3}(\gamma_1\alpha s), \\
F_{\sigma r \theta w n}^{(1)}(r, s) &= s\{\gamma_1\alpha rs(\gamma_1^{-2} + \alpha)R_{n3}(\gamma_1\alpha rs) \\
&\quad - (\gamma_1^{-2} - \alpha)M_n(\gamma_1\alpha rs)\}R_{n0}(s), \\
F_{\sigma r \theta v n}^{(0)}(r, s) &= F_{\sigma \theta r v n}^{(0)}(r, s) = 2sN\gamma_1^{-2}R_{n4}(rs)R_{n0}(\gamma_1\alpha s), \\
F_{\sigma r \theta v n}^{(1)}(r, s) &= s\{\gamma_1\alpha rs(\gamma_1^{-2} + \alpha)R_{n3}(\gamma_1\alpha rs) \\
&\quad - (\gamma_1^{-2} - \alpha)M_n(\gamma_1\alpha rs)\}R_{n1}(s), \\
F_{\sigma \theta r w n}^{(1)}(r, s) &= s\{\gamma_1\alpha rs(\gamma_1^{-2} - \alpha)R_{n3}(\gamma_1\alpha rs) \\
&\quad - (\gamma_1^{-2} + \alpha)M_n(\gamma_1\alpha rs)\}R_{n0}(s), \\
F_{\sigma \theta r v n}^{(1)}(r, s) &= s\{\gamma_1\alpha rs(\gamma_1^{-2} - \alpha)R_{n3}(\gamma_1\alpha rs) \\
&\quad - (\gamma_1^{-2} + \alpha)M_n(\gamma_1\alpha rs)\}R_{n1}(s), \\
F_{\mu r \vartheta w n}^{(1)}(r, s) &= s\alpha\gamma_1^2k_\omega[-R_{n1}(\gamma_1\alpha rs) - \eta R_{n0}(\gamma_1\alpha rs)]R_{n0}(s), \\
F_{\mu r \vartheta v n}^{(1)}(r, s) &= s\alpha\gamma_1^2k_\omega[-R_{n1}(\gamma_1\alpha rs) - \eta R_{n0}(\gamma_1\alpha rs)]R_{n1}(s), \\
F_{\mu \vartheta r w n}^{(1)}(r, s) &= s\alpha\gamma_1^2k_\omega[-\eta R_{n1}(\gamma_1\alpha rs) - R_{n0}(\gamma_1\alpha rs)]R_{n0}(s), \\
F_{\mu \vartheta r v n}^{(1)}(r, s) &= s\alpha\gamma_1^2k_\omega[-\eta R_{n1}(\gamma_1\alpha rs) - R_{n0}(\gamma_1\alpha rs)]R_{n1}(s), \\
F_{\mu \theta \vartheta w n}^{(1)}(r, s) &= -sN\alpha\gamma_1^2k_\omega R_{n0}(\gamma_1\alpha rs)R_{n0}(s), \\
F_{\mu \theta \vartheta v n}^{(1)}(r, s) &= -sN\alpha\gamma_1^2k_\omega R_{n1}(s)R_{n0}(\gamma_1\alpha rs), \\
F_{\mu \vartheta \theta w n}^{(1)}(r, s) &= -\eta F_{\mu \theta \vartheta w n}^{(1)}(r, s), F_{\mu \vartheta \theta v n}^{(1)}(r, s) = -\eta F_{\mu \theta \vartheta v n}^{(1)}(r, s).
\end{aligned} \tag{16.40}$$

The following polynomials are used here:

$$\begin{aligned}
R_{n0}(z) &= \sum_{k=0}^n A_{nk}z^{n-k}, \quad A_{nk} = \frac{(n+k)!}{2^k(n-k)!k!}, \quad R_{n1}(z) = R_{n+1,0}(z) - nR_{n0}(z), \\
R_{n3}(z) &= R_{n1}(z) - R_{n0}(z), \quad R_{n4}(z) = R_{n1}(z) + R_{n0}(z), \\
Q_n(z) &= [z^2 + N(1-\kappa)]R_{n0}(z) + 2(1-\kappa)R_{n1}(z), \\
K_n(z) &= \{(\kappa-1)R_{n1}(z) + [\kappa z^2 + N(\kappa-1)]R_{n0}(z)\}, \\
M_n(z) &= (N-1)R_{n0}(z) + R_{n1}(z).
\end{aligned}$$

It is fairly easy to verify that, in terms of displacements v, w and stresses σ_{rr} , up to the notation, the images coincide with the solution of a similar problem for an elastic medium given in [20], when replacing $\gamma_1\alpha$ by value γ_1 . Thus, in a linear approximation with respect to the elastic medium, the shear wave velocity changes and, naturally, additional components of the stress-strain state appear.

16.7 Originals of the Solution

It follows from (16.38), (16.39) and (16.40) that the coefficients in front of the exponents in the images of the influence functions are rational functions of the parameter s . An analysis of the powers of the numerators and denominators shows that all fractions except of $H_{wwn}^{(0)L}(r, s)$, $H_{\sigma rrwn}^{(0)L}(r, s)$, and $H_{\sigma rrvn}^{(0)L}(r, s)$ are correct. We distinguish the whole parts of these functions:

$$\begin{aligned}
 H_{wwn}^{(0)L}(r, s) &= \frac{1}{r} + H_{wwnr}^{(0)L}(r, s), \\
 H_{\sigma rrwn}^{(0)L}(r, s) &= -\frac{s}{r} + \frac{a_{rm}r + b_{rm}}{r^2} + H_{\sigma rrvnr}^{(0)L}(r, s), \\
 H_{\sigma rrvn}^{(0)L}(r, s) &= -\frac{N}{\gamma_{1\alpha}r} + H_{\sigma rrvnr}^{(0)L}(r, s), \\
 a_{rm} &= \frac{N}{2} + 1, \quad b_{rm} = 2(1 - \kappa) - \frac{N}{2}.
 \end{aligned}
 \tag{16.41}$$

where functions with an additional index « r » are regular fractions. The originals of such functions are quite simply found using residues. It should be borne in mind that they have a second-order pole at a point $s = 0$, as well as simple poles at the points $s = s_j$ —zeros of the polynomial $P_n(s)$.

The inverse of the Laplace transform for functions in (16.41) gives the following result [15]:

$$\begin{aligned}
 H_{wwn}^{(0)}(r, \tau) &= \frac{1}{r} \delta(\tau) + H_{wwnr}^{(0)}(r, \tau), \\
 H_{\sigma rrwn}^{(0)}(r, \tau) &= -\frac{1}{r} \delta'(\tau) + \frac{a_{rm}r + b_{rm}}{r^2} \delta(\tau) + H_{\sigma rrvnr}^{(0)}(r, \tau), \\
 H_{\sigma rrvn}^{(0)}(r, \tau) &= -\frac{N}{\gamma_{1\alpha}r} \delta(\tau) + H_{\sigma rrvnr}^{(0)}(r, \tau),
 \end{aligned}$$

where $\delta(\tau)$ is the Dirac delta function.

The originals of the influence functions in accordance with (16.38) and the transformation properties are as follows:

$$G_{\xi \zeta n}(r, \tau) = \sum_{k=0}^1 H_{\xi \zeta n}^{(k)}(r, \tau - \rho_k) H(\tau - \rho_k),$$

where $H(\tau)$ is the unit Heaviside function. The originals of the coefficients of the series according to (16.33) and (16.34) are the corresponding linear combinations of convolutions of the right-hand sides of the boundary conditions (16.16) with the influence functions.

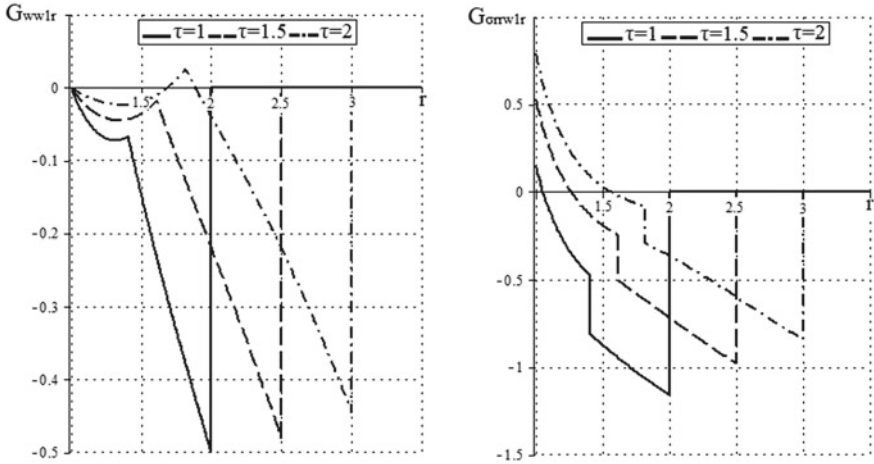


Fig. 16.1 Distribution of the regular component of the influence function G_{ww1r} and G_{σ_{rrw1r} along the radius at different points in time

16.8 Examples

As an example, we consider a medium in the form of a composite of aluminum fraction in an epoxy matrix with the following physical characteristics [19]:

$$\lambda = 7.59 \text{ MPa}, \quad \mu = 1.89 \text{ MPa}, \quad \gamma + \xi = 2.64 \text{ kN}, \quad J = 0.429 \times 10^{-3} \text{ kg/m}$$

Taking a characteristic linear size $L = 1 \text{ m}$, we obtain dimensionless parameters:

$$\gamma_1 = 2.45; \quad \gamma_2 = 0.92; \quad \alpha' = 0.66 \times 10^{-3}; \quad \delta = 5.1 \times 10^6.$$

As an example, Figs. 16.1 and 16.2 show graphs of changes in the influence functions corresponding to radial displacement and stress, along the radius and time, respectively. They are characterized by surges in stress and the derivative of displacement at the fronts $\tau = r - 1$ and $\tau = \gamma_{1\alpha} (r - 1)$ waves.

16.9 Conclusion

An analytical solution of the propagation problem of axisymmetric unsteady perturbations from a spherical cavity in a Cosserat medium was built by first-order approximation respectively to a small parameter connecting the fields of displacements and rotations. It is shown that there are two wave fronts corresponding to

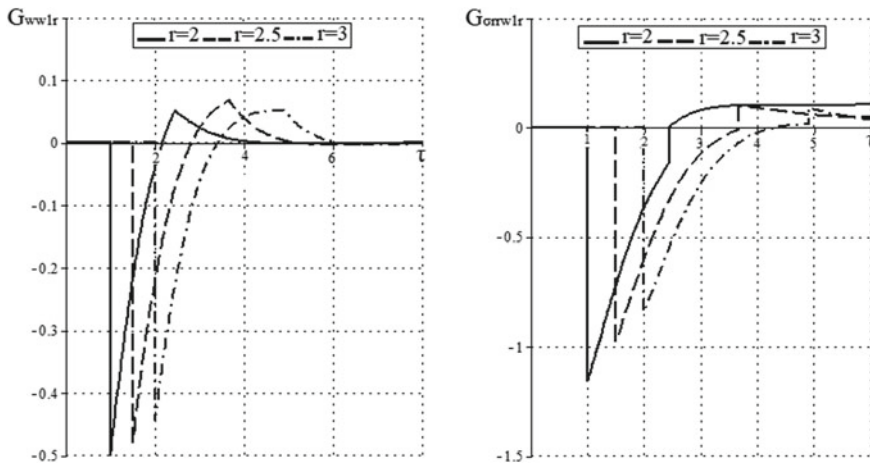


Fig. 16.2 Dependence of the regular component of the influence function G_{ww1r} and $G_{\sigma_{rrw1r}}$ on time for various values of the radius

a tensile-compression wave and a shear wave modified regarding to free rotation. The subject of further research may consider a subsequent approximation in order to assess the accuracy of the created solution.

Acknowledgements This was funded by the subsidy from RFBR (Project 17-08-00493).

References

1. Cosserat, E., Cosserat, F.: *Théorie des corps déformables*. Herman et Fils, Paris (1909). (in French)
2. Han, S.Y., Narasimhan, M.N.L., Kennedy, T.C.: Dynamic propagation of a finite crack in a micropolar elastic solid. *Acta Mech.* **85**(3–4), 179–191 (1990)
3. Sargsyan, S.H., Atoyán, A.A.: Problem of dynamics of thin plate on the basis of asymmetric theory of elasticity. *Izv. AS SSR Armenia Mech.* **57**(2), 18–33 (2004). (in Russian)
4. Vitali, G.: Fundamental solutions in the linear micropolar theory of elasticity. *Bul. Inst. politehn. Iasi.* **1**, 263–268 (1985)
5. Kumar, R., Singh, R., Chadha, T.K.: Eigenvalue approach to second dynamic problem of micropolar elastic solid. *Indian J. Pure Appl. Math.* **34**, 743–754 (2003)
6. Saxena, H.S., Dhaliwal, R.S.: Eigenvalue approach to axially-symmetric coupled micropolar thermoelasticity. *Bull. Pol. Acad. Sci. Tech. Sci.* **38**(1), 7–18 (1990)
7. Biršan, M.: Thermal stresses in cylindrical Cosserat elastic shells. *Eur. J. Mech. A/Solids* **28**(1), 94–101 (2009)
8. Sargsyan, S.H.: The general theory of magnetothermoelasticity of thin shells. *Proc. Natl. Acad. Sci. Armenia Mech.* **63**(3), 41–51 (2010). (in Russian)
9. Lai, T.T., Tarlakovskii, D.V.: Propagation of non-stationary kinematic perturbations from a spherical cavity in the Cosserat pseudocontinuum. *Mech. Compos. Mater. Struct.* **17**(2), 184–195 (2011)
10. Belonosov, S.M.: *Moment Theory of Elasticity*. Dal'nauka, Vladivostok (1993). (in Russian)

11. Bolshakov, V.I., Andrianov, I.V., Danishevs'kyy, V.V.: *Asymptotic Methods for Calculation of Composite Materials with Microstructure*. Porogi, Dnipropetrovs'k (2008). (in Russian)
12. Aero, E.L., Kuvshinskii, E.V.: Continuum theory of asymmetric elasticity. The equilibrium of an isotropic body. *Fizika Tverdogo* **6**(9), 2689–2699 (1964). (in Russian)
13. Aero, E.L., Kuvshinskii, E.V.: Fundamental equations of the theory of elastic media with rotationally interacting particles. *Fizika Tverdogo* **2**(7), 1399–1409 (1960). (in Russian)
14. Nowacki, V.: *Teoriya Uprugost*. Mir, Moscow, Russia (1975). (in Russian)
15. Gorshkov, A.G., Medvedsky, A.L., Rabinsky, L.N., Tarlakovsky, D.V.: *Volny v sploshnykh sredakh*. Fizmatlit, Moscow, Russia (2004). (in Russian)
16. Abramowitz, M., Stegun, I.A.: *Handbook of Mathematical Functions with Formulas, Graphs and Mathematical Tables*. U.S. Department of Commerce, National Bureau of Standards (1964)
17. Vestyak, V.A., Tarlakovskii, D.V.: Unsteady axisymmetric deformation of an elastic space with a spherical cavity under the action of body forces. *Moscow Univ. Mech. Bull.* **71**(4), 87–92 (2016)
18. Vestyak, V.A., Tarlakovskiy, D.V.: Elastic ball under non-stationary axially symmetrical volume forces. *ZAMM Z. Angew. Math. Mech.* **97**(1), 25–37 (2017)
19. Erofeev, V.I.: *Volnovye processy v tverdykh telakh s mikrostrukturoy*. MGU, Moscow, Russia (1999). (in Russian)
20. Gorshkov, A.G., Tarlakovsky, D.V.: *Nestacionarnaya aerouprugost tel sfericheskoy formy*. Nauka, Moscow, Russia (1990). (in Russian)

Chapter 17

The Equations of Coupled Dynamics of Electromagnetoelastic Thin Shells



Thong D. Pham, Dmitry V. Tarlakovskii and Vladimir A. Vestyak

Abstract In this paper, a coupled mathematical model of unsteady processes is constructed in a thin linearly elastic homogeneous anisotropic shell interacting with an electromagnetic field. The equations of its motion are used taking into account the rotation of the normal fiber and compression. They are supplemented by the three-dimensional Maxwell's equations, the generalized Ohm's law, expressions for the Lorentz force and the physical law taking into account the piezoelectric effects. These relations, like the mechanical values, are linearized along the transverse coordinate. As a result, a closed-form solution of system of equations is constructed. From it, the closed-form solutions of systems of equations for an isotropic shell and plate are also constructed as special cases.

Keywords Thin shell · Plate · Non-stationary processes · Rotation of a normal fiber · Coupled electromagnetoelasticity · Maxwell's equations · Generalized Ohm's law · Lorentz force · Piezo effects · Lateral linearization · Closed-form solution for system of equations

17.1 Introduction

At the present time, the most studied problems are the propagation of unsteady perturbations in classical elastic media without taking into account their interaction with fields of a different physical nature, including the electromagnetic fields considered in this work. In most well-known publications, this interaction is taken into account at the level of unrelated tasks. Issues related to the existence and uniqueness of solving problems of non-stationary coupled electromagnetoelasticity have been developed mainly from the middle and end of the 80s of the last century. The fundamental equations of electromagnetoelastic interactions, including the divergence equations, the

T. D. Pham (✉) · D. V. Tarlakovskii · V. A. Vestyak
Moscow Aviation Institute, Moscow, Russian Federation

D. V. Tarlakovskii
Institute of Mechanics, Lomonosov Moscow State University, Moscow, Russian Federation

© Springer Nature Switzerland AG 2020
H. Altenbach et al. (eds.), *Nonlinear Wave Dynamics of Materials and Structures*, Advanced Structured Materials 122,
https://doi.org/10.1007/978-3-030-38708-2_17

gradient equations, the constitutive relations, and the boundary and initial conditions for supplementing them, are given in the monograph of Parton and Kudryavtsev [1], as well as in the works of Korotkina [2], Pao and Yeh [3], Pao [4], Primenko and Vishnevskii [5], Ryu et al. [6], Altay and Cengiz Dökmeçi [7]. Integral equations are derived for some media and the basic properties are investigated.

Many works considered static problems for specific structural elements, for example, an analytical solution for electromagnetoelastic beams with different boundary conditions [8], an exact three-dimensional solution [9, 10], a state vector approach [11], a solution with a discrete layer [12, 13], and a partially mixed layer-by-layer finite element model [14] for multilayer electromagnetoelastic plates. Bardzokas and Senik in [15] described some general statements of problems of the theory of electromagnetoelasticity. As for this problem, they used the basic relations of the theory of elasticity and some additional relations for the coupling of electromagnetic and mechanical fields. Particular attention was paid to the construction of the theory of shells and plates from piezoelectric materials. Ambartsumyan et al. in [16] and Baghdasaryan and Danoyan in [17] used only the magnetic component to take into account the electromagnetic field to solve the Lamb problem and a number of problems of magnetoelasticity of shells and plates.

The next stage of complication of the problem is dynamic problems. Extensive research of dynamic problems of electromagnetoelasticity for different structural elements, for example, plates in [18–26], as well as cylindrical and spherical shells in [27–36]. Pan and Heyliger [21] solved the problem of vibration of a laminated rectangular plate with a simple support. Buchanan [27] determined and compared the natural frequencies of layered and different multiphase plate models using finite element analysis. Dynamic problems of electromagnetoelasticity for ceramic bodies were investigated by Shlyakhin in [37]. In this work, the problem of a circular radially polarized ceramic plate was considered. Storozhev and Bai [38] proposed a numerical-analytical approach to solving the problems of electromagnetoelasticity for a piezoceramic plate. The proposed approach allows to obtain a solution of the dispersion equation for any medium of the plate. Using the finite element method, Annigeri et al. [29] researched the free vibrations of layered and multiphase electromagnetoelastic shells, and Daga et al. [31] conducted a comparative study of the transient response of an electromagnetoelastic finite cylindrical shell at constant internal pressure. On the other hand, in the works of Green and Naghdi [39], they created nonlinear and linear thermomechanical theories of deformable shell bodies, which take into account the electromagnetic effect of a direct approach using the two-dimensional theory of direct media called a Cosserat surfaces. In [40], models of electromagnetic plates and shells of higher order were developed. Higher-order theory is based on the expansion of the three-dimensional equations of the linear theory of electromagnetic elasticity into Fourier series in terms of Legendre polynomials. All equations for the theory of higher orders of electromagnetoelastic plates in Cartesian and polar coordinates, as well as for cylindrical and spherical shells in the coordinates associated with the geometry of the shells, are developed and presented in detail in this work.

In this paper, unlike other works, in addition to the angle of rotation of a normal fiber, its compression, as well as the Lorentz force, is taken into account. We also used the generalized Ohm's law, and linearization of the normal coordinate of Maxwell's equations is carried out directly without using the functional. The resolving system of equations is given in an explicit form, which allows it to be used for specific problems without additional transformations.

17.2 Equations of Motion of the Elastic Shell at Given Loads

We consider a thin linearly elastic homogeneous anisotropic shell of thickness h with a smooth middle surface

$$\Pi : \mathbf{r} = \mathbf{r}_0(\xi^1, \xi^2), (\xi^1, \xi^2) \in D \subset \mathbb{R}^2 \quad (17.1)$$

where \mathbf{r} —radius vector and ξ^1, ξ^2 —curvilinear coordinates.

The basis π_1, π_2 of tangent space, the normal vector \mathbf{n} , the components of the curvature tensor b_{ij} , and the components of the metric basis tensor g_{ij} of basis π_1, π_2, \mathbf{n} are defined by the equalities:

$$\begin{aligned} \pi_j &= \frac{\partial \mathbf{r}_0}{\partial \xi^j}, \quad \mathbf{n} = \mathbf{N}/|\mathbf{N}|, \quad \mathbf{N} = [\pi_1, \pi_2], \quad b_{ij} = \left(\frac{\partial \pi_i}{\partial \xi^j}, \mathbf{n} \right) = \left(\frac{\partial \pi_j}{\partial \xi^i}, \mathbf{n} \right), \\ g_{ij} &= (\pi_i, \pi_j), \quad g_{i3} = 0, \quad g_{33} = 1. \end{aligned} \quad (17.2)$$

Hereinafter, unless otherwise indicated, the Latin indices take the values 1 and 2. The equations of motion of the sheath, taking into account the rotation of the normal fiber and its compression in the basis π_1, π_2, \mathbf{n} are written as follows in [41] (time derivatives are indicated by dots):

$$\begin{aligned} \rho h \ddot{u}^i &= \nabla_j T^{ji} - b_j^i \dot{Q}^j + q^i + q_e^i, \quad \rho h \ddot{w} = \nabla_i \dot{Q}^i + b_{ij} T^{ij} + q + q_e, \\ \rho I \ddot{\psi}^i &= \nabla_j M^{ij} - \dot{Q}^i + m^i + m_e^i, \quad \rho I \ddot{\psi}_3 = \nabla_i \mu^i - N + m + m_e, \quad I = h^3/12; \end{aligned} \quad (17.3)$$

$$Q^i = \hat{Q}^i + b_j^i \mu^j, \quad T^{ij} = \hat{T}^{ij} + b_k^i M^{kj}, \quad N = \hat{N} - b_{ij} M^{ij} \quad (17.4)$$

$$\begin{aligned} \hat{T}^{ij} &= \int_{-h/2}^{h/2} \sigma^{ij} dz, \quad M^{ij} = \int_{-h/2}^{h/2} z \sigma^{ij} dz, \quad \hat{Q}^i = \int_{-h/2}^{h/2} \sigma^{i3} dz, \\ \mu^i &= \int_{-h/2}^{h/2} z \sigma^{i3} dz, \quad \hat{N} = \int_{-h/2}^{h/2} \sigma^{33} dz; \end{aligned} \quad (17.5)$$

Here, the index 3 corresponds to the normal to the middle surface coordinate z ; ρ —material density; u_i and w —tangential and normal displacement; ψ_i —angles of

rotation normal to the fiber surface Π , ψ_3 —its deformation; σ^{ij} , σ^{i3} , σ^{33} —stress tensor components; $\mathbf{q}_e = q_e^i \pi_i + q_e \mathbf{n}$ and $\mathbf{m}_e = m_e^i \pi_i + m_e \mathbf{n}$ —vectors of surface pressure and referred to the unit area of the moment initiated by the electromagnetic field; $\mathbf{q} = q^i \pi_i + q \mathbf{n}$, $\mathbf{m} = m^i \pi_i + m \mathbf{n}$ —similar values of a different nature.

These equations are added kinematic relations

$$\begin{aligned} \varepsilon_{ij} &= \frac{1}{2} (\alpha_{ij} + \alpha_{ji}), \quad \kappa_{ij} = \frac{1}{2} (\beta_{ij} + \beta_{ji}), \\ \alpha_{ij} &= \nabla_i u_j - b_{ij} w, \quad \beta_{ij} = \nabla_i \psi_j - b_{ij} \psi_3 + b_i^k \alpha_{kj}, \\ -\vartheta_i &= \nabla_i w + b_i^k u_k, \quad \theta_k = \psi_k - \vartheta_k. \end{aligned} \tag{17.6}$$

where u_i and ε_{ij} —tangential displacements and deformations; w —normal displacement; κ_{ij} —components of the curvature change tensor; ψ_3 follows from the equation—relative elongation of normal fiber; ψ_i —angles between normal vector \mathbf{n} normal fiber in a deformed state.

Equalities Eq. (17.6) are obtained using the direct normal hypothesis, namely, approximate equalities for the displacement vector \mathbf{u} :

$$\begin{aligned} \mathbf{u}(\xi^1, \xi^2, z, t) &= [u_i(\xi^1, \xi^2, t) + \psi_i(\xi^1, \xi^2, t)z] \pi_i \\ &+ [w(\xi^1, \xi^2, t) + \psi_3(\xi^1, \xi^2, t)z] \mathbf{n} \end{aligned} \tag{17.7}$$

The boundary conditions for the system of Eqs. (17.3), (17.4), and (17.6) have the following forms [41] (the right parts are given):

$$\begin{aligned} u_i|_{\Gamma_u} &= u_{(0)i}, \quad w|_{\Gamma_u} = w_{(0)}, \quad \psi_i|_{\Gamma_u} = \psi_{(0)i}, \quad \psi_3|_{\Gamma_u} = \psi_{(0)3}, \\ T^{ji} v_j|_{\Gamma_\sigma} &= T_{(0)}^i, \quad M^{ij} v_j|_{\Gamma_\sigma} = M_{(0)}^i, \quad Q^i v_i|_{\Gamma_\sigma} = Q_{(0)}, \quad \mu^i v_i|_{\Gamma_\sigma} = \mu_{(0)} \end{aligned}$$

Here, $\partial\Pi = \Gamma = \Gamma_u \cup \Gamma_\sigma$; $\hat{\nu} = \nu_i \mathbf{e}^i$ —the unit normal vector to the lateral surface Π_b of the shell at $z = 0$ (at the intersection line $\Pi_b \cap \Pi = \Gamma$). Moreover, the curves Γ_u and Γ_σ can intersect only in the set of measure zero.

The necessary expressions for closed-form of system of Eqs. (17.3)–(17.6), expressions for the coordinates of the vector \mathbf{q}_e and the stresses σ^{ij} , σ^{i3} , σ^{33} are considered below.

17.3 Closed-Form Solution for System of Equations of an Electromagnetoelastic Shell

We use the following three-dimensional relations of electromagnetoelasticity in [42] as follows:

– Maxwell's equations

$$\operatorname{rot} \mathbf{E} = -\frac{1}{c} \frac{\partial \mathbf{B}}{\partial t}, \quad \operatorname{rot} \mathbf{H} = \frac{4\pi}{c} \mathbf{j} + \frac{1}{c} \frac{\partial \mathbf{D}}{\partial t}, \quad \operatorname{div} \mathbf{D} = 4\pi \rho_e \quad (17.8)$$

– Linearized with respect to the initial state (its components are indicated by the additional index «0») the generalized Ohm's law and the expression for the Lorentz force \mathbf{F}_e

$$\mathbf{j} = \sigma(\mathbf{E} + c^{-1}[\mathbf{v}, \mathbf{B}_0]) + \rho_e \mathbf{v}; \quad (17.9)$$

$$\mathbf{F}_e = F_e^i \pi_i + E_{e3} \mathbf{n} = \rho_{e0} \mathbf{E} + \rho_e \mathbf{E}_0 + c^{-1}([\mathbf{j}_0, \mathbf{B}] + [\mathbf{j}, \mathbf{B}_0]); \quad (17.10)$$

– Physical relations

$$\begin{aligned} D^i &= e^{ij} E_j + e^{i3} E_3 + \kappa^{ijk} \hat{\varepsilon}_{jk} + 2\kappa^{ij3} \hat{\varepsilon}_{j3} + \kappa^{i33} \varepsilon_{33}, \\ D_3 &= e^{3j} E_j + e^{33} E_3 + \kappa^{3jk} \hat{\varepsilon}_{jk} + 2\kappa^{3j3} \hat{\varepsilon}_{j3} + \kappa^{333} \varepsilon_{33}, \\ B^i &= \mu^{ij} H_j + \mu^{i3} H_3 + \gamma^{ijk} \hat{\varepsilon}_{jk} + 2\gamma^{ij3} \hat{\varepsilon}_{j3} + \gamma^{i33} \varepsilon_{33}, \\ B_3 &= \mu^{3j} H_j + \mu^{33} H_3 + \gamma^{3jk} \hat{\varepsilon}_{jk} + 2\gamma^{3j3} \hat{\varepsilon}_{j3} + \gamma^{333} \varepsilon_{33}, \\ \hat{\varepsilon}_{jk} &= \varepsilon_{jk} + z\kappa_{jk}, \quad \hat{\varepsilon}_{j3} = \theta_j + z \left(b_j^n \theta_n + \nabla_k \psi_3 \right), \quad \varepsilon_{33} = \psi_3; \end{aligned} \quad (17.11)$$

$$\begin{aligned} \sigma^{ij} &= C^{ijkl} \hat{\varepsilon}_{kl} + C^{ij33} \psi_3 - \left(\kappa^{ijk} E_k + \kappa^{ij3} E_3 + \gamma^{ijk} H_k + \gamma^{ij3} H_3 \right) / 4\pi, \\ \sigma^{i3} &= C^{i3k3} \hat{\varepsilon}_{k3} - \left(\kappa^{i3k} E_k + \kappa^{i33} E_3 + \gamma^{i3k} H_k + \gamma^{i33} H_3 \right) / 4\pi, \\ \sigma^{33} &= C^{33kl} \hat{\varepsilon}_{kl} + C^{3333} \psi_3 - \left(\kappa^{33k} E_k + \kappa^{333} E_3 + \gamma^{33k} H_k + \gamma^{333} H_3 \right) / 4\pi. \end{aligned} \quad (17.12)$$

where $\mathbf{E} = E^i \pi_i + E_3 \mathbf{n}$ and $\mathbf{H} = H^i \pi_i + H_3 \mathbf{n}$ —vectors of electric and magnetic fields; $\mathbf{D} = D^i \pi_i + D_3 \mathbf{n}$ and $\mathbf{B} = B^i \pi_i + B_3 \mathbf{n}$ —vectors of electric and magnetic induction; $\mathbf{j} = j^i \pi_i + j_3 \mathbf{n}$ —current density; c —speed of light; ρ_e —charge density; σ —conductivity coefficient; $\mathbf{v} = \dot{\mathbf{u}}$ —velocity of medium points; e^{ij} and μ^{ij} —dielectric and magnetic tensors; κ^{ijk} and γ^{ijk} —tensors of piezoelectric and piezomagnetic constants; C^{ijkl} ($i, j, k, l = 1, 2, 3$)—elastic constant tensor.

In this case, assume that in the initial state the electromagnetic parameters are independent of coordinate z and satisfy the following equalities ($i = 1, 2, 3$):

$$\begin{aligned} (\dot{\mathbf{B}})_0 &= 0, \quad (\dot{\mathbf{D}})_0 = 4\pi \mathbf{j}_{s0}, \quad \operatorname{rot} \mathbf{E}_0 = \mathbf{0}, \\ \operatorname{rot} \mathbf{H}_0 &= \frac{4\pi}{c} (\mathbf{j}_0 + \mathbf{j}_{s0}), \quad \operatorname{div} \mathbf{D}_0 = 4\pi \rho_{e0}, \quad \mathbf{j}_0 = \sigma \mathbf{E}_0, \end{aligned}$$

where \mathbf{j}_{s0} is the bias current.

One of the variants of the boundary conditions for the electromagnetic field in the three-dimensional region G has the following form [1, 2, 43–45] (the right parts are specified)

$$[\mathbf{B}, \nu]|_{\partial G} = \mathbf{P}, \quad (\mathbf{D}, \nu)|_{\partial G} = P \tag{17.13}$$

Another variant of the boundary conditions can be written through the potentials of the electromagnetic field. However, the rationale for this requires the use of appropriate functionality, which is not used here. At the same time, the boundary conditions can be specified as below:

$$\mathbf{E}|_{\Pi_E} = \mathbf{e}, \quad \mathbf{H}|_{\Pi_H} = \mathbf{h} \tag{17.14}$$

where $\partial G = \Pi_E \cup \Pi_H$. Moreover, the surfaces Π_E and Π_H can intersect only in the set of measure zero.

Included in the right parts of Eq. (17.3) components of the vectors \mathbf{q}_e and \mathbf{m}_e similar mechanical values in [41] are defined as follows:

$$q_e^i = \int_{-h/2}^{h/2} F_e^i dz, \quad q_e = \int_{-h/2}^{h/2} F_{e3} dz, \quad m_e^i = \int_{-h/2}^{h/2} z F_e^i dz, \quad m_e = \int_{-h/2}^{h/2} z F_{e3} dz \tag{17.15}$$

The components of the electromagnetic field present in a level of approximation formulas (17.5):

$$\begin{aligned} E_i &= e_i(\xi^1, \xi^2, t) + z\chi_i(\xi^1, \xi^2, t), \\ H_i &= h_i(\xi^1, \xi^2, t) + z\varphi_i(\xi^1, \xi^2, t), \\ D_i &= d_i(\xi^1, \xi^2, t) + z\delta_i(\xi^1, \xi^2, t), \\ B_i &= b_i(\xi^1, \xi^2, t) + z\beta_i(\xi^1, \xi^2, t), \\ j_i &= y_i(\xi^1, \xi^2, t) + z\nu_i(\xi^1, \xi^2, t), \\ \rho_e &= r_e(\xi^1, \xi^2, t) + z\lambda_e(\xi^1, \xi^2, t) \quad (i = 1, 2, 3). \end{aligned} \tag{17.16}$$

Substituting these equalities in Eqs.(17.11) and (17.12), taking into account Eq. (17.15), we obtain the following forms of physical laws for the shell:

$$\begin{aligned} d^i &= e^{ij}e_j + e^{i3}e_3 + \kappa^{ijk}\varepsilon_{jk} + \kappa^{ij3}\theta_j + \kappa^{i33}\psi_3, \\ b^i &= \mu^{ij}h_j + \mu^{i3}h_3 + \gamma^{ijk}\varepsilon_{jk} + \gamma^{ij3}\theta_j + \gamma^{i33}\psi_3, \\ \delta^i &= e^{ij}\chi_j + e^{i3}\chi_3 + \kappa^{ijk}\kappa_{jk} + \kappa^{ij3}\left(b_j^n\theta_n + \nabla_j\psi_3\right), \\ \beta^i &= \mu^{ij}\varphi_j + \mu^{i3}\varphi_3 + \gamma^{ijk}\kappa_{jk} + \gamma^{ij3}\left(b_j^n\theta_n + \nabla_j\psi_3\right) \quad (i, j, k = 1, 2, 3); \end{aligned} \tag{17.17}$$

$$\begin{aligned}
\hat{T}^{ij} &= h \left[(C^{ijkl} \varepsilon_{kl} + C^{ij33} \psi_3) - \frac{1}{4\pi} (\kappa^{ijk} e_k + \kappa^{ij3} e_3 + \gamma^{ijk} h_k + \gamma^{ij3} h_3) \right], \\
M^{ij} &= I \left[C^{ijkl} \kappa_{kl} - \frac{1}{4\pi} (\kappa^{ijk} \chi_k + \kappa^{ij3} \chi_3 + \gamma^{ijk} \varphi_k + \gamma^{ij3} \varphi_3) \right], \\
\hat{Q}^i &= h \left[C^{i3k3} \theta_k - \frac{1}{4\pi} (\kappa^{i3k} e_k + \kappa^{i33} e_3 + \gamma^{i3k} h_k + \gamma^{i33} h_3) \right], \\
\mu^i &= I \left[C^{i3k3} (b_k^l \theta_l + \nabla_k \psi_3) - \frac{1}{4\pi} (\kappa^{i3k} \chi_k + \kappa^{i33} \chi_3 + \gamma^{i3k} \varphi_k + \gamma^{i33} \varphi_3) \right], \\
\hat{N} &= h \left[C^{33kl} \varepsilon_{kl} + C^{3333} \psi_3 - \frac{1}{4\pi} (\kappa^{33k} e_k + \kappa^{333} e_3 + \gamma^{33k} h_k + \gamma^{333} h_3) \right].
\end{aligned} \tag{17.18}$$

In constructing the last relations in Eq. (17.18), it is assumed that the following symmetry holds:

$$C^{ijk3} = C^{i3kl} = C^{i333} = C^{33k3} = 0 \tag{17.19}$$

To linearize Eqs. (17.9) and (17.10) along coordinate z , we use the following equality for the vector product in [46]

$$[\mathbf{j}, \mathbf{B}] \sqrt{g} = (j_2 B_3 - j_3 B_2) \pi_1 + (j_3 B_1 - j_1 B_3) \pi_2 + (j_1 B_2 - j_2 B_1) \mathbf{n} \tag{17.20}$$

where g —second invariant of the metric tensor.

As a result, with the additional use of Eq. (17.17), we obtain an analog of Ohm's law:

$$\begin{aligned}
v^1 &= \sigma \left[e^1 + c_g \left(\dot{u}_2 B_{03} - \dot{w} \hat{B}_{02} \right) \right] + \rho_{e0} \dot{u}^1, \\
v^1 &= \sigma \left[\chi^1 + c_g \left(\dot{\psi}_2 B_{03} - \dot{\psi}_3 \hat{B}_{02} \right) \right] + \rho_{e0} \dot{\psi}^1, \\
v^2 &= \sigma \left[e^2 + c_g \left(\dot{w} \hat{B}_{01} - \dot{u}_1 B_{03} \right) \right] + \rho_{e0} \dot{u}^2, \\
v^2 &= \sigma \left[\chi^2 + c_g \left(\dot{\psi}_3 \hat{B}_{01} - \dot{\psi}_1 B_{03} \right) \right] + \rho_{e0} \dot{\psi}^2, \\
v_3 &= \sigma \left[e_3 + c_g \left(\dot{u}_1 \hat{B}_{02} - \dot{u}_2 \hat{B}_{01} \right) \right] + \rho_{e0} \dot{w}, \\
v_3 &= \sigma \left[\chi_3 + c_g \left(\dot{\psi}_1 \hat{B}_{02} - \dot{\psi}_2 \hat{B}_{01} \right) \right] + \rho_{e0} \dot{\psi}_3, \\
c_g &= c^{-1} g^{-1/2};
\end{aligned} \tag{17.21}$$

Using a similar procedure to Eq. (17.10), we obtain the components of the vectors \mathbf{q}_e and \mathbf{m}_e from Eq. (17.15)

$$\begin{aligned}
q_e^1 &= h [\rho_{e0} e^1 + r_e E_0^1 + c_g (j_{02} b_3 - j_{03} b_2 + y_2 B_{03} - y_3 B_{02})], \\
q_e^2 &= h [\rho_{e0} e^2 + r_e E_0^2 + c_g (j_{03} b_1 - j_{01} b_3 + y_3 B_{01} - y_1 B_{03})], \\
q_e &= h [\rho_{e0} e_3 + r_e E_{03} + c_g (j_{01} b_2 - j_{02} b_1 + y_1 B_{02} - y_2 B_{01})], \\
m_e^1 &= I [\rho_{e0} \chi^1 + \lambda_e E_0^1 + c_g (j_{02} \beta_3 - j_{03} \beta_2 + v_2 B_{03} - v_3 B_{02})], \\
m_e^2 &= I [\rho_{e0} \chi^2 + \lambda_e E_0^2 + c_g (j_{03} \beta_1 - j_{01} \beta_3 + v_3 B_{01} - v_1 B_{03})], \\
m_e &= I [\rho_{e0} \chi_3 + \lambda_e E_{03} + c_g (j_{01} \beta_2 - j_{02} \beta_1 + v_1 B_{02} - v_2 B_{01})].
\end{aligned} \tag{17.22}$$

In order to construct a «shell» analog of Eq. (17.8) for vector

$$\mathbf{u} = \hat{u}^i \pi_i + u_3 \mathbf{n} = \tilde{u}^i \mathbf{e}_i + \tilde{u}_3 \mathbf{n},$$

we use equalities in [46]

$$\begin{aligned}
\sqrt{g} \text{rot } \mathbf{u} &= (\tilde{\nabla}_2 \tilde{u}_3 - \tilde{\nabla}_3 \tilde{u}_2) \pi_1 + (\tilde{\nabla}_3 \tilde{u}_1 - \tilde{\nabla}_1 \tilde{u}_3) \pi_2 + (\tilde{\nabla}_1 \tilde{u}_2 - \tilde{\nabla}_2 \tilde{u}_1) \mathbf{n}, \\
\text{div } \mathbf{u} &= \tilde{\nabla}_i \tilde{u}^i + \tilde{\nabla}_3 \tilde{u}_3,
\end{aligned} \tag{17.23}$$

where $\mathbf{e}_1, \mathbf{e}_2, \mathbf{n}$ —the spatial basis, the first two vectors of which and the components $\tilde{g}_{ij}, \tilde{g}_{i3}, \tilde{g}_{33}$ of its metric tensor are defined as follows [42]:

$$\begin{aligned}
\mathbf{e}_j &= \frac{\partial}{\partial \xi^j} (\mathbf{r}_0 + z \mathbf{n}) = q_j^i \pi_i, \quad q_j^i = \delta_j^i - z b_j^i, \\
\tilde{g}_{ij} &= (\mathbf{e}_i, \mathbf{e}_j) = g_{ij} - 2z b_{ij}, \quad \tilde{g}_{i3} = 0, \quad \tilde{g}_{33} = 1, \quad \tilde{g}^{ij} = g^{ij} + 2z b^{ij}.
\end{aligned} \tag{17.24}$$

The covariant derivatives in Eq. (17.23) have the form:

$$\begin{aligned}
\tilde{\nabla}_i \tilde{u}_j &= \nabla_i \hat{u}_j - b_{ij} u_3 + z (c_{ij} u_3 - b_j^k \nabla_i \hat{u}_k), \quad c_{ij} = b_{ik} b_j^k, \\
\tilde{\nabla}_i \tilde{u}_3 &= \frac{\partial u_3}{\partial \xi^i} + b_i^k \hat{u}_k, \quad \tilde{\nabla}_3 \tilde{u}_i = \frac{\partial \hat{u}_i}{\partial z} - z b_i^k \frac{\partial \hat{u}_k}{\partial z}, \quad \tilde{\nabla}_3 \tilde{u}_3 = \frac{\partial u_3}{\partial z}.
\end{aligned} \tag{17.25}$$

This implies the following relation:

$$\tilde{\nabla}_i \tilde{u}^i = \tilde{g}^{im} \tilde{\nabla}_i \tilde{u}_m = \nabla_i \hat{u}^i - 2H u_3 + z [b^{ik} \nabla_i \hat{u}_k - 2(2H^2 - K) u_3], \tag{17.26}$$

where $H = (b_1^1 + b_2^2)/2$ and $K = (b_{11} b_{22} - b_{12}^2)/g$ —mean and Gaussian curvature of the surface Π .

Now, using Eqs. (17.23), (17.25), (17.26), and (17.17), from Eq. (17.8) we obtain:

$$\begin{aligned}
\frac{\partial e_3}{\partial \xi^2} + b_2^k e_k - \chi_2 &= -\frac{\sqrt{g}}{c} \dot{b}^1, \quad \chi_1 - \frac{\partial e_3}{\partial \xi^1} - b_1^k e_k = -\frac{\sqrt{g}}{c} \dot{b}^2, \\
\nabla_1 e_2 - \nabla_2 e_1 &= -\frac{\sqrt{g}}{c} \dot{b}_3;
\end{aligned} \tag{17.27}$$

$$\begin{aligned} \frac{\partial h_3}{\partial \xi^2} + b_2^k h_k - \varphi_2 &= \frac{\sqrt{g}}{c} (4\pi y^1 + \dot{d}^1), \quad \varphi_1 - \frac{\partial h_3}{\partial \xi^1} - b_1^k h_k = \frac{\sqrt{g}}{c} (4\pi y^2 + \dot{d}^2), \\ \nabla_1 h_2 - \nabla_2 h_1 &= \frac{\sqrt{g}}{c} (4\pi y_3 + \dot{d}_3); \end{aligned} \quad (17.28)$$

$$\nabla_i d^i - 2H d_3 + \delta_3 = 4\pi r_e; \quad (17.29)$$

$$\begin{aligned} \frac{\partial \chi_3}{\partial \xi^2} + b_2^k \chi_k + b_2^k \frac{\partial e_3}{\partial \xi^k} + c_2^k e_k &= -\frac{\sqrt{g}}{c} \dot{\beta}^1, \\ \frac{\partial \chi_3}{\partial \xi^1} + b_1^k \chi_k + b_1^k \frac{\partial e_3}{\partial \xi^k} + c_1^k e_k &= \frac{\sqrt{g}}{c} \dot{\beta}^2, \end{aligned} \quad (17.30)$$

$$\nabla_1 \chi_2 - \nabla_2 \chi_1 + b_1^k \nabla_k e_2 - b_2^k \nabla_k e_1 = -\frac{\sqrt{g}}{c} \dot{\beta}_3;$$

$$\begin{aligned} \frac{\partial \varphi_3}{\partial \xi^2} + b_2^k \varphi_k + b_2^k \frac{\partial h_3}{\partial \xi^k} + c_2^k h_k &= \frac{\sqrt{g}}{c} (4\pi v^1 + \dot{\delta}^1), \\ \frac{\partial \varphi_3}{\partial \xi^1} + b_1^k \varphi_k + b_1^k \frac{\partial h_3}{\partial \xi^k} + c_1^k h_k &= -\frac{\sqrt{g}}{c} (4\pi v^2 + \dot{\delta}^2), \\ \nabla_1 \varphi_2 - \nabla_2 \varphi_1 + b_1^k \nabla_k h_2 - b_2^k \nabla_k h_1 &= \frac{\sqrt{g}}{c} (4\pi v_3 + \dot{\delta}_3); \end{aligned} \quad (17.31)$$

$$\nabla_i \delta^i - 2H \delta_3 + b^{ik} \nabla_i d_k - 2(2H^2 - K) d_3 = 4\pi \lambda_e \quad (17.32)$$

Thus, the closed-form expressions for system of equations of motion of the anisotropic electromagnetoelastic shell include Eqs. (17.3), (17.4), (17.6), (17.17), (17.18), (17.21), (17.22), and (17.27)–(17.32).

To write the boundary conditions corresponding to the electromagnetic field, we first proceed to the scalar form of Eq. (17.13):

$$\begin{aligned} g^{-1/2} (\hat{B}_2 v_3 - B_3 v_2) \Big|_{\Pi_b} &= P^1, \quad g^{-1/2} (B_3 v_1 - \hat{B}_1 v_3) \Big|_{\Pi_b} = P^2, \\ g^{-1/2} (\hat{B}_1 v_2 - \hat{B}_2 v_1) \Big|_{\Pi_b} &= P^3, \quad (D^i v_i + D_3 v_3) \Big|_{\Pi_b} = P. \end{aligned} \quad (17.33)$$

Then, using linear approximations of the right parts of these equalities

$$P^i = P_0^i + zP_1^i \quad (i = 1, 2, 3), \quad P = P_0 + zP_1$$

and Eq. (17.16) we reduce these conditions to the following forms:

$$\begin{aligned} g^{-1/2} (b_2 v_3 - b_3 v_2) \Big|_{\Gamma} &= P_0^1, \quad g^{-1/2} (b_3 v_1 - b_1 v_3) \Big|_{\Gamma} = P_0^2, \\ g^{-1/2} (b_1 v_2 - b_2 v_1) \Big|_{\Gamma} &= P_0^3, \quad (d^i v_i + d_3 v_3) \Big|_{\Gamma} = P_0, \\ g^{-1/2} (\beta_2 v_3 - \beta_3 v_2) \Big|_{\Gamma} &= P_1^1, \quad g^{-1/2} (\beta_3 v_1 - \beta_1 v_3) \Big|_{\Gamma} = P_1^2, \\ g^{-1/2} (\beta_1 v_2 - \beta_2 v_1) \Big|_{\Gamma} &= P_1^3, \quad (\delta^i v_i + \delta_3 v_3) \Big|_{\Gamma} = P_1. \end{aligned}$$

Another variant of the boundary conditions follows from Eq. (17.14):

$$\begin{aligned} e_i|_{\Pi_E} &= e_{i0}, \quad e_3|_{\Pi_E} = e_{30}, \quad h_i|_{\Pi_E} = h_{i0}, \quad h_3|_{\Pi_E} = h_{30}, \\ \chi_i|_{\Pi_E} &= \chi_{i0}, \quad \chi_3|_{\Pi_E} = \chi_{30}, \quad \varphi_i|_{\Pi_E} = \varphi_{i0}, \quad \varphi_3|_{\Pi_E} = \varphi_{30}, \end{aligned}$$

Here, the linear approximations are used:

$$\mathbf{e} = (e_{i0} + z\chi_{i0}) \mathbf{e}^i + (e_{30} + z\chi_{30}) \mathbf{n}, \quad \mathbf{h} = (h_{i0} + z\varphi_{i0}) \mathbf{e}^i + (h_{30} + z\varphi_{30}) \mathbf{n}$$

17.4 Equations for an Isotropic Conductor Shell

Under isotropic conductors in [42] refers to a medium having the following physical characteristics (here $i, j, k, l = 1, 2, 3$):

$$\begin{aligned} C^{ijkl} &= \lambda g^{ij} g^{kl} + \mu (g^{ik} g^{jl} + g^{il} g^{jk}), \quad C^{i3k3} = \mu g^{ik}, \quad C^{ij33} = \mu g^{ij}, \quad C^{3333} = \lambda + 2\mu, \\ \kappa^{ijk} &= 0, \quad \gamma^{ijk} = 0, \quad e^{ij} = \varepsilon_e g^{ij}, \quad \mu^{ij} = \mu_e g^{ij}, \end{aligned} \tag{17.34}$$

where λ and μ —Lamé constants, ε_e and μ_e —dielectric permittivity and magnetic permeability coefficients.

In this case, Eqs. (17.11) and (17.17) are significantly simplified:

$$D^i = \varepsilon_e E^i, \quad D_3 = \varepsilon_e E_3, \quad B^i = \mu_e H^i, \quad B_3 = \mu_e H_3, \tag{17.35}$$

$$\begin{aligned} d^i &= \varepsilon_e e^i, \quad d_3 = \varepsilon_e d_3, \quad b^i = \mu_e h^i, \quad b_3 = \mu_e h_3, \\ \delta^i &= \varepsilon_e \chi^i, \quad \delta_3 = \varepsilon_e \chi_3, \quad \beta^i = \mu_e \varphi^i, \quad \beta_3 = \mu_e \varphi_3. \end{aligned} \tag{17.36}$$

In the above system, due to the last equalities, the number of unknown functions decreases, Eqs. (17.3), (17.4), and (17.6) are preserved, and the remaining Eqs. (17.18), (17.21), (17.22), and (17.27)–(17.32) take the following:

$$\begin{aligned} \hat{T}^{ij} &= h [\lambda (\varepsilon + \psi_3) g^{ij} + 2\mu \varepsilon^{ij}], \quad M^{ij} = I (\lambda g^{ij} \kappa + 2\mu \kappa^{ij}), \\ \hat{Q}^i &= \mu h \theta^i, \quad \mu^i = \mu I (b^{il} \theta_l + g^{ik} \nabla_k \psi_3), \quad \hat{N} = h [\lambda \varepsilon + (\lambda + 2\mu) \psi_3], \\ \varepsilon &= \varepsilon_1^1 + \varepsilon_2^2, \quad \kappa = \kappa_1^1 + \kappa_2^2; \end{aligned} \tag{17.37}$$

$$\begin{aligned} y^1 &= \sigma [e^1 + c_g \mu_e (\dot{u}_2 H_{03} - \dot{w} H_{02})] + \rho_{e0} \dot{u}^1, \\ y^2 &= \sigma [e^2 + c_g \mu_e (\dot{w} H_{01} - \dot{u}_1 H_{03})] + \rho_{e0} \dot{u}^2, \\ y_3 &= \sigma [e_3 + c_g \mu_e (\dot{u}_1 H_{02} - \dot{u}_2 H_{01})] + \rho_{e0} \dot{w}, \\ v^1 &= \sigma [\chi^1 + c_g \mu_e (\dot{\psi}_2 H_{03} - \dot{\psi}_3 H_{02})] + \rho_{e0} \dot{\psi}^1 \\ v^2 &= \sigma [\chi^2 + c_g \mu_e (\dot{\psi}_3 H_{01} - \dot{\psi}_1 H_{03})] + \rho_{e0} \dot{\psi}^2 \\ v_3 &= \sigma [\chi_3 + c_g \mu_e (\dot{\psi}_1 H_{02} - \dot{\psi}_2 H_{01})] + \rho_{e0} \dot{\psi}_3; \end{aligned} \tag{17.38}$$

$$\begin{aligned}
q_e^1 &= h [\rho_{e0} e^1 + r_e E_0^1 + c_g \mu_e (j_{02} h_3 - j_{03} h_2 + y_2 H_{03} - y_3 H_{02})], \\
q_e^2 &= h [\rho_{e0} e^2 + r_e E_0^2 + c_g \mu_e (j_{03} h_1 - j_{01} h_3 + y_3 H_{01} - y_1 H_{03})], \\
q_e &= h [\rho_{e0} e_3 + r_e E_{03} + c_g \mu_e (j_{01} h_2 - j_{02} h_1 + y_1 H_{02} - y_2 H_{01})], \\
m_e^1 &= I [\rho_{e0} \chi^1 + \lambda_e E_0^1 + c_g \mu_e (j_{02} \varphi_3 - j_{03} \varphi_2 + v_2 H_{03} - v_3 H_{02})], \\
m_e^2 &= I [\rho_{e0} \chi^2 + \lambda_e E_0^2 + c_g \mu_e (j_{03} \varphi_1 - j_{01} \varphi_3 + v_3 H_{01} - v_1 H_{03})], \\
m_e &= I [\rho_{e0} \chi_3 + \lambda_e E_{03} + c_g \mu_e (j_{01} \varphi_2 - j_{02} \varphi_1 + v_1 H_{02} - v_2 H_{01})];
\end{aligned} \tag{17.39}$$

$$\begin{aligned}
\frac{\partial e_3}{\partial \xi^2} + b_2^k e_k - \chi_2 &= -\frac{\mu_e \sqrt{g}}{c} \dot{h}^1, \quad \chi_1 - \frac{\partial e_3}{\partial \xi^1} - b_1^k e_k = -\frac{\mu_e \sqrt{g}}{c} \dot{h}^2, \\
\nabla_1 e_2 - \nabla_2 e_1 &= -\frac{\mu_e \sqrt{g}}{c} \dot{h}_3;
\end{aligned} \tag{17.40}$$

$$\begin{aligned}
\frac{\partial h_3}{\partial \xi^2} + b_2^k h_k - \varphi_2 &= \frac{\sqrt{g}}{c} (4\pi y^1 + \varepsilon_e \dot{e}^1), \\
\varphi_1 - \frac{\partial h_3}{\partial \xi^1} - b_1^k h_k &= \frac{\sqrt{g}}{c} (4\pi y^2 + \varepsilon_e \dot{e}^2), \\
\nabla_1 h_2 - \nabla_2 h_1 &= \frac{\sqrt{g}}{c} (4\pi y_3 + \varepsilon_e \dot{e}_3);
\end{aligned} \tag{17.41}$$

$$\nabla_i e^i - 2H e_3 + \chi_3 = 4\pi r_e / \varepsilon_e; \tag{17.42}$$

$$\begin{aligned}
\frac{\partial \chi_3}{\partial \xi^2} + b_2^k \chi_k + b_2^k \frac{\partial e_3}{\partial \xi^k} + c_2^k e_k &= -\frac{\mu_e \sqrt{g}}{c} \dot{\varphi}^1, \\
\frac{\partial \chi_3}{\partial \xi^1} + b_1^k \chi_k + b_1^k \frac{\partial e_3}{\partial \xi^k} + c_1^k e_k &= \frac{\mu_e \sqrt{g}}{c} \dot{\varphi}^2, \\
\nabla_1 \chi_2 - \nabla_2 \chi_1 + b_1^k \nabla_k e_2 - b_2^k \nabla_k e_1 &= -\frac{\mu_e \sqrt{g}}{c} \dot{\varphi}_3;
\end{aligned} \tag{17.43}$$

$$\begin{aligned}
\frac{\partial \varphi_3}{\partial \xi^2} + b_2^k \varphi_k + b_2^k \frac{\partial h_3}{\partial \xi^k} + c_2^k h_k &= \frac{\sqrt{g}}{c} (4\pi v^1 + \varepsilon_e \dot{\chi}^1), \\
\frac{\partial \varphi_3}{\partial \xi^1} + b_1^k \varphi_k + b_1^k \frac{\partial h_3}{\partial \xi^k} + c_1^k h_k &= -\frac{\sqrt{g}}{c} (4\pi v^2 + \varepsilon_e \dot{\chi}^2), \\
\nabla_1 \varphi_2 - \nabla_2 \varphi_1 + b_1^k \nabla_k h_2 - b_2^k \nabla_k h_1 &= \frac{\sqrt{g}}{c} (4\pi v_3 + \varepsilon_e \dot{\chi}_3);
\end{aligned} \tag{17.44}$$

$$\nabla_i \chi^i - 2H \chi_3 + b^{ik} \nabla_i e_k - 2(2H^2 - K) e_3 = 4\pi \lambda_e / \varepsilon_e \tag{17.45}$$

17.5 Equations of Motion of an Electromagnetoelastic Plate

In this case, it is necessary to consider the curvature tensor zero: $b_{ij} = 0$ [41]. Moreover, Eqs. (17.17), (17.21) and (17.22) do not change, equalities (17.4) are simplified: $Q^i = \hat{Q}^i$, $T^{ij} = \hat{T}^{ij}$, $N = \hat{N}$. Equations (17.3), (17.6), (17.18), and (17.27)–(17.32) are also transformed:

$$\begin{aligned} \rho h \ddot{u}^i &= \nabla_j T^{ji} + q^i + q_e^i, & \rho h \ddot{w} &= \nabla_i Q^i + q + q_e, \\ \rho I \ddot{\psi}^i &= \nabla_j M^{ij} - Q^i + m^i + m_e^i, & \rho I \ddot{\psi}_3 &= \nabla_i \mu^i - N + m + m_e; \end{aligned} \quad (17.46)$$

$$\varepsilon_{ij} = \frac{1}{2} (\nabla_i u_j + \nabla_j u_i), \quad \kappa_{ij} = \frac{1}{2} (\nabla_i \psi_j + \nabla_j \psi_i), \quad \theta_k = \psi_k + \nabla_k w_k; \quad (17.47)$$

$$\begin{aligned} T^{ij} &= h \left[(C^{ijkl} \varepsilon_{kl} + C^{ij33} \psi_3) - \frac{1}{4\pi} (\kappa^{ijk} e_k + \kappa^{ij3} e_3 + \gamma^{ijk} h_k + \gamma^{ij3} h_3) \right], \\ M^{ij} &= I \left[C^{ijkl} \kappa_{kl} - \frac{1}{4\pi} (\kappa^{ijk} \chi_k + \kappa^{ij3} \chi_3 + \gamma^{ijk} \varphi_k + \gamma^{ij3} \varphi_3) \right], \\ Q^i &= h \left[C^{i3k3} \theta_k - \frac{1}{4\pi} (\kappa^{i3k} e_k + \kappa^{i33} e_3 + \gamma^{i3k} h_k + \gamma^{i33} h_3) \right], \\ \mu^i &= I \left[C^{i3k3} \nabla_k \psi_3 - \frac{1}{4\pi} (\kappa^{i3k} \chi_k + \kappa^{i33} \chi_3 + \gamma^{i3k} \varphi_k + \gamma^{i33} \varphi_3) \right], \\ N &= h \left[C^{33kl} \varepsilon_{kl} + C^{3333} \psi_3 - \frac{1}{4\pi} (\kappa^{33k} e_k + \kappa^{333} e_3 + \gamma^{33k} h_k + \gamma^{333} h_3) \right]; \end{aligned} \quad (17.48)$$

$$\frac{\partial e_3}{\partial \xi^2} - \chi_2 = -\frac{\sqrt{g}}{c} \dot{b}^1, \quad \chi_1 - \frac{\partial e_3}{\partial \xi^1} = -\frac{\sqrt{g}}{c} \dot{b}^2, \quad \nabla_1 e_2 - \nabla_2 e_1 = -\frac{\sqrt{g}}{c} \dot{b}_3 \quad (17.49)$$

$$\frac{\partial h_3}{\partial \xi^2} - \varphi_2 = \frac{\sqrt{g}}{c} (4\pi y^1 + \dot{d}^1), \quad \varphi_1 - \frac{\partial h_3}{\partial \xi^1} = \frac{\sqrt{g}}{c} (4\pi y^2 + \dot{d}^2), \quad (17.50)$$

$$\nabla_1 h_2 - \nabla_2 h_1 = \frac{\sqrt{g}}{c} (4\pi y_3 + \dot{d}_3);$$

$$\nabla_i d^i + \delta_3 = 4\pi r_e; \quad (17.51)$$

$$\frac{\partial \chi_3}{\partial \xi^2} = -\frac{\sqrt{g}}{c} \dot{\beta}^1, \quad \frac{\partial \chi_3}{\partial \xi^1} = \frac{\sqrt{g}}{c} \dot{\beta}^2, \quad \nabla_1 \chi_2 - \nabla_2 \chi_1 = -\frac{\sqrt{g}}{c} \dot{\beta}_3; \quad (17.52)$$

$$\begin{aligned} \frac{\partial \varphi_3}{\partial \xi^2} &= \frac{\sqrt{g}}{c} (4\pi v^1 + \dot{\delta}^1), & \frac{\partial \varphi_3}{\partial \xi^1} &= -\frac{\sqrt{g}}{c} (4\pi v^2 + \dot{\delta}^2), \\ \nabla_1 \varphi_2 - \nabla_2 \varphi_1 &= \frac{\sqrt{g}}{c} (4\pi v_3 + \dot{\delta}_3); \end{aligned} \quad (17.53)$$

$$\nabla_i \delta^i = 4\pi \lambda_e. \quad (17.54)$$

Analysis of the system of Eqs. (17.18), (17.21), (17.22), and (17.46)–(17.54) shows that in the general case of the initial electromagnetic field, unlike the classical elastic plate, the bending and longitudinal motions are not separated.

Acknowledgements This work was funded by the subsidy from RFBR (Project 17-08-00493).

References

1. Kudryavtsev, B.A., Parton, V.Z.: Electromagnetoelasticity of Piezoelectric and Electrically Conductive Bodies. Nauka, Moscow (1988) (in Russian)
2. Korotkina, M.R.: Electromagnetoelasticity. MSU Publishing House, Moscow (1988) (in Russian)
3. Pao, Y.H., Yeh, C.S.: A linear theory for soft ferromagnetics elastic solids. *Int. J. Eng. Sci.* **11**, 415–436 (1983)
4. Pao, Y.H.: Electromagnetic forces in deformable continua. In: Nemat-Nasser, S. (ed.) *Mechanics Today*, vol. IV, pp. 209–305. Pergamon Press, London (1978)
5. Priimenko, V., Vishnevskii, M.: An initial boundary-value problem for model electromagnetoelasticity system. *J. Differ. Equ.* **235**, 31–55 (2007)
6. Ryu, J., Priya, S., Uchino, K., Kim, H.-E.: Magnetoelectric effect in composites of magnetostriptive and piezoelectric materials. *J. Electroceram.* **8**, 107–119 (2002)
7. Altay, G., Cengiz Dökmeçi, M.: On the fundamental equations of electromagnetoelastic media in variational form with an application to shell-laminae equations. *Int. J. Solids Struct.* **47**, 466–492 (2010)
8. Jiang, A., Ding, H.: Analytical solutions to magneto-electro-elastic beams. *Struct. Eng. Mech.* **18**, 195–209 (2004)
9. Pan, E.: Exact solution for simply supported and multilayered magnet-electroelastic plates. *ASME J. Appl. Mech.* **68**, 608–618 (2001)
10. Pan, E., Han, F.: Exact solution for functionally graded and layered magneto-electro-elastic plates. *Int. J. Eng. Sci.* **43**, 321–339 (2002)
11. Wang, J., Chen, L., Fang, S.: State vector approach to analysis of multilayered magneto-electro-elastic plates. *Int. J. Solids Struct.* **40**, 1669–1680 (2003)
12. Heyliger, P.R., Pan, E.: Static fields in magneto-electroelastic laminates. *AIAA J.* **42**, 1435–1443 (2004)
13. Heyliger, P.R., Ramirez, F., Pan, E.: Two dimensional static fields in magneto-electroelastic laminates. *J. Intell. Mater. Syst. Struct.* **15**, 689–709 (2004)
14. Garcia Lage, R., Mota Soares, C.M., Mota Soares, C.A., Reddy, J.N.: Layerwise partial mixed finite element analysis of magneto-electro-elastic plates. *Comput. Struct.* **82**, 1293–1301 (2004)
15. Bardzokas, D.I., Senik, N.A.: Contact problems of electroelasticity. *Mechanics of Contact Interactions*, pp. 583–606. Fizmatlit, Moscow (2001) (in Russian)
16. Ambartsumyan, S.A., Baghdasaryan, G.E., Belubekyan, M.V.: Magnetoelasticity of Thin Shells and Plates. The Main Edition of the Physical and Mathematical Literature of the Publishing House. Nauka, Moscow (1977) (in Russian)
17. Bagdasaryan, G.E., Danoyan, Z.N.: The flat magnetoelastic Lamb's problem. *Mechanics* (3), 68–76 (1983) (in Russian)
18. Kaloerov, S.A., Petrenko, A.V., Khoroshev, K.G.: Electromagnetoelastic problem for a plate with holes and cracks. *Prikladnaya Mekhanika* **46**(2), 93–105 (2010)
19. Kaloerov, S.A., Petrenko, A.V., Khoroshev, K.G.: Electromagnetoelastic problem for a plate with holes and cracks. *Prikladnaya Mekhanika i Tekhnicheskaya Fizika* **52**(5), 146–154 (2011)
20. Kaloerov, S.A., Samodurov, A.A.: Problem of electromagnetoviscoelasticity for multiply connected plates. *Prikladnaya Mekhanika* **51**(6), 23–41 (2015)

21. Pan, E., Heyliger, P.R.: Free vibrations of simply supported and multilayered magneto-electro-elastic plates. *J. Sound Vib.* **252**(3), 429–442 (2002)
22. Qing, G.-H., Qui, J.-J., Liu, Y.-H.: Mixed H-R mixed variational principle for magneto-electroelastic bodies and state-vector equation. *Appl. Math. Mech.* **26**(6), 722–728 (2005)
23. Chen, W.Q., Lee, K.Y., Ding, H.J.: On free vibration of non-homogeneous transversely isotropic magneto-electro-elastic plates. *J. Sound Vib.* **279**, 237–251 (2005)
24. Bhargale, R.K., Ganesan, N.: Free vibration of simply supported functionally graded and layered magneto- electro-elastic plates. *J. Sound Vib.* **294**, 1016–1038 (2006)
25. Chen, J., Chen, H., Pan, E., Heyliger, P.R.: Modal analysis of magneto-electroelastic plates using the state vector approach. *J. Sound Vib.* **304**, 722–734 (2007)
26. Chen, J.Y., Pan, E., Chen, H.L.: Wave propagation in magneto-electro-elastic multilayered plates. *Int. J. Solids Struct.* **44**, 1073–1085 (2007)
27. Buchanan, G.R.: Layered versus multiphase magneto-electro-elastic composites. *Compos. B: Eng.* **35**, 413–420 (2004)
28. Bhargale, R.K., Ganesan, N.: Free vibration studies of simply supported nonhomogeneous functionally graded magneto-electro-elastic finite cylindrical shells. *J. Sound Vib.* **288**, 412–422 (2005)
29. Annigeri, A.R., Ganesan, N., Swarnamani, S.: Free vibrations of simply supported layered and multiphase magneto-electro-elastic cylindrical shells. *Smart Mater. Struct.* **15**, 459–467 (2006)
30. Tsai, Y.H., Wu, C.P.: Dynamic responses of functionally graded magneto-electro-elastic shells with open-circuit surface conditions. *Int. J. Eng. Sci.* **46**(9), 843–857 (2008)
31. Daga, A., Ganesan, N., Shankar, K.: Comparative studies of the transient response for PECP, MSCP, Barium titanate, magneto-electro-elastic finite cylindrical shell under constant internal pressure using finite element method. *Finite Elem. Anal. Des.* **44**, 89–104 (2008)
32. Wu, C.P., Tsai, Y.H.: Static behavior of functionally graded magneto-electroelastic shells under electric displacement and magnetic flux. *Int. J. Eng. Sci.* **45**, 744–769 (2007)
33. Wu, C.P., Chiu, K.H., Wang, Y.M.: A mesh-free DRK-based collocation method for the coupled analysis of functionally graded magneto-electro-elastic shells and plates. *CMES Comput. Model. Eng. Sci.* **35**(3), 181–214 (2008)
34. Wu, C.P., Chiu, K.H., Wang, Y.M.: A review of the three-dimensional analytical approaches of multilayered and functionally graded piezoelectric plates and shells. *CMC Comput. Mater. Contin.* **8**(2), 93–132 (2008)
35. Dai, H.L., Fu, Y.M., Yang, J.H.: Electromagnetoelastic behaviors of functionally graded piezoelectric solid cylinder and sphere. *Acta. Mech. Sin.* **23**, 55–63 (2007)
36. Zhong, Z., Wang, X.: Exact solution for simply supported and multilayered magneto-electro-elastic cylindrical shells. In: *Mechanics of Electromagnetic Solids. Advances in Mechanics and Mathematics*, vol. 3, pp. 273–287 (2003)
37. Shlyakhin, D.A.: Unsteady axisymmetric electroelasticity problem for a piezoceramic plate. In: *Transactions of the 21st International Conference on the Theory of Shells and Plates*. Publishing House of the SSTU, pp. 242–248 (2005)
38. Bai, A.V., Storozhev, V.A.: Normal electroelastic waves in a layer of an arbitrary slice of a quartz piezocrystal. In: *Consonance 2003: Acoustic Symposium*, pp. 252–257 (2003)
39. Green, A.E., Naghdi, P.M.: On electromagnetic effects in the theory of shells and plates. *Philos. Trans. R. Soc. Lond. A* **309**, 559–610 (1983)
40. Zozulya, V.V.: Higher order theory of electro-magneto-elastic plates and shells. recent developments in the theory of shells. In: *Altenbach, H., Chróscielewski, J., Eremeyev, V., Wisniewski, K. (eds.) Recent Developments in the Theory of Shells. Advanced Structured Materials*, vol. 110, pp. 727–769 (2019)
41. Mihajlova, E.Yu, Tarlakovskii, D.V., Fedotenkov, G.V.: A generalized linear model of dynamics of thin elastic shells. *Uchenye Zapiski Kazanskogo Universiteta, Seriya Fiziko-Matematicheskie Nauki* **160**(3), 561–577 (2018)
42. Tarlakovskii, D.V., Vestyak, V.A., Zemskov, A.V.: Dynamic processes in thermo-electro-magneto-elastic and thermo-elasto-diffusive media. In: *Encyclopedia of Thermal Stresses*, vol. 2, pp. 1064–1071. Springer, Dordrecht, Heidelberg, New York, London (2014)

43. Selezov, I.T., Selezova, L.V.: Waves in Magnetoelastohydroelastic Media. Naukova Dumka, Kyiv (1975) (in Russian)
44. Nowacki, W.: Electromagnetic Effects in Solids. Panstwowe Wydawnictwo Naukowe, Warszawa (1983). (in Polish)
45. Morse, P.M., Feshbach, H.: Methods of Theoretical Physics. International Series in Pure and Applied Physics, Part 1. McGraw-Hill Book Company, New York (1953)
46. Gorshkov, A.G., Rabinskii, L.N., Tarlakovskii, D.V.: Fundamentals of Tensor Analysis and Continuum Mechanics. Publishing House Nauka, Moscow (2000) (in Russian)

Chapter 18

Nonlinear Dynamics of Two-Dimensional Lattices with Complex Structure



Alexey V. Porubov, Alena E. Osokina and Ilya D. Antonov

Abstract The dynamics of two-dimensional lattice structures is studied. The complexity of the structure includes non-neighboring interactions between the lattice masses, consideration of both translational and rotational interactions and also their nonlinear character (physical nonlinearity). The asymptotic procedures are developed to obtain the governing nonlinear equations of motion in the continuum limit. The equations obtained are studied both analytically and numerically. Of special interest are the propagation and transverse instability of the plane solitary strain waves. It is shown that the dynamics of longitudinal and shear waves is different in various two-dimensional lattices. The relationships for the elastic constants are obtained to characterize the type of the localized strain waves (tensile or compression), their transverse instability and possible auxetic behavior. Numerical solutions are obtained that describe unstable and stable dynamics of the plane longitudinal and shear waves.

Keywords Two-dimensional lattice · Nonlinear dynamics · Asymptotic solution

18.1 Introduction

When dealing with the problem of description of materials with a complex microstructure, one usually wants to take into consideration either the influence of some specific dynamic processes on the stress–strain behavior or the influence of a complex microstructure, additional degrees of freedom or non-neighboring interactions on the macro-parameters, and, in turn, on the model equations.

A. V. Porubov (✉) · I. D. Antonov
Institute for Problems in Mechanical Engineering,
Bolshoy 61, V.O., St. Petersburg, Russian Federation

A. V. Porubov · A. E. Osokina · I. D. Antonov
Peter the Great St. Petersburg Polytechnic University (SPbPU),
Polytechnicheskaya st., 29, St. Petersburg, Russian Federation

The modeling of the dynamic behavior of solid materials may be generally divided into two categories. Firstly, there are the discrete models, for which the equilibrium conditions, the kinematic conditions and the constitutive behavior are formulated for each individual micro-structural element (cell) with respect to its neighboring micro-structural elements [1–4]. Secondly, there are the continuum models, where the equilibrium conditions, the kinematic conditions and the constitutive behavior are formulated for an assembly of micro-structural elements, using the continuum concepts of stress and strain, see, e.g., [5–7].

A considerable advantage of discrete models in comparison to continuum models is that the inhomogeneous effects at the micro-level can be taken into account more accurately. The study of discrete models with non-neighboring interactions between the particles in the lattice has attracted considerable interest due to dispersion of the waves propagating in such a system [2, 5, 8–12]. In particular, this is also important for the study of an influence of a microstructure of the materials. Dynamic processes in the one-dimensional lattices are investigated more extensively both in the linear and nonlinear consideration [4, 5], while two-dimensional lattices are mainly considered in the linearized case [2, 4, 13]. Some two-dimensional processes may be modeled in one-dimensional approximation, like plane waves propagation, while their transverse instability requires two-dimensional consideration.

Considering everything mentioned above, it is obvious that discrete models can be utilized for the sake of accuracy. However, the number of representative micro-structural elements in a macro-structural configuration is usually very large, which causes the number of equations that has to be solved for a discrete system to become large as well. The discrete equations derived are very complex and stacked up, and cannot be solved analytically. So, the simplification and transition to some kind of a continuous model are needed in order to achieve a reasonable result for a further analysis.

In order to link the macroscopic and microscopic descriptions, it is necessary to understand how exactly the transition from one description to another has to be made, and how to derive continuous equations from the discrete ones.

One of the famous methods is described in the works of [2, 14]. In the linear case, both discrete and continuum equations may be considered analytically. However, only a few discrete nonlinear equations, like the Toda lattice equation or the Ablowitz–Ladik equation, possess exact solutions [15]. That is why an approach based on a continuum limit of an original discrete equation is needed to obtain governing nonlinear continuum equations. The familiar acoustic branch continuum limit requires the long-wavelength approximation and corresponds to the discrete model only for small wave numbers.

A well-known enhanced continuum formulation is the Cosserat continuum (or micro-polar continuum), which is an augmentation of the standard Boltzmann continuum by three rotational degrees of freedom. The rotational degrees of freedom introduce a “bending effect” in the constitutive formulations, and the characteristic length scale is therefore governed by the ratio between this additional bending stiffness and the normal stiffness. The development of the Cosserat continuum

formulation started at the beginning of this century with the concept of the inclusion of rotational degrees of freedom was introduced for the first time.

The problem of reasonable simplification when describing properties of materials is closely connected with the question of what can be neglected and what must be included. This can be resolved by utilizing a range of asymptotic methods. This is particularly important when dealing with nonlinear processes in crystal lattices [5, 8, 16–24].

Each of the approaches mentioned above has led to significant advances connected with higher precision of materials with microstructure description: from breathers and solitary waves to discovery of auxetic properties of 2D crystals [25].

In the following sections, authors show the asymptotic simplification procedure developed to make nonlinear analysis feasible. Later, it is applied to obtain Kadomtsev–Petviashvili [26] type equations and their solutions for the cases of generalized square and graphene lattices. Finally, it helps to describe the system's behavior in terms of stability and later utilize the findings in the numerical simulation.

18.2 Two-Dimensional Waves in a Generalized Square Lattice

18.2.1 Statement of the Problem

A generalized two-dimensional square lattice model considers additional long-range interactions of the central particle with mass M , see [22] for details. The model includes quadratic and cubic nonlinearity in the elastic inter-particle forces in addition to the conventional Hookean interaction. The central particle with the number m, n interacts with four horizontal and vertical neighbors by means of the elastic springs with the linear rigidity C_1 and the nonlinear rigidities Q and Q_3 . The relative distance in the unstrained state is assumed to be equal to l . Then the total potential energy is

$$\Pi = \Pi_1 + \Pi_2 + \Pi_3,$$

where Π_1 accounts for interactions with nearest four particles in the horizontal and vertical directions,

$$\Pi_1 = \frac{1}{2}C_1 \sum_{i=1}^4 \Delta l_i^2 + \frac{1}{3}Q \sum_{i=1}^4 \Delta l_i^3 + \frac{1}{4}Q_3 \sum_{i=1}^4 \Delta l_i^4,$$

where $x_{m,n}$, $y_{m,n}$ are the horizontal and vertical displacements of particle m, n . The expressions for elongations of the springs, Δl_i are [22]

$$\begin{aligned} \Delta l_1 &= x_{m+1,n} - x_{m,n}, \Delta l_2 = y_{m,n+1} - y_{m,n}, \Delta l_3 = x_{m,n} - x_{m-1,n}, \\ \Delta l_4 &= y_{m,n} - y_{m,n-1} \end{aligned}$$

where the springs are numbered counter-clockwise. Next group of interacting particles is composed by four diagonal neighboring particles, whose positions are described by the angles $\phi = \pi/4 + \pi k/2, k = 0, \dots, 3$. The linear rigidity of the connecting springs is C_2 while the nonlinear rigidities are P and P_3 . The contribution to the potential energy is

$$\Pi_2 = \frac{1}{2}C_2 \sum_{i=5}^8 \Delta l_i^2 + \frac{2\sqrt{2}}{3}P \sum_{i=5}^8 \Delta l_i^3 + P_3 \sum_{i=5}^8 \Delta l_i^4,$$

The expressions for elongations may be found in [22].

The final group consists of eight long-range particles, whose positions are characterized by the angles ψ, θ , so as $\tan \psi = 1/2, \tan \theta = 2$, see figure in [22]. Then the contribution to the energy is

$$\Pi_3 = \frac{1}{2}C_3 \sum_{i=9}^{16} \Delta l_i^2 + \frac{5\sqrt{5}}{3}S \sum_{i=9}^{16} \Delta l_i^3 + \frac{25}{4}S_3 \sum_{i=9}^{16} \Delta l_i^4,$$

where C_3 is the linear rigidity, S and S_3 are the nonlinear rigidities. The expressions for elongations may be found in [22].

The kinetic energy is

$$T = \frac{1}{2}M (\dot{x}_{m,n}^2 + \dot{y}_{m,n}^2).$$

Then the Lagrangian, $L = T - \Pi$, is composed, and the Hamilton–Ostrogradsky variational principle is applied to obtain the discrete governing equations of motion, see [22] for details.

18.2.2 Auxetic Behavior in the Linearized Model

For small wave numbers, one assumes that the continuum displacements of the central particle $x_{m,n}, y_{m,n}$ are $u(x, y, t), v(x, y, t)$, thus introducing predominantly longitudinal waves propagation. Then the Taylor series for the neighboring particles are

$$x_{m\pm 1, n\pm 1} = u \pm lu_x \pm ly_y + \frac{1}{2}l^2u_{xx} + l^2u_{xy} + \frac{1}{2}l^2u_{yy} + \dots$$

Then the two-dimensional linearized continuum equations are

$$\begin{aligned} M u_{tt} - \frac{l^2}{5} (5(C_1 + C_2) + 34C_3) u_{xx} - \frac{2l^2}{5} (5C_2 + 16C_3) v_{xy} \\ - \frac{l^2}{5} (5C_2 + 16C_3) u_{yy} = 0, \end{aligned} \quad (18.1)$$

$$\begin{aligned} M v_{tt} - \frac{l^2}{5} (5(C_1 + C_2) + 34C_3) v_{yy} - \frac{2l^2}{5} (5C_2 + 16C_3) u_{xy} \\ - \frac{l^2}{5} (5C_2 + 16C_3) v_{xx} = 0. \end{aligned} \quad (18.2)$$

Equations (18.1), (18.2) are related to the equations of motion of the cubic crystals provided that the elastic cubic constants C_{11} , C_{12} and C_{44} are connected with our constants C_1 , C_2 and C_3 as

$$\begin{aligned} C_{11} &= \frac{1}{5l} (5(C_1 + C_2) + 34C_3), \quad C_{44} = \frac{1}{5l} (5C_2 + 16C_3), \\ C_{12} + C_{44} &= \frac{2}{5l} (5C_2 + 16C_3). \end{aligned} \quad (18.3)$$

These relationships hold only if $C_{12} = C_{44}$ or for the Cauchy condition for materials with cubic symmetry when only central interactions are taken into account [1]. However, they fail, e.g., for cubic metals [27].

The relationships for the Poisson ratios of cubic crystals can be found in Ref. [25]. For the case $C_{12} = C_{44}$, they are

$$\begin{aligned} \nu_{<100,001>} &= \frac{C_{12}}{C_{11} + C_{12}}, \quad \nu_{<111,001>} = \frac{4C_{12}^2}{2C_{12}(C_{11} - C_{12}) + C_{11}(C_{11} + C_{12})}, \\ \nu_{<110,110>} &= \frac{(C_{11} + C_{12})(C_{11} - 2C_{12})}{(C_{11} - C_{12})(C_{11} + 2C_{12}) + 2C_{11}C_{12}}, \quad \nu_{<111,111>} = \frac{C_{11}}{2(C_{11} + 3C_{12})}. \end{aligned}$$

Using Eqs. (18.3), one obtains

$$C_{11} - C_{12} = \frac{l^2}{5M} (5C_1 + 18C_3), \quad C_{11} - 2C_{12} = \frac{l^2}{5M} (C_1 - C_2 + 2C_3).$$

Only the last expression can be negative giving rise to a negative value of $\nu_{<110,110>}$. One can see that the long-range interaction, described by the coefficient C_3 , adds positiveness in the relation $C_1 - C_2 + 2C_3$.

18.2.3 Continuum Nonlinear Equations

The equations of motion obtained from the variational principle are further reduced when the plane waves propagating in horizontal direction are studied [22]. For simplicity, let us consider nonlinear waves propagating in a horizontal direction along the x axis and weakly perturbed in the transverse direction along the y axis. The transverse weakness is characterized by the small parameter $\varepsilon \ll 1$, the continuum displacements are assumed to be the functions of the slow transverse variable $Y = \varepsilon y$. The same small parameter is used to account for the weakly nonlinear waves; however, its utilization depends on whether transverse variations of longitudinal or shear waves are studied.

18.2.3.1 Longitudinal Waves

For small wave numbers, one assumes that the continuum displacements of the central particle $x_{m,n}, y_{m,n}$ are $u(x, Y, t), v(x, Y, t)$. Of special interest are the localized waves keeping their shape and velocity on propagation. These waves exist under the balance between nonlinearity and dispersion. Dispersion terms are the higher-order linear derivative terms arising from the Taylor expansion. Their smallness may be ensured by choosing $l = \varepsilon h$. Nonlinear terms turn out to be of the same order under an assumption about smallness of the continuum displacement of the form $\varepsilon^2 u(x, Y, t), \varepsilon^3 v(x, Y, t)$, also the nonlinear rigidities should be $P = P/\varepsilon, Q = Q/\varepsilon, S = S/\varepsilon$, and cubic nonlinear terms are negligibly small for longitudinal waves. Higher power of the small parameter for v provides predominantly longitudinal waves propagation.

Then the Taylor series for the neighboring particles are

$$x_{m\pm 1, n\pm 1} = \varepsilon^2 u \pm \varepsilon^3 h u_x \pm \varepsilon^4 h u_Y + \frac{1}{2} h^2 \varepsilon^4 u_{xx} + \varepsilon^5 h^2 u_{xY} + \frac{1}{2} \varepsilon^5 h^2 u_{YY} + \dots$$

Substitution of these Taylor series into the discrete equations of motion gives rise to the continuum coupled nonlinear partial differential equations of motion for the functions $u(x, Y, t), v(x, Y, t)$, [22],

$$M u_{tt} - \frac{h^2}{5} \left(5(C_1 + C_2) + 34C_3 \right) u_{xx} - \varepsilon \frac{h^2}{5} \left(5C_2 + 16C_3 \right) (2v_{xY} + u_{YY}) - \frac{h^2}{12} (C_1 + C_3 + 26h^2 C_4) u_{xxxx} - 2h(2P + Q + 130S)u_x u_{xx} = O(\varepsilon^3) \tag{18.4}$$

$$M v_{tt} - \frac{h^2}{5} \left(5C_2 + 16C_3 \right) (v_{xx} + 2u_{xY}) = O(\varepsilon) \tag{18.5}$$

One assumes

$$u = G(\theta, T, Y); v = F(\theta, T, Y),$$

where $\theta = x - Vt, T = \epsilon^2 t$ are the fast and the slow variables, respectively. It allows us to obtain an asymptotic solution to Eqs. (18.4), (18.5) using expansions

$$G = G_0 + \epsilon^2 G_1 + \dots, F = F_0 + \epsilon^2 F_1 + \dots$$

Thus, one obtains in the leading order from Eqs. (18.4), (18.5), respectively,

$$G_{0,\theta\theta} (5C_1 + 5C_2 + 34C_3 - 5M V^2) = 0, \tag{18.6}$$

$$2G_{0,\theta Y} (5C_2 + 16C_3) + F_{0,\theta\theta} (5C_2 + 16C_3 - 5M V^2) = 0. \tag{18.7}$$

Equation (18.6) results in the solution for the phase velocity,

$$V = \frac{\sqrt{5C_1 + 5C_2 + 34C_3}}{\sqrt{5M}}. \tag{18.8}$$

Substitution of Eq. (18.8) into Eq. (18.7) allows us to express F_0 through G_0 ,

$$F_{0,\theta} = \frac{2(5C_2 + 16C_3)G_{0,Y}}{5C_1 + 18C_3}. \tag{18.9}$$

Next order solution to Eq. (18.4) results in the equation for the function G_0 ,

$$G_{0,\theta T} + A_1 G_{0,\theta} G_{0,\theta\theta} + A_2 G_{0,\theta\theta\theta\theta} + A_3 G_{0,Y Y} = 0, \tag{18.10}$$

where

$$A_1 = \frac{h(2P + Q + 130S)}{\sqrt{M} \sqrt{5C_1 + 5C_2 + 34C_3}}, A_2 = \frac{\sqrt{5}h^2(C_1 + C_2 + 26C_3)}{24\sqrt{M} \sqrt{5C_1 + 5C_2 + 34C_3}},$$

$$A_3 = \frac{(5C_2 + 16C_3)(5C_1 + 20C_2 + 82C_3)}{2\sqrt{5M}(5C_1 + 18C_3)\sqrt{5C_1 + 5C_2 + 34C_3}}.$$

Equation (18.10) may be rewritten in the form of the familiar Kadomtsev–Petviashvili equation, see [15] and references therein, for the strain function, $w = G_{0,\theta}$,

$$\left(w_T + A_1 w w_\theta + A_2 w_{\theta\theta\theta} \right)_\theta + A_3 w_{YY} = 0, \tag{18.11}$$

The coefficients A_2 and A_3 are always positive.

18.2.4 Shear Waves

The small parameter ε is introduced in a different way but using the same reasons as for the longitudinal waves considered before. Now predominantly, shear waves are considered, nonlinearity is weak and should balance dispersion, the waves are plane but disturbed in the transverse direction. Then the continuum displacements of the central particle $x_{m,n}, y_{m,n}$ are $\varepsilon^2 u(x, Y, t), \varepsilon v(x, Y, t)$. Again $l = \varepsilon h$ while for quadratic nonlinear rigidities, one has $P = \bar{P}/\varepsilon, Q = \bar{Q}/\varepsilon, S = \bar{S}/\varepsilon$, and for cubic nonlinear rigidities, one has $P_3 = \bar{P}_3/\varepsilon^2, Q_3 = \bar{Q}_3/\varepsilon^2, S_3 = \bar{S}_3/\varepsilon^2$. Substitution of the corresponding Taylor series to the continuum coupled nonlinear partial differential equations of motion gives rise to the equations for the functions $u(x, Y, t), v(x, Y, t)$,

$$Mu_{tt} - \frac{1}{5}(5C_1 + 5C_2 + 34C_3)u_{xx} - \frac{2}{5}(5C_2 + 16C_3)v_{x,Y} - 4h(\bar{P} + 20\bar{S})v_x v_{xx} = O(\varepsilon), \quad (18.12)$$

$$\begin{aligned} Mv_{tt} - \frac{1}{5}(5C_2 + 16C_3)v_{xx} - \varepsilon^2 \left(\frac{1}{5}(5C_1 + 5C_2 + 34C_3)v_{YY} + \frac{h^2}{12}(C_2 + 8C_3)v_{xxxx} \right. \\ \left. + \frac{2}{5}(5C_2 + 16C_3)u_{x,Y} + 4h(\bar{P} + 20\bar{S})(v_x(u_x + 2v_Y))_x + 6h^2(\bar{P}_3 + 32\bar{S}_3)v_x^2 v_{xx} \right) \\ = O(\varepsilon^3) \end{aligned} \quad (18.13)$$

The asymptotic solution to Eqs. (18.12), (18.13) is

$$u = G(\theta, T, Y); v = F(\theta, T, Y),$$

where the fast and slow variables are introduced similar to the case of longitudinal waves,

$$G = G_0 + \varepsilon^2 G_1 + \dots, F = F_0 + \varepsilon^2 F_1 + \dots$$

The leading order solution is

$$G_{0,\theta} = -\frac{2((5C_2 + 16C_3)F_{0,Y} + 5h(\bar{P} + 20\bar{S})F_{0,\theta}^2)}{5C_1 + 18C_3}$$

$$V = \sqrt{\frac{5C_2 + 16C_3}{5M}},$$

Nest order solution, $O(\varepsilon^2)$, gives rise to the model equation for F_0 ,

$$F_{0,\theta T} + B_1 F_{0,\theta}^2 F_{0,\theta\theta} + B_2 F_{0,\theta\theta\theta\theta} + B_3 F_{0,Y Y} + B_4 F_{0,Y} F_{0,\theta\theta} = 0, \quad (18.14)$$

where

$$\begin{aligned}
 B_1 &= \frac{3\sqrt{5}h^2 \left((5C_1 + 18C_3)(\bar{P}_3 + 32\bar{S}_3) - 20(\bar{P} + 20\bar{S})^2 \right)}{2(5C_1 + 18C_3)\sqrt{M}(5C_2 + 16C_3)}, \\
 B_2 &= \frac{\sqrt{5}h^2(C_2 + 8C_3)}{24\sqrt{M}(5C_2 + 16C_3)}, \\
 B_3 &= \frac{25(C_1^2 + C_1C_2 - 4C_2^2) + 10C_3(26C_1 - 55C_2) - 412C_3^2}{2\sqrt{5}(5C_1 + 18C_3)\sqrt{M}(5C_2 + 16C_3)}, \\
 B_4 &= \frac{2\sqrt{5}h(\bar{P} + 20\bar{S})(5C_1 - 2(5C_2 + 7C_3))}{(5C_1 + 18C_3)\sqrt{M}(5C_2 + 16C_3)}.
 \end{aligned}$$

The cubic nonlinear term coefficient, B_1 , may be of either sign due to the either sign of \bar{P} , \bar{S} and \bar{P}_3 , \bar{S}_3 ; the coefficient B_2 at the dispersion term is always positive. Both linear and nonlinear terms with transverse derivatives, B_3 and B_4 , may be of either sign, and now the sign of B_3 also depends on the long-range linear rigidity C_3 . The sign of B_1 defines the type of localized plane waves, a bell-shaped or a kink-shaped while the signs of B_3 and B_4 may be responsible for a transverse instability of plane waves.

18.3 Two-Dimensional Nonlinear Waves Propagation in Graphene Lattice

The two-dimensional graphene lattice consists of two interacting sub-lattices whose numbers are marked as “1” for the first sub-lattice and “2” for the second one. The sketch of the model can be found in [28]. The elements interaction is modeled by the translational springs with a linear stiffness C_1 and angular springs with a linear stiffness C_2 . The nonlinearity is introduced via additional elastic translational interaction with a stiffness Q . This model can be called “geometrically linear,” since the nonlinearity introduced in this paper takes into account deviations from the Hook’s law, which means the tensor of deformations is no longer linear and the additional mixed derivative occurs. This type is called physical nonlinearity. The geometrical nonlinearity is neglected for simplification’s sake.

When one tries to set up the nanoscale continuum theory for graphene, two main issues occur: the multi-body interatomic potential and the lack of centrosymmetry of hexagonal atomic structures. Zhang et al. [29] proposed a continuum theory that links the macroscopic deformation to the atomic structure of materials. The macroscopic behavior of the material is defined by the so-called Cauchy–Born rule of crystal elasticity by equating the strain energy function on the continuum level to the potential energy stored in the atomic bonds due to an imposed deformation on the discrete level.

The Cauchy–Born rule assumes that the atoms in a material subject to a homogeneous deformation move according to a single mapping from the undeformed to the deformed configuration. It should be pointed out that the Cauchy–Born rule that links the continuum model with particles interaction requires the atomic structure of the materials to be centrosymmetric because such a structure ensures the equilibrium of particles in a lattice. The hexagonal arrangement of atoms in a nanotube does not meet this requirement: when a carbon nanotube is under “homogeneous deformation” on the cell level, the deformation may not be homogeneous inside the cell [30].

An attempt to modify the Cauchy–Born rule to work for hexagonal atomic structure is to introduce a rigid body translation as an internal degree of freedom (DOF). A hexagonal lattice can be decomposed into two sub-lattices, each of which is centrosymmetric. Under a homogeneous deformation applied on the continuum level, each sub-lattice deforms according to the single mapping. However, the two sub-lattices move relative to each other by a certain rigid body translation, which is the internal DOF, to ensure the equilibrium of the atom. It is determined by the minimization of the strain energy density, which is equivalent to equilibrium of the atoms.

By introducing the internal DOF and enforcing the energy minimization, the equilibrium of each atom is ensured when subject to a deformation specified by the deformation gradient. In other words, neglecting the internal DOF is equivalent to applying some external constraints on top of the deformation. The stiffnesses or equivalently the elastic moduli of the graphene lattice are then reestimated because of the “external” constraints [30].

Therefore, in addition to the previously mentioned lattice models, the separation into two sub-lattices is used for the graphene modeling. Besides translational interactions, angular interactions are also taken into consideration.

Let us denote $x_{m,n}$, $y_{m,n}$ as the translational displacements of a central mass marked by 1 corresponding to the horizontal and vertical directions, respectively. The analogous displacements for the second sub-lattice are denoted by $X_{m,n}$ and $Y_{m,n}$. Then the potential energy is [28]

$$\begin{aligned}\Pi_{1Rot} &= C_1(\Delta l_1^2 + \Delta l_2^2 + \Delta l_3^2) + C_2 a^2(\phi^2 + \psi^2) + Q(\Delta l_1^3 + \Delta l_2^3 + \Delta l_3^3) \\ \Pi_{2Rot} &= C_1(\Delta L_1^2 + \Delta L_2^2 + \Delta L_3^2) + C_2 a^2(\Phi^2 + \Psi^2) + Q(\Delta L_1^3 + \Delta L_2^3 + \Delta L_3^3)\end{aligned}\tag{18.15}$$

where a is a distance between the particles, C_1 is the translational stiffness, C_2 is the rotational stiffness and Q is the nonlinear one.

The translational elongations for both sub-lattices can be found in [28].

The kinetic energy is

$$K_1 = \frac{M}{2} (\dot{x}^2 + \dot{y}^2) + J a^2 (\dot{\phi}^2 + \dot{\psi}^2), \quad (18.16)$$

where M is the mass of the particles in the lattice, J is the angular mass (moment of inertia).

In order to obtain the expressions for the angles ϕ , ψ , Φ , Ψ , the cosine formula was used in [28], where the expressions for connecting the angles and the displacements can be found. The physically nonlinear model assumes only small variations in the angular variables that result in the linearization of the expressions.

The discrete equations are obtained using the Hamilton–Ostrogradsky variational principle [28],

$$\begin{aligned} & (3J + M)\ddot{x}_{m,n} + \frac{\sqrt{3}}{2}J(\ddot{Y}_{m-1,n+1} - \ddot{Y}_{m-1,n-1} - \sqrt{3}(\ddot{X}_{m-1,n-1} - \ddot{X}_{m-1,n+1})) \\ & + \frac{C_1}{2}(6x_{m,n} - 4X_{m+1,n} - (X_{m-1,n-1} + X_{m-1,n+1}) + \sqrt{3}(Y_{m-1,n+1} - Y_{m-1,n-1})) \\ & + \frac{\sqrt{3}C_2}{2}(6x_{m,n} - 3(X_{m-1,n-1} + X_{m-1,n+1}) + \sqrt{3}(Y_{m-1,n+1} - Y_{m-1,n-1})) \\ & + \frac{3Q}{8}((x_{m,n} - X_{m-1,n-1})^2 + (x_{m,n} - X_{m-1,n+1})^2 + 3(y_{m,n} - Y_{m-1,n-1})^2 \\ & + 3(Y_{m-1,n+1} - y_{m,n})^2 + 2\sqrt{3}(x_{m,n} - X_{m-1,n-1})(y_{m,n} - Y_{m-1,n-1}) + 2\sqrt{3}(x_{m,n} \\ & - X_{m-1,n+1})(Y_{m-1,n+1} - y_{m,n}) - 8(x_{m,n} - X_{m+1,n})^2) = 0, \end{aligned} \quad (18.17)$$

$$\begin{aligned} & (J + M)\ddot{y}_{m,n} + \frac{J}{2}(\sqrt{3}(\ddot{X}_{m-1,n+1} - \ddot{X}_{m-1,n-1}) - (\ddot{Y}_{m-1,n-1} + \ddot{Y}_{m-1,n+1})) \\ & + \frac{C_1}{2}(6y_{m,n} + \sqrt{3}(X_{m-1,n+1} - X_{m-1,n-1}) - 3(Y_{m-1,n-1} + Y_{m-1,n+1})) \\ & + \frac{C_2}{2}(2y_{m,n} + \sqrt{3}(X_{m-1,n+1} - X_{m-1,n-1}) - (Y_{m-1,n-1} + Y_{m-1,n+1})) \\ & + \frac{3\sqrt{3}}{8}Q((x_{m,n} - X_{m-1,n-1})^2 - (x_{m,n} - X_{m-1,n+1})^2 + 3(y_{m,n} - Y_{m-1,n-1})^2 \\ & - 3(Y_{m-1,n+1} - y_{m,n})^2 + 2\sqrt{3}(x_{m,n} - X_{m-1,n-1})(y_{m,n} - Y_{m-1,n-1}) \\ & - 2\sqrt{3}(x_{m,n} - X_{m-1,n+1})(Y_{m-1,n+1} - y_{m,n})) = 0, \end{aligned} \quad (18.18)$$

$$\begin{aligned}
& (3J + M)\ddot{X}_{m,n} + \frac{\sqrt{3}}{2}J\left(\ddot{y}_{m+1,n-1} - \ddot{y}_{m+1,n+1} - \sqrt{3}(\ddot{x}_{m+1,n-1} - \ddot{x}_{m+1,n+1})\right) \\
& + \frac{C_1}{2}\left(6X_{m,n} - 4x_{m-1,n} - (x_{m+1,n-1} + x_{m+1,n+1}) + \sqrt{3}(y_{m+1,n-1} - y_{m+1,n+1})\right) \\
& + \frac{\sqrt{3}C_2}{2}\left(6X_{m,n} - 3(x_{m+1,n-1} + x_{m+1,n+1}) + \sqrt{3}(y_{m+1,n-1} - y_{m+1,n+1})\right) \\
& + \frac{3Q}{8}\left(8(x_{m,n} - X_{m-1,n})^2 - (x_{m+1,n+1} - X_{m,n})^2 - (x_{m+1,n-1} - X_{m,n})^2\right. \\
& - 3(y_{m+1,n+1} - Y_{m,n})^2 - 3(Y_{m,n} - y_{m+1,n-1})^2 - 2\sqrt{3}(x_{m+1,n+1} - X_{m,n})(y_{m+1,n+1} - Y_{m,n}) \\
& \left. - 2\sqrt{3}(x_{m+1,n-1} - X_{m,n})(Y_{m,n} - y_{m+1,n-1})\right) = 0,
\end{aligned} \tag{18.19}$$

$$\begin{aligned}
& (J + M)\ddot{Y}_{m,n} + \frac{J}{2}\left(\sqrt{3}(\ddot{x}_{m+1,n-1} - \ddot{x}_{m+1,n+1}) - (\ddot{y}_{m+1,n-1} + \ddot{y}_{m+1,n+1})\right) \\
& + \frac{C_1}{2}\left(6Y_{m,n} + \sqrt{3}(x_{m+1,n-1} - x_{m+1,n+1}) - 3(y_{m+1,n-1} + y_{m+1,n+1})\right) \\
& + \frac{C_2}{2}\left(2Y_{m,n} + \sqrt{3}(x_{m+1,n-1} - x_{m+1,n+1}) - (y_{m+1,n-1} + y_{m+1,n+1})\right) \\
& + \frac{3\sqrt{3}}{8}Q\left((x_{m+1,n-1} - X_{m,n})^2 - (x_{m+1,n+1} - X_{m,n})^2 + 3(Y_{m,n} - y_{m+1,n-1})^2\right. \\
& - 3(y_{m+1,n+1} - Y_{m,n})^2 + 2\sqrt{3}(x_{m+1,n-1} - X_{m,n})(Y_{m,n} - y_{m+1,n-1}) \\
& \left. - 2\sqrt{3}(x_{m+1,n+1} - X_{m,n})(y_{m+1,n+1} - Y_{m,n})\right) = 0.
\end{aligned} \tag{18.20}$$

Discrete nonlinear equations cannot be used for an analysis, and a continuum approximation of Eqs. (18.17)–(18.20) will be obtained in the following.

18.3.1 Continuum Limit for Weakly Transversely Perturbed Waves

18.3.1.1 Coupled Continuum Equations

The weak transverse variations along the vertical axis and small vertical displacements are studied. The discrete variables $x_{m,n}$, $y_{m,n}$, $X_{m,n}$, $Y_{m,n}$ are linked to the continuum functions $u(x, y, t)$, $v(x, y, t)$, $U(x, y, t)$ and $V(x, y, t)$, respectively, while the displacements of the neighboring particles are rewritten using the Taylor series expansion, like for the square lattice.

We consider predominantly longitudinal waves propagating along the horizontal axis. That is why we leave only the leading order nonlinear and dispersion terms in the equations of motions for u and U , and by analogy, only those terms that allow us to establish a connection between horizontal and vertical displacements are left in the equations of motion for the vertical displacements.

Then one obtains from Eqs. (18.17)–(18.20) [28]

$$\begin{aligned}
& (3J + M)u_{tt} + 3(C_1 + C_2)(u - U) - 3JU_{tt} - a(C_1 - 3C_2)U_x + 3JaU_{xtt} \\
& - \frac{3a^2}{2}(C_1 + C_2)U_{xx} + \sqrt{3}a(C_1 + C_2)V_y \\
& - \sqrt{3}a^2(C_1 + C_2)V_{xy} - \frac{a^2}{2}(C_1 + 3C_2)U_{yy} - \frac{3a^2}{2}JU_{xxtt} \\
& - \frac{a^3}{6}(C_1 - 3C_2)U_{xxx} - \frac{a^4}{8}(C_1 + C_2)U_{xxxx} - \frac{9Q}{4}(u - U)^2 \\
& + \frac{15Q}{2}a(u - U)U_x - \frac{9Q}{4}a^2(U_x)^2 = 0,
\end{aligned} \tag{18.21}$$

$$\begin{aligned}
& (3J + M)U_{tt} + 3(C_1 + C_2)(U - u) - 3Ju_{tt} + a(C_1 - 3C_2)u_x - 3Jau_{xtt} \\
& - \frac{3a^2}{2}(C_1 + C_2)u_{xx} - \sqrt{3}a(C_1 + C_2)v_y - \sqrt{3}a^2(C_1 + C_2)v_{xy} - \frac{a^2}{2}(C_1 + 3C_2)u_{yy} \\
& - \frac{3a^2}{2}Ju_{xxtt} + \frac{a^3}{6}(C_1 - 3C_2)u_{xxx} - \frac{a^4}{8}(C_1 + C_2)u_{xxxx} + \frac{9Q}{4}(u - U)^2 \\
& - \frac{15Q}{2}a(u - U)u_x + \frac{9Q}{4}a^2(u_x)^2 = 0.
\end{aligned} \tag{18.22}$$

$$(3C_1 + C_2)(v - V) + \sqrt{3}a(C_1 + C_2)U_y + a(3C_1 + C_2)V_x - \sqrt{3}a^2(C_1 + C_2)U_{xy} = 0 \tag{18.23}$$

$$(3C_1 + C_2)(V - v) - \sqrt{3}a(C_1 + C_2)u_y - a(3C_1 + C_2)v_x - \sqrt{3}a^2(C_1 + C_2)u_{xy} = 0 \tag{18.24}$$

The displacements responsible for the sub-lattices elements motion in the discrete equations are not physically reasonable in the continuum model. Then the transformation of variables

$$U_1 = \frac{u + U}{2}, \quad U_2 = \frac{u - U}{2},$$

$$V_1 = \frac{v + V}{2}, \quad V_2 = \frac{v - V}{2},$$

allows us to describe the dynamics using the macro-displacements U_1 , V_1 , and the micro-displacement variables u_1 , v_1 taking the microstructure into account. After the substitution and obvious manipulations with the equations (addition and subtraction), we obtain

$$\begin{aligned}
& MU_{1,tt} - \sqrt{3}a(C_1 + C_2)V_{2,y} - \frac{a^2}{2}(C_1 + 3C_2)U_{1,yy} + a(C_1 - 3C_2)U_{2,x} - 3aJU_{2,xtt} \\
& - \sqrt{3}a^2(C_1 + C_2)V_{1,xy} - \frac{3a^2}{2}(C_1 + C_2)U_{1,xx} - \frac{3a^2}{2}JU_{1,xtt} \\
& - \frac{a^3}{12}(C_1 - 3C_2)(U_{1,xxx} - U_{2,xxx}) - \frac{a^4}{16}(C_1 + C_2)(U_{1,xxxx}) \\
& - Qa^2 \left(\frac{15}{2}U_2U_{2,x} + \frac{9a}{4}U_{1,x}U_{2,x} + \frac{9a}{8}U_2U_{1,xx} \right) = 0,
\end{aligned} \tag{18.25}$$

$$\begin{aligned}
& (6J + M)U_{2,tt} + 6(C_1 + C_2) + \sqrt{3}a(C_1 + C_2)V_{1,y} + \frac{3a^2}{2}(C_1 + C_2)U_{2,xx} \\
& - a(C_1 - 3C_2)U_{1,x} + 3aJU_{1,xtt} + \sqrt{3}a^2(C_1 + C_2)V_{2,xy} - \\
& \frac{a^3}{12}(C_1 - 3C_2)(U_{1,xxx} - U_{2,xxx}) - \frac{a^4}{16}(C_1 + C_2)U_{1,xxxx} - \\
& Q \left(\frac{9}{2}U_2^2 + \frac{15}{2}aU_2U_{1,x} - \frac{9}{8}a^2(U_{1,x}^2 - U_{2,x}^2) + \frac{9}{8}a^2U_2(U_{1,xx} - U_{2,xx}) \right) = 0,
\end{aligned} \tag{18.26}$$

$$6(C_1 + C_2)U_2 + \sqrt{3}a(C_1 + C_2)V_{1,y} - a(C_1 - 3C_2)U_{1,x} = 0, \tag{18.27}$$

$$2(3C_1 + C_2)V_2 + \sqrt{3}a(C_1 + C_2)U_{1,y} + a(3C_1 + C_2)V_{1,x} = 0. \tag{18.28}$$

The slaving principle [31] will be applied below to obtain a single governing equation for a description of nonlinear dynamics of longitudinal strain waves.

18.3.1.2 Two-Dimensional Single Governing Equation

According to the slaving principle [31], we express U_2 through the other functions by separating terms by order in Eq. (18.26) and expanding U_2 , $U_2 = U_{21} + U_{22} + \dots$ so as

$$a(3C_2 - C_1)U_{1,x} + 6(C_1 + C_2)U_{21} = 0.$$

The solution is

$$U_{21} = \frac{a(C_1 - 3C_2)U_{1,x}}{6(C_1 + C_2)}. \tag{18.29}$$

Then the equation for U_{22} is

$$\begin{aligned}
& 3a^2(C_1 + C_2)U_{21,xx} + 2(6J + M)U_{21,tt} + a(6JU_{1,xtt} - (C_1 - 3C_2)U_{21,x}) \\
& + 15aQU_{1,x}U_{21} - 9QU_{21}^2 - \frac{1}{3}a^3(C_1 - 3C_2)U_{1,xxx} \\
& + 2\sqrt{3}a(C_1 + C_2)V_{1,y} + 12(C_1 + C_2)U_{22} = 0.
\end{aligned}$$

The solution is

$$U_{22} = \frac{a^2(C_1 - 3C_2)^2}{72(C_1 + C_2)^2} U_{1,xx} - \frac{\sqrt{3}a}{6} V_{1,y} - \frac{a^3(C_1 - 3C_2)}{72(C_1 + C_2)} U_{1,xx} - \frac{24aC_1 J + aM(C_1 - 3C_2)}{36(C_1 + C_2)^2} U_{1,xtt} - \frac{a^2Q(C_1 - 3C_2)(C_1 + 2C_2)}{12(C_1 + C_2)^3} U_{1,x}^2.$$

Equations (18.27), (18.28) are used to obtain the approximate relationships for V_1, V_2 . Equation (18.27) with Eq. (18.29) being taken into account is

$$-\frac{1}{3}a \left(\sqrt{3}a(7C_1 + 3C_2)U_{1,y} + 6(3C_1 + C_2)V_2 \right)$$

It gives rise to the solution for V_2 ,

$$V_2 = -\frac{a(7C_1 + 3C_2)U_{1,y}}{2\sqrt{3}(3C_1 + C_2)}$$

Equation (18.28) results in the solution for $V_{1,x}$,

$$V_{1,x} = \frac{4C_1U_{1,yy}}{\sqrt{3}(3C_1 + C_2)}$$

Substitution of all obtained solutions into Eq. (18.25) yields a single governing equation for the function U_1 ,

$$U_{1,tt} - \alpha_1 U_{1,xx} - \alpha_2 U_{1,x}U_{1,xx} - \alpha_3 U_{1,xtt} - \alpha_4 U_{1,xxxx} - \alpha_5 U_{1,yy} = 0, \tag{18.30}$$

where

$$\alpha_1 = \frac{8a^2C_1(C_1 + 3C_2)}{3(C_1 + C_2)}, \alpha_2 = \frac{5a^3Q(C_1 - 3C_2)^2}{12(C_1 + C_2)^2}, \alpha_3 = \frac{4a^2C_1J}{C_1 + C_2},$$

$$\alpha_4 = \frac{a^4(7C_1^2 + 30C_1C_2 - 9C_2^2)}{36(C_1 + C_2)}, \alpha_5 = \frac{4a^2C_1(C_1 + 2C_2)}{3C_1 + C_2}.$$

It is obvious from the expressions that the coefficients $\alpha_1, \alpha_3, \alpha_5$ are always positive, α_4 may be of either sign depending on the angular stiffness C_2 and the sign of the nonlinear term coefficient α_2 depends entirely on the sign of nonlinear stiffness Q .

Equation (18.30) can be rewritten in the form of the Kadomtsev–Petviashvili equation (18.11). We introduce the scales for the variables,

$$x = L\tilde{x}, y = a\tilde{y}, t = L/\sqrt{\alpha_1}\tilde{t}, U_1 = \varepsilon L\tilde{U}_1,$$

$$\alpha_3 = a^2 \tilde{\alpha}_3, \alpha_4 = a^2 \tilde{\alpha}_4.$$

where L is a typical horizontal size of the wave, $\varepsilon = a^2/L^2$ is a small parameter. We assume that $\tilde{U}_1 = \tilde{U}_1(\xi, \tilde{y}, T)$, where $\xi = \tilde{x} - \tilde{t}$, $T = \varepsilon \tilde{t}$. Then Eq. (18.30) at order ε is

$$(w_T + b_1 w w_\xi + b_2 w_{\xi\xi\xi})_\xi + b_3 w_{\tilde{y}\tilde{y}} = 0, \tag{18.31}$$

where $w = \tilde{U}_{1\xi}$,

$$b_1 = \frac{\alpha_2}{2\alpha_1}, b_2 = \frac{\tilde{\alpha}_3\alpha_1 + \tilde{\alpha}_4}{2\alpha_1}, b_3 = \frac{\alpha_5}{2\alpha_1}$$

The last equation is similar to Eq. (18.11) obtained for the extended square lattice.

18.4 Two-Dimensional Dynamical Strain Processes

18.4.1 Exact Solutions

The Kadomtsev–Petviashvili equation is integrable, and many analytical solutions are known, see, e.g., [15]. Of our interest is a particular exact plane traveling solitary wave solution to Eq. (18.11),

$$w = \frac{12A_2\beta^2}{A_1} \operatorname{sech}^2(\beta(\theta + mY - VT)), \tag{18.32}$$

where $V = 4\beta^2 A_2 + m^2 A_3$. The sign of the amplitude is defined by the sign of A_2 or by nonlinear stiffness of the springs of the lattice. The shape of the wave is described by one and the same expression for zero and nonzero m .

This is not the case of Eq. (18.14) for shear waves. Consider its plane traveling wave solution depending only on the phase variable $\xi = \theta + mY - VT$ and assume that $q = F_\xi$. Then Eq. (18.14) is transformed to the ordinary differential equation,

$$(-Vq_\xi + \frac{B_1}{3}(q^3)_\xi + B_2q_{\xi\xi\xi})_\xi + B_3m^2q_{\xi\xi} + \frac{B_4k}{2}(q^2)_{\xi\xi} = 0.$$

The solution is

$$q = \frac{A}{Q + \cosh(\beta\xi)}, \tag{18.33}$$

where

$$A = \pm \frac{6B_2\beta^2}{\sqrt{B_4^2m^2 + 6B_1B_2\beta^2}}, Q = \pm \frac{B_4m}{\sqrt{B_4^2m^2 + 6B_1B_2\beta^2}}, V = \beta^2B_2 + m^2B_3. \quad (18.34)$$

We consider only bounded solutions when $Q < 1$. It always happens when $B_1B_2 > 0$. Otherwise, only one set of parameters (18.34) corresponds to the bounded solution. The sign of Q depends on the sign of the parameter m responsible for the angle of the wave front propagation relative to the x -axis. However, the sign \pm discards an influence of this dependence on the solution. Also, the sign of the amplitude $A/(Q + 1)$ is not sensitive to the sign of m or the direction of the wave propagation.

For the wave propagating along x axis, $m = 0$ and $Q = 0$. Then the familiar solitary wave solution to the modified Korteweg–de Vries equation appears from (18.33),

$$q_m = \pm \frac{6B_2\beta}{\sqrt{6B_1B_2}} \cosh^{-1}(\beta\xi) \quad (18.35)$$

that exists only when $B_1B_2 > 0$.

18.4.2 Transverse Instability of Longitudinal and Shear Waves

Transverse instability of the longitudinal plane solitary wave to Eq. (18.11) is studied by an analysis of the solution [15]:

$$w = w_p + \delta w_i(\theta, T) \exp(\lambda T + \imath p Y), \quad (18.36)$$

where $\delta \ll 1$, w_p is plane solitary wave solution (18.32) to Eq. (18.11). An analysis performed in [22] gives rise to the solution for λ ,

$$\lambda^2 = -\frac{16A_2A_3\beta^2}{3}. \quad (18.37)$$

At $A_2 > 0$, $A_3 > 0$, $\lambda^2 < 0$, λ is imaginary number that corresponds to the stability which happens for a square lattice. For the graphene lattice, A_2 may be negative that gives rise to possible real values of λ and to the transverse instability.

Similarly, an instability of shear wave solutions to Eq. (18.14) can be studied [22],

$$q = q_p + \delta q_i(\theta, T) \exp(\lambda T + \imath p Y), \quad (18.38)$$

The localized bell-shaped solution q_p is exact solution (18.35) propagating along the x axis. The condition of the absence of secular terms in the next order solution gives rise to the solution of λ [22],

$$\lambda^2 = -4B_2 \beta^2 \left(B_3 + \frac{B_4^2}{108 B_1} \right).$$

Therefore, stability occurs for $B_3 > 0$, while positive value of λ may be achieved at negative B_3 that results in the transverse instability of plane shear waves in the lattice. Here, the linear stiffness coefficients C_2, C_3 of the long-range interactions may be responsible for instability.

18.4.3 Numerical Solutions

The analytical solutions presented in the previous section are the particular solutions which exist under specific initial conditions. More general solutions can be obtained numerically. The main aim is to reveal the difference between the dynamics of two-dimensional longitudinal and shear waves.

18.4.3.1 Simulation Technique

The model equations (18.11), (18.14) can be rewritten in the following form,

$$\partial_x \left(\partial_t u + c_1 \partial_{xxx} u + \frac{c_2}{p+1} \partial_x u^{p+1} \right) + f \partial_{yy} u + \gamma \partial_x \left(\partial_x u \int_{-\infty}^x \partial_y u \, dx' \right) = 0, \tag{18.39}$$

where c_1, c_2, f, γ are the coefficients related to those of either Eq.(18.11) or Eq.(18.14), $p = 1, 2$ correspondingly. For the last equation $u = F_{0,\theta}$.

For $p = 1$ Eq.(18.39) is the Kadomtsev–Petviashvili equation, a wide range of methods [32–37] was developed to numerically solve this equation and its generalizations studying solitons interactions, solutions stability, asymptotic regimes and other aspects. The Fourier spectral method is used here to numerically solve Eq.(18.39) in the domain $[-L_x, L_x] \times [-L_y, L_y]$ with the periodic boundary conditions. Applying the antiderivative ∂_x^{-1} and Fourier transform to Eq.(18.39) gives rise to

$$\partial_t \hat{u} - i \left(c_1 k_x^3 - f \frac{k_y^2}{k_x} \right) \hat{u} + i \frac{k_x}{p+1} \mathcal{F} (u^{p+1}) + \gamma \mathcal{F} \left[\partial_x u \int_{-\infty}^x \partial_y u \, dx' \right] = 0, \tag{18.40}$$

where $u(x, y, t) \xrightarrow{\mathcal{F}} \hat{u}(k, l, t)$, $k_x = \frac{2\pi k}{L_x}$ and $k_y = \frac{2\pi l}{L_y}$. This equation is solved using the Sanz–Serna discretization scheme and the fast Fourier transform for the nonlinear terms based on the method proposed in [38]. The numerical scheme is

$$\begin{aligned} & \frac{\hat{U}_{n+1} - \hat{U}_n}{\Delta t} - i \left(c_1 I_y \otimes K_x^3 - f K_y^2 \otimes \bar{K}_x^{-1} \right) \frac{\hat{U}_{n+1} + \hat{U}_n}{2} \\ & + i \frac{c_2}{p+1} (I_y \otimes K_x) \mathcal{F} \left[\left(\frac{U_{n+1} + U_n}{2} \right)^{p+1} \right] + \gamma \mathcal{F} \left[\left(I_y \otimes D_x \frac{U_{n+1} + U_n}{2} \right) \circ R \right] = 0, \end{aligned} \quad (18.41)$$

U_n denotes the approximation of u at time $n\Delta t$, I_x, I_y are identity matrices with the size N_x and N_y , respectively, R is the approximation of the last term of Eq. (18.40), D_* is the second-order central finite difference matrix of $\partial/\partial*$ operator with periodic boundary conditions, and K_x, K_y, \bar{K}_x^{-1} are diagonal matrices

$$\begin{aligned} K_{x,y} &= \frac{2\pi}{L_{x,y}} \text{diag} \left(0, 1, \dots, \frac{N_{x,y}}{2} - 1, -\frac{N_{x,y}}{2}, \dots, -1 \right), \\ \bar{K}_x^{-1} &= \frac{2\pi}{L_x} \text{diag} \left(0, 1, \dots, \frac{1}{N_x/2 - 1}, -\frac{2}{N_x}, \dots, -1 \right). \end{aligned}$$

The R is approximated as follows,

$$R(y) = \beta(y) + \sum_{x' \in [-L_x, x]} \left(D_y \otimes I_x \frac{U_{n+1} + U_n}{2} \right) \Delta x'. \quad (18.42)$$

When an influence of the borders of the numerical interval is being neglected then we obtain $u(-L_x, y, 0) = u(L_x, y, 0) = 0$. In this case, $\beta = 0$. Otherwise, we obtain $u(-L_x, y, t) = u(L_x, y, t)$, $u(x, -L_y, t) = u(x, L_y, t)$, $\int_{-L_x}^{L_x} \partial_y u \, dx = 0$. Then the following condition is used to define β ,

$$\int_{-L_x}^{L_x} R(y) \, dx = \text{const}. \quad (18.43)$$

Using the fixed point iteration method, Eq. (18.41) can be solved iteratively to find a solution at the next time step \hat{U}_{n+1} . Application of the inverse fast Fourier transform gives the solution u of Eq. (18.39).

18.4.3.2 Numerical Results for Longitudinal Waves

In order to check the numerical scheme given by Eq. (18.41) for $c_1 = 1$, $c_2 = 1$, $p = 1$, $f = 3$ and $\gamma = 0$, the values of the parameters are $N_x = N_y = 129$, time step $\Delta t = 0.005$ with two iterations per step.

The numerical solution shown in Fig. 18.1 demonstrates the stable propagation of the exact plane wave solution to the KP equation (18.11) when an initial condition is chosen in the form of (18.32) at $t = 0$. This is a test simulation for checking the scheme.

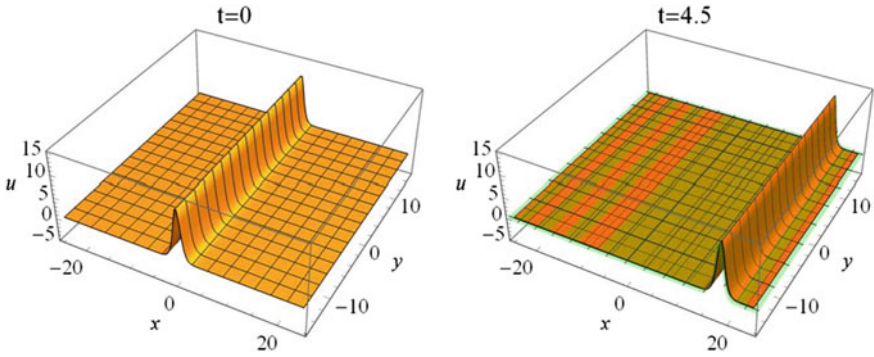


Fig. 18.1 Stable plane wave propagation. The shape and position of the plane wave solution at $t = 4.5$ do correspond to the numerical solution (orange colored) and the analytical one (green colored)

Perturbed plane solitary wave solution is studied using the initial condition developed on the basis of the asymptotic analysis (18.36),

$$u(x, y, 0) = 12\text{sech}^2(x - 4t) - 2.4\cos(y)\tanh(x) \text{sech}^2(x), \tag{18.44}$$

where $f = \pm 3$ is used in Eq. (18.39). According to the analytical solution, $f = 3$ corresponds to the stable case, while $f = -3$ relates to a transverse instability.

Comparing Figs. 18.1 and 18.2, one can see the stable propagation of the plane wave in Fig. 18.2 at the initially transversely perturbed plane wave. The wave in both figures propagates keeping its shape and velocity while initial perturbation at the wave in Fig. 18.2 disappears in time.

On the contrary, one can see in Fig. 18.3 that the initial condition with negative f provides serious transverse variations on the plane wave front. Initial small periodic perturbations suffer an increase in the amplitude, and initially, almost plane

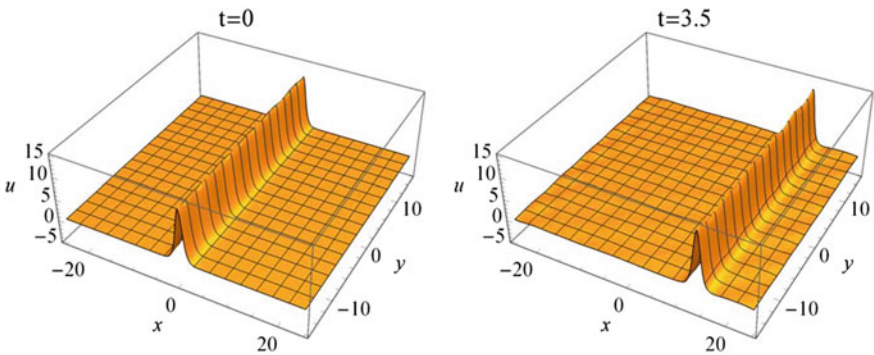


Fig. 18.2 Numerical solution for the initial condition $u(x, y, 0)$ for $f = 3$

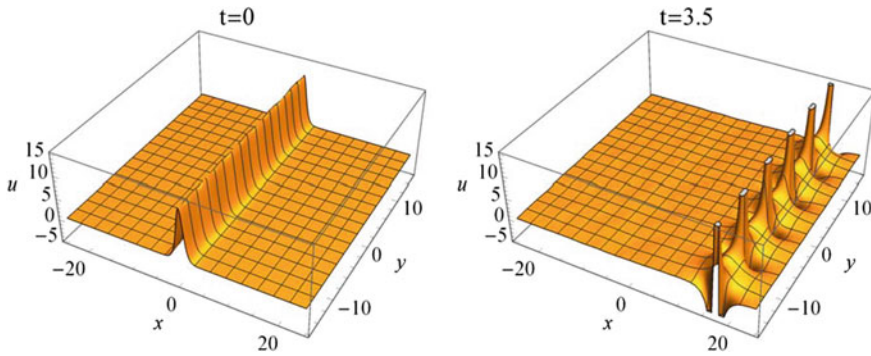


Fig. 18.3 Numerical solution for the initial condition $u(x, y, 0)$ for $f = -3$. The interpolation surface of the solution is cut off at $z = 15$ in order to save the scale

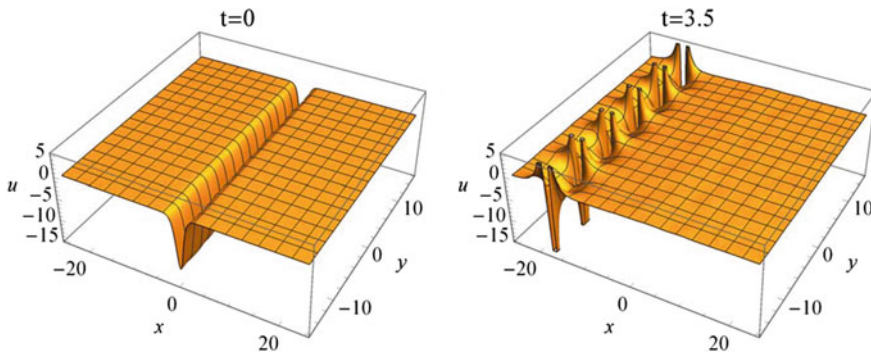


Fig. 18.4 Numerical solution for the initial condition $-u(x, y, 0)$ for $f = 3, c_1 = -1$. The interpolation surface of the solution is cut off at $z = -15$ in order to save the scale

wave evolves into a transversely modulated wave. This happens in agreement with the analysis. It was noted before that c_1 may be negative rather than f . However, transformation of variables, $t = -\tau, u = -v$, at negative c_1 and positive f results in the equation for v with positive c_1 and negative f corresponding to an unstable propagation of negative amplitude wave u (see Fig. 18.4).

18.4.3.3 Numerical Results for Shear Waves Equation

Consider Eq. (18.41) for $p = 2$ and $\gamma \neq 0$. For all simulations $N_x = 1025, N_y = 129$, time step $\Delta t = 0.003$ with two iterations per step. N_x is chosen to be higher than it was for previous simulations in order to increase the accuracy of evaluation of the term given by Eq. (18.42).

The parameters (18.34) of exact solution (18.33) depend on m responsible for propagation inclined to the x axis and two sets of parameters are possible. Therefore,

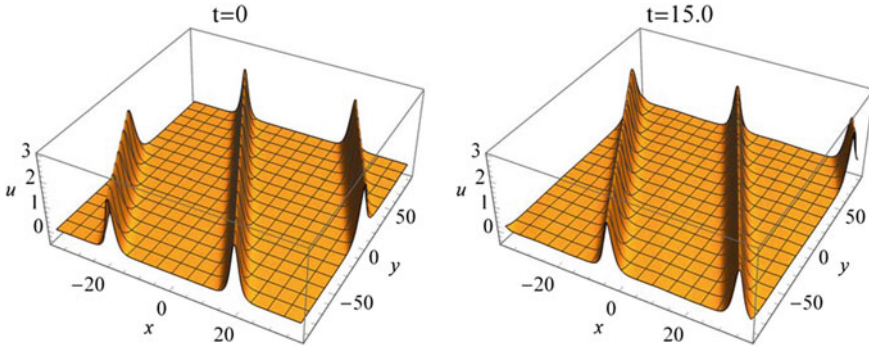


Fig. 18.5 Stable inclined plane shear wave propagation. The numerical solution corresponds to the sum of three analytical plane wave soliton solutions of Eq. (18.39) at $t = 15$

it is of interest to study inclined propagation of shear waves. For this purpose, the initial condition is constructed as the sums of three plane wave solitons (18.33) (at $t = 0$). The distance between them is chosen larger than their effective length, so the interaction between these solitons is very small. Also, the choice of the distance provides periodic conditions for y as it is seen in Fig. 18.5.

The calculation domain in x is increased in order to avoid the boundary influence.

$$L_x = 30\pi.$$

The initial condition is

$$u(x, y, 0) = u_{\text{exact}}(\xi) + u_{\text{exact}}(\xi - 2L_y \tan \phi) + u_{\text{exact}}(\xi + 2L_y \tan \phi), \quad (18.45)$$

where

$$u_{\text{exact}}(\xi) = \frac{A}{Q + \cosh(\xi)}, \quad (18.46)$$

$$A = \frac{6c_1}{\sqrt{6c_1c_2 + \gamma^2m^2}}, \quad Q = \pm \frac{\gamma m}{\sqrt{6c_1c_2 + \gamma^2m^2}},$$

$$\xi = x + my - Vt, \quad V = c_1 + fm^2, \quad m = \tan \phi, \quad \phi = 0.2;$$

$$c_1 = 1, \quad c_2 = 1, \quad f = 3, \quad \gamma = 2.$$

The results of stable propagation of the inclined plane waves are shown in Fig. 18.5. One can check that each of the inclined solitary waves corresponds to the single wave exact solitary wave solution.

To study the transverse instability, we consider propagation of a single solitary wave along the x axis. The perturbed initial condition is chosen according to the instability analysis of shear waves,

$$u(x, y, 0) = \sqrt{6} \operatorname{sech}(x) - \sqrt{6} \tanh(x) \operatorname{sech}(x) \cos(y), \quad (18.47)$$

The results are shown in Figs. 18.6, 18.7 and 18.8. The stable case is shown in Fig. 18.6. One can see that the initial perturbations on the front of the wave decrease while a two-dimensionally periodic tail develops behind the plane strain solitary wave.

The unstable plane shear wave propagation is shown in Figs. 18.7 and 18.8. In the former figure, one can see an evolution similar to that found for longitudinal waves: increase in the amplitude and deep transverse modulation of the plane wave front. The latter figure demonstrates an influence of the value of γ on the transverse instability. The oscillations on the front do not grow anymore while perturbations are developing both before and after the plane wave front.

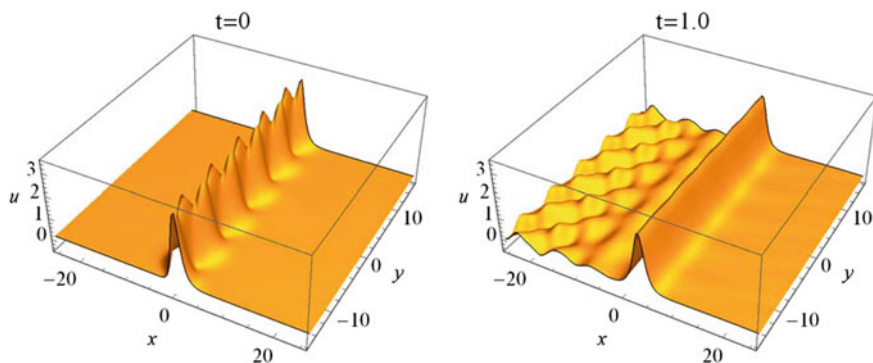


Fig. 18.6 Propagation of $u(x, y, 0)$ for $f = 3, \gamma = 2$

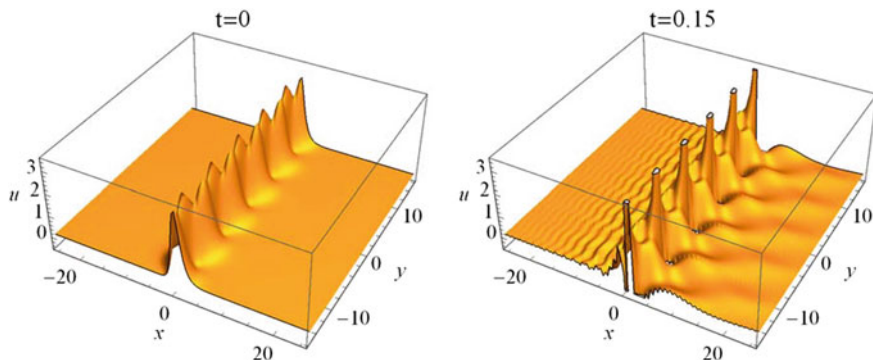


Fig. 18.7 Propagation of $u(x, y, 0)$ for $f = -3, \gamma = 1$

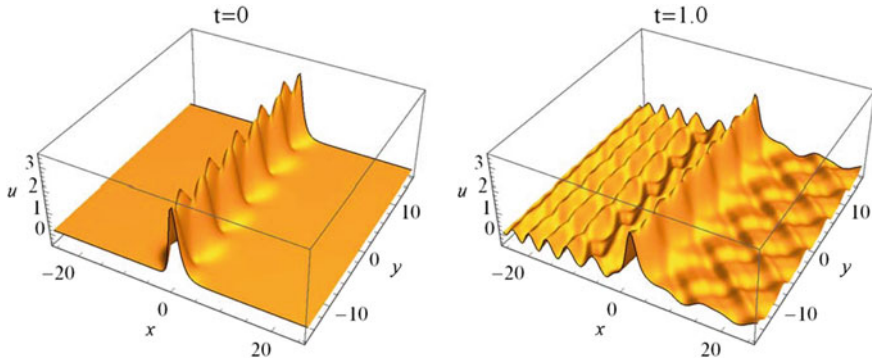


Fig. 18.8 Propagation of $u(x, y, 0)$ for $f = -3$, $\gamma = 2$

18.5 Conclusions

The asymptotic technique presented in this paper allows to reduce the coupled nonlinear continuum equations of 2D crystal lattices to a single nonlinear equation for strain waves, which allows to analyze only relevant terms in the new equations. Two types of lattices were considered: the generalized square lattice and the graphene lattice (the model is based on a consideration of two interacting sub-lattices with both translational and angular interactions being taken into account), and the governing two-dimensional equations for longitudinal and shear strain waves were obtained. Their exact plane wave solutions and their transverse stability have been revealed in numerical simulations.

Numerical simulations confirm that the angular stiffness in the original discrete model gives rise to various types of nonlinear waves localization depending on the coefficients values. Previous studies of the lattices of another structure revealed important variations in the governing equation from that of the longitudinal waves [22]. Extended interactions in the square lattice firstly produce additional extrema in the dispersion curve for linear longitudinal plane waves. They have a significant influence on the auxetic behavior of the material. One can note that the one-dimensional limits of the equations for longitudinal and shear waves differ only by nonlinear terms (quadratic or cubic) while two-dimensional consideration results in different transverse variation terms which are nonlinear for shear waves contrary to the linear term for longitudinal waves. Moreover, the sign of the coefficients in the governing equations may vary more for shear waves descriptions. It results in different stability criteria for longitudinal and shear localized plane strain waves.

This, in turn, allows us to predict different scenario of the wave amplification and localization due to a transverse instability caused by the values of the stiffness coefficients. In the stable case of the Kadomtsev–Petviashvili equation (18.11), two-dimensional localized wave amplification happens due to instability, see Figs. 18.3 and 18.4. An unstable case of Eq. (18.11) also results in the transverse periodic

modulation of the plane wave. Figure 18.3 demonstrated classic result for the corresponding negative sign at the term with derivatives with respect to y . However, this case is not realized for description of our lattice while the negative sign at the dispersion term can be achieved. This results in the dynamics shown in Fig. 18.4. The new results concern the transverse instability of nonlinear shear waves, see Figs. 18.7 and 18.8 which are different from that of longitudinal waves. The comparison of the numerical results for shear waves gives an explanation of how the coefficient at the quadratic nonlinearity influences the inclined plane solitary wave propagation and the transverse instability.

One of the potential extensions of this study is a short-range wave continualization. Previously, it was studied for a hexagonal lattice in Refs. [20, 21] where new model modulation two-dimensional equations were obtained. Also, nonlocal interactions will be of interest, in particular, utilization of the method of shift operators [11] for obtaining two-dimensional model equations for dynamical processes in nonlocal square lattice will be considered in the nearest future. Another extension of the model concerns an inclusion of the geometrical nonlinearity in the discrete model like it was done, e.g., in [39]. Furthermore, along with the geometrical nonlinearity and weakly transversely perturbed shear waves, the study can be extended to the case of nonlinear translational stiffnesses examination.

Acknowledgements The work was performed in IPME RAS, supported by the Russian Science Foundation (grant 19-41-04106).

References

1. Born, M., Huang, K.: *Dynamical Theory of Crystal Lattices*. Clarendon Press, Oxford (1954)
2. Askes, H., Metrikine, A.V.: Higher-order continua derived from discrete media: continualisation aspects and boundary conditions. *Int. J. Solids Struct.* **42**, 187–202 (2005)
3. Askar, A.: *Lattice Dynamical Foundations of Continuum Theories*. World Scientific, Singapore (1985)
4. Ostoja-Starzewski, M.: Lattice models in micromechanics. *Appl. Mech. Rev.* **55**, 35–60 (2002)
5. Maugin, G.A.: *Nonlinear Waves in Elastic Crystals*. Oxford University Press, Oxford, UK (1999)
6. Engelbrecht, J.: *Nonlinear Wave Dynamics. Complexity and Simplicity*. Kluwer, The Netherlands (1997)
7. Erofeev, V.I.: *Wave Processes in Solids with Microstructure*. World Scientific, Singapore (2002)
8. Manevich, A.I., Manevitch, L.I.: *The mechanics of nonlinear systems with internal resonances*. Imperial College Press (2005)
9. Andrianov, I.V., Awrejcewicz, J., Weichert, D.: Improved continuous models for discrete media. *Math. Probl. Eng. (Open Access)* 986242 (2010)
10. Kosevich, A.M., Savotchenko, S.E.: Peculiarities of dynamics of one-dimensional discrete systems with interaction extending beyond nearest neighbors, and the role of higher dispersion in soliton dynamics. *Low Temp. Phys.* **25**, 550–557 (1999)
11. Michelitsch, T.M., Collet, B., Wang, X.: Nonlocal constitutive laws generated by matrix functions: lattice dynamics models and their continuum limits. *Int. J. Eng. Sci.* **80**, 106–123 (2014)
12. Sharma, B.L., Eremeyev, V.A.: Wave transmission across surface interfaces in lattice structures. *Int. J. Eng. Sci.* **145**, 103173 (2019)

13. Tovstik, P.E., Tovstik, T.P.: Static and dynamic analysis of two-dimensional graphite lattices. *Mech. Solids* **47**, 517–524 (2012)
14. Suiker, A.S.J., Metrikine, A.V., de Borst, R.: Comparison of wave propagation characteristics of the Cosserat continuum model and corresponding discrete lattice models (2000)
15. Ablowitz, M., Segur, H.: *Solitons and Inverse Scattering Transform*. SIAM, Philadelphia (1981)
16. Zabusky, N.G., Deem, G.S.: Dynamics of nonlinear lattices I. Localized optical excitations, acoustic radiation, and strong nonlinear behavior. *J. Comput. Phys.* **2**, 126–153 (1967)
17. Engelbrecht, J.: *Nonlinear Wave Processes of Deformation in Solids*. Pitman, Boston (1983)
18. Zabusky, N.G., Kruskal, M.: Interaction of “solitons” in a collisionless plasma and the recurrence of initial states. *Phys. Rev. Lett.* **15**, 240–243 (1967)
19. Engelbrecht, J., Berezovski, A., Soomere, T.: Highlights in the research into complexity of nonlinear waves. *Proc. Est. Acad. Sci.* **59**, 61–65 (2010)
20. Porubov, A.V., Berinskii, I.E.: Nonlinear plane waves in materials having hexagonal structure. *Int. J. Non-Linear Mech.* **67**, 27–33 (2014)
21. Porubov, A.V., Berinskii, I.E.: Two-dimensional nonlinear shear waves in materials having hexagonal lattice structure. *Math. Mech. Solids* **21**(1), 94–103 (2016)
22. Porubov, A.V., Krivtsov, A.M., Osokina, A.E.: Two-dimensional waves in extended square lattice. *Int. J. Non-Linear Mech.* **99**, 281–287 (2018)
23. Porubov, A.V., Osokina, A.E., Michelitsch, T.M.: Operator approach to square lattice nonlinear dynamics. *Mater. Phys. Mech.* **35**(1), 139–144 (2018)
24. Porubov, A.V., Osokina, A.E., Michelitsch, T.: Nonlocal approach to square lattice dynamics. In: Altenbach, H., Pouget, J., Rousseau, M., Collet, B., Michelitsch, Th. (eds.) *Generalized Models and Non-Classical Approaches in Complex Materials*. *Advanced Structured Materials*, vol. 90, pp. 641–654. Springer International Publishing AG, part of Springer Nature (2018)
25. Erofeev, V.I., Pavlov, I.S.: Parametric identification of crystals having a cubic lattice with negative Poisson’s ratios. *J. Appl. Mech. Tech. Phys.* **56**(6), 1015–1022 (2015)
26. Kadomtsev, B.B., Petviashvili, V.I.: On the stability of solitary waves in a weakly dispersive media. *Sov. Phys. Dokl.* **15**, 539–541 (1970)
27. Thomas Jr., J.F.: Failure of the Cauchy relation in cubic metals. *Scr. Metall.* **5**, 787–790 (1971)
28. Porubov, A.V., Osokina, A.E.: Double dispersion equation for nonlinear waves in a graphenetype hexagonal lattice. *Wave Motion* **89**, 185–192 (2019)
29. Zhang, P., et al.: The elastic modulus of single-wall carbon nanotubes: a continuum analysis incorporating interatomic potentials. *Int. J. Solids Struct.* **39**, 3893–3906 (2002)
30. Peng, Z., Yonggang, H., Geubelle, P.H., Kelichikh, H.: On the continuum modelling of carbon nanotubes. *Acta Mech. Sin.* **18**, 528–536 (2002)
31. Porubov, A.V., Pastrone, F.: Nonlinear bell-shaped and kink-shaped strain waves in microstructured solids. *Int. J. Non-Linear Mech.* **39**, 1289–1299 (2004)
32. Porubov, A.V., Tsuji, H., Lavrenov, I.V., Oikawa, M.: Formation of the rogue wave due to nonlinear two-dimensional waves interaction. *Wave Motion* **42**, 202–210 (2005)
33. Lu, Z., Tian, E.M., Grimshaw, R.: Interaction of two lump solitons described by the Kadomtsev-Petviashvili I equation. *Wave Motion* **40**(2), 123–135 (2004)
34. Klein, C., Sparber, C., Markowich, P.: Numerical study of oscillatory regimes in the Kadomtsev-Petviashvili equation. *J. Nonlinear Sci.* **17**(5), 429–470 (2007)
35. Infeld, E., Senatorski, A., Skorupski, A.A.: Numerical simulations of Kadomtsev-Petviashvili soliton interactions. *Phys. Rev. E* **51**(4), 3183 (1995)
36. Kao, C.Y., Kodama, Y.: Numerical study of the KP equation for non-periodic waves. *Math. Comput. Simul.* **82**(7), 1185–1218 (2012)
37. Kodama, Y., Oikawa, M., Tsuji, H.: Soliton solutions of the KP equation with V-shape initial waves. *J. Phys. A Math. Theor.* **42**(31), 312001 (2009)
38. Chehab, J.P., Garnier, P., Mammeri, Y.: Numerical solution of the generalized Kadomtsev-Petviashvili equations with compact finite difference schemes (2016). arXiv preprint [arXiv:1605.03213](https://arxiv.org/abs/1605.03213)
39. Khusnutdinova, K., Samsonov, A.M., Zakharov, A.S.: Nonlinear layered lattice model and generalized solitary waves in imperfectly bonded structures. *Phys. Rev. E* **79**, 056606 (2009)

Chapter 19

Influence of First to Second Gradient Coupling Tensors Terms with Surface Effects on the Wave Propagation of 2D Network Materials



Yosra Rahali, Hilal Reda, Benoit Vieille, Hassan Lakiss
and Jean-François Ganghoffer

Abstract The influence of surface energy terms on the wave propagation characteristics of network materials is analyzed in this contribution. The asymptotic homogenization technique is extended to account for additional surface properties of network materials made of the periodic repetition of a unit cell consisting of beam type elements. The presence of a thin coating with specific properties give rise to surface effects that are accounted for by a strain gradient behavior at the mesoscopic level of an equivalent continuum. These effects emerge in the asymptotic expansion of the effective stress and hyperstress tensors versus the small scale parameters and the additional small parameters related to surface effects. The role of the coupling tensors between first and second order gradient kinematic terms, obtained by the homogenization, materials is pursued in this contribution, accounting for surface effects arising from the presence of a thin coating on the surface of the structural beam elements of the network. The lattice beams have a viscoelastic behavior described by a Kelvin voigt model and the homogenized second gradient viscoelasticity model reflects both the lattice topology, anisotropy and microstructural features in terms of its geometrical and micromechanical parameters. We formulate the dynamic equilibrium equations and compute the network materials' wave propagation attributes. We compute the influence of the coupling tensor terms on the wave propagation characteristics as a function of the propagation direction. Considerable differences between second gradient media description with and without the consideration of the coupling energy term contributions are observed for propagating modes along the non-centrosymmetric inner material direction. We assess the effect of coupling energy

Y. Rahali · B. Vieille · H. Lakiss

GPM, INSA Rouen, Université de Rouen, Avenue de L'université, Saint-Étienne-Du-Rouvray, France

e-mail: benoit.vieille@insa-rouen.fr

H. Reda

Faculty of Engineering, Section III, Lebanese University, Campus Rafic Hariri, Beirut, Lebanon

J.-F. Ganghoffer (✉)

LEM3, Université de Lorraine, CNRS, 7, rue Félix Savart, 57073 Metz, France

e-mail: jean-francois.Ganghoffer@univ-lorraine.fr

© Springer Nature Switzerland AG 2020

H. Altenbach et al. (eds.), *Nonlinear Wave Dynamics of Materials*

and Structures, Advanced Structured Materials 122,

https://doi.org/10.1007/978-3-030-38708-2_19

over a wide range of propagating directions, deriving useful overall conclusions on its role in the wave propagation features of 3D architected media.

Keywords Network materials · Homogenization · Wave propagation · Second gradient · Coupling energy · Dispersive behavior · Surface effects

19.1 Introduction

It is well-established that unusual and novel properties of nanomaterials emerge from their surface/interfacial properties. One well-known consequence of surface properties is the emerging size effect, that is the dependence of the effective mechanical properties on the size of the considered specimen, see, for example [1–5]. The presence of a coating in these surface metamaterials dramatically changes the surface physical properties of the material and in turn all the material properties. Let us briefly discuss the mathematical models and methods used in surface-related mechanics. The analysis of surface phenomena traces back to the pioneer works of Laplace [6, 7], Young [8] and Poisson [9] who introduced surface tension for fluids and formulated the corresponding boundary-value problems. Gibbs generalized later on the notion of surface tension in the case of solids [10]. For the recent state of the art in the theory of capillarity one can refer to [11, 12]. A model of surface elasticity for elastic solids undergoing large deformations was proposed by Gurtin and Murdoch [13, 14]; relying on the physical point of view of a nonlinear solid with an elastic membrane attached on its surface. The stress resultant tensor within the membrane receives the interpretation of surface stresses in the context of the Gurtin–Murdoch model. The Gurtin–Murdoch model found many applications in micro—and nanomechanics, and it predicts the size effects observed for nanosized materials [15], so in situations where the effective material properties deviate from the ones of the bulk corresponding materials. This model was generalized in [16, 17] to account for the bending stiffness of the thin film or coating attached onto the surface of the bulk material. The different models developed in the literature that incorporate surface effects involve enhanced constitutive equations including a description of the surface behavior, whereby the introduced surface stress tensor depends on the surface strain measure. More general surface models beyond the Gurtin–Murdoch model have been developed in the literature [18–26], like for instance the model of a Cosserat surface for material interfaces [27]. These extended models include additional material parameters that should be determined, and that do influence the actual properties of materials [28–34]. The presence of surface stresses leads especially to the stiffening of the material in the context of the linear theory of elasticity [35–41].

The main objective of this contribution is to analyze the wave propagation features in small scales (essentially the nanometric level) network materials for which surface effects are of importance. The effective anisotropic material properties of nanostructured network materials at the mesoscale of an effective continuum considering surface/interface properties have been described in the framework of strain

gradient effective continua. The asymptotic homogenization of periodic network materials modeled as beam networks leads to Cauchy and second gradient effective continua, enhanced by the consideration of surface effects. Based on the elaboration of small dimensionless parameters of geometrical or mechanical nature reflecting the different length scales, different homogenized models have been constructed, the relative importance of surface effects being ruled by the scaling relations between the introduced small parameters. The surface effects are incorporated into the homogenized strain gradient moduli. It has been evidenced that surface effects may become dominant for specific choices of the scaling laws of the introduced small parameters.

The outline of this contribution is as follows: In Sect. 19.2, we provide a clarification of the models developed in this work and we describe the homogenization process leading to the identification of the effective second order continuum for 2D viscoelastic structures accounting for surface effects and nodal rotations, based on a complete Euler-Bernoulli scheme [42]. The homogenized viscoelastic behavior of repetitive planar lattices consisting of viscoelastic Kelvin–Voigt type beams is also investigated. The effective constitutive laws are next introduced into the dynamical planar equilibrium equations (Sect. 19.3). 2D example illustrating the proposed viscoelastic second order homogenization scheme is presented in Sect. 19.3, and the dispersion relations and damping ratio evolutions versus the wave number are evaluated. Finally, we conclude in Sect. 19.4 by a summary of the main developments and perspectives for future developments.

19.2 Second Order Discrete Homogenization for Viscoelastic Network Materials

In order to determine the first and second order effective moduli of two-dimensional viscoelastic network materials accounting for surface effects and rotations at the lattices nodes, a discrete homogenization model is developed in the sequel for non-centrosymmetric structures. A dedicated code has been constructed in symbolic Maple software. The method enables to treat any repetitive lattice with an arbitrary architecture, relying on an input file describing the geometrical and mechanical properties of the beam lattice.

The discrete homogenization method requires the development of all geometrical variables (length, thickness, width) and kinematic variables (displacements) as Taylor series expansions versus a small parameter ε , defined as the ratio of unit cell size to a macroscopic length characteristic of the entire lattice. These expansions are thereafter inserted into the equilibrium equation of forces and moments, expressed in weak form. After resolution of the unknown displacements in the localization problem posed over the identified reference unit cell, the stress and hyperstress tensors are constructed versus their conjugated kinematic variables, respectively the

deformation and gradient of deformation tensors, thereby defining the homogenized constitutive law; this allows identifying the first and second order effective moduli for the equivalent continuum related to.

The different steps of the discrete homogenization method leading to the expression of the Cauchy stress and hyperstress tensors of the second gradient effective continuum are summarized in algorithmic format in the sequel (we refer the reader to [43, 44] for more details):

Regarding notations, vectors and second order tensors are denoted using boldface symbols.

- (1) For each beam b , write the expressions of the normal N and transverse T forces and moments M exerted on the beam extremities, including an elastic and a viscous part, summarized in the next Eqs. (19.1)–(19.6)

$$N_E^{\varepsilon b} = \tilde{k}_l^b (e^b \cdot (D_E^\varepsilon - D_O^\varepsilon)) + \frac{\mu_e \tilde{A}_b^\varepsilon}{l_b^\varepsilon} (e^b \cdot (\dot{D}_E^\varepsilon - \dot{D}_O^\varepsilon)) \tag{19.1}$$

$$N_O^{\varepsilon b} = -N_E^{\varepsilon b} \tag{19.2}$$

$$T_E^{\varepsilon b} = \tilde{k}_f^b \left(e^{b\perp} \cdot (D_E^\varepsilon - D_O^\varepsilon) - \frac{l_b^\varepsilon}{2} (\phi_E^\varepsilon + \phi_O^\varepsilon) \right) + \frac{12\mu_e \tilde{I}^{\varepsilon b}}{(l_b^\varepsilon)^3} \left(e^{b\perp} \cdot (\dot{D}_E^\varepsilon - \dot{D}_O^\varepsilon) - \frac{l_b^\varepsilon}{2} (\dot{\phi}_E^\varepsilon + \dot{\phi}_O^\varepsilon) \right) \tag{19.3}$$

$$T_O^{\varepsilon b} = -T_E^{\varepsilon b} \tag{19.4}$$

$$M_O^{\varepsilon b} e_3 = \left(\begin{array}{l} \frac{\tilde{k}_f l_b^\varepsilon}{6} (l_b^\varepsilon (2\phi_O^\varepsilon + \phi_E^\varepsilon) - 3 \cdot e^{b\perp} \cdot (D_E^\varepsilon - D_O^\varepsilon)) \\ + \frac{2\mu_e \tilde{I}^{\varepsilon b}}{(l_b^\varepsilon)^2} (l_b^\varepsilon (2\dot{\phi}_O^\varepsilon + \dot{\phi}_E^\varepsilon) - 3 \cdot e^{b\perp} \cdot (\dot{D}_E^\varepsilon - \dot{D}_O^\varepsilon)) \end{array} \right) \cdot e_3 \tag{19.5}$$

$$M_E^{\varepsilon b} e_3 = \left(\begin{array}{l} \frac{\tilde{k}_f l_b^\varepsilon}{6} (l_b^\varepsilon (\phi_O^\varepsilon + 2\phi_E^\varepsilon) + 3 \cdot e^{b\perp} \cdot (D_O^\varepsilon - D_E^\varepsilon)) \\ + \frac{2\mu_e \tilde{I}^{\varepsilon b}}{(l_b^\varepsilon)^2} (l_b^\varepsilon (\dot{\phi}_O^\varepsilon + 2\dot{\phi}_E^\varepsilon) - 3 \cdot e^{b\perp} \cdot (\dot{D}_E^\varepsilon - \dot{D}_O^\varepsilon)) \end{array} \right) e_3 \tag{19.6}$$

The subscripts O and E refer to the origin and extremity nodes of the beam. D , \dot{D} , ϕ^ε and $\dot{\phi}^\varepsilon$ are the displacement, the displacement velocity vectors, the nodal microrotation and the rotation velocity, respectively, μ_e the extensional viscosity and

$I^{\varepsilon b}, l_b^\varepsilon$ are respectively the quadratic moment and the length of the considered beam, \mathbf{e}^b the unit director along each beam and $\mathbf{e}^{b\perp}$ the normal unit vector. The index b refers to the beam.

ϕ^ε receives the following asymptotic expansion:

$$\begin{aligned}\phi_O^\varepsilon &= \phi_0^O \\ \phi_E^\varepsilon &= \phi_0^E + \varepsilon \left(\frac{\partial \phi_0^E}{\partial \lambda_i} \delta^{ib} \right)\end{aligned}$$

with $\phi_0^O = \phi_0^E = \phi_0 = \frac{\partial D_o(\lambda^\varepsilon)}{\partial \lambda_i} \mathbf{e}^{b\perp}$, the last relation linking the microrotation to the displacement gradient in the context of Bernoulli kinematics.

We consider a square section with area $\tilde{A} = t$, assuming a unit beam thickness. The tensile and flexural rigidities of the beam are expressed as (see [45]).

$$\tilde{k}_t^b = \frac{\tilde{E}_B \tilde{A}^{\varepsilon b}}{l_b^\varepsilon}; \tilde{k}_f^b = \frac{12 \tilde{E}_B \tilde{I}^{\varepsilon b}}{(l_b^\varepsilon)^3} \quad (19.7)$$

The tensile modulus of the base material E_B is enhanced by surface effects according to the relation (Eremeyev and Altenbach, 2015):

$$\tilde{E}_B = E_B \left(1 + \frac{l_s}{t} \right) = E_B \left(1 + \frac{l_s l_b}{l_b t} \right) = E_B \left(1 + \frac{\varepsilon^\alpha}{\eta} \right) \quad (19.8)$$

$\varepsilon^\alpha = \frac{l_s}{l_b}$ with $l_s = \frac{2E_s}{E}$ the ratio of (twice) the surface modulus of the coating to the bulk modulus of the beam material, called the characteristic length parameter in [46].

We consider that the slenderness ratio of the beam, parameter $\eta = \frac{t}{l_b}$, is finite.

(2) Write the asymptotic expansion of geometrical and kinematic variables of each beam, in curvilinear coordinates denoted λ in the sequel:

- The beam length and width respectively $l_b^\varepsilon = \varepsilon l_b, t^{\varepsilon b} = \varepsilon t_b$,
- The relative nodal displacement and velocity (see [42–44]).

$$\begin{aligned}(\mathbf{D}_O^\varepsilon - \mathbf{D}_E^\varepsilon) &= \varepsilon \left(\mathbf{D}_1^E - \mathbf{D}_1^O + L_i \delta_{ib} \frac{\partial D_o(\lambda^\varepsilon)}{\partial \lambda_i} \right) \\ &+ \varepsilon^2 \left(\mathbf{D}_2^E - \mathbf{D}_2^O + L_i \delta_{ib} \frac{\partial D_1^E(\lambda^\varepsilon)}{\partial \lambda_i} + \frac{L_i^2 \delta_{ib}^2}{2} \frac{\partial^2 D_o(\lambda^\varepsilon)}{\partial \lambda_i^2} \right) \quad (19.9)\end{aligned}$$

$$\begin{aligned}(\dot{\mathbf{D}}_E^\varepsilon - \dot{\mathbf{D}}_O^\varepsilon) &= \varepsilon \left(\dot{\mathbf{D}}_1^E - \dot{\mathbf{D}}_1^O + L_i \delta_{ib} \frac{\partial \dot{D}_o(\lambda^\varepsilon)}{\partial \lambda_i} \right) \\ &+ \varepsilon^2 \left(\dot{\mathbf{D}}_2^E - \dot{\mathbf{D}}_2^O + L_i \delta_{ib} \frac{\partial \dot{D}_1^E(\lambda^\varepsilon)}{\partial \lambda_i} + \frac{L_i^2 \delta_{ib}^2}{2} \frac{\partial^2 \dot{D}_o(\lambda^\varepsilon)}{\partial \lambda_i^2} \right) \quad (19.10)\end{aligned}$$

with δ_i the shift factor (equal to ± 1) for nodes belonging to a neighboring cell, and nil for nodes located inside the considered cell. The index $i \in \{1, 2\}$ indicating the considered axis e_1 or e_2 .

- (3) Passage of curvilinear to Cartesian coordinates (see [43]).
- (4) Writing the equilibrium of forces and moments in virtual power form

$$\sum_{v^i \in \mathbb{Z}^2} \sum_{b \in B_R} (T^b \dot{V} + N^b \dot{U}) = 0 \quad (19.11)$$

$$\sum_{v^i \in \mathbb{Z}^2} \sum_{b \in B_R} \left(M_O^b \cdot \mathbf{w}_O^b + M_E^b \cdot \mathbf{w}_E^b + \frac{l^b}{2} (\mathbf{e}^b \wedge \mathbf{F}_E^b) \cdot \mathbf{w}_C^b - \frac{l^b}{2} (\mathbf{e}^b \wedge \mathbf{F}_O^b) \cdot \mathbf{w}_C^b \right) = 0 \quad (19.12)$$

B_R refer to the set of beams within the reference unit cell, \mathbf{w} the virtual rotation velocity and $\mathbf{F}^b = N^b \mathbf{e}^b + T^b \mathbf{e}^{b\perp}$ the force exerted on the beam b .

- (5) Write the virtual power of internal forces over an elementary cell (on the boundary nodes, since the contribution of the internal nodes mutually cancel)

$$P_e = \sum_b (T_E (\dot{V}_E - \dot{V}_O) + N_E (\dot{U}_E - \dot{U}_O)) \quad (19.13)$$

with \dot{V}_i and \dot{U}_i therein the two components of the virtual velocity field.

- (6) Development of the expressions of the relative longitudinal and transverse velocities $(\dot{V}_E - \dot{V}_O)$ and $(\dot{U}_E - \dot{U}_O)$ using a Taylor series expansion (see Eq. (53) in [43]).
- (7) Write the continuous formulation of the virtual power by passing to the limit in (19.13). One can find after development

$$\begin{aligned} \lim_{\varepsilon \rightarrow 0} P &= \lim_{\varepsilon \rightarrow 0} \varepsilon^2 \sum_{c \in \mathbb{Z}} P_e \\ &= \int_{\Omega} P_e d\lambda = \int_{\Omega} \frac{1}{g} \sum_b \left[\begin{aligned} & \left(\left(T_E^1 L_i \delta_{ib} \frac{\partial \dot{V}_O(\lambda^\varepsilon)}{\partial \lambda_i} \right) + \left(N_E^1 L_i \delta_{ib} \frac{\partial \dot{U}_O(\lambda^\varepsilon)}{\partial \lambda_i} \right) \right) \\ & + \varepsilon \left(\left(T_E^1 \frac{L_i^2 \delta_{ib}^2}{2} \frac{\partial^2 \dot{V}_O(\lambda^\varepsilon)}{\partial \lambda_i^2} \right) + \left(T_E^2 L_i \delta_{ib} \frac{\partial \dot{V}_O(\lambda^\varepsilon)}{\partial \lambda_i} \right) \right) \\ & + \left(N_E^1 \frac{L_i^2 \delta_{ib}^2}{2} \frac{\partial^2 \dot{U}_O(\lambda^\varepsilon)}{\partial \lambda_i^2} \right) + \left(N_E^2 L_i \delta_{ib} \frac{\partial \dot{U}_O(\lambda^\varepsilon)}{\partial \lambda_i} \right) \right) \\ & + \varepsilon^2 \left(\left(T_E^2 \frac{L_i^2 \delta_{ib}^2}{2} \frac{\partial^2 \dot{V}_O(\lambda^\varepsilon)}{\partial \lambda_i^2} \right) + \left(N_E^2 \frac{L_i^2 \delta_{ib}^2}{2} \frac{\partial^2 \dot{U}_O(\lambda^\varepsilon)}{\partial \lambda_i^2} \right) \right) \end{aligned} \right] dV \end{aligned} \quad (19.14)$$

with $N_E = (\varepsilon N_E^1 + \varepsilon^2 N_E^2)$, $T_E = (\varepsilon T_E^1 + \varepsilon^2 T_E^2)$ and g is the Jacobean of the transformation from Cartesian to curvilinear coordinates. Parameter δ_i is the shift factor

equal to ± 1 for nodes belonging to a neighboring cell, and nil for nodes located inside the considered cell and L_i the periodic length, the index $i \in \{1, 2\}$ indicating the considered axis, e_1 or e_2 .

Previous expression involves three integrals of increasing powers with respect to the scale parameter ε , namely the zero order term lead to the Cauchy stress, the first order representing coupling terms and the second order associated to the hyperstress tensor contribution. Previous expression is next written in Cartesian coordinates (see the Appendix).

(8) Equivalence with a second order grade continuum [43, 47] in order to express the stress and hyperstress tensors

$$P^i = \int_{\Omega} ((\sigma - S \cdot \nabla) \cdot \nabla) \cdot \dot{D} dV = \int_{\Omega} \left(F^q \cdot \left(\frac{\partial \dot{D}}{\partial x_q} \right) - H^{pq} \cdot \left(\frac{\partial^2 \dot{D}}{\partial x_p \partial x_q} \right) \right) dV \quad (19.15)$$

with \dot{D} therein the virtual rate of deformation, σ Cauchy stress and S the third order hyperstress tensor with index symmetry $S_{ijk} = S_{ikj}$.

(9) Calculation of the stress and hyperstress tensors

$$\sigma = (\sigma_{iq} e_i) \otimes e_q = F^q \otimes e_q \quad (19.16)$$

$$S = (S_{kqp} e_k) \otimes e_q \otimes e_p = H^{pq} \otimes e_q \otimes e_p \quad (19.17)$$

The force vectors in (19.16) and (19.17) write for $q \in \{1, 2\}$,

$$F^1 = \left[\left(\frac{T_E^1 + N_E^1}{g} \right) + \varepsilon \left(\frac{T_E^2 + N_E^2}{g} \right) \right] (L_1 \delta_{1b} \cos \theta_1 + L_2 \delta_{2b} \cos \theta_2) \quad (19.18)$$

$$F^2 = \left[\left(\frac{T_E^1 + N_E^1}{g} \right) + \varepsilon \left(\frac{T_E^2 + N_E^2}{g} \right) \right] (L_1 \delta_{1b} \sin \theta_1 + L_2 \delta_{2b} \sin \theta_2) \quad (19.19)$$

with the pair of indices $(p, q) \in \{(1, 1), (2, 2), (1, 2)\}$,

$$H^{11} = \left[\varepsilon \left(\frac{T_E^1 + N_E^1}{g} \right) + \varepsilon^2 \left(\frac{T_E^2 + N_E^2}{g} \right) \right] \left(\frac{L_1^2 \delta_{1b}^2 \cos^2 \theta_1}{2} + \frac{L_2^2 \delta_{2b}^2 \cos^2 \theta_2}{2} \right) \quad (19.20)$$

$$H^{22} = \left[\varepsilon \left(\frac{T_E^1 + N_E^1}{g} \right) + \varepsilon^2 \left(\frac{T_E^2 + N_E^2}{g} \right) \right] \left(\frac{L_1^2 \delta_{1b}^2 \sin^2 \theta_1}{2} + \frac{L_2^2 \delta_{2b}^2 \sin^2 \theta_2}{2} \right) \quad (19.21)$$

$$\mathbf{H}^{12} = \left[\varepsilon \left(\frac{\mathbf{T}_E^1 + \mathbf{N}_E^1}{g} \right) + \varepsilon^2 \left(\frac{\mathbf{T}_E^2 + \mathbf{N}_E^2}{g} \right) \right] \left(L_1^2 \delta_{1b}^2 \cos \theta_1 \sin \theta_1 + L_2^2 \delta_{2b}^2 \sin \theta_2 \cos \theta_2 \right) \quad (19.22)$$

with $g = L_1 L_2 (\cos \theta_1 \sin \theta_2 - \sin \theta_1 \cos \theta_2)$ there above the determinant of the Jacobian matrix and $\mathbf{T}_E^1 = T_E^1 \mathbf{e}^{b\perp}$, $\mathbf{T}_E^2 = T_E^2 \mathbf{e}^{b\perp}$, $\mathbf{N}_E^1 = N_E^1 \mathbf{e}^b$; $\mathbf{N}_E^2 = N_E^2 \mathbf{e}^b$.

(10) Calculation of the stress and hyperstress tensors

$$\sigma = (\sigma_{iq} e_i) \otimes e_q = F^q \otimes e_q \quad (19.23)$$

$$S = (S_{kqp} e_k) \otimes e_q \otimes e_p = H^{pq} \otimes e_q \otimes e_p \quad (19.24)$$

The constitutive law for a homogeneous anisotropic viscoelastic second order grade continuum writes in index format as:

$$\begin{aligned} \{\sigma\} &= \underbrace{[A^e]\{\epsilon\} + [B^e]\{\kappa\}}_{\text{elastic part}} + \underbrace{[A^v]\{\dot{\epsilon}\} + [B^v]\{\dot{\kappa}\}}_{\text{viscous part}} \\ \{S\} &= \underbrace{[B^e]\{\epsilon\} + [D^e]\{\kappa\}}_{\text{elastic part}} + \underbrace{[B^v]\{\dot{\epsilon}\} + [D^v]\{\dot{\kappa}\}}_{\text{viscous part}} \end{aligned} \quad (19.25)$$

with σ_{ij} , S_{ijk} , ϵ_{pq} , κ_{pqr} , $\dot{\epsilon}_{pq}$, $\dot{\kappa}_{pqr}$ successively the stress and hyperstress tensors, and their conjugated kinematic quantities, namely (in component form) the first and second deformation gradients and their time derivatives, the first and second deformation velocity gradients.

The constitutive tensors A_{ijpq}^e , D_{ijkpqr}^e , B_{pqrij}^e , A_{ijpq}^v , D_{ijkpqr}^v , B_{pqrij}^v therein are respectively the first and second order elasticity and viscosity coefficients, the coupling moduli, which all depending on the specific considered lattices.

Note that the methodology presented in the current section is general, provided a repetitive unit cell of the repetitive network has been identified.

19.3 Wave Propagation Analysis in Non-centrosymmetric Architectures

The computation of the effective constitutive tensors form the basis for the subsequent dynamical analysis of network materials with surface effects. More precisely, the starting point is the writing of the equations of motion for a second gradient medium along both in-plane directions

$$\begin{aligned} \left(\frac{\partial \sigma_{11}}{\partial x_1} + \frac{\partial \sigma_{12}}{\partial x_2} \right) - \frac{\partial^2 S_{111}}{\partial x_1 \partial x_1} - \frac{\partial^2 S_{112}}{\partial x_1 \partial x_2} - \frac{\partial^2 S_{121}}{\partial x_2 \partial x_1} - \frac{\partial^2 S_{122}}{\partial x_2 \partial x_2} &= \rho^* \ddot{u} \\ \left(\frac{\partial \sigma_{21}}{\partial x_1} + \frac{\partial \sigma_{22}}{\partial x_2} \right) - \frac{\partial^2 S_{211}}{\partial x_1 \partial x_1} - \frac{\partial^2 S_{212}}{\partial x_1 \partial x_2} - \frac{\partial^2 S_{221}}{\partial x_2 \partial x_1} - \frac{\partial^2 S_{222}}{\partial x_2 \partial x_2} &= \rho^* \ddot{v} \end{aligned} \quad (19.26)$$

Parameter $\rho^* = \frac{M_1}{A_{\text{cell}}}$ in Eq. (19.26) is the effective density, with M_1 the mass of the set of lattice beams and A_{cell} the area of the periodic cell.

From Eq. (19.26), we obtain two roots that describe the propagation of longitudinal waves polarized in the direction of incident wave, and of shear waves polarized in a direction perpendicular to the direction of the incident wave.

We write the generalized displacement field for a harmonic wave propagating, at a point \mathbf{r} as

$$U = \widehat{U} e^{(\lambda t - i\mathbf{k} \cdot \mathbf{r})}, \quad V = \widehat{V} e^{(\lambda t - i\mathbf{k} \cdot \mathbf{r})} \quad (19.27)$$

In (19.27), \widehat{U} , \widehat{V} are the wave amplitudes, $\mathbf{k} = (k_1, k_2)$ is the wave vector and λ is a complex frequency function. Substitution of Eq. (19.27) in the equation of motion (19.26) delivers the system of equations

$$[D(k_1, k_2, \lambda)] \begin{Bmatrix} \widehat{U} \\ \widehat{V} \end{Bmatrix} = 0 \quad (19.28)$$

with \mathbf{k} the wave vector, chosen as a complex number. Any triad k_1, k_2, λ obtained by solving the eigenvalues problem in (19.28) represents plane waves propagating at the frequency λ . The characteristic equation of previous system is written as

$$\lambda^4 + a\lambda^3 + b\lambda^2 + c\lambda + d = 0 \quad (19.29)$$

The complex roots of Eq. (19.29) are

$$\lambda_s(k) = -\zeta_s(k) \cdot \omega_{ns}(k) \pm i \cdot \omega_{ns}(k) \sqrt{1 - \zeta_s^2} \quad (19.30)$$

Parameter s therein represents the branch type, $\omega_{ns}(k)$ is the natural frequency, $\omega_{ds}(k)$ the damped frequency and ζ_s is the damping factor. Relying on these expressions traducing the dispersion relation of the effective second gradient viscoelastic continuum, we shall plot the dissipated frequency and the damping ratio versus the wave vector \mathbf{k} .

In the current section, we apply the previously elaborated methodology to the 2D square-shaped unit-cell structure with two internal beams that do not intersect in their center, so that this unit cell is not centrosymmetric and coupling effects between first and second gradient contributions occur. The unit cell includes a total of 8 beam elements, as pictured on Fig. 19.1.

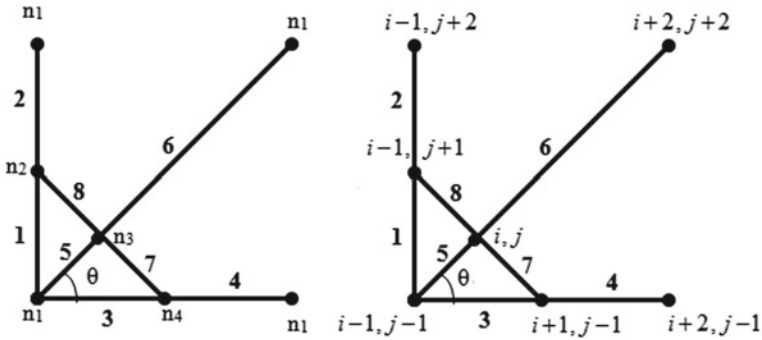


Fig. 19.1 Unit cell of the square structure with internal crossed beams

The vector including all beam lengths is elaborated as

$L_b = \left[\frac{L}{2}, \frac{L}{2}, \frac{L}{2}, \frac{L}{2}, \frac{L}{2\sqrt{2}}, \frac{3\sqrt{2}L}{4}, \frac{L}{2\sqrt{2}}, \frac{L}{2\sqrt{2}} \right]$, and the periodicity vectors are $Y_1 = \begin{bmatrix} 1 \\ 0 \end{bmatrix}$, $Y_2 = \begin{bmatrix} 0 \\ 1 \end{bmatrix}$ with respective lengths $L_1 = L_2 = L$. We adopt the angular value $\theta = 45^\circ$. The connectivity table of this lattice is provided in Table 19.1. All beams have the same mechanical properties.

The mechanical parameters selected in this example originate from experimental data for tensile tests of single crystal ZnO nanowires having a [0001] oriented wurtzite structure; the geometrical and mechanical parameters of the unit-cell structure are summarized in Table 19.2.

The constitutive law for an anisotropic second gradient viscoelastic continuum writes as follows:

$$\{\sigma\} = \underbrace{[A^e]\{\epsilon\} + [B^e]\{\kappa\}}_{\text{elastic part}} + \underbrace{[A^v]\{\dot{\epsilon}\} + [B^v]\{\dot{\kappa}\}}_{\text{viscous part}}$$

Table 19.1 Connectivity table of the square lattice

Beam	1	2	3	4	5	6	7	8
O(b)	1	2	1	4	1	3	4	3
E(b)	2	1	4	1	3	1	3	2
δ^1	0	0	0	1	0	1	0	0
δ^2	0	1	0	0	0	1	0	0

Table 19.2 Geometrical and mechanical parameters of the square lattice

Type	Geometric parameters of the beam	Mechanical properties
Square	$L = 10 \text{ mm}$, $\beta = 45^\circ$, $t = 1 \text{ mm}$ (width)	$E_B = 56.2 \text{ GPa}$, $\nu = 0.3$

$$\{S\} = \underbrace{[B^e]\{\epsilon\} + [D^e]\{\kappa\}}_{\text{elastic part}} + \underbrace{[B^v]\{\dot{\epsilon}\} + [D^v]\{\dot{\kappa}\}}_{\text{viscous part}} \tag{19.31}$$

We have introduced therein σ_{ij} , S_{ijk} , ϵ_{pq} and K_{pqr} the stress, hyperstress, deformation and gradient of deformation tensors respectively, which write in component form

$$\epsilon = \left[\frac{\partial U}{\partial x} \quad \frac{\partial V}{\partial y} \quad \frac{\partial U}{\partial y} \quad \frac{\partial V}{\partial x} \right]^T \text{ and } \kappa = \left[\frac{\partial^2 U}{\partial x^2} \quad \frac{\partial^2 V}{\partial y^2} \quad \frac{\partial^2 V}{\partial x^2} \quad \frac{\partial^2 U}{\partial y^2} \quad \frac{\partial^2 V}{\partial x \partial y} \quad \frac{\partial^2 U}{\partial y \partial x} \right]^T.$$

The elastic constitutive tensors A_{ijpq} , D_{ijkpqr} , B_{pqrij} in the previous (elastic) homogenized constitutive law (19.31) are the first and second order elasticity tensors and the coupling tensor respectively.

One obtains for this example exhibiting a non-centrosymmetric microstructure the following homogenized tensors:

For the elastic part:

$$[A^e] = \begin{bmatrix} 7872 & 2176 & 1848 & 2019 \\ 2002 & 7698 & 1844 & 1674 \\ 1510 & 1844 & 2096 & 2045 \\ 1958 & 1623 & 2158 & 2209 \end{bmatrix}; [B^e] = \begin{bmatrix} 39350 & 10880 & 9243 & 10090 & 0 & 0 \\ 10010 & 38480 & 9224 & 8375 & 0 & 0 \\ 9790 & 8119 & 10800 & 11040 & 0 & 0 \\ 7553 & 9224 & 10480 & 10230 & 0 & 0 \end{bmatrix}$$

$$[D^e] = \begin{bmatrix} 2.4410^5 & 94580 & 98570 & 1.0510^5 & 0 & 0 \\ 94580 & 2.4410^5 & 1.0510^5 & 94580 & 0 & 0 \\ 98570 & 1.0510^5 & 1.0510^5 & 2.4410^5 & 0 & 0 \\ 1.0510^5 & 94580 & 2.4410^5 & 1.0510^5 & 0 & 0 \\ 0 & 0 & 0 & 0 & 0 & 0 \\ 0 & 0 & 0 & 0 & 0 & 0 \end{bmatrix}$$

If we compare these results with those of the case without surface effects, one notes that the tensors **A** and **B** do not change while the components of the matrix **D** decreases by about 17%.

For the viscous part: two different values of the viscosity coefficient expressed versus the tensile modulus of the base material (of each beam) are considered in order to analyze its influence on the homogenized tensors.

- $\mu_e = \frac{10}{100} E_B$: this results in the effective viscous like constitutive tensor numerically given by

$$[A^v] = \begin{bmatrix} 787.2 & 217.6 & 184.8 & 201.9 \\ 200.2 & 769.8 & 184.4 & 167.4 \\ 151 & 184.4 & 209.6 & 204.5 \\ 195.8 & 162.3 & 215.8 & 220.9 \end{bmatrix}; [B^v] = \begin{bmatrix} 3935 & 1088 & 924.3 & 1009 & 0 & 0 \\ 1001 & 3848 & 922.4 & 837.5 & 0 & 0 \\ 979 & 811.9 & 1080 & 1104 & 0 & 0 \\ 755.3 & 922.4 & 1048 & 1023 & 0 & 0 \end{bmatrix}$$

$$[D^v] = \begin{bmatrix} 24450 & 9458 & 9857 & 10570 & 0 & 0 \\ 9458 & 24450 & 10570 & 9458 & 0 & 0 \\ 9857 & 10570 & 10570 & 24450 & 0 & 0 \\ 10570 & 9458 & 24450 & 10570 & 0 & 0 \\ 0 & 0 & 0 & 0 & 0 & 0 \\ 0 & 0 & 0 & 0 & 0 & 0 \end{bmatrix}$$

- $\mu_e = \frac{30}{100} E_B$: the effective viscous constitutive tensors are given by

$$[A^v] = \begin{bmatrix} 2361 & 652.8 & 554.5 & 605.6 \\ 600.7 & 2309 & 553.5 & 502.4 \\ 453.2 & 553.5 & 628.8 & 613.5 \\ 587.2 & 487.1 & 647.2 & 662.8 \end{bmatrix}; [B^v] = \begin{bmatrix} 11810 & 3264 & 2772 & 3027 & 0 & 0 \\ 3013 & 11550 & 2767 & 2512 & 0 & 0 \\ 2937 & 2435 & 3238 & 3312 & 0 & 0 \\ 2266 & 2767 & 3144 & 3068 & 0 & 0 \end{bmatrix}$$

$$[D^v] = \begin{bmatrix} 73200 & 28200 & 29500 & 31700 & 0 & 0 \\ 28200 & 73200 & 31700 & 9460.3 & 0 & 0 \\ 29500 & 31700 & 31700 & 73200 & 0 & 0 \\ 31700 & 9460.3 & 73200 & 31700 & 0 & 0 \\ 0 & 0 & 0 & 0 & 0 & 0 \\ 0 & 0 & 0 & 0 & 0 & 0 \end{bmatrix}$$

Throughout this work, one considers the material behavior at low frequencies (in the quasi-static regime), a frequency domain in which it makes sense to have recourse to the homogenized effective medium, since the wavelength is greater than the unit cell size. In Fig. 19.2, we represent the natural frequency band diagram versus the direction of propagation in the presence or absence of surface tension effects.

Figure 19.1 shows that the surface tension has an important role on the mode of propagation for both longitudinal and shear modes. An increase of the modes occurs due to surface tension caused by the increased rigidity of the material. We can note here that in presence of the second gradient terms, the influence of the surface gradient on wave propagation vanishes.

In Fig. 19.3 we represent the damped frequency band diagram and the damping ratio versus the dimensionless wave number kL and for two different directions of propagation.

The influence of the direction of propagation on both frequency and damping ratio is clearly observed in Fig. 19.3c, d for the shear mode. For the longitudinal mode, no influence of the direction of propagation on either frequency or damping ratio is observed. The cut-off mode is observed for the longitudinal mode beyond $kL = 1.2$ which means that waves are fully attenuated. The cut-off mode is observed for a

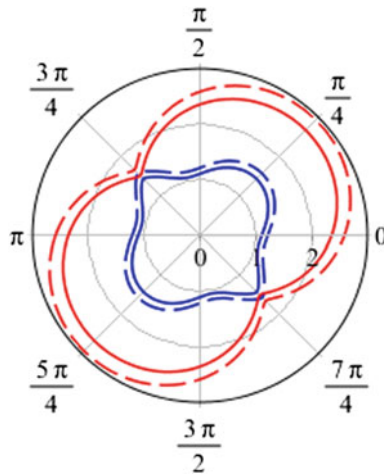


Fig. 19.2 Effect of surface tension on longitudinal and shear modes (frequency) in Cauchy medium (without the second gradient tensors). Red line: longitudinal mode—Blue line: shear mode. Continuous line: without surface tension surface—Dotted line: with the effect of surface tension

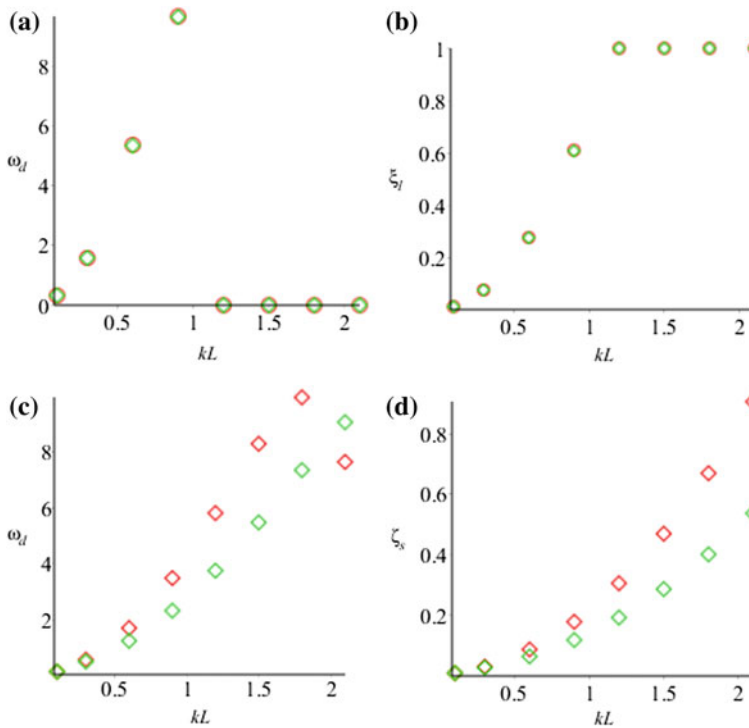


Fig. 19.3 frequency band structure versus dimensionless wave number kL . Red points: direction of propagation $\beta = \frac{\pi}{3}$; Green points: direction of propagation $\beta = \frac{\pi}{4}$. **a** Longitudinal damping frequency, **b** Longitudinal damping ratio, **c** Shear damping frequency, **d** Shear damping ratio

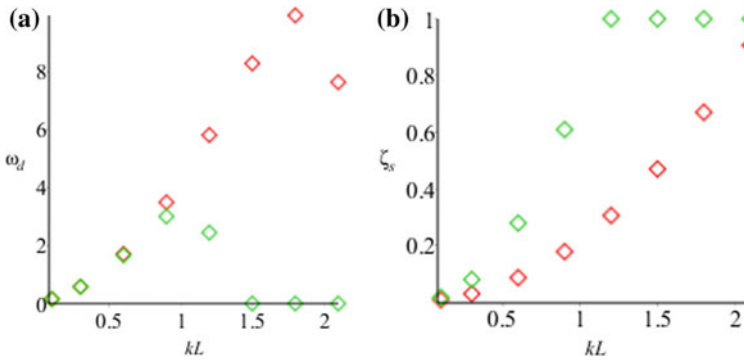


Fig. 19.4 Shear frequency band structure in function of the dimensionless wave number kL . Red points corresponding to $\mu_e = 0.1E_B$ and the green one corresponding to the higher damping coefficient $\mu_e = 0.3E_B$

damping ratio unity (Fig. 19.2b). For the shear mode, in the direction of propagation $\beta = \frac{\pi}{4}$, the frequency decreases beyond $kL = 2.1$ and vanishes when increasing the wave number.

In Fig. 19.4 we represent the damped frequency band diagram and the damping ratio versus the dimensionless wave number kL and for two different values of the viscosity.

The results in Fig. 19.4 evidence shifts in the frequency band diagrams due to the presence of damping, these shift being more pronounced as the viscosity coefficient increases. We also observe that the damping ratio values increase with the viscosity coefficient. The cut-off appears in the shear mode when increasing the viscosity beyond $kL = 1.5$, corresponding to a damping ratio unity.

19.4 Conclusion

Surface effects of repetitive network materials caused by a thin coating of the structural beam elements of the repetitive unit cell of the network have been accounted for by an effective strain gradient continuum, computed thanks to the discrete homogenization method. The proposed model of surface effects in network materials shall prove useful to predict the importance of surface contributions of network materials and architected media, especially at nanometers scales. Surface effects are accounted for by the ratio of the surface modulus of the coating to the bulk modulus of the beam material, and the ratio of the thickness coating to the beam length. These two parameters are related to the scaling parameter (ratio of the representative unit cell size to a macroscopic characteristic length) according to two different scaling laws, thereby introducing two scaling exponents. Thereby, surface effects appear in the second gradient contribution to the constitutive law (in the hyperstress tensor)

for non-negative values of the scaling exponents; this corresponds to the typical situation, described in the pioneering work of Mindlin [48] wherein the strain gradient continuum is motivated by its ability to incorporate surface effects.

Wave propagation in network materials with surface effects has next been analyzed on the basis of the computed homogenized properties and consideration of an effective first and second gradient viscous behavior. A significant surface effect on the frequency plot of both longitudinal and shear modes has been obtained. Therefore, one has to take surface effects into account when designing nanometric size components for acoustic applications.

Appendix: Transition from Curvilinear to Cartesian Coordinates

After development of Eq. (19.14) in Cartesian coordinates, one obtains

$$\lim_{\varepsilon \rightarrow 0} P = \int_{\Omega} \frac{1}{g} \sum_b \left[\begin{array}{l} \left(\begin{array}{l} T_E^1 \left(L_1 \delta_{1b} \left(c_{\theta_1} \frac{\partial \dot{V}_o}{\partial x} + s_{\theta_1} \frac{\partial \dot{V}_o}{\partial y} \right) + L_2 \delta_{2b} \left(c_{\theta_2} \frac{\partial \dot{V}_o}{\partial x} + s_{\theta_2} \frac{\partial \dot{V}_o}{\partial y} \right) \right) \\ + N_E^1 \left(L_1 \delta_{1b} \left(c_{\theta_1} \frac{\partial \dot{U}_o}{\partial x} + s_{\theta_1} \frac{\partial \dot{U}_o}{\partial y} \right) + L_2 \delta_{2b} \left(c_{\theta_2} \frac{\partial \dot{U}_o}{\partial x} + s_{\theta_2} \frac{\partial \dot{U}_o}{\partial y} \right) \right) \\ T_E^1 \left(\begin{array}{l} \frac{L_1^2 \delta_{1b}^2}{2} \left(c_{\theta_1}^2 \frac{\partial^2 \dot{V}_o}{\partial x^2} + s_{\theta_1}^2 \frac{\partial^2 \dot{V}_o}{\partial y^2} + 2s_{\theta_1} c_{\theta_1} \frac{\partial^2 \dot{V}_o}{\partial x \partial y} \right) \\ + \frac{L_2^2 \delta_{2b}^2}{2} \left(c_{\theta_2}^2 \frac{\partial^2 \dot{V}_o}{\partial x^2} + s_{\theta_2}^2 \frac{\partial^2 \dot{V}_o}{\partial y^2} + 2s_{\theta_2} c_{\theta_2} \frac{\partial^2 \dot{V}_o}{\partial x \partial y} \right) \end{array} \right) \\ + T_E^2 \left(L_1 \delta_{1b} \left(c_{\theta_1} \frac{\partial \dot{V}_o}{\partial x} + s_{\theta_1} \frac{\partial \dot{V}_o}{\partial y} \right) + L_2 \delta_{2b} \left(c_{\theta_2} \frac{\partial \dot{V}_o}{\partial x} + s_{\theta_2} \frac{\partial \dot{V}_o}{\partial y} \right) \right) \\ + N_E^1 \left(\begin{array}{l} \frac{L_1^2 \delta_{1b}^2}{2} \left(c_{\theta_1}^2 \frac{\partial^2 \dot{U}_o}{\partial x^2} + s_{\theta_1}^2 \frac{\partial^2 \dot{U}_o}{\partial y^2} + 2s_{\theta_1} c_{\theta_1} \frac{\partial^2 \dot{U}_o}{\partial x \partial y} \right) \\ + \frac{L_2^2 \delta_{2b}^2}{2} \left(c_{\theta_2}^2 \frac{\partial^2 \dot{U}_o}{\partial x^2} + s_{\theta_2}^2 \frac{\partial^2 \dot{U}_o}{\partial y^2} + 2s_{\theta_2} c_{\theta_2} \frac{\partial^2 \dot{U}_o}{\partial x \partial y} \right) \end{array} \right) \\ + N_E^2 \left(L_1 \delta_{1b} \left(c_{\theta_1} \frac{\partial \dot{U}_o}{\partial x} + s_{\theta_1} \frac{\partial \dot{U}_o}{\partial y} \right) + L_2 \delta_{2b} \left(c_{\theta_2} \frac{\partial \dot{U}_o}{\partial x} + s_{\theta_2} \frac{\partial \dot{U}_o}{\partial y} \right) \right) \\ + \varepsilon^2 \left(\begin{array}{l} T_E^2 \left(\begin{array}{l} \frac{L_1^2 \delta_{1b}^2}{2} \left(c_{\theta_1}^2 \frac{\partial^2 \dot{V}_o}{\partial x^2} + s_{\theta_1}^2 \frac{\partial^2 \dot{V}_o}{\partial y^2} + 2s_{\theta_1} c_{\theta_1} \frac{\partial^2 \dot{V}_o}{\partial x \partial y} \right) \\ + \frac{L_2^2 \delta_{2b}^2}{2} \left(c_{\theta_2}^2 \frac{\partial^2 \dot{V}_o}{\partial x^2} + s_{\theta_2}^2 \frac{\partial^2 \dot{V}_o}{\partial y^2} + 2s_{\theta_2} c_{\theta_2} \frac{\partial^2 \dot{V}_o}{\partial x \partial y} \right) \end{array} \right) \\ + N_E^2 \left(\begin{array}{l} \frac{L_1^2 \delta_{1b}^2}{2} \left(c_{\theta_1}^2 \frac{\partial^2 \dot{U}_o}{\partial x^2} + s_{\theta_1}^2 \frac{\partial^2 \dot{U}_o}{\partial y^2} + 2s_{\theta_1} c_{\theta_1} \frac{\partial^2 \dot{U}_o}{\partial x \partial y} \right) \\ + \frac{L_2^2 \delta_{2b}^2}{2} \left(c_{\theta_2}^2 \frac{\partial^2 \dot{U}_o}{\partial x^2} + s_{\theta_2}^2 \frac{\partial^2 \dot{U}_o}{\partial y^2} + 2s_{\theta_2} c_{\theta_2} \frac{\partial^2 \dot{U}_o}{\partial x \partial y} \right) \end{array} \right) \end{array} \right) \end{array} \right) dV \quad (A.1)$$

c_θ , s_θ , c_θ^2 and s_θ^2 stand for $\cos\theta$, $\sin\theta$, $\cos^2\theta$ and $\sin^2\theta$, they are the components of the periodicity vectors [43].

References

1. Chen, C., Shi, Y., Zhang, Y., Zhu, J., Yan, Y.: Size dependence of Young's modulus in ZnO nanowires. *Phys. Rev. Lett.* **96**(7), 075505 (2006)
2. Cuenot, S., Frétiigny, C., Demoustier-Champagne, S., Nysten, B.: Surface tension effect on the mechanical properties of nanomaterials measured by atomic force microscopy. *Phys. Rev. B* **69**(16), 165410 (2004)
3. Jing, G.Y., Duan, H.L., Sun, X.M., Zhang, Z.S., Xu, J., Wang, Y.D.L.J.X., Yu, D.P.: Surface effects on elastic properties of silver nanowires: contact atomic-force microscopy. *Phys. Rev. B* **73**(23), 235409 (2006)
4. He, J., Lilley, C.M.: Surface effect on the elastic behavior of static bending nanowires. *Nano Lett.* **8**(7), 1798–1802 (2008)
5. Liu, X., Luo, J., Zhu, J.: Size effect on the crystal structure of silver nanowires. *Nano Lett.* **6**(3), 408–412 (2006)
6. Laplace, P.S.: Sur l'action capillaire. Supplément à la théorie de l'action capillaire, In: *Traité de mécanique céleste*, vol. 4. Supplement 1, Livre X, 771–777. Gauthier-Villars et fils, Paris (1805)
7. Laplace, P.S.: À la théorie de l'action capillaire. Supplément à la théorie de l'action capillaire, In: *Traité de mécanique céleste*, vol. 4. Supplement 2, Livre X, 909–945. Gauthier-Villars et fils, Paris (1806)
8. Young, T.: An essay on the cohesion of fluids. *Philos. Trans. R. Soc. Lond.* **95**, 65–87 (1805)
9. Poisson, S.D.: Nouvelle théorie de l'action capillaire. Bachelier Père et Fils, Paris (1831)
10. Longley, W.R., Name, R.G.V. (eds.): *The Collected Works of J. Willard Gibbs, PH.D., LL.D. Vol. I Thermodynamics*. Longmans, New York (1928)
11. de Gennes, P.G., Brochard-Wyart, F., Quéré, D.: *Capillarity and Wetting Phenomena: Drops, Pearls, Bubbles, Waves*. Springer, New York (2004)
12. Rowlinson, J.S., Widom, B.: *Molecular Theory of Capillarity*. Dover, New York (2003)
13. Gurtin, M.E., Murdoch, A.I.: Addenda to our paper a continuum theory of elastic material surfaces. *Arch. Ration. Mech. Anal.* **59**(4), 389–390 (1975)
14. Gurtin, M.E., Murdoch, A.I.: A continuum theory of elastic material surfaces. *Arch. Ration. Mech. Anal.* **57**(4), 291–323 (1975)
15. Wang, J., Duan, H.L., Huang, Z.P., Karihaloo, B.L.: A scaling law for properties of nanostructured materials. *Proc. R. Soc. A* **462**(2069), 1355–1363 (2006)
16. Steigmann, D.J., Ogden, R.W.: Plane deformations of elastic solids with intrinsic boundary elasticity. *Proc. R. Soc. A* **453**(1959), 853–877 (1997)
17. Steigmann, D.J., Ogden, R.W.: Elastic surface–substrate interactions. *Proc. R. Soc. A* **455**(1982), 437–474 (1999)
18. Javili, A., McBride, A., Steinmann, P.: Thermomechanics of solids with lower-dimensional energetics: on the importance of surface, interface, and curve structures at the nanoscale, a unifying review. *Appl. Mech. Rev.* **65**(1), 010802–1–31 (2012)
19. Javili, A., dell'Isola, F., Steinmann, P.: Geometrically nonlinear higher-gradient elasticity with energetic boundaries. *J. Mech. Phys. Solids* **61**(12), 2381–2401 (2013)
20. Podio-Guidugli, P., Caffarelli, G.V.: Surface interaction potentials in elasticity. *Arch. Ration. Mech. Anal.* **109**, 345–385 (1990)
21. Povstenko, Y.: Mathematical modeling of phenomena caused by surface stresses in solids. In: Altenbach, H., Morozov, N.F. (eds.) *Surface Effects in Solid Mechanics*, 30, pp. 135–153. Springer, Berlin (2013)
22. Silhavý, M.: A direct approach to nonlinear shells with application to surface–substrate interactions. *Math. Mech. Complex Syst.* **1**(2), 211–232 (2013)
23. Lurie, S.A., Kalamkarov, A.L.: General theory of continuous media with conserved dislocations. *Int. J. Solids Struct.* **44**(22–23), 7468–7485 (2007)
24. Lurie, S.A., Belov, P.A.: Cohesion field: Barenblatt's hypothesis as formal corollary of theory of continuous media with conserved dislocations. *Int. J. Fract.* **150**(1–2), 181–194 (2008)

25. Lurie, S., Volkov-Bogorodsky, D., Zubov, V., Tuchkova, N.: Advanced theoretical and numerical multiscale modeling of cohesion/adhesion interactions in continuum mechanics and its applications for filled nanocomposites. *Comput. Mater. Sci.* **45**(3), 709–714 (2009)
26. Lurie, S., Belov, P.: Gradient effects in fracture mechanics for nano-structured materials. *Eng. Fract. Mech.* **130**, 3–11 (2014)
27. Rubin, M., Benveniste, Y.: A Cosserat shell model for interphases in elastic media. *J. Mech. Phys. Solids* **52**(5), 1023–1052 (2004)
28. Duan, H.L., Wang, J., Huang, Z.P., Karihaloo, B.L.: Size-dependent effective elastic constants of solids containing nanoinhomogeneities with interface stress. *J. Mech. Phys. Solids* **53**(7), 1574–1596 (2005)
29. Duan, H.L., Wang, J., Karihaloo, B.L., Huang, Z.P.: Nanoporous materials can be made stiffer than non-porous counterparts by surface modification. *Acta Mater.* **54**(11), 2983–2990 (2006)
30. Duan, H.L., Karihaloo, B.L.: Thermo-elastic properties of heterogeneous materials with imperfect interfaces: generalized Levin’s formula and Hill’s connections. *J. Mech. Phys. Solids* **55**(5), 1036–1052 (2007)
31. Duan, H.L., Wang, J., Karihaloo, B.L.: Theory of elasticity at the nanoscale. *Adv. Appl. Mech.* **42**, 1–68 (2009)
32. Kushch, V.I., Chernobai, V.S., Mishuris, G.S.: Longitudinal shear of a composite with elliptic nanofibers: local stresses and effective stiffness. *Int. J. Engng. Sci.* **84**, 79–94 (2014)
33. Kushch, V.I., Sevostianov, I., Chernobai, V.S.: Effective conductivity of composite with imperfect contact between elliptic fibers and matrix: Maxwell’s homogenization scheme. *Int. J. Eng. Sci.* **83**, 146–161 (2014)
34. Wang, J., Huang, Z., Duan, H., Yu, S., Feng, X., Wang, G., Zhang, W., Wang, T.: Surface stress effect in mechanics of nanostructured materials. *Acta Mech. Solida Sin.* **24**(1), 52–82 (2011)
35. Altenbach, H., Eremeyev, V.A.: On the shell theory on the nanoscale with surface stresses. *Int. J. Eng. Sci.* **49**(12), 1294–1301 (2011)
36. Altenbach, H., Eremeyev, V.A., Morozov, N.F.: Surface viscoelasticity and effective properties of thin-walled structures at the nanoscale. *Int. J. Eng. Sci.* **59**, 83–89 (2012)
37. Altenbach, H., Eremeyev, V.A., Morozov, N.F.: Mechanical properties of materials considering surface effects. In: Cocks, A., Wang, J. (eds.) *IU TAM Symposium on Surface Effects in the Mechanics of Nanomaterials and Heterostructures*, IUTAM Bookseries (closed), 31, pp. 105–115. Springer, Dordrecht (2013)
38. Eremeyev, V.A., Altenbach, H., Morozov, N.F.: The influence of surface tension on the effective stiffness of nanosized plates. *Doklady Phys.* **54**(2), 98–100 (2009)
39. Guo, J.G., Zhao, Y.P.: The size-dependent elastic properties of nanofilms with surface effects. *J. Appl. Phys.*, **98**(7), 074306 (2005)
40. Heinonen, S., Huttunen-Saarivirta, E., Nikkanen, J.P., Raulio, M., Priha, O., Laakso, J., Storgårds, E., Levänen, E.: Antibacterial properties and chemical stability of superhydrophobic silver-containing surface produced by sol–gel route. *Colloids Surf. A Physicochem. Eng. Aspects* **453**, 149–161 (2014)
41. Wang, Z.Q., Zhao, Y.P., Huang, Z.P.: The effects of surface tension on the elastic properties of nano structures. *Int. J. Eng. Sci.* **48**(2), 140–150 (2010)
42. Rahali, Y., Dos Reis, F., Ganghoffer, J.F.: Multiscale homogenization schemes for the construction of second order grade anisotropic continuum media of architected materials. *J. Multiscale Comput. Eng.* **15**(1), 35–78 (2017)
43. Rahali, Y., Giorgio, I., Ganghoffer, J.F., dell’Isola, F.: Homogenization à la Piola produces second gradient continuum models for linear pantographic lattices. *Int. J. Engng Sci.* **97**, 148–172 (2015)
44. Reda, H., Rahali, Y., Ganghoffer, J.F., Lakiss, H.: Analysis of dispersive waves in repetitive lattices based on homogenized second—gradient continuum models. *Compos. Struct.* **152**, 712–728 (2016)
45. Rahali, Y., Eremeyev V., Ganghoffer, J.F.: Surface effects of network materials based on strain gradient homogenized media. In: *Mathematics and Mechanics of Solids*. (in press) (2019)

46. Eremeyev, V.: On effective properties of materials at the nanoand microscales considering surface effects. *Acta Mech.* **227**(1), 29–42 (2015)
47. Forest, S.: *Milieux Continus Généralisés et Matériaux Hétérogènes*, Presses de l'École des Mines (2006)
48. Mindlin, R.D.: Second gradient of strain and surface-tension in linear elasticity. *Int. J. Solids Struct.* **1**(4), 417–438 (1965)

Chapter 20

A Short Review of Rotations in Rigid Body Mechanics



Wilhelm Rickert, Sebastian Glane and Wolfgang H. Müller

Abstract The representation of rotations and of the corresponding angular velocity commonly used in rigid body dynamics are revisited using an abstract tensorial approach. In order to do so, RODRIGUES' formula is recalled and the related angular velocity vector is derived. This paper focuses on the analysis of successive rotations and especially a proof of the addition theorem for the angular velocity of successive rotations is presented in a rational manner. Following the discussion of successive rotations and the proof of the addition theorem, the treatment of successive rotation in the current literature on rigid body mechanics is discussed in a review.

Keywords Rigid rotations · Euler angles · Rodrigues formula

20.1 Introduction

The field of rigid body dynamics was initiated and established by EULER in the eighteenth century. Nowadays rigid body dynamics is an integral part of the design process in engineering. This field is covered in every course on engineering mechanics. However, the theoretical aspects are often not discussed in detail. In particular, this applies to the analysis of rotations. A possible reason for this is given in the textbook of Taylor [14, p. 336]: “A detailed study of rotations is actually surprisingly complicated. Fortunately, we do not need many of the details, and some of the properties that are quite hard to prove are reasonably plausible and can be stated without proof.”

W. Rickert (✉) · S. Glane · W. H. Müller
Institute of Mechanics, Chair of Continuum Mechanics and Constitutive Theory,
Technische Universität Berlin, Einsteinufer 5, 10587 Berlin, Germany
e-mail: rickert@tu-berlin.de

S. Glane
e-mail: glane@tu-berlin.de

W. H. Müller
e-mail: wolfgang.h.mueller@tu-berlin.de

© Springer Nature Switzerland AG 2020
H. Altenbach et al. (eds.), *Nonlinear Wave Dynamics of Materials and Structures*, Advanced Structured Materials 122,
https://doi.org/10.1007/978-3-030-38708-2_20

Rotations are present in many dynamical systems, e.g., classical problems such as the pendulum or advanced applications ranging from aircraft dynamics [8], to motion capturing techniques [12]. In order to characterize the rotational movement of a rigid body, three degrees of freedom are introduced. Commonly used concepts are EULER angles, TAIT–BRYANT angles, EULER parameters and quaternions. The first two angle approaches divide the rotation of the body into three successive rotations around specified axes and hence introduce three corresponding axes. The EULER parameters and quaternions, however, describe a rotation with one axis and a rotation angle, see [15].

In the following representations of rotations in terms of three successive rotations with specified axes and its consequences regarding the kinematics are discussed. While the presentation and discussion of these rotations is rather uniform in the literature, differences arise when the angular velocities are introduced. These differences are due to inaccuracies related to the term *angular velocity*. Often this term is confused with *rotational velocities*. However, as will be shown in Sect. 20.4, the angular velocity and the rotational velocity are not the same in general. Moreover, additional confusion arises, because the angular velocity due to multiple successive rotation is (surprisingly) given by the sum of the corresponding elementary rotational velocities. Sometimes this result is referred to as the “addition theorem of angular velocities.” The validity of this theorem makes it hard to distinguish the concept of the angular velocity from the rotational velocity. Furthermore, this fact renders the distinction of these concepts obsolete if only the final result is considered. In order to clarify the relations, this paper reconsiders the successive rotations and their angular velocities in a rational manner.

This paper starts with a brief introduction to the representations of rotations using an abstract tensor notation. Then, the angular velocity is introduced based on a tensor-based approach as in [3, 17]. Subsequently, successive rotations are investigated and relations for the corresponding angular velocities are derived and the addition theorem is proved. Furthermore, the terms rotational velocity, elementary angular velocity and angular velocity are precisely defined and explained. Based on this framework, a literature review is given on rotations in rigid body dynamics.

20.2 Rotation and Change of Base

In the following, the concept of tensor rotations is introduced by using orthogonal transformations. Let \mathbf{Q} be a proper orthogonal tensor such that

$$\mathbf{Q} \cdot \mathbf{Q}^T = \mathbf{Q}^T \cdot \mathbf{Q} = \mathbf{1}, \quad \det(\mathbf{Q}) = 1, \quad (20.1)$$

where \mathbf{Q}^T denotes the transpose of \mathbf{Q} . Consider two orthonormal bases with proper orientation $\{\mathbf{e}'_i\}$ and $\{\mathbf{e}^0_i\}$. They are connected by the following transformation

$$\mathbf{e}'_i = \mathbf{Q} \cdot \mathbf{e}^0_i, \quad (20.2)$$

which is the rotation of \mathbf{e}_i^0 onto \mathbf{e}'_i . Therefore, the tensor \mathbf{Q} is also referred to as rotation tensor. Based on the identity tensor, $\mathbf{1} = \mathbf{e}'_i \otimes \mathbf{e}'_i = \mathbf{e}_i^0 \otimes \mathbf{e}_i^0$, one can derive a mixed representation of the rotation tensor

$$\mathbf{Q} = \mathbf{e}'_i \otimes \mathbf{e}_i^0, \quad (20.3)$$

where the EINSTEIN summation convention is applied. The component matrices Q' and Q^0 corresponding to the non-mixed base representations,

$$\mathbf{Q} = Q'_{ij} \mathbf{e}'_i \otimes \mathbf{e}'_j = Q^0_{ij} \mathbf{e}_i^0 \otimes \mathbf{e}_j^0, \quad (20.4)$$

can be found via the projections:

$$Q'_{ij} = \mathbf{e}'_i \cdot \mathbf{Q} \cdot \mathbf{e}'_j = \mathbf{e}_i^0 \cdot \mathbf{e}'_j, \quad Q^0_{ij} = \mathbf{e}_i^0 \cdot \mathbf{Q} \cdot \mathbf{e}_j^0 = \mathbf{e}_i^0 \cdot \mathbf{e}'_j. \quad (20.5)$$

Note that the result $Q = Q' = Q_0$ is remarkable and inherent to the rotation tensor.

20.2.1 Rotations of Tensors

After agreeing on the rotation of base vectors, the rotation of a vector \mathbf{a} is given by

$$\mathbf{b} = \mathbf{Q} \cdot \mathbf{a}. \quad (20.6)$$

In order to emphasize that \mathbf{b} is a new vector, we refrain from using \mathbf{a}' and instead introduce \mathbf{b} as the result. Both vectors can be represented in both bases $\{\mathbf{e}_i^0\}$ and $\{\mathbf{e}'_i\}$, respectively:

$$\mathbf{a} = a_i^0 \mathbf{e}_i^0 = a'_i \mathbf{e}'_i, \quad \mathbf{b} = b_i^0 \mathbf{e}_i^0 = b'_i \mathbf{e}'_i, \quad (20.7)$$

and the following transformation rules for the components arise

$$a_i^0 = Q_{ij} a'_j, \quad b_i^0 = Q_{ij} b'_j. \quad (20.8)$$

It is essential to note that the transformations in Eq. (20.8) do *not* correspond to real tensor rotations as introduced in Eq. (20.6). The components a_i^0 and a'_i are nothing but different representations of the same object, \mathbf{a} . Bearing in mind the nomenclature of Eq. (20.7), the rotation in Eq. (20.6) may be represented in various forms:

$$b_i^0 = Q_{ij} a_j^0 = Q_{ik} Q_{kj} a'_j, \quad b'_i = a_i^0 = Q_{ij} a'_j. \quad (20.9)$$

Note that the difference between a tensor rotation as in Eq. (20.6) cannot be distinguished from a change of base as in Eq. (20.7) if only the component equations are considered, cf., Eqs. (20.8) and (20.9). For example, the transformation of the components for the rotation $\mathbf{b} = \mathbf{Q} \cdot \mathbf{a}$ looks exactly the same as the component equa-

tion for the change of base of \mathbf{a} , i.e., Eq. (20.8)₁ is equal to Eq. (20.9)₂. However, the underlying interpretation is rather different.

Furthermore note that, from a mathematical point of view, one could conclude that it does not matter whether a change of the base or a vector rotation is considered. However, from a physical point of view the difference could be significant, e.g., if a change of observer is considered. Note that this is not considered in this article. The interested reader is referred to [7].

If rotations of higher order tensors are considered, the RAYLEIGH product “ $*$ ” is used conveniently. It is a non-commutative product between a tensor of second rank and a tensor of rank n , see [3],

$$\mathbf{Q} * \mathbf{C}^{(n)} = \mathbf{Q} * (C_{i_1 \dots i_n} \mathbf{e}_{i_1} \otimes \dots \otimes \mathbf{e}_{i_n}) := C_{i_1 \dots i_n} \mathbf{Q} \cdot \mathbf{e}_{i_1} \otimes \dots \otimes \mathbf{Q} \cdot \mathbf{e}_{i_n} . \quad (20.10)$$

Hence, the tensor of second rank is applied to every base vector of the second tensor. If \mathbf{Q} is a proper orthogonal tensor, its application with the RAYLEIGH product rotates any tensor. In particular, one has

$$\mathbf{Q} * \mathbf{a} = \mathbf{Q} \cdot \mathbf{a} , \quad \mathbf{Q} * \mathbf{A} = \mathbf{Q} \cdot \mathbf{A} \cdot \mathbf{Q}^T . \quad (20.11)$$

20.2.2 Representation of the Rotation Tensor

In order to construct the rotation tensor in terms of orientation parameters, the RODRIGUES formula is used,

$$\mathbf{Q} = \hat{\mathbf{Q}}(\psi, \mathbf{q}) = \mathbf{1} + \sin(\psi)\mathbf{D} + (1 - \cos(\psi))\mathbf{D}^2 , \quad (20.12)$$

where

$$\mathbf{D} = \mathbf{q} \times \mathbf{1} = -\mathbf{q} \cdot \boldsymbol{\epsilon}^{(3)} , \quad \|\mathbf{q}\| = 1 . \quad (20.13)$$

Therein, the vector \mathbf{q} is parallel to the axis of rotation, ψ is the angle of rotation and $\boldsymbol{\epsilon}^{(3)}$ is the LEVI-CIVITA tensor, see Appendix 20.7. The simple contraction of the tensor \mathbf{D} with a vector, \mathbf{x} , yields

$$\mathbf{D} \cdot \mathbf{x} = \mathbf{q} \times \mathbf{x} \quad \Rightarrow \quad \mathbf{D}^2 \cdot \mathbf{x} = \mathbf{D} \cdot (\mathbf{q} \times \mathbf{x}) = \mathbf{q} \times (\mathbf{q} \times \mathbf{x}) . \quad (20.14)$$

Hence, the action of a rotation tensor in the form (20.12) on a vector, \mathbf{x} , reads

$$\mathbf{Q} \cdot \mathbf{x} = \mathbf{x} + \sin(\psi)\mathbf{q} \times \mathbf{x} + (1 - \cos(\psi))\mathbf{q} \times (\mathbf{q} \times \mathbf{x}) . \quad (20.15)$$

Another useful representation is given by

$$\mathbf{Q} = \cos(\psi)\mathbf{1} + (1 - \cos(\psi))\mathbf{q} \otimes \mathbf{q} - \sin(\psi)\mathbf{q} \cdot \boldsymbol{\epsilon}^{(3)} . \quad (20.16)$$

20.3 Time Derivatives in Rotating Systems

In the preceding sections, tensors were treated as invariant regarding their representation. However, if time derivatives are concerned one has to clarify in which system the temporal change is measured. In the following, the notation $\dot{\mathbf{a}}$ denotes the time derivative in an inertial system. Consider a body-fixed system $\mathcal{B} = \{\mathbf{b}_i\}$ that differs from an inertial system $\mathcal{I} = \{\mathbf{e}_i^0\}$ by a rotation

$$\mathbf{b}_i(t) = \mathbf{Q} \cdot \mathbf{e}_i^0, \quad (20.17)$$

where $\mathbf{Q} = \hat{\mathbf{Q}}(t)$ is a proper orthogonal tensor. Then, if a vector \mathbf{a} is represented in the \mathcal{B} -base, one finds from the product rule:

$$\dot{\mathbf{a}} := \frac{d^{\mathcal{I}}\mathbf{a}}{dt} = \frac{d^{\mathcal{B}}\mathbf{a}}{dt} + a_i \frac{d^{\mathcal{I}}\mathbf{b}_i}{dt}, \quad \frac{d^{\mathcal{B}}\mathbf{a}}{dt} := \frac{d^{\mathcal{I}}a_i}{dt} \mathbf{b}_i. \quad (20.18)$$

Therein, the time derivative with respect to \mathcal{B} , $d^{\mathcal{B}}/dt$, can be interpreted as the measurement of the temporal change in the body-fixed system.

In order to further analyze $\dot{\mathbf{b}}_i$, the temporal change of the rotation tensor $\hat{\mathbf{Q}}$ is investigated and the angular velocity tensor is introduced as

$$\boldsymbol{\Omega} := \dot{\mathbf{Q}} \cdot \mathbf{Q}^T \quad \text{with} \quad \boldsymbol{\Omega} = -\boldsymbol{\Omega}^T. \quad (20.19)$$

Therefore, the time derivative of \mathbf{b}_i can be written as

$$\frac{d^{\mathcal{I}}\mathbf{b}_i}{dt} = \dot{\mathbf{Q}} \cdot \mathbf{e}_i^0 = \boldsymbol{\Omega} \cdot \mathbf{Q} \cdot \mathbf{e}_i^0 = \boldsymbol{\Omega} \cdot \mathbf{b}_i. \quad (20.20)$$

Since the angular velocity tensor is skew-symmetric, a corresponding axial vector, the angular velocity $\boldsymbol{\omega}$, is the solution of the axial equation for all $\mathbf{x} \neq \mathbf{0}$:

$$\boldsymbol{\Omega} \cdot \mathbf{x} = \boldsymbol{\omega} \times \mathbf{x} \quad \Rightarrow \quad \boldsymbol{\Omega} = -\boldsymbol{\omega} \cdot \boldsymbol{\epsilon} \quad \Rightarrow \quad \boldsymbol{\omega} = -\frac{1}{2} \boldsymbol{\Omega} \cdot \boldsymbol{\epsilon}, \quad (20.21)$$

where the double contraction is defined as $\mathbf{A} \cdot \mathbf{B} = A_{ij}B_{ij}$. Note that sometimes the so-called POISSON relation is stated as follows

$$\dot{\mathbf{Q}} = \boldsymbol{\Omega} \cdot \mathbf{Q} = \boldsymbol{\omega} \times \mathbf{Q} \quad (20.22)$$

for the ‘‘left angular velocity’’ and one might introduce a ‘‘right angular velocity,’’ which is shown in, e.g., [7, 17] but will not be used in the following. Note that in this paper $\boldsymbol{\Omega}$ is the angular velocity tensor and not the right angular velocity vector as in [7]. Furthermore, note that the inverse problem of determining the rotation tensor from a given angular velocity vector is also called DARBOUX problem.

With the angular velocity $\boldsymbol{\omega}$, the time derivative in Eq. (20.18) can be simplified:

$$\dot{\boldsymbol{a}} = \frac{d^{\mathcal{B}}\boldsymbol{a}}{dt} + \boldsymbol{\omega} \times \boldsymbol{a}. \quad (20.23)$$

Note that although only bold symbols are used this equation, it is system dependent because a system-dependent time derivative is involved.

It is worthwhile mentioning that the angular velocity is not a velocity in the usual sense, i.e., it is not a time derivative of some position or orientation. In order to see this, the angular velocity is computed in terms of the rotation angle and axis from RODRIGUES' formula. Since this computation is lengthy, it is detailed in Appendix 20.8. The angular velocity tensor as well as its axial vector are given by:

$$\begin{aligned} \boldsymbol{\Omega} &= (1 - \cos(\psi))[\dot{\boldsymbol{q}} \otimes \boldsymbol{q} - \boldsymbol{q} \otimes \dot{\boldsymbol{q}}] - (\dot{\psi}\boldsymbol{q} + \sin(\psi)\dot{\boldsymbol{q}}) \cdot \boldsymbol{\epsilon}^{(3)}, \\ \boldsymbol{\omega} &= \dot{\psi}\boldsymbol{q} + \sin(\psi)\dot{\boldsymbol{q}} + (1 - \cos(\psi))\boldsymbol{q} \times \dot{\boldsymbol{q}}. \end{aligned} \quad (20.24)$$

This result shows that the angular velocity is only coaxial to the current axis of rotation, i.e., the vector \boldsymbol{q} , if this axis is fixed in space, viz., $\dot{\boldsymbol{q}} = \mathbf{0}$. This is for example the case for two-dimensional settings in which the axis of rotation is always perpendicular to the plane under consideration and thus constant.

Consider a body-fixed axis of rotation \boldsymbol{q} with constant components in the \mathcal{B} system. From Eq. (20.23), it follows that $\dot{\boldsymbol{q}} = \boldsymbol{\omega} \times \boldsymbol{q}$. Bearing in mind Eq. (20.15), the insertion of this relation into Eq. (20.24)₂ yields:

$$\boldsymbol{\omega} = \dot{\psi}\boldsymbol{q} + \sin(\psi)\boldsymbol{\omega} \times \boldsymbol{q} + (1 - \cos(\psi))\boldsymbol{q} \times (\boldsymbol{\omega} \times \boldsymbol{q}) \Rightarrow \boldsymbol{Q} \cdot \boldsymbol{\omega} = \dot{\psi}\boldsymbol{q}. \quad (20.25)$$

There is another representation of the angular velocity that arises from Eq. (20.21)₃ if the representation from Eq. (20.3) is inserted:

$$\boldsymbol{\omega} = -\frac{1}{2}\boldsymbol{\epsilon}^{(3)} \cdot (\dot{\boldsymbol{Q}} \cdot \boldsymbol{Q}^T) = -\frac{1}{2}\dot{\boldsymbol{b}}_i \times \boldsymbol{b}_i = \frac{1}{2}\varepsilon_{ijk}(\dot{\boldsymbol{b}}_j \cdot \boldsymbol{b}_k)\boldsymbol{b}_i. \quad (20.26)$$

However, since the base \mathcal{B} is orthonormal, the time derivative applied to the condition $\boldsymbol{b}_i \cdot \boldsymbol{b}_j = \delta_{ij}$ reveals (no summation w.r.t. α)

$$\dot{\boldsymbol{b}}_\alpha \cdot \boldsymbol{b}_\alpha = 0, \quad \dot{\boldsymbol{b}}_1 \cdot \boldsymbol{b}_2 = -\boldsymbol{b}_1 \cdot \dot{\boldsymbol{b}}_2, \quad \dot{\boldsymbol{b}}_1 \cdot \boldsymbol{b}_3 = -\boldsymbol{b}_1 \cdot \dot{\boldsymbol{b}}_3, \quad \dot{\boldsymbol{b}}_2 \cdot \boldsymbol{b}_3 = -\boldsymbol{b}_2 \cdot \dot{\boldsymbol{b}}_3. \quad (20.27)$$

Hence, the angular velocity can be written as

$$\boldsymbol{\omega} = (\dot{\boldsymbol{b}}_2 \cdot \boldsymbol{b}_3)\boldsymbol{b}_1 + (\dot{\boldsymbol{b}}_3 \cdot \boldsymbol{b}_1)\boldsymbol{b}_2 + (\dot{\boldsymbol{b}}_1 \cdot \boldsymbol{b}_2)\boldsymbol{b}_3. \quad (20.28)$$

20.4 Analysis of Sequential Rotations

Hitherto a single rotation was considered. However, for (say) the EULER angle approach the total rotation is composed of three successive rotations. These rotations are referred to as elementary rotations \mathcal{Q}_α . Then, the total rotation tensor is given by

$$\mathcal{Q} = \mathcal{Q}_3 \cdot \mathcal{Q}_2 \cdot \mathcal{Q}_1, \quad (20.29)$$

with the respective elementary rotation tensors and elementary angular velocity tensors according to Eqs. (20.16) and (20.24)₁:

$$\begin{aligned} \mathcal{Q}_\alpha &= \cos(\psi_\alpha) \mathbf{1} + (1 - \cos(\psi_\alpha)) \mathbf{q}_\alpha \otimes \mathbf{q}_\alpha - \sin(\psi_\alpha) \mathbf{q}_\alpha \cdot \overset{(3)}{\boldsymbol{\epsilon}}, \\ \boldsymbol{\Omega}_\alpha &= (1 - \cos(\psi_\alpha)) [\dot{\mathbf{q}}_\alpha \otimes \mathbf{q}_\alpha - \mathbf{q}_\alpha \otimes \dot{\mathbf{q}}_\alpha] - (\dot{\psi}_\alpha \mathbf{q}_\alpha + \sin(\psi_\alpha) \dot{\mathbf{q}}_\alpha) \cdot \overset{(3)}{\boldsymbol{\epsilon}}, \end{aligned} \quad (20.30)$$

where the EINSTEIN summation convention does not apply to Greek indices. Then, the total angular velocity tensor follows as

$$\begin{aligned} \boldsymbol{\Omega} &= \dot{\mathcal{Q}} \cdot \mathcal{Q}^T \\ &= \dot{\mathcal{Q}}_3 \cdot \mathcal{Q}_3^T + \mathcal{Q}_3 \cdot \dot{\mathcal{Q}}_2 \cdot \mathcal{Q}_2^T + \mathcal{Q}_3 \cdot \mathcal{Q}_2 \cdot \dot{\mathcal{Q}}_1 \cdot \mathcal{Q}_1^T + \mathcal{Q}_3 \cdot \mathcal{Q}_2 \cdot \dot{\mathcal{Q}}_1 \cdot \mathcal{Q}_1^T \cdot \mathcal{Q}_2^T \cdot \mathcal{Q}_3^T \\ &= \boldsymbol{\Omega}_3 + \mathcal{Q}_3 * \boldsymbol{\Omega}_2 + (\mathcal{Q}_3 \cdot \mathcal{Q}_2) * \boldsymbol{\Omega}_1. \end{aligned} \quad (20.31)$$

In the Appendix, it is shown that the LEVI-CIVITA tensor is invariant under rotations, i.e., $\mathcal{Q} * \overset{(3)}{\boldsymbol{\epsilon}} = \overset{(3)}{\boldsymbol{\epsilon}}$ for all proper orthogonal tensors \mathcal{Q} , see Eq. (20.51). Hence, the rotation of $\boldsymbol{\Omega}_2$ can be simplified:

$$\begin{aligned} \mathcal{Q}_3 * \boldsymbol{\Omega}_2 &= -\mathcal{Q}_3 * (\boldsymbol{\omega}_2 \cdot \overset{(3)}{\boldsymbol{\epsilon}}) = -\mathcal{Q}_3 * (\boldsymbol{\omega}_2 \cdot \mathcal{Q}_3^T \cdot \mathcal{Q}_3 \cdot \overset{(3)}{\boldsymbol{\epsilon}}) \\ &= -\boldsymbol{\omega}_2 \cdot \mathcal{Q}_3^T \cdot (\mathcal{Q}_3 * \overset{(3)}{\boldsymbol{\epsilon}}) = -\boldsymbol{\omega}_2 \cdot \mathcal{Q}_3^T \cdot \overset{(3)}{\boldsymbol{\epsilon}} = -\overset{(3)}{\boldsymbol{\epsilon}} \cdot \mathcal{Q}_3 \cdot \boldsymbol{\omega}_2. \end{aligned} \quad (20.32)$$

The term $(\mathcal{Q}_3 \cdot \mathcal{Q}_2) * \boldsymbol{\Omega}_1$ in Eq. (20.31) is treated analogously such that

$$\boldsymbol{\Omega} = \boldsymbol{\Omega}_3 - \overset{(3)}{\boldsymbol{\epsilon}} \cdot \mathcal{Q}_3 \cdot \boldsymbol{\omega}_2 - \overset{(3)}{\boldsymbol{\epsilon}} \cdot \mathcal{Q}_3 \cdot \mathcal{Q}_2 \cdot \boldsymbol{\omega}_1. \quad (20.33)$$

Hence, the total angular velocity vector is then obtained via double contraction with the LEVI-CIVITA tensor $\overset{(3)}{\boldsymbol{\epsilon}}$,

$$\boldsymbol{\omega} = \boldsymbol{\omega}_3 + \mathcal{Q}_3 \cdot \boldsymbol{\omega}_2 + (\mathcal{Q}_3 \cdot \mathcal{Q}_2) \cdot \boldsymbol{\omega}_1, \quad (20.34)$$

where the elementary angular velocities are given according to Eq. (20.24)₂,

$$\boldsymbol{\omega}_\alpha = \dot{\psi}_\alpha \mathbf{q}_\alpha + \sin(\psi_\alpha) \dot{\mathbf{q}}_\alpha + (1 - \cos(\psi_\alpha)) \mathbf{q}_\alpha \times \dot{\mathbf{q}}_\alpha. \quad (20.35)$$

It is interesting to note that the total angular velocity is not given by the sum of the elementary angular velocities.

The formulas in Eqs. (20.24) and (20.34) are useful to solve the DARBOUX problem. Note that in some cases even closed-form analytical solutions can be derived. Examples are presented, among others, in [1] and [16]. In literature, the concept of a skew-symmetric spin tensor is commonly introduced, which corresponds to the angular velocity tensor $\boldsymbol{\Omega}$ in this paper. However, the angular velocity vector, instead of the “spin tensor,” and representations as in Eq. (20.34) can be very useful not only in rigid body mechanics but also in continuum mechanics. Indeed, some simple and transparent relationships for different angular velocity vectors, e.g., vorticity vector, rotation of principal directions of tensors and logarithmic strain can be derived, see [10, Sect. 4.1.3].

20.4.1 Simplification for Attached Axes

Commonly used descriptions of rotations, e.g., by the EULER angles, are based on fixed elementary axes of rotation, where the term “fixed” needs further explanation. Since the rotation is divided into three successive rotations, two intermediate systems, \mathcal{B}_1 and \mathcal{B}_2 , are generated before the inertial system is transformed into the body-fixed system:

$$\mathcal{I} \rightarrow \mathcal{B}_1 \rightarrow \mathcal{B}_2 \rightarrow \mathcal{B}.$$

The first elementary axis of rotation is usually spatially fixed and the second and third elementary axes are attached to the intermediate systems \mathcal{B}_1 and \mathcal{B}_2 , respectively. Hence, the time derivatives of these elementary axes are given by

$$\dot{\mathbf{q}}_1 = \mathbf{0}, \quad \dot{\mathbf{q}}_2 = \boldsymbol{\omega}_1 \times \mathbf{q}_2, \quad \dot{\mathbf{q}}_3 = (\boldsymbol{\omega}_2 + \mathbf{Q}_2 \cdot \boldsymbol{\omega}_1) \times \mathbf{q}_3. \quad (20.36)$$

These axes are therefore called “attached” rather than fixed. If these results are plugged into the angular velocities in Eq. (20.35), similar to the result in Eq. (20.25), one obtains

$$\begin{aligned} \boldsymbol{\omega}_1 &= \dot{\psi}_1 \mathbf{q}_1, & \boldsymbol{\omega}_2 &= \dot{\psi}_2 \mathbf{q}_2 + [\mathbf{1} - \mathbf{Q}_2] \cdot \boldsymbol{\omega}_1, \\ \boldsymbol{\omega}_3 &= \dot{\psi}_3 \mathbf{q}_3 + [\mathbf{1} - \mathbf{Q}_3] \cdot (\boldsymbol{\omega}_2 + \mathbf{Q}_2 \cdot \boldsymbol{\omega}_1). \end{aligned} \quad (20.37)$$

With these relations, the expression for the total angular velocity vector in Eq. (20.34) can be simplified such that all rotation tensors \mathbf{Q}_α cancel:

$$\boldsymbol{\omega} = \dot{\psi}_1 \mathbf{q}_1 + \dot{\psi}_2 \mathbf{q}_2 + \dot{\psi}_3 \mathbf{q}_3. \quad (20.38)$$

This final representation of the total angular velocity vector is much simpler than the first one in Eq. (20.34), but it is only obtained if the elementary axes of rotation are “attached” to the intermediate systems. Note that the products $\dot{\psi}_\alpha \mathbf{q}_\alpha$ are not necessarily angular velocities in the sense of the definition introduced above. The fact that for attached axes the simple addition rule holds was pointed out in [16] without detailed proof.

20.4.2 Summary for Sequential Rotations

The results of the foregoing analysis are summarized in the following. First the universal results read:

For a rotation tensor \mathbf{Q} expressed in terms of a rotation axis \mathbf{q} and a rotation angle ψ ,

$$\mathbf{Q} = \cos(\psi)\mathbf{1} + (1 - \cos(\psi))\mathbf{q} \otimes \mathbf{q} - \sin(\psi)\mathbf{q} \cdot \boldsymbol{\epsilon}^{(3)}, \quad (20.39)$$

where $\|\mathbf{q}\| = 1$, the angular velocity tensor and the corresponding angular velocity vector are given by:

$$\begin{aligned} \boldsymbol{\Omega} &= \dot{\mathbf{Q}} \cdot \mathbf{Q}^T = (1 - \cos(\psi))[\dot{\mathbf{q}} \otimes \mathbf{q} - \mathbf{q} \otimes \dot{\mathbf{q}}] - (\dot{\psi}\mathbf{q} + \sin(\psi)\dot{\mathbf{q}}) \cdot \boldsymbol{\epsilon}^{(3)}, \\ \boldsymbol{\omega} &= -\frac{1}{2}\boldsymbol{\epsilon}^{(3)} \cdot \boldsymbol{\Omega} = \dot{\psi}\mathbf{q} + \sin(\psi)\dot{\mathbf{q}} + (1 - \cos(\psi))\mathbf{q} \times \dot{\mathbf{q}}. \end{aligned} \quad (20.40)$$

If three successive rotations are considered, i.e., $\mathbf{Q} = \mathbf{Q}_3 \cdot \mathbf{Q}_2 \cdot \mathbf{Q}_1$, with their respective elementary axes and angles of rotation, then the following composition rule holds for the total angular velocity

$$\boldsymbol{\omega} = \boldsymbol{\omega}_3 + \mathbf{Q}_3 \cdot \boldsymbol{\omega}_2 + \mathbf{Q}_3 \cdot \mathbf{Q}_2 \cdot \boldsymbol{\omega}_1. \quad (20.41)$$

Therein, each elementary angular velocity $\boldsymbol{\omega}_\alpha$ is constructed by the formulae from Eq. (20.40)₂.

For commonly used descriptions of sequential rotations, e.g., the EULER angles, the following simplifications are possible:

If all axes are “attached,” i.e., have constant components in their intermediate bases,

$$\mathbf{q}_3 = q_i^3 \mathbf{Q}_2 \cdot \mathbf{Q}_1 \cdot \mathbf{e}_i^0, \quad \mathbf{q}_2 = q_i^2 \mathbf{Q}_1 \cdot \mathbf{e}_i^0, \quad \mathbf{q}_1 = q_i^1 \mathbf{e}_i^0, \quad \dot{q}_i^\alpha = 0, \quad (20.42)$$

for all $\alpha \in \{1, 2, 3\}$, where $\{\mathbf{e}_i^0\}$ is an inertial base, then the total angular velocity vector is given by

$$\boldsymbol{\omega} = \dot{\psi}_1 \mathbf{q}_1 + \dot{\psi}_2 \mathbf{q}_2 + \dot{\psi}_3 \mathbf{q}_3. \quad (20.43)$$

Following [11, p. 29], the products $\dot{\psi}_\alpha \mathbf{q}_\alpha$ (no summation) are referred to as elementary rotational velocity vectors. Hence, the addition theorem for the angular velocity vector of successive rotations can be restated as:

The angular velocity vector is given by the sum of the elementary rotational velocity vectors.

However, note that if one chooses to use three spatially fixed axes, all their time derivatives vanish and the associated angular velocities of the elementary rotations are simply given by

$$\boldsymbol{\omega}_1 = \dot{\psi}_1 \mathbf{q}_1, \quad \boldsymbol{\omega}_2 = \dot{\psi}_2 \mathbf{q}_2, \quad \boldsymbol{\omega}_3 = \dot{\psi}_3 \mathbf{q}_3. \quad (20.44)$$

In this case, the elementary angular velocity vectors are equal to the elementary rotational velocity vectors. However, according to the composition rule in Eq. (20.41) [in contrast to Eq. (20.43)] the following total angular velocity results

$$\boldsymbol{\omega} = \dot{\psi}_3 \mathbf{q}_3 + \dot{\psi}_2 \mathbf{Q}_3 \cdot \mathbf{q}_2 + \dot{\psi}_1 \mathbf{Q}_3 \cdot \mathbf{Q}_2 \cdot \mathbf{q}_1, \quad (20.45)$$

which is not the sum of the elementary rotational velocity vectors. Finally, note that spatially fixed axes are rarely used.

20.5 Treatment of Successive Rotations in the Literature

In this section, a review of several classical textbooks, which cover rigid body dynamics and successive rotations, is presented. In particular, the approaches of the different authors to the problem of successive rotations are discussed. Note that the given list is by far not complete and for this short review limited to the essentials.

First, one can note that most of the authors rely mostly on matrix calculus, e.g., [4, 6, 9, 11, 13, 15] in contrast to the ones using an abstract tensor notation, e.g., [3, 8, 14, 17]. Recalling the discussion in Sect. 20.2, it is therefore not certain if authors, who rely on a matrix-based approach, regard their equations in terms of a change of bases or in terms of a rotation of a vector. This requires a detailed investigation of each equation in terms of the meaning intended by the author.

Second, several authors do not introduce a precise definition of the angular velocity vector $\boldsymbol{\omega}$. If sequential rotations are considered a profound definition of $\boldsymbol{\omega}$ is required because otherwise confusion may arise. This confusion manifests itself in a mix of terms. For example, the rotational velocities are referred to as EULER angular velocities, angular, or elementary angular velocities in several sources. As outlined in Sect. 20.4 some of the terminology used in the literature is at least partially inconsistent, see [6, p. 176], [14, p. 402] and [15, Sect. 2.3]. In some of the exemplary literature cited in this paper, products of angle velocities, $\dot{\psi}_\alpha$, and corresponding axes of rotation, \mathbf{q}_α , are called “angular velocities.” In the classical book of Taylor [14, p. 337], the angular velocity is even introduced as $\boldsymbol{\omega} = \dot{\psi} \mathbf{q}$, which gives the impression of this statement being true in general. However, on the same page a comment is given on the possible time dependence of the axis of rotation and in the subsequent analysis the more general statement $\dot{\mathbf{e}} = \boldsymbol{\omega} \times \mathbf{e}$ for a body-fixed vector \mathbf{e} is used by Taylor.

In [11, p. 29] the products $\dot{\psi}_\alpha \mathbf{q}_\alpha$ are also introduced without any further comment, but they are called “elementary rotational velocities.” This nomenclature is precise

and is recommended to be used. Furthermore Schiehlen and Eberhard present a formula similar to Eq. (20.41), which is rarely seen in any textbook. However, they use a matrix notation and do not give a derivation. In [2, pp. 12–14], which is an introductory book for the same topic, several definitions for the angular velocity are given of the form $\dot{\psi} \mathbf{q}$, but ultimately on page 15 the author writes for a body-fixed vector, \mathbf{r} , a defining equation for the angular velocity, $\dot{\mathbf{r}} = \boldsymbol{\omega} \times \mathbf{r}$. All references have this definition in common. However, this definition is mentioned as a side note in [4, p. 23], which is a book for numerical applications of rigid body dynamics. It is curious that no definition on the angular velocity is given in [4].

Third, a rational proof of the addition theorem for the angular velocity vector of successive rotations is rarely presented in the literature considered in this review. The theorem is discussed mostly in context with specific examples like, for example, the EULER angles and it is established by determining the elementary components from a figure similar to the one in Fig. 20.1. While some authors present a derivation of the theorem for infinitesimal successive rotations, the requirements and restrictions related the addition theorem are often not specified. This is annoying, because for the EULER angles, for example, one could infer that the successive elementary axes of rotation need to be orthogonal since $\mathbf{i}_3 \perp \mathbf{j}_1$ and $\mathbf{j}_1 \perp \mathbf{k}_3$, see Fig. 20.1. In order to avoid such a misleading conclusion, the presentation of a derivation, which clearly states all assumptions, is didactically beneficial to the reader.

However, there is at least one example in the given literature list [8, p. 16], in which the angular velocity is defined formally in terms of a representation in a body-fixed base. Also Kane and Levinson distinguish between a general angular velocity and a simple one, namely $\dot{\psi} \mathbf{q}$. In contrast to some other authors, the authors always specify the angular velocity ${}^A \boldsymbol{\omega}^B$ as a quantity that conveys between two systems A and B . Hence, the time derivatives associated with ${}^A \boldsymbol{\omega}^B$ are measured with respect to A , even if A is a rotating system from an inertial point of view. Hence, for every vector \mathbf{a} fixed in B one can write

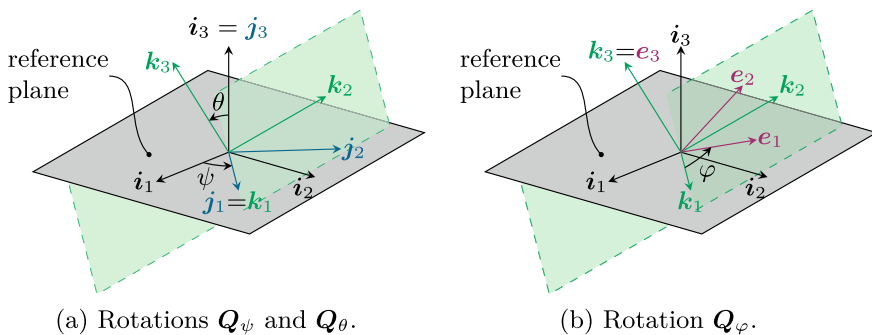


Fig. 20.1 Illustration of the rotations related the EULER angles ψ , θ and ϕ . The sequence of the elementary axes of rotation is given by $\mathbf{i}_3, \mathbf{j}_1$ and \mathbf{k}_3 . The $\{\mathbf{i}_i\}$ -system is the inertial system and the $\{\mathbf{e}_i\}$ -system the body-fixed one

$$\frac{d^A \mathbf{a}}{dt} = {}^A \boldsymbol{\omega}^B \times \mathbf{a} . \quad (20.46)$$

Therefore, with this different notion of the angular velocity, intermediate angular velocities for a gyroscope consisting of rotor and gimbal rings are introduced, see [8, p. 22]. These intermediate angular velocities are simple ones for a gimbal suspension, as two intermediate systems always share one common vector. Finally, the textbook [8, Sect. 2.4] is the only one from the given reference list, in which the addition theorem of angular velocities is stated, analyzed and proved. Bearing in mind the notion of an angular velocity that conveys between two “frames,” intermediate frames A_i are introduced such that

$${}^A \boldsymbol{\omega}^B = {}^A \boldsymbol{\omega}^{A_1} + {}^{A_1} \boldsymbol{\omega}^{A_2} + \dots + {}^{A_n} \boldsymbol{\omega}^B , \quad (20.47)$$

where the intermediate quantities ${}^{A_i} \boldsymbol{\omega}^{A_{i+1}}$ do not necessarily need to be simple. One should note that with the term frame a set of basis vectors is meant and not a frame of an observer as in [7]. Furthermore, it is correctly stated that: “Indeed, Eq. (20.1) represents precisely such a resolution of ${}^A \boldsymbol{\omega}^B$ into components. In no case, however, are these components themselves angular velocities of B in A , for there exists at any one instant only one angular velocity of B in A .” Together with Eq. (20.46) the addition rule in Eq. (20.47) is equivalent to our composition rule. Finally note that the quantity $\boldsymbol{\omega}$ in our paper conveys from an inertial system to the moving one and the angular velocities $\boldsymbol{\omega}_\alpha$ are the intermediate quantities ${}^{A_i} \boldsymbol{\omega}^{A_{i+1}}$ from [8], but measured only from an inertial system. Therefore, the definitions in [8] are more general, allow for less constrained terminology and may even be more useful for practical applications.

20.6 Conclusion

This paper revisited the description of rotations in general. Successive rotations, which commonly occur in engineering applications of rigid body dynamics, were considered in detail. The mathematical description of a single rotation by RODRIGUES’ formula was recalled and the related representations of the angular velocity tensor and the angular velocity vector were derived using an invariant notation.

The analysis of successive rotations focused on the addition theorem for the angular velocity vector, which was proved in a rational manner. Requirements and restrictions on the successive rotations related to the addition theorem were discussed. Moreover, the vectors of rotational velocity, elementary angular velocity and total angular velocity were defined and labeled clearly. Finally, a short literature review was presented and the treatment of successive rotations by several authors was put in context with the rational approach presented in this study. The literature review revealed that the addition theorem is rarely proved in classical textbooks covering the subject.

20.7 The LEVI-CIVITA Tensor

This section briefly presents important properties of the LEVI-CIVITA tensor $\epsilon^{(3)}$, which is given by

$$\epsilon^{(3)} = \epsilon_{ijk} \mathbf{e}_i \otimes \mathbf{e}_j \otimes \mathbf{e}_k = \tilde{\epsilon}_{ijk} \tilde{\mathbf{e}}_i \otimes \tilde{\mathbf{e}}_j \otimes \tilde{\mathbf{e}}_k . \quad (20.48)$$

In this equation, the components w.r.t. the \mathbf{e}_i -base are given by the permutation symbol ϵ_{ijk} , which has the properties as introduced, for example, in [5]. The components w.r.t. the $\tilde{\mathbf{e}}$ -base are denoted by $\tilde{\epsilon}_{ijk}$. These base vectors are connected to the ones of the \mathbf{e}_i -base by a proper rotation,

$$\tilde{\mathbf{Q}} \cdot \tilde{\mathbf{e}}_i = \mathbf{e}_i \quad \Rightarrow \quad \tilde{\mathbf{Q}} = \mathbf{e}_i \otimes \tilde{\mathbf{e}}_i = \tilde{Q}_{ij} \mathbf{e}_i \otimes \mathbf{e}_i , \quad \tilde{Q}_{ij} = \tilde{\mathbf{e}}_i \cdot \mathbf{e}_j . \quad (20.49)$$

In order to obtain a relation between these components, Eq. (20.48) is contracted with the triad $\tilde{\mathbf{e}}_i \otimes \tilde{\mathbf{e}}_j \otimes \tilde{\mathbf{e}}_k$ and scalar products of the different base vectors are replaced by the components of the orthogonal tensor. The resulting relation reads:

$$\tilde{\epsilon}_{ijk} = \epsilon_{lmn} \tilde{Q}_{il} \tilde{Q}_{jm} \tilde{Q}_{kn} = \det(\tilde{\mathbf{Q}}) \epsilon_{ijk} , \quad (20.50)$$

where the connection of the permutation symbol to the determinant was used in the second step, see [5, p. 184]. This equation implies that the components of the LEVI-CIVITA tensor w.r.t. the \mathbf{e} -base are the same as the ones of the $\tilde{\mathbf{e}}$ -base if the tensor $\tilde{\mathbf{Q}}$ is a proper orthogonal tensor, i.e., $\epsilon_{ijk} = \tilde{\epsilon}_{ijk}$ if $\det(\tilde{\mathbf{Q}}) = 1$.

Note that some authors tend to call the tensor $\epsilon^{(3)}$ a tensor density due to the component transformation rule in Eq. (20.50). The transformation rule for the components has the consequence that a RAYLEIGH product of the LEVI-CIVITA tensor with a proper orthogonal tensor is equal to the LEVI-CIVITA tensor, i.e., it is invariant under a rotation. This may be shown by the following calculation:

$$\tilde{\mathbf{Q}} * \epsilon^{(3)} = \tilde{\epsilon}_{ijk} (\tilde{\mathbf{Q}} \cdot \tilde{\mathbf{e}}_i) \otimes (\tilde{\mathbf{Q}} \cdot \tilde{\mathbf{e}}_j) \otimes (\tilde{\mathbf{Q}} \cdot \tilde{\mathbf{e}}_k) = \tilde{\epsilon}_{ijk} \mathbf{e}_i \otimes \mathbf{e}_j \otimes \mathbf{e}_k = \epsilon^{(3)} , \quad (20.51)$$

where $\det(\tilde{\mathbf{Q}}) = \det(\tilde{\mathbf{Q}}) = 1$ must hold true in order to substitute $\tilde{\epsilon}_{ijk}$ by ϵ_{ijk} in the last step.

20.8 Angular Velocity in Terms of Orientation Parameters

In this section, an expression of the angular velocity vector $\boldsymbol{\omega}$ in terms of the RODRIGUES parameters $\boldsymbol{\psi}$ and \mathbf{q} shall be derived. In order to do so, the time derivative of the tensor \mathbf{Q} in Eq. (20.16) is computed as

$$\begin{aligned} \dot{\mathbf{Q}} = & -\sin(\psi)\dot{\psi}(\mathbf{1} - \mathbf{q} \otimes \mathbf{q}) + (1 - \cos(\psi))(\mathbf{q} \otimes \dot{\mathbf{q}} + \dot{\mathbf{q}} \otimes \mathbf{q}) \\ & - (\cos(\psi)\dot{\psi}\mathbf{q} + \sin(\psi)\dot{\mathbf{q}}) \cdot \boldsymbol{\epsilon}^{(3)}. \end{aligned} \tag{20.52}$$

Furthermore, it is convenient to compute the products of $\dot{\mathbf{Q}}$ with the tensors on the right-hand side of Eq.(20.16), i.e., with $\mathbf{q} \otimes \mathbf{q}$ and $\mathbf{q} \cdot \boldsymbol{\epsilon}^{(3)}$. In order to simplify the resulting expression, the following identities related to LEVI-CIVITA tensor are required

$$\frac{1}{2} \boldsymbol{\epsilon}^{(3)} \cdot \boldsymbol{\epsilon}^{(3)} = \mathbf{1}, \quad \boldsymbol{\epsilon}^{(3)} \cdot \boldsymbol{\epsilon}^{(3)} = \mathbf{1} - \mathbf{T}^{(4)}, \tag{20.53a}$$

$$\mathbf{1} = \mathbf{e}_i \otimes \mathbf{e}_j \otimes \mathbf{e}_i \otimes \mathbf{e}_j, \quad \mathbf{T}^{(4)} = \mathbf{e}_i \otimes \mathbf{1} \otimes \mathbf{e}_i, \tag{20.53b}$$

$$\mathbf{1} \cdot \mathbf{A} = \mathbf{A}, \quad \mathbf{T}^{(4)} \cdot \mathbf{A} = \mathbf{A}^T, \tag{20.53c}$$

$$(\boldsymbol{\epsilon}^{(3)} \cdot \mathbf{a}) \cdot (\boldsymbol{\epsilon}^{(3)} \cdot \mathbf{b}) = \mathbf{a} \cdot \boldsymbol{\epsilon}^{(3)} \cdot \boldsymbol{\epsilon}^{(3)} \cdot \mathbf{b} = \mathbf{b} \otimes \mathbf{a} - (\mathbf{a} \cdot \mathbf{b})\mathbf{1}, \tag{20.53d}$$

$$\mathbf{a} \times \mathbf{b} = -\mathbf{a} \cdot \boldsymbol{\epsilon}^{(3)} \cdot \mathbf{b} = \boldsymbol{\epsilon}^{(3)} \cdot (\mathbf{a} \otimes \mathbf{b}). \tag{20.53e}$$

Note that the tensor $\mathbf{1}^{(4)}$ is referred as the identity tensor of rank four and that the tensor $\mathbf{T}^{(4)}$ is the “transposer,” i.e., a tensor of rank four representing to the transposition of a tensor of rank two. In addition, the GRASSMANN identities for the double cross product will be used in the following and may be expressed in terms of the LEVI-CIVITA tensor

$$\mathbf{a} \times (\mathbf{b} \times \mathbf{c}) = \boldsymbol{\epsilon}^{(3)} \cdot (\mathbf{a} \otimes (\mathbf{b} \times \mathbf{c})) = \mathbf{a} \cdot (\mathbf{c} \otimes \mathbf{b} - \mathbf{b} \otimes \mathbf{c}), \tag{20.53f}$$

$$(\mathbf{a} \times \mathbf{b}) \times \mathbf{c} = \boldsymbol{\epsilon}^{(3)} \cdot ((\mathbf{a} \times \mathbf{b}) \otimes \mathbf{c}) = \mathbf{c} \cdot (\mathbf{a} \otimes \mathbf{b} - \mathbf{b} \otimes \mathbf{a}). \tag{20.53g}$$

After same algebraic manipulations, the product of $\dot{\mathbf{Q}}$ with the tensor $\mathbf{q} \otimes \mathbf{q}$ is given by

$$\dot{\mathbf{Q}} \cdot \mathbf{q} \otimes \mathbf{q} = (1 - \cos(\psi))\dot{\mathbf{q}} \otimes \mathbf{q} + \sin(\psi)(\dot{\mathbf{q}} \times \mathbf{q}) \otimes \mathbf{q}. \tag{20.54}$$

The final expression for the product with the tensor $\boldsymbol{\epsilon}^{(3)} \cdot \mathbf{q}$ reads

$$\begin{aligned} \dot{\mathbf{Q}} \cdot (\boldsymbol{\epsilon}^{(3)} \cdot \mathbf{q}) = & -\sin(\psi)\dot{\psi}\boldsymbol{\epsilon}^{(3)} \cdot \mathbf{q} - (1 - \cos(\psi))\mathbf{q} \otimes (\dot{\mathbf{q}} \times \mathbf{q}) \\ & + \cos(\psi)\dot{\psi}[\mathbf{1} - \mathbf{q} \otimes \mathbf{q}] - \sin(\psi)\mathbf{q} \otimes \dot{\mathbf{q}}. \end{aligned} \tag{20.55}$$

Using the two previous relations, the angular velocity tensor $\boldsymbol{\Omega}$ can be expressed as

$$\begin{aligned} \boldsymbol{\Omega} = & \sin(\psi)(1 - \cos(\psi))[(\dot{\mathbf{q}} \times \mathbf{q}) \otimes \mathbf{q} - \mathbf{q} \otimes (\dot{\mathbf{q}} \times \mathbf{q})] - \\ & - [\dot{\psi}\mathbf{q} + \sin(\psi)\cos(\psi)\dot{\mathbf{q}}] \cdot \boldsymbol{\epsilon}^{(3)} + (1 - \cos(\psi))[\dot{\mathbf{q}} \otimes \mathbf{q} - \mathbf{q} \otimes \dot{\mathbf{q}}]. \end{aligned} \tag{20.56}$$

From this expression, the angular velocity vector $\boldsymbol{\omega}$ is obtained by computing the axial vector of $\boldsymbol{\Omega}$ according to Eq. (20.21),

$$\boldsymbol{\omega} = \dot{\psi} \mathbf{q} + \sin(\psi) \dot{\mathbf{q}} + (1 - \cos(\psi)) \mathbf{q} \times \dot{\mathbf{q}}. \quad (20.57)$$

By means of Eq. (20.21), the angular velocity tensor can be recomputed from Eq. (20.57)

$$\boldsymbol{\Omega} = (1 - \cos(\psi)) [\dot{\mathbf{q}} \otimes \mathbf{q} - \mathbf{q} \otimes \dot{\mathbf{q}}] - (\dot{\psi} \mathbf{q} + \sin(\psi) \dot{\mathbf{q}}) \cdot \boldsymbol{\epsilon}^{(3)}, \quad (20.58)$$

which is a simpler expression than the one in Eq. (20.56).

References

1. Altenbach, H., et al.: Influence of rotary inertia on the fiber dynamics in homogeneous creeping flows. *ZAMM* **87**(2), 81–93 (2007)
2. Amirouche, F.: *Fundamentals of Multibody Dynamics*. Birkhäuser, Boston (2006)
3. Bertram, A., Glüge, R.: *Solid Mechanics*. Springer, Berlin (2015)
4. Featherstone, R.: *Rigid Body Dynamics Algorithms*. Springer, Berlin (2008)
5. Flügge, W.: *Tensor Analysis and Continuum Mechanics*. Springer, Berlin (1972)
6. Goldstein, H., Poole, Ch., Safko, J.: *Classical Mechanics*. Addison-Wesley, Reading, MA (1980)
7. Ivanova, E., Vilchevskaya, E., Mueller, W.: A study of objective time derivatives in material and spatial description. In: Altenbach, H., Goldstein, R., Murashkin, E. (eds.) *Mechanics for Materials and Technologies. Advanced Structured Materials*, vol. 46, pp. 195–229. Springer, Cham (2017)
8. Kane, T.R., Levinson, D.A.: *Dynamics, Theory and Applications*. McGraw Hill (1985)
9. Magnus, K.: *Kreisel: Theorie und Anwendungen*. Springer, Berlin (1971)
10. Naumenko, K., Altenbach, H.: *Modeling High Temperature Materials Behavior for Structural Analysis*. Springer International Publishing (2016)
11. Schiehlen, W., Eberhard, P.: *Technische Dynamik*, 5th edn. Springer Vieweg, Wiesbaden (2017)
12. Spoor, C.W., Veldpaus, F.E.: Rigid body motion calculated from spatial co-ordinates of markers. *J. Biomech.* **13**(4), 391–393 (1980)
13. Stevens, B.L., Lewis, F.L., Johnson, E.N.: *Aircraft Control and Simulation: Dynamics, Controls Design, and Autonomous Systems*, 3rd edn. Wiley-Blackwell, Hoboken, NJ (2015)
14. Taylor, J.R.: *Classical Mechanics*. University Science Books, Sausalito, CA (2005)
15. Wittenburg, J.: Dynamics of systems of rigid bodies. In: Görtler, H. (ed.) *Leitfäden der angewandten Mathematik und Mechanik*, vol. 33. B. G. Teubner, Stuttgart (1977)
16. Zhilin, P.A.: A new approach to the analysis of free rotations of rigid bodies. *ZAMM J. Appl. Math. Mech./Z. Angew. Math. Mech.* **76**(4), 187–204 (1996)
17. Zhilin, P.A.: *Рациональная механика сплошных сред (Rational Continuum Mechanics)*. Санкт-Петербург Издательство Политехнического университета, St. Petersburg (2012) (in Russian)

Chapter 21

A Variant of the Description of the Acoustic and Optical Branches of the Dispersion Law of High-Frequency Waves in an Elastic Medium



Sergey N. Romashin, Margarita V. Khoroshilova and Vladimir S. Shorkin

Abstract This paper presents an alternative description of the acoustic and optical branches of the law of dispersion for high-frequency waves in an elastic medium. For longitudinal and transverse plane waves which propagate in an elastic media the dispersion law consists of two sections—acoustic and optical for large oscillation frequency values. The acoustic branch has a description both in mechanics of deformable solids and in solid-state physics. The optical branch is described only by solid-state physics. According to it, the oscillations of neighboring atoms in the crystal lattice for the optical branch occur in the antiphase. This can lead to the destruction of interatomic bonds and substance. Methods of solid physics for materials having complex chemical composition and structure are difficult to apply. Therefore, the description for the optical branch of the dispersion law in the framework of continuum mechanics is relevant. The paper uses a version of the moment elasticity theory which is a consequence of the nonlocal model of a continuous material, considering the pair and triple interactions between its infinitesimal particles. Another feature of the oscillations relevant for the optical branch includes by that they are similar to the thermal vibrations of atoms. They are characterized by anharmonicity—such a shift in the center of oscillations, that the average distance between atoms increases. The proposed model considers the influence of anharmonicity on the stress state of the material in the construction of the equation for conservation law of linear momentum. This equation is a balance equation for changing the total linear momentum of a substance particle for a finite, rather than infinitely small, time frame. This finite segment is a material constant. The method of its definition is specified in this work. The obtained theoretical results satisfactorily correspond to the experimental data available in the literature.

Keywords Dispersion law · Acoustic and optical branches · Anharmonicity · Moment theory · Nonlocal interactions · Conservation law of linear momentum

S. N. Romashin · M. V. Khoroshilova · V. S. Shorkin (✉)
Orel State University named after I.S. Turgenev, 29 Naugorskoe Shosse,
302020 Orel, Russian Federation

© Springer Nature Switzerland AG 2020
H. Altenbach et al. (eds.), *Nonlinear Wave Dynamics of Materials and Structures*, Advanced Structured Materials 122,
https://doi.org/10.1007/978-3-030-38708-2_21

21.1 Introduction

The elements of space technology structures and nuclear engineering during operation are exposed to x-ray and neutron irradiation. Under its influence, high-frequency longitudinal and transverse waves of phonons occur into the irradiated material [4]. Waves are characterized by dispersion law— $\omega = \omega(K)$ the dependence of the oscillation frequency ω on their wave number K [2]. The dispersion law has two branches—acoustic and optical. During the acoustic vibrations, neighboring atoms move in the same direction. With optical vibrations, neighboring atoms move toward each other. Their center of mass remains fixed, and the interatomic bond is stretched and can be destroyed. The destruction of interatomic bonds can lead to the destruction of a material similarly that occurs during the thermal atomic oscillation [3, 7, 11]. Therefore, the study of such oscillation is relevant. Real materials that are used in industry have a complex chemical composition and atomic-molecular structure. Therefore, when studying their behavior in different situations, it is convenient to use information about their phenomenological properties. In the framework of mechanics of deformable solids, the acoustic branch for the dispersion law is described in [10]. This paper presents an attempt to describe within the mechanics of continuous elastic solid media not only acoustic, but also the optical branch of the dispersion law for high-frequency waves.

21.2 General Provisions and Assumptions

21.2.1 An Elastic Medium Model

It is assumed that the studied solids B are obtained first by mental and then by real instantaneous separation from infinitely extended, homogeneous, isotropic continuous elastic media Ω . As a reference, configuration of bodies B is taken that they had Ω with mental isolation. This assumption is used to exclude from consideration the heterogeneity of material properties caused by proximity to the boundary.

In the reference configuration, the body B occupies an area V , and the centers of inertia of its particles dB have radius vectors $\mathbf{r} = x_j \mathbf{e}_j \in V$. The triple of unit vectors \mathbf{e}_j ($j = 1, 2, 3$) forms an orthonormal basis. Let $dB_1 \equiv dB$ and dB_2 is two arbitrary infinitely small particles of the body B . The position dB_2 relative to $dB_1 \equiv dB$ in the reference configuration is determined by the vector $\mathbf{l}_2 \equiv \mathbf{l}_{12} = \mathbf{r}_2 - \mathbf{r}_1$. When deforming the body, the particles $dB_1 \equiv dB$ and dB_2 at each time t acquire new positions $\mathbf{R}(t) = X_j(t) \mathbf{e}_j$ and displacement vectors $\mathbf{u}(t) = \mathbf{R}(t) - \mathbf{r}$. The position of the particle dB_2 relative to the particle dB will be determined by the vector $\mathbf{L}_{12} = \mathbf{R}_2 - \mathbf{R}_1 = (\mathbf{r}_2 - \mathbf{r}_1) + (\mathbf{u}_2 - \mathbf{u}_1) = \mathbf{l}_{12} + \Delta \mathbf{u}_{12}$. Here, $\Delta \mathbf{u}_{12} \equiv \Delta \mathbf{u}_2 = \mathbf{u}_2 - \mathbf{u}_1$ the displacement of the particle dB_2 relative to the particle dB . Changes in the relative orientation of the particles are not considered. For every particle, dB_j vectors $\Delta \mathbf{u}_j$ are represented as series in the external degrees of the vectors \mathbf{l}_j .

$$\Delta \mathbf{u}_j = \sum_{n=1}^{\infty} \frac{1}{n!} \left(\nabla_{l_j}^n \mathbf{u} \right) \overbrace{\dots}^{n \text{ step}} \mathbf{l}_j^n = \sum_{n=1}^{\infty} \frac{(-1)^n}{n!} \left(\nabla^n \mathbf{u} \right) \overbrace{\dots}^{n \text{ step}} (\mathbf{l}_j)^n, \quad (21.2.1)$$

Here, $\nabla = d \dots / d\mathbf{r}$ is differential operator Hamiltonian by \mathbf{r} vector, and $\nabla_{l_j} = d \dots / d\mathbf{l}_j$ —by the \mathbf{l}_j vector $\nabla = d \dots / d\mathbf{r} = -\nabla_{l_j} = d \dots / d\mathbf{l}_j$. Gradients $\nabla^n \mathbf{u}$ are defined at the center of inertia of the ΔB particle.

The temperature Θ and density ρ distributions of the material generally change over time. In the work this does not consider.

Each body B can be represented as a union of non-intersecting parts: $\Delta B_n (n = 1, \dots, N) : B = \bigcup_{n=1}^{n=N} \Delta B_n$.

Let

$$d_n = \text{diam} \Delta V_n \approx \sqrt[3]{\Delta V_n} \quad (21.2.2)$$

is the diameter of the part ΔB_n . Then properly:

$$(N \rightarrow \infty) \Rightarrow (\Delta B_n \equiv \Delta B_{(k)n} \rightarrow dB \equiv dB_{(k)}). \quad (21.2.3)$$

The system $\{\Delta B_n\}_N$ of particles ΔB_n is put in accordance with the system $\{b_n\}_N$ of b_n material points. The points b_n are located in the centers of inertia of the ΔB_n particles. They have the same mass, kinetic energy and linear momentum as the ΔB_n particles.

The potential energy of interaction $W_{(N)}$ between all parts ΔB_n is equal to the potential energy of interaction between all material b_n points. It is a function of the position of b_n points in space:

$$W_{(N)} = W(N)(\mathbf{R}_1, \dots, \mathbf{R}_N) \quad (21.2.4)$$

Under each partition of the body B into elementary parts ΔB_n , the equality is true

$$W = W(N)(\mathbf{R}_1, \dots, \mathbf{R}_N) \quad (21.2.5)$$

In accordance with [9], for N -point function (21.2.5) it is true to represent as a sum of all two-, three- and so on point functions $\Delta W_{(N)}^{ij}(\mathbf{R}_i, \mathbf{R}_j)$, $\Delta W_{(N)}^{ijk}(\mathbf{R}_i, \mathbf{R}_j, \mathbf{R}_k)$ which characterize, respectively, two-, three-, etc. partial potential interactions of ΔB_n particles.

It is assumed that there are limits that do not depend on the method N -partition.

$$\lim_{N \rightarrow \infty, d_{(N)} \rightarrow 0} \frac{\Delta W_{(N)}^{(ij)}}{\Delta V_{(N)}^{(i)} \Delta V_{(N)}^{(j)}} = \Phi^{(ij)}(\mathbf{R}_i, \mathbf{R}_j, \{\kappa^{(2)}\}), \quad (21.2.6)$$

$$\lim_{N \rightarrow \infty, d_{(N)} \rightarrow 0} \frac{\Delta W_{(N)}^{(ijk)}}{\Delta V_{(N)}^{(i)} \Delta V_{(N)}^{(j)} \Delta V_{(N)}^{(k)}} = \Phi^{(ijk)}(\mathbf{R}_i, \mathbf{R}_j, \mathbf{R}_k, \{\kappa^{(3)}\}).$$

Here, $\{\kappa^{(2)}(\Theta)\}$ and $\{\kappa^{(3)}(\Theta)\}$ are sets of parameters that determine the type of the pair and triple interaction potentials for specific materials at a given Θ temperature. The material under study is assumed to be homogeneous and isotropic. Therefore,

$$\begin{aligned} \Phi^{(ij)}(\mathbf{R}_i, \mathbf{R}_j) &= \Phi^{(2)}(|\mathbf{R}_1 - \mathbf{R}_j|) = \Phi^{(2)}(L_{1i}, \{\kappa^{(2)}\}), \\ \Phi^{(ijk)}(\mathbf{R}_i, \mathbf{R}_j, \mathbf{R}_k) &= \Phi^{(3)}(|\mathbf{R}_1 - \mathbf{R}_2|, |\mathbf{R}_1 - \mathbf{R}_3|) = \Phi^{(3)}(L_{1i}, L_{1j}, \{\kappa^{(3)}\}). \end{aligned} \tag{21.2.7}$$

Here, $L_{1j} = |\mathbf{R}_1 - \mathbf{R}_j|$ is the distance between the dB_1 and dB_j particles. The paper [6] presents one of the possible variants for these potentials and methods for determining the values of their parameters. The potential energy $dW(\mathbf{R}) = w(\mathbf{R})dV$ of the particle interaction with all other $dB \equiv dB_1$ particles of the body B is determined by equality

$$dW = w(\mathbf{R})dV = \left\{ \int_V \Phi^{(2)}(L_{(12)})dV_2 + \int_V dV_2 \int_V \Phi^{(3)}(L_{12}, L_{13})dV_3 \right\} dV \tag{21.2.8}$$

This expression will be used in the local description of the mechanical behavior of the material to establish the relationship between stresses and deformation.

The local description of a solids uses the description of the properties of not many particles, but only one dB particle. Its characteristics of deformed, stressed and energy states are determined at one point $\mathbf{R} \equiv \mathbf{R}_1$ – its center of inertia. The characteristics of the dB particle kinematics are gradients $\nabla^n \mathbf{u}$, $n = 1, \dots, M$. The number M of gradients stored in the decomposition (21.2.1) is determined by the need to suitable describe for the corresponding mechanical effect.

The acoustic branch for the dispersion law in [10] is described by using two stress tensors $P^{(1)} = \mathbf{e}_p \mathbf{e}_k P_{pk}^{(1)}$ and $P^{(2)} = \mathbf{e}_p \mathbf{e}_k \mathbf{e}_q P_{pkq}^{(2)}$. They are generalized forces that work on generalized displacements $\nabla \mathbf{u}$ and $\nabla^2 \mathbf{u}$, respectively. These tensors are also used in this paper. For their introduction [10] it is assumed that each infinitesimal dB particle of a continuous solid is exposed to the action of a volume distributed $\mathbf{f} = \mathbf{e}_k f_k$ force. In this paper, such forces are inertial forces.

It is assumed that the norm $\left[\sum_{i,j_1, \dots, j_n=1}^n (u_{i,j_1, \dots, j_n})^2 \right]^{1/2}$ of the tensor is a small value. Then the change in the volume of particles can be neglected and assume that in the coordinate system (x_1, x_2, x_3) occupied by the particle area dB is infinitely small parallelepiped. Its elementary volume dV is a differential antisymmetric basis 3-form [8].

$$dV = \frac{1}{3!} \varepsilon_{ijk} dx_i dx_j dx_k = dx_1 \wedge dx_2 \wedge dx_3. \tag{21.2.9}$$

(\wedge is sign antisymmetric multiplication, ε_{ijk} is Levi-Civita symbol). At an each value of the number k , the expression

$$dF_k = \varphi_k dV = \varphi_k dx_1 \wedge dx_2 \wedge dx_3 = (-f_k) dx_1 \wedge dx_2 \wedge dx_3. \quad (21.2.10)$$

is also a 3-form. In three-dimensional space its differential not symmetrical 4-form is equal to zero.

$$\partial(dF_k) = (\partial\varphi_k/\partial x_p) dx_p dx_1 \wedge dx_2 \wedge dx_3 = 0. \quad (21.2.11)$$

Therefore, according to the Poincare theorem [8] for a given value k , there is such a 2-form $d\Psi_k$ that is associated with equality:

$$\partial(d\Psi_k) = dF_k. \quad (21.2.12)$$

The form $d\Psi_k$ has the view:

$$d\Psi_k = \psi_{12k} dx_1 \wedge dx_2 + \psi_{23k} dx_2 \wedge dx_3 + \psi_{31k} dx_3 \wedge dx_1. \quad (21.2.13)$$

Here, ψ_{ijk} are the components of a differentiable tensor $\Psi = \mathbf{e}_p \mathbf{e}_k \mathbf{e}_q \psi_{pkq}$. Considering (21.2.11) and (21.2.12) the form (21.2.10) look as:

$$dF_k = \left(\frac{\partial\psi_{12k}}{\partial x_3} + \frac{\partial\psi_{23k}}{\partial x_1} + \frac{\partial\psi_{31k}}{\partial x_2} \right) dx_1 \wedge dx_2 \wedge dx_3. \quad (21.2.14)$$

Consequently, it turns out that

$$\varphi_k = \frac{\partial\psi_{12k}}{\partial x_3} + \frac{\partial\psi_{23k}}{\partial x_1} + \frac{\partial\psi_{31k}}{\partial x_2}. \quad (21.2.15)$$

So, such a tensor $\Psi = \mathbf{e}_p \mathbf{e}_k \mathbf{e}_q \psi_{pkq}$ for the vector $\boldsymbol{\varphi} = -\mathbf{e}_k f_k$ exists and for it the equality is fulfilled (21.2.15). The components ψ_{ijk} of the tensor $\Psi = \mathbf{e}_i \mathbf{e}_j \mathbf{e}_k \psi_{ijk}$ are invited to submit in the form:

$$\psi_{ijk} = \psi_{ijk}^{(1)} - \frac{\partial\psi_{ijkp}^{(2)}}{\partial x_p}. \quad (21.2.16)$$

By performing a double convolution of this representation with the Levi-Civita tensor ε_{ijp} , considering $\varepsilon_{ijq} \psi_{ijk}^{(1)} = P_{qk}^{(1)}$ and $\varepsilon_{ijq} \psi_{ijkp}^{(2)} = P_{qkp}^{(2)}$, we can obtain the equation

$$\nabla \cdot (P^{(1)} - \nabla \cdot P^{(2)}) + \mathbf{f} = 0. \quad (21.2.17)$$

This is the equation of the moment theory for elasticity during stresses. To use it, we need information about the relationship between stress tensors and displacement gradients, which take into account the peculiarities of the mechanical behavior of the material under the conditions under consideration.

21.2.2 Expansion Feature of Elastic Material Model

For the description of both branches of the dispersion law, it is proposed to use instead of the motion equation in the form of (21.2.17) the differential equation of motion in the form of

$$\rho \left(\frac{\partial \mathbf{v}}{\partial t} + \frac{1}{2} T \frac{\partial^3 \mathbf{v}}{\partial t^3} \right) = \nabla \cdot P \equiv \nabla \cdot (P^{(1)} - \nabla \cdot P^{(2)}). \quad (21.2.18)$$

Here, T is an additional material constant possessing the time dimension.

The equation of motion (21.2.18) is based on the following reasoning.

The oscillation frequencies of the medium particles for the optical branch of the dispersion law are of great importance. It is commensurate with the frequency of thermal vibrations by solids atoms in the crystal lattice. These oscillations have the property of anharmonicity [1, 5]. Its manifestations are the force of anharmonicity—the difference between the repulsion force of the medium particles and the force of their attraction, as well as such a displacement of the average distance between the interacting particles, at which the medium as a whole expands (thermal expansion with thermal vibrations of atoms). Quasi-harmonic approximation can be used to account for the anharmonic effects of optical wave oscillations [1, 5]. For this, as for the dependence of the temperature expansion of the material, it is necessary to determine the expansion associated with high-frequency anharmonic fluctuations. Then the oscillations about this state can be considered approximately harmonic and the expression (21.2.8) can be used to construct constitutional relations. External influences, which can be simultaneously with high-frequency oscillations, change over time the equilibrium state, which corresponds to a quasi-harmonic expansion. These changes occur very slowly compared to high-frequency oscillatory movements. Therefore, it is assumed that there is a segment $\eta \in [t - T/2; t + T/2]$ within which $P^{(1)}$, $P^{(2)}$ stress tensors and their gradients do not depend on time η . The parameter $T \geq 2\pi/\omega$ value is considered to be known. It is determined experimentally. The expansion, which is caused by high-frequency oscillations, is not determined.

For a segment $\eta \in [t - T/2; t + T/2]$, it is assumed that the particle dB velocity $\mathbf{v}(\eta) = \partial \mathbf{u} / \partial \eta$ is determined by equality

$$\mathbf{v}(\eta) = \mathbf{v}(t) + \frac{\partial \mathbf{v}(t)}{\partial t} \xi + \frac{1}{2} \frac{\partial^2 \mathbf{v}(t)}{\partial t^2} \xi^2, \quad \xi = \eta - t. \quad (21.2.19)$$

With this in mind, the volume density of the pulse obtained by the particle dB on the segment $\eta \in [t - T/2; t + T/2]$ is expressed by the formula

$$\rho \int_{t-T/2}^{t+T/2} \frac{\partial \mathbf{v}}{\partial \eta} d\eta = \rho \left(T \frac{\partial \mathbf{v}}{\partial t} + \frac{T^3}{2} \frac{\partial^3 \mathbf{v}}{\partial t^3} \right). \quad (21.2.20)$$

In this case, the impulse received from the environment at the same time is determined by equality

$$T\boldsymbol{\phi}(t) = T\nabla \cdot P(t) \equiv T\nabla \cdot (P^{(1)}(t) - \nabla \cdot P^{(2)}(t)). \quad (21.2.21)$$

Equating the right parts (21.2.20) and (21.2.21) the Eq. (21.2.18) can be obtained.

The expression of stress tensors included in (21.2.18), through the gradients of displacements the dependences $\Phi^{(2)}(L_{12})$ and $\Phi^{(3)}(L_{12}, L_{13})$, are represented as polynomials of the second degree with respect to the vector determined by the equality (21.2.1). On the basis of the obtained expressions, tensors $P^{(1)}$ and $P^{(2)}$ are determined by equalities [10]

$$P^{(n)} = \frac{\partial w}{\partial (\nabla^n \mathbf{u})} = P^{0(n)} + \sum_{m=1}^M (\nabla^m \mathbf{u}) \overbrace{\dots}^{n \text{ step}} C^{(m,n)}, \quad (21.2.22)$$

$$P^{0(n)} = \int_V (\nabla_{12} \Phi^{(2)}) \mathbf{I}_{12}^n dV_2 + \sum_{j=2}^3 \int_V \left[\int_V (\nabla_{1j} \Phi^{(3)}) \mathbf{I}_{1j}^n dV_2 \right] dV_3, \quad (21.2.23)$$

$$C^{(n,m)} = \int_V \mathbf{I}_{12}^n (\nabla_{12}^2 \Phi^{(2)}) \mathbf{I}_{12}^m dV_2 + \sum_{p,q=2}^3 \int_V \left[\int_V \mathbf{I}_{1p}^n (\nabla_{1p} \nabla_{1q} \Phi^{(3)}) \mathbf{I}_{1q}^m dV_2 \right] dV_3, \quad (21.2.24)$$

Anharmonicity can be accounted in these equations if a changing of the average distance $\Delta l_{ij}^{an}(\omega)$ between the interacting particles $dB \equiv dB_1$ and dB_j is used. To do this, it is necessary to use $\Phi^{(2)}(L_{1j} - \Delta l_{ij}^{an}(\omega), \{\kappa^{(2)}\})$ and $\Phi^{(3)}(L_{1i} - \Delta l_{ij}^{an}(\omega), L_{1j} - \Delta l_{ij}^{an}(\omega), \{\kappa^{(3)}\})$ dependencies. However, this is not done in this paper. In this paper, the value $\Delta l_{ij}^{an}(\omega)$ was not consider. The effect of anharmonicity is shown without taking into account the value $\Delta l_{ij}^{an}(\omega)$ only by using Eq. (21.2.18).

21.3 The Optical and Acoustic Branches Model for Dispersion Law

Flat wave

$$u = u_0 \exp[i(kx - \omega t)], \quad (21.3.1)$$

extends in the direction \mathbf{e}_1 . Here, $x \equiv x_1$, $i = \sqrt{-1}$, $\mathbf{u}_0 = \text{const}$. For longitudinal wave, $\mathbf{u}_0 = u_0 \mathbf{e}_1$, $\mathbf{u} = u \mathbf{e}_1$. For transverse wave, $\mathbf{u}_0 = u_0 \mathbf{e}_2$, $\mathbf{u} = u \mathbf{e}_2$. The scalar form of the one-dimensional equation (21.2.18) in this case has the following form.

$$\frac{1}{c^2} \left(\frac{\partial^2 u}{\partial t^2} + \frac{T}{2} \frac{\partial^4 u}{\partial t^4} \right) = \frac{\partial^2 u}{\partial x^2} + b^2 \frac{\partial^4 u}{\partial x^4}, \tag{21.3.2}$$

For the classical velocity of an acoustic longitudinal waves propagation $c = \sqrt{C_{1111}^{(1,1)}/\rho}$. This speed for the classical transverse waves is equal to $c = \sqrt{C_{1212}^{(1,1)}/\rho}$. The parameter b in the first case is calculated by the formula $b = \sqrt{\left(C_{111111}^{(1,3)} - C_{111111}^{(2,2)} + C_{111111}^{(3,1)}\right)/C_{1111}^{(1,1)}}$, and in the second case by formula $b = \sqrt{\left(C_{112112}^{(1,3)} - C_{112112}^{(2,2)} + C_{112112}^{(3,1)}\right)/C_{1212}^{(1,1)}}$. Material constants $C_{1111}^{(1,1)}$, $C_{111111}^{(1,3)}$, $C_{111111}^{(2,2)}$, $C_{111111}^{(3,1)}$, $C_{1212}^{(1,1)}$, $C_{112112}^{(1,3)}$, $C_{112112}^{(2,2)}$, $C_{112112}^{(3,1)}$ determined by Eq.(21.2.24). The type of dependences of the potentials of pair and triple interactions of the elastic medium, as well as the values of the parameters that concretize their type for the corresponding materials, are considered to be known [6]. During constructing the Eq.(21.3.2) for the $P^{(1)}$ tensor in decomposition (21.2.22) is $M = 3$ accepted, for $P^{(2)} - M = 2$ accepted. It is considered that in an infinitely extended medium at an odd value $m + n$ it is $C^{(n,m)} = 0$ true.

Substituting the expression (21.3.1) in (21.3.2) one can obtain the expression for the dispersion law.

$$\frac{\omega^2(1 - T^2\omega^2)}{c^2} = (K^2 - b^2K^4), \tag{21.3.3}$$

This is followed by expressions that describe not one but two branches of the dispersion law.

$$\omega_1(K) = \frac{1}{T\sqrt{2}}\sqrt{1 + \sqrt{1 - 4c^2T^2(K^2 - b^2K^4)}}, \tag{21.3.4}$$

$$\omega_2(K) = \frac{1}{T\sqrt{2}}\sqrt{1 - \sqrt{1 - 4c^2T^2(K^2 - b^2K^4)}} \approx c^2(K^2 - b^2K^4), \tag{21.3.5}$$

While $(T\omega) \rightarrow 0$ (21.3.3) represents the dispersion law possessing only one branch—acoustic [10]. If this is the case $K \rightarrow 0$, then (21.3.5) is a classical linear expression for the dispersion law.

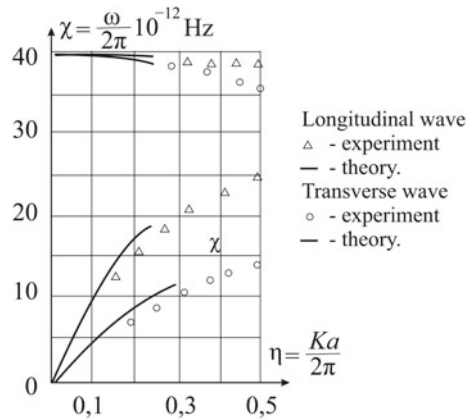
$$\omega = cK, \tag{21.3.6}$$

Approximate equality (21.3.3) is considered to be valid for each small values of the wave K number, including those when the equality is true (21.3.5). Therefore, substituting (21.3.5) in (21.3.3) , you can get:

$$b = cT, \tag{21.3.7}$$

This equality indicates that the parameter T is a material constant.

Fig. 21.1 Dispersion law for crystal of diamond in the direction [111]



21.4 Results and Experimental Data Comparison

The obtained theoretical results can be compared with the experimental data available in the literature. In [4] data for acoustic and optical branches of the law of dispersion of diamond crystal are given. For longitudinal and transverse waves, the optical branch begins at a point with coordinates $(\chi = \omega/2\pi, K) = (\chi_0, 0)$. By the value χ_0 and sound speed c for longitudinal and transverse waves, on the basis of equality $1 - T^2(\chi_0^2/4\pi^2) = 0$, true to the point $(\chi_0, 0)$, the parameter T value is determined. Then the parameter b value is calculated using (21.3.7). The obtained data make it possible to produce graphical dependencies $\omega_1(K)$ and $\omega_2(K)$. The results are shown in Fig. 21.1.

Calculations are carried out for the case when the waves propagate along the direction [111] of the diamond crystal for which $C_{11} = 10.76 \times 10^{11} \text{ N/m}^2$, $C_{12} = 1.25 \times 10^{11} \text{ N/m}^2$, $C_{44} = 5.76 \times 10^{11} \text{ N/m}^2$, $\rho = 3.5 \times 10^3 \text{ Kg/m}^3$. The comparison results of theoretical data obtained in this work and presented in [4] indicate to their qualitative coincidence and satisfactory quantitative compliance.

21.5 Conclusion

The description for both acoustic and optical branches of the dispersion law for low-amplitude and high-frequency waves is proposed within the framework of the mechanics of deformable solids. This description is made under the assumption the existence of medium oscillations anharmonicity that correspond to the optical branch. The quantitative and qualitative correspondence between theoretical results and experimental data available in the literature is obtained. The results of the work should be considered illustrative. Their practical application requires a more detailed theoretical analysis for the anharmonicity phenomenon in terms of continuum mechanics.

References

1. Born, M., Huang, H.: *Dynamical Theory of Crystal Lattices*. Clarendon Press, Oxford. <https://doi.org/10.1119/1.1934059>
2. Erofeeyev, V.I.: *Wave Processes in Solid with Microstructure*, p. 276. World Scientific Publishing Co Inc, Singapore (2003)
3. Jensen, E.M.: Combined multiscale creep strain and creep rupture modeling for composite materials. In: *Structural Dynamics, and Materials Conference AIAA 2015-1360*. Kissimmee, Florida (2015). <https://doi.org/10.2514/6.2015-1360>
4. Kittel, Ch.: *Introduction to Solid State Physics*. Wiley, New York (2004)
5. Leibfried, G., Ludwig, W.: Theory of anharmonic effect in crystal. In: Seitz, F., Turnbull, D. (eds.) *Solid State Physics XII*. Academic Press, New York (1961)
6. Presnetsova, VYu., Romashin, S.N., Frolenkova, LYu., Shorkin, V.S., Yakushina, S.I.: A variant of describing adhesion interaction in the probe-sample system of an atomic-force microscope. *Nanosci. Technol. Int. J.* **9**(4), 299–323 (2018). <https://doi.org/10.1615/NanoSciTechnolIntJ.201802671>
7. Regel, V.R., Slutsker, A.I., Tomashevsky, E.E.: *The Kinetic Nature of Solids*. Nauka, Moscow (1974)
8. Rudin, W.: *Principles of Mathematical Analysis*. McGraw-Hill, New York (1976)
9. Ruelle, D.: *Statistical Mechanics: Rigorous Results*. Benjamin, New York (1969). <https://doi.org/10.1142/4090>
10. Shorkin, V.S.: Nonlinear dispersion properties of high-frequency waves in the gradient theory of elasticity. *Mech. Solids* **46**(6), 898–912 (2011). <https://doi.org/10.3103/S0025654411060094>
11. Slutsker, A.I.: Characteristics of elementary acts in the kinetics of metal fracture. *Phys. Solid State* **46**(9), 1658–1666 (2004)

Chapter 22

Supercomputer Modeling of Wave Propagation in Blocky Media Accounting Fractures of Interlayers



Vladimir M. Sadovskii and Oxana V. Sadovskaya

Abstract To analyze the propagation of stress waves in structurally inhomogeneous materials, we use the method of direct numerical simulation based on a mathematical model of a blocky medium with elastic blocks interacting through compliant elastic-plastic interlayers, and a model of nonlinear theory of the orthotropic Cosserat continuum that takes into account the shear and rotational nature of irreversible deformation. The continuum model is formulated as a variational inequality, correctly describing both the state of an elastic-plastic flow of a material under active loading and the state of elastic unloading. In the model of a blocky medium, variational inequalities are used to describe the plastic deformation of interlayers between the blocks and to simulate cracks moving along the interlayers. Parallel computational algorithms and author's software codes for multiprocessor computer systems of cluster architecture are used in the numerical implementation of mathematical models. In 2D setting, a problem of pulse loading of a rectangular blocky rock mass of the masonry type through a platform is studied. A good correspondence between the results of computations is obtained on qualitative and quantitative levels.

Keywords Microstructure · Blocky medium · Interlayers · Dynamics · Elasticity · Plasticity · Fracture · Pulse loading · Cosserat continuum · Couple stresses · High-performance computing

V. M. Sadovskii (✉) · O. V. Sadovskaya
Institute of Computational Modeling SB RAS, Akademgorodok 50/44, Krasnoyarsk 660036,
Russian Federation
e-mail: sadov@icm.krasn.ru

O. V. Sadovskaya
e-mail: o_sadov@icm.krasn.ru

© Springer Nature Switzerland AG 2020
H. Altenbach et al. (eds.), *Nonlinear Wave Dynamics of Materials and Structures*, Advanced Structured Materials 122,
https://doi.org/10.1007/978-3-030-38708-2_22

22.1 Introduction

Most applications in the construction industry, mining, oil exploration and oil production are dedicated to the discrete and continuous modeling that imitates the behavior of inhomogeneous materials of layered and blocky structure. Modeling allows to reproduce the crack opening and joint sliding of the blocks which are responsible for the occurrence of the destruction. On a model level, a medium is considered as a set of the interacting blocks or particles [3, 5, 15]. Models of periodic media can be used for simulating of wave processes in soils and rocks as layered materials [14, 17, 18] or blocky materials [11]. A 3D masonry model was introduced in [6], where a medium is periodic in three orthogonal directions.

Simple and effective approach to the description of wave processes in structurally inhomogeneous media is based on the Cosserat continuum equations [7, 12, 20]. In these equations, along with the translational motion of particles of the material microstructure under the action of gradients of internal stresses, the rotational degrees of freedom due to the moment interactions of particles are taken into account in averaged form. We applied the Cosserat equations to the analysis of wave propagation in blocky media with elastic blocks interacting through compliant elastic interlayers [24]. Recently, we have simulated physically nonlinear plastic deformation of interlayers [23]. In this approach, fundamentally difficult is a problem of specification of the mechanical parameters of a continuum, which would correspond to a real blocky structure such as masonry or lumpy rock [4, 16, 19].

An alternative approach is to model blocks and interlayers independently as interconnected structural elements [1, 2, 28]. In geomechanics and geodynamics, it is developed starting from the fundamental work [21], in which, based on the analysis of an experimental material, the natural lumpiness of rocks was established.

As a result of modeling, a large system of equations is obtained, which describes the dynamics of blocks with internal boundary conditions of their contact through interlayers. This system occurs to be practically inaccessible for research by analytical methods, and it requires the use of high-performance computations. Developing this approach, we construct different versions of the model [26]: from the case of elastic, viscoelastic or plastic interlayers to the case of a porous material in interlayers, where the pores collapse under application of compressive stresses is considered, and the case of a fluid-saturated porous material. In the present contribution, the model of a blocky medium is generalized to take into account the propagation of a system of cracks along with interlayers. The deformation criterion of crack formation is used. Internal boundary conditions on the crack edges are formulated as variational inequalities describing contact of blocks without friction. Using MPI (Message Passing Interface) technology, parallel software is developed for modeling the dynamics of blocky media with cracks in 2D formulation. Results of computations of the cracks' growth caused by the rotation of blocks under the action of external pulse loads are presented.

22.2 Blocky Medium with Elastic-Plastic Interlayers

A plane deformation of a rock with the blocky structure, consisting of rectangular elastic blocks with the sides h_1, h_2 and interlayers of the thicknesses δ_1, δ_2 , is considered. The block sides are parallel to the axes x_1, x_2 of the Cartesian coordinate system (Fig. 22.1). The number of blocks in the directions of the axes is N_1 and N_2 , respectively.

A motion of each block is defined by the system of equations of an isotropic elastic medium, written in terms of the velocities v_k and stresses σ_{jk} :

$$\begin{aligned}
 \rho \dot{v}_1 &= \sigma_{11,1} + \sigma_{12,2} , \\
 \rho \dot{v}_2 &= \sigma_{12,1} + \sigma_{22,2} , \\
 \dot{\sigma}_{11} &= \rho c_1^2 (v_{1,1} + v_{2,2}) - 2 \rho c_2^2 v_{2,2} , \\
 \dot{\sigma}_{22} &= \rho c_1^2 (v_{1,1} + v_{2,2}) - 2 \rho c_2^2 v_{1,1} , \\
 \dot{\sigma}_{12} &= \rho c_2^2 (v_{2,1} + v_{1,2}) .
 \end{aligned}
 \tag{22.1}$$

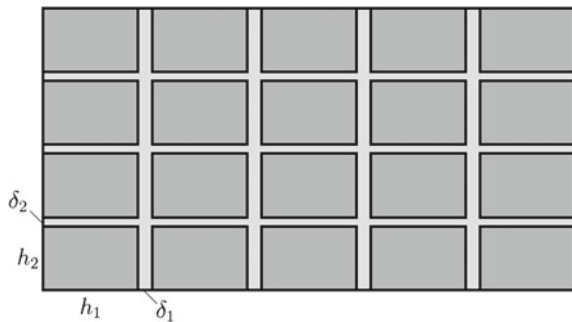
Here, ρ is the density of a blocky material, c_1 and c_2 are the velocities of longitudinal and transverse elastic waves in the blocks, respectively. Dot over a symbol denotes partial derivative with respect to time, and indices after a comma denote partial derivatives with respect to spatial variables.

An elastic interlayer between the horizontally located nearby blocks is described by the system of ordinary differential equations:

$$\begin{aligned}
 \rho' \frac{\dot{v}_1^+ + \dot{v}_1^-}{2} &= \frac{\sigma_{11}^+ - \sigma_{11}^-}{\delta_1} , & \frac{\dot{\sigma}_{11}^+ + \dot{\sigma}_{11}^-}{2} &= \rho' c_1'^2 \frac{v_1^+ - v_1^-}{\delta_1} , \\
 \rho' \frac{\dot{v}_2^+ + \dot{v}_2^-}{2} &= \frac{\sigma_{12}^+ - \sigma_{12}^-}{\delta_1} , & \frac{\dot{\sigma}_{12}^+ + \dot{\sigma}_{12}^-}{2} &= \rho' c_2'^2 \frac{v_2^+ - v_2^-}{\delta_1} .
 \end{aligned}
 \tag{22.2}$$

An interlayer between the vertically located nearby blocks is modeled using similar system:

Fig. 22.1 Scheme of a blocky medium



$$\begin{aligned} \rho' \frac{\dot{v}_2^+ + \dot{v}_2^-}{2} &= \frac{\sigma_{22}^+ - \sigma_{22}^-}{\delta_2}, & \frac{\dot{\sigma}_{22}^+ + \dot{\sigma}_{22}^-}{2} &= \rho' c_1'^2 \frac{v_2^+ - v_2^-}{\delta_2}, \\ \rho' \frac{\dot{v}_1^+ + \dot{v}_1^-}{2} &= \frac{\sigma_{12}^+ - \sigma_{12}^-}{\delta_2}, & \frac{\dot{\sigma}_{12}^+ + \dot{\sigma}_{12}^-}{2} &= \rho' c_2'^2 \frac{v_1^+ - v_1^-}{\delta_2}. \end{aligned} \quad (22.3)$$

Here, ρ' is the density of a material of the interlayer, and c_1' and c_2' are the velocities of longitudinal and transverse waves in the interlayers. Indices “+” and “-” in Eqs. (22.2) and (22.3) are related to the boundaries of interacting blocks. Due to the large aspect ratio between the size of blocks and the thickness of interlayers, the characteristic time scale of the physical processes within the interlayers is smaller as compared to characteristic time of the physical processes within the blocks. Hence, the stress state of the interlayers is described by the system of ordinary (not partial) differential equations (22.2) and (22.3).

It was shown [24] that these equations are thermodynamically consistent with the system (22.1) in the sense of fulfillment of the energy conservation law, where the sum of kinetic and potential elastic energy of the mass of blocks equals to the sum of kinetic and potential energies of the blocks and interlayers, and the work of external forces is calculated as an integral about the outer mass boundary. Thermodynamic consistency is an exceptionally important property of the mathematical model since its absence may lead to nonphysical effects.

To take into account the plasticity in accordance with the general approach suggested in [22], constitutive equations of the vertical elastic interlayer in (22.2) are replaced by the variational inequality:

$$(\delta\sigma_{11}^+ + \delta\sigma_{11}^-) \dot{\varepsilon}_{11}^p + (\delta\sigma_{12}^+ + \delta\sigma_{12}^-) \dot{\varepsilon}_{12}^p \leq 0. \quad (22.4)$$

Here, $\delta\sigma_{jk}^\pm = \tilde{\sigma}_{jk}^\pm - \sigma_{jk}^\pm$ are the variations of stresses,

$$\dot{\varepsilon}_{11}^p = \frac{v_1^+ - v_1^-}{\delta_1} - \frac{\dot{\sigma}_{11}^+ + \dot{\sigma}_{11}^-}{2\rho'c_1'^2}, \quad \dot{\varepsilon}_{12}^p = \frac{v_2^+ - v_2^-}{\delta_1} - \frac{\dot{\sigma}_{12}^+ + \dot{\sigma}_{12}^-}{2\rho'c_2'^2}$$

are the plastic strain rates. Along with the actual stresses σ_{jk}^\pm , the admissible stresses $\tilde{\sigma}_{jk}^\pm$ are subject to the constraint in the form:

$$f\left(\frac{\tilde{\sigma}_{11}^+ + \tilde{\sigma}_{11}^-}{2}, \frac{\tilde{\sigma}_{12}^+ + \tilde{\sigma}_{12}^-}{2}\right) \leq \tau(\chi), \quad (22.5)$$

where τ is the material yield point of interlayers, χ is a material parameter (or set of parameters) of hardening, and $f(\sigma_n, \sigma_\tau)$ is the equivalent stress function, in which arguments are normal and tangential stresses in the interlayer.

The variational inequality (22.4) allows to describe constitutive equations of elastic-plastic flow with isotropic hardening in accordance with the principle of maximum of plastic dissipation, which guarantees the fulfillment of basic principles

of irreversible thermodynamics. The strong inequality in (22.5) corresponds to the elastic state of the interlayer, while the equality is achieved in the plastic state.

Selection of the hardening parameter χ is not unique. The yield point for rocks depends significantly on the value of hydrostatic pressure or, in a simplified variant, on the value of normal stress $\chi = \sigma_n$. After such selection the yield criterion, which is described by the constraint (22.5), is the Mohr–Coulomb criterion adapted to the case of interlayers of small thickness. The simplest form of the constraint for a microfractured medium is as follows:

$$|\sigma_\tau| \leq \tau_s - \kappa_s \sigma_n, \quad (22.6)$$

where τ_s and κ_s are the material parameters. Under such constraint, in virtue of the arbitrariness of variation of the normal stress in (22.4), the transverse plastic deformation of the interlayer is identically equal to zero, while the shear deformation in the plastic state contains a nonzero irreversible component. Note, that the constraint (22.6) is applicable in a limited range of tensile normal stresses, where the yield point remains positive.

Similarly, constitutive equations of the horizontal elastic-plastic interlayer are formulated in the form of variational inequality:

$$(\delta\sigma_{12}^+ + \delta\sigma_{12}^-) \dot{\epsilon}_{12}^p + (\delta\sigma_{22}^+ + \delta\sigma_{22}^-) \dot{\epsilon}_{22}^p \leq 0.$$

The plastic strain rates are expressed as

$$\dot{\epsilon}_{12}^p = \frac{v_1^+ - v_1^-}{\delta_2} - \frac{\dot{\sigma}_{12}^+ + \dot{\sigma}_{12}^-}{2 \rho' c_2'^2}, \quad \dot{\epsilon}_{22}^p = \frac{v_2^+ - v_2^-}{\delta_2} - \frac{\dot{\sigma}_{22}^+ + \dot{\sigma}_{22}^-}{2 \rho' c_1'^2}.$$

The constraint takes the form:

$$f\left(\frac{\sigma_{22}^+ + \sigma_{22}^-}{2}, \frac{\sigma_{12}^+ + \sigma_{12}^-}{2}\right) \leq \tau(\chi).$$

In the same way, plastic deformation of a material inside the blocks can be taken into account. For this, one can use the principle of maximal power of dissipation, equivalent to the associated law of plastic flow, which also admits a formulation in the form of variational inequality. Numerical implementation of the variational inequality is carried out based on simple and efficient algorithms of solution correction (see, for example [20, 22]). However, in the case of pliable interlayers, plasticity in the blocks occurs much later than plasticity in the interlayers. Therefore, we do not take it into account in this chapter.

To solve the system (22.1)–(22.3) and a generalized system, in which the equations of Hook's law are replaced by the inequalities (22.4), (22.5), the computational algorithm has been developed. This algorithm is based on the two-cyclic splitting method by spatial variables and on the special procedure of correction of the stresses, which takes into account plastic effects.

Two-cyclic splitting in the blocks includes four consequently executing stages; each of them presumes the solution of 1D system of equations in the blocks with internal boundary conditions at the interblock boundaries. These stages are presented in [26] for a more general situation. The mentioned system of equations is solved in the blocks using the Godunov gap decay scheme with the uniform finite difference grid at maximum possible time step, defined by the Courant–Friedrichs–Lewy criterion: $\Delta t = \min\{\Delta x_1, \Delta x_2\}/c_1$. In the interlayers, a nondissipative unconditionally stable predictor–corrector scheme was used, constructed according to the method of Ivanov [13]. Considered 1D hybrid scheme for longitudinal waves (at least in the case of square grid) does not have energy dissipation caused by the approximation; such scheme does not lead to the amplitude attenuation of the traveling waves. The artificial nonphysical energy dissipation of transverse waves is reduced using special reconstruction of the solution.

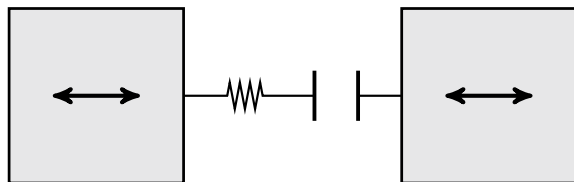
22.3 Simulation of Cracks in Interlayers

At the initial stage of destruction of a blocky medium with compliant interlayers, the cracks originate and move along the interlayers without disturbing the integrity of the blocks. We describe this process within the framework of a model with square elastic blocks. For simplicity, we will consider only the separation cracks, simulating fracture on the basis of the deformation criterion. For the vertical interlayers, this criterion is written in the form: $\varepsilon_{11} = \varepsilon_*$, where ε_* is the ultimate tensile strain. Until the destruction, when $\varepsilon_{11} < \varepsilon_*$, and at the contact of edges of the crack, which is already formed, deformation of the interlayer occurs according to the elastic–plastic law. Normal stress in the interlayer is continuous and satisfies the conditions of contact interaction. It is equal to zero in the opened crack, and it is negative in the case of contact. Tangential stress in the crack zone is absent if friction is not taking into account. Rheological scheme of the interaction of blocks after the formation of a crack is shown in Fig. 22.2.

Conditions of contact interaction of the crack edges are formulated as the variational inequality

$$\delta\sigma_{11} \left(\frac{1}{\rho'c_1'^2} \sigma_{11} - \varepsilon_{11} \right) \geq 0, \quad \dot{\varepsilon}_{11} = \frac{v_1^+ - v_1^-}{\delta_1}, \quad (22.7)$$

Fig. 22.2 Rheological scheme of contact interaction of blocks



with the constrains $\sigma_{11} \leq 0$ and $\tilde{\sigma}_{11} \equiv \sigma_{11} + \delta\sigma_{11} \leq 0$. If $\sigma_{11} < 0$, then the sign of the stress variation $\delta\sigma_{11}$ can be arbitrary; therefore, the inequality (22.7) goes into the equation of Hooke's law for the interlayer. This is fulfilled in the case of contact of the crack edges. If $\sigma_{11} = 0$, then, by virtue of the sign of variation $\delta\sigma_{11} \leq 0$, the condition $\varepsilon_{11} \geq 0$, corresponding to the state of opened crack, is fulfilled.

The algorithm of numerical implementation of the variational inequality (22.7) in the mesh of a finite difference grid is based on the equations:

$$\hat{\varepsilon}_{11} = \varepsilon_{11} + \frac{v_1^+ - v_1^-}{\delta_1} \tau, \quad z_1 v_1^+ + \sigma_{11}^+ = R_1^+, \quad z_1 v_1^- - \sigma_{11}^- = R_1^-, \quad (22.8)$$

where $z_1 = \rho c_1$ is the acoustic impedance, R_1^\pm are the Riemann invariants calculated in the border meshes of the interacting blocks. Hat over a symbol indicates that it belongs to a new layer by time. The first of equations (22.8) is obtained as a result of approximation of the equation for the strain rate, the others are relations on bicharacteristics of the system (22.1), which are used at the predictor step of the Godunov gap decay scheme.

Taking into account the closing equation: $\hat{\sigma}_{11} + \sigma_{11} = \sigma_{11}^+ + \sigma_{11}^-$, guaranteeing the absence of artificial dissipation in the Ivanov scheme, the inequality (22.7) can be reduced to the form:

$$(\tilde{\sigma}_{11} - \hat{\sigma}_{11}) \left(\kappa \hat{\sigma}_{11} - \varepsilon_{11} - \frac{R_1^+ - R_1^- - \sigma_{11}}{z_1 \delta_1} \tau \right) \geq 0, \quad \kappa = \frac{1}{\rho' c_1'^2} + \frac{\tau}{z_1 \delta_1}.$$

Hence, using elementary properties of variational inequalities, one can obtain a formula for stress correction in terms of the projection $\pi_-(\sigma) = (\sigma - |\sigma|)/2$ onto the semiaxis $\sigma \leq 0$:

$$\hat{\sigma}_{11} = \frac{1}{\kappa} \pi_-\left(\varepsilon_{11} + \frac{R_1^+ - R_1^- - \sigma_{11}}{z_1 \delta_1} \tau \right). \quad (22.9)$$

Application of this formula leads to automatic fulfillment at the discrete level of the condition of nonpenetration of crack edges into each other and the condition of positivity of a contact pressure. In addition, since the projector is a nonexpanding mapping, the stability condition of the finite difference scheme is preserved in the same form as for elastic or elastic-plastic interlayers without cracks.

Formula for recalculation of the transverse velocity in the uncracked interlayer is derived on the basis of the discrete equation of motion:

$$\rho' \frac{\hat{v}_1 - v_1}{\tau} = \frac{\sigma_{11}^+ - \sigma_{11}^-}{\delta_1},$$

the relations (22.9) on bicharacteristics and closing equation of a nondissipative scheme: $\hat{v}_1 + v_1 = v_1^+ + v_1^-$. It takes the following form:

$$\hat{v}_1 = \frac{(R_1^+ + R_1^-)\tau - (z_1\tau - \rho'\delta_1)v_1}{z_1\tau + \rho'\delta_1}. \quad (22.10)$$

After calculating \hat{v}_1 and $\hat{\sigma}_{11}$, the values of v_1^\pm and σ_{11}^\pm are determined as the solution of the system of equations:

$$\begin{aligned} v_1^+ + v_1^- &= \hat{v}_1 + v_1, & v_1^+ - v_1^- &= \frac{R_1^+ - R_1^- - \hat{\sigma}_{11} - \sigma_{11}}{z_1}, \\ \sigma_{11}^+ + \sigma_{11}^- &= \hat{\sigma}_{11} + \sigma_{11}, & \sigma_{11}^+ - \sigma_{11}^- &= R_1^+ + R_1^- - z_1(\hat{v}_1 + v_1). \end{aligned}$$

If $\hat{\sigma}_{11} = 0$, then the interlayer is divided by a crack into two noninteracting parts. Since the moment of crack generation, the stresses σ_{11}^\pm on the crack edges are zero. Edge velocities are found from the equations on bicharacteristics as $v_1^\pm = R_1^\pm/z_1$. Conditional velocity of the interlayer is calculated by the formula of inertial motion: $\hat{v}_1 = v_1$, which is consistent with (22.10).

Formulas for the calculation of cracks in the horizontal interlayers can be obtained by the cyclic replacement of indices in the formulas obtained above.

22.4 Elastic-Plastic Cosserat Continuum

Mathematical model of a blocky medium is easily generalized for the description of complex nonlinear mechanical factors such as a crack formation and fluid saturation in interlayers and can be effectively implemented numerically. But it is practically unsuitable for analytical research methods. It is impossible, for example, to obtain explicit expressions for the velocities of elastic and plastic waves, to apply a well-developed apparatus of dispersion analysis. Therefore, it is advisable to develop approaches to the description of the deformation and destruction of a blocky medium using the models of continuum mechanics. One of such models, taking into account rotational motions of the blocks, is the Cosserat model.

In the plane strain case, the equations of elastic Cosserat continuum have the following form [24]:

$$\begin{aligned} \rho_0 \dot{v}_1 &= \sigma_{11,1} + \sigma_{12,2}, \\ \rho_0 \dot{v}_2 &= \sigma_{21,1} + \sigma_{22,2}, \\ J_0 \dot{\omega}_3 &= \mu_{31,1} + \mu_{32,2} + \sigma_{21} - \sigma_{12}, \\ \dot{\sigma}_{11} &= a_1 v_{1,1} + b_1 v_{2,2}, \\ \dot{\sigma}_{22} &= a_1 v_{2,2} + b_1 v_{1,1}, \\ \dot{\sigma}_{21} &= a_2 (v_{2,1} - \omega_3) + b_2 (v_{1,2} + \omega_3), \\ \dot{\sigma}_{12} &= a_2 (v_{1,2} + \omega_3) + b_2 (v_{2,1} - \omega_3), \\ \dot{\mu}_{31} &= \alpha_2 \omega_{3,1}, \\ \dot{\mu}_{32} &= \alpha_2 \omega_{3,2}. \end{aligned} \quad (22.11)$$

They are written in Cartesian coordinates relative to the projections v_1, v_2 of the linear velocity vector, nonzero projection ω_3 of angular velocity, components σ_{jk} of the stress tensor and components μ_{jk} of the couple stress tensor ($j, k = 1, 2$). Here, ρ_0 is the density of the continuum, J_0 is the product of the moment of inertia of a particle (block) and a number of particles in a unit volume, a_1, b_1, a_2, b_2 and α_2 are the elastic moduli of an orthotropic material with planes of symmetry parallel to the coordinate planes. Elastic properties of the continuum are considered to be identical in the direction of the axes of coordinates, which corresponds to the model of a blocky medium with square blocks.

Constitutive equations for the stress rates can be represented in the reversed form:

$$\begin{aligned} \bar{a}_1 \dot{\sigma}_{11} - \bar{b}_1 \dot{\sigma}_{22} &= v_{1,1}, & \bar{a}_1 \dot{\sigma}_{22} - \bar{b}_1 \dot{\sigma}_{11} &= v_{2,2}, \\ \bar{a}_2 \dot{\sigma}_{21} - \bar{b}_2 \dot{\sigma}_{12} &= v_{2,1} - \omega_3, & \bar{a}_2 \dot{\sigma}_{12} - \bar{b}_2 \dot{\sigma}_{21} &= v_{1,2} + \omega_3, \end{aligned}$$

where $\bar{a}_1, \bar{b}_1, \bar{a}_2, \bar{b}_2$ are the moduli of elastic compliance of a material:

$$\bar{a}_1 = \frac{a_1}{a_1^2 - b_1^2}, \quad \bar{b}_1 = \frac{b_1}{a_1^2 - b_1^2}, \quad \bar{a}_2 = \frac{a_2}{a_2^2 - b_2^2}, \quad \bar{b}_2 = \frac{b_2}{a_2^2 - b_2^2}.$$

It allows to represent Eqs. (22.11) in the matrix form:

$$A \frac{\partial U}{\partial t} = B^1 \frac{\partial U}{\partial x_1} + B^2 \frac{\partial U}{\partial x_2} + Q U \tag{22.12}$$

with symmetric matrix-coefficients A, B^1, B^2 and antisymmetric matrix Q . When the inequalities

$$a_1 > |b_1|, \quad a_2 > |b_2|, \quad \alpha_2 > 0$$

are performed, the system of equations (22.12) belongs to the class of symmetric t -hyperbolic systems [8] and systems of thermodynamically consistent conservation laws [9, 10]. The system (22.12) is formulated with respect to the vector-function U , whose components $v_1, v_2, \omega_3, \sigma_{11}, \sigma_{22}, \sigma_{21}, \sigma_{12}, \mu_{31}, \mu_{32}$ are written in the column. Characteristic matrix of the system $n_1 B^1 + n_2 B^2 - c A$ is as follows:

$$\begin{bmatrix} -\rho_0 c & 0 & 0 & n_1 & 0 & 0 & n_2 & 0 & 0 \\ 0 & -\rho_0 c & 0 & 0 & n_2 & n_1 & 0 & 0 & 0 \\ 0 & 0 & -J_0 c & 0 & 0 & 0 & 0 & n_1 & n_2 \\ n_1 & 0 & 0 & -\bar{a}_1 c & \bar{b}_1 c & 0 & 0 & 0 & 0 \\ 0 & n_2 & 0 & \bar{b}_1 c & -\bar{a}_1 c & 0 & 0 & 0 & 0 \\ 0 & n_1 & 0 & 0 & 0 & -\bar{a}_2 c & \bar{b}_2 c & 0 & 0 \\ n_2 & 0 & 0 & 0 & 0 & \bar{b}_2 c & -\bar{a}_2 c & 0 & 0 \\ 0 & 0 & n_1 & 0 & 0 & 0 & 0 & -c/\alpha_2 & 0 \\ 0 & 0 & n_2 & 0 & 0 & 0 & 0 & 0 & -c/\alpha_2 \end{bmatrix}.$$

Setting c, n_1, n_2 as zeros and units, from this system one can express the symmetric matrix–coefficients. The antisymmetric matrix $Q = (q_{jk})$ is completely filled with zeros, except for its coefficients $q_{36} = -q_{63} = 1$ and $q_{37} = -q_{73} = -1$.

The characteristic equation $\det(n_1 B^1 + n_2 B^2 - c A) = 0$ has six nontrivial roots $c = \pm c_1, \pm c_2$ and $\pm c_3$, which determine three velocities of weak shock waves propagating in the direction of the unit vector (n_1, n_2) —longitudinal waves, transverse waves and waves of rotational motion:

$$c_1 = \sqrt{\frac{\lambda_1}{\rho_0}}, \quad c_2 = \sqrt{\frac{\lambda_2}{\rho_0}}, \quad c_3 = \sqrt{\frac{\alpha_2}{J_0}},$$

$$\lambda_{1,2} = \frac{a_1 + a_2}{2} \pm \sqrt{\left(\frac{a_1 - a_2}{2}\right)^2 (n_1^2 - n_2^2)^2 + (b_1 + b_2)^2 n_1^2 n_2^2},$$

and a triple zero root corresponding to the contact discontinuities.

Using the general approach developed in [20, 22], it is possible to construct a model of the elastic-plastic Cosserat continuum based on the system of equations (22.12) of the elasticity theory. Such model is formulated as a variation inequality:

$$(\tilde{U} - U) \cdot \left(A \frac{\partial U}{\partial t} - B^1 \frac{\partial U}{\partial x_1} - B^2 \frac{\partial U}{\partial x_2} - Q U \right) \geq 0, \quad \tilde{U}, U \in F. \quad (22.13)$$

Here, F is the set of admissible variations of the vector U , and \tilde{U} is an arbitrary element of F . The variational inequality is a formulation of the von Mises' principle of maximum power of plastic dissipation. The set F does not contain constraints on the velocity vector and angular velocity. The boundary of this set in the space of stresses and couple stresses is the yield surface of a material. If U lies inside F , then, due to the arbitrariness of variation, from (22.13) follows the system of equations (22.12) describing the elastic process. If U is a boundary point, then the associated law of plastic flow is fulfilled, in accordance with which the vector of plastic strain rate is directed along the outward normal to the boundary.

Since, within the framework of accepted model, the behavior of orthotropic continuum is completely determined by the deformation properties of the weakened interlayers of blocky structure, the yield criterion is used in the following form:

$$\begin{aligned} |\sigma_{21}| &\leq \tau_0 - \kappa_\tau \sigma_{11}, & |\sigma_{12}| &\leq \tau_0 - \kappa_\tau \sigma_{22}, \\ |\mu_{31}| &\leq \mu_0 - \kappa_\mu \sigma_{11}, & |\mu_{32}| &\leq \mu_0 - \kappa_\mu \sigma_{22}. \end{aligned} \quad (22.14)$$

In this criterion, τ_0 and μ_0 are the yield limits of a material of interlayers under shear and bending, and κ_τ and κ_μ are the phenomenological coefficients taking into account the increase in elastic properties under the action of compressive stresses. The normal stresses σ_{11} and σ_{22} are involved in (22.14) as unvariable hardening parameters of

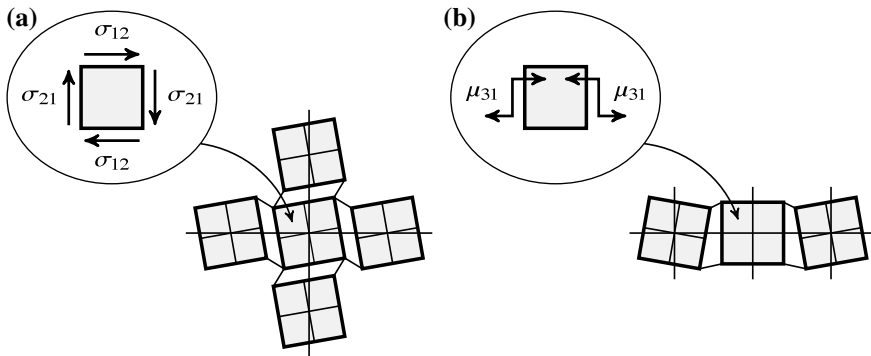


Fig. 22.3 Scheme of action of tangential stresses caused by rotations of the blocks (a), scheme of couple-stressed interactions (b)

a material. In the case of positive (tensile) normal stresses, the condition of plasticity makes sense only until the moment of separation, when the yield limits, decreasing with increase in stresses, become equal to zero.

The yield criterion limits the tangential components of the nonsymmetric stress tensor, which characterizes shear along the interlayers. This criterion also limits the couple stresses, and when their limit values are achieved, it leads to an irreversible change in the curvature characteristics of the deformed state of the continuum.

Transition to the plastic state occurs as one or more equalities in (22.14) are achieved. Figure 22.3 shows two schemes explaining the meaning of this criterion. The first of them illustrates how, due to the rotation of particles in the interlayers, the reaction forces arise that violate the symmetry of the stress tensor. Judging by this scheme, tangential stresses in the Cosserat continuum are caused by two factors—shear strain and rotation of particles.

Both factors influence the transition to plasticity; therefore, in the first line of inequalities (22.14) two tangential stresses are present independently. If the rotation field is nonuniform, then, as shown in the second scheme, couple stresses occur, which are taken into account in the second line of (22.14).

22.5 Results of Computation

The methods of solution of dynamic problems for a blocky medium and for the Cosserat continuum were implemented as software packages in the Fortran language by means of the MPI library. Technology of parallelization is based on the uniform distribution of computational domain between the nodes of a cluster. Two-dimensional decomposition of computational domain is used for the considered problems. Each node of a cluster on each time step performs similar computations consisting of mutually coordinated step-by-step realization of the space-variable splitting

method. The exception is represented by the processes which, in addition, perform the pasting together of solutions on the inner boundaries of blocks. Data interchange between the processes is carried out at the predictor step of the finite difference scheme on stages of the two-cyclic splitting method. Parallel programs were registered in Rospatent [25, 27].

The developed program codes were applied to solve a series of problems related to the waves propagation in a blocky medium under intensive loads. In the plane strain approximation, the destruction of a vertical brick wall, whose length is 20 m and height is 10 m, with weakened connecting seams was simulated due to a pulse action through a loading platform of width 5 m on the upper boundary. Figures 22.4, 22.5 and 22.6 demonstrate the stress fields in the blocks, zones of plasticity and zones of fracture in the interlayers, which vary as soon as the head wave passes through blocks and reflects from interlayers, for three successive time moments. U -shaped pulse of pressure $p_0 = 500$ MPa, uniformly distributed over the contact surface, acted for the time $t_0 = 0.5$ ms. Lateral sides of the brick wall were considered as free of stresses. At the lower boundary, conditions of adhesion with an absolutely rigid foundation were set. Besides the uniformly distributed pressure, the case of a linear distribution of $p(x_1) = p_0 + \kappa_p(x_1 - x_1^0)/l$ with different values of κ_p was considered separately, simulating the rotation of the platform around the middle point x_1^0 of the upper side of the wall. Computations were performed for blocks of the size $0.1 \text{ m} \times 0.1 \text{ m}$ and interlayers of the thickness $\delta = 1 \text{ mm}$ with the parameters: $\rho = 3700 \text{ kg/m}^3$, $c_1 = 3500$, $c_2 = 2100 \text{ m/s}$ (for blocks) and $\rho' = 1200 \text{ kg/m}^3$, $c'_1 = 1500$, $c'_2 = 360 \text{ m/s}$, $\tau_s = 0.86 \text{ MPa}$, $\kappa_s = 0$, $\varepsilon_* = 3\%$ (for interlayers). The considered brick wall consisted of 200×100 square blocks. Each block was covered by a grid of 20×20 meshes.

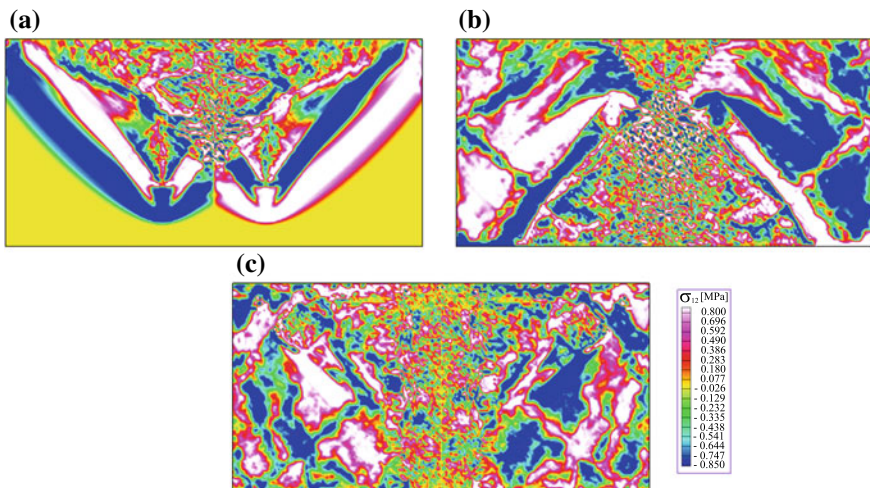


Fig. 22.4 Level curves of tangential stress σ_{12} under U -shaped pulse loading at different time moments: $t = 2.7$ ms (a), 5.4 ms (b) and 8.1 ms (c)

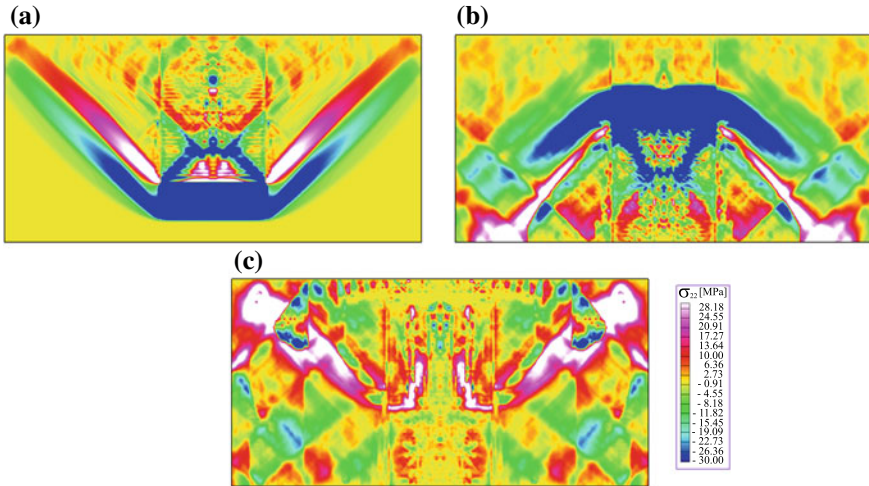


Fig. 22.5 Level curves of normal stress σ_{22} under *U*-shaped pulse loading at different time moments: $t = 2.7$ ms (a), 5.4 ms (b) and 8.1 ms (c)

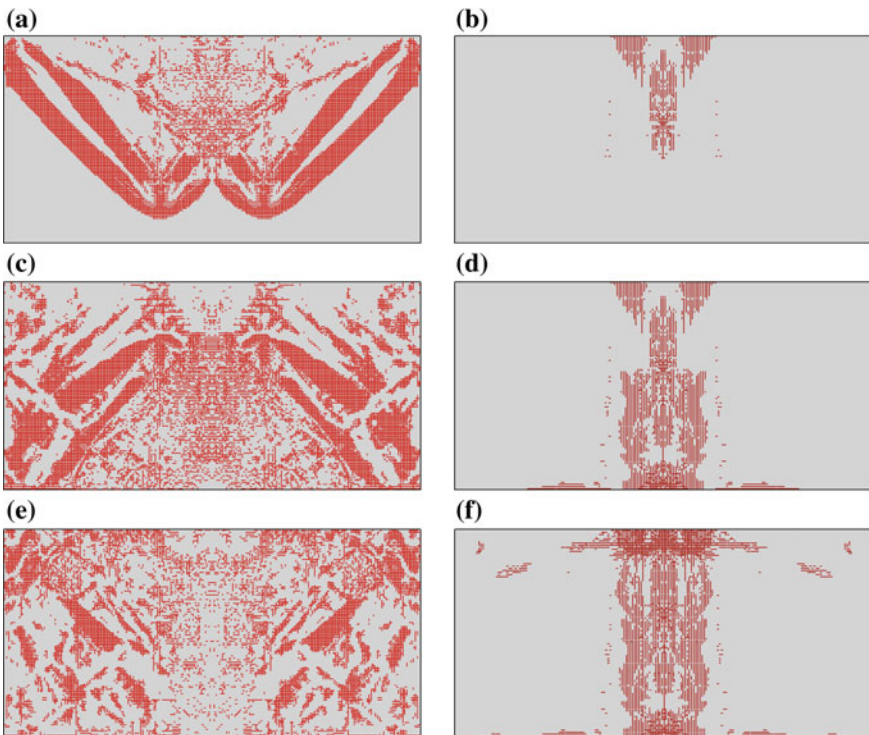


Fig. 22.6 Configuration of plastic zones (a, c, e) and of fracture zones (b, d, f) under *U*-shaped pulse loading at different time moments: $t = 2.7$ ms (a, b), 5.4 ms (c, d) and 8.1 ms (e, f)

The clusters of the MVS series of the Institute of Computational Modeling SB RAS (Krasnoyarsk) and the Joint Supercomputer Center of the Russian Academy of Sciences (Moscow) were used for computations.

For a linear pressure profile, the pattern of distribution of plastic zones remains approximately the same as for uniform distribution, but the fracture zones change significantly. Due to the rotational motion of a medium under platform, cracks develop near the region of maximum pressure.

Computations were also performed for a Δ -shaped pulse in time variable with the same action time and twice pressure (in order to preserve constant integral momentum of the load). Characteristic difference of the results is that the cracks originate in the middle of the wall and their number practically does not grow with time (see Fig. 22.7).

For comparison, the problem of loading the brick wall by U -shaped pressure pulse without fractures was solved. Numerical results are represented in Figs. 22.8, 22.9 and 22.10. The difference from Figs. 22.4, 22.5, 22.6 and 22.7 is that in intact material there is no fine-dispersed diffraction of waves, and therefore, their reflection from the upper side of the wall, as from a free surface, is more clearly seen.

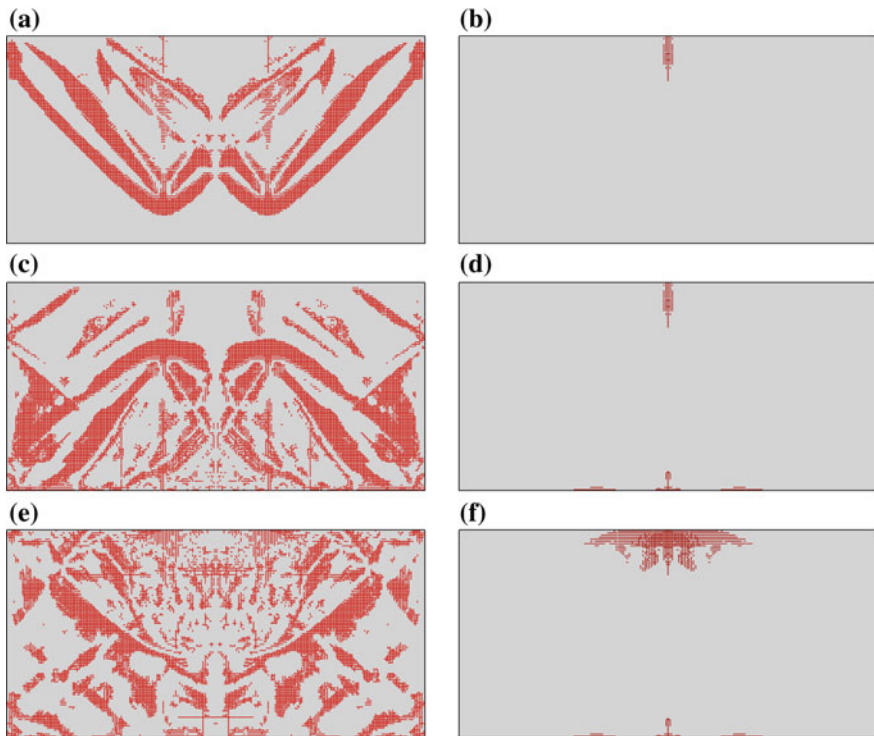


Fig. 22.7 Configuration of plastic zones (a, c, e) and of fracture zones (b, d, f) under Δ -shaped pulse loading at different time moments: $t = 2.7$ ms (a, b), 5.4 ms (c, d) and 8.1 ms (e, f)

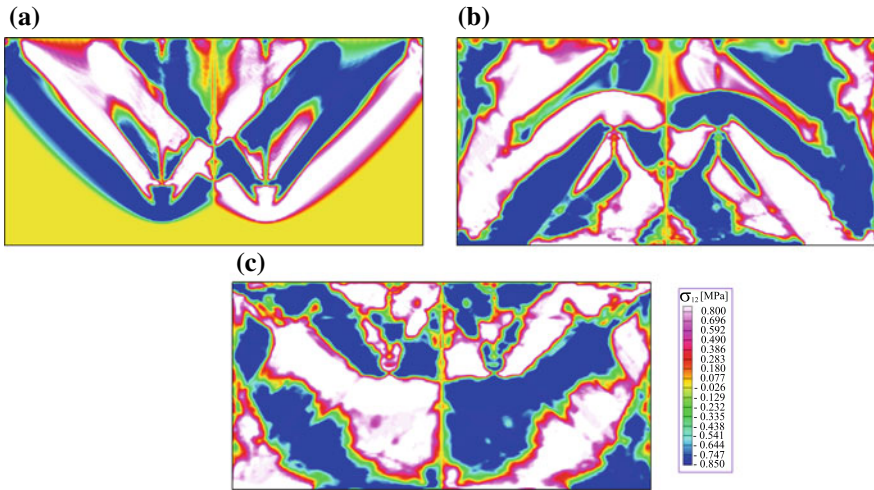


Fig. 22.8 Level curves of tangential stress σ_{12} without fractures under *U*-shaped pulse loading at different time moments: $t = 2.7$ ms (a), 5.4 ms (b) and 8.1 ms (c)

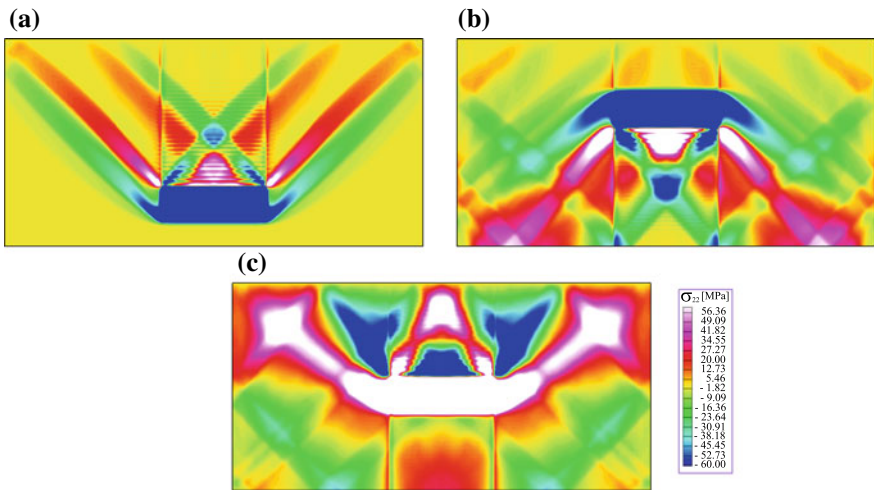


Fig. 22.9 Level curves of normal stress σ_{22} without fractures under *U*-shaped pulse loading at different time moments: $t = 2.7$ ms (a), 5.4 ms (b) and 8.1 ms (c)

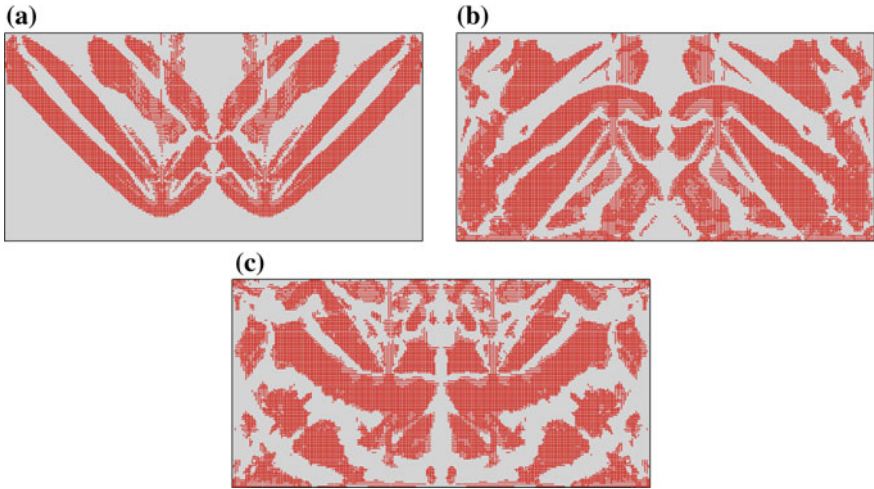


Fig. 22.10 Configuration of plastic zones without fractures under U -shaped pulse loading at different time moments: $t = 2.7$ ms (a), 5.4 ms (b) and 8.1 ms (c)

In general, computations have shown that the pulse shape as a function of time and the distribution of pressure under the platform have a significant influence on the cracking pattern, although the stress state, including the configuration of plasticity zones, varies only slightly.

The considered problems of wave propagation in the brick wall (with and without fractures) are pure methodological, they are not correspond to any real situation. The main goal was to compare the results obtained using the blocky medium model and the Cosserat continuum theory.

In Figs. 22.11, 22.12 and 22.13, one can see the results of computations, obtained within the framework of model of the elastic-plastic Cosserat continuum.

A rather fine grid of 500×250 meshes was used, the size of which is consistent with the characteristic linear scale $r_0 = \sqrt{6J_0/\rho_0} \approx 0.1$ m of the material microstructure in the sense that this size of particles corresponds to approximately five meshes of the grid. For reliability, the results were recalculated on a half finer grid. No major changes were detected.

The mechanical parameters given in Table 22.1 from [24] for the same blocky material were used in computations. Here, c_1'' , c_2'' , c_3'' are the velocities of elastic waves for the Cosserat continuum in the coordinate directions. The shear and bending yield limits were assumed to be 0.86 MPa and 8.8 kPa m, respectively. Material hardening due to the compression was not taken into account. Yield limits are two orders of magnitude lower than the maximum stresses in the elastic problem. In fact, the ratio of yield limits, which primarily depends on the mechanical properties of material of the seams, can vary over a wide range. Therefore, to analyze the influence on the deformation process of various factors such as shear deformations and curvature

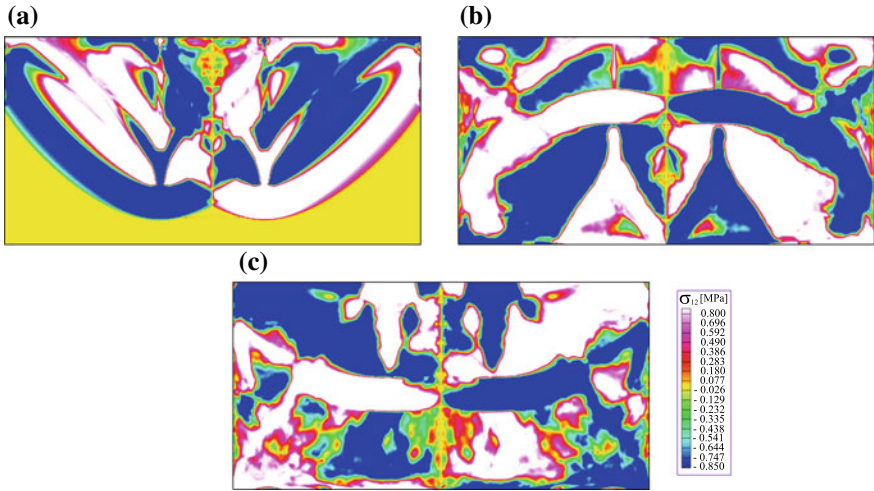


Fig. 22.11 Level curves of tangential stress σ_{12} for the Cosserat continuum: $t = 2.7$ ms (a), 5.4 ms (b) and 8.1 ms (c)

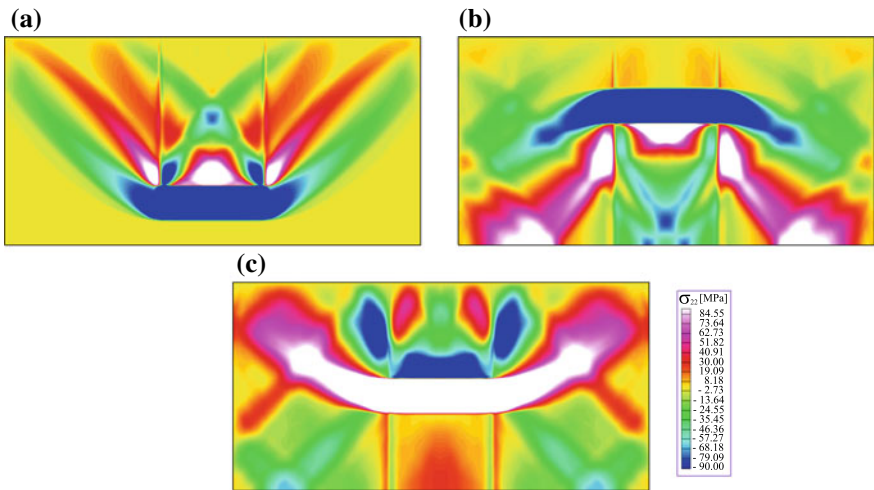


Fig. 22.12 Level curves of normal stress σ_{22} for the Cosserat continuum: $t = 2.7$ ms (a), 5.4 ms (b) and 8.1 ms (c)

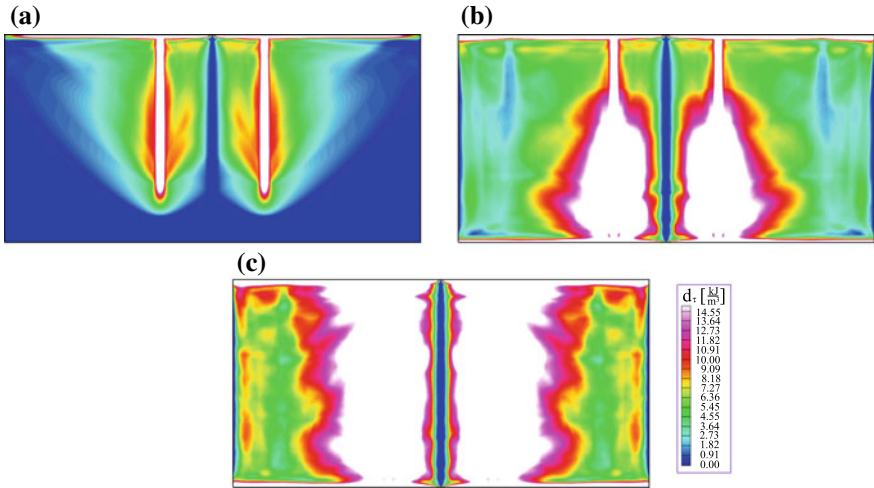


Fig. 22.13 Level curves of energy of plastic dissipation for the Cosserat continuum: $t = 2.7$ ms (a), 5.4 ms (b) and 8.1 ms (c)

Table 22.1 Mechanical parameters of the Cosserat continuum

δ , mm	ρ_0 , kg/m ³	J_0 , kg/m	a_1 , GPa	b_1 , GPa	a_2 , GPa	b_2 , GPa	α_2 , MN	c''_1 , m/s	c''_2 , m/s	c''_3 , m/s
0.1	3690	6.15	44.5	19.1	14.8	6.77	22.2	3470	2000	1900
1.0	3650	6.05	38.6	16.5	6.46	4.05	9.60	3250	1330	1260
5.0	3470	5.59	23.8	10.2	2.33	0.53	3.39	2620	820	780

characteristics, one of the two yield limits was assigned the value exceeding the level of elastic stresses.

In Figs. 22.11, 22.12 and 22.13, the stress fields and the configuration of plastic zones are depicted. Comparison with Figs. 22.8, 22.9 and 22.10 shows a good qualitative and even quantitative correspondence of the results obtained by the model of a discrete-continuous blocky medium and by the model of a continuum. As a hypothesis, we may suggest that the formation and growth of cracks in a blocky medium can be modeled on the basis of equations of the elastic-plastic Cosserat continuum by means of adequately specifying the parameter κ_μ in the criterion of plasticity (22.14) to describe the separation effect. Testing this hypothesis requires computations of many variants of the problem on the selection of the parameter, which is beyond the scope of this chapter.

22.6 Concluding Remarks

To study wave processes in structurally inhomogeneous media, a discrete-continuous model of a blocky structure composed of elastic blocks interacting through thin compliant elastic-plastic interlayers is proposed. In this model, the deformation of blocks is simulated on the basis of a system of equations of dynamic theory of elasticity. In interlayers, the simplified physically nonlinear governing relations thermodynamically consistent with the main system are used. Alternative approach is developed based on the model of the orthotropic Cosserat continuum, taking into account plastic deformation of a material and independent rotations of the particles (blocks). Comparative analysis of these models using supercomputer technologies in solving the problem of pulse loading of a brick wall showed that by appropriate choosing the mechanical parameters of the Cosserat continuum, it is possible to achieve correspondence of the results both on qualitative and quantitative levels. The model of a blocky medium is generalized for the description of crack formation in the interlayers. It is also suitable for taking into account the more complex effects of the porosity of the interlayers and fluid saturation in combination with the destruction due to the pore pressure and deformation processes caused by the external influence. Developed computational algorithms and software can be used to test the adequacy of the formulas for calculating the parameters of the Cosserat continuum of blocky-layered structures obtained as a result of using the homogenization procedures.

References

1. Aleksandrova, N.I., Chernikov, A.G., Sher, E.N.: Experimental investigation into the one-dimensional calculated model of wave propagation in block medium. *J. Min. Sci.* **41**(3), 232–239 (2005)
2. Ayzenberg-Stepanenko, M.V., Sher, E.N.: Modeling of wave phenomena in periodic structures. *Fiz. Mezomekh.* **10**(1), 47–57 (2007)
3. Azevedo, J., Sincraian, G., Lemos, J.V.: Seismic behavior of blocky masonry structures. *Earthq. Spectra* **16**(2), 337–365 (2000)
4. Boutin, C., Hans, S.: Homogenization of periodic discrete medium: application to dynamics of framed structures. *Comput. Geotech.* **30**(4), 303–320 (2003)
5. Brekhovskikh, L.M.: *Waves in Layered Media*, Applied Mathematics and Mechanics, vol. 16. Academic Press, New York, London (1980)
6. Cecchi, A., Sab, K.: Out of plane model for heterogeneous periodic materials: the case of masonry. *Eur. J. Mech. A/Solids* **21**(5), 715–746 (2002)
7. Erofeev, V.I.: *Wave Processes in Solids with Microstructure*. Series on Stability, Vibration and Control of Systems, Series A, vol. 8. World Scientific Publishing, New Jersey (2003)
8. Friedrichs, K.O.: Symmetric hyperbolic linear differential equations. *Commun. Pure Appl. Math.* **7**(2), 345–392 (1954)
9. Godunov, S.K.: *Elementy Mekhaniki Sploshnoi Sredy* (Elements of Continuum Mechanics). Nauka, Moscow (1978)
10. Godunov, S.K., Romenskii, E.I.: *Elements of Continuum Mechanics and Conservation Laws*. Kluwer Academic/Plenum Publishers, New York (2003)
11. Goldin, S.V.: *Seismicheskie Volny v Anizotropnykh Sredakh* (Seismic Waves in Anisotropic Media). SB RAS Publishing, Novosibirsk (2008)

12. Grekova, E.F.: Nonlinear isotropic elastic reduced Cosserat continuum as a possible model for geomedium and geomaterials. Spherical prestressed state in the semilinear material. *J. Seismol.* **16**(4), 695–707 (2012)
13. Ivanov, G.V., Volchkov, Y.M., Bogulskii, I.O., Anisimov, S.A., Kurguzov, V.D.: *Chislennoe Reshenie Dinamicheskikh Zadach Uprugoplasticheskogo Deformirovaniya Tverdykh Tel* (Numerical Solution of Dynamic Elastic-Plastic Problems of Deformable Solids). Sibirskoe Universitetskoe Izdatelstvo, Novosibirsk (2002)
14. Kunin, I.A.: *Elastic Media with Microstructure II: Three-Dimensional Models*, Solid-State Sciences, vol. 44. Springer, Berlin (1983)
15. Lemos, J.V.: Discrete element modeling of masonry structures. *Int. J. Archit. Herit.* **1**(2), 190–213 (2007)
16. Lourenço, P.B., Milani, G., Tralli, A., Zucchini, A.: Analysis of masonry structures: review of and recent trends in homogenization techniques. *Can. J. Civ. Eng.* **34**(11), 1443–1457 (2007)
17. Molotkov, L.A., Khilo, A.E.: Single-phase and multiphase effective models describing periodic media. *J. Math. Sci.* **32**(2), 173–185 (1986)
18. Nikitin, I.S.: Dynamic models of layered and block media with slip, friction, and separation. *Mech. Solids* **43**(4), 652–661 (2008)
19. Pasternak, E., Dyskin, A.: Measuring of Cosserat effects and reconstruction of moduli using dispersive waves. In: Maugin, G.A., Metrikine, A.V. (eds.) *Mechanics of Generalized Continua: One Hundred Years After the Cosserat*, Advanced in Mechanics and Mathematics, vol. 21, pp. 71–78. Springer, Heidelberg (2010)
20. Sadovskaya, O., Sadovskii, V.: Mathematical modeling in mechanics of granular materials. In: Altenbach, H. (ed.) *Advanced Structured Materials*, vol. 21. Springer, Heidelberg (2012)
21. Sadovskii, M.A.: Natural lumpiness of a rock. *Dokl. Akad. Nauk SSSR* **247**(4), 829–831 (1979)
22. Sadovskii, V.M.: *Razryvnye Resheniya v Zadachakh Dinamiki Uprugoplasticheskikh Sred* (Discontinuous Solutions in Dynamic Elastic-Plastic Problems). Fizmatlit, Moscow (1997)
23. Sadovskii, V.M., Guzev, M.A., Sadovskaya, O.V., Qi, C.: Modeling of plastic deformation based on the theory of an orthotropic Cosserat continuum. *Fiz. Mezomekh.* **22**(2), 59–66 (2019)
24. Sadovskii, V.M., Sadovskaya, O.V.: Modeling of elastic waves in a blocky medium based on equations of the Cosserat continuum. *Wave Motion* **52**, 138–150 (2015)
25. Sadovskii, V.M., Sadovskaya, O.V., Chentsov, E.P.: Parallel program system for numerical modeling of dynamic processes in multi-blocky media on cluster systems (2Dyn_Blocks_MPI): certificate of state registration of computer program no. 2016615178. In: RU OBPBT, vol. 6(116). FIPS, Moscow (2016)
26. Sadovskii, V.M., Sadovskaya, O.V., Lukyanov, A.A.: Modeling of wave processes in blocky media with porous and fluid-saturated interlayers. *J. Comput. Phys.* **345**, 834–855 (2017)
27. Sadovskii, V.M., Sadovskaya, O.V., Varygina, M.P.: Parallel program system for the solution of 2D dynamic problems of the Cosserat elasticity theory (2Dyn_Cosserat): certificate of state registration of the computer program no. 2012614823. In: RU OBPBT, vol. 3(80), p. 415. FIPS, Moscow (2012)
28. Saraikin, V.A., Chernikov, A.G., Sher, E.N.: Wave propagation in two-dimensional block media with viscoelastic layers (theory and experiment). *J. Appl. Mech. Tech. Phys.* **56**(4), 688–697 (2015)

Chapter 23

Structural and Micropolar Beam Models of Nanocrystalline Materials (One-Dimensional Case)



Samvel H. Sargsyan

Abstract In the present paper, linear atomic chain is studied. It is assumed that there is a non-central force and moment interaction between the atoms of the chain. The discrete model of the chain is constructed with the main equations and Hamilton principle. Further, the limit procedure to the continual (beam) model is performed. It is shown that the continual (beam) model of the linear chain of atoms is identical to the applied beam model, which is constructed based on the moment (micropolar) theory of elasticity. Elastic constants of the micropolar beam are determined through the elastic parameters of the discrete model of the linear chain of atoms.

Keywords Linear chain of atoms · Discrete · Continual-moment model · Beam-applied model · Moment elasticity · Elastic parameters

23.1 Introduction

In connection with the development of nanotechnology, mathematical modeling of carbon materials (nanotube, graphene, etc.) is of great interest. The molecular dynamics method is the most common one to study atomic or molecular systems of larger sizes [1, 2]. In computational nanotechnologies, the molecular dynamics method (in case of static problems—the molecular mechanics method) allows to calculate new and perspective materials at the atomic–molecular level and creates nanomaterials with required physical–mechanical properties.

It should be noted that in recent decades, methods of mechanics of a deformable solid body are widely used for modeling the nanomaterials. For example [3], during the calculation of the stress–strain state of nanotubes, the classical theory of elastic thin shells without consideration of the microstructure of the material is used. In other cases, by using the theory of elastic shells [4, 5], the elastic modules of the shell are determined as a result of studying a discrete model where only the force interaction between the tube-forming atoms is taken into account. However, [6–8], the existence of a single-layer nanotube and grapheme speaks about the need to take

S. H. Sargsyan (✉)
Shirak State University, Gyumri, Armenia

© Springer Nature Switzerland AG 2020
H. Altenbach et al. (eds.), *Nonlinear Wave Dynamics of Materials and Structures*, Advanced Structured Materials 122,
https://doi.org/10.1007/978-3-030-38708-2_23

into account the moment interaction between atoms (otherwise, the atomic layer, forming the nanotube or grapheme, would not have flexural rigidity, which is not true).

On the other hand, it is known that, in principle, it is impossible to define the thickness of nanomaterials (nanotube, graphene, etc.). Despite this fact, to study nanotubes or graphene, both the above-mentioned shell models [3–5] and the beam models, constructed in papers [9–15], contain the concept of their thickness. From this point of view, it is important to construct such mechanical models; in this case “beam” ones, which, on the one hand, would take into account the moment interactions between the atoms of the nanomaterial and, on the other hand, would not use the concept of their thickness.

In this paper, based on consideration of non-central force and moment interaction between atoms, a discrete model of a nanocrystalline chain of atoms is constructed and, further, by performing limit passage, its continuous one-dimensional (“beam”) model is constructed, where the thickness of the “beam” plays no role. In this micropolar “beam” continual model, all elastic constants are expressed by the parameters of the atomic discrete model of the considered chain.

Taking into account that in [16, 17], the simple, physically understandable, and illustrative one-dimensional model of a micropolar elastic beam, where (in case of free vibrations) the concept of the thickness of this beam does not participate, is constructed. Using the asymptotic method, the elastic constants of the micropolar beam are determined through the parameters of the atomic discrete model of the chain by comparing with the continuous “beam” model of the atomic chain.

23.2 Discrete-Moment Model of the Atom Chain. Hamilton’s Principle

A polyatomic molecule is considered, when atoms (with the same mass and moment of inertia) of the given molecule are located with an equal interval a along one straight line (such molecule is called a linear or atomic chain). Let the axis x be located on this straight line. We will take into account the interaction of each atom only with its nearest neighbors. The acting forces and moments on the atom with the number k from the neighboring atoms with the numbers $k-1$ and $k+1$ are noted as follows. Since the mentioned forces are of non-central nature, components along the axis x are marked with a letter N components along the axis y —with a letter Q the moments—with a letter L . The movement of the atoms of the chain runs in a plane xy (longitudinal deformation—along the axis x , bending deformation—along the axis y).

The motion equations of the atom with the number k as a body-point [18] will be expressed as follows (free oscillations are considered):

$$N^{(k+1)} - N^{(k)} = m \frac{\partial^2 u_1^{(k)}}{\partial t^2}, \quad (23.1)$$

$$\begin{aligned} Q^{(k+1)} - Q^{(k)} &= m \frac{\partial^2 u_2^{(k)}}{\partial t^2}, L_3^{(k+1)} - L_3^{(k)} + Q^{(k)} \frac{1}{2} a \\ &+ Q^{(k+1)} \frac{1}{2} a = I_3 \frac{\partial^2 \omega_3^{(k)}}{\partial t^2}. \end{aligned} \quad (23.2)$$

Here, m and I_3 are the mass and moment of inertia of each atom, $N^{(k)}$ —the longitudinal force, $Q^{(k)}$ —the shear force, $L_3^{(k)}$ —the bending moment, $(u_1^{(k)}, u_2^{(k)})$ —the components of displacement vector of the atom with the number k , $\omega_3^{(k)}$ —the free rotation of the k th atom around the axis z . In the second equation from the system (23.2), (i.e., in the equation of moments) for shear forces, $Q^{(k)}$ and $Q^{(k+1)}$ middle points between neighboring atoms are taken as points of their application.

In the literature (e.g., [11]), expressions for the potential energy of many molecules are well known in the linear approximation (i.e., if we accept that the elastic forces and moments depend on the deformation displacements and rotations by the linear law). This expression for the considered chain of atoms can be written as follows:

$$V = \frac{1}{2} \sum_k C_1 (d_1^{(k)})^2 + \frac{1}{2} \sum_k C_2 (d_2^{(k)})^2 + \frac{1}{2} \sum_k C_3 (\theta^{(k)})^2, \quad (23.3)$$

where C_i , $i = 1, 2, 3$ —are the elastic constants for the corresponding deformations (longitudinal or bending), $d_1^{(k)}$ —longitudinal relative displacements, $d_2^{(k)}$ —relative bending linear displacements, $\theta^{(k)}$ —relative angular free displacements, i.e.,

$$\begin{aligned} d_1^{(k)} &= u_1^{(k+1)} - u_1^{(k)}, d_2^{(k)} = u_2^{(k+1)} - u_2^{(k)} - \frac{1}{2} a (\omega_3^{(k+1)} + \omega_3^{(k)}), \\ \theta^{(k)} &= \omega_3^{(k+1)} - \omega_3^{(k)}. \end{aligned} \quad (23.4)$$

The expression of the potential energy (23.3) is usually used to calculate the vibration spectra of polyatomic molecules, and the elastic constants C_i ($i = 1, 2, 3$) can be considered as known in advance (experimentally) for many molecules [14].

It is easy to see, that

$$\begin{aligned} N^{(k+1)} - N^{(k)} &= -\frac{\partial V}{\partial u_1^{(k)}}, Q^{(k+1)} - Q^{(k)} = -\frac{\partial V}{\partial u_2^{(k)}}, \\ L_3^{(k+1)} - L_3^{(k)} &= -\frac{\partial V}{\partial \omega_3^{(k)}}. \end{aligned} \quad (23.5)$$

Thus, Hooke's law for the considered linear molecule can be written as follows:

$$N^{(k)} = C_1(u_1^{(k)} - u_1^{(k-1)}), \quad (23.6)$$

$$\begin{aligned} Q^{(k)} &= C_2 \left[(u_2^{(k)} - u_2^{(k-1)}) - \frac{1}{2}a(\omega_3^{(k)} + \omega_3^{(k-1)}) \right], \\ L_3^{(k)} &= C_3(\omega_3^{(k)} - \omega_3^{(k-1)}). \end{aligned} \quad (23.7)$$

Thus, the discrete model (molecular dynamics model) for the considered linear molecule is constructed: In the case of longitudinal oscillations, this is the motion Eq. (23.1) and the elasticity law (23.6) and in the case of bending oscillations, this is the motion Eq. (23.2) and the elasticity law (23.7).

For the considered linear molecule, the kinetic energy will have the following expression:

$$K = \frac{1}{2} \sum_k \left[m \left(\frac{du_1^{(k)}}{dt} \right)^2 + m \left(\frac{du_2^{(k)}}{dt} \right)^2 + I_3 \left(\frac{d\omega_3^{(k)}}{dt} \right)^2 \right]. \quad (23.8)$$

From the expressions (23.3), (23.4), and (23.8), the Lagrangian L for the considered linear molecule is equal to

$$\begin{aligned} L = K - V &= \frac{1}{2} \sum_k \left\{ \left[m \left(\frac{du_1^{(k)}}{dt} \right)^2 + m \left(\frac{du_2^{(k)}}{dt} \right)^2 + I_3 \left(\frac{d\omega_3^{(k)}}{dt} \right)^2 \right] \right. \\ &\quad \left. - \left\{ C_1(u_1^{(k+1)} - u_1^{(k)})^2 + C_2 \left[u(u_2^{(k+1)} - u_2^{(k)}) - \frac{1}{2}a(\omega_2^{(k+1)} + \omega_2^{(k)}) \right]^2 \right. \right. \\ &\quad \left. \left. + C_3(\omega_3^{(k+1)} - \omega_3^{(k)})^2 \right\} \right\}, \end{aligned} \quad (23.9)$$

and the Hamilton's principle will be expressed as follows:

$$\delta \int_{t_1}^{t_2} L dt = \delta \int_{t_1}^{t_2} (K - V) dt = 0. \quad (23.10)$$

It is easy to see that the Euler–Lagrange equations, obtained from the Hamilton principle (23.10) (with consideration of (23.9)) are the motion Eqs. (23.1) and (23.2).

23.3 One-Dimensional (“Bending”) Continual Model of Linear Chain of Atoms. Hamilton’s Principle for the Continual Model

To construct a continual model of a linear molecule, the Lagrangian of the discrete model (23.9) will be presented in the following form:

$$\begin{aligned}
 L = \frac{1}{2} \sum_k a \left\{ \left[\frac{m}{a} \left(\frac{du_1^{(k)}}{dt} \right)^2 + \frac{m}{a} \left(\frac{du_2^{(k)}}{dt} \right)^2 + \frac{I_3}{a} \left(\frac{d\omega_3^{(k)}}{dt} \right)^2 \right] \right. \\
 \left. - \left\{ C_1 a \left(\frac{u_1^{(k+1)} - u_1^{(k)}}{a} \right)^2 + C_2 a \left[\frac{u_3^{(k+1)} - u_3^{(k)}}{a} - \frac{1}{2} (\omega_3^{(k+1)} + \omega_3^{(k)}) \right]^2 \right. \right. \\
 \left. \left. + C_3 a \left(\frac{\omega_3^{(k+1)} - \omega_3^{(k)}}{a} \right)^2 \right\} \right\} \quad (23.11)
 \end{aligned}$$

The special form, in which the Lagrangian of the discrete model (23.9) is written, is chosen for the convenience of limit transition to the case of a continual (continuous) model, i.e., when $a \rightarrow 0$.

Regarding the multiplier a , which stands under the sum in front of the big brackets in formula (23.11), it should be replaced by $\Delta x = dx$, and the summation by k should be replaced by the integral by x . Further, it is clear that the index k , characterizing the number of the atom, should turn into a continuous coordinate x , when moving to the continual model. Therefore, instead of variables $u_1^{(k)}(t)$, $u_2^{(k)}(t)$ and $\omega_3^{(k)}(t)$, we will now have variables $u(x, t)$, $w(x, t)$ and $\Omega(x, t)$. As for the quantities $C_i \cdot a$, $i = 1, 2, 3$, we will see below that their limiting values, when $a \rightarrow 0$, are constant, which will be noted as follows:

$$C_i \cdot a, = \tilde{C}_i, \quad i = 1, 2, 3. \quad (23.12)$$

Acting in the above-mentioned way because of the passage to the limit, when $a \rightarrow 0$, Eq. (23.11) turns into a Lagrangian of continuum model, for which we will have:

$$\begin{aligned}
 L = \frac{1}{2} \int_0^\ell \left\{ \left[\tilde{\rho} \left(\frac{\partial u}{\partial t} \right)^2 + \tilde{\rho} \left(\frac{\partial w}{\partial t} \right)^2 + \tilde{I} \left(\frac{\partial \Omega}{\partial t} \right)^2 \right] \right. \\
 \left. - \left(\tilde{C}_1 \varepsilon_x^2 + \tilde{C}_2 \gamma^2 + \tilde{C}_3 \chi^2 \right) \right\} dx. \quad (23.13)
 \end{aligned}$$

Here

$$\varepsilon_x = \frac{\partial u}{\partial x} = \lim_{a \rightarrow 0} \frac{u_1^{(k+1)} - u_1^{(k)}}{a}, \quad (23.14)$$

$$\gamma = \frac{\partial w}{\partial x} - \Omega = \lim_{a \rightarrow 0} \left[\frac{u_2^{(k+1)} - u_2^{(k)}}{a} - \frac{1}{2} \left(\omega_3^{(k+1)} + \omega_3^{(k)} \right) \right], \quad (23.15)$$

$$\chi = \frac{\partial \Omega}{\partial x} = \lim_{a \rightarrow 0} \frac{\omega_3^{(k+1)} - \omega_3^{(k)}}{a}, \quad (23.16)$$

$$\tilde{\rho} = \lim_{a \rightarrow 0} \frac{m}{a}, \quad \tilde{I} = \lim_{a \rightarrow 0} \frac{I}{a}, \quad (23.17)$$

$\tilde{\rho}$ —is the linear density of the chainmass, \tilde{I} —the linear density of its moment of inertia, ε_x —the relative longitudinal deformation, γ —shear deformation, and χ —the curvature of the chain.

To obtain the motion equation, the elasticity and geometric relations for the continual model, the motion Eqs. (23.1), (23.2), and the elasticity relation (23.7) are expressed as follows:

Motion equation

$$\frac{N^{(k+1)} - N^{(k)}}{\alpha} = \frac{m}{a} \frac{\partial^2 u_1^{(k)}}{\partial t^2}, \quad (23.18)$$

$$\begin{aligned} \frac{Q^{(k+1)} - Q^{(k)}}{\alpha} &= \frac{m}{a} \frac{\partial^2 u_2^{(k)}}{\partial t^2}, \\ \frac{L_3^{(k+1)} - L_3^{(v)}}{\alpha} + \frac{1}{2} Q^{(k)} + \frac{1}{2} Q^{(k+1)} &= \frac{I_3}{a} \frac{\partial^2 \omega_3^{(k)}}{\partial t^2} \end{aligned} \quad (23.19)$$

Elasticity relations

$$N^{(k)} = c_1 a \frac{u_1^{(k)} - u_1^{(k-1)}}{a}, \quad (23.20)$$

$$\begin{aligned} Q^{(k)} &= c_2 a \left[\frac{u_2^{(k)} - u_2^{(k-1)}}{a} - \frac{1}{2} \left(\omega_3^{(k)} + \omega_3^{(k-1)} \right) \right], \\ L_3^{(k)} &= c_3 a \frac{\omega_3^{(k)} - \omega_3^{(k-1)}}{a}. \end{aligned} \quad (23.21)$$

Passing to the limit, when $\alpha \rightarrow 0$, we obtain the motion equations, the elasticity, and geometric relations for the continual model:

Motion equation

$$\frac{\partial N}{\partial x} = \tilde{\rho} \frac{\partial^2 u}{\partial t^2}, \quad (23.22)$$

$$\frac{\partial Q}{\partial x} = \tilde{\rho} \frac{\partial^2 w}{\partial t^2}, \quad \frac{\partial L_3}{\partial x} + Q = \tilde{I} \frac{\partial^2 \Omega}{\partial t^2}; \quad (23.23)$$

Elasticity relations

$$N = \tilde{c}_1 \varepsilon_x, \quad (23.24)$$

$$Q = \tilde{c}_2 \gamma, \quad L_3 = \tilde{c}_3 \chi, \quad (23.25)$$

Geometric relations

$$\varepsilon_x = \frac{\partial u}{\partial x}, \quad (23.26)$$

$$\gamma = \frac{\partial w}{\partial x} - \Omega, \quad \chi = \frac{\partial \Omega}{\partial x}. \quad (23.27)$$

Equations (23.22), (23.24), and (23.26) relate to longitudinal vibrations and Eqs. (23.23), (23.25), and (23.27)—to bending vibrations. The initial and boundary conditions should be added to these groups of equations.

For longitudinal oscillations, values for u and $\frac{\partial u}{\partial t}$ are given initial conditions when $t = 0$, and for bending oscillations values for w , Ω and $\frac{\partial w}{\partial t}$, $\frac{\partial \Omega}{\partial t}$ are given as initial conditions at the beginning of the movement.

The boundary conditions are given at $x = 0$ or $x = l$:

1. The conditions for displacements and free rotation, for example, if one of these edges is rigidly fixed, then we have the following boundary conditions:

$$u = 0 \quad (23.28)$$

for longitudinal vibrations,

$$w = 0, \quad \Omega = 0 \quad (23.29)$$

for bending vibrations.

2. For the free edge

$$N = 0 \quad (23.30)$$

for longitudinal vibrations,

$$Q = 0, \quad L = 0 \quad (23.31)$$

for bending vibrations.

There may also be mixed boundary conditions. It should be said that the motion Eqs. (23.22), (23.23) and the boundary conditions (23.30), (23.31) can be obtained based on the Hamilton principle (23.10), (23.13) for the continual model.

If the formulas of geometric relations (23.26), (23.27) are substituted into relations of elasticity (23.24), (23.25) and the obtained expressions are substituted into the equations of motion (23.22), (23.23), we will obtain the following equations (relative to the function $u = u(x, t)$ in case of longitudinal vibrations, and $w(x, t)$, $\Omega(x, t)$ in case of bending vibrations):

Equations of longitudinal vibrations

$$\tilde{c}_1 \frac{\partial^2 u}{\partial x^2} = \tilde{\rho} \frac{\partial^2 u}{\partial t^2}; \quad (23.32)$$

Equations of bending vibrations

$$\tilde{c}_2 \left(\frac{\partial^2 w}{\partial x^2} - \frac{\partial \Omega}{\partial x} \right) = \tilde{\rho} \frac{\partial^2 w}{\partial t^2}; \quad \tilde{c}_3 \frac{\partial^2 \Omega}{\partial x^2} + \tilde{c}_2 \left(\frac{\partial w}{\partial x} - \Omega \right) = \tilde{I} \frac{\partial^2 \Omega}{\partial t^2}. \quad (23.33)$$

The model (23.22), (23.24), (23.26), (23.28), or (23.30) for the longitudinal vibrations of the chain of atoms, and the model (23.23), (23.25), (23.27), (23.29), or (23.31) for bending vibrations of atomic chains represent, respectively, one-dimensional-continual (“beam”) models for vibrations of the atomic chains. The equations of these models do not contain the concept of the thickness of the “beams.” This is a very important result for nanomaterials, particularly for a graphene, if we assume that the material is located in the plane xz , that all atoms synchronously move along the axis z , and vibrations are in the plane xy along x —the longitudinal ones and along y —bending ones.

Equations (23.32) for longitudinal vibrations or (23.33) for bending vibrations of a chain of atoms can be compared with the corresponding equations of the simple models of vibrations of micropolar thin beams.

23.4 Equations of the Simple Applied Theory of Micropolar Elastic Thin Beams with Free Fields of Displacements and Rotations. Comparison of the Constructed Models and Determination of the Micropolar Elastic Parameters

In [16, 17], based on the asymptotic approach, the simple version of the applied theory of micropolar elastic thin beams is constructed for problems of statics and dynamics. The determining system of equations of the applied theory of micropolar elastic thin beams with free vibrations is expressed as follows:

Equation for longitudinal vibrations

$$E \frac{\partial^2 u}{\partial x^2} = \rho \frac{\partial^2 u}{\partial t^2}, \quad (23.34)$$

where E is Young's modulus and ρ —volume density of the material mass.

Equations for bending vibrations

$$\begin{aligned} \frac{4\mu\alpha}{\mu + \alpha} \left(\frac{\partial^2 w}{\partial x^2} - \frac{\partial \Omega}{\partial x} \right) &= \rho \frac{\partial^2 w}{\partial t^2}, \\ B \frac{\partial^2 \Omega}{\partial x^2} + \frac{4\mu\alpha}{\mu + \alpha} \left(\frac{\partial w}{\partial x} - \Omega \right) &= I \frac{\partial^2 \Omega}{\partial t^2}, \end{aligned} \quad (23.35)$$

where μ is the classical module of shear, α —micropolar module of shear, B —micropolar elastic constant of the studied material, and I —volume density of the moment of inertia.

As we will see, Eqs. (23.32) and (23.34), as well as Eqs. (23.33) and (23.35), are quite similar to each other. The main difference is that in Eqs. (23.32) and (23.33), $\tilde{\rho}$ is the linear mass density and \tilde{I} —the linear density of the moment of inertia, and in Eqs. (23.34) and (23.35), ρ is the volume density of the mass and I —the volume density of the moment of inertia. It is clear that in the left parts of these equations, the coefficients will also be physically different.

To make a comparison of Eqs. (23.32) and (23.34), as well as (23.33) and (23.35), we assume that the representative volume for the studied material is a cube with a size a then $\frac{\tilde{\rho}}{a^3}$ will be an approximate value of the volume density of the material, and $\frac{\tilde{I}}{a^2}$ —of volume density of the moment of inertia.

After such reasoning, Eqs. (23.34) and (23.35) will be as follows:

Equation for longitudinal vibrations

$$E \frac{\partial^2 u}{\partial x^2} = \frac{\tilde{\rho}}{a^2} \frac{\partial^2 u}{\partial t^2}; \quad (23.36)$$

Equations for bending vibrations

$$\begin{aligned} \frac{4\mu\alpha}{\mu + \alpha} \left(\frac{\partial^2 w}{\partial x^2} - \frac{\partial \Omega}{\partial x} \right) &= \frac{\tilde{\rho}}{a^2} \frac{\partial^2 w}{\partial t^2}, \\ B \frac{\partial^2 \Omega}{\partial x^2} + \frac{4\mu\alpha}{\mu + \alpha} \left(\frac{\partial w}{\partial x} - \Omega \right) &= \frac{\tilde{I}}{a^2} \frac{\partial^2 \Omega}{\partial t^2}. \end{aligned} \quad (23.37)$$

Now, comparing Eqs. (23.32) and (23.36), and (23.33) and (23.37), we will obtain:

$$Ea^2 = \tilde{c}_1, \quad (23.38)$$

$$\frac{4\mu\alpha}{\mu + \alpha}a^2 = \tilde{c}_2, Ba^2 = \tilde{c}_3. \quad (23.39)$$

From where

$$E = \frac{\tilde{c}_1}{a^2}, \quad (23.40)$$

$$\frac{4\mu\alpha}{\mu + \alpha} = \frac{\tilde{c}_2}{a^2}, B = \frac{\tilde{c}_3}{a^2}. \quad (23.41)$$

Equations (23.40) and (23.41) represent the connections between the physical macro parameters and the micro (nano) parameters of the material during the longitudinal and bending vibrations. Equation (23.41) makes it possible to calculate the mechanical constants of the micropolar substance through the parameters of the atomic–molecular structure of this substance.

23.5 Conclusion

In the present work, assuming that the force interaction between the atoms of the chain is non-central, and that moment interaction is present, the structural (discrete) and continual (moment)—“beam” models are constructed for the atomic chain. The continuum (moment)—“beam” model corresponds to the simple demonstrative model of a micropolar elastic thin beam with free fields of displacements and rotations constructed earlier [16, 17]. Based on these correspondence, elastic constants, including micropolar ones are expressed by the characteristic features of the atomic structure. The constructed micropolar—“beam” model can be used to develop applied finite-element software packages with the purpose of studying flat nanostructures (e.g., for graphene).

References

1. Blase, X.: Numerical simulation. In: Blase, X., Delerue, C. (eds.) *Nanoscience. Nanotechnologies and Nanophysics*. Springer, Berlin (2007)
2. Liu, W.K.: Computational nanomechanics of materials. In: Liu, W.K., Jun, S., Quian, D. (eds.) *Handbook of Theoretical and Computational Nanotechnology*. American Scientific Publishers (2005)
3. Yakobson, B.I., Brabeck, C.I., Bernholc, J.: Nanomechanics of carbon tubes: Instabilities beyond linear response. *Phys. Rev. Lett.* **75**, 2511–2514 (1996)
4. Ru, C.Q.: Effective bending stiffness of carbon nanotubes. *Phys. Rev. B.* **62**(15), 9973–9976 (2000)
5. Ru, C.Q.: Elastic buckling of single-walled carbon nanotubes ropes under high pressure. *Phys. Rev. B.* **62**(15), 10405–10408 (2000)

6. Ivanova, E.A., Krivtsov, A.M., Morozov, N.F., Firsova, A.D.: Inclusion of the moment interaction in the calculation of the flexural rigidity of nanostructures. *Dokl. Phys.* **48**(8), 455–458 (2003)
7. Ivanova, E.A., Krivtsov, A.M., Morozov, N.F.: Derivation of macroscopic relations of the elasticity of complex crystal lattices taking into account the moment interactions at the microlevel. *J. Appl. Math. Phys.* **71**(4), 543–561 (2007)
8. Berinskii, I.E., Ivanova, E.A., Krivtsov, A.M., Morozov, N.F.: Application of moment interaction to the construction of a stable model of graphite crystal lattice. *Mech. Solids* **42**(5), 663–671 (2007)
9. Odegard, G.M., Gates, T.S., Nicholson, L.M., Wise K.E.: Equivalent-Continuum Modeling of Nano-Structured Materials. NASA Langley Research Center. Technical Memorandum NASA/TM-2001-210863 (2001)
10. Goldstein, R.V., Chentsov, A.V.: Discrete-continuous model of a nanotube. *Mech. Solids* **40**(4), 45–59 (2005)
11. Li, C.A., Chou, T.W.: A structural mechanics approach for the analysis of carbon nanotubes. *Int. J. Solids Struct.* **40**, 2487–2499 (2003)
12. Berinskiy, I.E.: The Beam model of the crystal lattice of graphene. *Sci. Tech. J. StPSPU.* **104**, 13–20 (2010). (in Russian)
13. Wan, H., Delale, F.: A structural mechanics approach for predicting the mechanical properties of carbon nanotubes. *Mechanics* **45**, 43–51 (2010)
14. Scarp, F., Adhikari, S., Srikantha, Phari A.: Effective elastic mechanical properties of single layer grapheme sheets. *Nanotechnology* **20**, 065709 (2009)
15. Tserpes, K.I., Papanikos, P.: Finite element modeling of single-walled carbon nanotubes. *Composites* **36**, 468–477 (2005)
16. Sargsyan, S.H.: Applied one-dimensional beam theories based on the asymmetric theory of elasticity. *Phys. Mesomech.* **11**(5), 41–54 (2008) (in Russian)
17. Sargsyan, S.H.: Thin beams based on asymmetric theory of elasticity. In: Proceedings “Problems of the Mechanics of a Deformable Solid”. Dedicated to 85th Anniversary of the Academician NAS Armenia S.H. Ambardzumyan. pp. 177–183. Publishing house of NAS Armenia, Yerevan (2007) (in Russian)
18. Zhilin, P.A.: Theoretical mechanics. *Fundamental Laws Mechanics*, vol. 340. Publishing house StPSPU, St. Petersburg (2003) (in Russian)

Chapter 24

Circuit Analogies in the Search for New Metamaterials: Phenomenology of a Mechanical Diode



Mario Spagnuolo

Abstract The pantographic metamaterial, a particular metamaterial, composed of two orthogonal families of fibers, with remarkable deformation properties, presents, in case the interconnections between the two layers of fibers are perfect hinges, a mechanical response that recalls by analogy the law characteristic of diodes, in the theory of electrical circuits. In this sense, the pantographic metamaterial represents a sort of mechanical diode.

Keywords Metamaterials synthesis · Pantographic structures · Higher gradient models · Extension tests · Diode

24.1 Introduction

Technological breakthroughs in additive manufacturing have allowed the creation of highly complex designs for structures and objects. With this particular capability, 3D printing has substantially improved the realization and investigation of metamaterials, i.e. materials that have exotic mechanical features with an a priori chosen microstructure [26, 32, 33]. A particular group of metamaterials is constituted by the so-called pantographic metamaterials.

Such pantographic architectures are constituted by two families of parallel fibers that are joined by some pivots. Recently several samples have been moulded in Polyamide substituting the standard pivots (cylinders with a certain torsional stiffness) with perfect pivots, which are equivalent to hinges (free rotations). Details of this research are given in [10, 14, 29, 54, 60, 61, 65, 67–69].

Pantographic structures with perfect pivots are the object of the present study. In this paper we present some phenomenological observations on the mechanical behaviour of the aforementioned pantographic structures with perfect pivots. In fact, through numerical simulations and experimental tests, it is observed that the curve of the force-displacement plot in the case of perfect pivots takes on an extremely peculiar

M. Spagnuolo (✉)

International Research Center M&MoCS & Università degli Studi dell'Aquila, L'Aquila, Italy

form. By analogy with electrical circuits, the shape of the mechanical response of the pantographic metamaterial is reminiscent of that of the voltage-current rule in diodes.

24.2 Continuum Model of Pantographic Structures

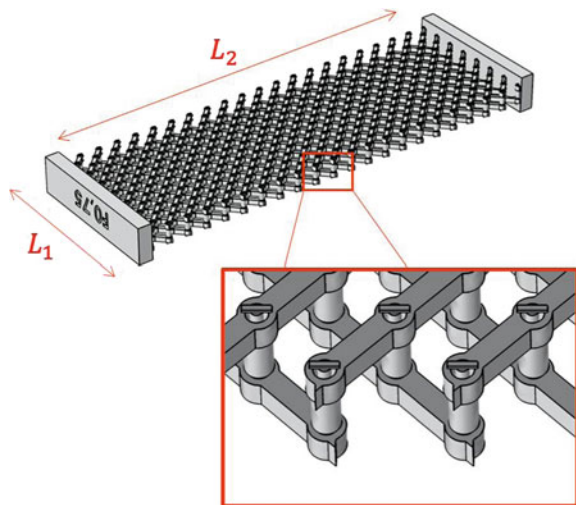
A typical procedure in the synthesis of new metamaterials is to specify the properties and mechanical responses required to the sought metamaterial by means of appropriately chosen equations. As a second step, the microstructure that, when properly homogenized, produces the above specified mechanical response is searched for.

In the practical case of pantographic structures, the sought behaviour consists in having a material whose elongation can be produced with no energy expense. In [1, 63] it is proven that such a material can be obtained by homogenisation of a pantographic microstructure (see Fig. 24.1).

Similarly to what Casal did in the case of the deformation energy of a beam [18, 19], in Sepecher et al. [63] a grid of fibres as the one of Fig. 24.1 was proposed as the fundamental cell of the microstructure to be homogenised to obtain a second gradient macroscopic model with the following properties:

- i. it consists of two families of mutually orthogonal fibers, which intersect by means of some cylinders called pivots (see Fig. 24.1);
- ii. the pivots, in theory, have no torsional energy;
- iii. when clamping the short sides of the structure, its elongation corresponds to elongation and flexion of the fibers; the latter one is modeled by a second gradient energetic term.

Fig. 24.1 CAD design of a pantographic structure with perfect pivots and detail of the pivots



As a result of points (i)–(iii), the homogenised model corresponding to the pantographic structure has a deformation energy depending on second gradient of the displacement [8, 17, 27, 28, 38–40, 46, 59].

24.2.1 Deformation Energy of a Pantographic Sheet

In dell’Isola et al. [31] it has been illustrated how to reach a macroscopic model of second gradient continuum by means of a process of homogenisation (which actually consists in performing a procedure of identification of the energy of macro-deformation, which is a macroscopic lagrangian density, in terms of constitutive parameters appearing in the postulated expressions of the micro-deformation energy) of a postulated micromodel. If we assume a 2D continuum whose reference configuration is given by a rectangular domain $\Omega = [0, L_1] \times [0, L_2] \subset \mathfrak{N}^2$ (for example, in Fig. 24.1 L_1 and L_2 represent the lengths of the sides of the ideal rectangle which contains the pantographic structure) and assuming the planar motion, the current configuration of Ω is described by the planar macroplacement

$$\chi: \Omega \rightarrow \mathfrak{N}^2 \quad (24.1)$$

In dell’Isola et al. [31] it has been shown that the continuum deformation energy of a pantographic structure can be written as

$$\begin{aligned} \mathcal{W}(\chi) = & \int_{\Omega} \sum_{\alpha} \frac{K_e}{2} (\|\mathbf{F}\mathbf{D}_{\alpha}\| - 1)^2 \, d\Omega \\ & + \int_{\Omega} \sum_{\alpha} \frac{K_b}{2} \left[\frac{\nabla \mathbf{F} | \mathbf{D}_{\alpha} \otimes \mathbf{D}_{\alpha} \cdot \nabla \mathbf{F} | \mathbf{D}_{\alpha} \otimes \mathbf{D}_{\alpha}}{\|\mathbf{F}\mathbf{D}_{\alpha}\|^2} - \left(\frac{\mathbf{F}\mathbf{D}_{\alpha}}{\|\mathbf{F}\mathbf{D}_{\alpha}\|} \cdot \frac{\nabla \mathbf{F} | \mathbf{D}_{\alpha} \otimes \mathbf{D}_{\alpha}}{\|\mathbf{F}\mathbf{D}_{\alpha}\|} \right)^2 \right] d\Omega \end{aligned}$$

In Eq. (24.1) it has been defined $\mathbf{F} = \nabla \chi$ and no sum over repeated α is intended. Moreover, a reference configuration has been introduced, whose unit base vectors, $(\mathbf{D}_1, \mathbf{D}_2)$, are oriented along the fiber directions in the reference configuration. K_e and K_b represent the elongation and bending stiffnesses, respectively.

If the interconnecting pivots are not perfect hinges, a further energetic term has to be included into the model formulation, describing the torsion of the pivots (at the micro-level) and the shear of the metamaterial (at the macro-level). Eventually, it could be considered a last term that model the relative sliding between the two fibre layers in correspondence of the interconnections. In this work, the sliding effect is neglected, while it has been experimentally observed and theoretically investigated in previous works [7, 64].

Equation (24.1) can be used to perform numerical finite element simulations. These simulations can be compared with the experiments and thus offer the possibility of validating the proposed model. Figure 24.2 shows the geometric shape of a

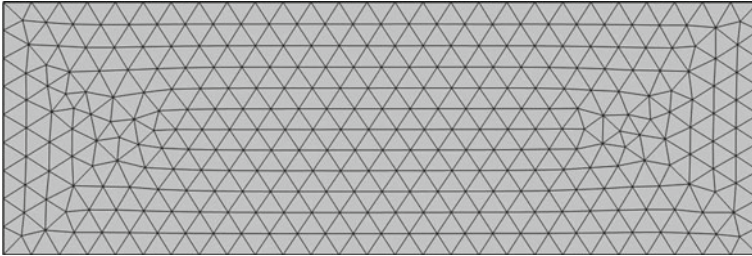


Fig. 24.2 The geometric shape of a rectangle with the sides in a ratio of 1:3 (as in a pantographic structure) is shown. On this rectangle the triangular finite elements used in the numerical code are displayed

rectangle with the sides in a ratio of 1:3 (as in a pantographic structure) and on which the triangular finite elements used in the numerical code are displayed.

24.3 A Mechanical Diode

In several applications of interest, the voltage-current behaviour of an ideal diode, under static conditions, can be approximated by a piecewise linear function. In this approximation, the current can be considered null if the voltage between anode and cathode is less than or equal to a certain threshold value V_γ ; if on the contrary the voltage is higher, the diode can be approximated to a voltage generator, whose current is imposed by the circuit to which it is subordinated.

In the field of mechanics, a response formally identical to that exhibited by the diode in electrical circuits is shown by the pantographic metamaterial. In fact, the macroscopic deformation of the pantographic metamaterial is translated, at the micro level (i.e. at the level of architecture), by the deformation of its basic constituents, i.e. fibers and pivots. If the pivots are perfect (see Fig. 24.3) and their torsional stiffness is therefore zero or negligible, then the overall deformation of the structure results in the simple deformation of the fibers, which can primarily bend and secondly stretch.

When deforming a perfect pivot pantographic structure in a BIAS extension test, it will be observed (i) the flexion of the fibers coupled with an extremely negligible elongation of the fibers and then, after the fibers in the central part of the structure have come into contact, (ii) an elongation of the fibers (see Fig. 24.4). From the model's point of view, the fact that the fibres in the central part of the structure come into contact is countered by the activation of the various deformation terms in the strain energy. In fact, if on the one hand in the practical implementation through 3D printing the fibers are clearly recognizable, on the other hand the model concerns a continuous two-dimensional medium and it is still referred to as fibers only as mathematical artifices that allow to write the strain energy as shown above.

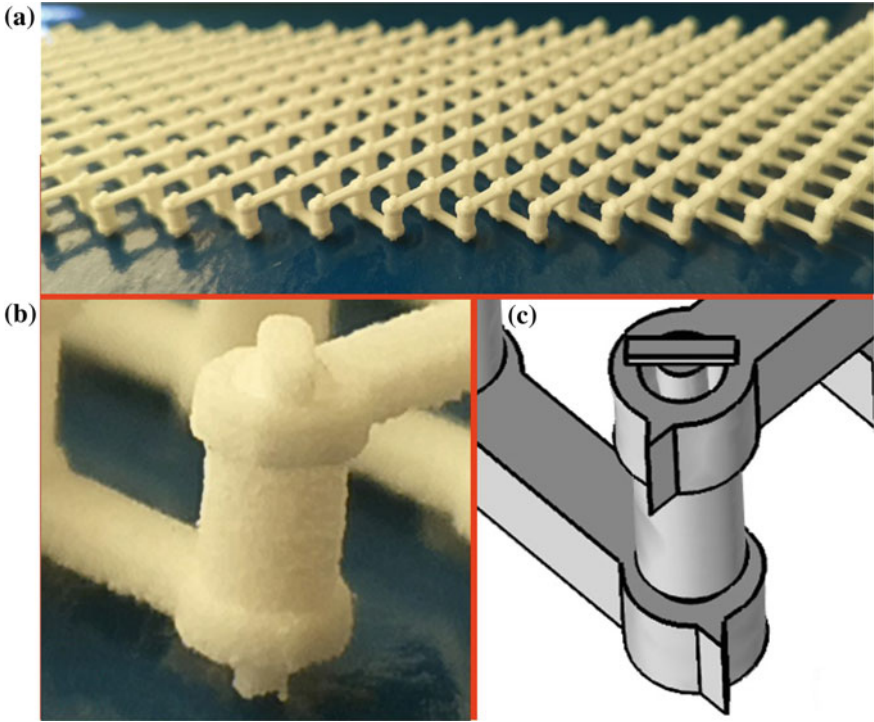


Fig. 24.3 Real sample of a Polyamide printed pantographic structure with perfect pivots (a). Detail of the pivot (b) and comparison with the CAD design (c)

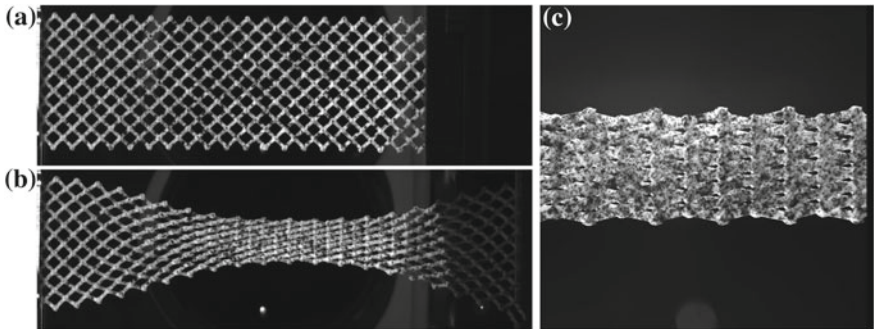


Fig. 24.4 Bias extension test of a pantographic structure with perfect pivots. Reference configuration (a), deformed configuration with fibres at contact in the center of the specimen (b) and detail showing the contact of the fibres (c)

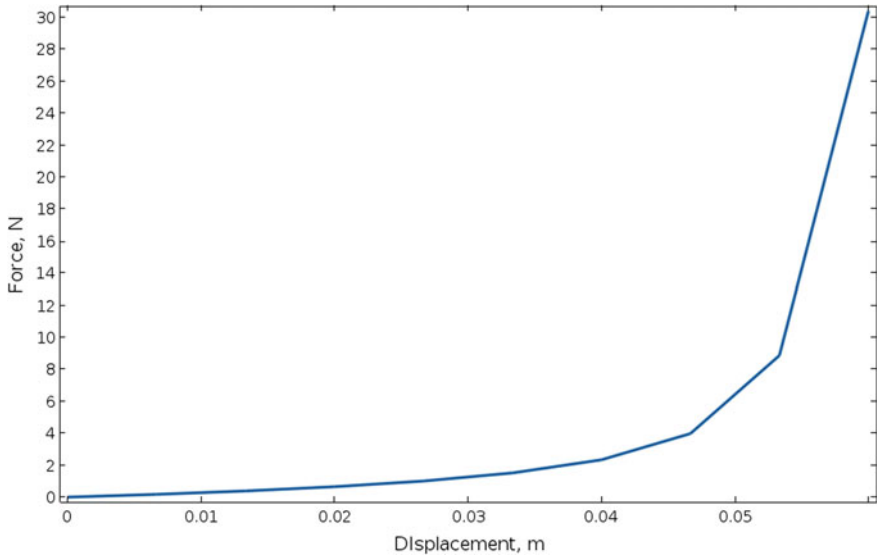


Fig. 24.5 Numerical simulation of the force-displacement plot for a pantographic structure with perfect pivots

If we plot the reaction force exerted by the pantographic metamaterial during the BIAS extension test, we theoretically obtain a response composed basically of two steps: in the first part the force will be due only to the flexion of the fibres and will be of a very low value (almost negligible if compared with the value of the maximum force); in the second part, after the contact between the fibres, the energy contribution of elongation will be activated and the force will change its slope until it reaches very high values (see Fig. 24.5).

An experimental analysis was carried out to verify the reliability of theoretical forecasts and numerical simulations. A polyamide pantographic structure with perfect pivots was used in a BIAS extension test and the reaction force was measured. The result obtained is presented in Fig. 24.6.

As can be easily seen from the image, up to 30 mm of elongation the measured force is practically zero or of the order of experimental noise. After this first stage of extension, the force increases almost linearly (until the sample breaks, which occurs by successive ruptures of the structural elements, but which we do not intend to talk about here). This can be explained simply by using the model introduced previously. In the first part of the extension, the preferred deformation mechanism is the bending of the fibres which, observing Eq. (24.1), is represented by a highly non-linear term (hence the non-linearities of the curve) weighted by a very low K_b stiffness, so that the average value of the measured force is in this first phase of the extension very small (almost zero, if one considers the sensitiveness of the experimental apparatus). In the second phase of the extension test, after the fibres in the central part of the structure have come into contact, the extension mechanism

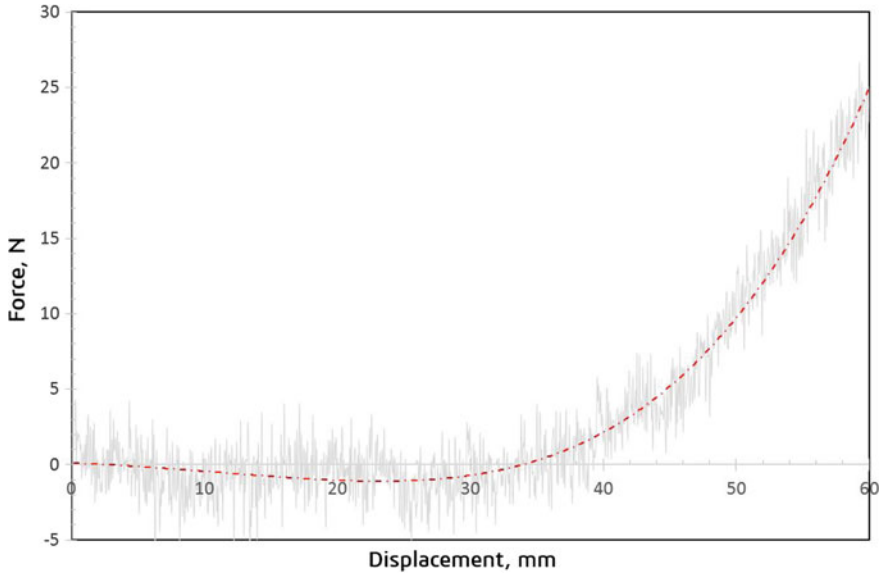


Fig. 24.6 Experimental force-displacement plot for a pantographic structure with perfect-pivots (grey line) and interpolation (red, dash-dotted line)

of the individual fibres is activated. This deformation is represented in Eq. (24.1) by the elongation energy term, which is quadratic in extension and which is weighted by a stiffness K_e much higher than K_b . For this reason, at the activation of this term, the bending term can be considered negligible and, from a theoretical point of view, the observed response should be linear (because the energy is basically that of elongation, which is quadratic). Clearly, the bending energy continues to play a role, even if considerably less than the elongation one, and for this reason it is observed, both in the measured curve (Fig. 24.6) and in the simulated one (Fig. 24.5), a trend that is not precisely linear.

The force plot displayed in Fig. 24.6 shows a peculiar feature of the pantographic metamaterial: this specific metamaterial can be stretched in a certain range (which depends only on the geometric characteristics of the architecture) with no or negligible energy and, if stretched outside this range, it will exert a reaction force that varies linearly with the elongation (up to the emergence of damage).

24.4 Conclusion

In this article a peculiar characteristic of the pantographic metamaterial has been presented. In the presence of perfect pivots, which at a macroscopic level imply a shear deformation at zero energy in the homogenised material, the force-displacement

graph characteristic of this metamaterial is very similar to the voltage-current law of diodes. The pantographic metamaterial is, in this sense, an example of a mechanical diode. It can be adopted in applications related to structures or systems where structural elements that exert reaction forces are necessary only for stretching values above a certain threshold (i.e. applications in earthquake-proof construction, in structures subject to stress due to vibrations such as parts designed for aeronautical or aerospace construction). In the different fields of applications, it could be useful to consider the coupling with other kind of materials, i.e. granular materials [12, 34, 45, 48, 49, 66, 70], laminate plates [3–6, 24], micropolar materials [2, 35, 52].

The study here presented can be completed by an analysis of the damage in pantographic structures. General discussions to investigate the damage in higher gradient theories can be found in [53, 56–58]. Problems related to modeling and simulation of metamaterials like the one presented in this article can be greatly simplified by the introduction of appropriate numerical tools [9, 11, 20–23, 25, 41–44, 47, 50, 55].

Finally, the problem briefly presented in this article can be investigated and many of its applications can be designed and tested. This requires accurate theoretical analyses that find in the literature several points of reference [13, 15, 16, 30, 36, 37, 51, 62].

Acknowledgements The author would like to thank Prof. F. Hild and Dr. X. Pinelli (LMT, ENS Paris-Saclay/CNRS/Univ. Paris-Saclay) for their help in the experimental analyses conducted on pantographic structures. The author would also like to thank Prof. T. Lekszycki (Warsaw University of Technology) for providing him with the samples used in the experiment.

References

1. Alibert, J.J., Seppecher, P., dell’Isola, F.: Truss modular beams with deformation energy depending on higher displacement gradients. *Math. Mech. Solids* **8**(1), 51–73 (2003)
2. Altenbach, H., Eremeyev, V.: On the linear theory of micropolar plates. *ZAMM-J. Appl. Math. Mech./Zeitschrift für Angewandte Mathematik und Mechanik* **89**(4), 242–256 (2009)
3. Altenbach, H., Eremeyev, V.A.: Direct approach-based analysis of plates composed of functionally graded materials. *Arch. Appl. Mech.* **78**(10), 775–794 (2008)
4. Altenbach, H., Eremeyev, V.A.: On the bending of viscoelastic plates made of polymer foams. *Acta Mech.* **204**(3–4), 137 (2009b)
5. Altenbach, H., Eremeyev, V.A.: Thin-walled structures made of foams. In: *Cellular and Porous Materials in Structures and Processes*. Springer, pp 167–242 (2010)
6. Altenbach, H., Eremeyev, V.A., Naumenko, K.: On the use of the first order shear deformation plate theory for the analysis of three-layer plates with thin soft core layer. *ZAMM-J. Appl. Math. Mech./Zeitschrift für Angewandte Mathematik und Mechanik* **95**(10), 1004–1011 (2015)
7. Andreus, U., Spagnuolo, M., Lekszycki, T., Eugster, S.R.: A Ritz approach for the static analysis of planar pantographic structures modeled with nonlinear euler-bernoulli beams. *Continuum Mech. Thermodyn.* **30**(5), 1103–1123 (2018)
8. Auffray, N., dell’Isola, F., Eremeyev, V., Madeo, A., Rosi, G.: Analytical continuum mechanics à la Hamilton-Piola least action principle for second gradient continua and capillary fluids. *Math. Mech. Solids* **20**(4), 375–417 (2015)

9. Balobanov, V., Niiranen, J.: Locking-free variational formulations and isogeometric analysis for the Timoshenko beam models of strain gradient and classical elasticity. *Comput. Methods Appl. Mech. Eng.* **339**, 137–159 (2018)
10. Barchiesi, E., Ganzosch, G., Liebold, C., Placidi, L., Grygoruk, R., Müller, W.H.: Out-of-plane buckling of pantographic fabrics in displacement-controlled shear tests: experimental results and model validation. *Continuum Mech. Thermodyn.* 1–13 (2018)
11. Beirão Da Veiga, L., Hughes, T., Kiendl, J., Lovadina, C., Niiranen, J., Reali, A., Speleers, H.: A locking-free model for Reissner-Mindlin plates: analysis and isogeometric implementation via NURBS and triangular NURPS. *Math. Models Methods Appl. Sci.* **25**(08), 1519–1551 (2015)
12. Bilotta, A., Morassi, A., Rosset, E., Turco, E., Vessella, S.: Numerical size estimates of inclusions in Kirchhoff-Love elastic plates. *Int. J. Solids Struct.* **168**, 58–72 (2019)
13. Bouchitté, G., Mattei, O., Milton, G.W., Seppecher, P.: On the forces that cable webs under tension can support and how to design cable webs to channel stresses. *Proc. R. Soc. A* **475**(2223), 20180781 (2019)
14. Boutin, C., Giorgio, I., Placidi, L., et al.: Linear pantographic sheets: asymptotic micro-macro models identification. *Math. Mech. Complex Syst.* **5**(2), 127–162 (2017)
15. Camar-Eddine, M., Seppecher, P.: Non-local interactions resulting from the homogenization of a linear diffusive medium. *C. R. de l'Académie des Sci. Ser. I-Math.* **332**(5), 485–490 (2001)
16. Camar-Eddine, M., Seppecher, P.: Determination of the closure of the set of elasticity functionals. *Arch. Ration. Mech. Anal.* **170**(3), 211–245 (2003)
17. Carcaterra, A., dell'Isola, F., Esposito, R., Pulvirenti, M.: Macroscopic description of microscopically strongly inhomogeneous systems: a mathematical basis for the synthesis of higher gradients metamaterials. *Arch. Ration. Mech. Anal.* **218**(3), 1239–1262 (2015)
18. Casal, P.: La capillarité interne. *Cahier du groupe Français de rhéologie, CNRS VI* **3**, 31–37 (1961)
19. Casal, P.: Theory of second gradient and capillarity. *C r hebdomadaire des séances Acad. Sci. A* **274**(22), 1571 (1972)
20. Cazzani, A., Malagù, M., Turco, E.: Isogeometric analysis: a powerful numerical tool for the elastic analysis of historical masonry arches. *Continuum Mech. Thermodyn.* **28**(1–2), 139–156 (2016)
21. Cazzani, A., Malagù, M., Turco, E.: Isogeometric analysis of plane-curved beams. *Math. Mech. Solids* **21**(5), 562–577 (2016)
22. Cazzani, A., Malagù, M., Turco, E., Stochino, F.: Constitutive models for strongly curved beams in the frame of isogeometric analysis. *Math. Mech. Solids* **21**(2), 182–209 (2016)
23. Cazzani, A., Stochino, F., Turco, E.: An analytical assessment of finite element and isogeometric analyses of the whole spectrum of Timoshenko beams. *ZAMM-J. Appl. Math. Mech./Zeitschrift für Angewandte Mathematik und Mechanik* **96**(10), 1220–1244 (2016)
24. Cazzani, A., Serra, M., Stochino, F., Turco, E.: A refined assumed strain finite element model for statics and dynamics of laminated plates. *Continuum Mech. Thermodyn.* **3**, 1–28 (2018). <https://doi.org/10.1007/s00161-018-0707-x>
25. Cuomo, M., Contrafatto, L., Greco, L.: A variational model based on isogeometric interpolation for the analysis of cracked bodies. *Int. J. Eng. Sci.* **80**, 173–188 (2014)
26. Del Vescovo, D., Giorgio, I.: Dynamic problems for metamaterials: review of existing models and ideas for further research. *Int. J. Eng. Sci.* **80**, 153–172 (2014)
27. dell'Isola, F., Seppecher, P., Madeo, A.: How contact interactions may depend on the shape of Cauchy cuts in Nth gradient continua: approach “à la D'Alembert”. *Zeitschrift für angewandte Mathematik und Physik* **63**(6), 1119–1141 (2012)
28. dell'Isola, F., Andreaus, U., Placidi, L.: At the origins and in the vanguard of peridynamics, non-local and higher-gradient continuum mechanics: an underestimated and still topical contribution of Gabrio Piola. *Math. Mech. Solids* **20**(8), 887–928 (2015)
29. dell'Isola, F., Steigmann, D., Della Corte, A.: Synthesis of fibrous complex structures: Designing microstructure to deliver targeted macroscale response. *Appl. Mech. Rev.* **67**(6), 060804 (2015)

30. dell'Isola, F., Della Corte, A., Esposito, R., Russo, L.: Some cases of unrecognized transmission of scientific knowledge: from antiquity to Gabrio Piola's peridynamics and generalized continuum theories. In: *Generalized Continua as Models for Classical and Advanced Materials*. Springer, pp. 77–128 (2016)
31. dell'Isola, F., Giorgio, I., Pawlikowski, M., Rizzi, N.: Large deformations of planar extensible beams and pantographic lattices: heuristic homogenization, experimental and numerical examples of equilibrium. *Proc. R. Soc. A* **472**(2185), 20150790 (2016)
32. dell'Isola, F., Seppecher, P., Alibert, J.J., Lekszycki, T., Grygoruk, R., Pawlikowski, M., Steigmann, D., Giorgio, I., Andreaus, U., Turco, E., Golaszewski, M., Rizzi, N., Boutin, C., Eremeyev, V.A., Misra, A., Placidi, L., Barchiesi, E., Greco, L., Cuomo, M., Cazzani, A., Corte, A.D., Battista, A., Scerrato, D., Eremeeva, I.Z., Rahali, Y., Ganghoffer, J.F., Müller, W., Ganzosch, G., Spagnuolo, M., Pfaff, A., Barcz, K., Hoschke, K., Neggers, J., Hild, F.: Pantographic metamaterials: an example of mathematically driven design and of its technological challenges. *Continuum Mech. Thermodyn.* **31**(4), 851–884 (2019)
33. dell'Isola, F., Seppecher, P., Spagnuolo, M., Barchiesi, E., Hild, F., Lekszycki, T., Giorgio, I., Placidi, L., Andreaus, U., Cuomo, M., Eugster, S., Pfaff, A., Hoschke, K., Langkemper, R., Turco, E., Sarikaya, R., Misra, A., Angelo, M.F., D'Annibale, F., Bouterf, A., Pinelli, X., Misra, A., Desmorat, B., Pawlikowski, M., Dupuy, C., Scerrato, D., Peyre, P., Laudato, M., Manzari, L., Göransson, P., Hesch, C., Hesch, S., Franciosi, P., Dirrenberger, J., Maurin, F., Vangelatos, Z., Grigoropoulos, C.P., Mellissinaki, V., Farsari, M., Muller, W., Abali, B.E., Liebold, C., Ganzosch, G., Harrison, P.G., Drobnicki, R., Igumnov, L.A., Alzahrani, F., Hayat, T.: Advances in pantographic structures: design, manufacturing, models, experiments and image analyses. *Continuum Mech. Thermodyn.* **31**, 1231–1282 (2019)
34. Eremeyev, V.A.: On the material symmetry group for micromorphic media with applications to granular materials. *Mech. Res. Commun.* **94**, 8–12 (2018)
35. Eremeyev, V.A., Pietraszkiewicz, W.: Material symmetry group and constitutive equations of micropolar anisotropic elastic solids. *Math. Mech. Solids* **21**(2), 210–221 (2016)
36. Eugster, S., Hesch, C., Betsch, P., Glocker, C.: Director-based beam finite elements relying on the geometrically exact beam theory formulated in skew coordinates. *Int. J. Numer. Methods Eng.* **97**(2), 111–129 (2014)
37. Eugster, S., Steigmann, D., et al.: Continuum theory for mechanical metamaterials with a cubic lattice substructure. *Math. Mech. Complex Syst.* **7**(1), 75–98 (2019)
38. Eugster, S.R., dell'Isola, F.: Exegesis of the introduction and sect. I from “Fundamentals of the mechanics of continua” ** by E. Hellinger. *ZAMM-J. Appl. Math. Mech./Zeitschrift für Angewandte Mathematik und Mechanik* **97**(4):477–506 (2017)
39. Eugster, S.R., dell'Isola, F.: Exegesis of sect. II and III. A from “Fundamentals of the mechanics of continua” by E. Hellinger. *ZAMM-J. Appl. Math. Mech./Zeitschrift für Angewandte Mathematik und Mechanik* **98**(1):31–68 (2018)
40. Eugster, S.R., dell'Isola, F.: Exegesis of sect. III. B from “Fundamentals of the mechanics of continua” by E. Hellinger. *ZAMM-J. Appl. Math. Mech./Zeitschrift für Angewandte Mathematik und Mechanik* **98**(1):69–105 (2018)
41. Giorgio, I.: Numerical identification procedure between a micro-cauchy model and a macro-second gradient model for planar pantographic structures. *Zeitschrift für angewandte Mathematik und Physik* **67**(4):95 (2016)
42. Greco, L., Cuomo, M.: B-Spline interpolation of Kirchhoff-Love space rods. *Comput. Methods Appl. Mech. Eng.* **256**, 251–269 (2013)
43. Greco, L., Cuomo, M., Contrafatto, L.: A quadrilateral G1-conforming finite element for the Kirchhoff plate model. *Comput. Methods Appl. Mech. Eng.* **346**, 913–951 (2019a)
44. Greco, L., Cuomo, M., Contrafatto, L.: Two new triangular G1-conforming finite elements with cubic edge rotation for the analysis of Kirchhoff plates. *Comput. Methods Appl. Mech. Eng.* **356**, 354–386 (2019b)
45. Jia, H., Misra, A., Poorsolhjoui, P., Liu, C.: Optimal structural topology of materials with micro-scale tension-compression asymmetry simulated using granular micromechanics. *Mater. Des.* **115**, 422–432 (2017)

46. Khakalo, S., Niiranen, J.: Form II of Mindlin's second strain gradient theory of elasticity with a simplification: For materials and structures from nano-to macro-scales. *Eur. J. Mech.A/Solids* **71**, 292–319 (2018)
47. Luongo, A., Zulli, D., Piccardo, G.: Analytical and numerical approaches to nonlinear galloping of internally resonant suspended cables. *J. Sound Vibr.* **315**(3), 375–393 (2008)
48. Misra, A., Poorsolhjoui, P.: Granular micromechanics model for damage and plasticity of cementitious materials based upon thermomechanics. *Math. Mech. Solids* 1081286515576821 (2015)
49. Misra, A., Poorsolhjoui, P.: Grain-and macro-scale kinematics for granular micromechanics based small deformation micromorphic continuum model. *Mech. Res. Commun.* **81**, 1–6 (2017)
50. Niiranen, J., Balabanov, V., Kiendl, J., Hosseini, S.: Variational formulations, model comparisons and numerical methods for euler-bernoulli micro-and nano-beam models. *Math. Mech. Solids* **24**(1), 312–335 (2019)
51. Pideri, C., Seppecher, P.: A second gradient material resulting from the homogenization of an heterogeneous linear elastic medium. *Continuum Mech. Thermodyn.* **9**(5), 241–257 (1997)
52. Pietraszkiewicz, W., Eremeyev, V.: On natural strain measures of the non-linear micropolar continuum. *Int. J. Solids Struct.* **46**(3), 774–787 (2009)
53. Placidi, L., Barchiesi, E.: Energy approach to brittle fracture in strain-gradient modelling. *Proc. R. Soc. A* **474**(2210), 20170878 (2018)
54. Placidi, L., Barchiesi, E., Turco, E., Rizzi, N.L.: A review on 2D models for the description of pantographic fabrics. *Zeitschrift für angewandte Mathematik und Physik* **67**(5), 121 (2016)
55. Placidi, L., Barchiesi, E., Battista, A.: An inverse method to get further analytical solutions for a class of metamaterials aimed to validate numerical integrations. In: *Mathematical Modelling in Solid Mechanics*. Springer, pp 193–210 (2017)
56. Placidi, L., Barchiesi, E., Misra, A.: A strain gradient variational approach to damage: a comparison with damage gradient models and numerical results. *Math. Mech. Complex Syst.* **6**(2), 77–100 (2018a)
57. Placidi, L., Misra, A., Barchiesi, E.: Simulation results for damage with evolving microstructure and growing strain gradient moduli. *Continuum Mech. Thermodyn.* 1–21 (2018)
58. Placidi, L., Misra, A., Barchiesi, E.: Two-dimensional strain gradient damage modeling: a variational approach. *Zeitschrift für angewandte Mathematik und Physik* **69**(3), 56 (2018c)
59. Rahali, Y., Giorgio, I., Ganghoffer, J., dell'Isola, F.: Homogenization à la Piola produces second gradient continuum models for linear pantographic lattices. *Int. J. Eng. Sci.* **97**, 148–172 (2015)
60. Scerrato, D., Giorgio, I., Rizzi, N.L.: Three-dimensional instabilities of pantographic sheets with parabolic lattices: numerical investigations. *Zeitschrift für angewandte Mathematik und Physik* **67**(3), 53 (2016)
61. Scerrato, D., Zhurba Eremeeva, I., Lekszycki, T., Rizzi, N.: On the shear stiffness influence for modelling of deformations of pantographic sheets. In: *Shell Structures: Theory and Applications Volume 4: Proceedings of the 11th International Conference Shell Structures: Theory and Applications (SSTA 2017)*, pp 161–164, 11–13 October 2017, Gdansk, Poland, CRC Press (2017)
62. Seppecher, P.: Moving contact lines in the Cahn-Hilliard theory. *Int. J. Eng. Sci.* **34**(9), 977–992 (1996)
63. Seppecher, P., Alibert, J.J., dell'Isola, F.: Linear elastic trusses leading to continua with exotic mechanical interactions. *J. Phys. Conf. Ser.* **319**(1), 012018 (2011)
64. Spagnuolo, M., Barcz, K., Pfaff, A., dell'Isola, F., Franciosi, P.: Qualitative pivot damage analysis in aluminum printed pantographic sheets: numerics and experiments. *Mech. Res. Commun.* **83**, 47–52 (2017)
65. Steigmann, D., dell'Isola, F.: Mechanical response of fabric sheets to three-dimensional bending, twisting, and stretching. *Acta Mech. Sin.* **31**(3), 373–382 (2015)
66. Turco, E.: In-plane shear loading of granular membranes modeled as a Lagrangian assembly of rotating elastic particles. *Mech. Res. Commun.* **92**, 61–66 (2018)
67. Turco, E., dell'Isola, F., Cazzani, A., Rizzi, N.: Hencky-type discrete model for pantographic structures: numerical comparison with second gradient continuum models. *Zeitschrift für angewandte Mathematik und Physik* **67** (2016)

68. Turco, E., Golaszewski, M., Giorgio, I., D'Annibale, F.: Pantographic lattices with non-orthogonal fibres: experiments and their numerical simulations. *Compos. Part B Eng.* **118**, 1–14 (2017)
69. Turco, E., Misra, A., Pawlikowski, M., dell'Isola, F., Hild, F.: Enhanced Piola-Hencky discrete models for pantographic sheets with pivots without deformation energy: numerics and experiments. *Int. J. Solids Struct.* **147**, 94–109 (2018)
70. Turco, E., dell'Isola, F., Misra, A.: A nonlinear Lagrangian particle model for grains assemblies including grain relative rotations. *Int. J. Numer. Anal. Methods Geomech.* **43**(5), 1051–1079 (2019)

Chapter 25

Damping of Oscillations by a Vibro-Impact System with Serial Magnetic Impact Pairs



Yuri M. Zamuragin, Alexander M. Gousskov and Vitaly L. Krupenin

Abstract The body vibration damping process with a dynamic shock vibration damper containing a system of successive shock pairs in which the colliding elements are magnets is considered. The projected parameters' effect of the vibration damper on the body oscillations is considered. The features of setting up the system in the mode of wideband vibration damping are described.

Keywords Impact vibration damping · Magnetic impact pair · Series impact pair · Impact interaction force

25.1 Introduction

The creation of modern high-performance machines and high-speed vehicles, forced by power, loads, and other defining performance, inevitably leads to an increase in the intensity and expansion of the generated vibration spectrum and vibroacoustic fields, causing unwanted vibration, the appearance of which leads to disruption of the proper functioning of the systems. In this case, methods and means of reducing the existing vibration and the vibration activity of the mechanisms and machine units are important [1].

The method of dynamic oscillation damping consists in attaching additional devices to the vibration protection object to change its vibration state in a certain frequency range of external influence [1, 2]. In this paper, the problem of using a multi-mass system with magnetic elements as a dynamic vibration damper and study the dynamics of the entire system was considered.

A dynamic shock damper with one shock pair was considered in [1, 3–5]. Issues related to the use of magnetic elements (an element consisting of a magnetorheological fluid) to reduce vibration are considered in [6]. The magnetic element in

Y. M. Zamuragin · A. M. Gousskov
N.E. Bauman Moscow State Technical University (BMSTU), Moscow, Russian Federation

A. M. Gousskov · V. L. Krupenin (✉)
A.A. Blagonravov Mechanical Engineering Research Institute of the RAS (IMASH RAN),
Moscow, Russian Federation

this paper is represented by a damping element, the damping coefficient of which depends on the external magnetic field acting on the element [7].

In this paper, we consider a system with many successive shock pairs, which include magnetic elements. The fundamentals of the theory of vibro-impact systems of a similar structure were laid in papers [8, 9]. One-dimensional chains of different structures were studied, in particular, in papers [10–13]. In addition, in papers [10, 11], chains containing a large number of shock pairs were considered. As a result of research and numerical modeling revealed a number of significant facts. In particular, it is shown that the vibration damper can be regulated by changing the distance between the elements at the equilibrium state. Such a setting provides effective damping of the body oscillations in the required frequency spectrum.

25.2 Problem Statement

A device, which is considered in this work to use as a dynamic vibration damper with many shock pairs, is shown in Fig. 25.1a. Identical magnets are located inside the cylindrical tube. Magnets are oriented at each other by opposite poles, so that repulsive forces act between them. Two boundary magnets are rigidly fixed at the ends of body (tube). Each pair of nearby magnetic poles with the same name creates an elastic one-way connection. When they approach, after overcoming the repulsive force, impacts are possible. This system has n degrees of freedom and n natural frequencies. Movable elements are represented as solid bodies. Depending on the value of external load, determined by the movement of the body, the impact pairs may not work simultaneously. There are various possible modes of work of the dynamic system. With periodic external load of the main body, periodic movements without collisions can occur. Periodic motions with different number of impact pairs are also possible. At a high level of external load, complex movements with multiple impacts can be observed: Since the finite nature of the phase space, the movements can be quasi-periodic and, apparently, chaotic. This paper offers the result of numerical simulation of the dynamics of the system under consideration.

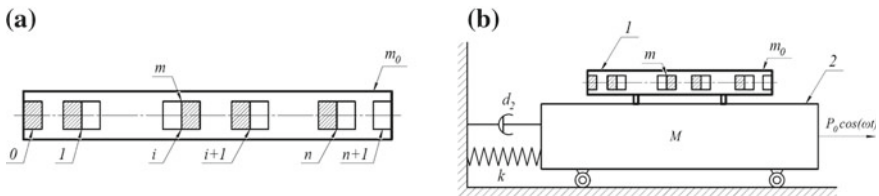


Fig. 25.1 **a** Mechanical model of the damper; **b** mechanical model of the body, with an installed damper

25.3 Motion Equations

The motion equation of the i -th movable element in the tube, with harmonic kinematic load $u(t) = B \cos(\omega t)$ on the tube with elements, takes the following form:

$$m\ddot{x}_i + d_1\dot{x}_i = F_i - F_{i+1} + mB\omega^2 \cos \omega t, \quad i = 1, \dots, n, \quad (25.1)$$

where

m —mass of i -th magnet, [kg],

$x_i, \dot{x}_i, \ddot{x}_i$ —displacement, velocity, and acceleration of i -th magnet relative to equilibrium states, [m], [m/s], and [m/s²],

d_1 —damping factor for magnets, [kg/s],

F_i, F_{i+1} —force, acting on i -th magnet from $(i-1)$ -th and $(i+1)$ -th magnets, respectively, [N],

B —amplitude of external kinematic load, [m],

ω —frequency of external kinematic load, [s⁻¹].

The function repulsive force versus distance is taken as follows (for more details, see Appendix)

$$F_i = F(z_i) = \frac{F_0 z_i}{(1 + z_i^2)^\beta}, \quad z_i = \frac{X_i}{a}, \quad X_i = A + x_i - x_{i-1}, \quad (25.2)$$

where

A —distance between magnets in the equilibrium state, [m],

$F_0, [N], a, [m], \beta, [1]$ —experimentally or analytically defined magnetic parameters,

$X_*, [m]$ and $T_*, [s]$ are chosen as linear and time scales, respectively, for mathematical models (25.1) and (25.2), where $X_* = a, T_* = \sqrt{\frac{ma}{F_0}}$. The following dimensionless complexes $\alpha, \gamma, \nu, \zeta$ and variables ξ, τ were introduced:

$$\alpha = \frac{A}{X_*}, \quad \gamma = \frac{B}{X_*}, \quad \nu = \omega T_*, \quad \zeta_1 = \frac{T_* d_1}{2m}, \quad \xi = \frac{x}{X_*}, \quad \tau = \frac{t}{T_*}$$

Equations (25.1) and (25.2) could be written as:

$$\begin{aligned} \ddot{\xi}_i + 2\zeta \dot{\xi}_i &= \Phi_i - \Phi_{i+1} + \gamma \nu^2 \cos \nu \tau, \quad i = 1, 2, \dots, n \\ \Phi_i &= \Phi(\xi_i, \xi_{i-1}) = \frac{z_i}{(1 + z_i^2)^\beta}; \quad z_i = \alpha + \xi_i - \xi_{i-1}, \quad i = 2, \dots, n-1 \end{aligned} \quad (25.3)$$

The dimensionless period of external load T_0 for setting integration interval was introduced:

$$T_0 = 2\pi \nu^{-1}$$

Since the boundary magnets are fixed in tube, following expressions are valid for first and last (n -th) magnets:

$$\Phi_1 = \Phi(\xi_1, 0) = \frac{(\alpha + \xi_1)}{(1 + (\alpha + \xi_1)^2)^\beta}$$

$$\Phi_{n+1} = \Phi(0, \xi_n) = \frac{(\alpha - \xi_n)}{(1 + (\alpha - \xi_n)^2)^\beta}$$

System consisting of n magnets (25.3) could be linearized near stationary (equilibrium) state (position of magnets without external loading). Then, equations were derived to matrix form (25.4), and natural frequencies spectrum and mode shapes of small oscillations were gained [13].

$$m\ddot{\xi} + r\xi = 0, \xi = \{\xi_1, \xi_2, \dots\}^T, \tag{25.4}$$

where

- m —mass matrix,
- r —rigidity matrix,
- ξ —system state vector.

The characteristics of this system were considered in [15]. The parameters at which the impact modes in the system occur were estimated.

It is necessary to solve the equation for the distance between the magnets α at the stationary state to obtain dynamic damper with certain one of natural frequencies. Natural frequencies values vs distance between magnets in stationary state is shown in Fig. 25.2. In order to ensure that the required natural frequency of the system

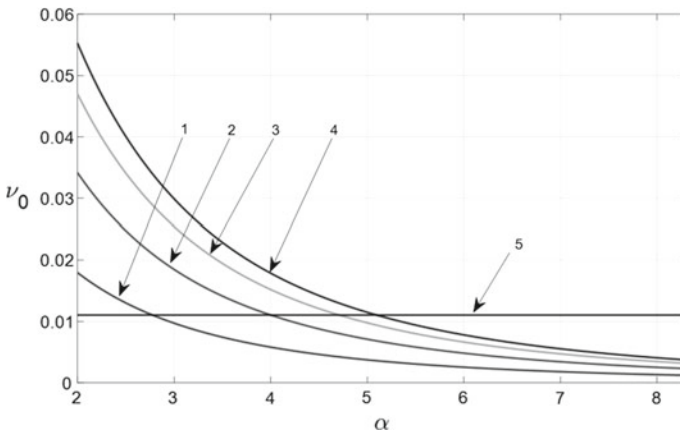


Fig. 25.2 Natural frequencies vs distance between magnets in stationary state function for system consisting of four elements (1–4—natural frequencies numbers, 5—external load frequency)

is equal to the frequency of external load, it is necessary to find the intersection of line 5 (external load frequency) and one of the natural frequencies (curves 1–4). Appropriate value α as distance between magnets in stationary state should be taken.

Let us consider to use the described device as a dynamic vibration damper. The device is installing on a damped body of mass M , which oscillations must be reduced. The mechanical model of this system is shown in Fig. 25.1b. Motion equation system damper-damped body takes the following form:

$$\begin{cases} \eta_1 (\ddot{\xi}_1 + \ddot{\xi}_{n+1}) + 2\zeta_1 \dot{\xi}_1 + \Phi_2 - \Phi_1 = 0 \\ \dots \\ \eta_i (\ddot{\xi}_i + \ddot{\xi}_{n+1}) + 2\zeta_1 \dot{\xi}_i + \Phi_{i+1} - \Phi_i = 0, i = 2, \dots, n - 1 \\ \dots \\ \eta_n (\ddot{\xi}_n + \ddot{\xi}_{n+1}) + 2\zeta_1 \dot{\xi}_n + \Phi_{n+1} - \Phi_n = 0 \\ \ddot{\xi}_{n+1} + \sum_{i=1}^n \eta_i \ddot{\xi}_i + 2\zeta_2 \dot{\xi}_{n+1} + \kappa \xi_{n+1} - \Pi(\tau) = 0 \end{cases} \quad (25.5)$$

The variable ξ_{n+1} denotes the displacement of damped body. Also there were used following symbols:

$$\eta_i = \frac{m_i}{\left(\sum_{j=1}^n m_j + M + m_0\right)}, \kappa = \frac{ka}{F_0}, \Pi_0 = \frac{P_0}{F_0}, \zeta_2 = \frac{T_* d_2}{2m},$$

where

- m_0 —mass of the tube without magnets,
- m_i, m_j — i -th and j -th magnets' masses,
- d_2 —damping factor for body, [kg/s],
- n —the number of moving magnets in the damper.

For numerical integration, the system of Eq. (25.5) is presented in matrix form (25.6).

$$\dot{Y} = AY + g(\xi, t); Y = \left\{ \xi^T, \dot{\xi}^T \right\}^T \quad (25.6)$$

To describe the interaction of elements of the system at impact, Newton's theory of elastic impact was used [14]. When two adjacent elements ($i - 1$) and i impact, their coordinates and velocities are changing as follows in accordance with [14]:

$$\begin{cases} \xi_{i-1}^+ = \xi_{i-1}^- \\ \dot{\xi}_i^+ = \dot{\xi}_i^- \\ \dot{\xi}_{i-1}^+ = \frac{(m_{i-1} - r m_i) \dot{\xi}_{i-1}^- + m_i (1+r) \dot{\xi}_i^-}{m_{i-1} + m_i} \quad i = 2, \dots, n - 1 \\ \dot{\xi}_i^+ = \frac{m_{i-1} (1+r) \dot{\xi}_{i-1}^- + (m_i - r m_{i-1}) \dot{\xi}_i^-}{m_{i-1} + m_i} \end{cases}$$

In addition, for magnets $i = 1$ and $i = n$, since they impact with the body. The difference is explained by the fact that the displacement of magnets is counted in the moving coordinate system (relative to the moving body to which the device is attached), and the coordinates of the body are counted in an absolute, fixed coordinate system.

$$\begin{cases} \xi_{n+1}^+ = \xi_{n+1}^- \\ \xi_i^+ = \xi_i^- \\ \dot{\xi}_{n+1}^+ = \dot{\xi}_{n+1}^- + \frac{m_i(1+r)\dot{\xi}_i^-}{M+m_i} \quad i = 1, i = n \\ \dot{\xi}_i^+ = \frac{(m_i-rM)\dot{\xi}_i^-}{M+m_i} \end{cases}$$

Laws of motion according to parameters (25.7) are shown in Fig. 25.3 (magnets in damper) and in Fig. 25.5 (body with damper and without damper). The following parameters are assumed

$$\begin{aligned} n = 4, \alpha = 2.78, v_0 = 0.11, v = v_0, \mu = 25.43, \zeta = 4.78 \times 10^{-5}, \\ \zeta_1 = 4.78 \times 10^{-4}, r = 0.95, \Pi_0 = 0.0226 \end{aligned} \tag{25.7}$$

In Fig. 25.4, the big black points indicate the moments of impact between adjacent magnets in the selected Fig. 25.3 area.

In Fig. 25.5, the body oscillations' amplitude is shown, with the dynamic damper installed, with used parameters decreased about ten times compared to the body without damper.

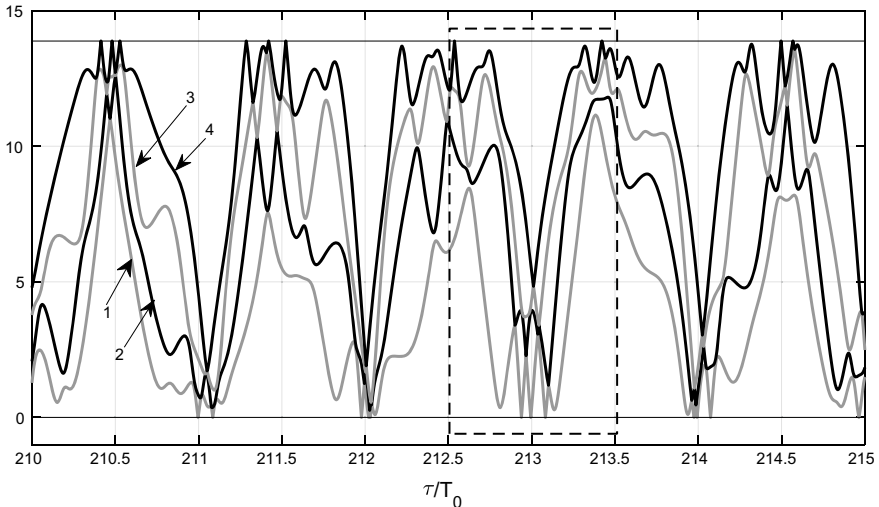


Fig. 25.3 Movements of magnets in the system implementation (numbers correspond to magnets' laws of motion, respectively)

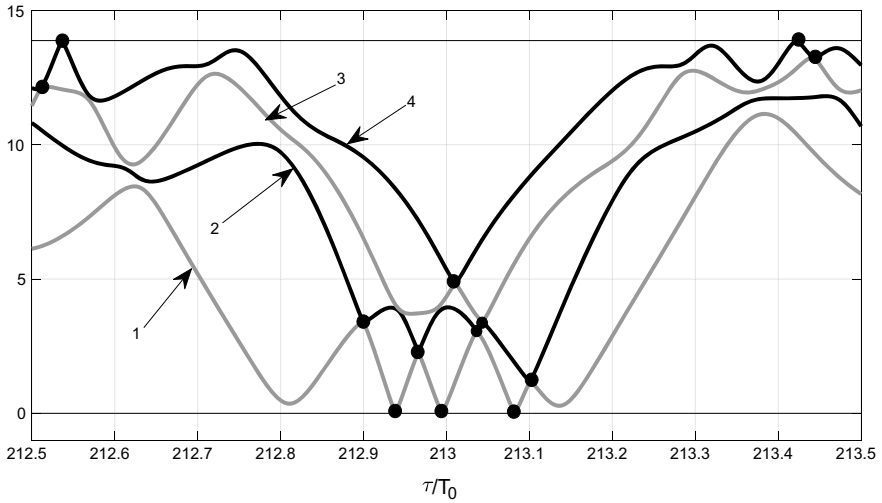


Fig. 25.4 Moments of impacts between magnets (numbers correspond to magnets' laws of motion, respectively)

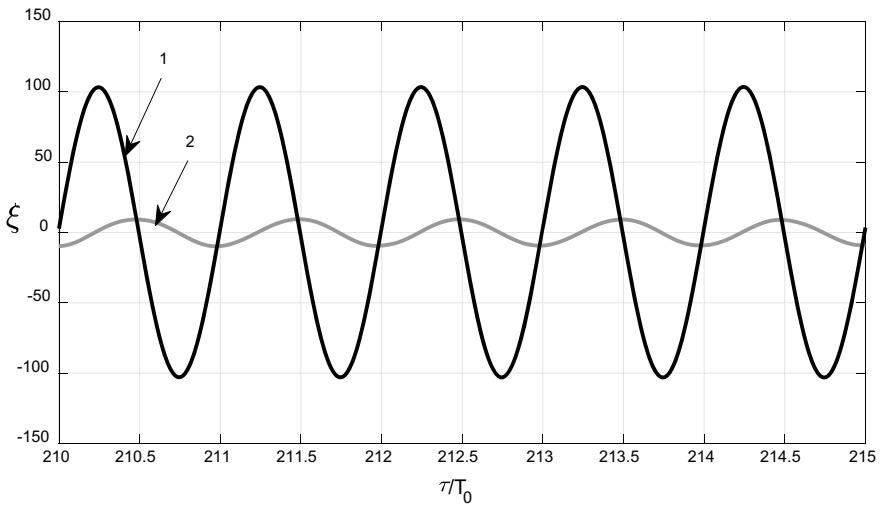


Fig. 25.5 Movements of body with damper (2) and body with similar mass without damper (1) with external frequency equal to natural

25.4 Frequency Response

To estimate the effectiveness of this device as an oscillation damper, it is advisable to build the frequency response of two bodies. First body with mass M , with dynamic

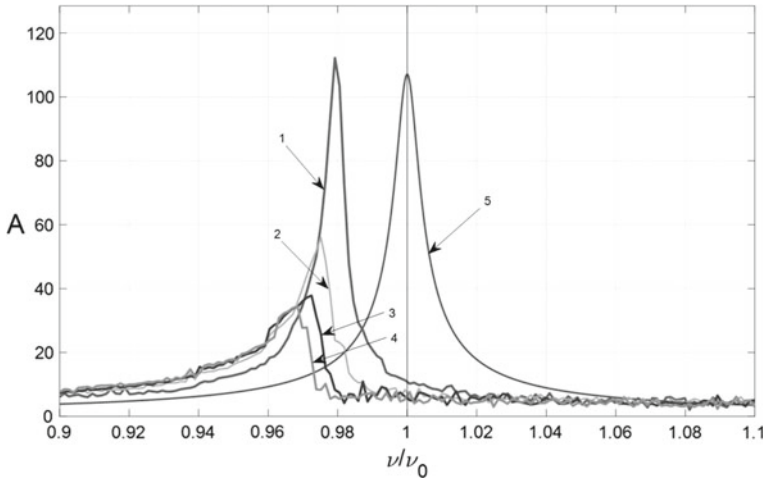


Fig. 25.6 Frequency responses' comparison

damper installed on with mass M_1 , is calculated by Eq. (25.8). The second one has mass M_2 , which is equal to full mass of first one (body and dynamic damper)

$$M_1 = m_0 + \sum_{j=1}^n m_j \quad (25.8)$$

Five frequency responses of bodies with dynamic damper consisting of four magnets are presented in Fig. 25.6 for comparison.

Numbers in Fig. 25.6 mean the following:

- 1—the first natural frequency of the device is set to the frequency of external load;
- 2—the second natural frequency of the device is set to the frequency of external load;
- 3—the third natural frequency of the device is set to the frequency of external load;
- 4—the fourth natural frequency of the device is set to the frequency of external load;
- 5—frequency response of body without damper.

The results obtained with numerical simulation of the system's motion (Fig. 25.6) show that by setting the second, third, or fourth natural frequency of dynamic damper to the frequency of external load (by setting distance between magnets in stationary state), it is possible to effectively reduce oscillations of the protected body in a wide frequency range. In particular, when $\nu_{(4)} \approx \nu_0$ in the range $\nu \in [0.98, 1.1]\nu_0$, almost complete damping of the oscillations of the main body occurs.

25.5 Conclusion

The use of the proposed device as a dynamic damper effectively reduces the amplitude of oscillations of a damped body. It is necessary to set the second, third, or fourth natural frequency of the device to body natural frequency.

Acknowledgements The Russian Science Foundation supported the work (project No. 19-19-00065).

Appendix

Analytical function for magnetic characteristic was found according to Biot–Savart–Laplace principle and current circuit interaction principle (for more details, see [16]). Following expression is obtained:

$$F(X) = \frac{3}{2} \frac{\pi B_M^2 r^4 h^2 X}{\mu_0 (r^2 + X^2)^{5/2}},$$

where

B_M —remanence of material [T],
 r —magnet radius, [m],
 h —magnet height, [m],
 μ_0 —magnetic constant, [$m \cdot \text{kg} \cdot \text{s}^{-2} \text{A}^{-2}$],
 X —distance between magnets, [m].

After some manipulations, one obtains:

$$F(z) = \frac{F_0 z}{(1 + (z)^2)^{5/2}} F_0 = \frac{3 \pi B_M^2 h^2}{2 \mu_0} z = \frac{X}{r} \quad (25.9)$$

The best match with the experiment for specific magnets shows the following function:

$$F(z) = \frac{F_0 \left(z - \frac{h}{(2r)} \right)}{\left(1 + \left(z - \frac{h}{(2r)} \right)^2 \right)^3}$$

This one was used in the numerical simulation of the device.

References

1. Vibratsii v tekhnike, T. 6 Zashchita ot vibratsii i udarov [Vibrations in technique, vol. 6: Vibration and impact protection]. Moscow, Mashinostroenie Publ (1995). (in Russ.)
2. Braun, S. (ed.): Encyclopedia of Vibration. Academic (2002)
3. Kobrinsky, A.A.: Mechanisms with Elastic Connections and Impact Systems. Ilife Books Ltd., London (1969)
4. Babitsky, V.I.: Ntheory of Vibro-Impact Systems and Applications. Springer, Berlin (1998)
5. Timofeev, G.A., Lyuminarskiy, I.E., Lyuminarskiy, S.E.: To calculation of shock vibration suppressors of unilateral action. Herald Bauman Moscow State Tech. Univ., Series Mech. Eng. **1**, 90–100 (2019)
6. Yancheng, L., Jiong, W.: Linfang nonlinear characteristics of magnetorheological damper under base excitation. In: Nonlinear Science and Complexity (2007)
7. Spaggiari, A.: Properties and applications of Magnetorheological fluids, *Frattura ed Integrità Strutturale* **23** 57–61 (2013) (IGF-ESIS.23.06 Scilla 2012—The Italian research on smart materials and MEMS)
8. Kobrinsky, A.A., Kobrinsky, A.E.: Vibro-Impact Systems. Nauka, Moscow (1973). (in Russ.)
9. Nagaev, R.F., Khodzhaev, KSh: Vibrations of Mechanical Systems with Periodic Structure. FAN, Tashkent (1973). (in Russ.)
10. Krupenin, V.L.: To the theory of strongly non-linear vibro-conduct. *Mashinovedenie* **1**, 25–32 (1987). (in Russ.)
11. Krupenin, V.L.: On the description of strongly nonlinear vibroconducting and vibrogenerating media. *J. Mach. Manuf. Reliab.* **4**, 9–19 (2016)
12. Erofeev, V.I., Kolesov, D.A., Malkhanov, A.O.: Nonlinear localized waves of deformation in the class of metamaterials as set as the mass-in-mass chain, advanced structured materials. In: Abali, B.E., Altenbach, H., dell’Isola, F., Eremeyev, V.A., Ochsner, A. (eds.) *Advanced Structured Materials series/ A Tribute to Wolfgang, H. Muller*, vol. 108, pp. 105–116. Springer Nature Switzerland AG. Part of Springer. Cham. Switzerland
13. Erofeev, V.I., Kolesov, D.A., Malkhanov, A.O.: Nonlinear strain waves in a metamaterial defined a mass-to-mass chain. In: *IOP Conference Series: Materials Science and Engineering* (2019) (in Press)
14. Panovko, Y.G.: *Osnovy prikladnoy teorii kolebaniy i udara* [Fundamentals of applied theory of oscillation and impact]. Leningrad, Mashinostroenie Publ., 1976 (in Russ.)
15. Zamuragin, Y.M., Gousov, A.M.: Vibro-impact system with magnetic elements frequency response. XXX International Innovation Conference of Young Scientists and Students IICYSS-2018: Conference proceedings (Moscow, 20–23 Nov 2018), Moscow: Publ., A.A Blagonravov MERI RAS, 2019, pp. 304–307 (in Russ.)
16. Irodov, I.E.: *Basic Principles of Electromagnetism. Tutorial for students*. Moscow, High School, 1991 (in Russ.)

Chapter 26

Exact Solutions of Cubic-Quintic Modified Korteweg-de-Vries Equation



Alexander I. Zemlyanukhin and Andrey V. Bochkarev

Abstract We study a nonintegrable modified Korteweg-de-Vries equation containing a combination of third- and fifth-degree nonlinear terms that simulate waves in a three-layer fluid, as well as in spatially one-dimensional nonlinear-elastic deformable systems. It is established that this equation passes the Painlevé test in a weak form. After the traveling wave transformation, this equation reduces to a generalized Weierstrass elliptic function equation, the right side of which is determined by a sixth-order polynomial in the dependent variable. Determined by the structure of the polynomial roots, the general solution of the equation is expressed in terms of the Weierstrass elliptic function or its successive degenerations—rational functions depending on the exponential functions of the traveling wave variable or directly on traveling wave variable. The classification of exact solitary-wave and periodic solutions is carried out, and the ranges of parameters necessary for their physical feasibility are revealed. An approach is proposed for constructing approximate solitary-wave and periodic solutions to generalized Weierstrass elliptic equation with a polynomial right-hand side of high orders.

Keywords Modified Korteweg-de-Vries equation · Exact solutions · Approximate solutions · Weierstrass elliptic function

26.1 Introduction

In the study of problems of nonlinear wave dynamics of continuous media, generalizations of equations that are integrable by the inverse scattering method often arise [1]. The simplest generalization is the Gardner integrable equation containing

A. I. Zemlyanukhin (✉) · A. V. Bochkarev
Yuri Gagarin State Technical University of Saratov,
Politeknicheskaya st. 77, Saratov 410054, Russian Federation
e-mail: zemlyanukhinai@sstu.ru

A. V. Bochkarev
e-mail: ab2009sar@list.ru

© Springer Nature Switzerland AG 2020
H. Altenbach et al. (eds.), *Nonlinear Wave Dynamics of Materials and Structures*, Advanced Structured Materials 122,
https://doi.org/10.1007/978-3-030-38708-2_26

quadratic and cubic nonlinearity. This equation revealed a new type of solitary-wave solutions—solitons of limiting amplitude, having a plate-like form [2]. The practical significance of such decisions is the ability to predict the occurrence of rogue waves in the ocean and the conditions for their prevention on the basis of a numerical experiment.

Of the nonintegrable generalizations in recent years, the modified Korteweg-de Vries (mKdV) equation containing a combination of nonlinear third- and fifth-degree terms (cubic-quintic mKdV or mKdV 3-5) attracts much attention. This equation has exact solutions in the form of solitary waves of different polarity, which at small amplitudes are close to the solitons of the mKdV equation, and at large amplitudes to the solitons of the Gardner equation [3].

The mKdV 3-5 equation first appeared when describing waves in a three-layer fluid with symmetric stratification. However, it also naturally arises in modeling the propagation of longitudinal waves in thin rods, plates and shells when the dependence of the stress intensity on the strain intensity has the form of a fifth-degree polynomial [4, 5].

In this paper, using the Painlevé analysis [6], we study the analytical structure of equation, obtained from the mKdV 3-5 equation by transition to a traveling wave variable, build its solution, expressed in terms of the Weierstrass elliptic function [7–9], classify exact and approximate partial solitary-wave and periodic solutions and plot the corresponding graphs.

26.2 Painlevé Analysis

Consider a nonlinear third-order partial differential equation, known as the mKdV 3-5 equation:

$$u_t + \alpha_1 u^2 u_x + \alpha_3 u^4 u_x + \beta u_{xxx} = 0. \quad (26.1)$$

After the transition to a running variable $z = x - ct$ and the subsequent integration over the variable z , we obtain a nonlinear second-order equation

$$\beta u_{zz} + \frac{\alpha_3}{5} u^5 + \frac{\alpha_1}{3} u^3 - cu - \frac{\beta}{2} C_1 = 0. \quad (26.2)$$

The first two terms of the equation are its leading terms. The substitution $u = u_0 z^{-p}$ in the leading terms shows that the balance between them is achieved with a fractional value $p = \frac{1}{2}$ for the pole of exact solution. Consequently, Eq. (26.2) does not pass the Painlevé test, and its general solution does not decompose into a Laurent series. However, the continuation of the Painlevé analysis gives the integer values $-1, 3$ for Fuchs indices and shows that the decomposition of $u(z)$ into the Puiseux series $\sum_{n=0} u_n (z - z_0)^{(n-1)/2}$ contains two arbitrary constants z_0 and u_6 . Thus, Eq. (26.2) passes the Painlevé test in a weak form, and this fact allows us to hope for obtaining single-valued partial solutions in a closed form [6].

After term-by-term multiplication by u_z , Eq. (26.2) can be integrated again:

$$(u_z)^2 = a_6u^6 + a_4u^4 + a_2u^2 + a_1u + a_0, \tag{26.3}$$

where

$$a_6 = -\frac{\alpha_3}{15\beta}, \quad a_4 = -\frac{\alpha_1}{6\beta}, \quad a_2 = \frac{c}{\beta}, \quad a_1 = \frac{C_1}{2}, \quad a_0 = C_2 \tag{26.4}$$

and C_1, C_2 are the integration constants.

Equation (26.3) contains an incomplete sixth-order polynomial in the dependent variable and can be considered as a generalization of the canonical equation for Weierstrass elliptic functions [10]. The representation of the general solution to Eq. (26.3) in a closed form for arbitrary values of the coefficients is unknown. We obtain its solutions in particular cases.

26.3 Case 1. $a_1 = 0, a_0 \neq 0$. Periodic and Soliton Solutions

In this case, the exact solution of Eq. (26.3) is expressed in terms of the Weierstrass elliptic function or its successive degenerations—simple periodic, rational in $\exp(z)$ or rational in z functions. The specific form of the solution depends on the structure of the roots of the polynomial on the right side of the equation.

Substituting $a_1 = 0$ into (26.3), after passing to the new dependent variable $u(z) = v(z)^{-\frac{1}{2}}$, we get

$$(v_z)^2 = 4a_0v^3 + 4a_2v^2 + 4a_4v + 4a_6. \tag{26.5}$$

Applying to $v(z)$ shift and scaling operation $v(z) = by(z) + c$, we select the following parameter values

$$b = \frac{1}{a_0}, \quad c = -\frac{a_2}{3a_0}, \tag{26.6}$$

in order to exclude from Eq. (26.5) the term containing v^2 and obtain the coefficient 4 for the higher term. As a result, we come to the canonical equation for Weierstrass elliptic functions:

$$(y_z)^2 = 4y^3 - g_2y - g_3, \tag{26.7}$$

where

$$g_2 = \frac{4}{3}a_2^2 - 4a_0a_4, \quad g_3 = -\frac{8}{27}a_2^3 + \frac{4}{3}a_0a_2a_4 - 4a_0^2a_6. \tag{26.8}$$

The general solution of Eq. (26.7) is the Weierstrass elliptic function

$$y(z) = \wp(\pm z + C_3, g_2, g_3), \tag{26.9}$$

containing an arbitrary constant C_3 , which can have a complex value. After returning to the original dependent variable $u(z)$, we obtain the general solution of Eq. (26.3):

$$u(z) = \left(\frac{a_0}{\wp(\pm z + C_3, g_2, g_3) - a_2/3} \right)^{1/2}, \tag{26.10}$$

where the invariants g_2, g_3 are determined by equalities (26.8).

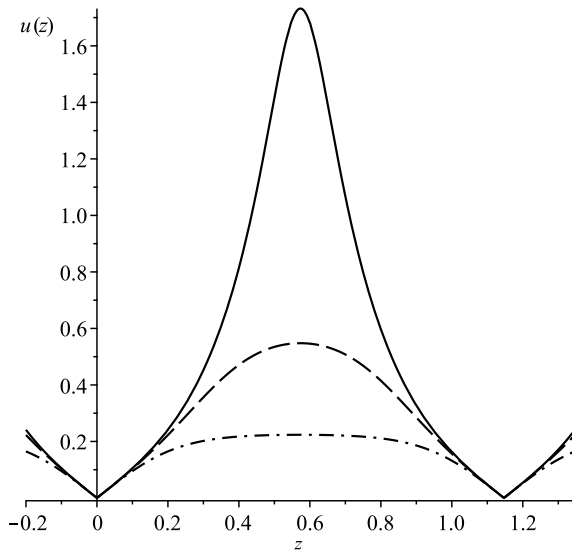
We define the ranges of the coefficients (26.4) for which the solution (26.10) is a real bounded function, considering the parameters $\alpha_1, \alpha_3, \beta$ of the original equation to be real. In this case, the invariants g_2, g_3 are also real [10], and depending on the sign of the discriminant $\Delta = g_2^3 - 27g_3^2$, three cases are possible.

If $\Delta > 0$, then the third degree polynomial

$$4y^3 - g_2y - g_3 \tag{26.11}$$

has three different real roots $y_3 < y_2 < y_1$. These roots define two ranges $y_1 \leq y$ and $y_3 \leq y \leq y_2$, in each of which the value of the polynomial (26.11) is non-negative and Eq. (26.7), which contains the square of the derivative in the left-hand side, can have a real solution. Each of these ranges corresponds to one real branch of the Weierstrass elliptic function (26.9). The first branch of the solution, which corresponds to an unlimited range $y_1 \leq y$, is a real periodic bounded function of the variable z when $C_3 = C, C \in \mathbb{R}$ in (26.10) and the conditions $a_0 > 0, a_2 < 3y_1$ are satisfied. The forms of one period of the function (26.10) at $y_1 = 10, y_2 = 9, a_0 = 1, C_3 = 0$ and three different values of a_2 are shown in Fig. 26.1.

Fig. 26.1 Form of one period of the function (26.10) at $y_1 = 10, y_2 = 9, a_0 = 1, C_3 = 0$ and $a_2 = 29$ (solid), $a_2 = 20$ (dashed), $a_2 = -30$ (dash-dotted)



The second branch of the function (26.9), corresponding to a limited range $y_3 \leq y \leq y_2$, is a real function when choosing a complex value for a constant C_3 :

$$C_3 = C + \omega_3 = C - i \int_{-\infty}^{y_3} (g_3 + g_2y - 4y^3)^{-1/2} dy, \quad C \in \mathbb{R}, \quad (26.12)$$

where ω_3 is the imaginary half period of the function $\wp(z, g_2, g_3)$. In this case, the solution (26.10) is real and bounded in the ranges $a_0 < 0, a_2 > 3y_2$ or $a_0 > 0, a_2 < 3y_3$. The corresponding graphs for each range are shown in Fig. 26.2a, b. We note that, in contrast to cnoidal waves of the first branch, which lose the continuity of the first derivative at the minimum points (Fig. 26.1), the second branch corresponds to smooth waves (Fig. 26.2).

If $\Delta < 0$, then the polynomial (26.11) has one real root y_1 and a pair of complex conjugate roots $y_{Re} \pm iy_{Im}$. There is a single range $y \geq y_1$ in which there is a real solution to Eq. (26.7). The corresponding solution (26.10) of Eq. (26.3) is real and bounded when $a_0 > 0, a_2 < 3y_1, C_3 = C, C \in \mathbb{R}$. At the same time, the form of the solution essentially depends on the ratio between y_1 and y_{Re} . In case $y_1 > y_{Re}$, the shape of graph of the polynomial (26.11) in the region $y \geq y_1$ (Fig. 26.3, dashed) differs little from that in the case considered earlier and the form of the solution curve resemble those shown in Fig. 26.1. In case $y_1 < y_{Re}$, the graph of polynomial in region $y \geq y_1$ is no longer monotonically increasing and receives a local minimum. As a result, the shape of the cnoidal wave changes and acquires a ‘‘plateau’’ zone, in the middle of which a peak rises (Fig. 26.4a).

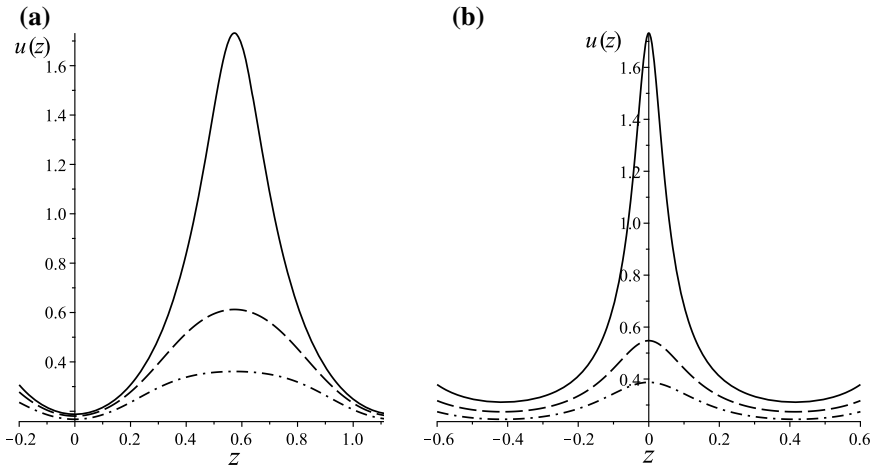


Fig. 26.2 Form of one period of the function (26.10) at $y_1 = 10, C_3 = \omega_3$: **a** $y_2 = 9, a_0 = -1$; $a_2 = 28$ (solid), $a_2 = 35$ (dashed), $a_2 = 50$ (dash-dotted), **b** $y_3 = -10, a_0 = 1$; $a_2 = -31$ (solid), $a_2 = -40$ (dashed), $a_2 = -50$ (dash-dotted)

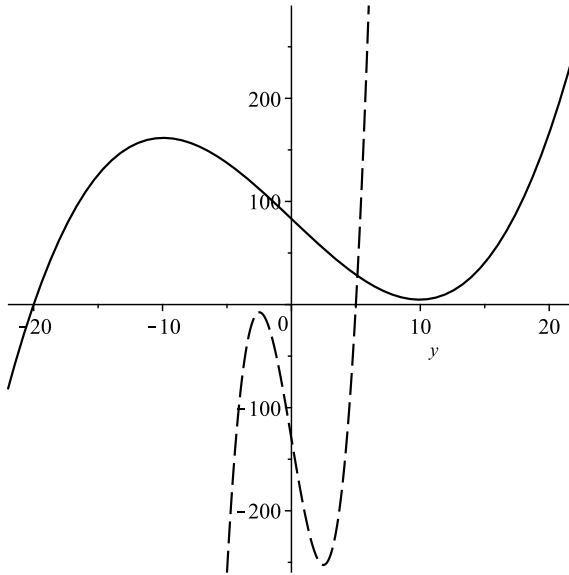


Fig. 26.3 Value of the polynomial (26.11) at $y_1 = 5$, $y_{Re} = -2.5$, $a_0 = 1$, $a_2 = 14$ (dashed) and $y_1 = -20$, $y_{Re} = 10$, $a_0 = 1$, $a_2 = -61$ (solid)

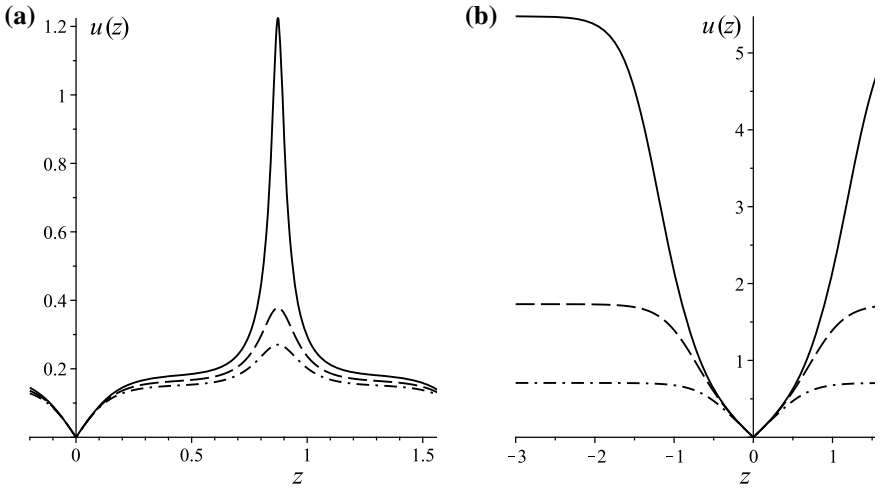


Fig. 26.4 **a** Form of one period of the function (26.10) at $y_1 = 5$, $y_{Re} = -2.5$, $a_0 = 1$, $a_2 = 14$ (dashed) and $y_1 = -20$, $y_{Re} = 10$, $a_0 = 1$, $a_2 = -61$ (solid); **b** Graphs of the solution (26.13) at $y_1 = 4$, $a_0 = 1$, $C_3 = 0$ and $a_2 = 5.9$ (solid), $a_2 = 2$ (dashed) and $a_2 = 0$ (dash-dotted)

If $\Delta = 0$, then with roots of (26.11), there are three possible situations: (1) there are simple root y_1 and double root y_2 , and $y_1 > y_2$, (2) there are double root y_1 and simple root y_2 , and $y_1 > y_2$, and (3) there is a triple root y_1 .

In situation 1, there is a periodic solution corresponding to the range $y \geq y_1$, the shape of which resembles Fig. 26.1. In situation 2, there are already two ranges: the limited $y_2 \leq y \leq y_1$ and semi-infinite $y \geq y_1$, each of which is limited by the value of the double root y_1 . The polynomial right-hand side of (26.3) ensures that derivatives $u^{(n)}$ of any order at the points corresponding to the multiple roots of the right-hand side vanish. At the same time, at the points of simple roots, the second and higher derivatives $u^{(n)}$ are nonzero. Therefore, in the finite or semi-infinite ranges that come into contact with simple roots only, periodic solutions appear since unstable stationary points of the solution correspond to simple roots. If one and only one of the boundaries of the range corresponds to a multiple root, then solitary-wave solutions arise in this range since multiple roots give points of indifferent equilibrium. Finally, if both boundaries of the range are bounded by multiple roots, then a solution in the form of a kink is observed.

In situation 2, Eq. (26.7) can be represented in the form

$$(y_z)^2 = 4(y + y_1) \left(y - \frac{y_1}{2}\right)^2, \tag{26.13}$$

where $y_1 > 0$. The general solution of Eq. (26.12) is expressed in terms of the hyperbolic sine

$$u(z) = \left(\frac{a_0}{\frac{y_1}{2} \left(1 + 3\sinh^{-2} \frac{\sqrt{6}y_1}{2} (z + C_3)\right) - \frac{a_2}{3}} \right)^{1/2}. \tag{26.14}$$

The function (26.13) is a degeneration of the solution (26.10), expressed in terms of the Weierstrass elliptic function (26.9). For $a_0 > 0$, $a_2 < 3y_1/2$, $C_3 \in \mathbb{R}$ solution (26.13) that corresponds to a semi-infinite range $y \geq y_1$ is real, bounded and has the form of a “dark” cnoidal soliton (Fig. 26.4b).

To obtain a solution for a finite range $y_2 \leq y \leq y_1$, it suffices to use the property of the periodicity of a function $\sinh^{-2}(z + C_3)$ along the imaginary axis—it has real values not only for $C_3 \in \mathbb{R}$ but also for a shift by half of the imaginary period $C_3 = C + i\pi/2$, $C \in \mathbb{R}$. With this shift, the function $\sinh^{-2}(z + C_3)$ becomes bounded and determines smooth solitary waves at $a_0 > 0$, $a_2 < -3y_1$ or at $a_0 < 0$, $a_2 > 3y_1/2$. The first group of conditions determines the “light” solitons, and the second - the “dark” ones, which differ from those shown in Fig. 26.4b by smoothness of form.

Finally, in the third situation, when the polynomial (26.11) has a single triple root, Eq. (26.7) is simplified to

$$(y_z)^2 = 4y^3 \tag{26.15}$$

with rational solution

$$y(z) = \wp(z + C_3, 0, 0) = (z + C_3)^{-2}. \tag{26.16}$$

The last equality gives for Eq. (26.3) a solution

$$u(z) = \left(\frac{a_0}{(z + C_3)^{-2} - a_2/3} \right)^{1/2}, \tag{26.17}$$

corresponding to a rational dark cnoidal soliton with a graph similar to that shown in Fig. 26.4b by dash-dotted line.

26.4 Case 2. $a_1 = 0, a_0 = 0$. Periodic and Soliton Solutions

Assuming that $4a_6 - a_4^2/a_2 > 0$ and using the substitution $v(z) = b_1y(z) + b_2$, we select the constants b_1 and b_2 so that for the function $y(z)$ we obtain the equation

$$(y_z)^2 = 4a_2y^2 + 1, \tag{26.18}$$

whose general solution is

$$y = \frac{1}{2\sqrt{a_2}} \sinh 2\sqrt{a_2} (z + C_3). \tag{26.19}$$

When $a_2 < 0, a_4 > 0$, equality (26.19) defines a real bounded periodic solution of Eq. (26.3):

$$u = \left(\frac{2a_2}{\sqrt{a_4^2 - 4a_2a_6} \sin 2\sqrt{-a_2} (z + C_3) - a_4} \right)^{1/2}. \tag{26.20}$$

When the condition $4a_6 - a_4^2/a_2 < 0$ is satisfied, Eq. (26.5) is reduced to

$$(y_z)^2 = 4a_2y^2 - 1, \tag{26.21}$$

whose general solution has the form

$$y = \frac{1}{2\sqrt{a_2}} \cosh 2\sqrt{a_2} (z + C_3). \tag{26.22}$$

The corresponding expression for function $u(z)$ determines solution of Eq. (26.3)

$$u = \left(\frac{2a_2}{\sqrt{a_4^2 - 4a_2a_6} \cosh 2\sqrt{a_2}(z + C_3) - a_4} \right)^{1/2}, \tag{26.23}$$

that is real in two cases. Under condition $a_2 > 0, a_4 > 0, a_6 < 0$ function (26.23) describes a soliton whose amplitude tends to infinity and width tends to zero at $a_6 \rightarrow 0$. Under condition $a_2 > 0, a_4 < 0, a_6 < a_4^2/4a_2$, we have a soliton with a flat top (table-like solution), whose amplitude does not exceed $\sqrt{2a_2}/-a_4$, and width increases indefinitely when a_6 tends to its maximum allowable value. An analytical representation and corresponding graphs of the table-like solution were obtained in [3]. Numerical analysis revealed the inelasticity of the interaction of flat top solitons.

26.5 Case 3. Kink-Shaped Solution

Replacement $u(z) = v(z)^{-1/2}$, used in cases 1 and 2, requires that the function $u(z)$ is non-negative and does not allow finding solutions of Eq. (26.3) in the form of a kink. Therefore, it is now necessary to work directly with Eq. (26.3). As mentioned earlier, a solution in the form of a kink can occur in a finite range, limited at the ends by two multiple roots of the right-hand side polynomial of (26.3). As a simple analysis shows, there are only three variants of the structure of the polynomial roots, for which such a range exists.

In the first variant, there are two triple roots $\pm u_1$. Equation (26.3) takes the form

$$(u_z)^2 = a_6(u - u_1)^3(u + u_1)^3 \tag{26.24}$$

and when $a_6 < 0$, it has as a general solution the “rational” kink

$$u = u_1^3(z + C_3) \left(\frac{a_6}{a_6 u_1^4(z + C_3)^2 - 1} \right)^{1/2}. \tag{26.25}$$

In the second variant, there are three double roots $\pm u_1$ and $u_2 = 0$. Equation (26.3) takes the form

$$(u_z)^2 = a_6 u^2(u - u_1)^2(u + u_1)^2 \tag{26.26}$$

and has two branches of solutions in the form of kinks at $-u_1 \leq u \leq 0$ and at $0 \leq u \leq u_1$ when $a_6 > 0$. In the particular case, for example, when $a_2 = a_6 = 1$, these solutions are determined by the equations

$$u = \pm \frac{1}{\sqrt{C_3 \exp(\pm 2z) + 1}}. \tag{26.27}$$

Finally, in the third version, there are two real double roots $\pm u_1$ and a pair of imaginary roots $\pm iu_{\text{Im}}$:

$$(u_z)^2 = a_6 (u^2 + u_{\text{Im}}^2) (u - u_1)^2 (u + u_1)^2. \tag{26.28}$$

The exact solution (26.28) is cumbersome and is written in an implicit form. In particular, when $a_6 = u_1 = 1$, $u_{\text{Im}} = (2\sqrt{6})^{-1}$, this solution looks like

$$z - \frac{\sqrt{6}}{5} \sum_{k=1}^2 \operatorname{arctanh} \left(\frac{\sqrt{6} (-1)^k + 24u}{5 \sqrt{6 + 144u^2}} \right) = C_3. \tag{26.29}$$

26.6 Case 4. $a_1 \neq 0$, $a_0 \neq 0$. Approximate Solution

The complete Eq. (26.3), all five terms of which are nonzero, is integrated in quadratures as a first-order equation, but the analytical representation of its general solution through elementary or special functions is unknown. Meanwhile, we can propose a simple method for constructing an analytical representation of its approximate solution.

Suppose that among the roots of the right-hand side of (26.3) as a sixth-order polynomial in the function u , there are two simple or multiple real roots u_A and u_B , $u_A < u_B$:

$$(u_z)^2 = (u - u_A)^{k_A} (u - u_B)^{k_B} p_m(u), \tag{26.30}$$

where $m = 6 - k_A - k_B$ is the order of the polynomial $p_n(u)$. Let the right-hand side of (26.30) be non-negative in the range $u_A \leq u \leq u_B$. Then, in this range, there is a bounded real solution of Eq. (26.30). Replace Eq. (26.30) with an approximate equation

$$(u_z)^2 = (u - u_A)^{k_A} (u - u_B)^{k_B} q_n(u), \tag{26.31}$$

the right side of which contains polynomial $q_n(u)$, has order in u not higher than fourth and is close in the range $u_A \leq u \leq u_B$ to the right side (26.30). The exact solution of Eq. (26.31) is expressed in terms of the Weierstrass elliptic function or its degenerations and gives an analytical representation of an approximate solution to Eq. (26.30).

To solve (26.31), following [10], we group the right-hand side of (26.31) in powers of u :

$$(u_z)^2 = a_4 u^4 + a_3 u^3 + a_2 u^2 + a_1 u + a_0 \tag{26.32}$$

and represent it in the form

$$(u_z)^2 = A_1 (u - u_A) + A_2 (u - u_A)^2 + A_3 (u - u_A)^3 + A_4 (u - u_A)^4 \tag{26.33}$$

Expressing $A_1 - A_4$ through $a_0 - a_4$, after substituting $u(z) = 1/v(z) + u_A$ for function $v(z)$, we have the equation

$$(v_z)^2 = A_1 v^3 + A_2 v^2 + A_3 v + A_4, \tag{26.34}$$

similar to Eq. (26.5). Repeating the steps described above for (26.5), we solve (26.34) and present the general solution (1.30) in the form

$$u(z) = u_A - \frac{3A_1}{A_2 - 12\wp(z + C_3, g_2, g_3)}, \tag{26.35}$$

where

$$\begin{aligned} A_1 &= 4q_4 u_A^3 + 3q_3 u_A^2 + 2q_2 u_A + q_1, & A_2 &= \frac{1}{2} \frac{dA_1}{du_A}, & A_3 &= \frac{1}{3} \frac{dA_2}{du_A}, & A_4 &= q_4, \\ g_2 &= \frac{1}{12} (A_2^2 - 3A_1 A_3), & g_3 &= -\frac{1}{432} (2A_2^3 - 9A_1 A_2 A_3 + 27A_1^2 A_4). \end{aligned} \tag{26.36}$$

Equality (26.35) with conditions (26.36) is an analytical representation of an approximate solution of Eq. (26.30).

Consider an example. Let the right-hand side of (26.30) be

$$\begin{aligned} P &= (u - u_1)(u - u_2)(u - u_3)(u - u_4)(u - u_5)(u - u_6) \\ &= \left(u + \frac{13}{4} + \frac{3\sqrt{65}}{52}\right) \left(u + \frac{13}{4} - \frac{3\sqrt{65}}{52}\right) \left(u + \frac{1}{2}\right) (u - 1)(u - 2)(u - 4) \\ &\approx u^6 - 21.4u^4 + 98.1u^2 - 36.3u - 41.4. \end{aligned} \tag{26.37}$$

On the graph of the function (26.37) (Fig. 26.5), there are two suitable ranges: $\Delta_1 = \{u, u_4 \leq u \leq u_5\}$ and $\Delta_2 = \{u, u_2 \leq u \leq u_3\}$. To find an approximate solution corresponding to, for example, Δ_1 , we consider a fourth order polynomial

$$Q = (u - u_4)(u - u_5)(q_2 u^2 + q_1 u + q_0) \tag{26.38}$$

and choose arbitrary constants q_0, q_1, q_2 so that the values of the polynomials P and Q are close to each other on range Δ_1 . The closeness criterion can be chosen differently. Since the solution function $u(z)$ “spends” the longest time near the boundaries of the range due to the proximity of the derivative u_z to zero there, it seems reasonable to require that at the boundaries of the range not only the values of P and Q polynomials but also the its first derivatives coincide:

$$\left. \frac{dQ}{du} \right|_{u=u_4, u_5} = \left. \frac{dP}{du} \right|_{u=u_4, u_5}. \tag{26.39}$$

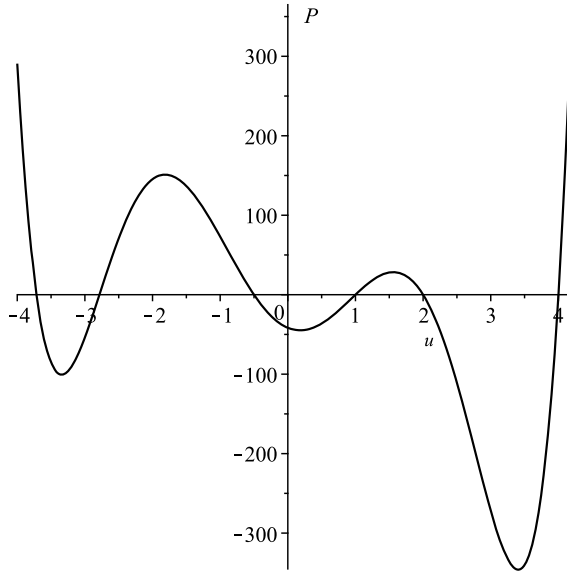


Fig. 26.5 Graph of the function (26.37)

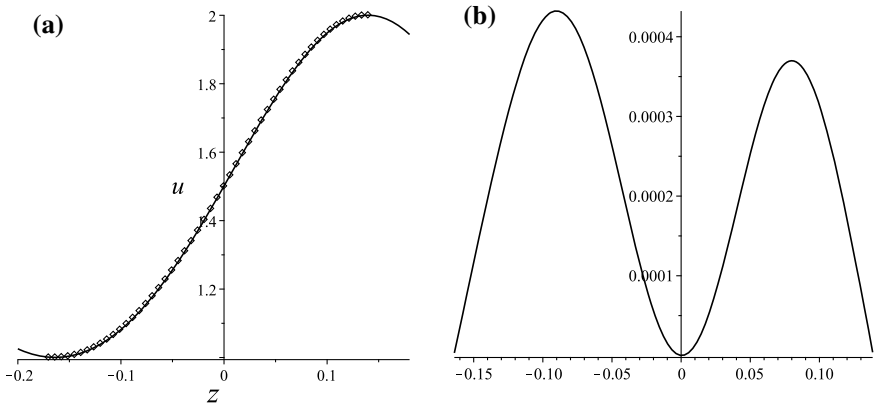


Fig. 26.6 **a** Numerical solution (box) and an approximate analytical solution (solid), **b** Difference between the numerical and approximate analytical solutions

Adding a couple of conditions (26.39) with the requirement that the standard deviation be zero:

$$\int_{u_4}^{u_5} (P - Q)^2 du = 0, \tag{26.40}$$

we obtain the system from which we determine the constants $q_0 - q_2$:

$$Q = (u - 1)(u - 2) \left(\frac{7361}{572}u^2 - \frac{54357}{572}u + \frac{265}{143} \right). \quad (26.41)$$

The general solution of Eq. (26.31) with the right side (26.41) is determined by the expression (26.35), which gives an analytical representation of the approximate solution of the original Eq. (26.30) with the right side (26.37) for the range Δ_1 . Comparison of the results of numerical integration of Eq. (26.30) with an approximate analytical solution (26.35) shows that the absolute error of the approximate solution within half of the period in z does not exceed 5×10^{-4} , while the oscillation range reaches unity (Fig. 26.6).

Funding The reported study was funded by RFBR, project number 20-01-00123.

References

1. Bagdoev, A.G., Erofejev, V.I., Shekoyan, A.V.: Wave Dynamics of Generalized Continua. Springer, Heidelberg (2016)
2. Pelinovskii, E.N., Slyunyaev, A.V.: Generation and interaction of large-amplitude solitons. *Jetp Lett.* **67**(9), 655–661 (1998)
3. Kurkina, O.E., Kurkin, A.A., Ruvinskaya, E.A., Pelinovsky, E.N., Soomere, T.: Dynamics of solitons in a nonintegrable version of the modified Korteweg-de Vries equation. *Jetp Lett.* **95**(2), 91–95 (2012)
4. Bochkarev, A.V., Zemlyanukhin, A.I., Mogilevich, L.I.: Solitary waves in an inhomogeneous cylindrical shell interacting with an elastic medium. *Acoust. Phys.* **63**(2), 148–153 (2017)
5. Zemlyanukhin, A.I.: Exact solutions of the fifth-order non-linear evolution equation. *Reg. Chaotic Dyn.* **4**(3), 67–69 (1999)
6. Conte, R., Musette, M.: The Painlevé Handbook. Springer, New York (2008)
7. Porubov, A.V.: Exact travelling wave solutions of nonlinear evolution equation of surface waves in a convecting fluid. *J. Phys. A Math. Gen.* **26**, L797–L800 (1993)
8. Porubov, A.V.: Periodical solution to the nonlinear dissipative equation for surface waves in a convecting liquid layer. *Phys. Lett. A* **221**(6), 391–394 (1996)
9. Samsonov, A.M.: Travelling wave solutions for nonlinear waves with dissipation. *Appl. Anal.* **57**, 85–100 (1995)
10. Whittaker, E.T., Watson, G.N.: A Course of Modern Analysis. Cambridge University Press, Cambridge (1996)

Chapter 27

Modelling of Unsteady Elastic Diffusion Oscillations of a Timoshenko Beam



Andrei V. Zemskov and Dmitry V. Tarlakovskii

Abstract We study unsteady oscillations of a Timoshenko beam considering mass transfer. In a general case, the beam is subjected to tensile forces, bending moments and shear forces applied to its ends. Densities of diffusion fluxes are also defined at the ends of the beam. All aforementioned force factors lie in the beam's plane of bending. We define the problem using a model of unsteady flat bending of an elastodiffusive beam. Solution for the problem is obtained using Laplace transform and Fourier series.

Keywords Elastic diffusion · Coupled problem · Unsteady problem · Green's function · Integral transformation · Multicomponent continuum · Timoshenko beam

27.1 Introduction

Currently, there are many publications devoted to modelling effects associated with the interaction of fields of various physical nature. Among them, one can mention works on thermoelasticity [1, 2], electroelasticity and electromagnetoelasticity, as well as thermoelectromagnetoelasticity [3–10].

From the second half of the 20th century to the present, there has been an urgent problem associated with the influence study of diffusion processes on the medium stress–strain state and structural elements. It is also interesting to considering of other fields: temperature, electromagnetic, etc. Among the most recent publications, it can be noted [11–20].

In these articles, the interaction problems of physical fields are mainly considered in a static or stationary formulation for space, half-space or a layer. At the same time, real structural elements usually have finite dimensions (rods, plates or shells). In

A. V. Zemskov (✉) · D. V. Tarlakovskii
Moscow Aviation Institute, Moscow, Russian Federation

Institute of Mechanics, Lomonosov Moscow State University, Moscow, Russian Federation

addition, real loads can be non-stationary in nature, which also needs to be considered when choosing a calculation model.

We note that the solution of unsteady problems (in particular, mechanodiffusion problems) is associated with great computational difficulties. When constructing analytical solutions, a problem arises with the Laplace transform inversion. Issues related to this problem are discussed in detail in [21]. When using numerical methods, questions arise related to the stability of difference schemes, as well as the study of their convergence.

In this article, we study the unsteady oscillation of a Timoshenko beam with considering of mass transfer. We also propose an analytical method for solving the problem based on series expansion in eigenfunctions of the elastic diffusion operator.

27.2 Problem Formulation

We consider the flat unsteady oscillations problem of a Timoshenko beam with mass transfer effects. The beam is subjected to tensile forces, bending moments and shear forces applied to its ends. Densities of diffusion fluxes are also defined at the ends of the beam. Figure 27.1 shows the orientation of Cartesian axes as well as how the forces and the bending moments are applied to the beam.

For the problem formulation, we use the coupled elastic diffusion continuum model in a rectangular Cartesian coordinate system, which has the next form [11–13, 16, 18–20, 22–24]:

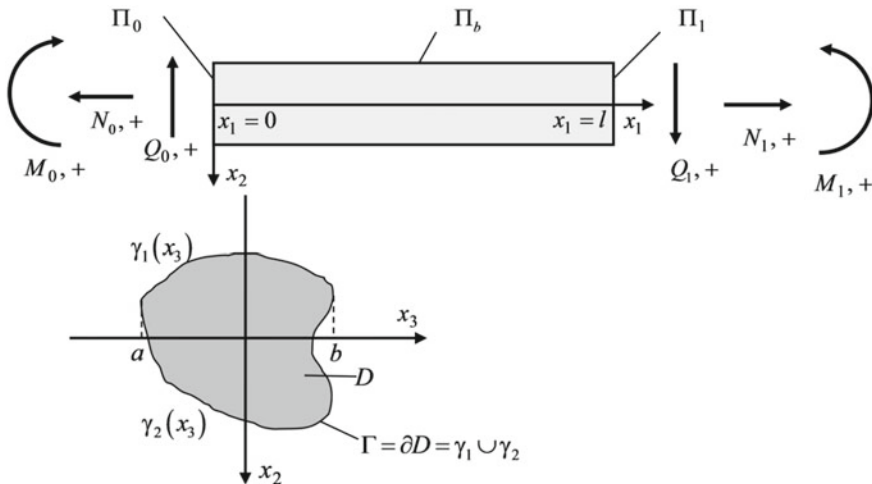


Fig. 27.1 Forces and bending moments acting upon the beam

$$\begin{aligned}
\ddot{u}_i - \frac{\partial \sigma_{ij}}{\partial x_j} - F_i &= 0, \quad \dot{\eta}^{(q)} + \frac{\partial J_i^{(q)}}{\partial x_i} - Y^{(q)} = 0, \quad (x_1, x_2, x_3) \in G \subset \mathfrak{R}^3, \\
\sigma_{ij} n_j \Big|_{\Pi_\sigma} &= P_i, \quad J_i^{(q)} \Big|_{\Pi_J} = I_i^{(q)}, \quad \partial G = \Pi_\sigma \cup \Pi_J, \\
u_i \Big|_{\tau=0} &= 0, \quad \frac{\partial u_i}{\partial \tau} \Big|_{\tau=0} = 0, \quad \eta^{(q)} \Big|_{\tau=0} = 0, \quad \frac{\partial \eta^{(q)}}{\partial \tau} \Big|_{\tau=0} = 0 \quad (q = \overline{1, N}),
\end{aligned} \tag{27.1}$$

where σ_{ij} and $J_i^{(q)}$ are components of stress tensor and diffusion flux vector which are the defined by ($q = \overline{1, N}$) [22–25]:

$$\sigma_{ij} = C_{ijkl} \frac{\partial u_k}{\partial x_l} - \sum_{q=1}^N \alpha_{ij}^{(q)} \eta^{(q)}, \quad J_i^{(q)} = - \sum_{t=1}^N D_{ij}^{(q)} g^{(qt)} \frac{\partial \eta^{(t)}}{\partial x_j} + \Lambda_{ijkl}^{(q)} \frac{\partial^2 u_k}{\partial x_j \partial x_l}. \tag{27.2}$$

All the variables in these formulas are dimensionless values and are defined as seen below

$$\begin{aligned}
x_i &= \frac{x_i^*}{l}, \quad u_i = \frac{u_i^*}{l}, \quad \tau = \frac{Ct}{l}, \quad C_{ijkl} = \frac{C_{ijkl}^*}{C_{1111}^*}, \quad C^2 = \frac{C_{1111}^*}{\rho}, \quad \alpha_{ij}^{(q)} = \frac{\alpha_{ij}^{*(q)}}{C_{1111}^*}, \\
D_{ij}^{(q)} &= \frac{D_{ij}^{*(q)}}{Cl}, \quad \Lambda_{ijkl}^{(q)} = \frac{m^{(q)} D_{ij}^{*(q)} \alpha_{kl}^{*(q)} n_0^{(q)}}{\rho RT_0 Cl}, \quad F_i = \frac{\rho l F_i^*}{C_{1111}^*}, \quad Y^{(q)} = \frac{l Y^{*(q)}}{C},
\end{aligned}$$

where t is time; x_i^* are Cartesian coordinates; u_i^* are displacement vector components; l is the length of the beam; $\eta^{(q)} = n^{(q)} - n_0^{(q)}$ are concentration increments for the q -th substance component of an N -component medium; $n^{(q)}$ and $n_0^{(q)}$ are actual and initial concentrations of q -th component; C_{ijkl}^* are components of the elastic constant tensor; ρ is density; $\alpha_{ij}^{*(q)}$ are coefficients characterizing volume changing of the medium due to diffusion; $D_{ij}^{*(q)}$ are coefficients of diffusion; R is universal gas constant; T_0 is the temperature of the medium; $m^{(q)}$ is molar mass; P_i and $I_i^{(q)}$ are surface disturbances; F_i^* and $Y_i^{*(q)}$ are volume disturbances; n_i are components of the outer normal unit vector to $\partial G = \Pi_\sigma \cup \Pi_J$.

The beam oscillation equations are obtained using the Lagrange–D’Alembert principle. Using equations (27.1), we obtain:

$$\begin{aligned}
\int_G \left(\ddot{u}_i - \frac{\partial \sigma_{ij}}{\partial x_j} - F_i \right) \delta u_i dG + \sum_{q=1}^N \int_G \left(\dot{\eta}^{(q)} + \frac{\partial J_i^{(q)}}{\partial x_i} - Y^{(q)} \right) \delta \eta^{(q)} dG \\
+ \iint_{\Pi_\sigma} (\sigma_{ij} n_j - P_i) \delta u_i dS + \sum_{q=1}^N \iint_{\Pi_J} (J_i^{(q)} - I_i^{(q)}) n_i \delta \eta^{(q)} dS = 0.
\end{aligned} \tag{27.3}$$

To construct the equations of bending, we assume the following:

- material of the beam is uniform and isotropic (λ and μ are Lamé coefficients, δ_{qr} is the Kronecker symbol)

$$C_{ijkl} = \lambda \delta_{ij} \delta_{kl} + \mu (\delta_{ik} \delta_{jl} + \delta_{il} \delta_{jk}), \quad \Lambda_{\alpha\alpha\beta\beta}^{(q)} = \Lambda_q, \quad \alpha_{\alpha\alpha}^{(q)} = \alpha_q, \quad D_{\alpha\alpha}^{(q)} = D_q.$$

- the transverse deflections of the beam are small. Sections normal to the axis of the beam before deformation remain flat after deformation (flat sections hypothesis). In this case, linearization of desired values in respect to x_2 will give the following (approximate equality becomes exact equality) [22–24, 26]

$$\begin{aligned} u_1(x_1, x_2, \tau) &= u(x_1, \tau) + x_2 \chi(x_1, \tau), \\ u_2(x_1, x_2, \tau) &= v(x_1, \tau) + x_2 \psi(x_1, \tau), \\ \eta^{(q)}(x_1, x_2, \tau) &= N_q(x_1, \tau) + x_2 H_q(x_1, \tau). \end{aligned} \tag{27.4}$$

- there are no loads on the side surface. This allows us to use the hypothesis of the beam incompressibility in the transverse direction. In this case, $\psi(x_1, \tau) \equiv 0$. (27.4) can be written as

$$\begin{aligned} u_1(x_1, x_2, \tau) &= u(x_1, \tau) - x_2 \chi(x_1, \tau), \quad u_2(x_1, x_2, \tau) = v(x_1, \tau), \\ \eta^{(q)}(x_1, x_2, \tau) &= N_q(x_1, \tau) + x_2 H_q(x_1, \tau). \end{aligned} \tag{27.5}$$

The components of the stress tensor and the diffusion flux vector (27.2) will have the form [24]

$$\begin{aligned} \sigma_{11} &= \frac{\partial u_1}{\partial x_1} + \lambda \frac{\partial u_2}{\partial x_2} - \sum_{q=1}^N \alpha_q \eta^{(q)} = (u' - x_2 \chi') - \sum_{q=1}^N \alpha_q (N_q + x_2 H_q), \\ \sigma_{22} &= \lambda \frac{\partial u_1}{\partial x_1} + \frac{\partial u_2}{\partial x_2} - \sum_{q=1}^N \alpha_q \eta^{(q)} = \lambda (u' - x_2 \chi') - \sum_{q=1}^N \alpha_q (N_q + x_2 H_q), \\ \sigma_{12} &= \mu \frac{\partial u_1}{\partial x_2} - \mu \frac{\partial u_2}{\partial x_1} = \mu (v' - \chi), \quad \frac{\partial \sigma_{12}}{\partial x_2} = 0, \end{aligned} \tag{27.6}$$

$$\begin{aligned} J_1^{(q)} &= -D_q \frac{\partial \eta^{(q)}}{\partial x_1} + \Lambda_q \frac{\partial^2 u_1}{\partial x_1^2} + \Lambda_q \frac{\partial^2 u_2}{\partial x_1 \partial x_2} \\ &= -D_q (N_q' + x_2 H_q') + \Lambda_q (u'' - x_2 \chi''), \\ J_2^{(q)} &= -D_q \frac{\partial \eta^{(q)}}{\partial x_2} + \Lambda_q \frac{\partial^2 u_2}{\partial x_2^2} + \Lambda_q \frac{\partial^2 u_1}{\partial x_1 \partial x_2} = -D_q H_q - \Lambda_q \chi' \quad (q = \overline{1, N}). \end{aligned} \tag{27.7}$$

Substituting (27.5) and (27.6) into (27.3), we obtain the model of unsteady plane bending of an elastodiffusive Timoshenko beam:

- the problem of uniaxial tension–compression of the rod with diffusion

$$\ddot{u} - u'' + \sum_{q=1}^N \alpha_q N'_q - n = 0, \quad \dot{N}_q - D_q N''_q + \Lambda_q u''' - y^{(q)} = 0; \quad (27.8)$$

$$\left(u' - \sum_{q=1}^N \alpha_q N_q \right) \Big|_{x_1=0} = \frac{N_0}{F}, \quad \left(u' - \sum_{q=1}^N \alpha_q N_q \right) \Big|_{x_1=1} = \frac{N_1}{F}; \quad (27.9)$$

$$\left(\Lambda_q u'' - D_q N'_q \right) \Big|_{x_1=0} = \frac{\Gamma_0^{(q)}}{F}, \quad \left(\Lambda_q u'' - D_q N'_q \right) \Big|_{x_1=1} = \frac{\Gamma_1^{(q)}}{F}, \quad (27.10)$$

- the problem of beam deflections with diffusion

$$\begin{aligned} \ddot{v} - \mu (v'' - \chi') - \frac{q}{F} &= 0, \\ \ddot{\chi} - \chi'' - \frac{F}{J_3} \mu (v' - \chi) - \sum_{q=1}^N \alpha_q H'_q - \frac{m}{J_3} &= 0, \end{aligned} \quad (27.11)$$

$$\dot{H}_q - D_q H''_q - \Lambda_q \chi''' - \frac{z^{(q)}}{J_3} = 0;$$

$$(v' - \chi) \Big|_{x_1=0} = \frac{Q_0}{\mu F}, \quad (v' - \chi) \Big|_{x_1=1} = \frac{Q_1}{\mu F}; \quad (27.12)$$

$$\left(\chi' + \sum_{q=1}^N \alpha_q H_q \right) \Big|_{x_1=0} = -\frac{M_0}{J_3}, \quad \left(\chi' + \sum_{q=1}^N \alpha_q H_q \right) \Big|_{x_1=1} = -\frac{M_1}{J_3}; \quad (27.13)$$

$$\left(\Lambda_q \chi'' + D_q H'_q \right) \Big|_{x_1=0} = -\frac{\Omega_0^{(q)}}{J_3}, \quad \left(\Lambda_q \chi'' + D_q H'_q \right) \Big|_{x_1=1} = -\frac{\Omega_1^{(q)}}{J_3}, \quad (27.14)$$

where F is cross section area, J_3 is beam's moment of inertia relative to Ox_3 , $m(x_1, \tau)$ is distributed lineal moment, $q(x_1, \tau)$ is distributed lineal transverse load; $n(x_1, \tau)$ is the linearly distributed axial load; $z^{(q)}(x_1, \tau)$ and $y^{(q)}(x_1, \tau)$ is density of volume sources of mass transfer. The other force factors are shown as follows

$$N_0(\tau) = \iint_D P_1(0, x_2, x_3, \tau) dx_2 dx_3, \quad N_1(\tau) = \iint_D P_1(1, x_2, x_3, \tau) dx_2 dx_3,$$

$$M_0(\tau) = \iint_D P_1(0, x_2, x_3, \tau) x_2 dx_2 dx_3, \quad M_1(\tau) = \iint_D P_1(1, x_2, x_3, \tau) x_2 dx_2 dx_3,$$

$$Q_0(\tau) = \iint_D P_2(0, x_2, x_3, \tau) dx_2 dx_3, \quad Q_1(\tau) = \iint_D P_2(1, x_2, x_3, \tau) dx_2 dx_3,$$

$$\begin{aligned} \Gamma_0^{(q)}(\tau) &= \iint_D I_1^{(q)}(0, x_2, x_3, \tau) dx_2 dx_3, \\ \Gamma_1^{(q)}(\tau) &= \iint_D I_1^{(q)}(1, x_2, x_3, \tau) dx_2 dx_3, \\ \Omega_0^{(q)}(\tau) &= \iint_D x_2 I_1^{(q)}(0, x_2, x_3, \tau) dx_2 dx_3, \\ \Omega_1^{(q)}(\tau) &= \iint_D x_2 I_1^{(q)}(1, x_2, x_3, \tau) dx_2 dx_3. \end{aligned}$$

In more accurate models [for this, it is necessary to take into account terms of a higher order of smallness in (27.4)], Equations (27.11) are written as

$$\begin{aligned} \ddot{v} - \mu k^2 (v'' - \chi') - \frac{q}{F} &= 0, \\ \ddot{\chi} - \chi'' - \frac{F}{J_3} \mu k^2 (v' - \chi) - \sum_{q=1}^N \alpha_q H'_q - \frac{m}{J_3} &= 0, \\ \dot{H}_q - D_q H''_q - \Lambda_q \chi''' - \frac{z^{(q)}}{J_3} &= 0, \end{aligned} \tag{27.15}$$

where k —coefficient taking into account the uneven distribution of shear stresses over the beam section. If the shear stresses are distributed according to the Zhuravsky formula, then for the rectangular cross section beam with a height h and unit thickness, we have [26]

$$k^2 = \frac{5}{6}.$$

In accordance with the Lagrange variational principle, the boundary conditions (27.9), (27.10), (27.12)–(27.14) are considered in conjunction with the kinematic boundary conditions

$$u|_{x_1=0} = U_0(\tau), \quad u|_{x_1=1} = U_1(\tau); \tag{27.16}$$

$$N_q|_{x_1=0} = N_{q0}(\tau), \quad N_q|_{x_1=1} = N_{q1}(\tau); \tag{27.17}$$

$$v|_{x_1=0} = V_0(\tau), \quad v|_{x_1=1} = V_1(\tau); \tag{27.18}$$

$$H_q|_{x_1=0} = H_{q0}(\tau), \quad H_q|_{x_1=1} = H_{q1}(\tau); \tag{27.19}$$

$$\chi|_{x_1=0} = X_0(\tau), \quad \chi|_{x_1=1} = X_1(\tau).$$

The solution of problems (27.8)–(27.10), (27.16), (27.17) was considered in [25]. Here, we will consider initial-boundary value problems for Eq. (27.15).

27.3 Integral Representation of the Solution

We represent the solution to (27.15), (27.13), (27.18), (27.19) as ($k = \overline{1, N+1}$) [24]:

$$\begin{aligned}
 v(x, \tau) &= \sum_{k=1}^{N+2} \int_0^\tau [G_{1k}(x, \tau-t)f_{k1}(t) + G_{1k}(1-x, \tau-t)f_{k2}(t)] dt \\
 &\quad + \sum_{k=1}^{N+2} \int_0^\tau \int_0^1 \tilde{G}_{1k}(x, \xi, \tau-t) F_k(\xi, t) d\xi dt, \\
 \chi(x, \tau) &= \sum_{k=1}^{N+2} \int_0^\tau [G_{2k}(x, \tau-t)f_{k1}(t) - G_{2k}(1-x, \tau-t)f_{k2}(t)] dt \\
 &\quad + \sum_{k=1}^{N+2} \int_0^\tau \int_0^1 \tilde{G}_{2k}(x, \xi, \tau-t) F_k(\xi, t) d\xi dt, \tag{27.20}
 \end{aligned}$$

$$\begin{aligned}
 H_q(x, \tau) &= \sum_{k=1}^{N+2} \int_0^\tau [G_{q+2,k}(x, \tau-t)f_{k1}(t) + G_{q+2,k}(1-x, \tau-t)f_{k2}(t)] dt \\
 &\quad + \sum_{k=1}^{N+2} \int_0^\tau \int_0^1 \tilde{G}_{q+2,k}(x, \xi, \tau-t) F_k(\xi, t) d\xi dt.
 \end{aligned}$$

Here, $x = x_1$; $F_k(x, \tau)$ are body force factors present in equations (27.15); $f_{kl}(\tau)$ are surface disturbances from boundary conditions (27.13), (27.18), (27.19); $G_{mk}(x, \tau)$ are surface Green's functions which satisfy equations [24]

$$\begin{aligned}
 \ddot{G}_{1k} - \mu k^2 (G''_{1k} - G'_{2k}) &= 0, \\
 \ddot{G}_{2k} - G''_{2k} - \frac{F}{J_3} \mu k^2 (G'_{1k} - G_{2k}) - \sum_{q=1}^N \alpha_q G'_{q+2,k} &= 0, \tag{27.21} \\
 \dot{G}_{q+2,k} - D_q G''_{q+2,k} - \Lambda_q G'''_{2k} &= 0,
 \end{aligned}$$

and boundary conditions ($\delta(\tau)$ are Dirac delta function):

$$\begin{aligned}
 G_{1k}|_{x=0} &= \delta_{1k} \delta(\tau), \quad G_{1k}|_{x=1} = 0, \\
 G_{q+1,k}|_{x=0} &= \delta_{q+1,k} \delta(\tau), \quad G_{q+1,kl}|_{x=1} = 0, \\
 \left(G'_{2k} + \sum_{j=1}^N \alpha_j G_{j+1,k} \right) \Big|_{x=0} &= \delta_{2k} \delta(\tau), \quad \left(G'_{2k} + \sum_{j=1}^N \alpha_j G_{j+1,k} \right) \Big|_{x=1} = 0. \tag{27.22}
 \end{aligned}$$

$\tilde{G}_{mk}(x, \xi, \tau)$ are the bulk Green's functions that satisfy equations

$$\begin{aligned} \ddot{\tilde{G}}_{1k} - \mu k^2 \left(\tilde{G}''_{1k} - \tilde{G}'_{2k} \right) - \delta_{1k} \delta(x - \xi) \delta(\tau) &= 0, \\ \ddot{\tilde{G}}_{2k} - \tilde{G}'_{2k} - \frac{F}{J_3} \mu k^2 \left(\tilde{G}'_{1k} - \tilde{G}_{2k} \right) - \sum_{q=1}^N \alpha_q \tilde{G}'_{q+2,k} - \delta_{2k} \delta(x - \xi) \delta(\tau) &= 0, \\ \dot{\tilde{G}}_{q+2,k} - D_q \tilde{G}_{q+2,k} - \Lambda_q \tilde{G}'''_{2k} - \delta_{q+2,k} \delta(x - \xi) \delta(\tau) &= 0, \end{aligned}$$

and homogeneous boundary conditions corresponding to (27.22).

27.4 Solution Algorithm

We consider the problem of finding the surface Green’s functions $G_{mk}(x, \tau)$. By applying Laplace transform to (27.21) and (27.22), we get

$$\begin{aligned} s^2 G^L_{1k} - \mu k^2 \left(G''^L_{1k} - G'^L_{2k} \right) &= 0, \\ s^2 G^L_{2k} - G''^L_{2k} - \mu \frac{F}{J_3} k^2 \left(G'^L_{1k} - G^L_{2k} \right) - \sum_{q=1}^N \alpha_q G'^L_{q+2,k} &= 0, \\ s G^L_{q+2,k} - D_q G''^L_{q+2,k} - \Lambda_q G'''^L_{2k} &= 0; \\ \left(G^L_{1k} \Big|_{x=0} = \delta_{1k}, \quad G^L_{1k} \Big|_{x=1} = 0, \right. \\ \left. \left(G'^L_{2k} + \sum_{j=1}^N \alpha_j G^L_{j+2,k} \right) \Big|_{x=0} = \delta_{2k}, \quad \left(G'^L_{2k} + \sum_{j=1}^N \alpha_j G^L_{j+2,k} \right) \Big|_{x=1} = 0, \right. \\ \left. G^L_{q+2,k} \Big|_{x=0} = \delta_{q+2,k}, \quad G^L_{q+2,k} \Big|_{x=1} = 0. \right. \end{aligned}$$

Then, we represent all functions $G^L_{mk}(x, s)$ as series ($\lambda_n = \pi n$):

$$\begin{aligned} \left\{ \begin{array}{l} G^L_{1k}(x, s) \\ G^L_{q+2,k}(x, s) \end{array} \right\} &= \sum_{n=1}^{\infty} \left\{ \begin{array}{l} G^{Ls}_{1k}(\lambda_n, s) \\ G^{Ls}_{q+2,k}(\lambda_n, s) \end{array} \right\} \sin \lambda_n x, \\ G^L_{2k}(x, s) &= \frac{G^{Lc}_{2k}(0, s)}{2} + \sum_{n=1}^{\infty} G^{Lc}_{2k}(\lambda_n, s) \cos \lambda_n x, \end{aligned}$$

As a result, we obtain a system of linear algebraic equations of functions $G^{Ls}_{mk}(\lambda_n, s)$ ($m, k = 1, N + 1$):

$$\begin{aligned} k_1 G^{Ls}_{1k} - \mu \lambda_n k^2 G^{Lc}_{2k} &= F_{1k}, \\ -\mu k^2 \lambda_n \frac{F}{J_3} G^{Ls}_{1k} + k_2 G^{Lc}_{2k} - \lambda_n \sum_{q=1}^N \alpha_q G^{Ls}_{q+2,k} &= F_{2k}, \\ -\Lambda_q \lambda_n^3 G^{Lc}_{2k} + k_{q+2} G^{Ls}_{q+2,k} &= F_{q+2,k}, \end{aligned}$$

$$k_1(\lambda_n, s) = s^2 + \mu k^2 \lambda_n^2, \quad k_2(\lambda_n, s) = s^2 + \lambda_n^2 + \mu k^2 \frac{F}{J_3}, \quad k_{q+2}(\lambda_n, s) = s + D_q \lambda_n^2,$$

$$F_{1k}(\lambda_n) = 2\mu k^2 \lambda_n \delta_{1k}, \quad F_{2k}(\lambda_n) = -2\mu k^2 \frac{F}{J_3} \delta_{1k} - 2\delta_{2k},$$

$$F_{q+2,k}(\lambda_n) = 2\Lambda_q \lambda_n \delta_{2k} + 2\lambda_n \left(D_q \delta_{q+2,k} - \Lambda_q \sum_{j=1}^N \alpha_j \delta_{j+2,k} \right).$$

The solution to this system is the following ($q, p = \overline{1, N}, k = \overline{1, N+1}$) [24]:

$$G_{ik}^{Ls}(\lambda_n, s) = \frac{P_{ik}(\lambda_n, s)}{P(\lambda_n, s)} \quad (i = 1, 2),$$

$$G_{q+2,1}^{Ls}(\lambda_n, s) = \frac{P_{q+2,1}(\lambda_n, s)}{P(\lambda_n, s)}, \quad G_{q+2,2}^{Ls}(\lambda_n, s) = \frac{2\Lambda_q \lambda_n}{k_{q+2}} + \frac{P_{q+2,2}(\lambda_n, s)}{Q_q(\lambda_n, s)},$$

$$G_{q+2,p+2}^{Ls}(\lambda_n, s) = \frac{2\lambda_n (D_q \delta_{pq} - \Lambda_q \alpha_p)}{k_{q+2}} + \frac{P_{q+2,p+2}(\lambda_n, s)}{Q_q(\lambda_n, s)}, \quad (27.23)$$

where

$$P(\lambda_n, s) = \left[k_1(\lambda_n, s) k_2(\lambda_n, s) - \mu^2 k^4 \lambda_n^2 \frac{F}{J_3} \right] \Pi(\lambda_n, s) - \lambda_n^4 k_1(\lambda_n, s) \sum_{j=1}^N \alpha_j \Lambda_j \Pi_j(\lambda_n, s),$$

$$Q_q(\lambda_n, s) = k_{q+2}(\lambda_n, s) P(\lambda_n, s);$$

$$P_{11}(\lambda_n, s) = 2\mu k^2 \lambda_n \left[\left(k_2(\lambda_n, s) - \mu k^2 \frac{F}{J_3} \right) \Pi(\lambda_n, s) - \lambda_n^4 \sum_{j=1}^N \alpha_j \Lambda_j \Pi_j(\lambda_n, s) \right],$$

$$P_{12}(\lambda_n, s) = -2\mu k^2 \lambda_n \left[\Pi(\lambda_n, s) - \lambda_n^2 \sum_{j=1}^N \alpha_j \Pi_j(\lambda_n, s) \Lambda_j \right],$$

$$P_{1,q+2}(\lambda_n, s) = 2\mu k^2 \alpha_q \lambda_n^3 \left[\Pi_q(\lambda_n, s) D_q - \sum_{j=1}^N \alpha_j \Lambda_j \Pi_j(\lambda_n, s) \right],$$

$$P_{21}(\lambda_n, s) = 2\mu k^2 \frac{F}{J_3} \Pi(\lambda_n, s) [\mu k^2 \lambda_n^2 - k_1(\lambda_n, s)],$$

$$P_{22}(\lambda_n, s) = -2k_1(\lambda_n, s) \left[\Pi(\lambda_n, s) - \lambda_n^2 \sum_{j=1}^N \alpha_j \Lambda_j \Pi_j(\lambda_n, s) \right],$$

$$P_{2,q+2}(\lambda_n, s) = 2\lambda_n^2 \alpha_q k_1(\lambda_n, s) \left[\Pi_q(\lambda_n, s) D_q - \sum_{j=1}^N \alpha_j \Lambda_j \Pi_j(\lambda_n, s) \right],$$

$$\begin{aligned}
 P_{q+2,1}(\lambda_n, s) &= 2\mu k^2 \Lambda_q \lambda_n^3 \frac{F}{J_3} [\mu k^2 \lambda_n^2 - k_1(\lambda_n, s)] \Pi_q(\lambda_n, s), \\
 P_{q+2,2}(\lambda_n, s) &= -2\Lambda_q \lambda_n^3 k_1(\lambda_n, s) \left[\Pi(\lambda_n, s) - \lambda_n^2 \sum_{j=1}^N \alpha_j \Lambda_j \Pi_j(\lambda_n, s) \right], \\
 P_{q+2,p+2}(\lambda_n, s) &= 2\alpha_p \Lambda_q \lambda_n^4 k_1(\lambda_n, s) \left[\Pi_p(\lambda_n, s) D_p - \sum_{j=1}^N \alpha_j \Lambda_j \Pi_j(\lambda_n, s) \right], \\
 \Pi(\lambda_n, s) &= \prod_{j=1}^N k_{j+1}(\lambda_n, s), \quad \Pi_j(\lambda_n, s) = \prod_{r=1, r \neq j}^N k_{r+1}(\lambda_n, s).
 \end{aligned}$$

Originals of Green’s functions in (27.23) are as following [24]:

$$\begin{aligned}
 G_{ik}^s(\lambda_n, \tau) &= \sum_{j=1}^{N+4} A_{ik}^{(j)}(\lambda_n) e^{s_j(\lambda_n)\tau}, \quad A_{ik}^{(j)}(\lambda_n) = \frac{P_{ik}(\lambda_n, s_j)}{P'(\lambda_n, s_j)}, \\
 G_{q+2,1}^s(\lambda_n, \tau) &= \sum_{j=1}^{N+4} A_{q+2,1}^{(j)}(\lambda_n) e^{s_j(\lambda_n)\tau}, \quad A_{q+2,1}^{(l)}(\lambda_n) = \frac{P_{q+2,1}(\lambda_n, s_l)}{P'(\lambda_n, s_l)}, \\
 G_{q+2,2}^s(\lambda_n, \tau) &= -2\Lambda_q \lambda_n e^{-D_q \lambda_n^2 \tau} + \sum_{j=1}^{N+5} A_{q+2,2}^{(j)}(\lambda_n) e^{s_j(\lambda_n)\tau}, \\
 G_{q+2,p+2}^s(\lambda_n, \tau) &= 2\lambda_n (D_q \delta_{pq} - \Lambda_q \alpha_p) e^{-D_q \lambda_n^2 \tau} + \sum_{l=1}^{N+5} A_{q+2,p+2}^{(l)}(\lambda_n) e^{s_l(\lambda_n)\tau}, \\
 A_{q+2,p+2}^{(l)}(\lambda_n) &= \frac{P_{q+2,p+2}(\lambda_n, s_l)}{Q'_q(\lambda_n, s_l)}, \quad A_{q+2,2}^{(l)}(\lambda_n) = \frac{P_{q+2,2}(\lambda_n, s_l)}{Q'_q(\lambda_n, s_l)}.
 \end{aligned}$$

Here, $s_j(\lambda_n)$ are zeros of polynomial $P(\lambda_n, s)$, $s_{N+3}(\lambda_n) = -D_q \lambda_n^2 \tau$.

Body Green functions are found in a similar way. Substituting the found expressions for the Green functions into convolutions (27.20), we obtain the solution to the problem of the bending of the Timoshenko beam (27.15), (27.13), (27.18), (27.19).

27.5 Example of Computation

We consider the beam that has the rectangular cross section: height $h = 10^{-2}$ m, width $b = 5 \times 10^{-3}$ m, length $l = 10^{-1}$ m. We done the calculation example for two-component ($N = 2$) duralumin medium [27], with the following dimensionless characteristics

$$\lambda = 4.92 \times 10^{-1}, \quad \mu = 2.54 \times 10^{-1}, \quad \alpha_1 = 1.50 \times 10^{-4}, \quad \alpha_2 = 5.92 \times 10^{-4}, \\ D_1 = 1.27 \times 10^{-16}, \quad D_2 = 5.02 \times 10^{-21}, \quad \Lambda_1 = 2.77 \times 10^{-18}, \quad \Lambda_2 = 5.50 \times 10^{-23}.$$

The geometric dimensionless characteristics of the rectangular cross section of this beam are as follows:

$$F = bh = 5.00 \times 10^{-3}, \quad J_3 = 4.17 \times 10^{-6}.$$

Design parameters in boundary conditions ($q = 1, 2$):

$$\left. \begin{aligned} \left(\chi' + \sum_{j=1}^2 \alpha_j H_j \right) \\ \left(\chi' + \sum_{j=1}^2 \alpha_j H_j \right) \end{aligned} \right|_{x=0} = -\frac{M_0}{J_3} = f_{11}(\tau) = H(\tau), \\ = -\frac{M_0}{J_3} = f_{12}(\tau) = H(\tau),$$

$$v|_{x=0} = V_0 = f_{21}(\tau) = 0, \quad v|_{x=1} = V_1 = f_{22}(\tau) = 0,$$

$$H_q|_{x=0} = H_{q0} = f_{q+2,1}(\tau) = 0, \quad H_q|_{x=1} = H_{q1} = f_{q+2,2}(\tau) = 0.$$

The calculation of convolutions (27.20)

$$v(x, \tau) = \int_0^\tau [G_{11}(x, \tau - t) + G_{11}(1 - x, \tau - t)] H(t) dt \\ = 2 \sum_{n=1}^{\infty} \sin \frac{\lambda_n}{2} \cos \left[\lambda_n \left(\frac{1}{2} - x \right) \right] \sum_{j=1}^4 A_{11}^{(j)}(\lambda_n) \frac{e^{s_j(\lambda_n)\tau} - 1}{s_j(\lambda_n)}, \\ \chi(x, \tau) = \int_0^\tau [G_{21}(x, \tau - t) - G_{21}(1 - x, \tau - t)] H(t) dt \\ = 2 \sum_{n=1}^{\infty} \sin \frac{\lambda_n}{2} \sin \left[\lambda_n \left(\frac{1}{2} - x \right) \right] \sum_{j=1}^4 A_{21}^{(j)}(\lambda_n) \frac{e^{s_j(\lambda_n)\tau} - 1}{s_j(\lambda_n)}, \\ H_q(x, \tau) = \int_0^\tau [G_{q+2,1}(x, \tau - t) + G_{q+2,1}(1 - x, \tau - t)] H(t) dt \\ = 2 \sum_{n=1}^{\infty} \sin \frac{\lambda_n}{2} \cos \left[\lambda_n \left(\frac{1}{2} - x \right) \right] \sum_{j=1}^4 A_{q+2,1}^{(j)}(\lambda_n) \frac{e^{s_j(\lambda_n)\tau} - 1}{s_j(\lambda_n)}.$$

The calculation results are shown in Figs. 27.2, 27.3 and 27.4.

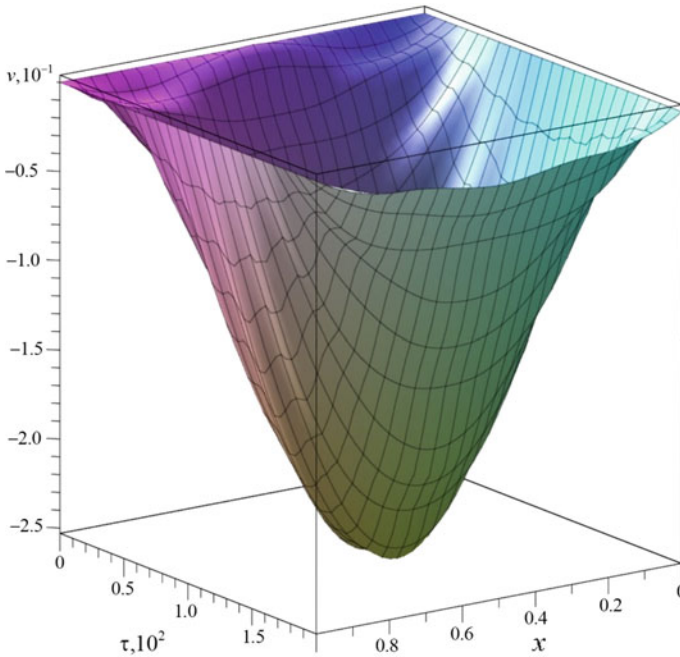


Fig. 27.2 Beam deflections

27.6 Conclusions

Thus, the coupled unsteady model of elastodiffusive Timoshenko beam oscillations is presented. An algorithm for constructing the surface Green functions of the problem is proposed. The use of the unknown functions expansion into series by eigenfunctions allows us to solve the problem associated with the Laplace transform inversion. Such an approach makes it possible to find an analytical solution to the oscillation problem of an elastic diffusion Timoshenko beam.

Based on the developed model, the interaction of mechanical and diffusion fields is investigated. The results of calculations are presented in analytical and graphical forms.

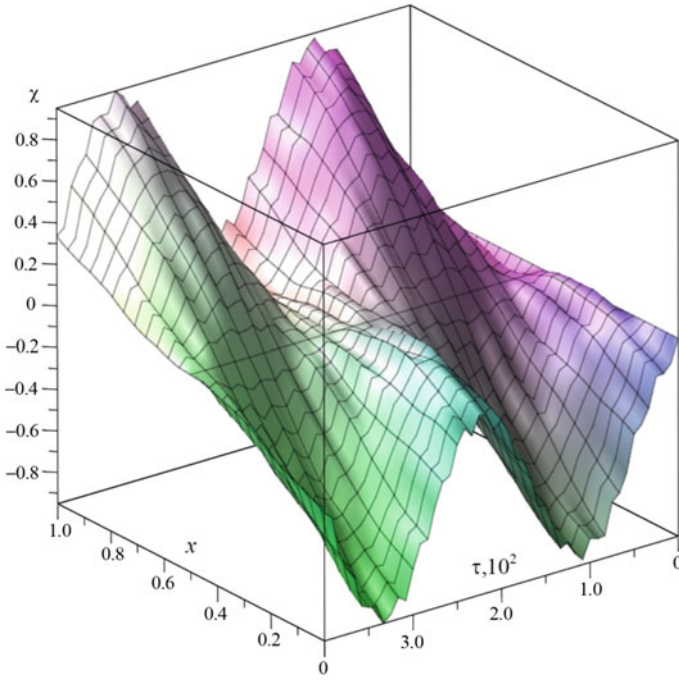
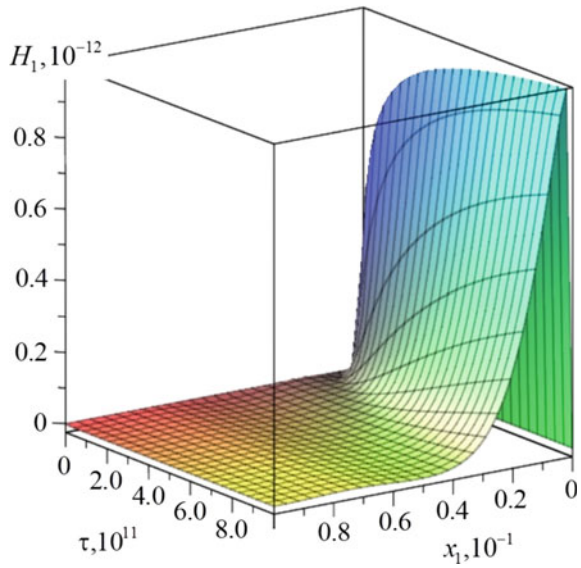


Fig. 27.3 Angle of rotation of the normal to the mid-surface of the beam

Fig. 27.4 Concentration increment



References

1. Chen, W.Q., Ding, H.J., Ling, D.S.: Thermoelastic field of transversely isotropic elastic medium, containing a penny-shaped crack: exact fundamental solution. *Int. J. Solids Struct.* **41**, 69–83 (2004)
2. Kumar, R., Vashisth, A.K., Suniti, S.: Waves in anisotropic thermoelastic medium with phase lag, two-temperature and void. *Mater. Phys. Mech.* **35**, 126–138 (2018)
3. Aouadi, M.: Hybrid Laplace transform-finite element method to a generalized electromagneto-thermoelastic problem. *Appl. Math. Model.* **31**, 712–726 (2007)
4. Chen, T., Lin, F.Z.: Boundary integral formulations for three-dimensional anisotropic piezoelectric solid. *Comput. Mech.* **15**, 485–496 (1995)
5. Chu, H.J., Pan, E., Ramsey, J.J., Wang, J., Xue, C.X.: A general perturbation method for in homogeneities in anisotropic and piezoelectric solids with applications to quantum-dot nanostructures. *Int. J. Solids Struct.* **48**, 673–679 (2011)
6. Hou, P.F., Yi, T., Wang, L.: 2D General Solution and Fundamental Solution for Orthotropic Electro-Magneto-Thermo-elastic Materials. *J. Therm. Stresses* **31**, 807–822 (2008)
7. Igumnov, L., Markov, I., Vorobtsov, I., Litvinchuk, S., Bragov, A.: Three-dimensional BEM for transient dynamic analysis of piezoelectric and anisotropic elastic solids. In: *EPJ Web of Conferences*, vol. 94, pp. 04025 (2015)
8. Kaloski, S., Nowacki, W.: Wave Propagation of Thermo-Magneto-Microelasticity. *Bulletin of the Polish Academy of Sciences Technical Sciences* **18**, 155–158 (1970)
9. Pan, E.: Three-dimensional Green's functions in anisotropic magneto-electro-elastic bimetals. *Z. angew. Math. Phys.* **53**, 815–838 (2002)
10. Vestyak, V.A., Hachkevych, A.R., Tarlakovskii, D.V., Terletskii, R.F.: Elastic half plane under the action of nonstationary surface kinematic perturbations. *J. Math. Sci.* **203**(2), 202–214 (2014)
11. Afram, A.Y., Khader, S.E.: 2D problem for a half-space under the theory of fractional thermoelastic diffusion. *Am. J. Sci. Ind. Res.* **6**(3), 47–57 (2014)
12. Aouadi, M.: A generalized thermoelastic diffusion problem for an infinitely long solid cylinder. *Int. J. Math. Math. Sci.* **2006**, 1–15 (2006)
13. Atwa, S.Y., Egypt, Z.: Generalized thermoelastic diffusion with effect of fractional parameter on plane waves temperature-dependent elastic medium. *J. Mater. Chem. Eng.* **1**(2), 55–74 (2013)
14. Belova, I.V., Murch, G.E.: Thermal and diffusion-induced stresses in crystalline solids. *J. Appl. Phys.* **77**(1), 127–134 (1995)
15. Deswal, S., Kalkal, K.: A two-dimensional generalized electro-magneto-thermoviscoelastic problem for a half-space with diffusion. *Int. J. Therm. Sci.* **50**(5), 749–759 (2011)
16. Elhagary, M.A.: Generalized thermoelastic diffusion problem for an infinitely long hollow cylinder for short times. *Acta Mech.* **218**, 205–215 (2011)
17. Indeitsev, D.A., Semenov, B.N., Sterlin, M.D.: The phenomenon of localization of diffusion process in a dynamically deformed solid. *Doklady Phys.* **57**(4), 171–173 (2012)
18. Knyazeva, A.G.: Model of medium with diffusion and internal surfaces and some applied problems. *Mater. Phys. Mech.* **7**(1), 29–36 (2004)
19. Kumar, R., Chawla, V.: Study of fundamental solution in orthotropic thermodiffusive elastic media. *Int. Commun. Heat Mass Transfer* **38**, 456–462 (2011)
20. Sherief, H.H., El-Maghraby, N.M.: A thick plate problem in the theory of generalized thermoelastic diffusion. *Int. J. Thermophys.* **30**, 2044–2057 (2009)
21. Poroshina, N.I., Ryabov, V.M.: Methods for Laplace transform inversion. *Vestn. St. Petersburg Univ. Math.* **44**(3), 214–222 (2011)
22. Zemskov, A.V., Tarlakovskii, D.V.: Unsteady vibration model of the Euler-Bernoulli beam taking into account diffusion. *J. Phys. Conf. Ser.* **1158**, 042043 (2019)
23. Tarlakovskii, D.V., Zemskov, A.V.: An elastodiffusive orthotropic Euler-Bernoulli beam with considering diffusion flux relaxation. *Math. Comput. Appl.* **24**(1), 23 (2019)

24. Afanasieva, O. A., Gafurov, U.S., Zemskov, A.V.: Unsteady elastic diffusion oscillations of a Timoshenko beam with considering the diffusion relaxation effects. In: Proceedings of the Second International Conference on Theoretical, Applied and Experimental Mechanics, pp. 193–199. Springer Nature Switzerland AG (2019)
25. Davydov, S.A., Zemskov, A.V.: Unsteady one-dimensional perturbations in multicomponent thermoelastic layer with cross-diffusion effect. *J. Phys. Conf. Ser.* **1129**, 012009 (2018)
26. Mikhailova, E.Yu., Tarlakovskii, D.V., Fedotenkov, G.V.: *Obshchaya teoriya uprugikh obolochek*. Moscow, MAI, Russia (2018). [In Russian]
27. Grigoriev, I.S., Meylikhov I.Z. (eds.): *Fizicheskiye velichiny: Spravochnik*. Moscow, Energoatomizdat, Russia (1991) [In Russian]
28. Gorshkov, A.G., Medvedsky, A.L., Rabinsky, L.N., Tarlakovsky, D.V.: *Volny v sploshnykh sredakh*. Moscow. Fizmatlit, Russia (2004). [In Russian]